AD NUMBER
AD368640
CLASSIFICATION CHANGES
TO: **UNCLASSIFIED**
FROM: **CONFIDENTIAL**
LIMITATION CHANGES
TO: **Approved for public release; distribution is unlimited.**
FROM: **Distribution authorized to U.S. Gov't. agencies and their contractors; Administrative/Operational Use; DEC 1965. Other requests shall be referred to Air Force Rocket Propulsion Lab., Attn: Research and Technology Div., Edwards AFB, CA 93525.**
AUTHORITY
31 Dec 1977, Group-4, DoDD 5200.10, per document marking AFRPL ltr dtd 7 May 1973

SECURITY MARKING

The classified or limited status of this report applies to each page, unless otherwise marked.
Separate page printouts MUST be marked accordingly.

THIS DOCUMENT CONTAINS INFORMATION AFFECTING THE NATIONAL DEFENSE OF THE UNITED STATES WITHIN THE MEANING OF THE ESPIONAGE LAWS, TITLE 18, U.S.C., SECTIONS 793 AND 794. THE TRANSMISSION OR THE REVELATION OF ITS CONTENTS IN ANY MANNER TO AN UNAUTHORIZED PERSON IS PROHIBITED BY LAW.

NOTICE: When government or other drawings, specifications or other data are used for any purpose other than in connection with a definitely related government procurement operation, the U. S. Government thereby incurs no responsibility, nor any obligation whatsoever; and the fact that the Government may have formulated, furnished, or in any way supplied the said drawings, specifications, or other data is not to be regarded by implication or otherwise as in any manner licensing the holder or any other person or corporation, or conveying any rights or permission to manufacture, use or sell any patented invention that may in any way be related thereto.

CONFIDENTIAL

Report AFRPL-TR-65-191

HIGH CHAMBER PRESSURE ROCKETRY PROGRAM (u)

Final Report

Contract AF 04(611)-8191

Book One
of Two

Prepared for

ROCKET PROPULSION LABORATORY
Research and Technology Division
Air Force Systems Command
United States Air Force
Edwards, California

AIR FORCE PROGRAM STRUCTURE NO. 750G
AFSC PROJECT NO. 3058
AFSC TASK NO. 305802

CONFIDENTIAL

CONFIDENTIAL

December 1965

Report AFRPL-TR-65-191

AGC Report 8191-F

HIGH CHAMBER PRESSURE ROCKETRY PROGRAM (u)

Final Report

Contract AF 04(611)-8191

Book One
of Two

Prepared for

ROCKET PROPULSION LABORATORY
Research and Technology Division
Air Force Systems Command
United States Air Force
Edwards, California

AIR FORCE PROGRAM STRUCTURE NO. 750G
AFSC PROJECT NO. 3058
AFSC TASK NO. 305802

6381T

AEROJET-GENERAL CORPORATION
A SUBSIDIARY OF THE GENERAL TIRE & RUBBER COMPANY

CONFIDENTIAL

Book One

FOREWORD

The High Chamber Pressure Rocketry Program, Contract AF 04(611)-8191, was performed by Aerojet-General Corporation, Sacramento, California. Program structure number is 750G; AFSC project number is 3058. The work covered the period 1 May 1962 through 15 June 1965.

The program was conducted by the Advanced Storable Engine Division of the Liquid Rocket Operations. The program manager was Mr. R. Beichel. Technical managerial control was provided by Mr. R. A. Hankins, Project Manager. The Project Engineer was Mr. H. B. Scammon.

The Air Force Project Officer for this contract was Mr. R. R. Weiss, Rocket Propulsion Laboratory, Edwards, California.

This report contains no classified information extracted from other classified documents except for that taken from monthly and quarterly reports previously published for this contract.

The report number assigned to this document by the Aerojet-General Corporation is 8191-F.

This report has been published in two books. Book One contains Sections 1 through VII and Book Two contains Sections VIII through XII.

This technical report has been reviewed and is approved.

Book One

ABSTRACT

The objective of this program was to investigate, by both experimental testing and supporting analytical studies, the feasibility and degree of advantage of high chamber pressure rocket engines using nitrogen tetroxide/50% UDMH--50% N_2H_4 propellants. Both uncooled and cooled thrust chambers were test-fired at the 3000-psia pressure level; supporting studies included a study of the gas-side heat transfer coefficient, a propellants investigation which included some advanced propellant combinations, and system studies to determine the degree of advantage of high chamber pressure. Two injector concepts were developed using uncooled chambers, one of which attained a performance level of 97% c*. Cooling systems investigated during cooled chamber t sting included regenerative cooling with both oxidizer and fuel, film cooling with oxidizer, thermal barrier coatings, and vortex cooling. Based on the test results and supporting studies, it is concluded that operation of engines at high chamber pressure is feasible, and that the optimum chamber pressure is in the range of 2500 to 3500 psia. The best potential cooling system for future advanced high-pressure engines is regenerative cooling using N_2O_4 in combination with a thermal barrier coating and film cooling.

Book One

TABLE OF CONTENTS

TABLE OF CONTENTS (cont.)

Book One

TABLE OF CONTENTS (cont.)

Book One

FIGURE LIST

FIGURE LIST (cont.)

FIGURE LIST (cont.)

FIGURE LIST (cont.)

FIGURE LIST (cont.)

FIGURE LIST (cont.)

FIGURE LIST (cont.)

I. INTRODUCTION

1. INTRODUCTION

Book One

I. INTRODUCTION

This is the final report submitted in fulfillment of Contract AF 04(611)-8191, "High Chamber Pressure Rocketry Program." The period covered by this report is from 1 May 1962 through 15 June 1965, which was the technical effort period of performance. Eleven quarterly progress reports were submitted during the course of the program, which provided a summary of accomplishments, discussed problem areas, and presented planned programs for the periods covered.

The objective of the program was to provide the study, analysis, design, and combustion research required to establish the feasibility and degree of advantage of high chamber pressure rocket engines using nitrogen tetroxide/50% UDMH--50% N_2H_4 (N_2O_4/AeroZINE 50) propellants. It was also the purpose of the program to determine a reasonable upper limit to high chamber pressure rocketry, above which development effort, production costs, and increasing propulsion package weight negate additional performance gains.

The results of the program are summarized in Section II. The final work statement to which the program was performed is presented in Section III. Complete technical discussions covering all aspects of the program are reported in Sections IV through XII.

II. PROGRAM SUMMARY

A. INTRODUCTION

The program technical effort consisted of five main tasks: Propellants Investigation, Gas-Side Heat Transfer Study, Uncooled Chamber Program, Cooled Chamber Program, and System Studies. Results of the overall program are discussed in Section II,B; program accomplishments for each of the major tasks are summarized in Sections II,C through II,G. The master program schedule, which shows the time period during which each phase of the effort was performed, is shown in Figure II-A-1. The occurrence of each test is also noted on this schedule. A cumulative summary of the test results for all thrust chamber testing performed in this program is given in Figure II-A-2.

B. OVERALL PROGRAM RESULTS

The feasibility of high chamber pressure rocket engines using nitrogen tetroxide/50% UDMH--50% N_2H_4 was demonstrated in this program. Both uncooled and cooled thrust chambers, operating at chamber pressures in the range of 3000 psia, were evaluated during the test program which encompassed 48 tests. The propellants were supplied to the thrust chamber by high-pressure centrifugal turbopumps that had lightweight rotating components.

Based upon the test results, together with the results of analytical investigations performed as a part of this program, the following conclusions are made.

1. Operation of engines at high chamber pressure is feasible. In this program, stable injector performance of 97% of c* at 3000 psia was achieved; all portions of a cooled combustion chamber, including the chamber, throat, and expansion nozzle sections, were operated successfully under thermal steady-state conditions.

II, B, Overall Program Results (cont.)

2. The best potential cooling system for future advanced high-pressure engines is regenerative cooling using N_2O_4 in combination with a thermal barrier coating and film cooling. Results from this program, together with data from several other programs conducted by Aerojet-General as well as by other contractors, form the basis for this selection. Recent investigations conducted under Contract AF 04(611)-10830, "Advanced Rocket Engine, Storable," indicate that transpiration cooling with N_2O_4 also potentially offers a practical high performance cooling system design.

3. The staged-combustion engine cycle, in combination with high chamber pressure, offers significant payload increases over conventional systems. For single-stage vehicles, a potential payload increase of 75% is possible. Analytical studies indicated optimum chamber pressure is approximately 3500 psia. However, differences in payload between 2500 and 4500 psig are very small (less than 1/2%), and practical considerations dictate the best chamber pressure to be near the low end of this range. High chamber pressure in combination with the gas generator cycle offers a maximum payload improvement of 50% (single-stage vehicle). Optimum chamber pressure with this system is 2000 psia. For either staged-combustion or gas generator cycle engines, operating at any pressure, the choice of thrust chamber nozzle--Delaval or forced-deflection--will depend on the specific vehicle and application. No one nozzle type showed clear performance gains over the other.

4. Large payload gains are potentially achievable by the use of advanced propellants in combination with high chamber pressure and the staged-combustion engine cycle. Recommended propellant systems for development in the near future are N_2O_4/Alumizine and 98% H_2O_2/Alumizine. For the systems studied, the highest payload gains were with 98% H_2O_2/beryllium hydride. However, this fuel is still in the phase of basic research development.

II, Program Summary (cont.)

C. PROPELLANTS INVESTIGATION

The Propellants Investigation was conducted during the period from May 1962 through January 1963. Its goals were to establish the theoretical performance and heat-transfer design criteria as well as to define the problem areas likely to result from the use of N_2O_4/AeroZINE 50 and selected additive propellant combinations in high-pressure rocket engines. The selected additive propellants were N_2O_4/N_2H_4 + Al, N_2O_4/N_2H_4 + AlH_3, N_2O_4/N_2H_4 + Be, N_2O_4/N_2H_4 + BeH_2, 98% H_2O_2/N_2H_4 + Al, 98% H_2O_2/N_2H_4 + AlH_3, 98% H_2O_2/N_2H_4 + Be, and 98% H_2O_2/N_2H_4 + BeH_2.

Extensive theoretical performance calculations and the extension of significant propellant physical properties utilizing estimation techniques were made to provide the basic data required for more detailed heat-transfer analyses and system studies. These data were compiled into a special report issued under this contract.* This report constitutes the contractural commitment for the reporting of this effort, and as such, becomes a part of this final report. On the basis of a literature and experience review and the performance and properties calculations, the more desirable propellants were selected for the study of likely problem areas. After identifying the more significant problem areas, research and development programs were recommended which would overcome the problems and lead to the successful development of the better metalized propellants.

D. GAS-SIDE HEAT-TRANSFER STUDY

A detailed study of the gas-side heat transfer coefficient was performed with the high-pressure thrust chamber design used in this program. The objectives of this study were three-fold:

* Aerojet-General Report LRP 302, 1 March 1963 (conf). Performance and Properties of N_2O_4 AeroZINE 50 and Selected Metalized Storables (u).

II, D, Gas-Side Heat-Transfer Study (cont.)

1. To evaluate existing analytical methods of determining gas-side heat-transfer coefficients for application to high-pressure engines.

2. To investigate specialized techniques for experimental measurement of gas-side heat-transfer coefficients.

3. Using instrumentation based on the results of 2., above, obtain experimental measurements of the gas-side heat-transfer coefficients and compare them with the analytical predictions.

In the analytical studies, gas-side heat-transfer coefficients were determined by three analytical methods: the Bartz short form; twice-Bartz short form diminishing linearly; the Mayer's approximation. In the cylindrical section of the combustion chamber, the Bartz short form yields the lower heat-transfer coefficient values, whereas in the convergent and divergent section of the nozzle, Mayer's approximation yields the lowest values. The twice-Bartz short form diminishing linearly is the most conservative of the three analytical methods, and was the method selected for determining the heat-transfer characteristics in the various cooling studies conducted in this program. Using this method, the resulting gas-side heat-transfer coefficients in the chamber and throat section of a 50,000-lb-thrust 3000-psia thrust chamber were calculated to be 0.006 and 0.016 Btu/sec-in.^{2}-°F, respectively.

Prior to conducting the test firings, an investigation of available instrumentation revealed that no present state-of-the-art heat flux calorimeters could withstand the environment of high chamber pressure thrust chambers. Gas-side coefficients can be calculated from the transient temperature characteristics of the chamber wall using the "Schmidt Plot" analysis. It was decided to attempt to obtain the experimental data by measuring the temperature at various points in the chamber wall using special fast-response high-temperature thermocouples. The thermocouples were imbedded into graphite of known thermal conductivity at measured distances from the gas-side wall.

II, D, Gas-Side Heat-Transfer Study (cont.)

Measurements were first attempted in uncooled chambers having graphite liners. However, failure of the liners precluded the obtaining of any heat flux measurements. The choice chamber liners was subsequently changed to ablative materials; thermocouples were then imbedded into graphite plugs which were installed into the chamber wall. Two thrust chamber firings were conducted in which data were recorded. The temperature measurements recorded by the thermocouple located in the cylindrical portion of the chamber corresponded to the twice-Bartz correlation prediction. Other data indicated that the coefficients were five to ten times lower than the analytical values, which must be considered invalid. It was concluded that the ablation gases issuing from the chamber liner were responsible for the invalid data. It was hoped that the graphite plug would provide enough isolation of the thermocouple from the liner so that true uncooled conditions would be recorded; unfortunately this was not the case. No further attempts were made to determine the gas-side coefficient.

E. UNCOOLED THRUST CHAMBER PROGRAM

The broad objective of the Uncooled Thrust Chamber Program was to investigate the performance, heat transfer, and general operating characteristics of N_2O_4/AeroZINE 50 at a combustion chamber pressure of approximately 3000 psia. The information and data gained from this effort was then to be used as a reference for the evaluation of high-pressure operation with cooled thrust chamber hardware.

To meet this objective, a program was formulated and conducted which included the following elements:

1. Design and development of an uncooled thrust chamber capable of operating for short durations (up to 5 sec) in the environment produced by extremely high chamber pressure (3000 to 5000 psia).

II, E, Uncooled Thrust Chamber Program (cont.)

2. Design of several injector concepts for high-pressure operation and test evaluation of the most promising concepts to determine their performance, combustion characteristics, and overall design adequacy.

3. Using the results of the analytical investigations performed in the Gas-Side Heat Transfer Studies, experimentally determine the gas-side heat-transfer coefficients in the combustion chamber.

Based upon the above criteria, the Uncooled Chamber Program was conducted. The program is summarized in Figure II-E-1. Twenty tests were performed, of which 15 reached steady-state conditions to produce valid data. This testing demonstrated the feasibility of obtaining high performance, stable combustion at chamber pressures in the range of 3000 psia. (One injector tested demonstrated 97% of c* at 3050 psia with peak-to-peak chamber pressure oscillations below 2% of the nominal pressure.) In addition, a vast amount of design information was derived which, properly utilized, can be of great benefit to the design of future high-pressure engines. A brief summary describing the type of specific design information derived for the uncooled chamber components follows:

1. Injectors

a. Performance and combustion characteristics were determined for three injectors, including concentric-ring, vortex, and a swirl transpiration face-cooled concept.

b. Means of preventing injector element and face erosion for large-element-type injectors were evaluated, with a solution obtained and specific design recommendations formulated.

II, E, Uncooled Thrust Chamber Program (cont.)

2. Chamber Construction

a. The relative adequacy of several liner materials for use in various parts of high-pressure chambers, including the chamber, throat, and exit sections were determined. Design and erosion data for those materials which can successfully withstand the environment were obtained.

b. A step-joint, designed to prevent combustion gas leakage between the chamber or injector and the liner material was developed.

c. The use of the "Conoseal," a metal belleville washer-type seal, was determined very satisfactory for use with high-pressure heavyweight hardware. The HiPc chamber, which has sealing diameters up to 14 in., never experienced a combustion gas leak throughout the entire program.

The design and development of the uncooled chamber hardware components are discussed in detail in Section VI, below. Uncooled thrust chamber performance is discussed jointly with cooled thrust chamber performance in Section VIII. The combustion stability characteristics of both uncooled and cooled chambers are jointly discussed in Section IX. The experimental measurement of the gas-side heat-transfer coefficients is discussed as a portion of the Gas-Side Heat Transfer Studies, Section V.

II, Program Summary (cont.)

F. COOLED THRUST CHAMBER PROGRAM

The overall objective of the Cooled Thrust Chamber Program was to establish and evaluate suitable methods for cooling the chamber and the nozzle using N_2O_4/AeroZINE 50 propellants at a chamber pressure of approximately 3000 psia. The basic approach established was to use segmented thrust chambers incorporating replaceable cooled sections in the chamber, throat, and expansion portions of the nozzle. This enabled the investigation of each cooling technique by itself in conjunction with uncooled chamber segments, as well as in combination with other cooling techniques during the same test.

A design and analytical investigation was first conducted in which prospective cooling concepts were analyzed for application to high-pressure engines. As a result of this investigation, the following concepts were selected for experimental evaluation in thrust chamber hardware: regenerative cooling, film cooling, thermal barrier coatings, vortex cooling, and ablative cooling. Other cooling techniques considered but not selected for testing in this program included transpiration cooling, hot-gas cooling, and high-temperature resistant materials.

Segmented thrust chambers employing the selected cooling methods were designed, fabricated, and evaluated in the test program. Included were the following components:

1. Drilled chamber L* segment (regeneratively cooled with AeroZINE 50 in combination with a thermal barrier coating and film cooling).

2. Vortex chamber L* segment (vortex cooling).

3. Convergent nozzle and throat segment (film cooled by N_2O_4).

4. Sea-level expansion nozzle (regeneratively cooled with N_2O_4).

5. Expansion nozzle skirt (ablative cooled)

II, F, Cooled Thrust Chamber Program (cont.)

A total of 28 tests were conducted in the Cooled Chamber Program, of which 18 produced valid steady-state data. The program is summarized in Figure II-F-1. A brief summary of the test results for each component is given in the following paragraphs.

1. Drilled L* Segment

The drilled L* segment was regeneratively cooled with AeroZINE 50, supplemented by a small amount of oxidizer film cooling. A thermal barrier coating covering the inside chamber wall was also used in two of the three valid tests performed with this unit. Satisfactory operation and adequate cooling were demonstrated in all tests. Test durations were up to 2-sec pressure steady-state, sufficiently long to achieve thermal steady-state conditions.

2. Vortex Chamber L* Segment

In this application of the vortex cooling concept, all propellants are tangentially injected directly onto the combustion chamber wall. In the injection area, the wall is film cooled by the fuel and oxidizer propellants. Below this, additional cooling is provided by the resulting vortexing gas flow, which keeps the cooler gases (which are heavier) on the chamber wall by centrifugal force. Once combustion is complete, no further cooling is provided. Two tests were conducted with the vortex L* segment, of which one reached steady-state chamber pressure. Unfortunately, an interchannel propellant leak and resulting fire developed in the propellant manifold during the one valid test, which locally damaged the unit beyond repair. The post-fire condition of that portion of the chamber wall not in the area of the interchannel leak was in excellent condition, which proved that the chamber was being adequately cooled; however, no quantitative heat-transfer data were obtained.

II, F, Cooled Thrust Chamber Program (cont.)

3. Convergent Nozzle and Throat Segment

This chamber segment was entirely film-cooled with oxidizer. Fourteen valid tests were performed, during which film coolant was reduced in steps until burnout occurred. The data produced by these tests was used to develop mathematical models relating the effects of film cooling on performance and heat transfer for high chamber pressure engines. These models are now being used in the Advanced Storable Engine Program, Contract AF 04(611)-10830, currently underway at Aerojet.

4. Sea-Level Expansion Nozzle

The expansion nozzle is a tube bundle regeneratively cooled by oxidizer; the nozzle extends to an area ratio of 21:1. It was tested in conjunction with the convergent nozzle and throat segment during seven valid tests. These tests demonstrated cooling of the expansion nozzle portion of a high-pressure chamber with supercritical N_2O_4.

5. Expansion Nozzle Skirt

The expansion nozzle skirt, constructed of ablative material, extended from an area ratio of 21:1 to an area ratio of 70:1. It was used in conjunction with the cooled throat and sea-level expansion nozzle in one short-duration test. The test objective was to obtain performance data with a high area ratio nozzle; the test duration was not long enough to provide ablative cooling data.

The design and development of the cooled chamber hardware components are discussed in detail in Section VII. Cooled thrust chamber performance is discussed in Section VIII.

II, F, Cooled Thrust Chamber Program (cont.)

From the test results obtained in this program, together with recent data from several other programs conducted by Aerojet-General as well as by other contractors, it is concluded that oxidizer regenerative cooling used in combination with film cooling and a thermal barrier coating, offers one cooling system with potentially high performance for high-pressure engines. Recent studies conducted under contract AF 04(611)-10830 indicate that transpiration cooling using N_2O_4 may provide another very efficient system. Recent data for supercritical N_2O_4, together with new fabrication concepts for transpiration-cooled chambers are responsible for this renewed interest in transpiration cooling. As to vortex cooling, insufficient data was obtained in this program to allow any firm conclusions to be made; however, no negative results were obtained as to its cooling capability with the limited testing performed.

II, Program Summary (cont.)

G. SYSTEM STUDIES

The System Studies had as its objective the determination of the practical upper limit of chamber pressure and the selection of the best nozzle area ratio and propellant mixture ratio. These parameters were to be selected upon the basis of vehicle performance, cost, and weight. The study included comparisons of both altitude-compensating and DeLaval nozzles, as well as the gas generator and staged-combustion engine cycles. The propellants used in the basic investigation were N_2O_4/AeroZINE 50. The results were then extended to include selected metalized propellant systems.

The system studies were conducted in two parts: the Preliminary System Studies and the Final System Studies. The preliminary studies were performed early in the program; at this time the basic investigations were made, including a complete engine cycle analysis, a vehicle and engine performance and weight study, and the development of a cost model. Also included was an investigation to determine potential payload gains through the use of selected metalized propellant systems. The final studies, which had the same objective as the preliminary studies, were performed at the end of the program, and included the results from this and other recent programs. The analysis was conducted using the latest parametric weight data and theoretical specific impulse data corrected for known real effects. Two additional effects were included as a result of data that were available only recently: (1) a film-cooling model reflecting the effect of film cooling on specific impulse as a function of chamber pressure and (2) non-ideal compensation in forced-deflection nozzles. The final studies were restricted to N_2O_4/AeroZINE 50 propellants.

The final results, presented in Figures XI-F-7 through -9, clearly show the benefit of using high chamber pressure and staged-combustion cycle engines. These curves are relatively flat between 2500 and 5000 psia, with some variation in optimum pressure depending on the stage application. Payload variations within

II, G, System Studies (cont.)

the range are probably within the accuracy of the analysis. Therefore, selection of chamber pressure within this range should be influenced by other practical factors not included in this analysis. Use of existing facilities and experience would dictate selection of a chamber pressure of 3000 psia or below. Similar conclusions were reached in the Preliminary Systems Studies. However, unlike the results of the earlier study, the altitude compensating nozzles show no benefit. This was partially a result of non-ideal compensation effects not being considered in the Preliminary Systems Studies and partially a result of the choice of 20 modules for the engine system studied. This required use of a large base-area, which results in higher performance losses attributable to the nozzles. Use of eight modules might still show significant benefit for the forced-deflection nozzle. Therefore, the conclusion regarding altitude compensating nozzles is that the best nozzle to use will depend on the specific application.

Engine mixture ratio was optimized at the mixture ratio corresponding to maximum specific impulse for all values of chamber pressure. Optimum area ratio varied as a function of chamber pressure (Figure XI-F-6).

A detailed investigation of the effects of cost considerations on the selection of the optimum chamber pressure showed that cost is not a major consideration in the selection of optimum chamber pressure; the selection should be based upon performance advantages.

Detailed discussions of the Preliminary and Final System Studies are given in Sections X and XI, respectively.

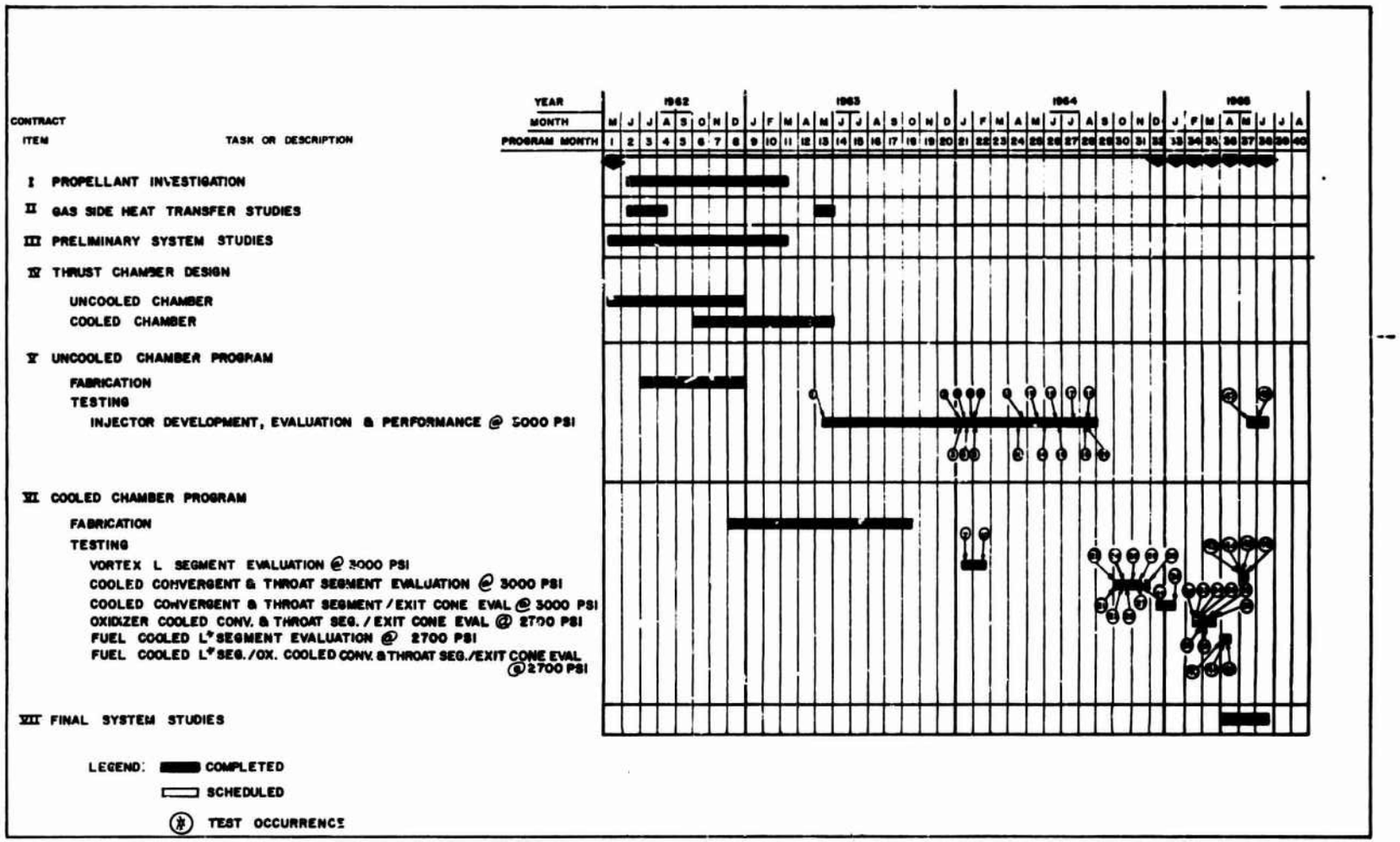

Figure II-A-1

Master Program Schedule

Book One

Cumulative Summary of TCA Testing (u)

Test Number	Date	Injector Type	L* in.	A_e/A_t At Data Point	P_c psia	MR	$\dot{w}_T$ lb/sec	$\dot{w}_F$ lb/sec	$\dot{w}_O$ lb/sec	F lb	c* ft/sec	% Theo c*	I_s sec	% Theo I_s	Duration sec	Remarks	Reported In Report
Uncooled Chamber Progr.m																	
1.2-01-YAM-001	5/31/63	Vortex (Original Design)	70	4.463	2628.5	2.675	164.6	44.8	119.8	37,182	5190	94.9	225.8	82.1	2.235	Oxidizer pump and gas-generator assembly ware destroyed; injector face eroded.	8191-M-13
1.2-01-YAM-002	1/3/64	Vortex (Mod I)	70	---	---	---	---	---	---	---	---	---	---	---	0.550	Gas-generator valve malfunction; no hardware damage.	8191-M-20
1.2-01-YAM-003	1/3/64	Vortex (Mod I)	70	---	---	---	---	---	---	---	---	---	---	---	0.891	Gas-generator valve malfunction; graphite-liner erosion.	8191-M-20
1.2-01-YAM-004	1/4/64	Concentric-Ring (Original Design)	70	---	---	---	---	---	---	---	---	---	---	---	0.659	Gas-generator malfunction; no hardware damage.	8191-M-20
1.2-01-YAM-005	1/4/64	Concentric-Ring (Original Design)	70	4.400	3128.2	1.81	211.45	75.25	136.20	44,750	4818	83.1	211.6	72.9	1.440	CSM shutdown due to an erroneous signal; minor erosion of the injector, graphite liner, end steinless pressure vessel.	8191-M-20
1.2-01-YAM-006	1/10/64	Vortex (Mod I)	70	---	---	---	---	---	---	---	---	---	---	---	0.945	Grephite L* liner was destroyed.	8191-M-20
1.2-01-YAM-008	1/30/64	Concentric-Ring (Mod I)	100	19.5	3205	1.67	196.0	73.8	122.2	54,381	5476 to 5793	94.0 to 99.7	280.5	91.6	1.841	Injector erosion; throat damage.	8191-M-21
1.2-01-YAM-009	1/31/64	Vortex (Mod I)	70	---	3704	---	---	---	---	40,810	---	---	---	---	1.850	Injector face eroded; throat was damaged; eblative end-cover was damaged.	8191-M-21
1.2-02-YAM-001	4/11/64	Concentric-Ring (Mod II)	100	21.3	2782	2.875	170.1	44.1	126.6	43,800	5190	95.8	257	87.8	1.863	Minor injector-face erosion; loss of outer eblative injector-face cover; inner-channel leakage.	8191-M-23
1.2-02-YAM-002	4/13/64	Vortex (Mod II)	70	---	2958	---	---	---	---	40,900	---	---	216	---	1.773	Injector feiled during the start trensient; eblative end-cover was destroyed; no useful performance data ware obtsined.	8191-M-23

Figure II-A-2, Sheet 1 of 6

Test Number	Date	Injector Type	L^* in.	A_c/A_t At Data Point	P_c psia	MR	$\dot{W}_F$ lb/sec	$\dot{W}_F$ lb/sec	$\dot{W}_O$ lb/sec	F lb	C^* ft/sec	$\%$ Theo C^*	I_s sec	$\%$ Theo I_s	Duration sec	Remarks	Reported In Report
Uncooled Chamber Program, (cont.)																	
1.2-02-YAM-003	5/26/64	Concentric-Ring (Mod III)	100	20.3	2974	1.76	183.2	66.4	116.8	49,390	5530	95.4	269	87.4	1.884	Part of the ablative injector-face cover was destroyed; combustion occurred in the outer oxidizer manifold ring. Fuel-ring erosion occurred.	SID 64-825
1.2-02-YAM-004	5/27/64	Concentric-Ring (Mod IV)	100	4.50	3020	1.93	179.9	61.4	118.5	43,440	5640	97.4	241.4	84.8	1.883	Weld failure permitted the Rigimesh outer injector face ring to deform, offsetting injection and cooling patterns; minor Rigimesh erosion was experienced. Fuel-ring erosion occurred.	SID 64-825
1.2-02-YAM-005	6/22/64	Concentric-Ring (Mod V)	100	---	---	---	---	---	---	---	---	---	---	---	0.910	High transient-pressure shut-down device was mismanaged and initiated premature shutdown. No hardware damage.	SID 64-826
1.2-02-YAM-006	6/23/64	Concentric-Ring (Mod V)	100	18.4	2838	1.82	196.1	69.7	126.4	49,102	5390	91.1	250.4	80.0	1.863	Minor erosion of outer weld on outer oxidizer ring. Significant ablation of ablative material at connection of L^* to injector. All other thrust-chamber components in refirable condition.	SID 64-826
1.2-02-YAM-007	7/14/64	Concentric-Ring (Mod VI)	100	17.6	2997	2.07	215.4	70.2	145.2	53,515	5376	93.2	248.5	80.0	1.854	Minor erosion of outer weld on outer oxidizer ring. Significant ablation of ablative material at connection of L^* to injector. All other thrust-chamber components in refirable condition.	SID 64-826
1.2-02-YAM-008	8/25/64	Concentric-Ring (Mod VII)	100	20.4	2931	2.35	182.9	54.7	128.2	46,610	5840	93.2	256	82.8	1.593	No hardware damage sustained.	SID 64-828

Cumulative Summary of TCA Testing (u)

Figure II-A-2, Sheet 2 of 6

Test Number	Date	Injector Type	L* in.	A_e/A_t At Data Point	P_c psia	MR	$\dot{w}_T$ lb/sec	$\dot{w}_F$ lb/sec	$\dot{w}_O$ lb/sec	F lb	c* ft/sec	% Theo c*	I_s sec	% Theo I_s	Duration sec	Remarks	Reported In Report
Uncooled Chamber Program (cont.)																	
1.2-02-YAM-009	8/27/64	Concentric-Ring (Mod VII)	100	19.3	2782	2.52	180.2	51.2	129	45,975	5420	97.8	255.1	86.8	2.17	Minor erosion of outer Rigimesh ring.	8191-M-28
1.2-02-YAM-010	8/28/64	Concentric-Ring (Mod VIII)	100	4.54	2869	2.55	171.4	48.3	123.1	39,678	5180	93.8	231.5	82.0	1.668	Peripheral weld joining the oxidizer center plug and the centar Rigimesh failed.	8191-M-28
1.2-02-YAM-037	5/20/65	Transpiration Cooled	100	---	2481	2.08	179.6	58.4	121.2	43,306	---	---	241.0	---	2.575	Successful test of transpiration cooled injector. Used eblative throat insert mechanicelly feiled end destroyed during startup.	8191-M-35
1.2-02-YAM-038	5/27/65	Transpiration Cooled	100	20.81	3054	2.15	173.2	55.0	118.2	46,316	5700	99.5	267.0	84.3	2.111	Successful test of transpiration cooled injector. No test hardware damage was sustained.	8191-M-35
Cooled Chamber Program																	
1.2-01-YAM-007	1/11/64	Vortex L*	70	---	---	---	---	---	---	---	---	---	---	---	0.918	Shutdown by CSM, Graphite L* liner end part of eblative face cover were destroyed.	8191-M-20
1.2-01-YAM-010	2/11/64	Vortex L*	70	2.665	2902	2.03	189.6	62.6	127.0	43,000	5431	94.3	226.8	80.0	1.264	Vortex L* was destroyed by inter-channel propellant leakage in the manifold.	8191-M-21
1.2-02-YAM-011	10/8/64	Concentric-Ring (Mod VIII-A)	100	---	---	---	---	---	---	---	---	---	---	---	0.849	Gas generator valve malfunction ceusing premature shutdown; no hardware damage.	8191-M-29
1.2-02-YAM-012	10/9/64	Concentric-Ring (Mod VIII-A)	100	8.28	2940	3.16	210.5	50.5	160	42,547	4340	86.1	198.5	70.6	1.865	Successful test; all objectivee meet; no hardware damage.	8191-M-29
1.2-02-YAM-013	10/16/64	Concentric-Ring (Mod VIII-A)	100	---	---	---	---	---	---	---	---	---	---	---	1.186	Erroneous signal to the high transient pressure sensing device initieted. Premature shutdown; no hardware damage.	8191-M-30
1.2-02-YAM-014	10/16/64	Concentric-Ring (Mod VIII-A)	100	8.28	2990	3.17	212.9	51.0	161.9	42,380	4440	86.5	199	69.4	2.373	Successful test; no hardware damage.	8191-M-30
1.2-02-YAM-015	10/19/64	Concentric-Ring (Mod VIII-A)	100	8.28	3052	3.06	217.5	52.6	163.9	43,160	4430	86.2	199	71.4	4.0335	Successful test. Screws securing inner oxidizer ring Rigimesh plate failed during test; no other hardware damage.	8191-M-30

Figure II-A-2, Sheet 3 of 6

Cumulative Summary of TCA Testing (u)

Test Number	Date	Injector Type	L* In.	A_e/A_t At Data Point	P_c psia (ave)	MR	$\dot{w}_T$ lb/sec	$\dot{w}_F$ lb/sec	$\dot{w}_O$ lb/sec	F lb	c* ft/sec	% Theo c*	I_s sec	% Theo I_s	Duration Sec	Remarks	Reported In Report
Cooled Chamber Program (cont.)																	
1.2-02-YAM-016	11/26/64	Reworked Mod VIII-A Concentric Ring	100	8.28	--	--	--	--	--	--	--	--	--	--	--	Thrust Chamber valve timer malfunction; premature shutdown; no test hardware damage; no test data obtained.	8191-M-31
1.2-02-YAM-017	11/26/64	Reworked Mod VIII-A Concentric Ring	100	8.28	3018	3.39	222.9	50.7	172.2	43265	4536	86.2	194.1	71.9	3.022	No test hardware damage; coolant flow rate was higher than anticipated; $\dot{w}_c$ = 57.9 lb/sec.	8191-M-31 & 8191-M-32
1.2-02-YAM-018	11/30/64	Reworked Mod VIII-A Concentric Ring	100	8.28	2963	3.07	224.1	55.0	169.1	42505	4358	81.3	189.7	68.0	2.524	Coolant flow rate was higher than anticipated; $\dot{w}_c$ = 49.4 lb/sec.	8191-M-32
1.2-02-YAM-019	12/2/64	Reworked Mod VIII-A Concentric Ring	100	8.28	--	--	--	--	--	--	--	--	--	--	--	Gas generator valve malfunction; premature shutdown; no test hardware damage; no test data obtained.	8191-M-31
1.2-02-YAM-020	12/2/64	Reworked Mod VIII-A Concentric Ring	100	8.28	2809	2.56	217.7	61.1	156.6	48104	--	92.3*	221.0	--	2.067	Severe throat segment erosion; steady-state pressure operation was not achieved.	8191-M-31 & 8191-M-32
1.2-02-YAM-021	1/9/65	Mod VIII-B Concentric Ring	100	21.28	3054	3.13	209.2	50.6	158.6	45629	4732	85.4	218.1	73.7	2.197	Oxidizer pump exploded at Fs-1 + 2.1055 sec; minor test hardware damage.	8191-M-32

*Single point data

Cumulative Summary of TCA Testing (u)

Figure II-A-2, Sheet 4 of 6

Cumulative Summary of TCA Testing (u)

Test Number	Date	Injector Type	L* in.	A_c/A_t at Data Point	P_c psia (avg)	MR_{TCA}	$\dot{w}_{TCA}$ lb/sec	$\dot{w}_F$ lb/sec	$\dot{w}_{O_{TCA}}$ lb/sec	F lb	c* ft/sec	% Theo c*	I_s sec	% Theo I_s	Dur sec	Remarks	Reported In Report
Cooled Chamber Program (cont.)																	
1.2-02-YAM-022	2/15/65	Mod VIII-B Concentric-Ring	100	21.28	1148	.362	187.8	100.9	86.9	15,602	2012.2	37.3	83.07	28.6	2.678	High-pressure flexible inlet line on oxidizer regeneratively cooled exit cone failed, causing a reduced plenum pressure for duration of test. No test hardware damage.	8191-M-34
1.2-02-YAM-023	2/19/65	Mod VIII-B Concentric-Ring	100	21.28	2686	3.083	184.5	45.2	139.3	40,119	4874.4	90.5	217.44	76.8	2.953	Successful test; no test hardware damage.	8191-M-34
1.2-02-YAM-024	2/[illegible]/65	Mod VIII-B Concentric-Ring	100	21.28	2305	2.20	180.5	56.4	124.1	33,795	4205.8	73.2	187.23	61.0	3.514	Gas generator valve malfunction, causing a reduced plenum pressure for duration of test. No test hardware damage.	8191-M-34
1.2-02-YAM-025	3/2/65	Mod VIII-B Concentric-Ring	100	21.28	2749	3.077	185.7	45.6	140.1	40,983	4890.6	91.1	220.69	78.0	3.506	Successful test, no test hardware damage.	8191-M-34
1.2-02-YAM-026	3/5/65	Mod VIII-B Concentric-Ring	100	21.28	---	---	---	---	---	---	---	---	---	---	---	Plenum pressure transducer malfunction. Erroneous signal sent to the high-transient-pressure-sensing device; premature shutdown; no hardware damage; no test data obtained.	8191-M-34
1.2-02-YAM-027	3/8/65	Mod VIII-B Concentric-Ring	100	21.28	2610	3.16	178.5	42.9	135.6	38,413	4823.3	90.6	215.2	77.2	3.522	Successful test; no test hardware damage.	8191-M-34
1.2-02-YAM-028	3/12/65	Mod VIII-B Concentric-Ring	100	21.28	---	---	---	---	---	---	---	---	---	---	---	Test stand gas generator valve malfunctioned, causing premature shutdown; no hardware damage.	8191-M-34
1.2-02-YAM-029	3/15/65	Mod VIII-B Concentric-Ring	100	70.00	2532	3.66	174.8	37.5	137.3	33,234	4745.0	93.2	190.2	80.6	3.008	Successful test; no test hardware damage.	8191-M-34

Figure II-A-2, Sheet 5 of 6

Test Number	Date	Injector Type	L^* in.	A_e/A_t At Data Point	P_c psia	MR	$\dot{w}_T$ lb/sec	$\dot{w}_F$ lb/sec	$\dot{w}_O$ lb/sec	F lb	c* ft/sec	% Theo c*	I_s sec	% Theo I_s,	Duration sec	Remarks	Reported In Report
Cooled Chamber Program (cont.)																	
1.2-02-YAM-030	3/23/65	Mod VIII-B Concentric-Ring	100	4.3	2573	2.43	162.8	47.3	115.3	36,792	5280	94.5	226.0	81.3	2.139	Successful test of regeneratively cooled L^* segment. No test hardware damage was sustained.	8191-M-35
1.2-02-YAM-031	3/29/65	Mod VIII-B Concentric-Ring	100	4.1	2456	2.23	164.8	51.1	113.7	38,421	5310	93.4	218.2	78.8	3.519	Successful test of regeneratively cooled L^* segment. Refractory coating in chamber was found to be loose after disassembly. No other damage was sustained.	8191-M-35
1.2-02-YAM-032	4/14/65	Mod VIII-B Concentric-Ring	100	21.28	1700	---	---	---	---	---	---	---	---	---	2,347	Test stand malfunction initiated premature engine shutdown. Steady-state was not obtained.	8191-M-35
1.2-02-YAM-033	4/14/65	Mod VIII-B Concentric-Ring	100	21.28	2615	3.33	189.6	43.0	146.6	38,752	4475	86.9	204.4	73.3	3.524	Minor erosion of the cooled throat segment was sustained.	8191-M-35
1.2-02-YAM-034	4/20/65	Mod VIII-B Concentric-Ring	100	17.10	2475	2.10	178.5	57.5	121.0	43,479	5470	95.4	243.6	78.2	3.583	Successful test of uncooled regeneratively cooled L^* segment. No test hardware damage was sustained.	8191-M-35
1.2-02-YAM-035	5/18/65	Mod VIII-B Concentric-Ring	100	---	---	---	---	---	---	---	---	---	---	---	---	Test stand malfunction initiated premature engine shutdown. Steady-state was not obtained.	8191-M-35
1.2-02-YAM-036	5/19/65	Mod VIII-B Concentric-Ring	100	19.40	2651	2.85	166.7	43.4	123.3	38,688	4900 to 5200	91.0 to 96.5	232	80.2	2.580	Cooled-throat segment was damaged beyond repair by erosion during this test.	8191-M-35

Cumulative Summary of TCA Testing (u)

Figure II-A-2, Sheet 6 of 6

OBJECTIVE	TEST HARDWARE	TEST OBJECTIVE	TEST CONDITIONS			TEST NUMBER	TEST DATE	TEST RESULTS	
			PC PSIA	L* IN.	S.S. DUR. SEC.			VALID	INVALID
INJECTOR EVALUATION, TCA PERFORMANCE, AND CHAMBER HEAT FLUX @ 3000 PSIA	VORTEX INJECTOR	INJECTOR EVALUATION	2628	70	0.88	1.2-01-YAM-001	31 MAY 1983	X	
	VORTEX INJECTOR, MOD I	INJECTOR EVALUAVION	----	70	----	1.2-01-YAM-002	3 JANUARY 1984		X
			----	70	----	1.2-01-YAM-003	3 JANUARY 1984		X
			----	70	----	1.2-01-YAM-006	10 JANUARY 1984		X
			3074	70	0.55	1.2-01-YAM-009	31 JANUARY 1984	X	
	VORTEX INJECTOR MOD II	INJECTON EVALUATION	2958	70	0.44	1.2-02-YAM-002	13 APRIL 1984	X	
	CONCENTRIC RING INJECTOR	INJECTOR EVALUAVION	----	70	----	1.2-01-YAM-004	4 JANUARY 1984		X
			3129	70	0.43	1.2-01-YAM-004	4 JANUARY 1984	X	
	CONCENTRIC RING INJECTOR, MOD I	INJECTOR EVALUAVION	3205	100	0.54	1.2-01-YAM-008	30 JANUARY 1984	X	
	CONCENTRIC RING INJECTOR, MOD II	INJECTOR EVALUAVION	2782	100	0.60	1.2-02-YAM-001	11 APRIL 1984	X	
	CONCENTRIC RING INJECTOR, MOD III	INJECTOR EVALUAVION & CHAMBER HEAT FLUX	2974	100	0.64	1.2-02-YAM-003	26 MAY 1984	X	
	CONCENTRIC RING INJECTOR MOD IV	INJECTON EVALUATION & CHAMBER HEAT FLUX	3020	100	0.66	1.2-02-YAM-004	27 MAY 1984	X	
	CONCENTRIC RING INJECTON, MOD V	INJECTOR EVALUATION	----	100	----	1.2-02-YAM-005	22 JUNE 1984		X
			2838	100	0.59	1.2-02-YAM-006	22 JUNE 1984	X	
	CONCENTRIC RING INJECTOR MOD VI	INJECTOR EVALUATION	2997	100	0.52	1.2-02-YAM-007	14 JULY 1984	X	
	CONCENTRIC RING INJECTOR, MOD VII	INJECTOR EVALUATION	2931	100	0.22	1.2-02-YAM-008	24 AUGUST 1984	X	
			2782	100	0.96	1.2-02-YAM-009	27 AUGUST 1984	X	
	CONCENTRIC RING INJECTOR, MOD VIII	INJECTOR EVALUAVION	2869	100	0.40	1.2-02-YAM-010	28 AUGUST 1984	X	
	TRANSPIRATION COOLED INJECTOR	INJECTOR EVALUATION	2406	100	0.90	1.2-02-YAM-037	20 MAY 1985	X	
			2039	100	0.50	1.2-02-YAM-037	27 MAY 1985	X	

Figure II-E-1

Uncooled Chamber Program Summary

Book One

OBJECTIVES	TEST HARDWARE	TEST OBJECTIVES	TEST CONDITIONS			TEST NO.	TEST DATE	TEST RESULTS	
			PC PSIA	L* IN.	S.S. DURATION		CONDUCTED (SCHEDULE)	VALID	INVALID
EVALUATE COOLED HARDWARE COMPONENTS, OPTIMIZE COOLING, PERFORMANCE.	VORTEX L* SEGMENT	EVALUATE VORTEX L* SEGMENT	----	TO	NONE	1.2-01-YAM-007	11 JANUARY 1984		X
			2902	TO	0.05	1.2-01-YAM-010	12 FEBRUARY 1984	X	
	COOLED CONVERGENT AND THROAT SEGMENT	EVALUATE COOLED CONVERGENT AND THROAT SEGMENT, ACHIEVE THERMAL STEADY STATE, EVALUATE MOD. VIII-A CONCENTRIC RING INJECTOR.	----	100	NONE	1.2-02-YAM-011	9 OCTOBER 1984		X
			2940	100	0.630	1.2-02-YAM-012	9 OCTOBER 1984	X	
			----	100	NONE	1.2-02-YAM-013	16 OCTOBER 1984		X
			2990	100	2.829	1.2-02-YAM-014	16 OCTOBER 1984	X	
			3062	100	1.360	1.2-02-YAM-015	19 OCTOBER 1984	X	
			----	100	NONE	1.2-02-YAM-016	25 NOVEMBER 1984		X
			3032	100	1.830	1.2-02-YAM-017	26 NOVEMBER 1984	X	
		REDUCE FILM COOLANT	2903	100	1.324	1.2-02-YAM-018	30 NOVEMBER 1984	X	
			----	100	NONE	1.2-02-YAM-019	1 DECEMBER 1984		X
			2909	100	0.867	1.2-02-YAM-020	2 DECEMBER 1984	X	
	COOLED CONVERGENT AND THROAT SEGMENT, COOLED EXIT CONE (EXIT CONE OXIDIZER REGENERATIVE COOLANT RETURNS TO INJECTOR)	EVALUATE COOLED EXIT CONE	3054	100	0.210	1.2-02-YAM-021	9 JANUARY 1985	X	
		REDUCE FILM COOLANT IN FILM COOLED CONVERGENT AND THROAT SEGMENT	1148	100	0.770	1.2-02-YAM-022	15 FEBRUARY 1985		X
			2686	100	0.553	1.2-02-YAM-023	19 FEBRUARY 1985	X	
			2304	100	1.204	1.2-02-YAM-024	26 FEBRUARY 1985	X	
			2749	110	1.125	1.2-02-YAM-025	2 MARCH 1985	X	
			----	100	NONE	1.2-02-YAM-026	6 MARCH 1985		X
			2609	100	1.073	1.2-02-YAM-027	9 MARCH 1985	X	
			----	110	NONE	1.2-02-YAM-028	15 MARCH 1985		X
			2532	110	0.572	1.2-02-YAM-029	15 MARCH 1985	X	
			----	110	NONE	1.2-02-YAM-032	14 APRIL 1985		X
			2615	100	0.130	1.2-02-YAM-033	14 APRIL 1985	X	
			----	100	NONE	1.2-02-YAM-035	19 MAY 1985		X
			2637	100	1.094	1.2-02-YAM-036	19 MAY 1985	X	
	REGENERATIVELY COOLED L* SEGMENT	EVALUATE REGENERATIVELY COOLED L* SEGMENT (COOLED WITH OXIDIZER)	2573	100	0.439	1.2-02-YAM-030	23 MARCH 1985	X	
			2456	100	2.043	1.2-02-YAM-031	29 MARCH 1985	X	
			2475	100	1.711	1.2-02-YAM-034	30 APRIL 1985	X	

Figure II-F-1

Cooled Chamber Program Summary

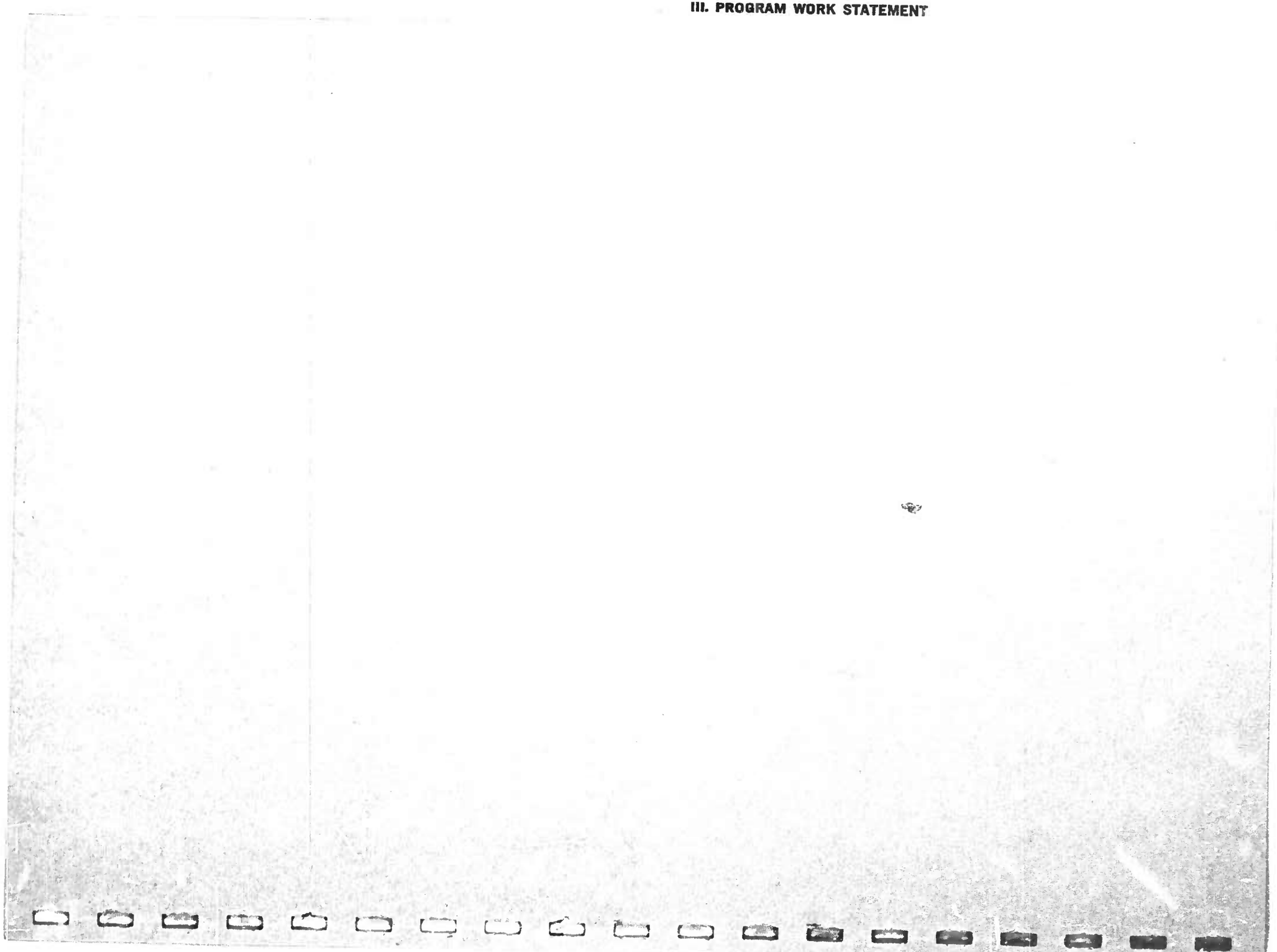

III. PROGRAM WORK STATEMENT

The final work statement to which this program was performed is presented below. It is included in this report to serve as a concise summary of the overall program scope and the individual program tasks.

TECHNICAL REQUIREMENTS

INTRODUCTION:

This applied research program is for investigation into high chamber pressure rocketry utilizing storable propellants. High chamber pressure rocket engines permit the use of large expansion area ratio nozzles at sea level, and maintain high specific impulse at lift-off and altitude conditions. As a result, trajectory averaged specific impulse can be increased quite significantly over those presently attainable at current chamber pressures. Furthermore, the nozzle throat size is reduced to such an extent that greatly increased nozzle area ratios can be realized for a given engine envelope. The objective of the program is to provide the study, analysis, design and combustion research required to establish the feasibility and degree of advantage of high chamber pressure rocket engines using nitrogen tetroxide/ 50% UDMH - 50% N_2H_4 propellants. It is also the purpose of this program to determine a reasonable upper limit to high chamber pressure rocketry above which development effort, production costs, and increasing propulsion package weight negate additional performance gains.

SCOPE:

The N_2O_4/(50% N_2H_4 - 50% UDMH) propellant combination shall be used throughout except as noted in Item I for the below-defined technical program. Maximum use shall be made of existing hardware and information.

III, Program Work Statement (cont.)

1. Item I - A literature review shall be made in the technical areas of combustion and heat transfer at conditions encountered in thrust chamber operating at 1,500 - 10,000 psi with N_2O_4/50% N_2H_4 - 50% UDMH propellants. This shall be followed by analytical studies to define problem areas and to determine theoretical combustion performance and heat transfer design criteria at chamber pressure up to 10,000 psi. Effects of additives to fuel and oxidizer shall be considered in the performance and heat transfer analyses.

2. Item II - A detailed analytical study shall be conducted on the gas-side heat transfer coefficient. Existing empirical data shall be collected and correlated with analytical predictions to establish a basis for extrapolation to the high chamber pressures. Also, specialized techniques for measurement of the gas-side heat transfer coefficient shall be evaluated for application to this program.

3. Item III - A preliminary determination of a practical upper chamber pressure limit, and a mixture ratio and area ratio selection for a high-pressure, pump-fed storable rocket engine shall be made. Comparisons between advanced and DeLaval nozzles and various turbine drive cycles shall be included. The selection of these parameters shall be based upon analytical weight, performance and cost studies, along with preliminary mission studies defined under Item VII. A comparison of incremental performance increase versus the attendant increase in propulsion system cost, weight and technological advances required in chamber cooling techniques and materials application will be shown. Propulsion costs shall include facility costs specifically attributable to increased pressure.

4. Item IV

a. Based upon the results of Items I, II, and III, detailed designs shall be prepared of cooled and uncooled thrust chamber assemblies for experimental

III, Program Work Statement (cont.)

test firings. The chambers shall be designed so as to achieve maximum utilization of the hardware and maximum versatility for investigating the ignition, combustion, performance, cooling techniques, materials and heat transfer characteristics.

b. The thrust chambers shall be designed nominally for a thrust of 50,000 pounds with a combustion pressure of 3,000 psia. The designs shall include three injection concepts. The thrust chambers shall be of the segmented type incorporating individual injector, chamber, nozzle, and divergent sections.

c. The design and materials selection shall be based on a careful analysis of the heat transfer, strength, and environmental requirements. Supporting data in terms of cost, flexibility, and maximum usage shall be provided to substantiate the design and hardware selection.

d. Final test hardware designs will be reviewed by the responsible Air Force Project Engineer before fabrication of any hardware except that components which may be required regardless of the peculiar design selected will not require prior Air Force review.

5. Item V - Uncooled Testing

a. The broad objective of this item of work is to investigate the performance, heat transfer, and general operating characteristics of nitrogen tetroxide and 50% N_2H_4 - 50% UDMH at a combustion pressure of approximately 3000 psia. The test firings for these investigations shall be of short duration and shall be made with uncooled thrust chambers and selected injector types designed to operate at approximately 50,000 pound thrust and 3,000 psia. Tests shall be conducted at different values of characteristic length.

b. The thrust stand and nozzles shall be equipped with suitable instrumentation for measuring the important performance and heat transfer parameters.

III, Program Work Statement (cont.)

c. Approximately 18 tests shall be planned for uncooled chamber testing. Approximately 13 of these tests shall be for scheduled objectives; and 5 for contingency tests. If test data obtained during the program dictates that maximum technical benefits can be achieved by modifying the original testing plan, including numbers and/or objectives of tests, such modifications may be accomplished, commensurate with the remaining contract funds, providing approval is obtained from the Procuring Contracting Officer.

The major objectives to be achieved on the uncooled chamber tests are as follows:

Evaluate two injectors of different design at a chamber pressure of approximately 3000 psia, for performance, combustion characteristics, and overall design adequacy.

6. Item VI - Cooled Testing

a. The broad objective of this item of work is to evaluate and establish suitable methods for cooling the chamber and the nozzle for a combustion pressure of approximately 3000 psia. For this purpose, tests shall be conducted utilizing cooled thrust chambers designed to produce 50,000 pound thrust (at 3,000 psia). Segmented thrust chambers incorporating replaceable cooled sections in the chamber and throat portions of the nozzle will be employed to enable the investigation of several different cooling techniques during each run. Different cooling techniques to be tested in the segmented chamber include a vortex chamber segment, regeneratively cooled chamber segment, film cooled convergent nozzle and throat segment, regeneratively cooled sea-level expansion nozzle segment, and ablative skirt extension. Tests shall be conducted at a chamber pressure of approximately 3000 psia.

III, Program Work Statement (cont.)

b. The thrust stand and nozzle shall be equipped with suitable instrumentation for measuring the important performance, stability and heat transfer parameters, including film coolant flow rates and wall temperatures.

c. Approximately 27 tests shall be planned for cooled chamber testing. Approximately 20 of these tests shall be for scheduled objectives, and 7 for contingency tests. If test data obtained during the program dictates that maximum technical benefits can be achieved by modifying the original testing plan, including numbers and/or objectives of tests, such modification may be accomplished, commensurate with the remaining contract funds, providing approval is obtained from the Procuring Contracting Officer. The major objectives to be achieved in the cooled chamber program are as follows:

(1) Evaluate each of the cooled chamber components for cooling capability and overall design adequacy at approximately 3000 psia chamber pressure. These components shall include the following: vortex chamber segment, regeneratively cooled chamber segment, film cooled convergent nozzle and throat segment, and regeneratively cooled sea-level expansion nozzle segment.

(2) Using the best cooled chamber components as determined from testing in Paragraph 6,c,(1) above, a cooled thrust chamber assembly that operates at approximately 3000 psia chamber pressure will be evaluated. An uncooled L* segment may be used in this thrust chamber assembly to provide the L* required for relative high injector performance (based on uncooled tests). The objective of these tests shall be to demonstrate cooled thrust chamber operation, establish the minimum film coolant flow rates required to cool the chamber segments, and to determine the effect of the film cooling on performance, heat transfer, and combustion stability.

III, Program Work Statement (cont.)

(3) Investigate the effect of a high expansion ratio skirt (of the order of 70:1) on thrust chamber performance using the cooled thrust chamber tested in Paragraph 6,c,(2) above, and operated at the approximate same conditions.

7. Item VII

a. Based upon analytical weight studies and results from the thrust chamber test data, a determination of a practical upper limit of the thrust chamber pressure and a selection of the best operating mixture ratio and area ratio at this chamber pressure shall be made. A comparison of incremental performance increases versus the attendant increases in propulsion system cost, weight and technological advances required in chamber cooling techniques and materials application shall be shown. Included shall be comparisons between advanced and DeLaval nozzles and various turbine drive cycles. This will be accomplished by determining the variation of payload and cost with chamber pressure for both one- and two-stage vehicles for 300 nautical mile orbit missions. Propulsion system costs shall include facility costs specifically attributable to increased pressures.

b. Single stage vehicles analyzed shall utilize both the high pressure propulsion concept and conventional chamber pressure systems. Two stage systems shall utilize high pressure propulsion in both stages, high pressure propulsion for a boost stage with a second stage of conventional chamber pressures, and high pressure propulsion for a second stage boosted by a propulsion system of conventional chamber pressures. The thrust level of the first stage shall be mutually agreed upon between the Contractor and the Procuring Contracting Officer.

IV. PROPELLANT INVESTIGATION

The propellant investigation had as its goals the establishment of theoretical performance and heat-transfer design criteria, as well as the definition of the problem areas likely to result from the use of N_2O_4/AeroZINE 50 (50% N_2H_4 + 50% UDMH) and selected additive propellant combinations in high chamber pressure rocket engines. The program conducted toward this end involved three tasks: (1) literature review, performance calculations, and physical property calculations, (2) qualitative definition of problem areas, and (3) recommendation of programs required to resolve the important problem areas. The selected propellant combinations containing additives covered by this investigation included N_2O_4/N_2H_4 + Al, N_2O_4/N_2H_4 + AlH_3, N_2O_4/N_2H_4 + Be, N_2O_4/N_2H_4 + BeH_2, 98% H_2O_2/N_2H_4 + Al, 98% H_2O_2/N_2H_4 + AlH_3, 98% H_2O_2/N_2H_4 + Be, and 98% H_2O_2/N_2H_4 + BeH_2. Although the propellant investigation was conducted only during the period from May 1962 through January 1963, much additional work has been conducted since that time under various other contracts and independent investigations. Where the latter work has contributed significantly to the propellant aspects covered by this contract or invalidated portions of the information presented in previous reports, the new contributions and revisions in thinking or information are summarized in this report.

On the basis of the propellant investigation, the following conclusions can be made:

(1) Of the propellant systems studied, 98% H_2O_2/N_2H_4 + BeH_2 has the highest performance potential. Other systems, in order of decreasing performance, are as follows: N_2O_4/N_2H_4 + BeH_2; 98% H_2O_2/N_2H_4 + Be; N_2O_4/N_2H_4 + Be; 98% H_2O_2/N_2H_4 + AlH_3; N_2O_4/N_2H_4 + AlH_3; 98% N_2O_4/N_2H_4 + Al; N_2O_4/N_2H_4 + Al; N_2O_4/AeroZINE 50;

Note that 98% H_2O_2 is superior to N_2O_4 for all fuel combinations.

(2) Both N_2O_4 and 98% H_2O_2 are fully developed propellants and have no known major problems to preclude their use in rocket engine systems.

(3) The state-of-the-art of Alumizine (N_2H_4 + Al) and Beryllizine (N_2H_4 + Be) is sufficiently advanced to warrant increased effort in advanced technology programs for rocket application. Of the two fuels, Alumizine is the most developed. It does not present a toxic hazard as does Beryllizine and is less costly. However, it does not have as high a performance potential.

(4) Aluminum hydride and beryllium hydride fuels, N_2H_4 + AlH_3 and N_2H_4 + BeH_2, are still in the early state of laboratory development at this time. Difficulty has been experienced with both of these propellants in obtaining the stability and chemical compatibility required of a storable, gelled propellant. However, improvements are currently being made in this area. Also, maximum performance with these fuels requires metal loading in the range of 60 to 80% by weight, which is beyond current capabilities.

(5) The final recommendations issuing from this study are as follows:

(a) A laboratory program should be performed to define the high-pressure heat-transfer characteristics of N_2O_4, AeroZINE 50, 98% H_2O_2, and Alumizine.

(b) Feasibility demonstration programs should be performed at high pressures and for extended durations. Propellant combinations should include N_2O_4/AeroZINE 50, 98% H_2O_2/Alumizine, and N_2O_4/Alumizine.

(c) Propellant development of the more advanced fuels, aluminum hydride and beryllium hydride, should be continued, and if proved successful and practical, then applied to feasibility demonstration programs.

A. LITERATURE AND EXPERIENCE REVIEW

1. Nitrogen Tetroxide and AeroZINE 50

Experience with these propellants is very broad but, prior to the inception of this contract, was largely obtained by either direct or indirect

contractual support of the Titan II weapon system development program and, thus, was somewhat limited in respect to pressure. This contract and the integrated components program contracts (Phase I, AF 04(611)-8017 and Phase II, AF 04(611)-8548) have greatly extended experience with these propellants in the high-pressure region, and development of Transtage and Apollo engines has since provided extensive experience in the low-pressure region. The combination of all these programs and others has brought the experience level of N_2O_4 and AeroZINE 50 far beyond that of any other high-performance storable propellant combination.

Many documents are available concerning the properties and use of these materials as rocket propellants. One of these many documents, Storable Liquid Propellants, Nitrogen Tetroxide/AeroZINE 50, Aerojet-General Corporation, Liquid Rocket Plant Report LRP 198, Second Edition, June 1962, provides a comprehensive review particularly valuable as a reference for physicochemical property data and for descriptions of the proper methods of storing, handling, and using these propellants in rocket engines. While the information presented in this reference is primarily oriented toward the Titan II system, the information is equally applicable in most cases to the use of N_2O_4 and/or AeroZINE 50 in high chamber pressure rocket engines. It was noted early, however, that physical-property data from all sources fail to extend into the high-pressure region of primary interest to this program. Thus, to fill this gap, specific gravities, viscosities, thermal conductivities, and heat capacities were calculated as a part of this program. Later, improved calculation techniques and experimental laboratory work brought about significant revisions in the N_2O_4 properties. This work is discussed further in Section IV,C.

The problem areas that have been encountered in utilizing N_2O_4 and AeroZINE 50 in large, moderately high-pressure (900-psia) rocket engines and the methods employed in overcoming these problems to develop an operational engine system are described in detail under Contract AF 04(647)-521. Although a review of the particulars of that contract was beyond the scope of the propellant

IV, A, Literature and Experience Review (cont.)

investigation, two significant problems were encountered which should be recognized. These problems involved the achievement of adequate thrust-chamber cooling and combustion stability within the stringent weight and performance requirements of the program. Both of these problems were satisfactorily overcome through design modifications; the details of the modifications are given in reports generated under Contract AF 04(647)-521.

2. Hydrogen Peroxide

The use of hydrogen peroxide (H_2O_2) as an oxidizer for rocket engines dates back to the early German efforts of World War II; however, their hydrogen peroxide was neither high strength (i.e., a 98% pure product of interest in this program) nor was it applied to high-pressure engines. Probably the largest use of and greatest experience with 98% H_2O_2 was obtained at Aerojet-General in connection with more than 100 firings of 98% H_2O_2/B_5H_9 at a nominal 5000-lb thrust level under the AMC Product Improvement Program, Contract AF 33(600)-38470. This work indicated that 98% H_2O_2 could be safely and relatively easily used in a rocket engine. Although this work did not extend beyond approximately 900 psia, it did not suggest that H_2O_2 would create unique problems by reason of high-pressure usage.

The properties of H_2O_2 have been given in a comprehensive product bulletin of the Food Machinery and Chemical Corporation, Becco Division. Again, it was evident that physical properties at high pressures were not available and, therefore, by necessity, were calculated as a part of this program.

The storability of high-strength H_2O_2 has been a subject of study for a number of years by several organizations (e.g., Becco, Shell, and M.I.T.). These studies have brought forth stabilizers and equipment passivation procedures that have grossly improved the storability of H_2O_2. Recent laboratory work at Becco under Contract AF 04(611)-6342 indicates that high-strength H_2O_2.

IV, A, Literature and Experience Review (cont.)

can now be stored with only about one-sixth as much decomposition and pressure rise as was previously possible using standard inhibitors and passivation techniques.

3. Alumizine and Beryllizine

Alumizine and Beryllizine are the names given to thixotropic gels of aluminum and beryllium powders in hydrazine (N_2H_4), respectively. These metalized fuels had been under development at Aerojet-General for approximately four years at the time of the propellant investigation and were essentially ready for engine development work. At that time the work was continuing under Contract AF 04(647)-652, SA 4. The properties of Alumizine and Beryllizine had been defined over a limited temperature and pressure range and their feasibility as rocket engine fuels had been partially demonstrated with N_2O_4 as the oxidizer at a nominal 5000-lb thrust level and at moderate chamber pressures (about 500 psia). Results of the early work had been reported in References 1 through 4. Although testing to that date had been limited, the work indicated that the unique rheological properties of the gelled fuels may present problems in injection, atomization, and heat transfer (if the fuel were to be considered as a regenerative coolant).

As previously mentioned, the properties of Alumizine and Beryllizine had been defined only at moderate temperatures and pressures from prior work and the then-current work under Contract AF 04(647)-652, SA 4. Some properties at

---

Ref 1 Laboratory Investigation of Advance Mixed Oxidizers and Metalized Fuels, Aerojet-General Corporation, Liquid Rocket Plant, Report 8160-01Q-67, Volume 2, Contract AF 33(600)-38470 (Confidential)

Ref 2 Development of Slurries as Next-Generation Storable Propellants, Aerojet-General Corporation, Liquid Rocket Plant, Proposal LR61000, 19 July 1961 (Confidential)

Ref 3 Design Criteria for Advanced Propellant Systems, Aerojet-General Corporation, Liquid Rocket Plant, Proposal LR62067, 18 March 1962 (Confidential)

Ref 4 Gelled Metalized Propellant Demonstration Program, Aerojet-General Corporation, Liquid Rocket Plant, Report 9660-18, 5 July 1962 (Confidential)

IV, A, Literature and Experience Review (cont.)

elevated temperatures and pressures were calculated under this contract. The properties data calculated included specific gravities and heat capacities for the thixotropic gels consisting of 62.5% N_2H_4 + 37.5% Al, 57% N_2H_4 + 43% Al, 76% N_2H_4 + 24% Be, and 69% N_2H_4 + 31% Be. Unfortunately, no methods existed for estimating viscosities or thermal conductivities of Alumizine or Beryllizine. To provide the necessary basis for estimating the specific gravities and heat capacities of the metallized gels and to provide rough-order-of-magnitude values for viscosities and thermal conductivities of the matalized gels, the specific gravities, viscosities, thermal conductivities, and heat capacities of hydrazine were calculated and used.

From the work conducted to develop Alumizine under Contract AF 04(647)-652, SA 4 (1 April 1962 to 1 April 1963), a number of conclusions were reached. These conclusions were reported in Reference 5 and are given in the following paragraphs.

The results of work conducted with Alumizine during Contract AF 04(647)-652, SA 4, and previous programs (reported in References 1 and 4) show that Alumizine formulations exist which meet the requirements for a storable fuel. Additionally, the quality-control procedures and measuring devices have been developed so that uniformity can be assured from batch to batch and within small tolerances. Alumizine mixing equipment and preparation procedures have been scaled up to enable construction of a mixing facility that will support engine testing at 80,000-lb thrust. A large mixing facility was constructed by a facilities contract (AF 33(600)-29926) during the following Contract AF 04(647)-652, SA 4, efforts.

Ref 5 Product Engineering Final Report, Metalized Thixotropic Propellants, Aerojet-General Corporation, Liquid Rocket Plant, Report 652/SA4-2.2-F-1, Vol 5, 26 June 1963 (Confidential)

IV, A, Literature and Experience Review (cont.)

Engineering evaluations conducted during Contract AF 04(647)-652, SA 4, indicated that the problems associated with the application of metalized non-Newtonian fluids to liquid rocket engine systems are not unsolvable. For example: (1) The flow of Alumizine can be measured with a conventional flowmeter if sufficient calibration data are available; (2) on the basis of small-scale and two-variable testing, the expulsion efficiency of a hemispherical-bottom tank appears to be approximately the same as for that of some current vehicles; and (3) Alumizine appears to be usable as a regenerative coolant within certain regions of heat flux; however, more basic data are required before the practicability can be determined. Alumizine flow has been mathematically described, and tentative Alumizine shear diagrams have been successfully plotted with experimental data.

Test data from the 5000-lb thrust-chamber assembly firings indicate that injectors must be designed specifically to efficiently break up Alumizine. This means that proper injector design is one of the major keys to high performance.

Some problems that were encountered with the ball-type thrust-chamber valves were caused by the worn condition of the internal parts. These valves and actuators were extensively used on previous programs. Before this program, all nonmetallic seats and seals were replaced, but wear of the metallic bearing and sealing surfaces resulted in clearances greater than those specified. Leakage, nonrepetitive operating characteristics, and mechanical failures sometimes resulted in fuel leads into the thrust chamber and premature test terminations.

Low-frequency chamber pressure oscillations were experienced during testing, indicating a phenomenon related to a fluctuating feed system. Problems of this type are usually attributable to some orifice or pressure relationship phenomenon, and can ordinarily be eliminated by using the classic higher-pressure-drop injector.

IV, A, Literature and Experience Review (cont.)

Pressure pulses (spikes) were noted during testing, and appeared likely to be closely coupled to the injection process. Several 100-lb-thrust firings were performed during a company-sponsored program (Reference 4) which support this apparent relationship. The propellants were N_2O_4 and Alumizine-33 (33% aluminum). First firings with the four-on-one injector resulted in the same type of pressure spikes that occurred during the 5000-lb-thrust firings. The firings with a swirler to break up the Alumizine were very smooth and pressure-pulse-free. This is further evidence that a high degree of Alumizine breakup is mandatory.

The specific-impulse data from test firings with Alumizine containing 25% aluminum were lower on the average than those obtained with Alumizine containing 33% aluminum as theoretically predicted. Theoretical analysis conducted to determine the performance losses attributable to two-phase flow indicates that the difference between the two Alumizine formulations is insignificant.

The preparations required to test at 80,000-lb thrust were accomplished. The majority of components necessary to convert a Titan II second-stage workhorse thrust-chamber assembly for use with Alumizine were fabricated.

A preliminary design analysis showed that an elongated Titan II missile using N_2O_4/Alumizine (containing 45% aluminum) could deliver twice the present payload over the current maximum range. Other analyses disclosed that further component and subsystem investigations are warranted, but there are no problems which are considered to be insurmountable. A two-phase program was recommended for development of an Alumizine engine. A predevelopment program should be conducted first to provide data and solutions to potential problem areas prior to full-scale development.

IV, A, Literature and Experience Review (cont.)

Following the work of Contract AF 04(647)-652, SA 4, the improved Titan II Predevelopment Program Contract AF 04(694)-212 was conducted. The latter program brought Alumizine development, engine component demonstration, and breadboard engine demonstration to the point that a full engine-development program could be undertaken with N_2O_4 as the oxidizer. The major accomplishments and conclusions reached from that program are given below; details are available in the final report. Alumizine proved to be a practical propellant by its properties and characteristics, its larger-scale production and use, and by the fact that it can, in general, be used in components based on conventional design concepts. Subscale thrust-chamber tests (nominal 15,000-lb thrust and 1500-psia chamber pressure) demonstrated injector designs capable of delivering greater than 90% of theoretical specific impulse, good stability, and good durability. These tests also provided valuable heat-transfer information. Heat-transfer and thermal barrier investigations provided confidence that a regeneratively cooled chamber using N_2O_4 as coolant and thermal barriers could be developed. Uncooled, full-scale (nominal 120,000-lb thrust) breadboard engine and component tests demonstrated the feasibility of both components and engine; however, separate gas generation propellants were utilized. One test with a full-scale N_2O_4 regeneratively cooled chamber having a thermal barrier coating was performed, which resulted in tube burnout in the convergent region of the chamber upstream of the throat. It was concluded that the thermal barrier spalled off during the test, causing the tube burnout to occur.

Relatively little significant work on Beryllizine has been accomplished since the conclusion of the propellant investigation except that it has been further shown that beryllium is more difficult to burn efficiently than aluminum. In other respects, Beryllizine continues to bear strong behavioral resemblance to Alumizine. Currently, Beryllizine propellant development and subscale performance evaluation with N_2O_4 and 98% H_2O_2 is being conducted by Aerojet-General Corporation by Contract AF 04(611)-10783.

IV, A, Literature and Experience Review (cont.)

Numerous other organizations have worked with N_2H_4-Al and/or N_2H_4-Be gels; however, their conclusions and accomplishments are not directly cited because they tend to only further substantiate the results of the efforts already described. Good reviews of virtually all gelled propellant development efforts are given in References 6, 7, and 8.

4. N_2H_4-AlH_3 and N_2H_4-BeH_2

Thixotropic gels of N_2H_4 and aluminum hydride (AlH_3) or beryllium hydride (BeH_2) were still in an early state of laboratory development at the conclusion of the propellant investigation. In the case of N_2H_4-AlH_3 gels, their development into a usable storage fuel did not appear to present any insurmountable problems. There was one possible exception, however, that was noted at that time. Some samples of AlH_3 were found to decompose rather rapidly and appeared to be somewhat incompatible with N_2H_4, whereas others appeared quite acceptable from both standpoints. The fact that some samples of AlH_3 were relatively stable in N_2H_4 indicated that certain crystalline modifications and purity levels would satisfy the stability and chemical compatibility requirements of a storable, gelled propellant. Thus, with proper development of the AlH_3 production processes and on the basis of N_2H_4-Al gel knowledge, it was concluded that AlH_3 gels did not present a formidable development task.

Ref 6 Metalized Gelled Propellants Conference, AFRPL, Edwards, California, 10-12 June 1963, CPIA Publication 33 (Confidential)

Ref 7 Second Metallized Gelled Propellants Conference, AFRPL, Edwards, California 26-28 August 1964, CPIA Publication 64 (Confidential)

Ref 8 Proceedings of AIAA Propulsion Joint Specialist Conference, Colorado Springs, Colorado, 14-18 June 1965

IV, A, Literature and Experience Review (cont.)

Additional work on AlH_3-N_2H_4 gels has since been conducted; however, the effort has been of limited scope. The recent work indicates that AlH_3 production processes have improved and, in general, resulted in AlH_3 with better thermal stability and chemical compatibility with N_2H_4. Thus it is currently possible to prepare N_2H_4-AlH_3 gels that are satisfactory for test work, but that cannot be considered entirely storable. Further propellant development is required to achieve sufficient chemical and mechanical stability for long-term storage. N_2H_4-AlH_3 gels have been found to provide optimum theoretical performance with N_2O_4 and 98% H_2O_2 when the AlH_3 concentration in the fuel is near 55 and 70% by weight, respectively. Such concentrations present definite formulation problems within the bounds of acceptable flow characteristics. Aerojet-General, under IR&D effort, has achieved 55 to 60% loading level in small combustors improvement in flow characteristics of such highly loaded fuels and the achie of even higher loading requires further effort. The current very high cost of AlH_3 (near $700/lb) and limited availability present significant hindrances to the near-term development of N_2H_4-AlH_3 gel fuels.

In the case of N_2H_4-BeH_2 gels, a definite chemical compatibility probelm was found to exist with the BeH_2 available at the time of the propellant investigation. The reason for the incompatibility of BeH_2 with N_2H_4 was not determined and presented a perplexing problem since BeH_2 was compatible with water, UDMH, MMH, and apparently compatible with some N_2H_4-H_2O mixtures of high N_2H_4 concentrations. Such incompatibility could arise from either a unique N_2H_4-BeH_2 reaction or from impurities in either product. Additional work with N_2H_4 and BeH_2 was found to be definitely required, but the then-current knowledge indicated that BeH_2 could ultimately be incorporated into some gelled carrier of high N_2H_4 concentration, if not in commercially pure N_2H_4.

An appreciable amount of additional work has been devoted to the development of a gel fuel containing BeH_2; however, emphasis has shifted toward the use of monomethylhydrazine (MMH) rather than N_2H_4 as the carrier to avoid the severe

compatibility problem noted earlier. By using MMH, a BeH_2 gel fuel can be prepared which has sufficient chemical and mechanical stability for testing purposes. Aerojet-General Corporation is currently under contract to prepare 20 lb of a BeH_2-MMH gel containing 45% by weight BeH_2 under Contract AF 04(611)-10763 for testing purposes. Although this gel appears to be storable for extended periods of time, additional effort will be necessary to develop or prove long-term storability. BeH_2 gels, like AlH_3 gels, provide maximum performance when BeH_2 concentration in the fuel is relatively high, near 45 and 65% by weight with N_2O_4 and 98% H_2O_2 oxidizers, respectively. Efforts to achieve such high loadings have resulted in the preparation of gels containing up to approximately 51% BeH_2 in MMH with reasonable flow characteristics, but a 45 to 47% loading represents a more real upper limit, taking into account the flow characteristics normally desired in gelled propellants. The achievement of higher loadings and/or the use of N_2H_4 as the carrier (theoretically more desirable than MMH) presents definite challenges, but some hope is seen. The hope is based primarily on the anticipated development of crystalline BeH_2. By analogy to AlH_3, crystalline BeH_2 would be expected to be more compatible with N_2H_4 than the currently available amorphous material, and should be more dense, which would enhance increased loading. Some progress is being made in the preparation of crystalline BeH_2, and the benefits of such a material should soon be a subject of testing for proof.

The properties of N_2H_4-AlH_3 and N_2H_4-BeH_2 gels have not been well defined; however, the two-phase gelled fuels (Alumizine and Beryllizine) have densities which agree well with those calculated on the assumption that each component occupies its normal volume. This same assumption has been used to calculate the densities of N_2H_4-AlH_3 and N_2H_4-BeH_2 gels. Heat capacities have been estimated on the basis of additive molar heat capacities for the components. These properties were calculated as a part of this program.

IV, Propellant Investigation (cont.)

B. PERFORMANCE CALCULATIONS

The theoretical performance of N_2O_4/AeroZINE 50, N_2O_4/N_2H_4 + Al, N_2O_4/N_2H_4 + AlH_3, N_2O_4/N_2H_4 + Be, N_2O_4/N_2H_4 + BeH_2, 98% H_2O_2/N_2H_4 + Al, 98% H_2O_2/N_2H_4 + AlH_3, 98% H_2O_2/N_2H_4 + Be, and 98% H_2O_2/N_2H_4 + BeH_2 was computed as a part of the propellant investigation. These computations covered the chamber-pressure range of 1000 to 10,000 psia, various mixture ratios, and various concentrations of solid additive in the fuel, where applicable. As a result of these computations the effects of additive concentration, chamber pressure, and mixture ratio on specific impulse (optimum sea level), combustion temperature, and bulk propellant density were defined. Additionally, vacuum performance at various area ratios was defined at optimum additive concentration and mixture ratio (for sea-level operation) for each combination at each of several chamber pressures. These data were compiled into a special report (Reference 9) and issued under this contract. Because of the large volume of data presented, only a summary will be given here.

The optimum concentration of solid additive in the fuel (for sea-level operation) for each combination is shown in Figure IV-B-1 as a function of chamber pressure. Note that the optimum additive loadings for AlH_3 and BeH_2 are significantly higher than for Al and Be, and that when the fuels are oxidized by 98% H_2O_2, the optimum loadings are higher than with N_2O_4 oxidation. Also note that the optimum loadings of the hydrides increase with chamber pressure more rapidly than they do with the parent metals. From the discussion (Section IV,A) regarding the ability to achieve high loadings of the hydrides in carriers, it can be readily recognized that operation with 98% H_2O_2/N_2H_4 + AlH_3 and 98% H_2O_2/N_2H_4 + BeH_2 at optimum loading is not within current capabilities. Further, it should be recalled that the observed incompatibility of BeH_2 and N_2H_4 rules out the use of

---

Ref 9 Performance and Properties of N_2O_4/AeroZINE 50 and Selected Metalized Storables, Report LRP 302, Aerojet-General, Liquid Rocket Plant, 1 March 1963 (Confidential)

IV, B, Performance Calculations (cont.)

any BeH_2-N_2H_4 gel at the present time. Although the preceding conclusions would normally lead one to believe that AlH_3 and BeH_2 gels have little future, it must be recognized that operation below optimum loading or with a carrier other than N_2H_4 (e.g., MMH) does not degrade performance capabilities to the point that they become unattractive. For example, the optimum loading of AlH_3 in the fuel for the 98% H_2O_2/N_2H_4 + AlH_3 system at 3000-psia chamber pressure is approximately 73%, but operation with a fuel containing 55% AlH_3 (an achievable concentration) degrades specific impulse only about 5 sec.

Optimum mixture ratios at optimum additive concentration are shown for each combination as a function of chamber pressure in Figure IV-B-2. It is interesting to note that combinations containing Al, Be, and AlH_3 all operate at mixture ratios far below that of N_2O_4/AeroZINE 50 (less than 0.8 compared to approximately 2.0), whereas BeH_2 combinations operate somewhat intermediately but still closer to the other metalized propellants than to AeroZINE 50. The mixture ratios increase with chamber pressure in direct proportion to the increase in the optimum additive loading as pressure increases. Although it is not obvious from Figure IV-B-2, volumetric mixture ratios for the eight metalized propellant combinations can readily be shown to be extremely close to the same value at a given pressure. This fact indicates that interchangeability between these metalized propellants of hardware designed for any one would be relatively easy.

Optimum sea-level specific impulses for the various propellants is shown in Figure IV-B-3 as a function of chamber pressure. From this figure it can be readily seen that very significant performance advantage can be gained with increasing pressure for each propellant and that performance increases with the various fuels in the following order: AeroZINE 50, N_2H_4 + Al, N_2H_4 + AlH_3, N_2H_4 + Be, N_2H_4 + BeH_2. Also notice that 98% H_2O_2 is better than N_2O_4 with any of the metalized fuels when they are individually optimized for the particular oxidizer. The difference between the two oxidizers, however, is relatively small with N_2H_4 + Al (about 2 sec) but becomes progressively more significant in going to N_2H_4 + AlH_3

IV, B, Performance Calculations (cont.)

to N_2H_4 + Be to N_2H_4 + BeH_2 where the difference is approximately 21 sec. It must be pointed out, however, that the optimum additive loadings with 98% H_2O_2 are higher than with N_2O_4, and where loadability limits come into play, as is the case with AlH_3 and BeH_2, the potential advantage of 98% H_2O_2 over N_2O_4 can be significantly reduced as a result of this limit. For example, approximately 55% AlH_3 in N_2H_4 is the current achievable loading limit, and at this level the performance at 3000 psia with 98% H_2O_2 is only 1.3 sec better than with N_2O_4. Without a loadability limitation, 98% H_2O_2 would be an advantage of about 6 sec. The same type of limitation applied to BeH_2 at a 45% by weight loading level shows that the potential advantage of 98% H_2O_2 is reduced from approximately 21 to 11 sec. Recent work taking into account the fact the BeH_2 cannot currently be carried in N_2H_4, but can be used in MMH, shows that 98% H_2O_2/0.55 MMH + 0.45 BeH_2 provides the current practicable upper limit on storable specific impulse, and that this performance closely coincides with the values shown for N_2O_4/N_2H_4 + BeH_2 in Figure IV-B-3.

The theoretical combustion temperatures for the optimized propellant combinations are shown in Figure IV-B-4 as a function of chamber pressure. From this figure it is evident that the metalized propellants burn at nearly the same temperature as does N_2O_4/AeroZINE 50 when chamber pressure is near 1000 psia, but become 300 to 1000°R higher as the chamber pressure reaches 10,000 psia. In all cases, 98% H_2O_2 produces lower combustion temperatures than the corresponding N_2O_4 oxidized systems even though additive concentrations are consistently higher.

The bulk propellant densities for these combinations are shown in Figure IV-B-5. It is interesting to note that the BeH_2 systems have significantly lower bulk densities than does N_2O_4/AeroZINE, but that all other additives provide improvements over N_2O_4/AeroZINE 50. Al and AlH_3 systems produce the greatest bulk densities.

IV, Propellant Investigation (cont.)

C. EXTENSION OF PHYSICAL-PROPERTY DATA

Because little or no property data for the propellant of interest in this investigation were available at the high temperatures and pressures of importance to this program, various techniques for calculating physical properties were used extensively. The properties considered included heat capacity, viscosity, thermal conductivity, and density from saturation pressure to 10,000 psia. The propellants covered included the oxidizers N_2O_4 and 98% H_2O_2; and the fuels, AeroZINE 50, N_2H_4, N_2H_4 + Al, N_2H_4 + AlH_3, N_2H_4 + Be, and N_2H_4 + BeH_2.

It is known that the property data generated by the various calculation techniques employed are subject to relatively large errors, particularly where two-phase, non-Newtonian fluids are involved. Therefore, such data were utilized only in heat-transfer calculations where the possible property errors are probably less significant on the results of the heat-transfer calculation than are the inherent errors found in the heat-transfer coefficient correlations used in such calculations.

The properties thus generated and the techniques employed in their calculation are given in Reference 9. Because of their somewhat limited applicability and relatively large volume, they are not repeated here.

Since the conclusion of the propellant investigation conducted under this program, the properties of N_2O_4 have been redetermined on the basis of recent laboratory measurements of densities at high temperatures and pressures and upon new calculations which take N_2O_4 dissociation into account. This much-improved set of properties is given in Reference 10.

Ref 10 Baker, L., Namikawa, K., and Petrozzi, P. J., Physical Properties of Nitrogen Tetroxide, Aerojet-General Corporation, Liquid Rocket Operations, 1 December 1964

IV, C, Extension of Physical-Property Data (cont.)

Very little work has been done in the intervening period on the properties of 98% H_2O_2 at high temperatures and pressures; however, such work has very recently been undertaken as a part of the "High Energy Propellants Program" (Contract AF 04(611)-10785). The extensive effort planned is anticipated to provide not only improved properties information but also complete evaluation of the applicability of 98% H_2O_2 to high-pressure engines.

No significant new properties data at high temperatures and pressures have become available on the metalized gelled fuels. This is, however, not unexpected in view of the analytically predicted and partially demonstrated poor heat-transfer characteristics of such fuels.

D. SELECTION OF ADVANCED STORABLE PROPELLANT SYSTEMS

Because N_2O_4/AeroZINE 50 is the highest performing and most widely used state-of-the-art storable propellant system, an investigation of its applicability to high-chamber-pressure rocket engines provided a natural starting point for similar investigations of the advanced metalized propellant systems. Thus, the primary effort throughout the program was directed toward the N_2O_4/AeroZINE 50 propellant combination, and, secondarily, toward the metalized propellant combinations.

The various metalized propellant combinations considered are neither equally desirable from a theoretical performance standpoint as shown in Section IV,B, nor are they equally ready for application to high-pressure rocket engines as shown in Section IV,A. Unfortunately, those combinations most desirable on a performance basis (AlH_3,Be and BeH_2 combinations) are least ready for application to any rocket engine and, conversely, those with the lower performance potential (Al combinations) are more nearly ready for engine development. The selection of the most desirable advanced metalized propellant combinations is further complicated by two facts: (1) Be and BeH_2 have higher performance potential than Al and AlH_3, respectively, but they are now, or potentially, more expensive and are highly toxic, and (2) the

IV, D, Selection of Advanced Storable Propellant Systems (cont.)

use of H_2O_2 as an oxidizer provides a performance gain over the N_2O_4 (particularly in AlH_3, Be, and BeH_2 systems), but it is more expensive and less experience is available to define the extent of its applicability to advanced engines. It thus becomes apparent that one cannot judiciously select a "best" advanced metalized propellant combination without knowledge of the relative importance of system performance, required operational date, cost, and toxicity. Since it appears doubtful that anyone can properly assess the relative importance of the above-mentioned considerations for more than specific missions, one must conclude that the fuels containing Al, Be, AlH_3, and BeH_2 and the oxidizers N_2O_4 and 98% H_2O_2 may each occupy a prominent position at some time in storable propellant development as advancement is made from N_2O_4/AeroZINE 50 toward 98% H_2O_2/N_2H_4 + BeH_2 (potentially the highest performing storable propellant).

In view of the preceding facts, the best one can do in selecting advanced storable propellants for other than specific missions is to select propellant combinations that will quickly and economically lead to the development of the best performing propellant and, at the same time, yield one or more combinations of intermediate performance in the interim that could be made operational relatively easily if such a requirement became apparent. N_2O_4/N_2H_4 + Al offers about 5% higher performance than current state-of-the art storables (N_2O_4/AeroZINE 50), and as discussed in Section IV,A, has become essentially ready for conventional engine development. Thus, N_2O_4/N_2H_4 + Al was considered to be the most logical choice as the first metalized propellant to be considered in advanced engine concepts. The early, original choice of a fuel containing aluminum over a fuel containing beryllium was based upon a lower propellant cost and a lower development facility cost by reason of the elimination of the toxicity problem associated with beryllium use, and the choice of N_2O_4 and the very small performance advantage (0.3%) of 98% over H_2O_2 over N_2O_4 containing aluminum.

IV, D, Selection of Advanced Storable Propellant Systems (cont.)

The specific order of importance of other metalized propellants was not defined in the propellant investigation; however, further investigation of 98% H_2O_2/N_2H_4 + AlH_3 and 98% H_2O_2/N_2H_4 + Be was suggested because of their high performances and the benefits they could give toward the potential development of 98% H_2O_2/BeH_2 containing gel. For example, work with 98% H_2O_2/N_2H_4 + AlH_3 would define the methods for proper utilization of 98% H_2O_2 and the differences between the utilization of metals (Al) and metal hydrides (AlH_3), and work with 98% H_2O_2/N_2H_4 + Be would define the problems of handling and utilizing the toxic beryllium-containing liquid fuels and means of achieving good beryllium combustion.

Because of the very high cost and poor availability of AlH_3, it has since become apparent that no large-scale investigations of 98% H_2O_2/N_2H_4 + AlH_3 can be undertaken in the near future. The strong similarity between the various metalized fuels, however, indicates that Alumizine (N_2H_4 + Al) can serve as a very economical and satisfactory simulant. The 98% H_2O_2/N_2H_4 + Al system itself is of interest, though, because of its good performance (slightly better than N_2O_4/N_2H_4 + Al) and apparently easier utilization in advanced cycle engines than corresponding N_2O_4 systems if 98% H_2O_2 is suitable as a coolant.

E. DEFINITION OF PROBLEM AREAS

1. N_2O_4/AeroZINE 50

The potential problem areas related to the use of N_2O_4/AeroZINE 50 in high-pressure engines were briefly reviewed as a part of the early propellant investigation. Increased problems in chamber cooling and gas generation were foreseen, while combustion stability problems were expected to be no worse and possibly reduced. These areas have been studied in detail in other portions of this program and in the Integrated Component Program (Contracts AF 04(611)-8017 and AF 04(611)-8548).

IV, E, Definition of Problem Areas (cont.)

2. N_2O_4/N_2H_4 + Al

The problem areas related to utilization of this propellant combination were studied in considerable depth. The magnitude of the possible problems anticipated in various engine components were described and solutions were presented where possible. Since the study was completed, experimental verification has been achieved in almost all cases under Contracts AF 04(647)-652, SA 4, and AF 04(694)-212 and has given good agreement with prediction. Results of these recent programs are summarized in Section IV, A.

3. Other Metalized Propellants

The other more important metalized propellants considered in the problem definition phase included 98% H_2O_2/N_2H_4 + AlH_3, 98% H_2O_2/N_2H_4 + Be, and 98% H_2O_2/N_2H_4 + BeH_2. This study indicated that problem areas similar to those for N_2O_4/N_2H_4 + Al would exist with a few exceptions. Thrust-chamber cooling appeared to be possibly less of a problem, assuming 98% H_2O_2 decomposition at high pressures does not occur to an appreciable extent. The beryllium-containing system appeared to present a greater ignition and combustion problem. Gas generation was expected to be simplified because of the monopropellant capabilities of H_2O_2. Handling and storing of 98% H_2O_2 appeared to present more of a problem than with N_2O_4. The Be and BeH_2 systems presented new toxicity problems. The AlH_3 and BeH_2 systems required further fuel development effort to achieve chemical and mechanical stability of the fuels.

F. RECOMMENDED RESEARCH AND DEVELOPMENT PROGRAMS

Based upon the review of experience, performance, properties, and known and anticipated problem areas related to the various propellants of interest in this program, it was recommended that both laboratory and feasibility demonstration programs be either initiated or continued and expanded. The scope of these recommended efforts is outlined below.

IV, F, Recommended Research and Development Programs (cont.)

The laboratory effort should include the clear definition of the high-pressure heat-transfer characteristics of N_2O_4, AeroZINE 50, 98% H_2O_2, and Alumizine. Laboratory effort should also be directed toward the development of usable N_2H_4 + AlH_3 and N_2H_4 + BeH_2 gelled fuels (i.e., those with suitable chemical and mechanical stabilities).

Feasibility demonstration programs should include entire engine demonstrations at high pressures and for extended durations. N_2O_4/AeroZINE 50 should be used in the first demonstrations to establish basic high-pressure design criteria for thrust chambers, gas generators, turbines, pumps, and system controls. The effort necessarily should be oriented to consider novel concepts, which could eliminate some of the major problem areas known or anticipated. Following or simultaneously with this effort, emphasis should be placed upon the N_2O_4/N_2H_4 + Al and the 98% H_2O_2/N_2H_4 + Al propellant combinations to define the design modifications required to incorporate metalized, gelled propellants into high-pressure engines, to demonstrate the performance capabilities of the metalized fuels in high-pressure engines, and to evaluate 98% H_2O_2 as an oxidizer. After the successful demonstration of these propellant combinations, effort should then be centered on 98% H_2O_2/N_2H_4 + AlH_3 and 98% H_2O_2/N_2H_4 + Be to define any further design modifications required to utilize AlH_3 and Be in the fuel. This latter effort should then allow for the demonstration of the 98% H_2O_2/N_2H_4 + BeH_2 combination.

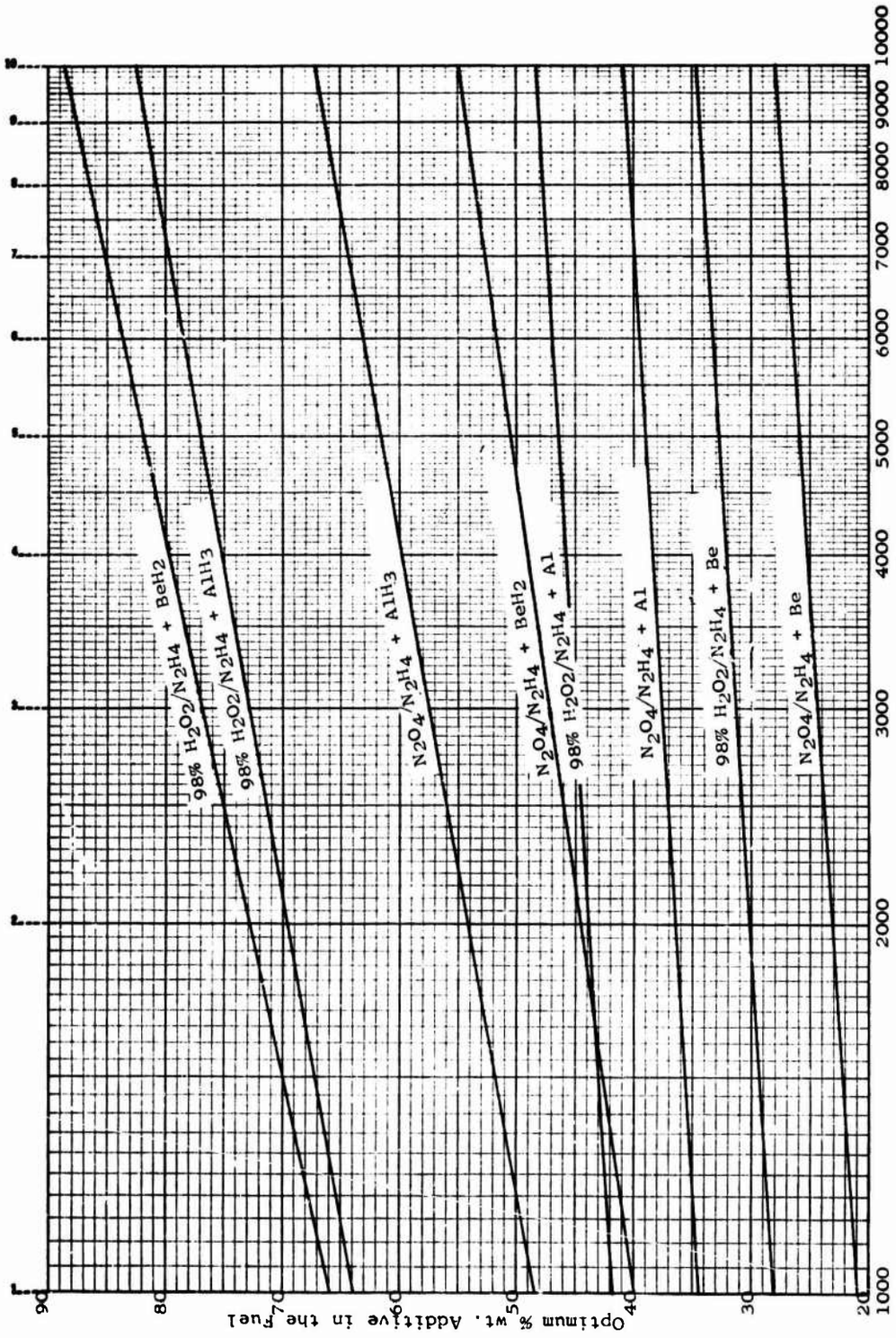

Optimum Additive Concentration in the Fuel of Various Metalized Storables vs Chamber Pressure (u)

Figure IV-B-1

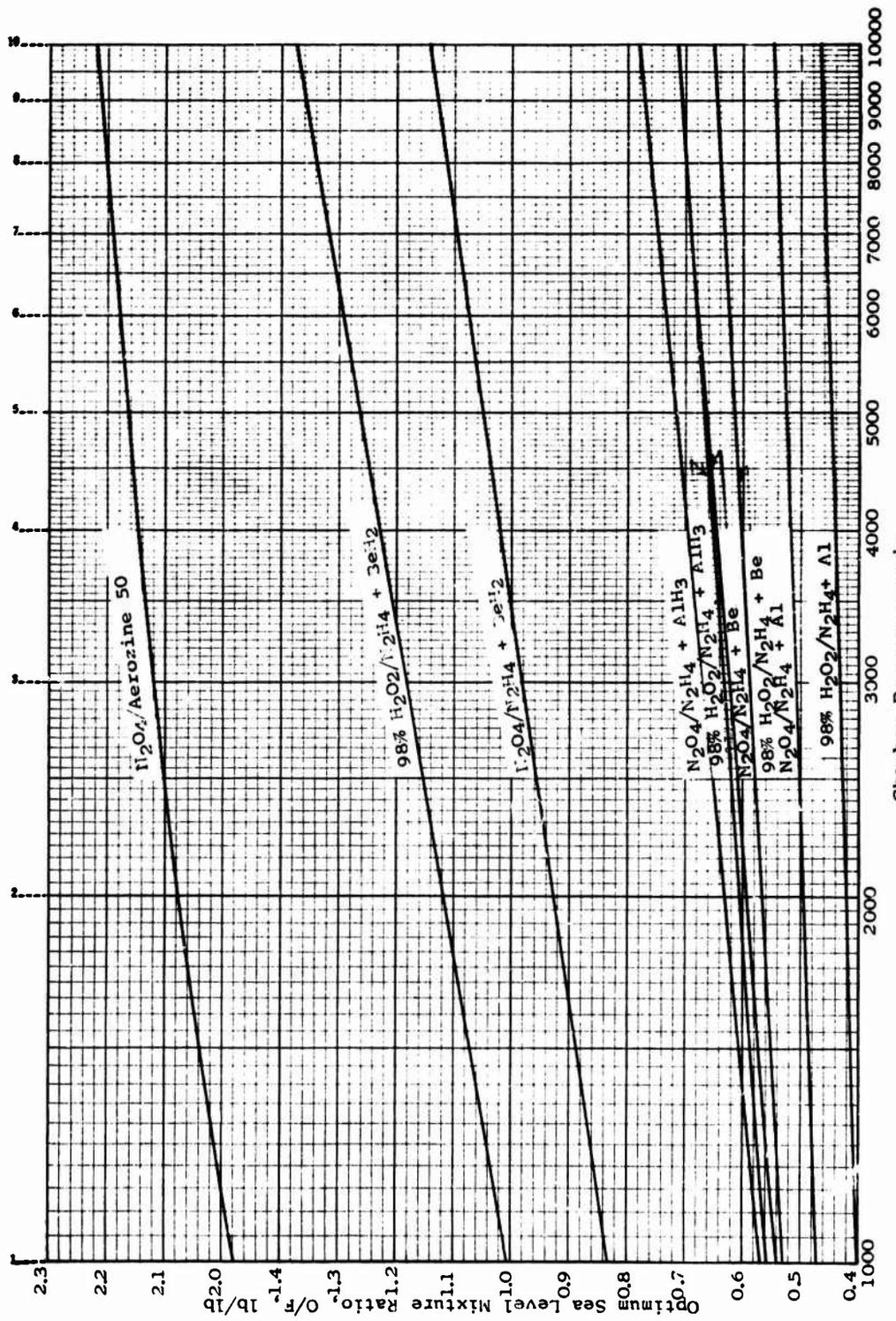

Optimum Sea-Level Mixture Ratio of Various Metalized Storables
at Optimum Additive Concentration vs Chamber Pressure (u)

Figure IV-B-2

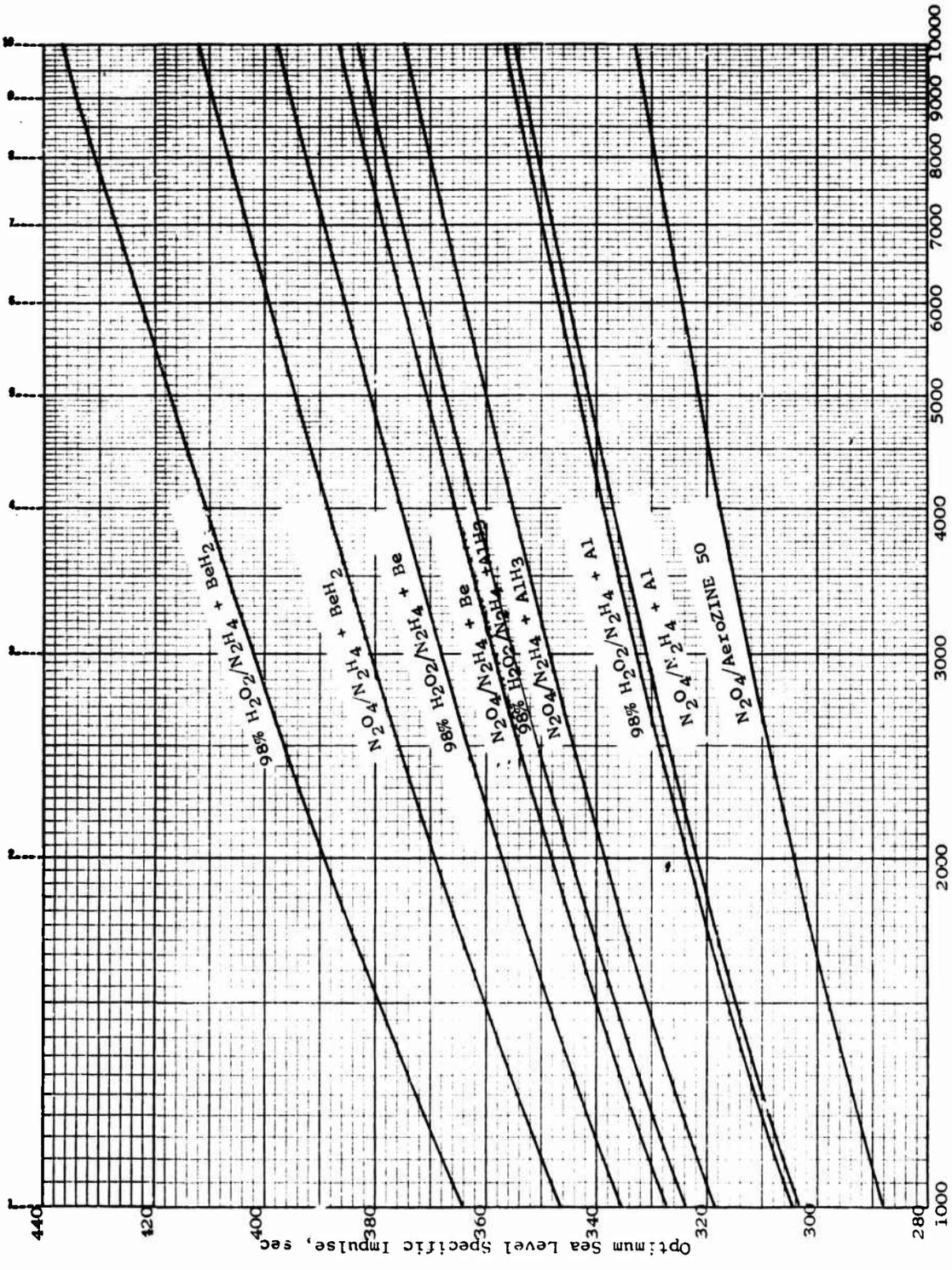

Optimum Sea-Level Specific Impulse of Various Metalized Storables vs Chamber Pressure (u)

Figure IV-B-3

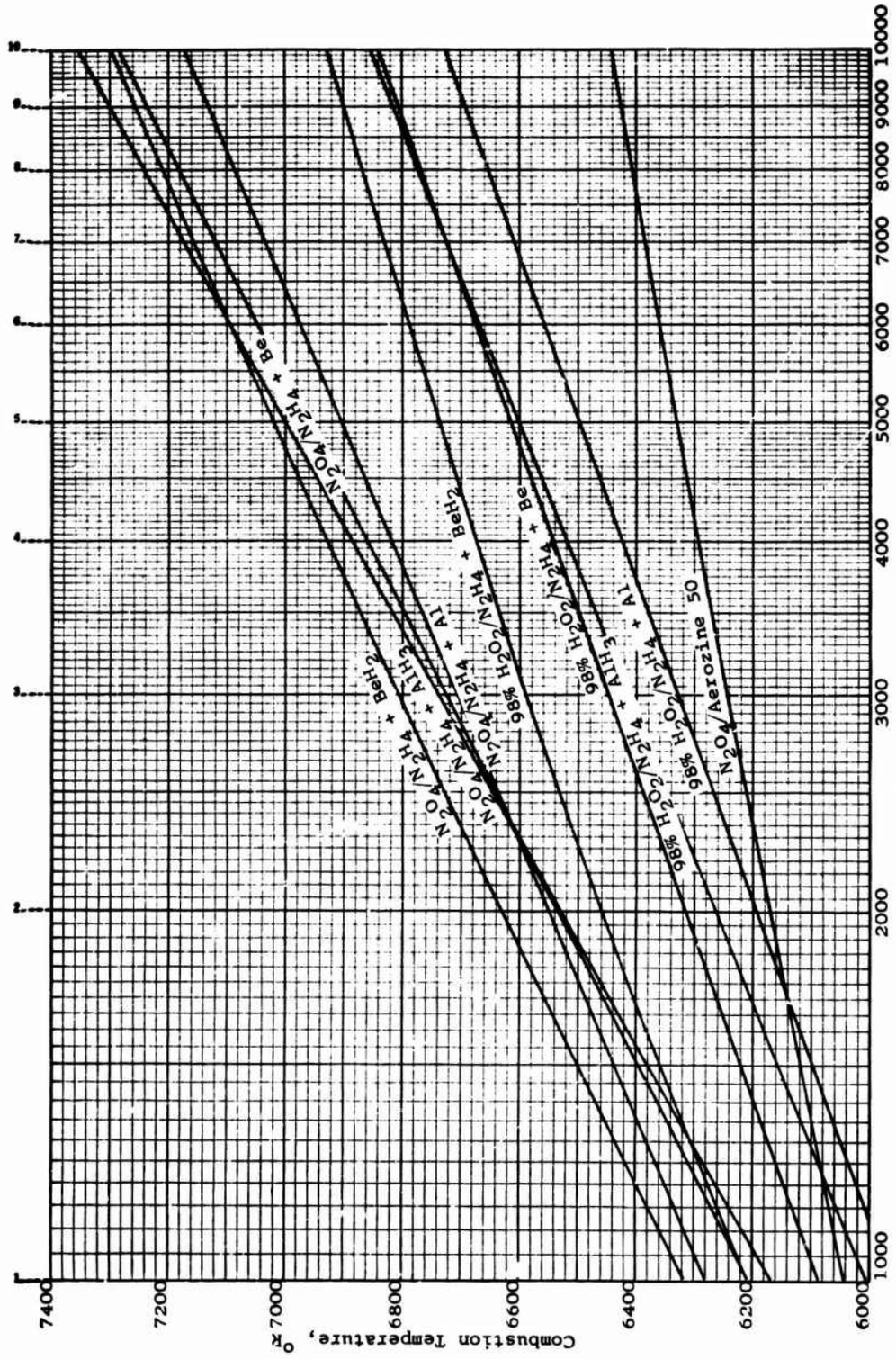

Combustion Temperature of Various Metalized Storables at Optimum Sea-Level Mixture Ratio and Additive Concentration vs Chamber Pressure (u)

Figure IV-B-4

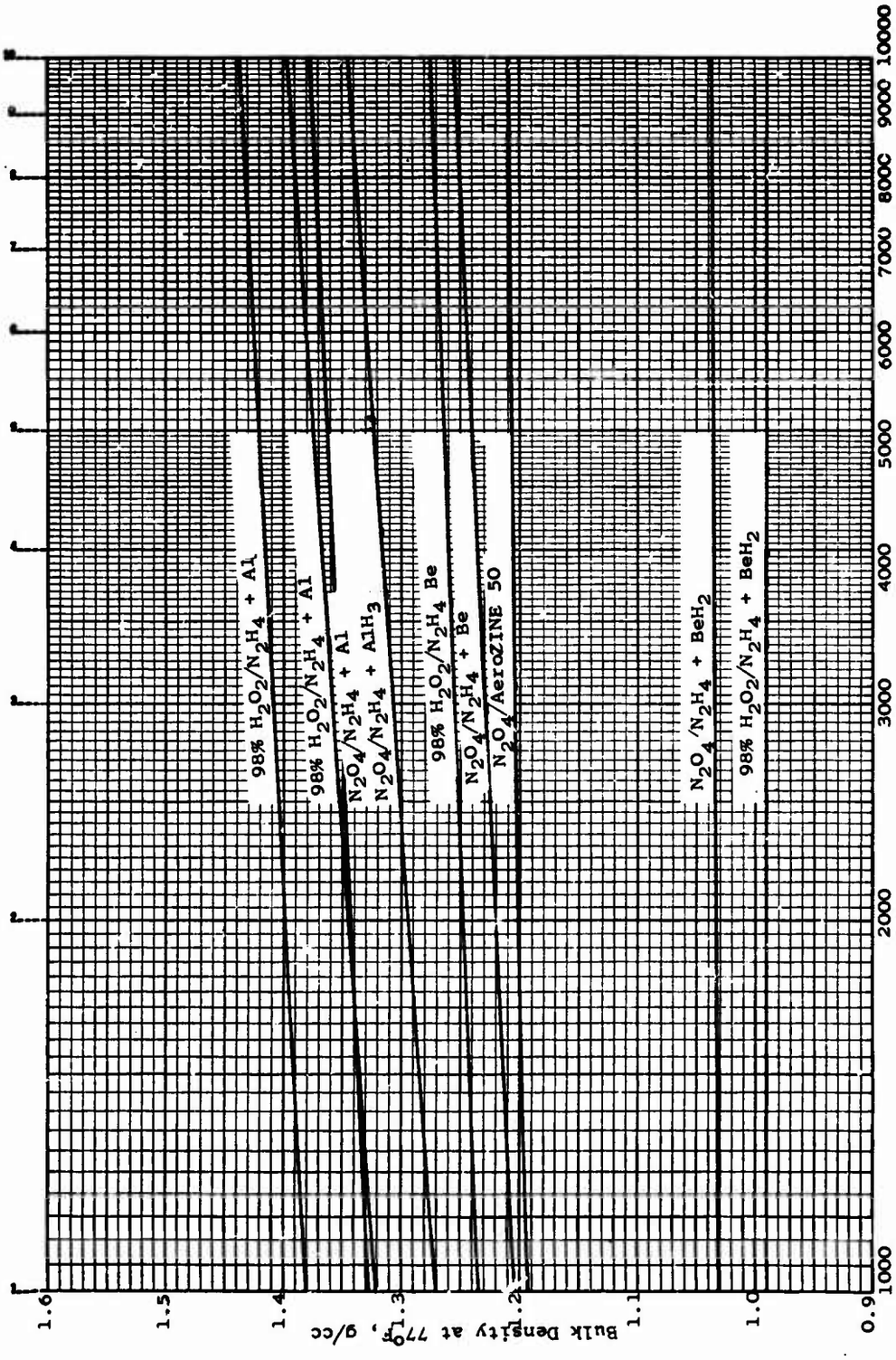

Bulk Density of Various Metalized Storables at Optimum Sea-Level Mixture Ratio and Additive Concentration vs Chamber Pressure (u)

Figure IV-B-5

V. GAS-SIDE HEAT-TRANSFER STUDY

V. GAS-SIDE HEAT-TRANSFER STUDY

A detailed program was conducted as a part of the High Chamber Pressure Rocketry Program to study the gas-side heat-transfer coefficient as applied to thrust chambers operating at high chamber pressures. This program consisted of three parts:

1. A detailed study of the existing analytical methods for the determination of the gas-side heat-transfer coefficient.

2. A study of the techniques to experimentally determine the gas-side heat-transfer coefficient in a high chamber pressure thrust chamber.

3. An experimental program to evaluate the most promising heat-flux measuring technique for determining the actual gas-side heat-transfer coefficient, and to correlate it with the analytically obtained coefficient.

Based upon the study conducted, the following conclusions are made:

1. Three analytical methods currently exist for determining gas-side heat-transfer coefficients including the Bartz general boundary layer method, the simplified Bartz method, and Mayer's approximation. Of these, the simplified Bartz method, used in conjunction with a correction factor multiplier based upon experimental data, is the most simple method to apply and gives generally accurate results.

2. No heat-flux instrument exists today which is capable of directly measuring the gas-side heat-transfer coefficient in a high-pressure rocket engine. There are techniques for computing heat flux from wall temperature measurements; however, these techniques are not fully developed either.

3. Some heat-transfer measurements were made in the experimental program to determine the gas-side heat-transfer coefficients. One measurement agreed with the simplified Bartz method using a multiplier of 2.0; other measurements yielded

V, Gas-Side Heat-Transfer Study (cont.)

values that were an order of magnitude too low. It must be concluded that experimental measurement of the gas-side heat-transfer coefficients was generally unsuccessful, mainly because of difficulty in maintaining the heat-transfer instruments in place during testing, as well as ablative gases from the uncooled chamber walls that significantly affected the boundary layer temperatures.

Book One

V, Gas-Side Heat-Transfer Study (cont.)

A. ANALYTICAL METHODS FOR DETERMINING GAS-SIDE HEAT-TRANSFER COEFFICIENTS

The first published attempt to predict gas-side heat-transfer coefficients in convergent-divergent nozzles was presented by Bartz (Ref 1) from a solution of the general boundary layer equations. Because such computations are quite complicated, Bartz subsequently presented a simplified method (Ref 2) which is essentially a form of the conventional pipe-flow equation. While the latter equation has been widely used, the results are not completely reliable because the effects of combustion chamber characteristic length (L*) and nozzle convergence angle are not expressed in the equation.

It is evident that high heat-transfer coefficients occur near the injector; this is demonstrated by the frequent necessity for film cooling in this region. A boundary layer analysis predicts high heat-transfer coefficients where the boundary layer growth originates, i.e., in the undeveloped flow region.

The simplified Bartz method predicts coefficients which agree very closely with those of the complete boundary layer analysis, except in the region where boundary layer growth originates. In this region the complete analysis predicts higher heat transfer coefficients. It has been the general practice, therefore, to compute coefficients by the simplified method, and then multiply these values by a factor to account for this effect. This factor has been shown to range from 1.5 and 2.0 depending on specific engine operating characteristics.

A simplified boundary layer analysis has been published by Mayer (Ref 3). In this analysis, the boundary layer development originates at the injector face and, as expected, indicates the existence of an infinite coefficient due to the zero thickness

Ref 1. Bartz, D.R., "An Approximate Solution of Compressible Turbulent Boundary Layer Development and Convective Heat Transfer in Convergent-Divergent Nozzles," Transactions of the ASME, November, 1955.

Ref 2. Bartz, D.R., "Simple Equation for Rapid Estimation of Rocket Nozzle Convective Heat Transfer Coefficients," Jet Propulsion, January, 1957.

Ref 3. Mayer, E., "Analysis of Convective Heat Transfer in Rocket Nozzles," ARS Journal, July, 1961.

of the boundary layer. Because of this, the computation of the required integrals is initiated at an arbitrary distance from the injector face.

It is reasoned that because the combustion process requires some finite time, and, therefore, distance, a region of relatively cooler gas exists near the injector face that permits establishment of the momentum boundary layer prior to establishment of the thermal boundary layer.

This scheme is admittedly artificial; however, extrapolation yields injector face coefficients which are generally consistent with practical experience. This method appears to make allowances for opposing criteria such as L* and nozzle convergence.

During the analytical studies undertaken on the High Chamber Pressure Program, gas-side heat-transfer coefficients were calculated for MR = 2.0 and Pc = 3000 psia, using both the Bartz short form approximation, the two-times Bartz, and the Mayer simplified boundary-layer method. The form of the Bartz approximation method is based on the assumption of a fully developed turbulent flow. Because of this assumption, the gas-side heat-transfer coefficient (h_g) is essentially constant in the cylindrical section of the chamber, increasing in the convergent section of the nozzle, and having a maximum value at the throat, where the mass velocity is maximum.

The upper limit of the Bartz method was obtained by multiplying these values by the above-mentioned factor (in this case 2.0) and diminishing it linearly in the convergent section to 1.0 at the throat. The results of the Bartz approximation, two-times Bartz, and the Mayer method are shown in Figure V-A-1.

In general, the values obtained by the Mayer method are between the Bartz values and the two-times Bartz values. The Mayer method of calculation gives somewhat lower values at the throat section, but, while the throat section is usually a critical

area with respect to heating, it has been experimentally established that the Bartz equation may be, under some conditions, conservative in predicting the gas-side heat-transfer coefficients in the throat.

Downstream of the throat, some designers use the Bartz equation with physical properties corrected in terms of the film temperature, i.e., the arithmetic average of the free stream and wall temperatures or Eckert's reference temperature (Ref 4). (In the case where Eckert's reference temperature is used, the gas-side heat-transfer coefficients are approximately 40% lower than those based on the film temperature, especially at large area ratios.) The Mayer simplified boundary-layer method, which is based on the use of Eckert's reference temperature, yields the lowest gas-side heat-transfer coefficients. The difference is probably not significant from an engineering standpoint under the conditions for which the two methods are compared.

A more important question is that of the proper temperature at which to establish transport and physical properties. In view of the nature of the problems involved, and the source of Eckert's reference correction, it is probable that the use of the film temperature leads to unnecessarily high gas-side heat-transfer coefficients downstream of the throat.

In general, it is preferable to use the Eckert reference temperature because, with an externally cooled wall, the boundary layer temperature reaches a local maximum which is greater than either the corresponding free stream temperature or the wall temperature, whereas the film temperature is defined as the average of the two temperatures.

The effect of mixture ratio is expected to be quite small (approximately 4% for mixture ratios in the range 1.6 to 2.4) because a variation in mixture ratio causes small variations in combustion temperature and appears in the Bartz equation in the form of a variation in characteristic velocity, c*. As long as the mixture ratio does not differ greatly from stoichiometric, variations in combustion temperature and, therefore, c*, are relatively small.

Ref 4. Eckert, E.R.G., "Survey of Boundary-Layer Heat Transfer at High Velocities and High Temperatures," WADC Technical Report 59-624, April 1960.

V, A, Analytical Methods for Determining Gas-Side Heat-Transfer Coefficients (cont.)

Another small effect results from variation in physical and transport properties caused by different fractions of combustion products. The effect is considered negligible because the effect of temperature variations would be further depressed where either the film temperature or reference temperature is used. The empirical formula for correcting the gas-side heat-transfer coefficient to different mixture ratios is

$$\frac{h_g \text{ MR} = x}{h_g \text{ MR} = 2.0} = 0.1 (MR_x) + 0.8$$

where:

h_g MR = X = heat transfer coefficient at some MR = x

h_g MR = 2.0 = heat-transfer coefficient at MR = 2.0

MR = x = injector mixture ratio other than 2.0

The effect of chamber pressure on the gas-side heat-transfer coefficient can be expressed directly in terms $h_{g2} = h_{g1} \frac{P_{c2}}{P_{c1}}$

where:

h_{g2} = heat transfer coefficient at some chamber pressure P_{c_2}

h_{g1} = heat transfer coefficient at some chamber pressure P_{c_1}

P_{c_2} = chamber pressure at h_{g2}

P_{c_1} = chamber pressure at h_{g1}

V, Gas-Side Heat-Transfer Study (cont.)

B. EXPERIMENTAL TECHNIQUES FOR DETERMINING GAS-SIDE HEAT-TRANSFER COEFFICIENTS

The most direct method for determining the gas-side heat-transfer coefficients is the use of heat flux calorimeters. During the course of the program, all known manufacturers of heat flux calorimeters were contacted. It was found that no manufacturers had instruments capable of operating in the severe temperature and pressure environment encountered in a high-pressure thrust chamber.

Some of the instruments could not absorb the anticipated heat fluxes, while others lacked the mechanical integrity required to withstand the turbulent flow and the high pressures experienced in the thrust chamber. The use of high-temperature, high-response thermocouples was then investigated.

Thermocouples and their mounting assemblies, when properly designed and adequately developed, can provide temperature data from which heat flux and gas-side heat-transfer coefficient can be determined. There are two ways by which the gas-side heat-transfer coefficient can be determined from thermocouple data.

One of these methods is to inbed the thermocouple at a known distance (L) from the "hot" surface of a material whose conductivity (k) is known and record the transient temperature history at that point. Then, by using the infinite slab case of the Schmidt plot method (Ref 5), the heat flux and thus the heat-transfer coefficient can be determined.

The other method is to install two thermocouples in the same plane at a known radial distance (L) from each other in a material whose conductivity (k) is known. The heat flux and the gas-side heat-transfer coefficient is then calculated from L, k, and ΔT.

Ref 5. Kreith, Frank, Principles of Heat Transfer, p. 153, International Textbook Company, Scranton, Pennsylvania, 1958.

V, B, Experimental Techniques for Determining Gas-Side Heat-Transfer Coefficients (cont.)

In both cases an effort has to be made, in the thermocouple installation design, to ensure uniplanar heat flow in the specimens. In rocket motors, it means that the heat flow should be purely radial. In case the thermocouple is not directly installed into the thrust chamber liner, the "plug" must be large enough in cross-section to inhibit "cross-heat" flow (due to the difference in conductivity between the chamber liner and plug) at the thermocouple during the anticipated data period.

The single thermocouple method was selected for use during this program. The thermocouple used in these investigations was custom-made by the NANMAC Corporation, New Jersey. This thermocouple was made of tungsten/74% tungsten-26% rhenium and had a body of ATJ graphite. The thermocouple was capable of giving accurate temperature readings even when it was eroding. The design is shown in Figure V-B-1.

Initially, three thermocouples were installed in an ATJ-graphite thrust-chamber liner and were located at different points along the chamber contour and at known distances from the gas-side wall. The installation is shown in Figure V-B-2. The material and grain orientation of these thermocouples was identical to the material and grain orientation of the thrust chamber liner in which they were installed. The thermocouples were lapped and cemented in place with a commercial product cement (C-9). This cement has thermal conductivity close to that of ATJ graphite.

The graphite chamber-liner segments, however, did not survive the engine start transient (in most cases the graphite cracked and was ejected through the nozzle), and consequently meaningful heat-transfer data were not obtained. Further use of the thermocouples was suspended until a satisfactory liner material was found.

Subsequent chamber development showed that ablative materials were very satisfactory as thrust chamber liners. (These materials were originally considered but rejected because of the possible effects of liner ablation on heat-transfer data). Attempts to determine the gas-side heat-transfer coefficients experimentally were then resumed. The thermocouples were embedded in ATJ-graphite plugs which were bonded to the ablative liner. The installation is shown in Figures V-B-3 and -4.

V, B, Experimental Techniques for Determining Gas-Side Heat-Transfer Coefficients (cont.)

The plug was designed so that a relatively large graphite area surrounded the thermocouple at the chamber wall surface. This was done in an attempt to isolate the thermocouple from the ablating chamber surface as much as possible, a condition which could obscure the temperature data. The surrounding graphite also provided a material of known conductivity between the thermocouple and chamber wall surface, which is necessary for heat transfer calculations.

Five thermocouples were installed for testing; they were located and numbered as shown in Figure V-B-5.

V, Gas-Side Heat-Transfer Study (cont.)

C. EXPERIMENTAL INVESTIGATION OF GAS-SIDE HEAT-TRANSFER COEFFICIENTS

Tests 1.2-02-YAM-003 and 1.2-02-YAM-004 were conducted with the ablative-lined thrust chambers to provide heat-transfer data. The temperature-vs-time plots are shown in Figures V-C-1 and V-C-2.

The raw data were reduced using the graphical Schmidt plot method to analyze transient heat transfer. By this method, the temperature-vs-time history is plotted throughout the material and its surface, because the temperature-time history at any point was known. The intersection of these curves with the corresponding gas or driving temperature yields the corresponding k/h_g value, where k is the material thermal conductivity at that particular time and temperature, and h_g is the corresponding gas-side heat-transfer coefficient.

To determine the validity of the obtained h_g, the Heissler chart (Ref 6) method was used. In this method, the h_g that was obtained from the Schmidt plot technique was used to obtain the corresponding wall temperature. The wall temperature that was calculated in this manner had to be identical to the experimentally measured temperature if the h_g was correct. The calculated temperatures were in good agreement with the measured values.

Slight differences did occur, however, and this was expected because the Heissler charts were developed for tests where the time is measured in hours, and the Forier modulus ($Fo = t/L^2$), which is one of the ordinates of the plot, is very small and near the convergent section of the available curves. The original equations could have been solved to generate an expanded set of curves, but the differences were not significant enough to warrant the time and cost involved.

Ref 6. "Heat and Mass-flow Analyzer Laboratory," Columbia University, Presented at the Semi-Annual Meeting of the American Society of Mechanical Engineers, Detroit, Michigan, June 17 to 20, 1946.

V, C, Experimental Investigation of Gas-Side Heat-Transfer Coefficients (cont.)

The resulting h_g was then compared with those obtained analytically in Figure V-C-3. The reduced data are presented in three plots: (1) Figure V-C-4 is the plot of the hot-gas-side wall temperature (T_{wg}) vs time, (2) Figure V-C-5 is the plot of the gas-side heat-transfer coefficient (h_g) vs time, and (3) Figure V-C-6 is the plot of the heat flux (q) vs time.

As can be seen in Figure V-C-3, the data obtained from the thermocouple located in the first L* segment (T_{c5}) is in agreement with that obtained analytically by doubling the Bartz values, while the others are too low by a factor of from five to ten.

Figure V-C-4, which is the plot of the hot-gas-side wall temperatures (T_{wg}), indicates that throughout the test the wall temperatures were lower than expected at all thermocouples except T_{c-5}.

Thermocouple T_{c-5} was located at the forward end of the chamber near the injector face, an area where little or no ablation of the thrust chamber liner was experienced in short duration tests. The other thermocouples, however, were located in the convergent section of the chamber, an area in which major ablation begins during the latter portion of the start transient.

It is therefore concluded that only thermocouple T_{c-5} recorded the true temperature conditions; the other data reflected the effect of the relatively cool gases produced by the ablating wall, which acted as a film coolant and caused a sharp reduction in wall temperatures.

No further measurements of the gas-side heat-transfer coefficients were attempted. The use of the ablative liners, which proved so successful for evaluation of injectors and for determination of uncooled thrust-chamber performance, preclude the measurement of accurate wall temperature data.

V, C, Experimental Investigation of Gas-Side Heat-Transfer Coefficients (cont.)

Additional heat-transfer experiments were conducted, however, with some of the cooled hardware components. These experiments are discussed under the subsections in Section VII, "Cooled Thrust Chamber Design and Development," and in Section VIII,D, "Effectiveness of Film Cooling."

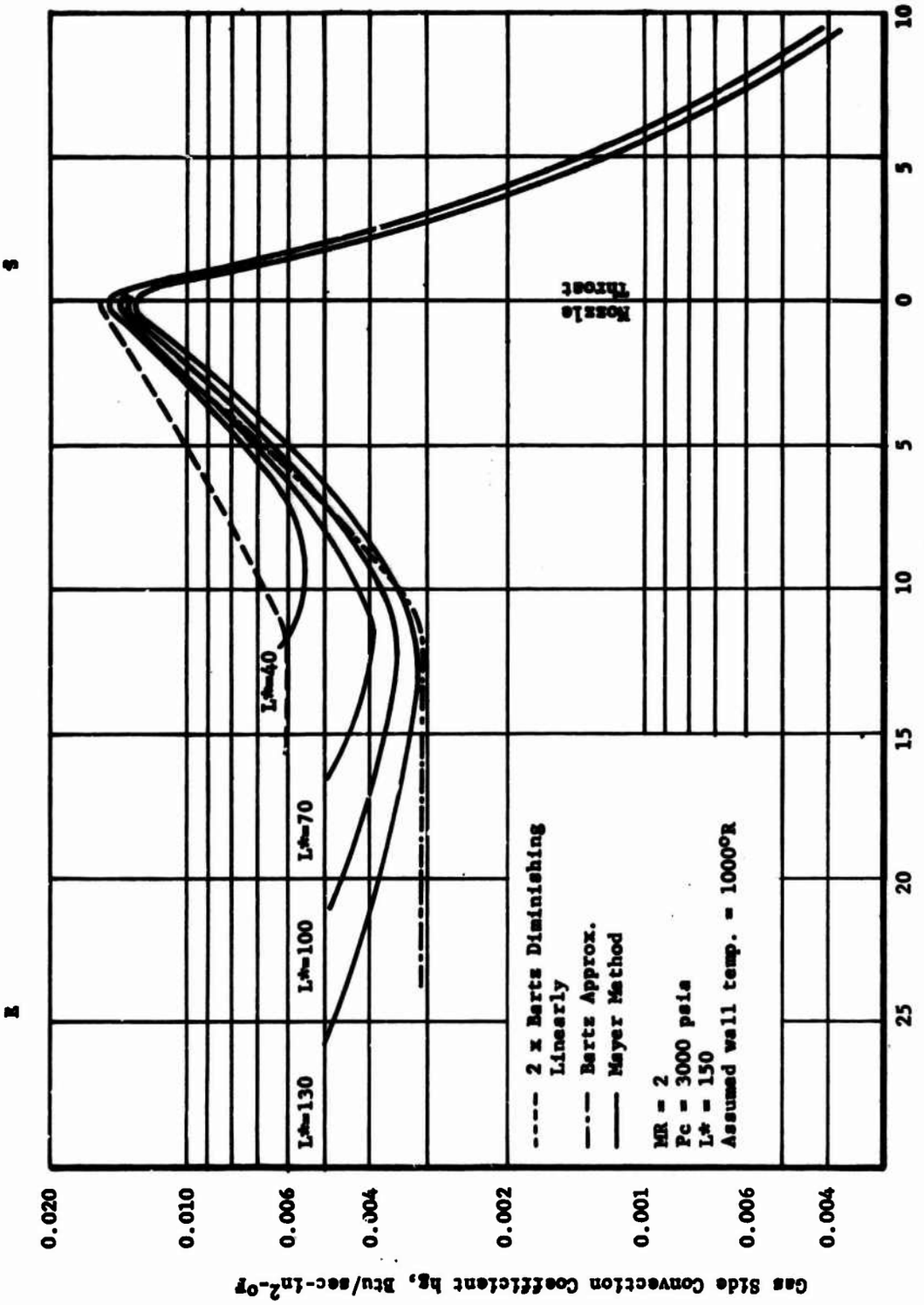

Effect of Chamber Length on Gas-Side Heat Transfer Coefficients

Figure V-A-1

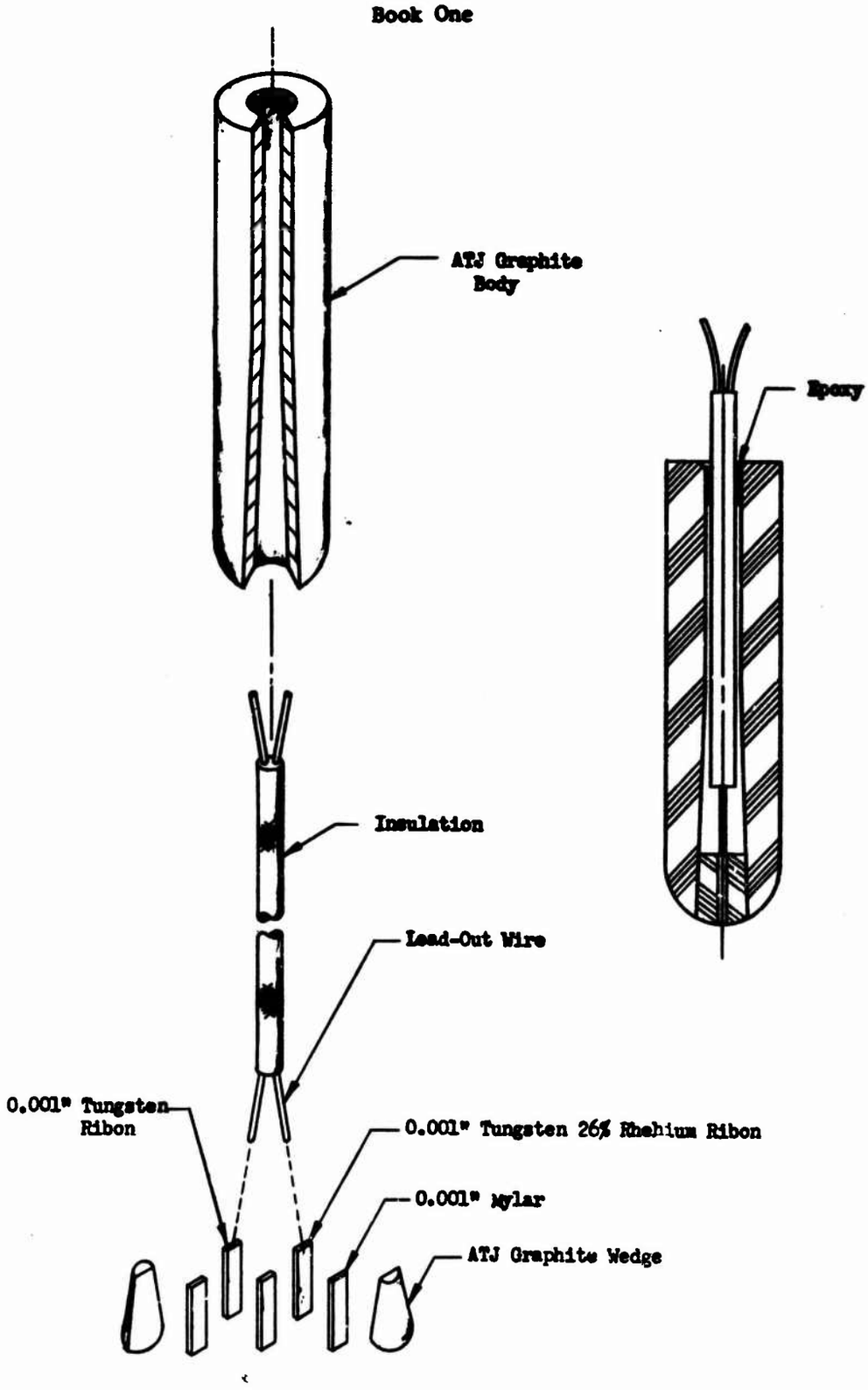

Graphite Bodied Thermocouple Design

Figure V-B-1

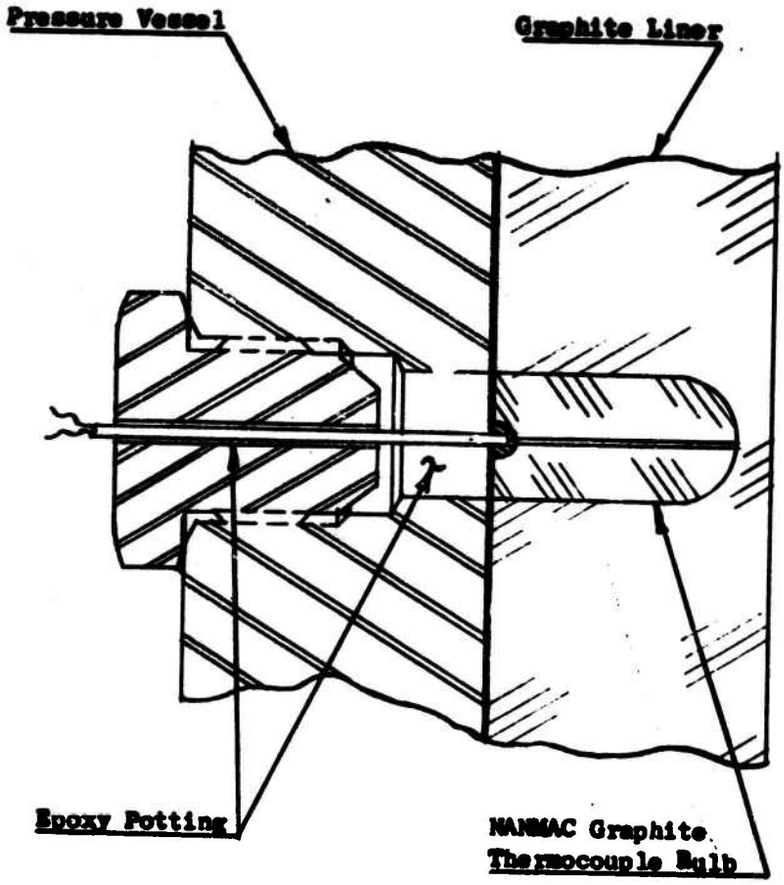

Graphite Liner Thermocouple Installation Design

Figure V-B-2

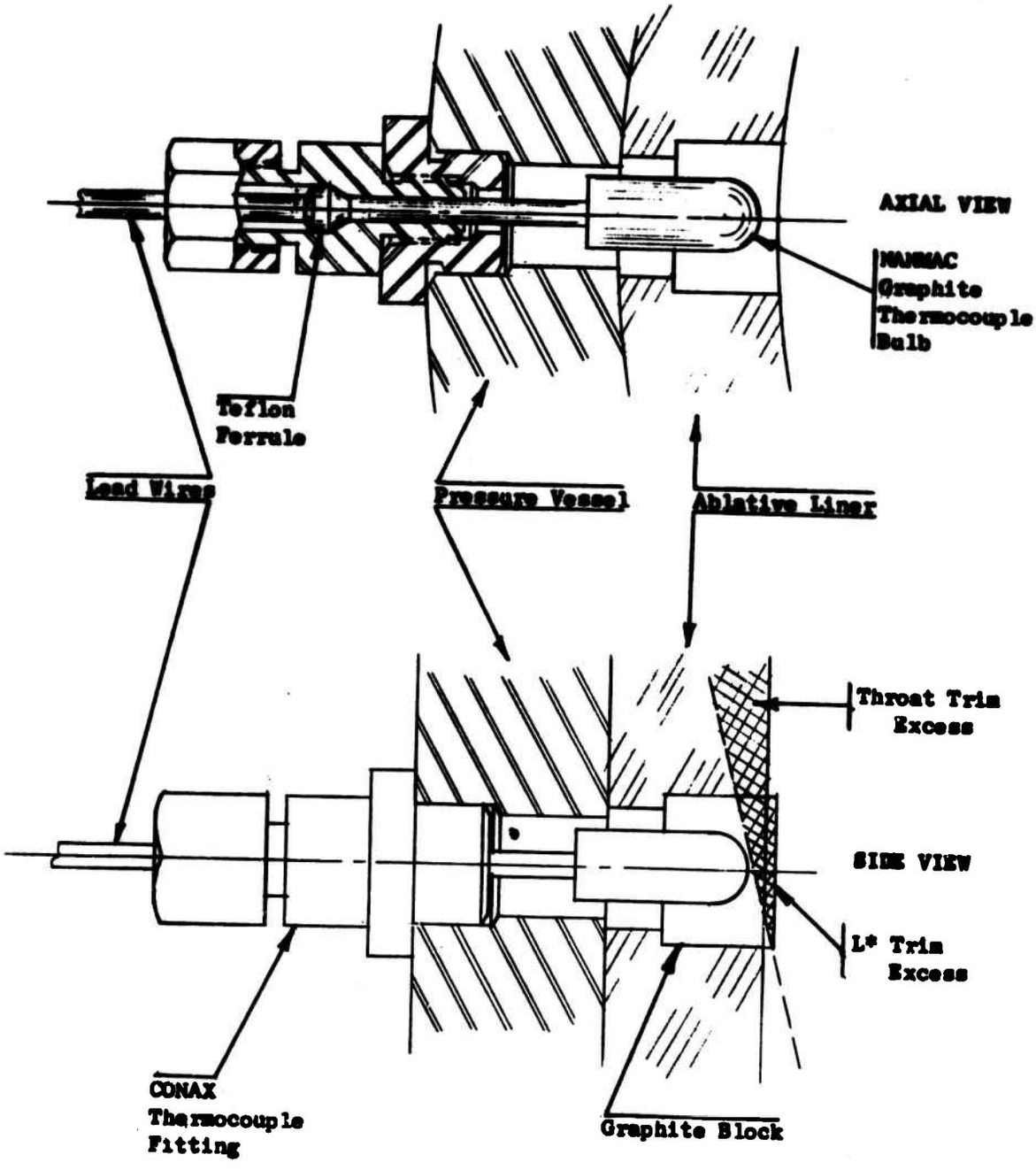

Ablative Liner Thermocouple Installation Design

Figure V-B-3

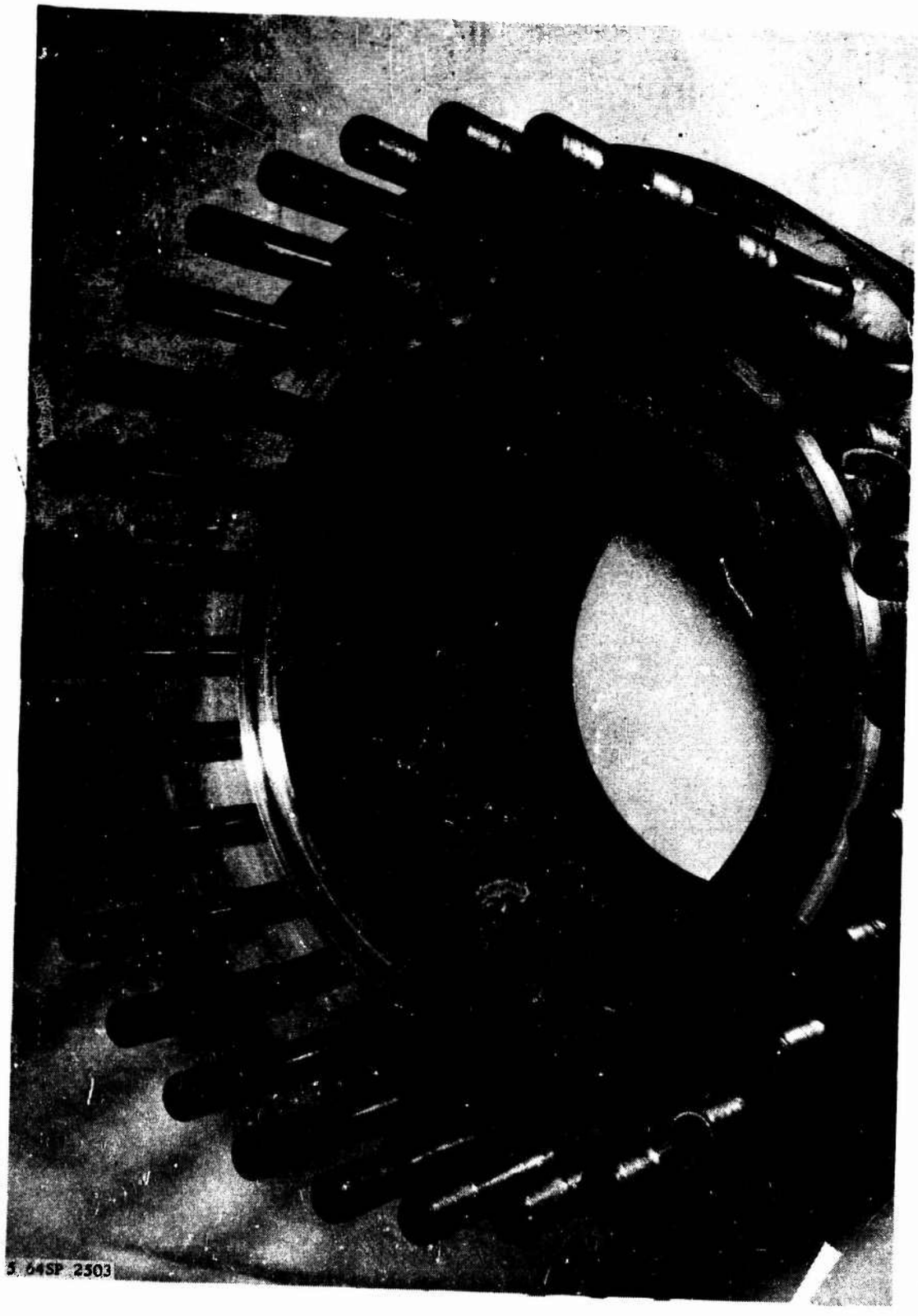

Ablative Liner Thermocouple Installation

Figure V-B-4

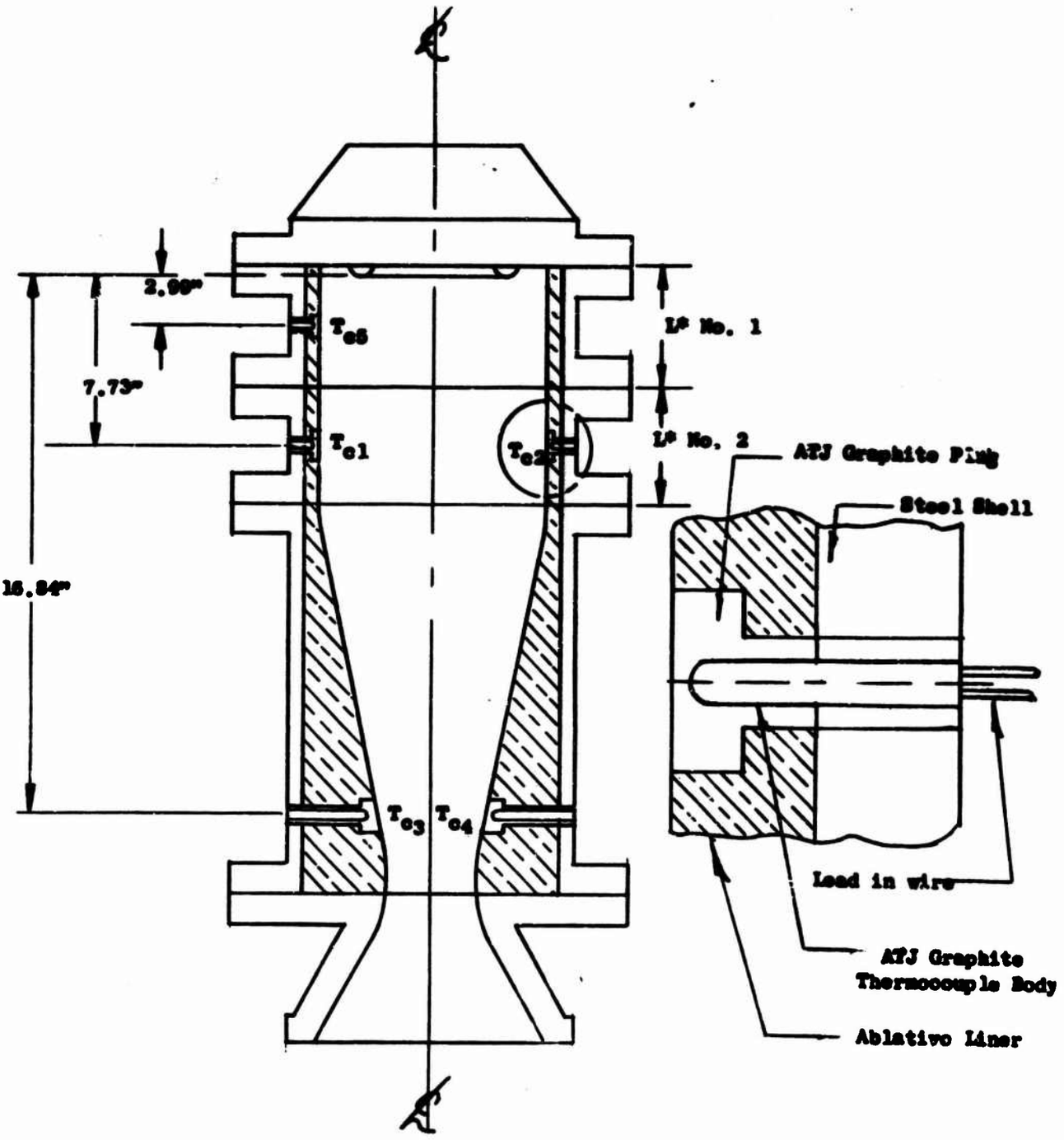

Thermocouple Locations, Uncooled Chamber

Figure V-B-5

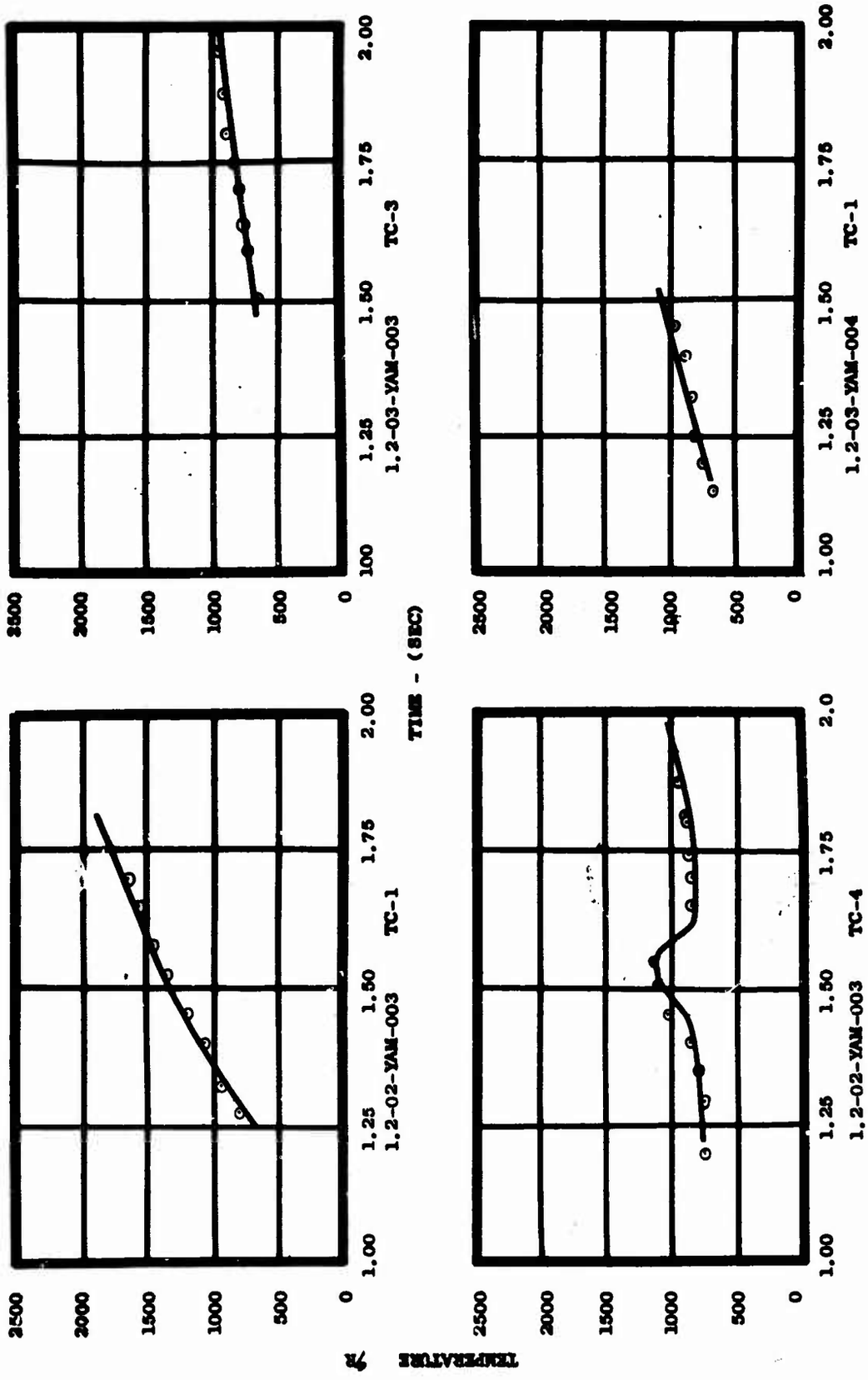

Thermocouple Data, Uncooled Chamber

Figure V-C-1

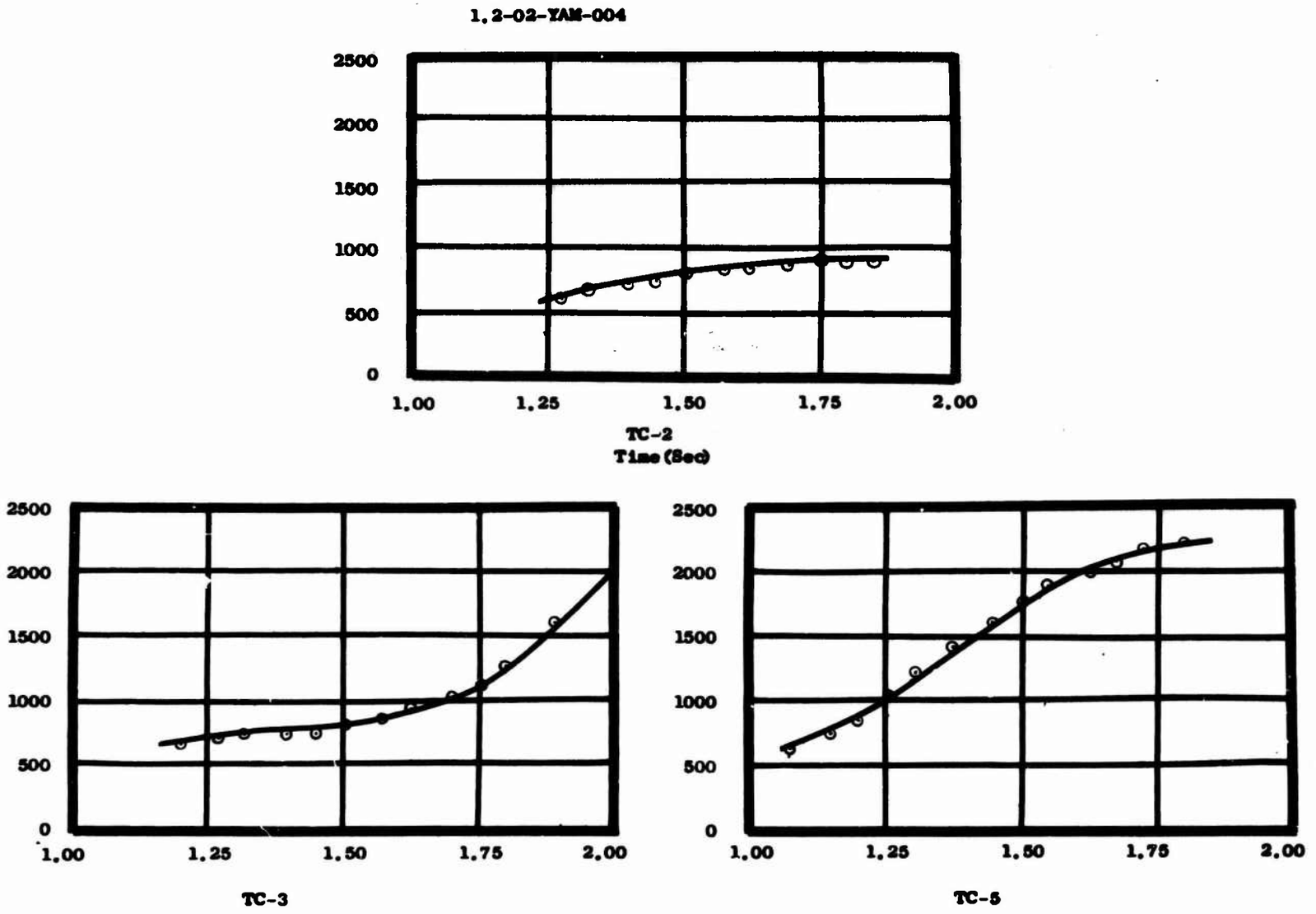

Figure V-C-2

Thermocouple Data, Uncooled Chamber

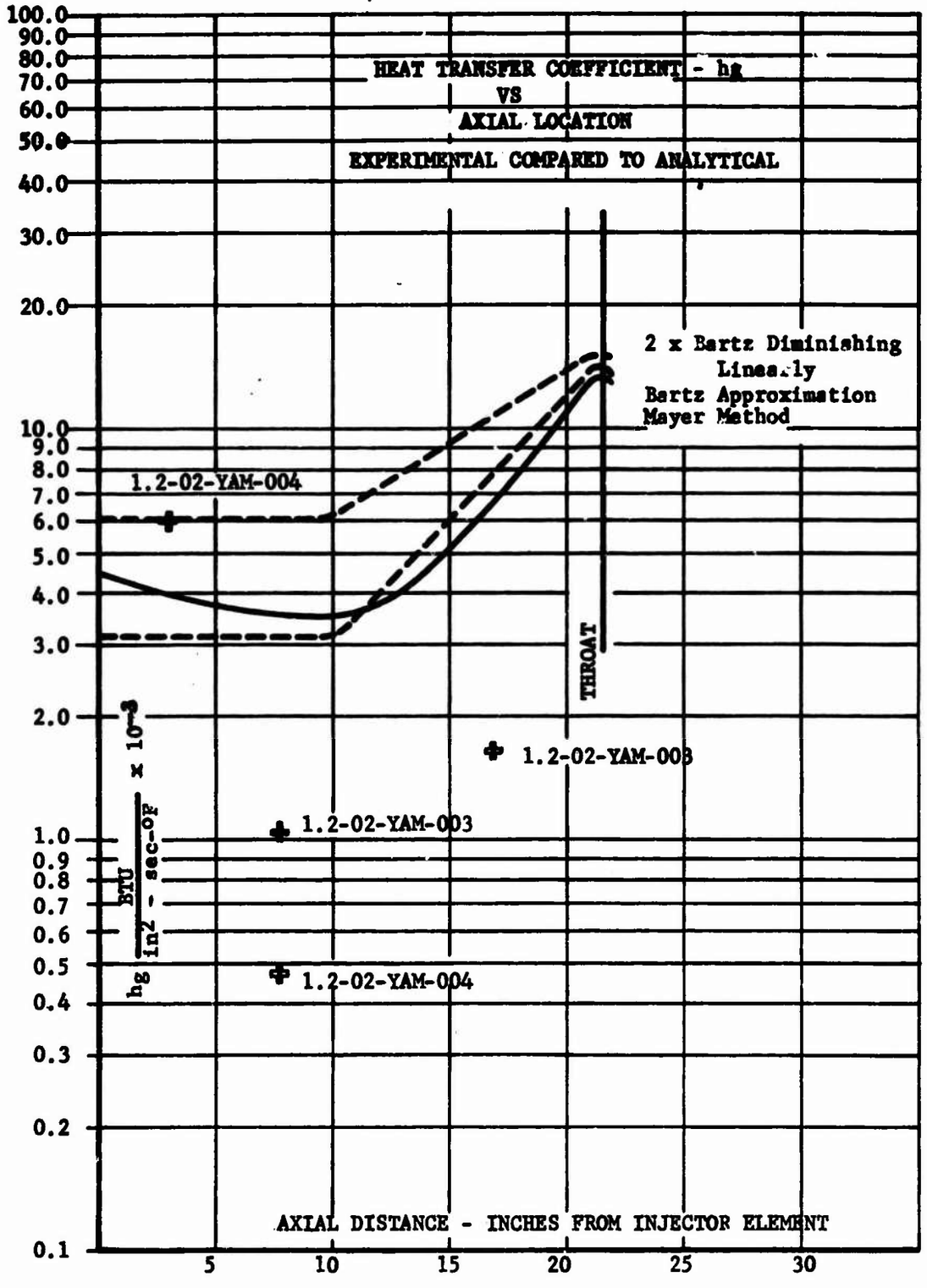

Gas-Side Heat-Transfer Coefficient, h_g, vs Axial Location, Experimental Compared to Analytical (u)

Figure V-C-3

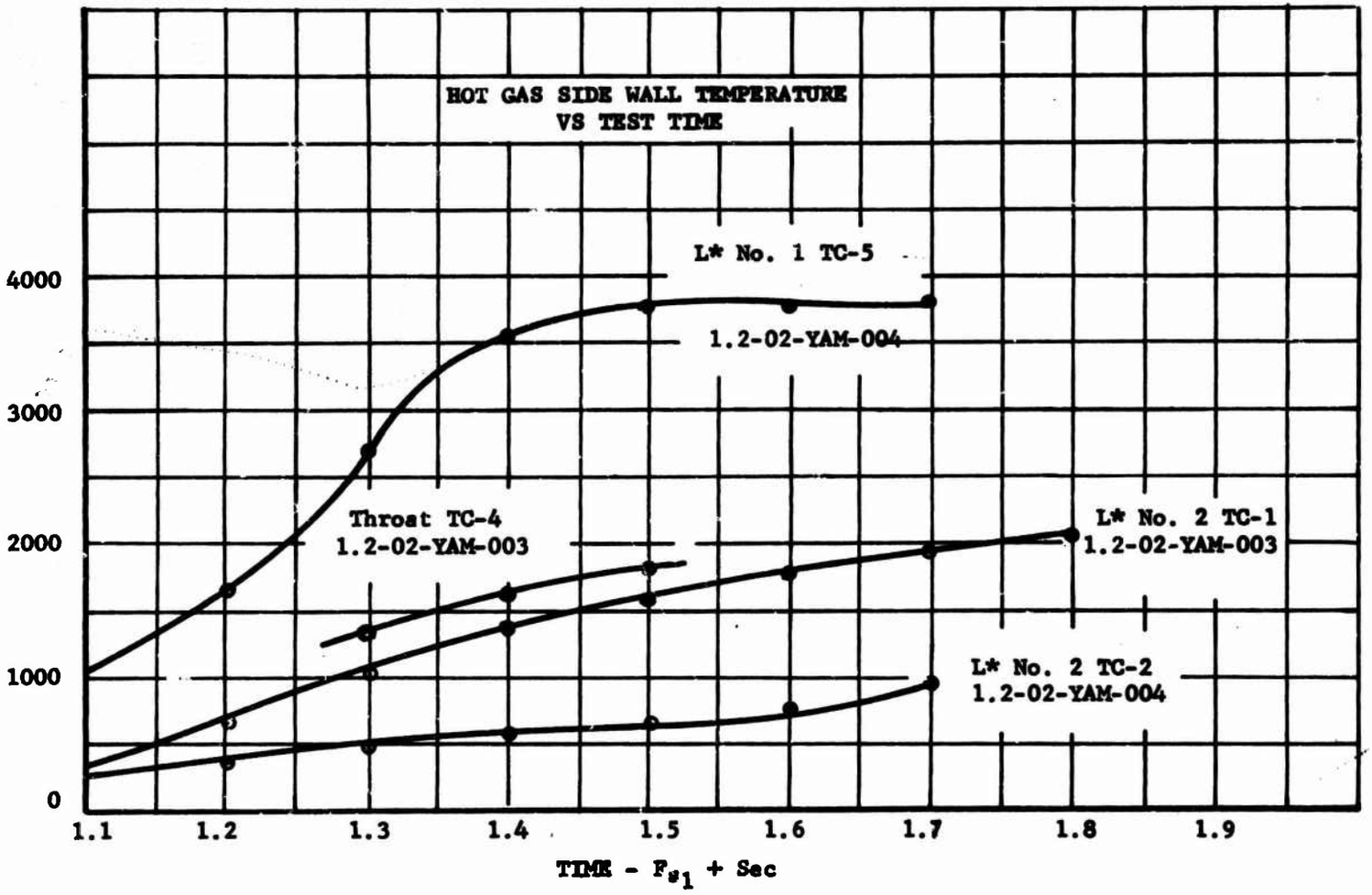

Figure V-C-4

Hot Gas-Side Wall Temperature vs Test Time

Book One

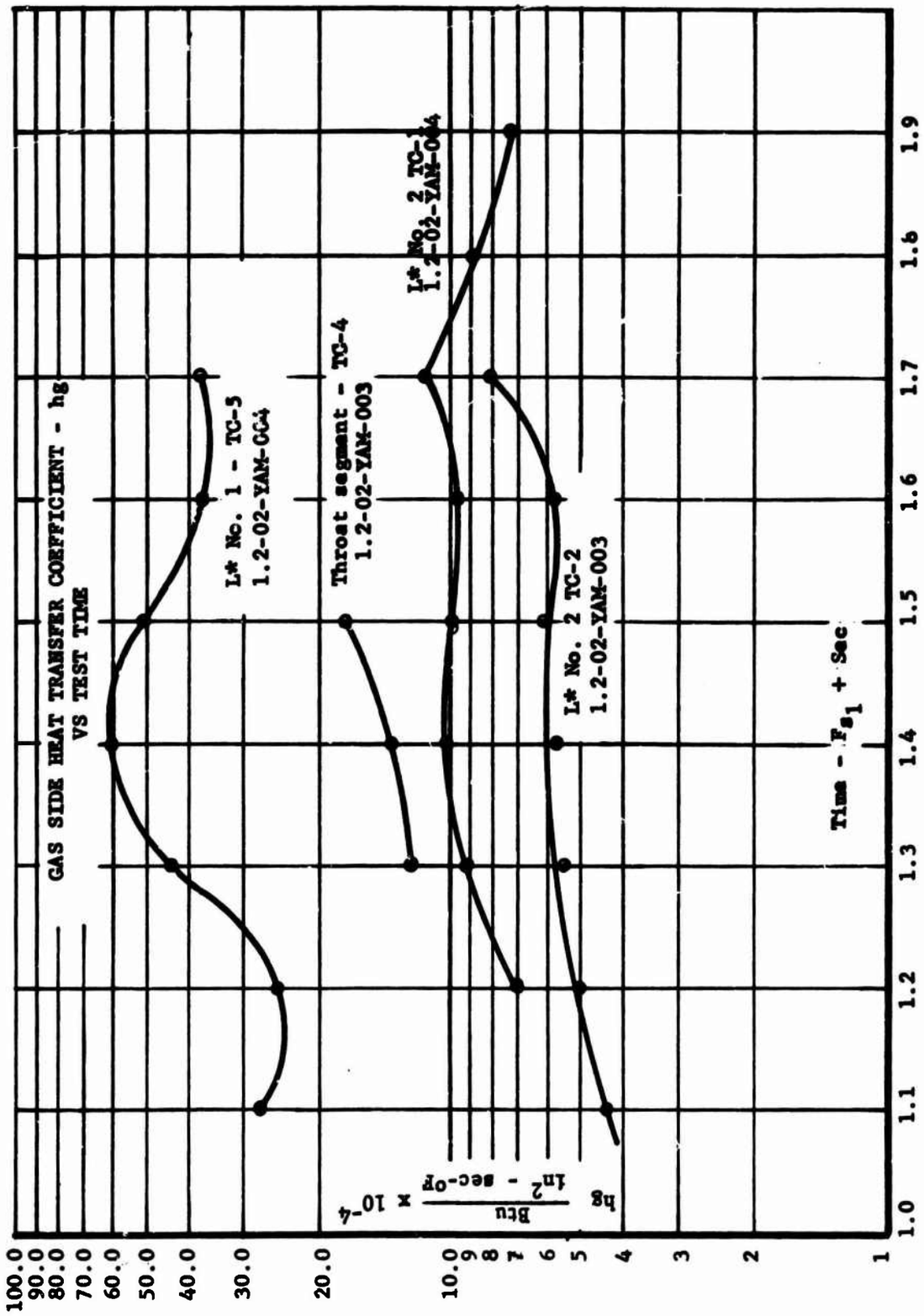

Gas-Side Heat-Transfer Coefficient vs Test Time

Figure V-C-5

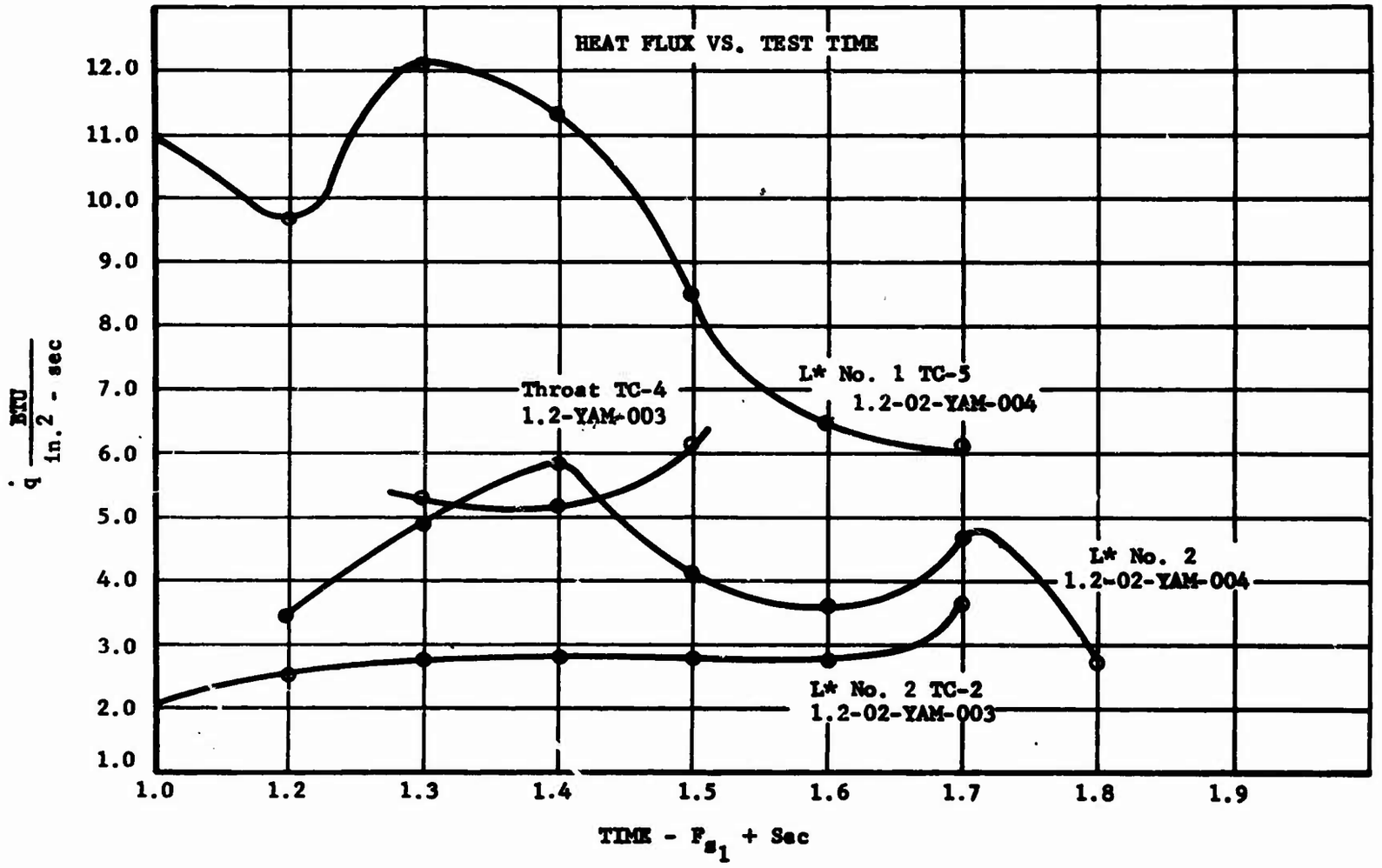

Heat Flux vs Test Time

Figure V-C-6

Book One

VI. UNCOOLED THRUST CHAMBER DESIGN AND DEVELOPMENT

VI. UNCOOLED THRUST CHAMBER DESIGN AND DEVELOPMENT

The basic objective of the Uncooled Chamber Program was to investigate the performance, heat transfer, and general operating characteristics of N_2O_4 and Aerozine 50 at a combustion pressure of 3000 psia. To achieve this objective, a 50,000-lb-thrust experimental thrust chamber of segmented design was designed, built, and tested.

The first task in the program was to define the operating specification, chamber contour, and basic materials of construction suitable for use in a high-pressure uncooled combustion chamber. This effort is discussed in Section VI,A, following. From this investigation, detailed components were designed and evaluated in the test program. These components included injectors, a chamber segment, a throat segment, and an exit nozzle segment. Design descriptions for each of the program components are discussed in Sections VI,B and C. Also included in these sections are discussions of the test results and design changes required in the development program for each of the components.

The thrust chamber performance obtained with the uncooled hardware is given in Section VIII, which is a combined discussion of all performance obtained in the program, including both uncocled and cooled hardware. Combustion stability data obtained has also been consolidated, and is given in Section IX.

VI, Uncooled Thrust Chamber Design and Development (cont.)

A. DESIGN CRITERIA

1. Operating Specifications

The nominal operating specifications to which the uncooled chamber was designed are as follows:

Thrust	50,000 lb at sea level
Chamber pressure	3000 psia
Mixture ratio	2.0
Combustion efficiency	0.97
Nozzle efficiency	0.97

From these values, the following design parameters were derived:

Oxidizer flow rate	114 lb/sec
Fuel flow rate	57 lb/sec
Throat area	9.92 $in.^2$

2. Chamber Contour

The selected chamber contour is shown in Figure VI-A-1. The values of the basic dimensions are given below:

Throat diameter	3.55 in.
Chamber diameter	9.0 in.
Convergent angle	15.0°
Contraction ratio	6.42
Chamber L*	Variable; 40 in., 70 in., 100 in., 130 in.
Exit diameter	7.47 in. (stub closure), 16.34 in. (exit cone)

VI, A, Design Criteria (cont.)

The chamber diameter of 9 in. was selected as the result of an investigation in which chamber diameters from 7 to 9 in. were evaluated. This investigation included the following elements: dependence of combustion chamber configuration upon contraction ratio; effect of L/D upon mode of instability; effect of length upon longitudinal mode; effect of diameter upon transverse modes; effect of nozzle upon stability; and effect of injection density. Studies of combustion stability which were used in the investigation are given in Ref 1 through 6. It was concluded that the relatively high contraction ratio (6.42) associated with the 9-in. chamber is not likely to produce instability problems, and may have a somewhat stabilizing effect. For a given convergence angle, a smaller diameter chamber would yield a shorter convergence section length, thereby reducing the area of that high heat-transfer region. The resultant increase of heat transfer coefficient in the chamber section, however, is felt to be a predominant consideration, thereby indicating the choice of the larger-diameter chamber.

The selection of the convergence angle was based upon stability and heat-transfer considerations. Theoretical studies, supported by test data, indicate that the incidence of longitudinal modes of instability are minimized when small convergence angles are used (Ref 1 through 6). Also, it was found in the Titan program that the use of large convergence angles increase the incidence of erosion above the throat. While the cause of the erosion is not fully understood, it is felt that the boundary layer is disturbed by the scrubbing effect of the gas flow, which increases with the turning angle.

Ref 1 Berman and Cheney, "Combustion Studies in Rocket Motors," Jet Propulsion, March 1953, Vol. 23, No. 3, pp. 89-93.
Ref 2 Crocco and Cheng, "High Frequency Instability in Rocket Motors," Jet Propulsion, October 1953, Vol. 23, No. 1, p. 301.
Ref 3 Crocco and Cheng, "Theory of Combustion Instability in Liquid Propellant Rocket Motors," AGARDOgraph, No. 8, Buttersworths London, 1956 (Princeton).
Ref 4 Crocco, Grey, and Harrje, "Theory of Liquid Propellant Rocket Combustion Instability and its Experimental Verification," ARS Journal, February 1960, Vol. 30, No. 2, pp. 159-168 (Princeton).
Ref 5 Zucrow and Osborn, "An Experimental Study of High Frequency Combustion Pressure Oscillations," Jet Propulsion, October 1958, Vol. 28, No. 10, (Purdue).
Ref 6 Priem and Morrell, "Application of Similarity Parameters for Correlating High Frequency Instability Behavior of Liquid Propellant Combustors," ARS Paper No. 1721-161, presented at Propellant, Combustion, and Liquid Rocket Conference, Palm Beach, Florida, April 1961, (NASA-Lewis).

VI, A, Design Criteria (cont.)

The chamber was designed so that the characteristic length (L*) could be varied to permit evaluation of the effect of L* upon combustion efficiency and to facilitate determination of the optimum L* at high pressures. The chamber lengths were adjusted by the addition of chamber inserts which were designed to change the characteristic length in multiples of 30 in.

The expansion nozzle was designed to meet the requirements of both the uncooled and cooled chamber programs. It extened to an overall area-ratio of 70:1, (used in part of the cooled chamber testing). For the uncooled chamber program and for part of the cooled chamber program, a truncated section of the nozzle was used, extending to an area ratio of approximately 21, which corresponds to an exit pressure of 14.7 psia. For injector evaluation, a very short stub closure was used, which terminates at an area ratio of 4.5.

3. Materials Investigation

Prior to completing the uncooled thrust chamber design activity, heat-transfer analyses were performed for various candidate materials of construction. Both metallic and nonmetallic materials were considered. The analyses were based on the predicted heat-transfer coefficients as shown in Figure VI-A-2 and VI-A-3. Metallic chamber materials were found to be unsatisfactory as chamber liners. Nonmetallic material analysis centered around various types of graphite. Ablative materials were considered as possible chamber liners, but were excluded from selection because the "gassing off" effect of the material was thought to seriously affect the thermal measurements that were to be made. Graphite materials therefore were selected for use as uncooled chamber liners. A complete discussion of the chamber heat transfer is given in Section V. Detailed discussions of metallic and nonmetallic chamber liner materials investigation are presented in the following subparagraphs.

VI, A, Design Criteria (cont.)

a. Metallic Chamber Liners

Six metallic chamber liner materials were studied: copper, aluminum, molybdenum, tungsten, cast iron, and chrome steel. A transient plot of temperature versus time was made for these materials, assuming an adiabatic outer wall and one-dimensional heat transfer. Figure VI-A-4 clearly illustrates failure of these materials before 5-sec duration. Conditions in the throat would be more severe, so no evaluation was made for that area.

Copper, the best of the metallics studied, was evaluted with a 0.005-in. coating of zirconium oxide. The transient plot, Figure VI-A-5 shows failure of the 1-in.-thick copper layer at the copper-zirconia interface at 1.5 sec.

b. Nonmetallic Chamber Liners

The principal nonmetallic material considered was graphite. It offers the advantages of high upper temperature limit (5000°F), good heat-sink capacity, good heat-transfer capabilities, and resistance to thermal shock.

Transient heat transfer calculations were made for ATJ-type material to determine the thickness of graphite necessary to obtain the required heat sink. The limiting assumptions were 5000°F graphite surface temperature and 1000°F inner pressure vessel wall temperature. Temperature profiles are shown in Figures VI-A-6 and VI-A-7 for the chamber and throat, respectively. It can be seen that ATJ material appeared satisfactory in the chamber but marginal at the throat. ZTA and pyrolytic graphite offered better erosion characteristics, but were higher in cost (10 times the cost of ATJ for pyrolytic material). In addition, the pyrolytic graphite offered a slightly increased heat-sink capacity.

VI, A, Design Criteria (cont.)

It was decided that the initial chambers would be fabricated with chamber and throat liners made of ATJ graphite. This was to continue until the injector development phase was over, at which time the throat was to be constructed of pyrolytic graphite. A transient plot for a pyrolytic throat is illustrated in Figure VI-A-8.

Graphite material was expected to react with water formed in the combustion products. Various coating materials were investigated for service as a protective boundary between the combustion gases and graphite chamber liner. These materials were tantalum carbide, silicon carbide, and zirconium oxide, and were to be tested as L* protective materials until a coating method was formulated. The carbides were deposited on graphite blocks by diffusion, and the zirconium oxide was plasma-sprayed.

Ablative materials were not considered initially because the hot-gas boundary layer would be disturbed by the ablation gases, which would make accurate measurements of the gas-side heat-transfer coefficients difficult. Development test experience obtained later in the program made it necessary to change from graphite materials to ablative materials. Actual materials used for chamber liner and throat construction are discussed in Section VI-C.

VI, Uncooled Thrust Chamber Design and Development (cont.)

B. INJECTOR DESIGN AND DEVELOPMENT

The basic objective of this portion of the uncooled chamber program was to design and develop a high-performance 50,000-lb-thrust-size injector to use N_2O_4 and AeroZINE 50 propellants and operate at a nominal chamber pressure of 3000 psia.

The general approach followed to meet this objective was: (1) consider all promising liquid-liquid injection techniques, (2) select three of the most promising injection techniques and complete designs through the engineering design layout stage, (3) select the two most promising designs, prepare detailed drawings, fabricate the injectors and retain the third design for possible backup use, (4) conduct development tests on the two selected injector designs in uncooled thrust chambers and evaluate injectors from standpoint of performance, stability, and erosion-free operation (variation of MR, P_c, L*, etc. is considered in evaluation of these designs), and (5) select the better of the two injector designs and use this design and its base-line performance figure for evaluation of chamber cooling techniques during the cooled chamber test program.

The three injectors that were initially designed were the pentad (Figure VI-B-1), the vortex (Figure VI-B-2), and the concentric-ring (Figure VI-B-3). These injectors conformed to the basic guidelines that were established early in the program between the Aerojet-General Corporation and the USAF Project Office. Basic guidelines included: (1) injector designs should include the large-thrust-per-element concept; (2) only flat-face injectors should be considered to minimize the heat-transfer area; (3) injectors should have the capability of replacing the orifice elements without major modification; and (4) injectors should have provisions for the incorporation of film cooling passages so that they can be used with only minor modification with the cooled thrust chamber program test hardware.

VI, B, Injector Design and Development (cont.)

The vortex injector and the concentric-ring injector were the designs that were selected for fabrication. The fabricated injectors are shown in Figures VI-B-4 and -5, respectively. The pentad injector design was retained for possible use as a backup design. The vortex injector, in addition to being a promising injector technique, offered the additional potential of providing chamber wall cooling. Experiments conducted at Thiokol Corporation indicated that vortex-type injectors provide cool boundary layers on the chamber wall.(1) Heat flux to the chamber wall in the area of the throat were reported to have been significantly reduced over that of conventional injectors that provide no supplemental film cooling to the wall.

The concentric-ring injector was selected on the basis of good test results obtained at Aerojet-General Corporation on the Unique Injector Concepts Program (Contract AF 04(611)-7410) where concentric-ring injectors (20,000-lb thrust) produced high performance.

All of the injector designs incorporated common features which made them interchangeable with one another, i.e., the vortex, pentad, and concentric-ring body design (that portion of the injector consisting of the injector pattern and internal housing) all fit into the same injector external housing design. This greatly simplified the TCA design, minimized installation problems on the test stand, and substantially reduced the total cost of fabrication and testing.

When development testing commenced, it was determined, after conducting several tests on each injector, that the vortex injector had a greater tendency toward producing erosion than did the concentric-ring injector. This was due to the failure of the ablative protective cap resulting from the severe vortex forces present in the chamber. From the limited test data obtained, however, the vortex injector achieved higher performance in 70-in. L* chambers than did the concentric-ring injector

(1) Vortex Combustion, Thiokol Chemical Corporation Report, Contract AF 04(611)-5682, April 1962.

VI, B, Injector Design and Development (cont.)

design, (95% of theoretical c* as compared with 84% of theoretical c*). Two modifications of the original vortex injector design were made to eliminate the ablative covers failure and the resulting erosion tendency of this design. With each attempt, protective covers continued to fail, the erosion problem remained, and no improvements in elimination or reduction of erosion were noted.

In conjunction with vortex injector modification and testing, concentric-ring injector modification and testing was taking place. With each refinement in the design of the concentric-ring injector, a noticeable improvement in the erosion problem occurred. Because of the high costs of continuing parallel development of the two injector designs and the extra time required for this parallel development effort, it was decided to suspend further design modification and testing of the vortex injector and concentrate all design and development effort on improving the concentric-ring injector.

At this same point in time, the overall injector development effort was reviewed and the impact of injector development on the entire program was studied. It was decided that while maximum effort should be expended on the continued design refinement of the concentric-ring injector, effort should be started on a backup injector in the event that the remaining development problems of the concentric-ring injector could not be resolved within allowable time periods. Several backup designs were studied including the previously designed pentad injector. A new injector concept, the transpiration-cooled injector (Figure VI-B-6) was selected as the backup design offering the most promise (experience on the Titan II-A Program with an injector of a very similar design gave high confidence in this injector concept). The transpiration-cooled injector was designed, fabricated, and held on standby while development testing of the concentric-ring injector continued. The fabricated injector is shown in Figure VI-B-7.

VI, B, Injector Design and Development (cont.)

Eight design modifications of the concentric-ring injector were required before a completely erosion-free design was produced. This satisfactory design was designated the Mod VIII concentric-ring injector. As soon as Mod VIII was established as a quality design and a valid base-line performance figure was available, the cooled chamber testing program commenced. All testing with cooled chamber components, other than the vortex chamber segment, was conducted using the Mod VIII concentric-ring injector.

Following the conclusion of the cooled chamber test program, the transpiration cooled injector was test-evaluated. This injector performed excellently. Absolutely no erosion of the injector resulted and very high performance was obtained (97% of theoretical c* based on one test sample).

In summarizing the results of the injector design and development activity conducted on this program, the following conclusions can be made.

1. Vortex injectors present severe gas recirculation forces and thermal problems in the combustion chamber and on the injector face. A transpiration-cooled vortex injector face might be the solution to compensate for the severe pressure forces and thermal conditions encountered with this design.

2. It could not be confirmed that vortex injectors reduce heat flux on the chamber wall (instrumentation techniques used were unsatisfactory to either validate or invalidate any claimed reduction in heat flux).

3. Additional development testing of vortex injectors is required before the full potential of this concept can be evaluated.

VI, B, Injector Design and Development (cont.)

4. Vortex injectors appear to give higher performance than concentric-ring injectors in chambers of the same L*.

5. Concentric-ring injectors require large L* in order to obtain high performance (L*s of 100 in. gave 95% of theoretical c* when injectors were face-cooled with 16% of total oxidizer flow).

6. Concentric-ring injectors produce chamber pressure oscillations of approximately 10% of P_c.

7. Porous-face cooling provides a satisfactory solution to injector face erosion.

8. Ablative materials are not satisfactory as an injector face protection device.

9. The transpiration-cooled injector design gives very high performance (97% of theoretical c* at 100 in. L*, based on a one test sample).

10. Combustion stability of the transpiration cooled injector is far superior to that of the concentric-ring or vortex injectors.

11. The transpiration-cooled injector operates relatively very cool and is free from erosion.

12. Any future thrust chamber work at high pressure using liquid-liquid N_2O_4/AeroZINE 50 propellants should strongly consider use of a transpiration-cooled injector design similar to the concept designed and development tested in this program.

VI, B, Injector Design and Development (cont.)

In the following subsections, each of the four injector designs is discussed. A design description is given for the pentad injector, whereas both design description and development testing experience are given for the vortex, concentric-ring, and transpiration-cooled injector designs.

1. Pentad Injector

The pentad injector design is shown in Figure VI-B-1. The pattern features four oxidizer orifices impinging on a central fuel orifice. Propellant mixing depends upon forced liquid impingement of large streams of propellant, and high performance is dependent upon maximum recirculation of combusting gases.

The pentad injector design was carried only to design layout stage. It was considered a backup injector only, and would be fabricated only in the event other injectors could not be developed. The eventual success of the concentric-ring injector eliminated the need for any further design activity for the pentad injector.

For a discussion of development testing conducted on a similar pentad injector design, reference is given to the final report of the Unique Injector Concepts Program, Aerojet-General Corporation, Contract AF 04(611)-7410.

2. Vortex Injector

The vortex injector was one of two injector designs initially selected for fabrication and development testing on this program. The original injector design is shown in Figure VI-B-2. In this concept the fuel is injected tangentially around the periphery of the injector at the chamber diameter. The oxidizer is introduced from the center portion of the injector and impinged radially onto the tangential fuel stream. The result is a vortexing mixture which moves in a spiral motion down the chamber.

VI, B, Injector Design and Development (cont.)

The vortex injector is unique in that it may provide thrust chamber wall cooling in addition to being the propellant injection mechanism. The vortexing gas stream is pressed against the thrust chamber wall by centrifugal force, and the cooler uncombusted elements, which are heavier than the combustion products, are freed to the outside, providing the cooling. The initial report of this method propellant injection and resulting cooling effect was presented by Thiokol Chemical Corporation. The cooling action is especially significant in the upper portion of the chamber, prior to complete combustion. Some cooling may also be provided in the throat region, since the remaining uncombusted products will still be to the outside, whereas in a conventional system they are homogeneously mixed throughout the gas stream.

Three tests were performed with the vortex injector. All tests were performed at 70-in. L*. Valid steady-state performance data was obtained in one test, in which 95% combustion efficiency was achieved.

The principal problem encountered with the vortex injector was in maintaining a protective cover over the center of the injector face. In all three tests conducted, the ablative protective cover was destroyed early in the firing, resulting in severe erosion of the oxidizer injection ring. The cover was redesigned following each test in an effort to prevent failure, but success was not achieved. The protective cover failures were not caused by erosion; the covers failed by mechanical shock. They appeared to be ripped from their position, indicating very great force is present in the center of the combustion chamber. Similar covers remained intact when tested with the concentric-ring injector.

VI, B, Injector Design and Development (cont.)

After development testing of the vortex injector was suspended, a design was prepared in which the center portion was replaced with a porous, transpiration-cooled section. No fabrication or testing of this design was conducted, however. The vortex injector with the porous cooled face is illustrated in Figure VI-B-5.

A complete tabular summary of the design features of all vortex injectors is presented in Figure IV-B-9. This figure also summarizes the performance data obtained on the vortex injector design. A cumulative summary of all development testing is presented in Figure II-A-2.

The following paragraphs discuss the detailed design features and the development testing experience obtained on each of the vortex injector configurations.

a. Vortex Injector (Original Design)

The original design vortex injector is shown in Figure VI-B-4. In this design oxidizer is fed through orificed cylindrical channels and is then ejected through a vertically slotted ring at a velocity of 109 ft/sec. This ring is capped by a thin stainless-steel cover plate, and the cover plate is protected by an ablative cap made from a molded phenolic resin, designated MX4566. The cap is secured to the cover plate with an epoxy resin.

The fuel is fed to a tangentially-slotted ring located on the periphery of the propellant premix chamber. Fuel injection velocity is 88 ft/sec. Two injector face pressure taps are located in the bottom of the propellant premix chamber.

VI, B, Injector Design and Development (cont.)

The injector was tested during Test 1.2-01-YAM-001. Posttest condition of this injector is shown in Figure VI-B-6. Severe erosion resulted across the injector face. Because of this erosion, a redesign of the oxidizer circuit was necessary.

b. Vortex Injector (Mod 1)

The Mod 1 design, shown in Figure VI-B-8, differed from the original design as follows: The volume of the premix chamber was reduced; the pure radial injection of the oxidizer was modified to have a radial velocity component in the same direction as the fuel; the resultant injection velocity of the oxidizer was increased (the radial component remained unchanged however); and the ablative face cover was mechanically attached to the injector face by metal fasteners.

In reducing the volume of the premix chamber, the oxidizer injection ring was increased in diameter and beveled at the surface of oxidizer ejection. A substantial reduction in cross-sectional area of the premix chamber resulted from this change. The oxidizer orifices were now positioned so that the oxidizer strikes the tangentially injected fuel stream headed in the same direction and at an impingement angle of 51°, compared to an impingement angle of 90° for the original design vortex injector. The velocity of fuel and oxidizer propellant injection was now 105 ft/sec and 121 ft/sec, respectfully, as compared to an injection velocity of 105 ft/sec for both propellants in the original design.

The original oxidizer circuit cover plate was replaced by a solid section of stainless steel, and protected by a 1-in.-thick ablative cap made from a molded phenolic commonly known as MX4566. This cap is held in place by six socket head machine screws and washers that are countersunk into the cap and protected by ablative plugs fabricated from an ablative material commonly known as Polytherm. The new ablative cover is shown in Figure VI-B-9.

VI, B, Injector Design and Development (cont.)

c. Vortex Injector (Mod II)

The Mod II design is shown in Figures VI-B-13 and VI-B-14. A summary of design changes from the Mod I design is as follows: The ablative protector cap covering the oxidizer circuit cover plate has been reinforced and more positively connected to the injector face. The injector premix cavity has been changed back to a rectangular configuration. The oxidizer propellant is injected through a vertically slotted ring, thus giving a true radial injection (same as the original design), and the extra metal stock below the oxidizer injection slot has been eliminated in order to prevent erosion as occurred in the original oxidizer injection-ring design.

The oxidizer center-plug ablative protective cap is now molded of MX4566, and contains a stainless-steel reinforcing plate that is internally threaded and screws into the oxidizer center plug as shown in Figure VI-B-14. The ablative protective cap is secured in place by the threads and by a bond of RTV-60 between the back side of the ablative cap and the oxidizer circuit metal cover plate.

Figure VI-B-14 shows that one of the injector face pressure taps remained in the center of the ablative face cap and the other pressure tap has been moved to the bottom of the injector premix chamber.

This injector was tested during Test 1.2-02-YAM-002. The posttest condition of the injector is shown in Figure VI-B-15 and Figure VI-B-16. Severe erosion occurred across the complete face of this injector even though steady-state operation had not been obtained. The test was prematurely shut down when a malfunction device sensed the injector failure.

VI, B, Injector Design and Development (cont.)

Further development of the vortex injector was terminated at the conclusion of the Mod II test. As previously noted, the basic reason for termination of the vortex injector development work was the severe erosion of the injector face. Other influencing factors included (1) the development effort required to solve this ablative cover failure problem and resulting erosion could further delay the completion of the uncooled chamber program and the initiation of cooled thrust chamber testing, and (2) the development of the concentric-ring injector which was being tested concurrently with the vortex injector program was experiencing considerably less erosion problems, and it was strongly believed that the erosion problem encountered with the concentric-ring injector would be resolved with continued injector design refinement.

The following section discusses the design and development of the concentric-ring injectors.

3. Concentric-Ring Injector

The concentric-ring injector was one of the two injector designs initially selected for fabrication and development testing for this program. The original design concentric-ring injector is shown in Figure VI-B-3. The basic concentric-ring injector pattern consists of a single slotted annular triplet element, composed of inner and outer oxidizer streams impinging on an axially directed annular fuel stream. The included angle between the intersecting streams of oxidizer is 90°. This basic injection pattern remained essentially unchanged throughout the development test program; however, minor modifications to the injection element design were made.

VI, B, Injector Design and Development (cont.)

During the testing program, two basic design problems were manifested and resolved: (1) erosion of the element and (2) erosion of the injector face. Ten modifications to the original injector design were required (Mod I through Mod VIII and Mod VIII-A and B) before a completely satisfactory injector design was produced that had no erosion tendencies. Specific problems and solutions are briefly summarized below.

The slotted oxidizer element design used on the inner and outer ring on the original and Mod I injector design proved to be unsatisfactory. In all tests conducted with this type of oxidizer slot configuration, local erosion surrounding the slots was present. This was corrected by changing to complete annuli for the oxidizer injection rings. A typical example of the new oxidizer ring configuration is shown in Figure VI-B-17.

The graphite pieces used to protect the injector face on the original injector design cracked and were destroyed during the firing. On design modifications I, II and III the graphite face protecting device was replaced by an ablative-type face-protecting device. Ablative materials also proved unsatisfactory in protecting the injector face. The erosion of the ablative material indicates a very severe recirculation pattern exists at the outer periphery of the injector. The problem was resolved by transpiration-cooling the injector face with N_2O_4. "Rigimesh", a porous material made from compacted screen wire, was used as the face material. A typical example of a concentric-ring injector design using transpiration face cooling is shown in Figure VI-B-17.

The fuel injection ring configuration eroded during some tests. This problem was corrected by changing the fuel ring configuration so that the element was film cooled by N_2O_4. Figure VI-B-17 also illustrates this feature.

VI, B, Injector Design and Development (cont.)

Of all the uncooled tests conducted with the concentric-ring injector, only one was conducted at less than 100-in. L*. Performance values for uncooled chambers using concentric-ring injectors at 100-in. L* yielded theoretical c* in the range 91 to 98%. A discussion of the performance obtained with the concentric-ring injector is given in Section VIII, below. This definitely indicates that for concentric-ring injectors of the type used with a storable liquid-liquid propellant system at high pressures, very low L* would be unsatisfactory.

A complete tabular summary of design features of all concentric-ring injectors designed and tested on this program is presented in Figure VI-B-18. Figure VI-B-18 also summarizes the performance data obtained from each injector design. A cumulative summary of all development testing is presented in Figure II-A-2.

The following paragraphs discuss the detailed design features and the development testing experience obtained from each of the injector configurations.

a. Concentric-Ring Injector (Original Design)

The original concentric-ring injector design is shown in Figure VI-B-5. In this injector configuration the oxidizer rings consist of a series of eloxed slots rather than a continuous slot. The ribs between slots were designed to help resist thermal distortion and resulting changes in slot width when subjected to the severe thermal conditions encountered during firing. The fuel ring, however, is a continuous slot, and is located midway between and concentric with the two oxidizer rings.

The central portion of the injector face plate and the extreme outer edge are protected by a layer of MX5700 insulation covered by ATJ graphite. The MX5700 insulation is bonded to the injector face while the graphite is mechanically attached by countersunk machine screws that are protected by graphite plugs as shown in Figure VI-B-5.

VI, B, Injector Design and Development (cont.)

Two pressure taps are located in the center of the injector (Figure VI-B-5). Pressure taps are also located in the injector fuel and oxidizer propellant inlet lines.

This injector was tested during Test 1.2-01-YAM-005. The posttest condition of the original design concentric-ring injector is shown in Figure VI-B-19. It is noted that the graphite protecting the center of the injector face was completely destroyed. The graphite protecting the outer edge of the injector face was eroded, cracked, and not capable of being refired. As a result of this graphite failure and the severity of erosion over the face of the injector protected by the graphite, it was concluded that the injector face protective device would have to be redesigned. It was decided to replace the graphite by an ablative center cap and an ablative circumferential ring. It was also concluded that the basic concept of propellant injection and impingement was satisfactory and would remain unchanged.

b. Concentric-Ring Injector (Mod I)

The Mod I design, shown in Figure VI-B-20, is identical to the original design, with the exception that an ablative cap is now mechanically attached to the center face portion of the injector (replacing the formerly used graphite disc), and an ablative ring replaces the segmented graphite ring located circumferentially and adjoining the outer oxidizer ring.

The ablative center cap and outer oxidizer circuit protective ring was molded phenolic material designated MX4566, which is mechanically held to the injector face by countersunk machine screws that are protected by Polytherm material.

VI, B, Injector Design and Development (cont.)

The Mod I design was tested during Test 1.2-01-YAM-008. The posttest condition of this injector is shown in Figure VI-B-21. It is noted that although rated steady-state operation of this injector was obtained, severe erosion occurred over the injector center ablative cap, and the outer ablative injector face protective ring failed mechanically over approximately 180° of its circumference. Also, all the support ribs located on the inner oxidizer orifice slots cracked.

After a thorough examination of the test hardware, and expecially after examining the severity of the injector face erosion, it was concluded that a redesign of the oxidizer circuit and a better method of protecting the injector face were required.

c. Concentric-Ring Injector (Mod II)

The Mod II design, shown in Figures VI-B-22 and -23, represents a major redesign and rework of the Mod I design. The basic method of injecting the fuel and oxidizer propellants and their respective flow rates and velocities remain unchanged. The redesign of this injector included the removal of the slotted inner and outer oxidizer rings and replacing these rings with complete concentric annuli whose slot width can be changed externally by the addition or removal of shims as shown in Figure VI-B-23. The center of the injector body has been bored and threaded to receive a screw in type inner oxidizer ring, and the injector body has been machined to receive a new outer oxidizer ring and ring retainer. Also, the injector ablative center cap contains a stainless-steel reinforcing plate around which ablative material is molded. This assembly screws into the injector oxidizer center plug and commercial product RTV-60 provides a bond between the back side of the ablative cap and the metal injector face.

VI, B, Injector Design and Development (cont.)

The injector face pressure taps have been removed from the center of the injector and relocated within the outer oxidizer ring. Also, a thermal barrier coating of zirconium oxide, 0.020 in. thick, is applied to the entire injector face to prevent injector face erosion.

The injector outer oxidizer ring is protected by an ablative cover which protrudes toward the center of the injector. This protective device is an integral part of the chamber L* ablative liner (Figure VI-B-23).

This injector was tested during Test 1.2-02-YAM-001. Rated steady-state operation was obtained during this injector test. Figure VI-B-24 shows the posttest condition of this injector. Minor erosion occurred on the inner oxidizer ring and ablative face cover, and extensive erosion occurred on the outer oxidizer ring. This extensive erosion of the outer oxidizer ring is the result of the failure of the outer oxidizer ring ablative face cover (an integral part of the ablative L* segment). Additionally, as a result of this localized ablative chamber liner failure, innerchannel burning in the outer oxidizer ring manifold occurred during this test. This was due to either hot-gas leakage into the oxidizer circuit through the pressure tap holes or inner-channel leakage from the fuel circuit. It was noted that the primary erosion pattern of previous concentric-ring injector designs was localized around the outer edge of the inner and outer oxidizer ring, and this erosion pattern was attributed to the ribs on each oxidizer slot. On this design with the ribs removed, no such erosion was present and, therefore, it was concluded that this problem was resolved.

In order to render the concentric-ring injector satisfactory for extended duration and multiple testing, two problems had to be resolved: (1) innerchannel fuel leakage or hot-gas leakage in the outer oxidizer ring manifold, and (2) the failure of ablative covers on the injector center cap and outer oxidizer ring. The Mod III design attempted to eliminate these problems.

VI, B, Injector Design and Development (cont.)

d. Concentric-Ring Injector (Mod III)

The Mod III design is shown in Figure VI-B-25. The Mod III design incorporated an ablative center cap that is integrally molded to a metal reinforcing ring that screws into the center oxidizer ring and is flush with the inner oxidizer ring. The outer oxidizer ring is protected by an ablative material known as MX4566 that is integrally molded to the ring. The outer oxidizer ring is attached to the injector body by 24 internal wrenching machine screws.

An O-ring seal is used to seal the joint between the outer oxidizer ring and the injector body. Also the two injector face pressure taps have been removed from the injector body.

This injector was tested during Test 1.2-02-YAM-003. The posttest condition of this injector is shown in Figure VI-B-26. Severe injector damage was sustained during this test. The inner oxidizer ring ablative protective cover was completely intact, but not in a refirable condition. The outer oxidizer-ring ablative-face protective cover experienced severe erosion over a 270° section. Also, wherever this ablative material was severely eroded, metal erosion occurred on the surface of the outer oxidizer ring.

It was apparent from the results of this test that the basic problems of injector face erosion had not been resolved. Therefore, a new concentric-ring injector concept incorporating an injector face cooling technique was designed, fabricated and designated the Mod IV design.

e. Concentric-Ring Injector (Mod IV)

The Mod IV design is shown in Figure VI-B-27. The basic method of injecting the fuel and oxidizer propellants remain unchanged except a new face cooling technique has been employed. Four percent of the total injector liquid

VI, B, Injector Design and Development (cont.)

oxidizer flow is transpired through the porous (Rigimesh) face of the inner and outer oxidizer injection rings.

The center and outer oxidizer rings have been redesigned to permit liquid oxidizer to flow behind the Rigimesh face. This Rigimesh face is attached to the center oxidizer ring by a continuous weld around the periphery of the ring and by 12 countersunk screws spaced uniformly about the Rigimesh face. The outer oxidizer ring Rigimesh face is attached by a continuous weld on its inner and outer diameter surface. The slot width of both the inner and outer oxidizer rings is controlled by shims between these rings and the injector body.

The cavity surrounding the fuel injection slot is protected by a thermal-barrier coating (zirconium oxide) approximately 0.020-in. thick.

This injector was tested during Test 1.2-02-YAM-004. Figure VI-B-28 shows that minor erosion occurred on the inner oxidizer ring Rigimesh face, and extensive erosion occurred on the face of the outer oxidizer ring. Also, the weld securing the outer edge of the oxidizer-ring Rigimesh face failed over an approximate 90° sector. The fuel injection ring incurred severe erosion; the characteristics of this erosion were identical to those of the fuel-ring erosion that occurred on the Mod III injector. It was concluded that the most probable cause of this fuel-ring erosion was due to a new hot-gas recirculation pattern set up by the Mod IV pattern design.

After a thorough examination of the injector face erosion pattern, it was concluded that an insufficient amount of oxidizer propellant was used to cool the porous injector face. Therefore, the Mod V design injector was revised to increase the percentage of total oxidizer flow for face cooling.

VI, B, Injector Design and Development (cont.)

f. Concentric-Ring Injector (Mod V)

The Mod V design is shown in Figures VI-B-29 and -30. This is also a Rigimesh face-cooled injector design, and is very similar to the Mod IV design. The principal differences are: (1) The quantity of oxidizer face cooling has been increased by a factor of 4 (from slightly less than 4% to slightly more than 16% of the total oxidizer weight flow to the injector). (2) The fuel injection ring configuration has been extended beyond the face of the injector as shown in Figure VI-B-30. This permits the injected oxidizer to film-cool the fuel ring and possibly eliminate a hot-gas recirculation path.

The outer oxidizer ring Rigimesh face is secured to the ring body by countersunk stainless-steel screws and a continuous weld on the inner and outer edge of this ring. The center oxidizer "screws in" ring is retained within the injector body by a nonmetallic tapered jam key. All the countersunk screws used to secure the Rigimesh to the injector face are tack-welded to the Rigimesh to prevent the possibility of its coming loose during testing.

No thermal barrier coating was applied to the injection area of the fuel or oxidizer injection ring of the Mod V design. The oxidizer-injection slot widths have been decreased in order to maintain the same momentum ratio and to adjust for the reduced flow through the main oxidizer injection slots as a result of the increased oxidizer used for Rigimesh face cooling.

Also installed on the fuel and oxidizer inlet side of the injector manifold are Kistler 701 high-frequency transducers.

This injector was tested during Test 1.2-02-YAM-006, and steady-state pressure operation was obtained.

VI, B, Injector Design and Development (cont.)

Figure VI-B-31 shows the posttest condition of this injector. The only damage sustained by the injector occurred on the outer oxidizer ring. The erosion was probably due to the lack of a sufficient quantity of oxidizer coolant sweeping over the outer weld on the oxidizer ting, thus causing hot gases to recirculate over this outer weld and eroding this weld area.

By increasing the flow rate of liquid oxidizer coolant through the Rigimesh injector face from 4 lb/sec in the Mod IV design to 16 lb/sec for the Mod V design, all injector face erosion was eliminated. Also, no erosion or discoloration occurred on the fuel injection ring. It was concluded that by extending the fuel injection ring beyond the injector face film cooling the fuel ring and eliminating a possible path for hot gas recirculation, the fuel-ring erosion problem was resolved.

The method of locking the inner oxidizer ring with a non-metallic jam key proved to be inadequate and the inner oxidizer ring loosened during this test.

The Mod VI injector design attempted to resolve the outer oxidizer ring weld erosion problem and provide positive locking for the inner oxidizer ring.

g. Concentric-Ring Injector (Mod VI)

The Mod VI design is shown in Figure VI-B-32. The basic changes in the Mod VI design as compared with the Mod V concentric-ring injector design include the following: The weld securing the Rigimesh to the outer oxidizer

ring was changed to an intermittent weld, thus allowing oxidizer coolant to flow over and cool the intermittent welds and the adjacent area. The intermittent welds were used to minimize the deflection of the Rigimesh face between the countersunk face support screws. The number of countersunk stainless-steel screws used to support the outer oxidizer ring Rigimesh face was increased from 16 to 32.

The oxidizer coolant flow that transpires through the outer Rigimesh ring was increased by approximately 3 lb/sec. This increase in coolant flow necessitated the reduction of the slot width of the outer oxidizer ring from 0.034 to 0.032 in. in order to retain the same propellant injection velocity.

The locking device for the "screw in" inner oxidizer ring was changed to a soft aluminum wedge that is jammed into a locking position.

The Mod VI design was tested during Test 1.2-02-YAM-007, and steady-state operation was obtained. The posttest condition of this injector is shown in Figure VI-B-33. The only damage sustained by this injector occurred on the outer oxidizer ring in the area of the intermittent welds and on the bolt circle that secures the outer oxidizer ring to the injector body. The erosion occurred over two separate areas spaced approximately 180° apart. Outer oxidizer-ring erosion was attributed to severe hot-gas recirculation patterns (radial openings occurred between the Rigimesh and the outer oxidizer ring, causing oxidizer to spray out of the openings and onto the hot interface surface adjacent to the ablative chamber and injector face.

The inner oxidizer ring was found to be loose, indicating the locking device had not given positive locking.

VI, B, Injector Design and Development (cont.)

h. Concentric-Ring Injector (Mod VII)

The Mod VII design is shown in Figure VI-B-34. The basic external change is in the outer oxidizer ring. The design of the outer oxidizer Rigimesh ring is oriented 45° with respect to the normal injector face in an attempt to minimize the recirculation of the combustion gases and eliminate erosion tendencies in the outer edge of this outer oxidizer ring.

Approximately 50% more oxidizer is transpired through the outer Rigimesh ring as compared with the Mod VI design.

The inner oxidizer ring plug is welded to the injector body on the back side, therefore eliminating the wedge-lock method of securing this plug within the injector body.

Two tests were conducted with the Mod VII design. The first test of 0.3 sec steady-state pressure operation was a completely satisfactory test. No erosion was present. To confirm that the erosion problem had been eliminated, a second test was conducted with the same test hardware at an extended duration of approximately 1.0 sec steady-state chamber pressure. Erosion of the outer oxidizer ring occurred on this test.

The posttest condition of this injector is shown on Figure VI-B-35. Erosion occurred over a 48° sector of the outer oxidizer ring Rigimesh retaining section. It was noted that the ablative chamber liner failed in the identical area in which erosion occurred on the outer oxidizer ring. It was concluded that injector failure was preempted by the ablative chamber liner failure, which in turn permitted a severe hot-gas recirculation pattern around the edge of the outer oxidizer ring and caused erosion of the ring.

VI, B, Injector Design and Development (cont.)

Fabrication of a Mod VIII design was nearing completion, and was the next design tested. It was planned to continue work on the Mod VII design if the Mod VIII did not prove satisfactory.

i. Concentric-Ring Injector (Mod VIII)

The Mod VIII design is shown in Figure VI-B-36. This design retains the flat face outer oxidizer ring (similar to the Mod VI design) but has 120 small-diameter (0.025 in.) holes located around the periphery of the ring to provide a uniform sheet of coolant to the thrust chamber wall. The film coolant ejected from the outer oxidizer ring impinges on a stainless-steel ring that acts as a splash plate and is located at the upper edge of the ablative L* chamber liner as shown in Figure VI-B-37. This design directs liquid oxidizer film coolant to an area where erosion has been a continuing problem on the past several injector designs.

The inner oxidizer ring and the fuel ring design remained unchanged, and are identical to the Mod VII design. The outer Rigimesh ring is attached to the outer oxidizer ring by intermittent welds on both inner and outer edges and by 32 countersunk screws.

The total oxidizer flow rate through the outer oxidizer ring for the Mod VIII design is approximately 17.5 lb/sec, (5.5 lb/sec less than the total oxidizer flow rate through the outer oxidizer ring for the Mod VII design).

A 0.4 sec steady-state pressure duration test was conducted on this design. The posttest condition of the Mod VIII design is shown in Figure VI-B-38. No injector erosion was experienced during this test. The only problem with this injector was the mechanical failure of the weld securing

VI, B, Injector Design and Development (cont.)

the inner oxidizer ring Rigimesh. This weld failed over its entire length, and it was concluded that insufficient weld penetration of the Rigimesh was the cause of this failure. Also 90% of the tack welds securing countersunk screws on the Rigimesh face cracked.

The minor injector structural problems remaining on the Mod VIII concentric-ring injector were to be resolved on the Mod VIII-A design.

j. Concentric-Ring Injector (Mod VIII-A)

The Mod VIII-A design (Figure VI-B-39) is a minor rework of the original Mod VIII design. The inner oxidizer ring Rigimesh face was removed and new Rigimesh face was installed and mechanically attached to the center oxidizer ring by 28 countersunk stainless-steel screws. This center oxidizer ring Rigimesh face could not be reattached by welding because it would distort the oxidizer slot width and give a nonuniform propellant distribution. The countersunk screws securing this Rigimesh face are double-tack-welded to prevent loosening.

The rework of the outer oxidizer ring included the following: Each of the Rigimesh face attachment screws is welded in place from the back side of the outer oxidizer ring, therefore eliminating the tack welds previously used on the head of these screws. Also, a multipass intermittent groove weld is used at 32 attachment points to secure the Rigimesh to the outer oxidizer ring.

This injector was tested during three tests: Tests 1.2-03-YAM-012, -014, and -015. This injector remained in a "like new" condition with no cracks, erosion, or severe discoloration evident upon completion of the first two tests. On the third test, minor injector damage was sustained, as shown in Figure VI-B-40. The center oxidizer ring Rigimesh face became partially detached from the

VI, B, Injector Design and Development (cont.)

injector face, and 27 of its 28 mounting screws were broken. A close examination of the center plug revealed peening marks on the center plug Rigimesh face seating surface. Because of these marks and the fact that some of the failed screws did not "neck down" as in a typical tensile type of failure, it was concluded that the Rigimesh face vibrations caused fatigue failure of several of the screws and the increased load on the remaining screws caused total failure of the Rigimesh face.

To eliminate the remaining mechanical problems encountered with the Mod VIII-A design, a minor redesign of the inner and outer oxidizer rings was incorporated and designated the Mod VIII-B design.

k. Concentric Ring Injector (Mod VIII-B)

The Mod VIII-B design is shown in Figure VI-B-41. This design differs from the Mod VIII-A design only in mechanical improvements that have been incorporated into a new inner and outer oxidizer ring.

The outer oxidizer ring has also undergone several minor mechanical changes. The diameters of the inner and outer countersunk screw circle have been changed to improve the mechanical support of the Rigimesh face. All flat-head countersunk screws are backed up with bushings, and are welded in place from the back side of the outer oxidizer ring. A continuous multipass weld is used to secure the inner diameter surface of the Rigimesh ring to the parent material. The outer diameter surface of this Rigimesh ring is retained by intermittent multi-pass welds. The film cooling holes and the method of lockwiring the outer oxidizer ring retaining bolts are identical to those of the Mod VIII-A design.

Inspection of the Mod VIII-B injector after its first test indicated the injector was completely free of erosion and no structural failures were present. With each succeeding test conducted, erosion-free operation and absence

VI, B, Injector Design and Development (cont.)

of structural problems were noted. Concentric-ring injector development had been completed. The cooled chamber testing program would now commence and cooling techniques could be evaluated. In the course of conducting the cooled chamber program, the Mod VIII-B design was tested on Tests 1.2-02-YAM-021 through -036.

The posttest condition of this injector upon conclusion of the above test series is shown in Figure VI-B-42. The Mod VIII-B injector was subjected to a total of 12 full-duration tests and for a total cumulative test duration of 36.7 sec. At the completion of this test series, it was concluded that the Mod VIII-B design was in excellent condition and capable of additional testing.

A complete set of detailed fabrication drawings of the Mod VIII-B injector design are presented in Figure VI-B-43.

4. Transpiration-Cooled Injector

a. Design, Fabrication, and Testing

The transpiration-cooled injector was fabricated as a backup assembly for the concentric-ring injector. It was planned to replace the concentric ring with the transpiration-cooled injector in the event that the continuing erosion problems on the concentric-ring injector could not be resolved. As noted in the previous section, with continued design refinement, the erosion problems on the concentric-ring injectors were eliminated.

An uncooled thrust chamber containing the transpiration-cooled injector was fabricated and held as a standby unit during the uncooled and cooled chamber test program. At the conclusion of the cooled chamber test program, remaining funds permitted the testing of the transpiration-cooled injector design.

VI, B, Injector Design and Development (cont.)

The transpiration-cooled injector incorporates 84 evenly spaced fuel spray nozzles in a flat porous (Rigimesh) injector face. All fuel is passed through these 84 spray nozzles. All of the oxidizer passes through the Rigimesh face and mixes with the fuel spray without any discrete impingement pattern. The injector hydraulic schematic is shown in Figure VI-B-46. A photograph of the completed injector is shown in Figure VI-B-7.

The injector was designed for a fuel flow rate of 57 lb/sec, or 0.679 lb/sec per spray nozzle. At this flow rate the fuel circuit design pressure drop is 188 psia. Figure VI-B-44 illustrates a water flow test of one of these spray nozzles at the equivalent fuel design flow rate. The water (or fuel) is atomized into a fine spray, and therefore provides a large total surface area for excellent mixing with the oxidizer. Figure VI-B-45 illustrates a water flow test of the entire fuel circuit at the equivalent fuel design flow rate. Note the excellent distribution of the fuel spray.

A total flow rate of 114 lb/sec of oxidizer passes through the Rigimesh face. At this flow rate the oxidizer circuit design pressure drop is 222 psia. The porosity of the injector face is uniform, and thus provides a uniform oxidizer injection density of 2.0 lb/sec/in.^{2}. Figure VI-B-46 illustrates a water flow test of the oxidizer circuit at the equivalent oxidizer design flow rate. Both fuel and oxidizer circuits are shown flowing simultaneously in Figure VI-B-47.

The uniform and fine distribution of the fuel and the complete and uniform distribution of the oxidizer across the injector face were planned to provide an injector with a wide area of propellant mixing and a resultant maximum energy release. It was known from injector design and development experience on other programs that a wide area of maximum energy release produces stable combustion. In addition, by passing oxidizer through the porous injector face, complete face cooling was assured.

VI, B, Injector Design and Development (cont.)

The basic transpiration-cooled injector design concept was patterned after an injector design used on the Aerojet-General Titan II-A Program, Contract AF 04(696)-212. The Titan II-A design used N_2O_4 and Alumizine as propellants. The Alumizine was ejected through showerhead orifices, whereas the oxidizer transpired through the porous face. The Titan II-A injector consistently gave high performance and was erosion-free. Good combustion dynamics was also a feature of this injector. One problem encountered with the injector, however, was the tendency for the porous injector face to plug with small foreign particles (10 to 50 microns and larger), resulting in variable hydraulic resistance of the oxidizer circuit. This, in turn, caused difficulty in controlling the desired injector mixture ratio. With the design of the High Chamber Pressure Program transpiration-cooled injector, where a greater porosity injector face was used (approximately 2.5 more porous than the Titan II-A injector design), it was believed that with mild precaution for cleanliness and the use of filtered water and propellants, plugging of the porous face would not present a problem. With the limited hydraulics testing and engine testing subsequently conducted on this injector, no plugging of the porous material was detected.

With high confidence in this new injector from a performance, stability and erosion-free operation standpoint, two test firings were conducted, Tests 1.2-02-YAM-037 and -038. Both tests provided excellent injector evaluation data. The first test of this injector, Test 1.2-02-YAM-037, 2.58-sec duration, was valid. There was no injector face erosion as can be seen by Figure VI-B-48, a posttest photograph of the injector. Although this test gave an indication of performance and stability characteristics of this injector, it failed to give truly accurate and reliable data because the ablative throat insert failed early in the test, and, consequently, no uniform chamber contour or chamber throat area was present during the steady-state portion of the test. Steady-state chamber pressure during this test was 2458 psia. After repairing the chamber and reassembling the TCA, the second injector evaluation test was conducted, Test 1.2-02-YAM-038. This test,

VI, B, Injector Design and Development (cont.)

2.10-sec duration at a steady-state chamber pressure of 3040 psia, yielded valid and complete test data. High combustion efficiency as evidenced by a characteristic exhaust velocity of 97.0% of the theoretical value was obtained. (In order to confirm the validity of the high-performance data obtained on this test, two special examinations were made. A check was made to verify the propellant flow rate to the injector. To confirm these flow rate values, orifices in the pump discharge lines were flow-calibrated with water in the hydraulics laboratory after completion of the test. These flow calibrations confirmed the flow rates data previously obtained by using known injector flow calibration values (K_w). Secondly, the throat diameter and chamber pressure were rechecked and reconfirmed.) Excellent combustion stability was apparent from the high-frequency transducer data. Mild pressure oscillations (amplitudes less than 2% of chamber pressure and random frequencies, probably background amplifier noise) were present. Figure IX-D-1 illustrates a typical portion of the combustion stability records obtained from this test. Absolutely no erosion was present on the injector after this test. Detail performance data on this injector is presented in Figure II-A-2. Detail information on the injector and design features are presented in Figure VI-B-49. Fabrication drawings are presented in Figure VI-B-50.

b. Conclusions and Recommendations

From the results of the two tests conducted on this injector, several conclusions can be made: (1) the injector operates very cool and is erosion free, (2) high combustion performance, indicated by characteristic exhaust velocity, c*, is inherent in this injector design (c* = 97.0% of theoretical at 100 in. L*, based on a one test sample), (3) combustion stability is superior to that of the concentric-ring and vortex injectors (chamber pressure oscillation, peak to peak were less than 2% of chamber pressure, and frequencies were random).

VI, B, Injector Design and Development (cont.)

The transpiration-cooled injector concept offers real promise as an optimized high chamber pressure injector for storable liquid-liquid propellants. It is strongly recommended that any future injector development work at high pressure and with liquid-liquid propellants give serious consideration to the use of the transpiration-cooled injector concept designed and development-tested on this program.

VI, Uncooled Thrust Chamber Design and Development (cont.)

C. UNCOOLED COMBUSTION CHAMBERS

1. Introduction and Summary

The basic purpose for the uncooled combustion chamber, designed and development-tested in this program, was to provide a device with which injectors could be test-fired, evaluated, developed, and from which base-line thrust chamber performance data could be obtained for cooled chamber testing. A second purpose was to provide a device for experimentally determining gas-side heat-transfer coefficients.

To accomplish these purposes most effectively, a segmented chamber design was selected. It is composed of a cylindrical L* segment, a convergent and throat segment, and an exit nozzle segment. These segments are removable from one another. Each segment is composed of a steel pressure vessel and a chamber liner. Figure VI-B-37 illustrates a typical thrust chamber assembly buildup using an injector, two L* segments, a convergent and throat segment, and an exit nozzle segment. Figure VI-C-1 shows the uncooled chamber with the ablative end-cover assembly instead of the exit nozzle. As can be seen from these figures, most design features are common among the several components. Bolt circles are common, attachment of steel shells is accomplished by using high-strength studs and nuts; seals are the conical seal type (Conoseals), and are used at each interface. Heavy-wall construction is used because these components are all designed for "workhorse" test conditions.

There was an alternative design for the exit-cone segment. A metal end-plate with an ablative end-stub closure was often used in place of the exit-cone segment. Chamber liners are retained within the steel pressure vessels by the end plate or the exit cone. These components are of smaller inside diameter than the L* segments and convergent and throat segments, and provide a locking effect on the chamber liners when assembled in a complete thrust chamber assembly.

VI, C, Uncooled Combustion Chambers (cont.)

The segmented chamber design permits simple removal of injector assemblies, easy replacement of chamber liner materials, L* variation capability, and maximum utilization of test hardware. Numerous fabrication and assembly benefits were also features of this segmented construction concept. Attachment of instrumentation probes to bosses machined in the steel pressure vessels of each segment permitted the gathering of heat-transfer data. (Uncooled-heat-transfer discussions are presented in Section V.)

The uncooled combustion chamber was designed to operate at chamber pressures up to 5000 psia and for test durations up to 5 sec of steady state operation.

The initial chamber designs used graphite chamber liners that were recommended from the material investigation study. Graphite was selected primarily because of its high-temperature properties. Ablative materials were not considered initially because the "gassing off" effect of ablating resins was thought to seriously affect the accuracy of temperature measurement taken on the chamber liner wall. Later in the development testing program, however, it was found necessary to use ablative chamber liners to resolve continuing chamber liner problems inherent in the graphite liner design. Section VI,A,3 discusses the chamber liner materials investigation.

In summarizing the results of the uncooled combustion chamber design and development activity conducted on this program, the following conclusions can be made.

1. Of the numerous types of uncoated graphite material used for chamber liners, i.e., ATJ, ZTA, pyrolytic, and others, none proved satisfactory. Cracking, erosion, and general destruction of the graphite occurred on every test where used.

2. Coating of graphite liners for improved oxidation resistance of the graphite proved unsatisfactory. Silicon carbide, tantalum carbide, and zeronium oxide were used as protective coatings. None of these coatings were intact after a

single short-duration test. Difference in thermal expansion coefficients of the coating material and the basic graphite parent material was identified as the major reason for coating failure (cracking) and subsequent graphite erosion. Failure of the basic graphite by cracking was also evident in all tests where coated graphite was used.

3. Failure of graphite chamber liners by oxidation and thermal and mechanical shock makes accurate measurement of thrust chamber performance extremely difficult and prevents obtaining any reliable chamber temperature or heat-transfer data.

4. Ablative materials make excellent chamber liners because they are well suited for short-duration high-chamber-pressure testing with storable propellants. Of three ablative materials tested on this program (MX 4566, 150 RPD, and phenolic-resin-impregnated graphite cloth) MX 4566, a silicon-impregnated chopped roving, proved most satisfactory. MX 4566 was used most extensively and had the lowest ablation rate. Very limited data indicated that 150 RPD ablates about 20% faster than MX 4566 under identical test conditions. A resin-impregnated graphite cloth throat insert was found to ablate nearly 3 times faster than an MX 4566 throat insert.

5. Ablative chambers with removable throat inserts are less costly and require less repair (turn-around) time than integral ablative chamber inserts. Throat areas are subjected to the most severe ablation, and replaceable throat inserts permit continued reuse of other chamber liner material, i.e., cylindrical, convergent, and divergent nozzle sections.

6. Experience indicates that a step-joint design at all ablative joints is far superior to butt-type joints. Ablation and gas leakage is considerably reduced by using a step-joint design.

VI, C, Uncooled Combustion Chambers (cont.)

7. Excellent sealers and fillers are available for use at all ablative joints. RTV 60, a silicon rubber compound, has been found to be an excellent gas sealant at all ablative-to-ablative and ablative-to-metal joints. Zinc chromate putty was extensively used as a filler at the joint of the ablative liner to the injector assembly.

In the subsections that follow, chamber liner, throat insert, and exit nozzle materials development is discussed. This is the area where major development effort was expended on the uncooled combustion chambers. Mechanical design details of the workhorse pressure vessels are not discussed except in those cases where development work was required.

2. Development of Chamber Liner Materials

a. Graphite Chamber Liners

A materials investigation was conducted early in uncooled thrust chamber programs to select a chamber liner material that would offer good heat-sink and heat-transfer capacities and thermal shock resistance, and would provide a good medium in which to measure wall temperature. The conclusion of this materials investigation was that graphite offered the advantages of a high upper-temperature limit (5000°F) and would withstand the thermal and mechanical shocks of test firings and the chemical environment within the thrust chamber.

It was also determined that graphite would react with the water formed in the combustion products of N_2O_4/AeroZINE 50, but the degree of reaction was not known. Graphite was selected as the chamber liner material. It was planned to pursue a two-phase approach in using graphite as a chamber liner. The first approach was to evaluate various types of uncoated graphite; the second was to evaluate coated graphite liners which would have improved oxidation resistance over uncoated graphite.

VI, C, Uncooled Combustion Chambers (cont.)

The basic graphite-lined thrust chamber configuration used in the uncooled combustion chamber is shown in Figure VI-C-1. This chamber contains two major chamber segments: the L* segment, and convergent and throat segment. Each component is individually loaded with graphite and then assembled into the complete thrust chamber configuration.

The thrust chamber graphite liner consists of three individual 120° graphite sectors that are premachined to the thrust chamber contour and then assembled, with C-9 cement used as a binding agent, into a continuous graphite ring. The graphite ring is then wrapped with MX 5700 (a phenolic-impregnated asbestos felt), and is finished-machined for an interference fit into the steel chamber pressure vessels. The ablative wrap surrounding the graphite chamber liner provides a hot-gas seal between the graphite and the stainless-steel chamber pressure vessel. The radial expansion of the graphite liner is provided for by sectoring the graphite liner or "precracking" as shown in Figure VI-C-2.

(1) Uncoated Chamber Graphite Liner Material Evaluation

ATJ and ZTA types of uncoated commercial graphite were used in the graphite-lined thrust chamber configurations. The ATJ graphite was used in the L* segment and the convergent segment. The ZTA graphite was used in chamber convergent section only because it offered considerably better erosion characteristics than ATJ graphite. (The cost of ZTA is approximately 10-times greater than ATJ graphite.) ZTA and ATJ graphites were also used as throat insert materials; this is discussed in Section VI,C,3.

The above types of graphite were used extensively in the thrust chamber configurations up to and including Test 1.2-01-YAM-009. Figure VI-C-3 illustrates a typical graphite liner failure. Note that the graphite 120° sectors are severely cracked and eroded. The most severe erosion occurred along axial glue lines. In an attempt to reduce the erosion and cracking, some chamber graphite liner segments were assembled with all the glue lines aligned as shown in Figure VI-C-2.

VI, C, Uncooled Combustion Chambers (cont.)

Aligning of the glue lines slightly reduced but in no way eliminated the cracking of the graphite liners. Figure VI-C-4 shows the posttest condition of a ZTA-lined convergent section and an ATJ-lined throat. It is noted that extensive erosion and cracking of the graphite liner occurred, and this convergent and throat segment is not in a refirable condition. It was concluded on completion of Test 1.2-01-YAM-009 that uncoated graphite, regardless of type, configuration, or its physical location within the thrust chamber contour, cannot survive the thrust chamber chemical environment or thermal and mechanical shock when subjected to operating characteristics of N_2O_4/AeroZINE 50 propellants at a combustion chamber pressure of approximately 3000 psia. Similar conclusions were reached concurrently about coated-type graphite. The coated-type graphite material evaluation is presented in the next section.

(2) Coated Chamber Graphite Liner Material Evaluation

As previously discussed, the analytical results of the uncooled materials investigation concluded that graphite material, when used as a chamber liner in a storable propellant (N_2O_4/AeroZINE 50) atmosphere, would react with water formed in the combustion products. The degree of reaction, however, was not known. It was decided that protective coating materials should be investigated for their service as a protective boundary between the combustion gases and the graphite chamber liner. Three coating materials (silicon carbide, tantalum carbide, and zirconium oxide) were applied to individual graphite 120° L* sections. These sectors were located within the chamber L* segment as shown in Figure VI-C-2. Figure VI-C-5 shows the posttest condition of the L* segment with coated graphite. It is noted that approximately 70% of the silicon carbide coating and 30% of the zirconium oxide coating remained, but the tantalum carbide coating eroded completely from the graphite liner segment. Additional testing of coated graphite yielded results similar to that shown in Figure VI-C-5.

VI, C, Uncooled Combustion Chambers (cont.)

It was concluded after a thorough evaluation of these graphite liner coatings, that if it were possible for the coating to remain attached to the graphite liner and not crack and then erode away, the coating would protect the graphite from the combustion products. The major problem was the fact that the difference in thermal expansion between the coating and the basic graphite material causes cracks to develop in the coating and exposes the graphite base to oxidation during testing. It was further concluded that it is uneconomical and impractical to coat graphite liners operating in a storable propellant (N_2O_4/AeroZINE 50) atmosphere.

As was the case with uncoated graphite, it soon became evident that a graphite-lined thrust chamber, regardless of the type of graphite used, its orientation within the thrust chamber, and whether it is coated or uncoated, is not capable of operating, even for short duration, in the environment produced by high-chamber-pressure rocket engines with storable propellants.

b. Ablative Chamber Liners

The use of ablative material as uncooled combustion chamber liners not only solved the erosion and complete-liner-failure problems experienced with graphite, but also provided refire capability.

The following discussion covers in detail the design, development, and test experience of the ablative uncooled combustion chamber.

(1) Ablative Chamber Liner Design and Development

The one similarity that exists between the design of ablative- and graphite-lined thrust chamber assemblies is the basic thrust chamber contour. The ablative combustion chamber design concept (Figure VI-B-37) incorporates a minimum of chamber liner joints, thus reducing the potential problem of

hot-gas leakage. L* segments, convergent segments, and throat inserts are separate and independent ablative segments. The throat insert, discussed in Section VI,C,3, extends into the ablative exit nozzle. The technique of using an independent throat insert requires a minimum of chamber rework time and expense in the event that throat replacement is required.

The ablative chamber design also incorporates an ablative stepped spacer between the L* segment and the convergent section, shown in Figure VI-B-37. This stepped spacer design provides an efficient hot-gas seal that was used extensively throughout the uncooled and cooled thrust chamber test program, in which ablative thrust chamber components were used.

All joints between the chamber ablative liner components are sealed by the application of RTV-60 silicone rubber. The interface between the metal injector and the ablative L* liner uses zinc chromate putty as a joint filler and sealer medium.

(2) Ablative Materials Investigation

Although it was not the objective of the uncooled thrust chamber program to investigate ablative chamber liner materials, it was concluded after the first ablative-lined, uncooled thrust chamber test that ablative material should be used in all succeeding uncooled chambers. Three types of ablative materials were used in the ablative chamber configurations and subjected to full-duration tests. These included MX 4566 (silicone-impregnated chopped roving), 150 RPD (phenolic-impregnated chopped asbestos), and phenolic-resin-impregnated graphite cloth. The following brief discussion covers a description and evaluation of MX 4566 and 150 RPD. Graphite cloth was used only as a throat insert material and therefore is discussed in Section VI,C,3.

VI, C, Uncooled Combustion Chambers (cont.)

(a) MX 4566 (Silicone Impregnated Chopped Roving)

This ablative material is a silicone-impregnated chopped roving that is compression-molded into the required chamber configuration. Figure VI-C-6 shows an MX 4566-lined 60-in. L* segment in its prefire condition. The MX 4566 material was used extensively as a basic ablative chamber liner material throughout the uncooled thrust chamber assemblies. It had the lowest erosion rate of either the 150 RPD (phenclic-impregnated asbestos) or graphite-impregnated cloth. It was evident from posttest condition, shown in Figure VI-C-7, that this ablative material did not experience any detrimental effects from either thermal or mechanical shock.

(b) 150 RPD (Phenolic Impregnated Asbestos)

150 RPD is a phenolic-impregnated chopped asbestos that is compression-molded into the required chamber configurations. This ablative material was used only in the 60-in. L* segment; the posttest condition of this liner material is shown in Figure VI-C-8. It is noted that ablative liner material separation occurred in the center of this chamber. This separation is due primarily to the preforming technique used in fabricating the liner and not to failure of the phenolic-impregnated asbestos material. The erosion rate of the 150 RPD lined 100-in. L* segment was approximately 20% greater than of the same chamber lined with MX 4566 under identical thrust chamber test conditions.

(3) Test Experience

In the first ablative-lined uncooled thrust chamber tests which used the ablative exit cone, hot-gas leaks developed at the joint between the L* segment liner and the convergent throat segment and at the butt-joint between the throat segment and the ablative exit cone. In order to eliminate hot-gas leaks at each ablative joint, all individual chamber ablative liners were

redesigned to incorporate a "step-joint," shown in Figure VI-B-37. On completion of the above modification, the ablative-lined thrust chamber assemblies performed exceptionally well throughout this program. No further hot-gas leakage occurred. Six valid tests totaling 16.181 sec were performed on one MX 4566-lined 60-in. L* segment.

3. Uncooled Throat Insert

The throat area of any thrust chamber is subjected to the most severe erosive environment of any portion of the thrust chamber. The chamber wall construction in this area causes a corresponding increase in hot-gas velocity and a decrease in the thickness of the gas boundary layer adjacent to the wall. The greatest mass flow per unit of surface area exists in the chamber throat, tending to increase chemical erosion of the throat. In addition, the decreased boundary layer thickness increases the heat-transfer rate and, therefore, increases the rate of thermal decomposition at the throat. Solid particles in the hot-gas stream commonly cause extensive mechanical damage or erosion in the throat area, whereas the cylindrical section and large-diameter converging sections of the thrust chamber are relatively unaffected.

The preceding three mechanisms illustrate why the uncooled thrust chamber throat offered the most severe erosive environment of any portion of the uncooled thrust chamber. The following paragraphs describe the evaluation of materials and methods used to create an uncooled throat insert capable of withstanding hot storable propellant gases at 3000 psia chamber pressure.

a. Graphite

Pressed carbon and pyrolytic graphite were used as throat insert materials during the course of the test program. Graphite cloth was also used as a throat insert, but it is discussed under ablative materials since it was held together with a phenolic binder.

VI, C, Uncooled Combustion Chambers (cont.)

(1) Pressed Carbon

ZTA and ATJ graphite were used to construct the throat inserts tested on the vortex injector thrust chamber (Test 1.2-01-YAM-001) and the concentric-ring thrust chamber (Test 1.2-01-YAM-005). Both of these throat inserts used three 120° graphite segments to form the throat insert. The throat insert pieces were cemented together with C-9 cement, and then cemented to the convergent section, wrapped with MX 5700 ablative material, and cured and machined to fit the pressure vessel. Throat insert materials and convergent section materials were evaluated jointly in these tests. A butt-joint existed between the graphite liner and ablative end-plate.

Figure VI-C-9 is a posttest photograph showing the ZTA convergent segment and ATJ throat insert. The staggered glue lines can be seen along with the extension of those lines into the middle of the adjacent carbon pieces. The carbon block glue lines were weak spots and promoted failure in the body of the next row of blocks.

To reduce failure of the adjacent carbon blocks on the convergent segment and throat insert on the next buildup, the glue lines were aligned along the axis of the thrust chamber and retested along with the concentric-ring injector (Test 1.2-01-YAM-008). However, as shown in Figure VI-C-4, the construction was still unsatisfactory. Segmented graphite appeared to be too weak structurally to support the stresses induced by uncooled chamber testing, and the system was abandoned.

The next throat insert development involved the use of a monolithic piece of ZTA graphite in combination with a convergent section of phenolic-impregnated fiber glass. This construction was tested along with the vortex L* thrust chamber (Test 1.2-01-YAM-010). Figure VI-C-10 shows the result of this firing. Again, the graphite throat insert failed mechanically. This was the last test-firing with any kind of solid graphite material.

VI, C, Uncooled Combustion Chambers (cont.)

(2) Pyrolytic Graphite

Pyrolytic graphite is a material normally produced by deposition into flat plates from vapor and possessing unique physical properties. It is an excellent thermal conductor, but only conducts well parallel to the plane of deposition. It also possesses excellent qualities as a heat-sink material. Pyrolytic graphite has the highest strength of any known material at temperatures above 3000°F, and it is about ten-times stronger than tungsten at 5000°F. Although it has good ductility at higher temperatures, it is quite brittle at low temperatures.

The pyrolytic throat insert used on this program was constructed of 0.250-in.-thick wafers, cemented together with C-9 cement and encased in graphite impregnated felt. The construction is illustrated in Figure VI-C-11. For economy, the pyrolytic graphite throat insert was contained in an outer cylinder of ATJ graphite.

This throat insert was tested in conjunction with a convergent section of staggered ATJ graphite blocks and the Mod I vortex injector (Test 1.2-01-YAM-006). The graphite wafers failed mechanically during this test. Figure VI-C-12 is a posttest photograph of this failed throat insert. The difference in diameter between the ATJ graphite blocks and the pyrolytic graphite wafers is the result of the loss of the pyrolytic wafers in between the two points.

An identical pyrolytic throat insert was tested together with a phenolic-impregnated fiber-glass-lined chamber and convergent section (Test 1.2-01-YAM-009). Figure VI-C-13 is a photograph illustrating the results of this test. As before, the pyrolytic wafers failed mechanically and were ejected through the throat and end plate. The end plate was also damaged. Further testing of pyrolytic graphite throat inserts was abandoned.

VI, C, Uncooled Combustion Chambers (cont.)

b. Ablative Material

All but one of the ablative throat inserts were fabricated from phenolic-impregnated chopped fiber-glass fabric, which was a phenolic-impregnated edge-grain graphite-cloth throat insert.

(1) Glass-Cloth-Phenolic

All glass-phenolic molded pieces were fabricated from MX 4566, a formulation of the Fiberite Co. The segmented construction is illustrated in Figure VI-C-14. The size and shape of the segments were selected so that currently available molded pieces of the ablative material could be used. All segment joints and the outside cylinder-pressure vessel joint were sealed with RTV-60 silicone rubber sealer. RTV-60 sealer was completely successful in preventing hot-gas leaks in the throat area as well as in the remainder of the thrust chamber.

The outside diameter of the throat insert was of a size that could be molded in Aerojet presses and dies. This permitted easy replacement of the throat inserts. The design of the throat insert piece differed from the design of the graphite throats in that there were no seams at the throat itself. Instead, the ablative throat insert was machined with a smooth, continuous contour from the convergent cone to the divergent exit cone or end plate. The prefire condition of a typical unit is shown in Figure VI-C-15. The success of this method of construction is seen in a posttest photograph, Figure VI-C-16. A single convergent and throat segment and exit cone of this construction was tested five times without failure. All throat development work was discontinued at this point.

(2) Graphite Cloth-Phenolic

One throat insert was fabricated from phenolic-impregnated graphite cloth because it was the only material available at the time. The billet of

material was made of graphite cloth laid down normal to the centerline of the molded cylinder. This produced a throat insert wherein the layers of graphite cloth were perpendicular to the direction of hot-gas flow.

The insert performed satisfactorily as evidenced in Figure VI-C-17, but the throat diameter increased at about three times the rate of the ablative throat inserts. The graphite-cloth throat insert eroded radially at the rate of 0.224 in./sec, whereas the phenolic-impregnated glass-cloth inserts eroded radially at an average rate of 0.082 in./sec. The above data is a result of short-duration testing and is not intended to represent longer-duration ablation rates.

4. Uncooled Thrust Chamber Exit Nozzle

Two thrust chamber exit nozzles were designed, fabricated, and tested in the uncooled thrust chamber program. These consisted of an ablative end-closure assembly and an ablative exit cone. The end-closure assembly was designed to be an inexpensive stub closure; it provided the functions of retaining the ablative throat and protecting the metal plate retainer from the hot combustion gases. The ablative exit cone was designed to have the identical nozzle contour of the regenerative cooled expansion nozzle, a component of the cooled chamber program. The exit cone thereby provided a means of directly comparing uncooled and cooled thrust chamber performance, in addition to providing the functions of the ablative end-closure assembly.

Brief design descriptions for each of the exit nozzle configurations are given in Sections VI,C,4,a and b below. A summary of the test experience is discussed in Section VI,C,4,c.

VI, C, Uncooled Combustion Chambers (cont.)

a. Ablative End-Closure Assembly

The end-closure assembly is shown installed on the TCA in Figure VI-C-18. It consists of an end-plate, Figure VI-C-19, and an ablative protective cover, Figure VI-C-20. The cover is mechanically attached to the end plate by twelve countersunk machine screws. A commercial product, silicon rubber, RTV-60, is used as a hot-gas sealant between the ablative cover and the end-plate. The protective cover is compression-molded into its finished configuration. It is made from MX 4566 material, a chopped high silica woven roving impregnated with a phenolic resin.

When used in conjunction with the ablative throat, the end-closure provides a thrust chamber expansion ratio of 4.5.

b. Ablative Exit Cone

The ablative exit cone is shown in Figures VI-C-21 and VI-C-22. It consists of a conical ablative liner contained in a steel shell and retained by a metal ring on the aft end. The liner contour is identical to that of the regeneratively cooled expansion nozzle, which is a 35° half-angle cone extending to an area ratio of 21.3. The liner is fabricated from a phenolic-impregnated tape, MX 2600. This tape is wound at a 20° angle to the longitudinal axis of the exit cone and molded to the required nozzle contour.

c. Test Experience

In the first uncooled thrust chamber test, which used the ablative exit cone, a hot-gas leak developed at the butt-type joint between the throat segment and the ablative exit cone liner. The ablative throat and exit cone liners were subsequently redesigned to provide a step-joint. This redesign, shown in Figure VI-C-14, provided an ablative throat insert, extending beyond the throat, which blended into the contour of the ablative exit cone.

VI, C, Uncooled Combustion Chambers (cont.)

Following this one modification, both ablative exit nozzle configurations performed satisfactorily throughout the program. Three valid tests totaling 7.5 sec were accumulated using the end-closure assembly; nine tests totaling 19.5 sec were performed with the exit cone assembly. No replacement of the exit cone ablative liner was ever necessary during the program.

From the results of the development test program and supporting studies, the following conclusions can be made for cooling systems of high-chamber-pressure engines:

(1) Regenerative cooling with either oxidizer (N_2O_4) of fuel (AeroZINE 50), supplemented by film-cooling and/or a thermal-barrier coating, is feasible for cooling high-chamber-pressure engines. In this program, the cylindrical portion of the chamber was fuel-cooled and the expansion nozzle was oxidizer-cooled. Experimental heat-transfer laboratory tests (not performed as part of this program) show that supercritical N_2O_4 is superior to AeroZINE 50 as a regenerative coolant; hence, less supplemental film coolant is required. On this basis, oxidizer regenerative cooling, with supplemental oxidizer film cooling, is the recommended system.

(2) A high-chamber-pressure engine can be cooled entirely by film-cooling the thrust chamber walls with oxidizer. However, for the design configuration tested in this program, the performance loss associated with the amount of film-cooling required to maintain the walls at an acceptable temperature level is too great to result in a practical cooling system. However, the performance and heat-transfer models derived from the test data of this configuration show that if the number of injection points could be substantially increased (approaching transportation cooling), the coolant flow rate could be reduced to a level commensurate with a very high performance level. Such a configuration is currently being pursued at Aerojet under Contract AF 04(611)-10830 "Advanced Rocket Engine, Storable."

VI, C, Uncooled Combustion Chambers (cont.)

(3) Recent developments with thermal-barrier coatings, in combination with regenerative and film cooling, now make this approach feasible. A new tungsten-based coating was successfully tested in this program, but only in short-duration tests. There may be a comparibility problem with this coating when used in conjunction with oxidizer film cooling; therefore additional testing at extended durations must be made before firm conclusions can be made.

(4) Vortex cooling, wherein all propellants are tangentially injected onto the combustion chamber wall, shows potential as a combination high-performance injector-cooling system. However, the test experience with this concept was very limited, and further development testing is required before any conclusions can be drawn.

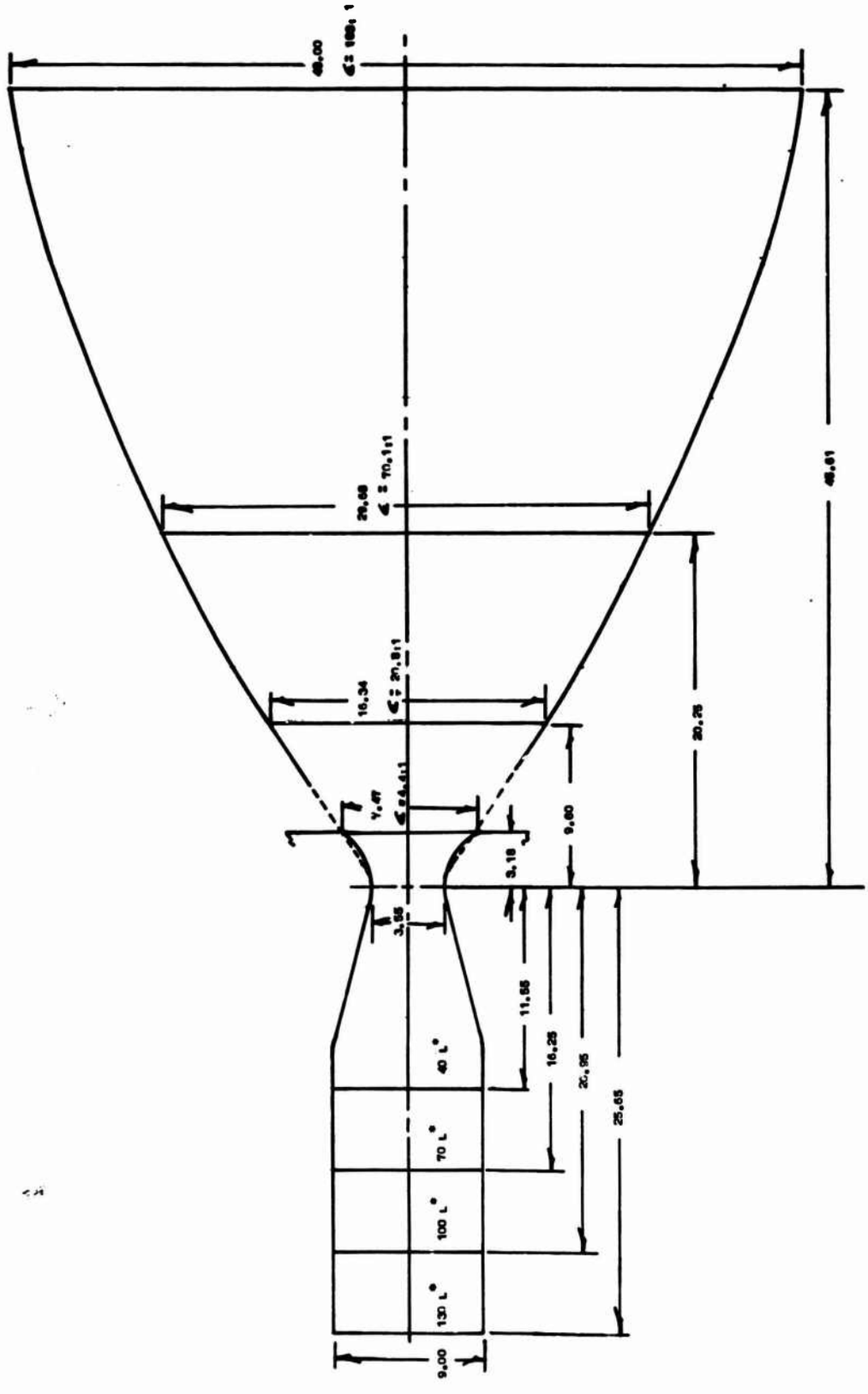

Thrust Chamber Contour

Figure VI-A-1

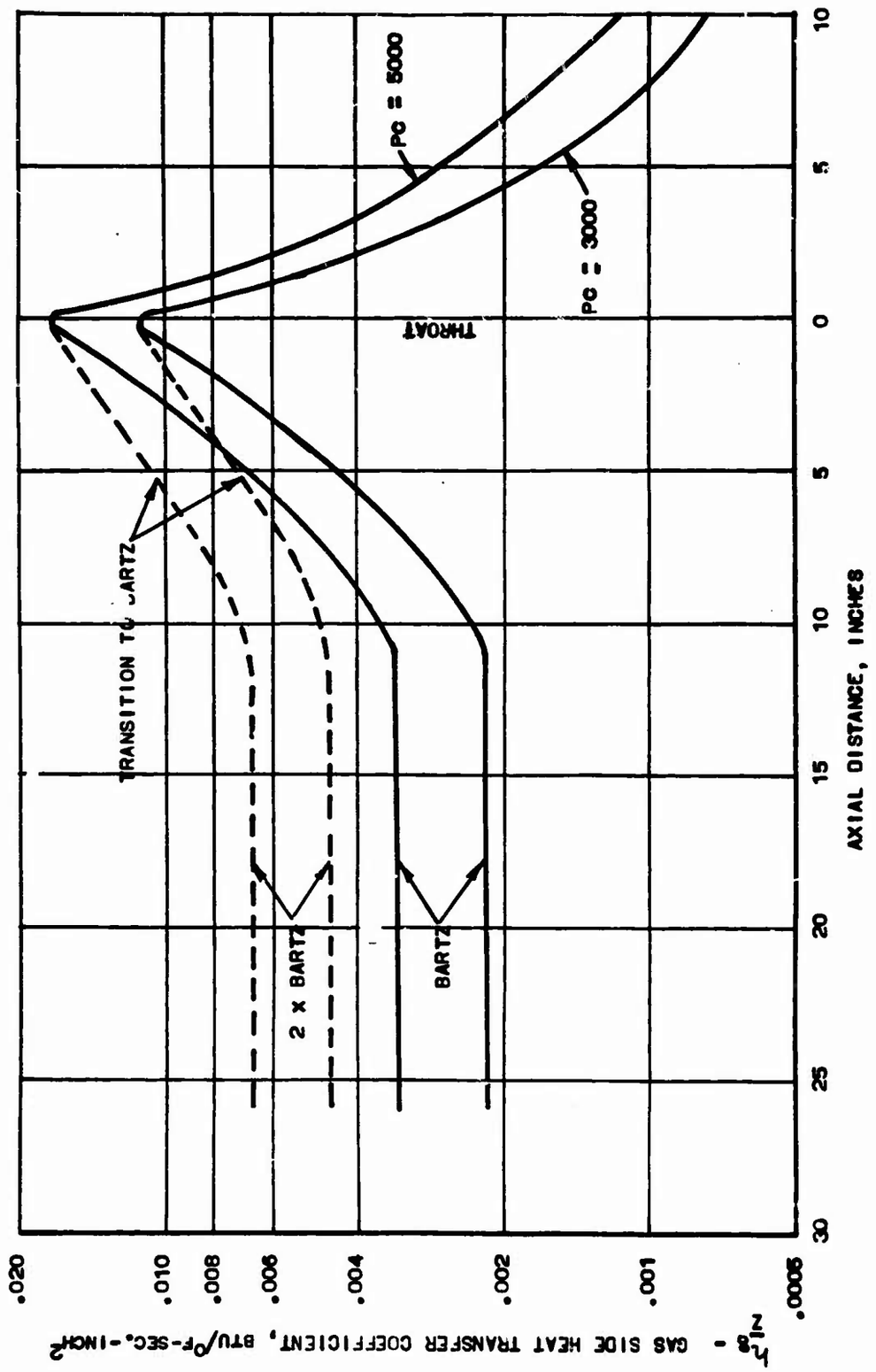

Gas-side Heat Transfer Coefficient vs Axial Chamber Length

Figure VI-A-2

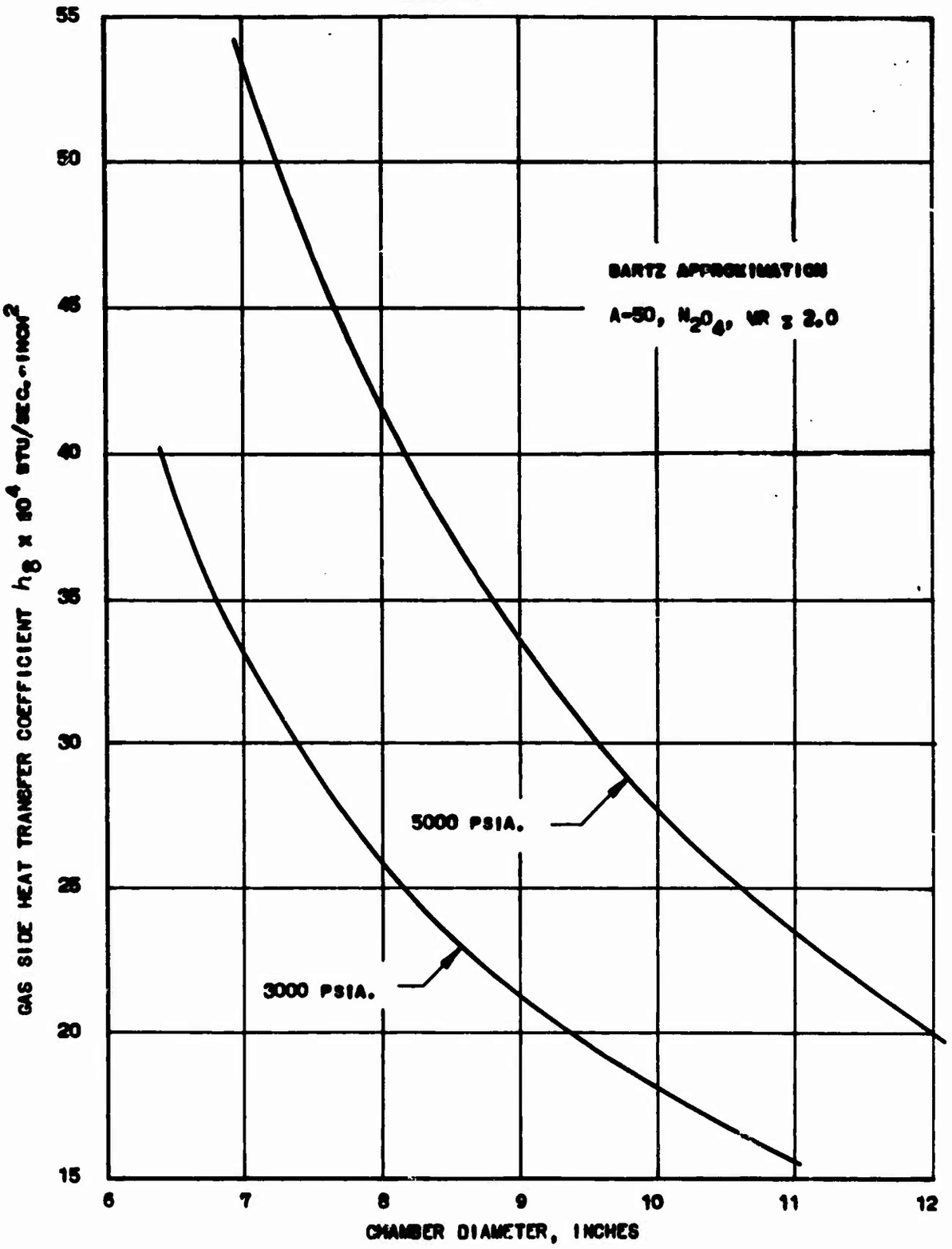

Gas-side Heat Transfer Coefficient vs Chamber Diameter

Figure VI-A-3

MATERIAL THICKNESS = .625 INCHES

CHAMBER PRESSURE = 3000 PSIA.

MIXTURE RATIO = 2.0

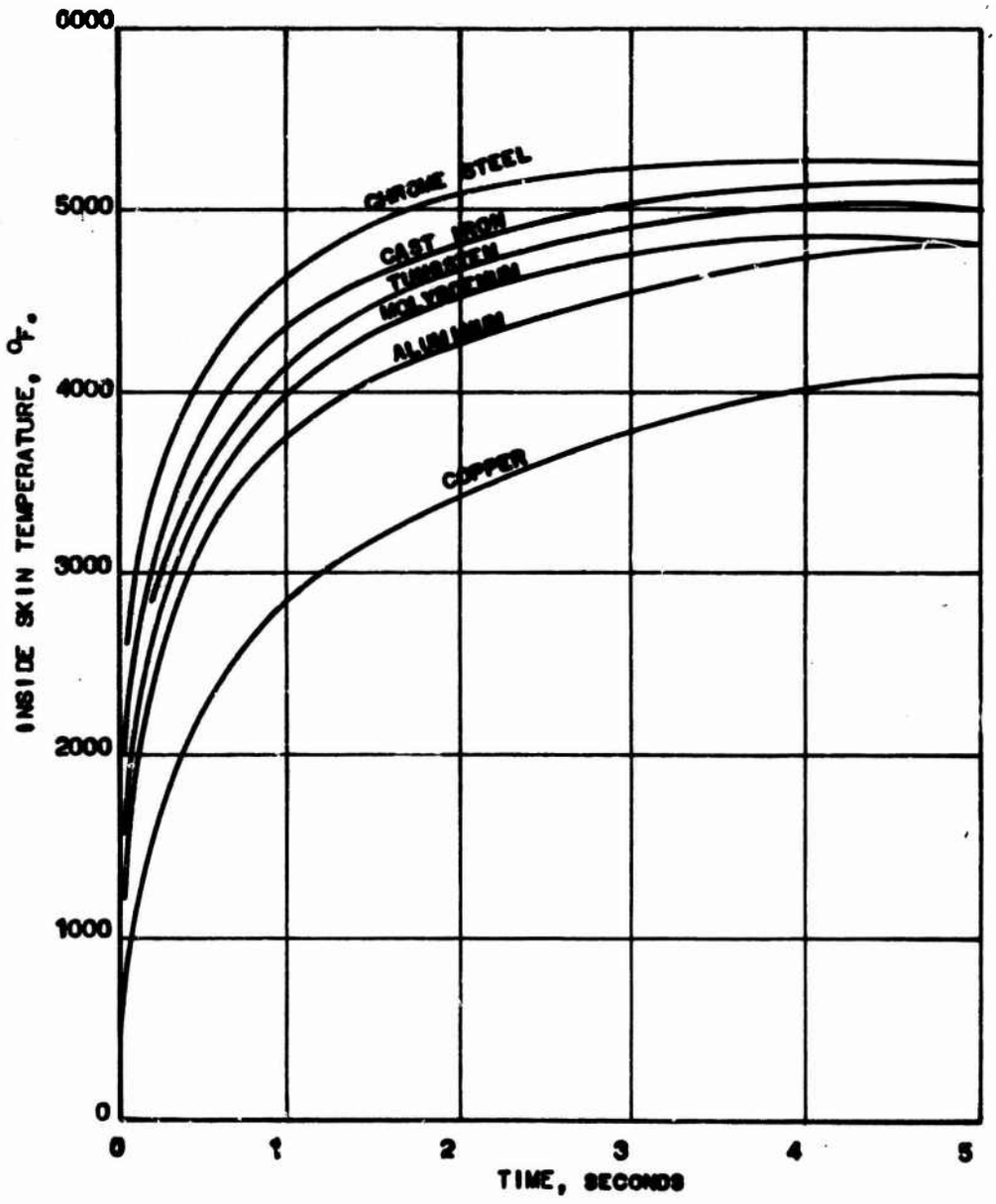

Inside Skin Temperature of Various Materials vs Time

Figure VI-A-4

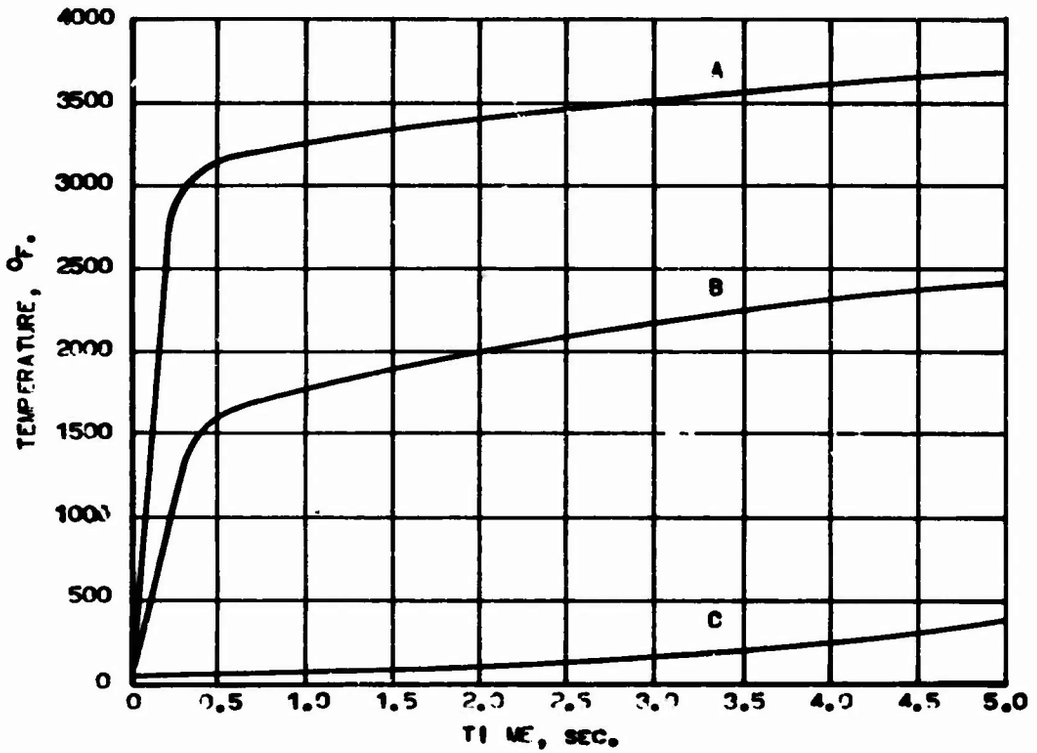

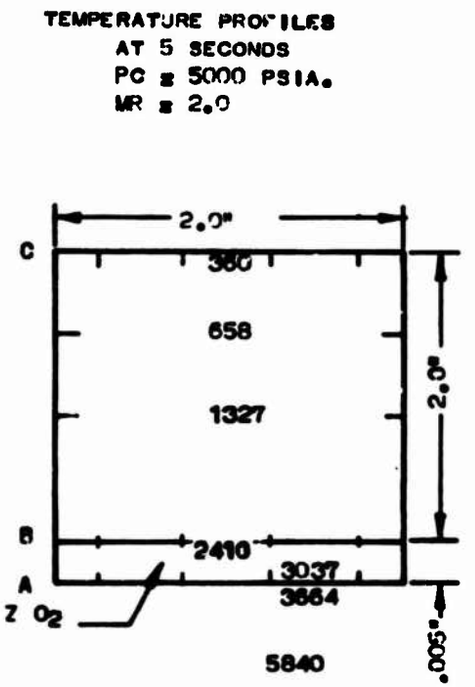

Copper Skin Temperature vs Time

Figure VI-A-5

Book One

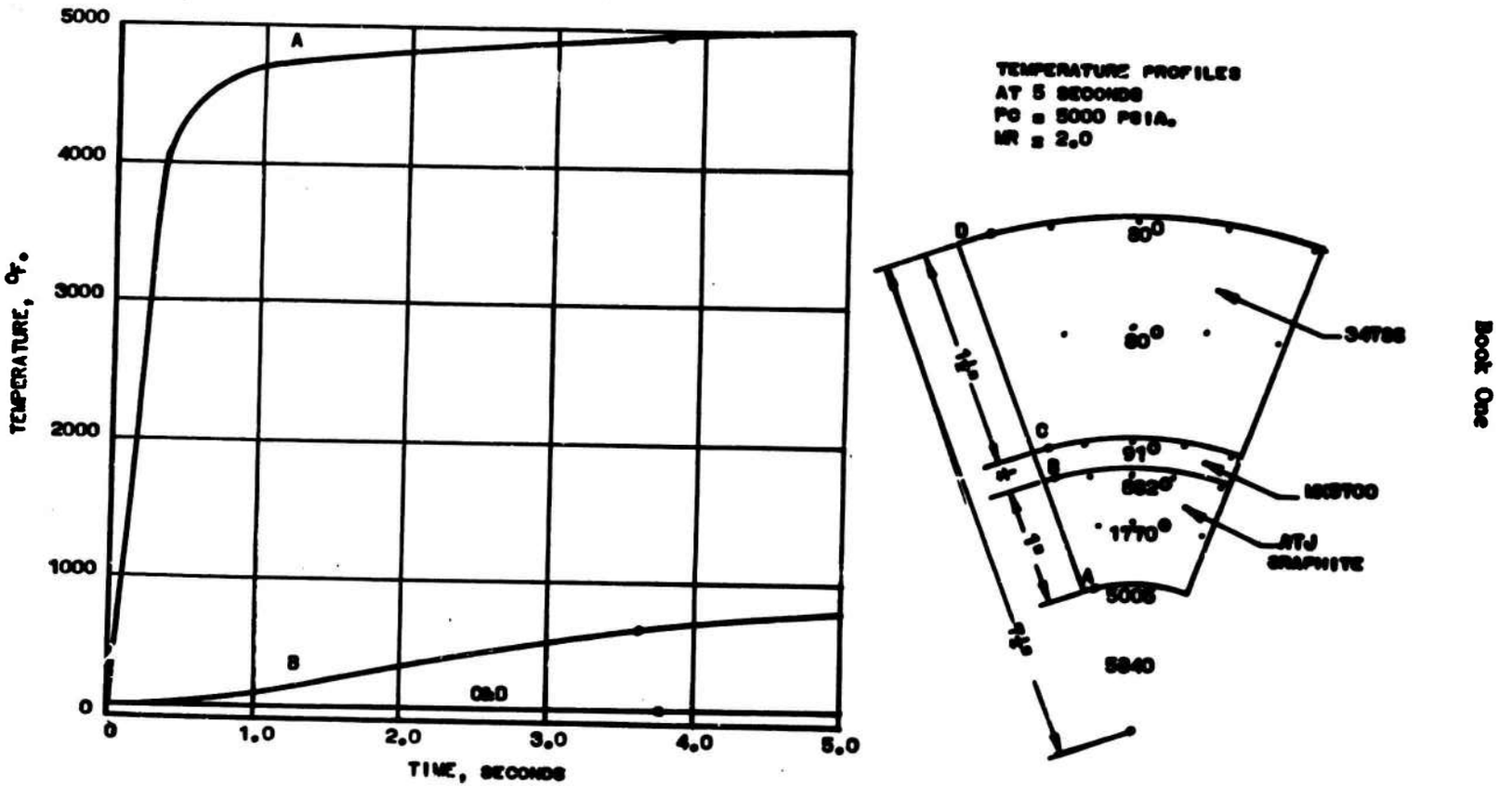

Figure VI-A-6

ATJ Chamber Skin Temperature vs Time

Book One

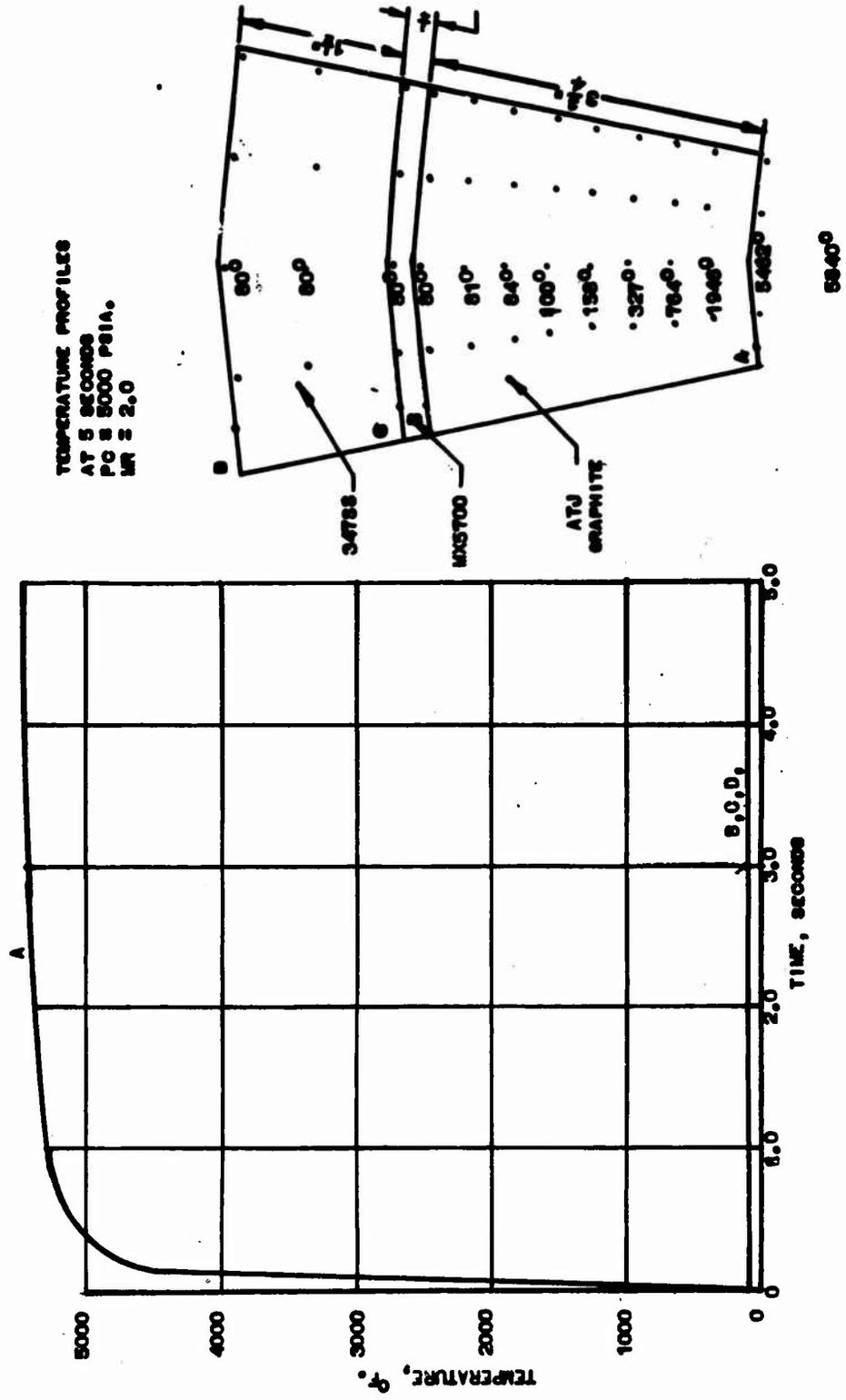

ATJ Throat Skin Temperature vs Time

Figure VI-A-7

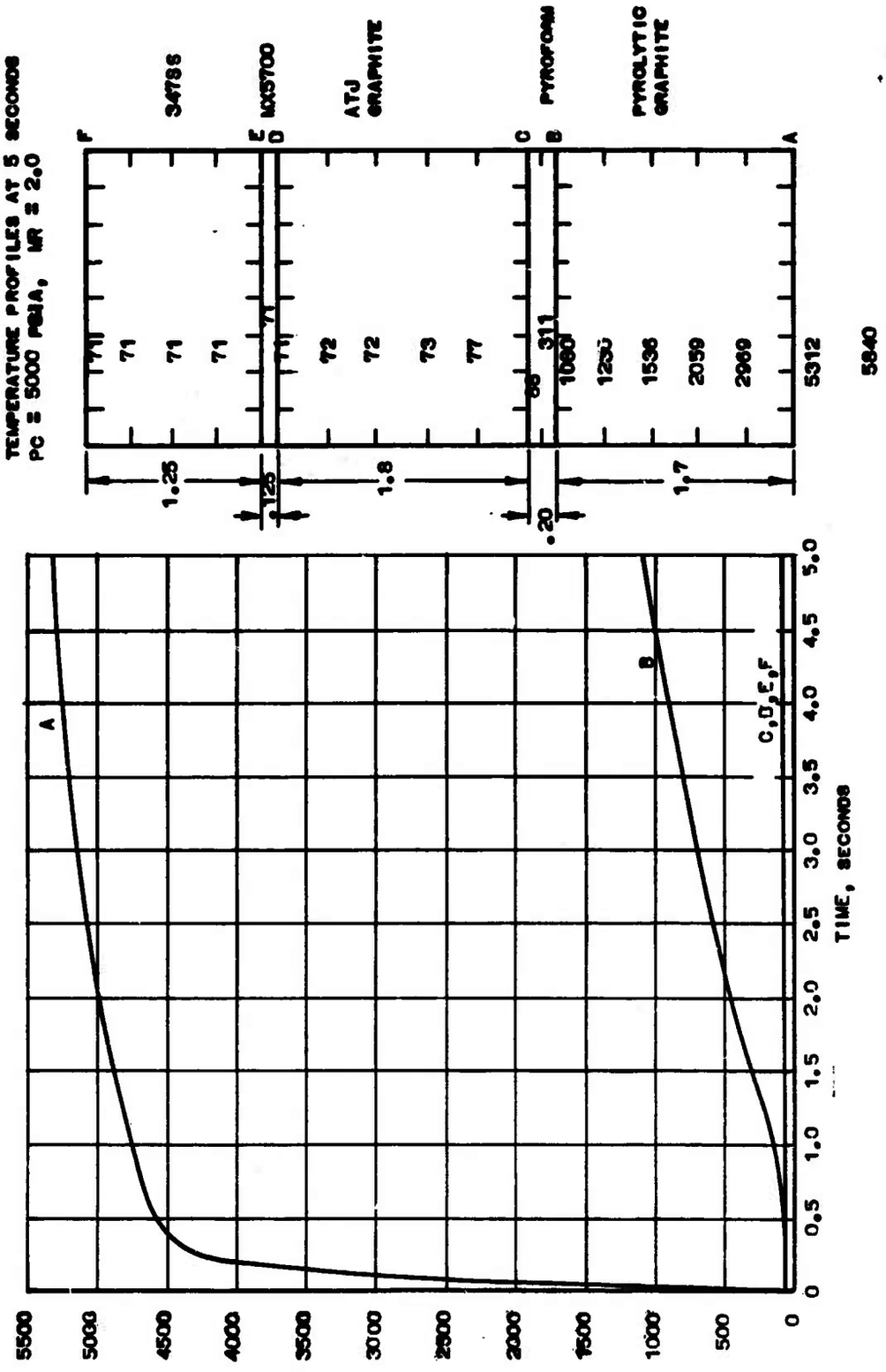

Pyrolytic Throat Skin Temperature vs Time

Figure VI-A-8

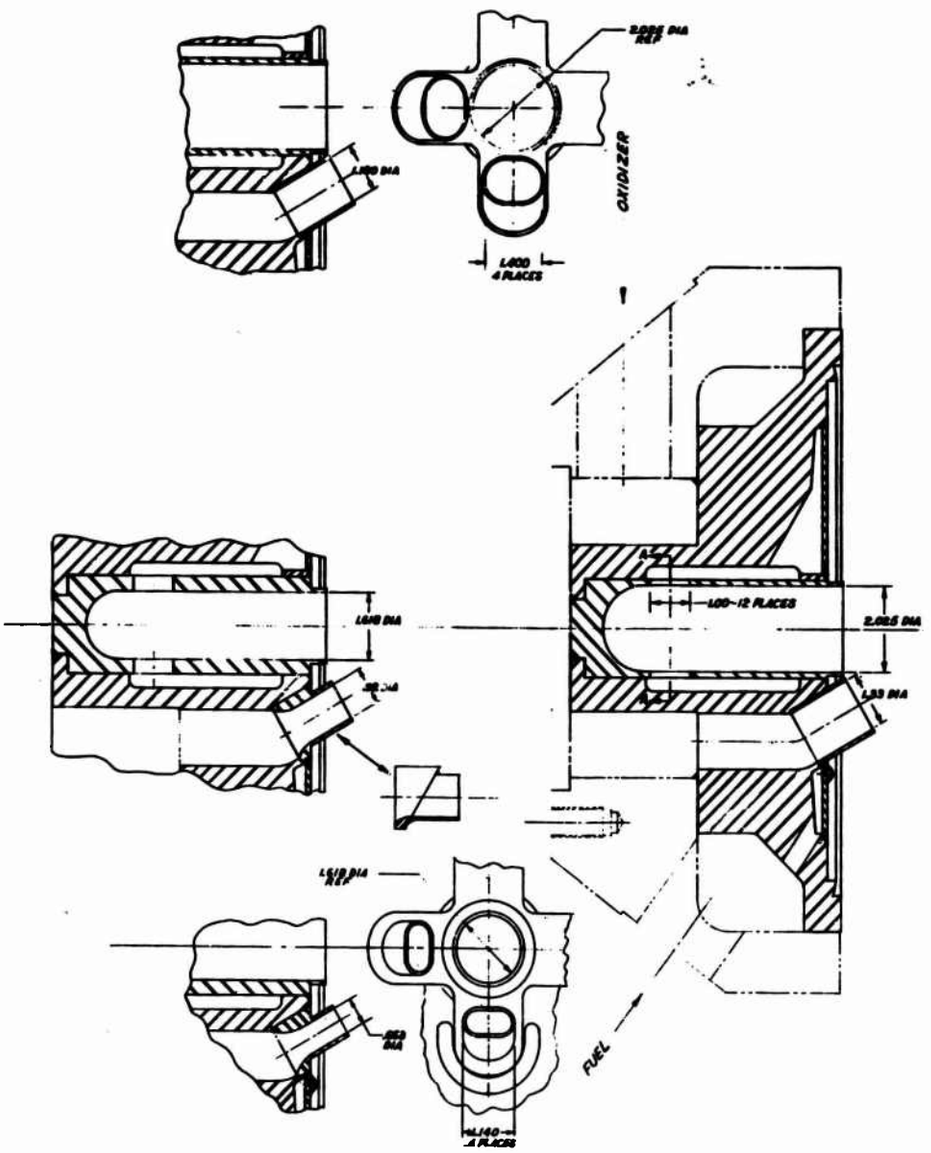
OXIDIZER
FUEL

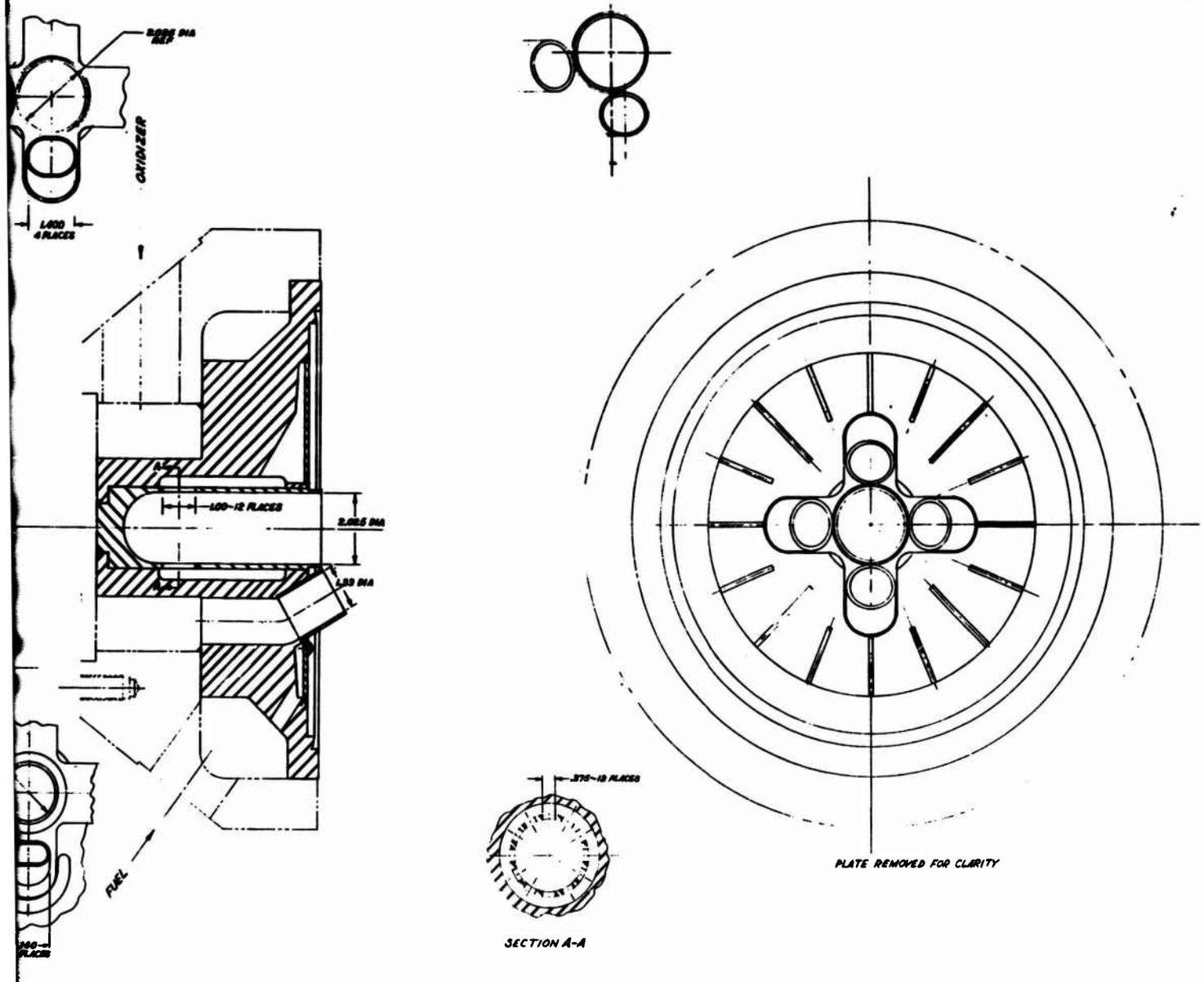

Pentad Injector Design (u)

Figure VI-B-1

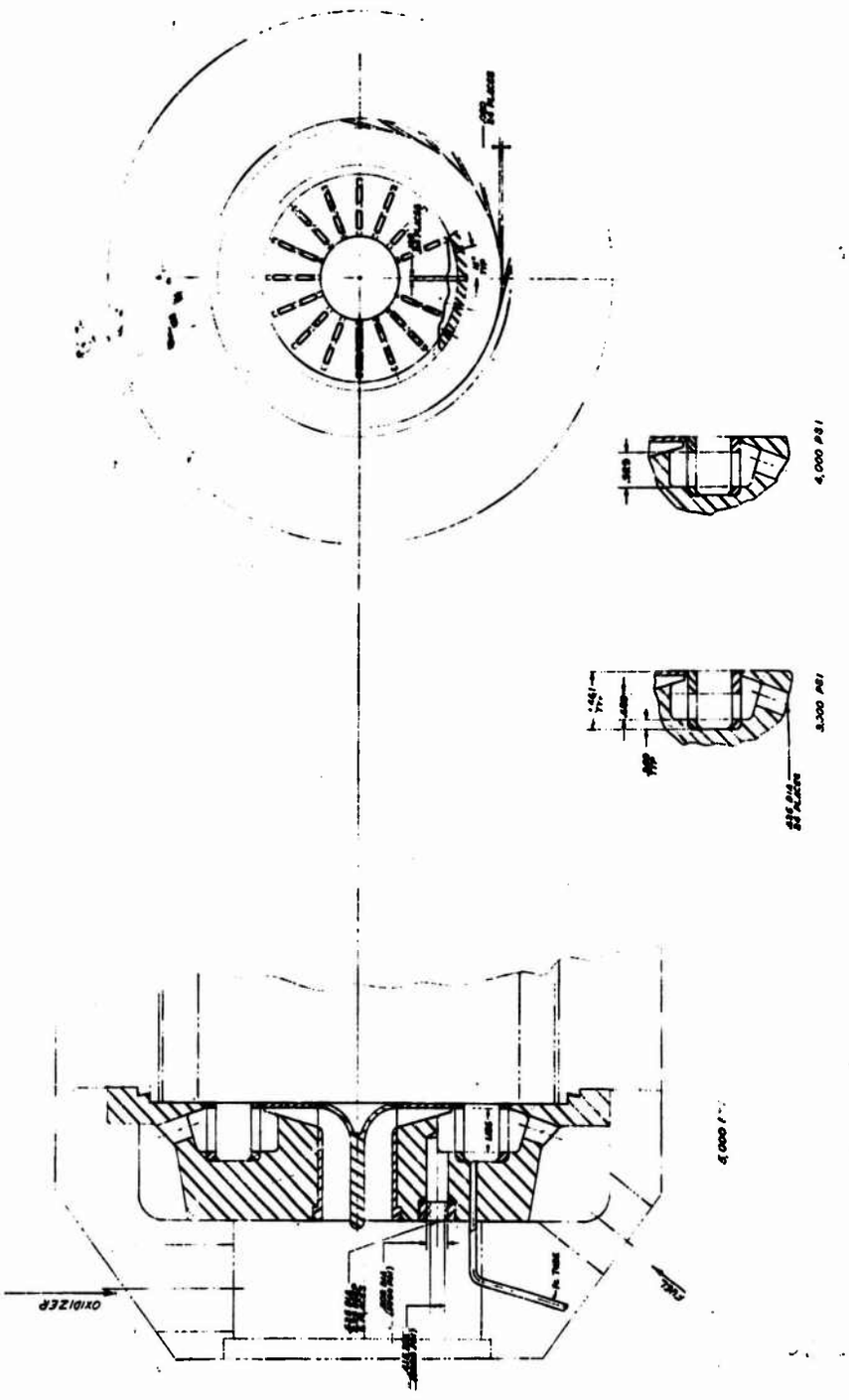

Vortex Injector Design (u)

Figure VI-B-2

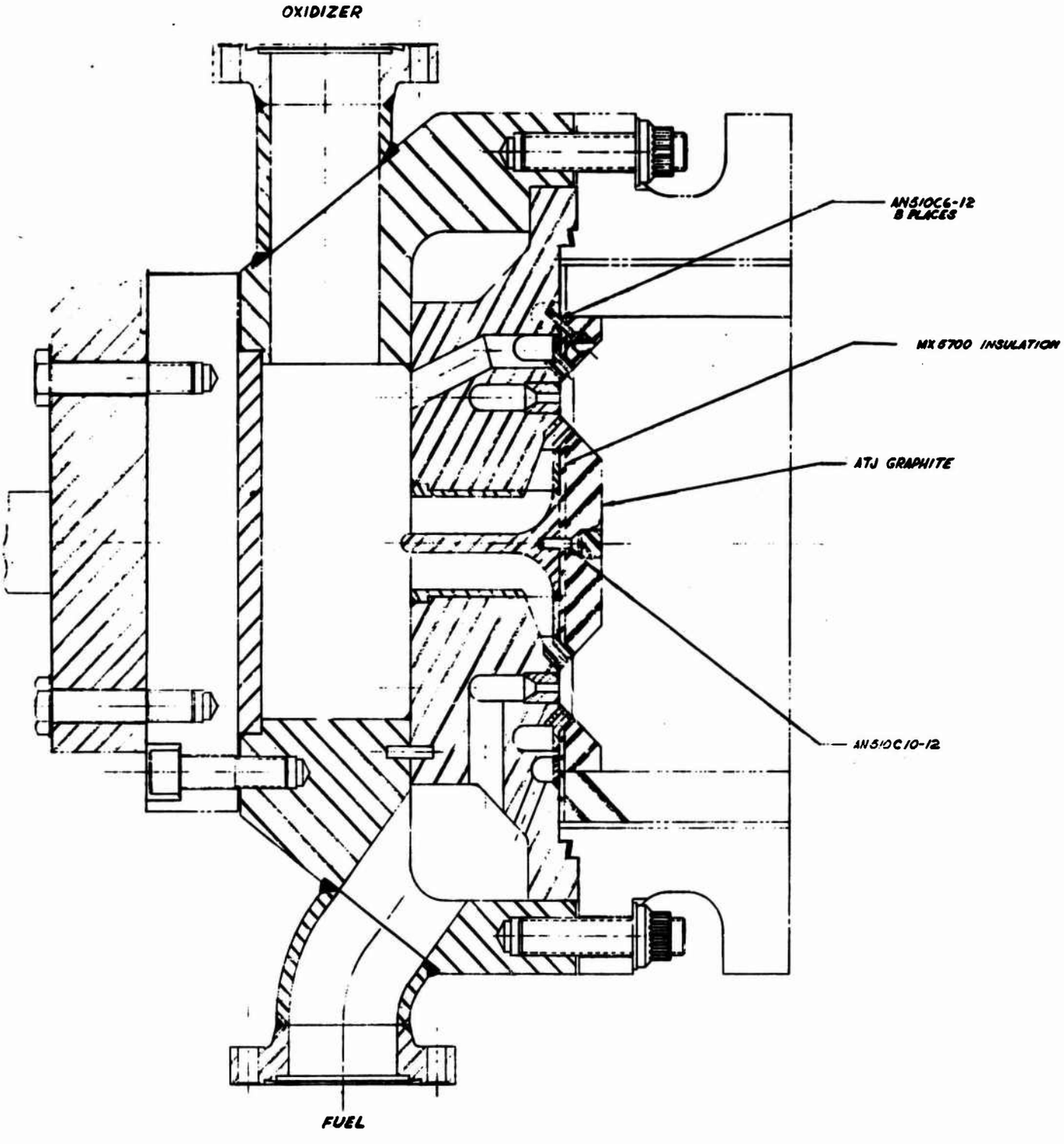

Concentric Ring Injector Design (u)

Figure VI-B-3

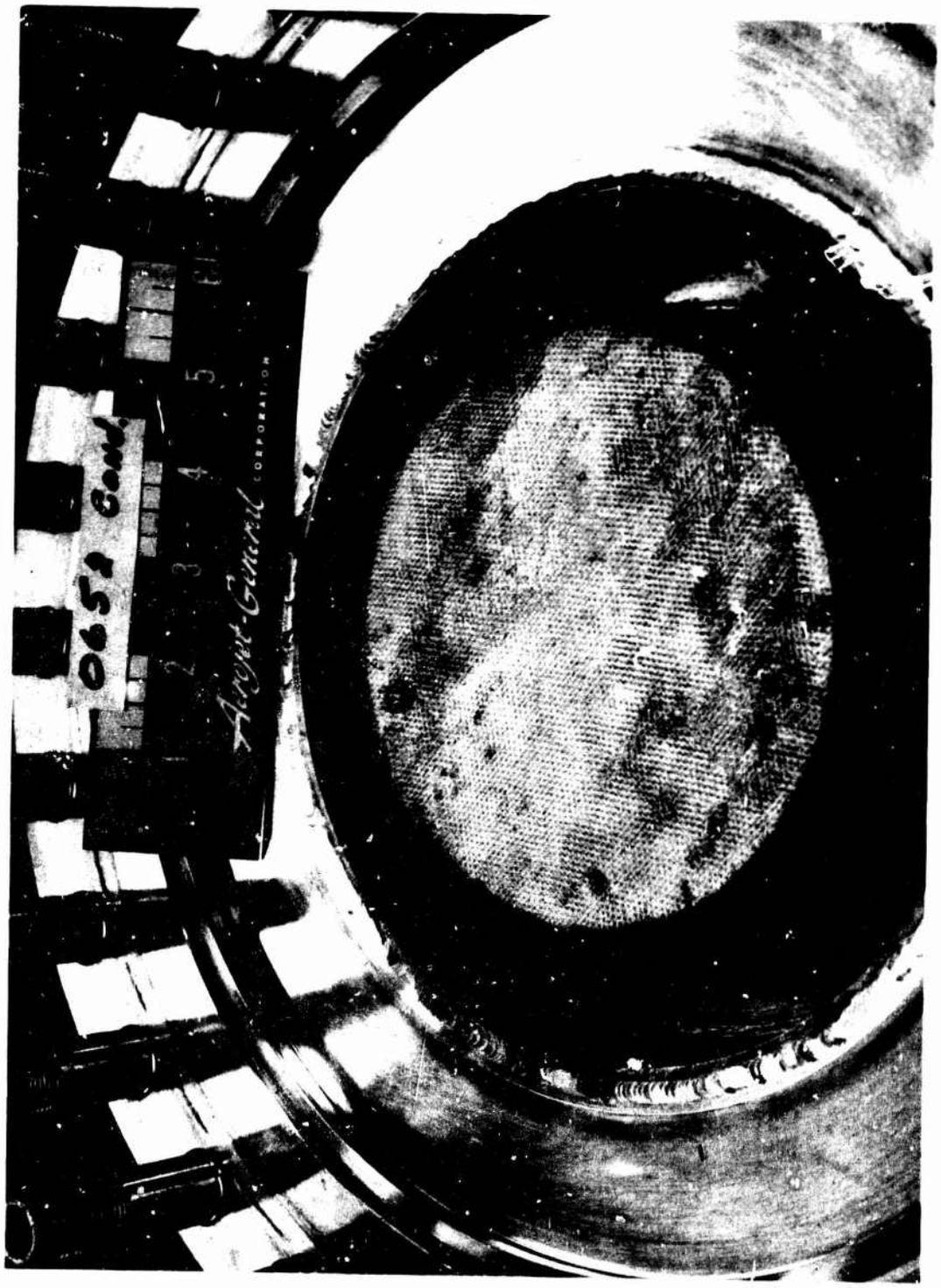

Vortex Injector (u)

Figure VI-B-4

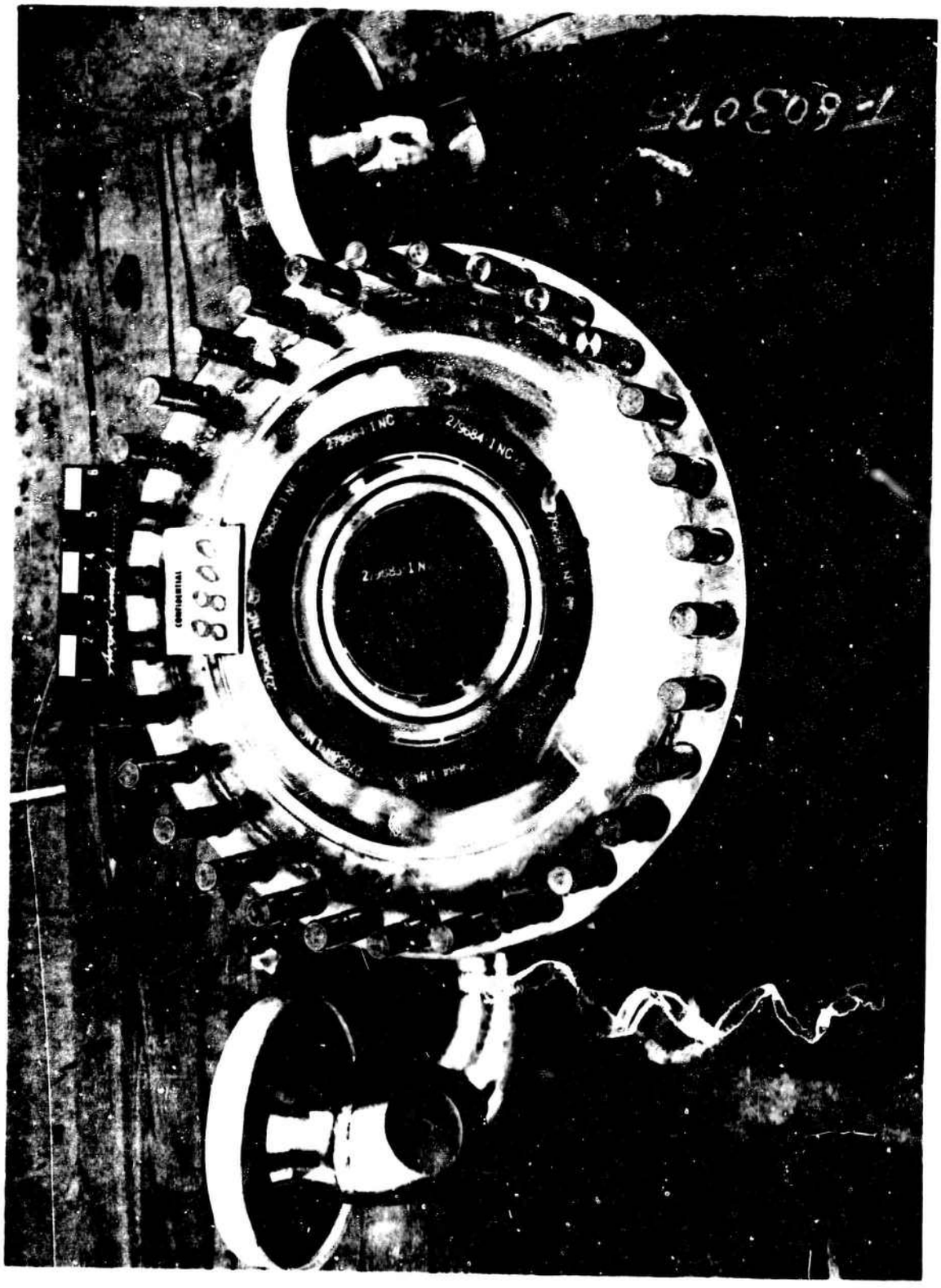

Concentric Ring Injector (u)

Figure VI-B-5

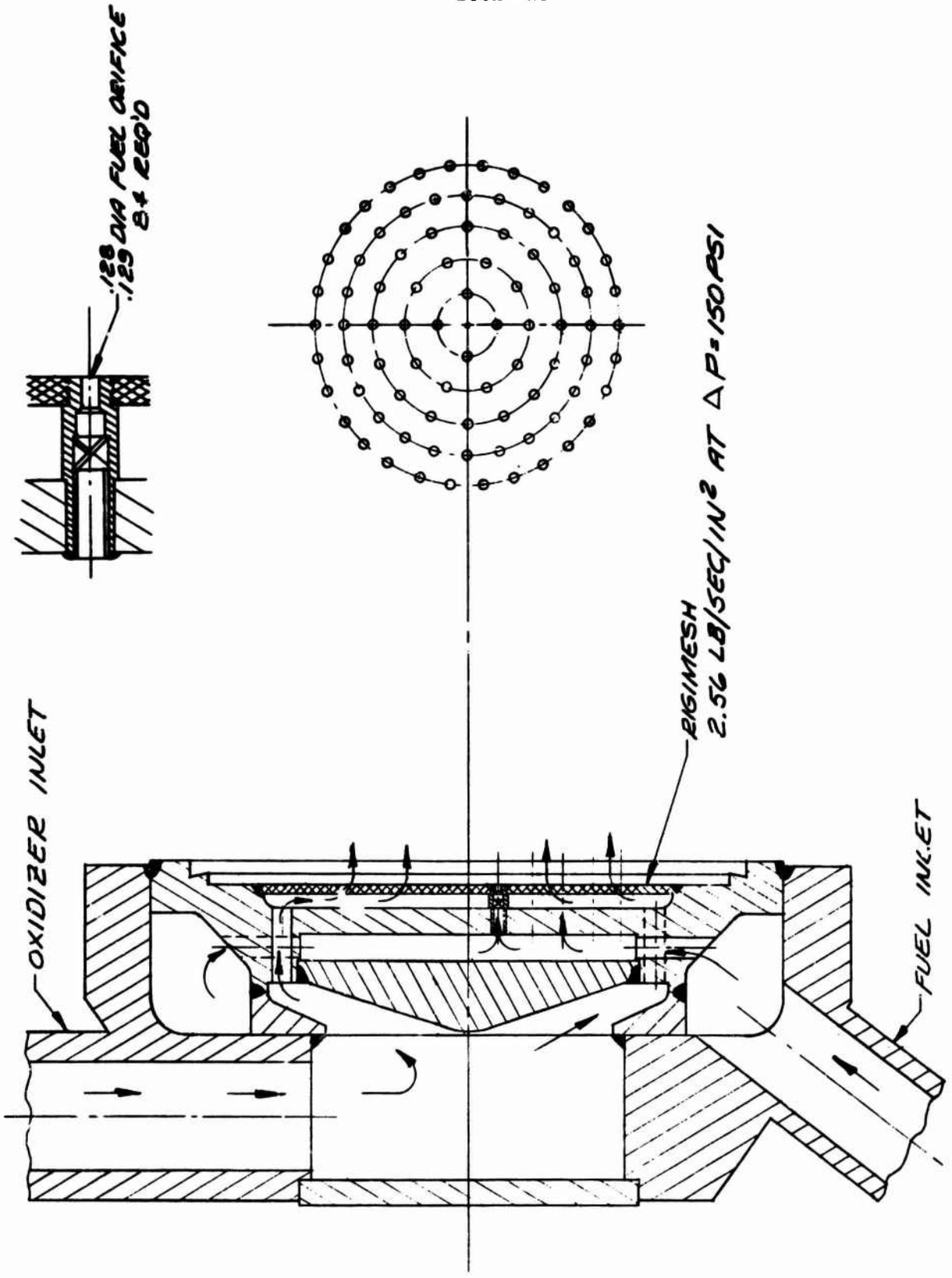

Transpiration-cooled Injector Design (u)

Figure VI-B-6

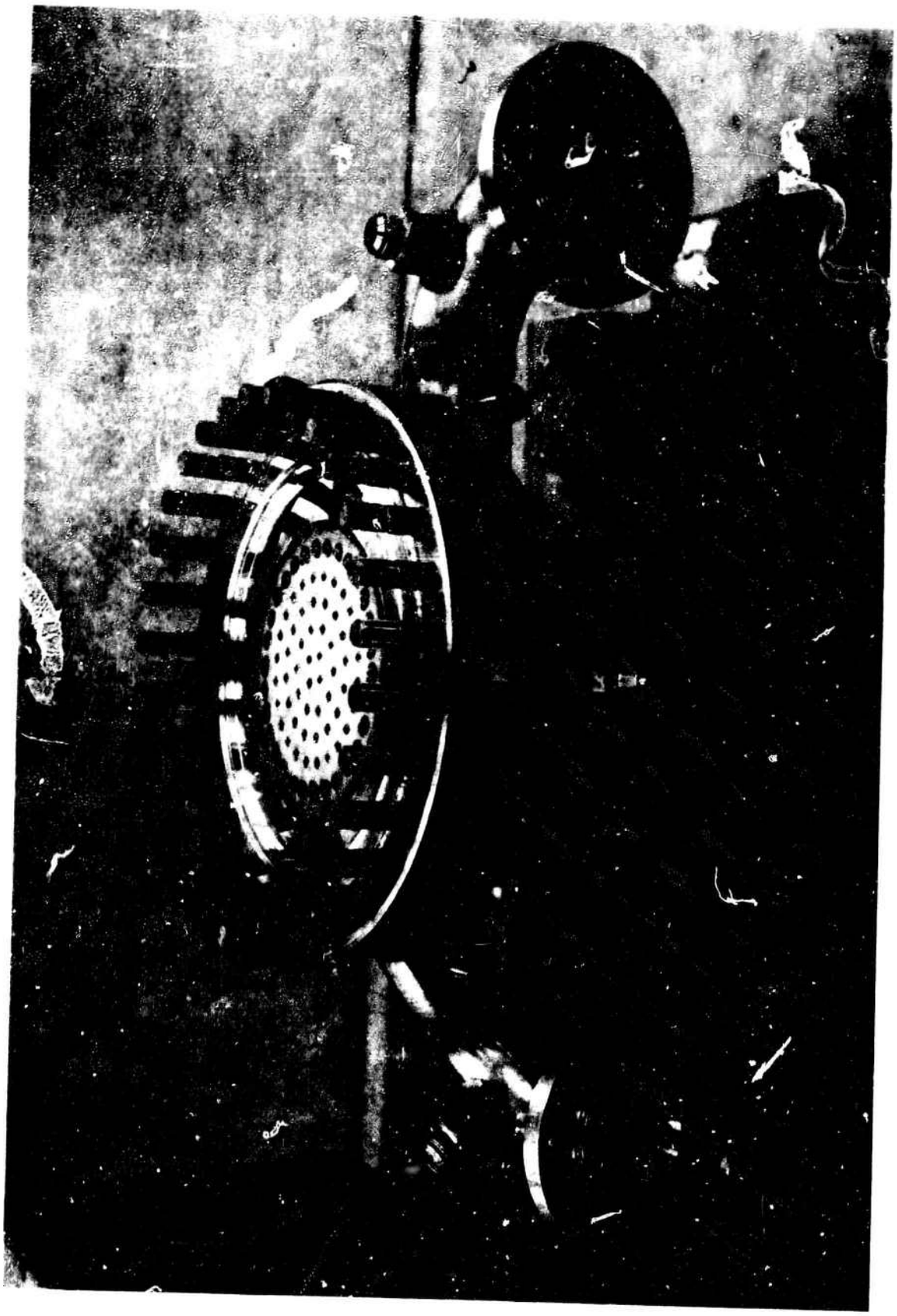

Transpiration-cooled Injector

Figure VI-B-7

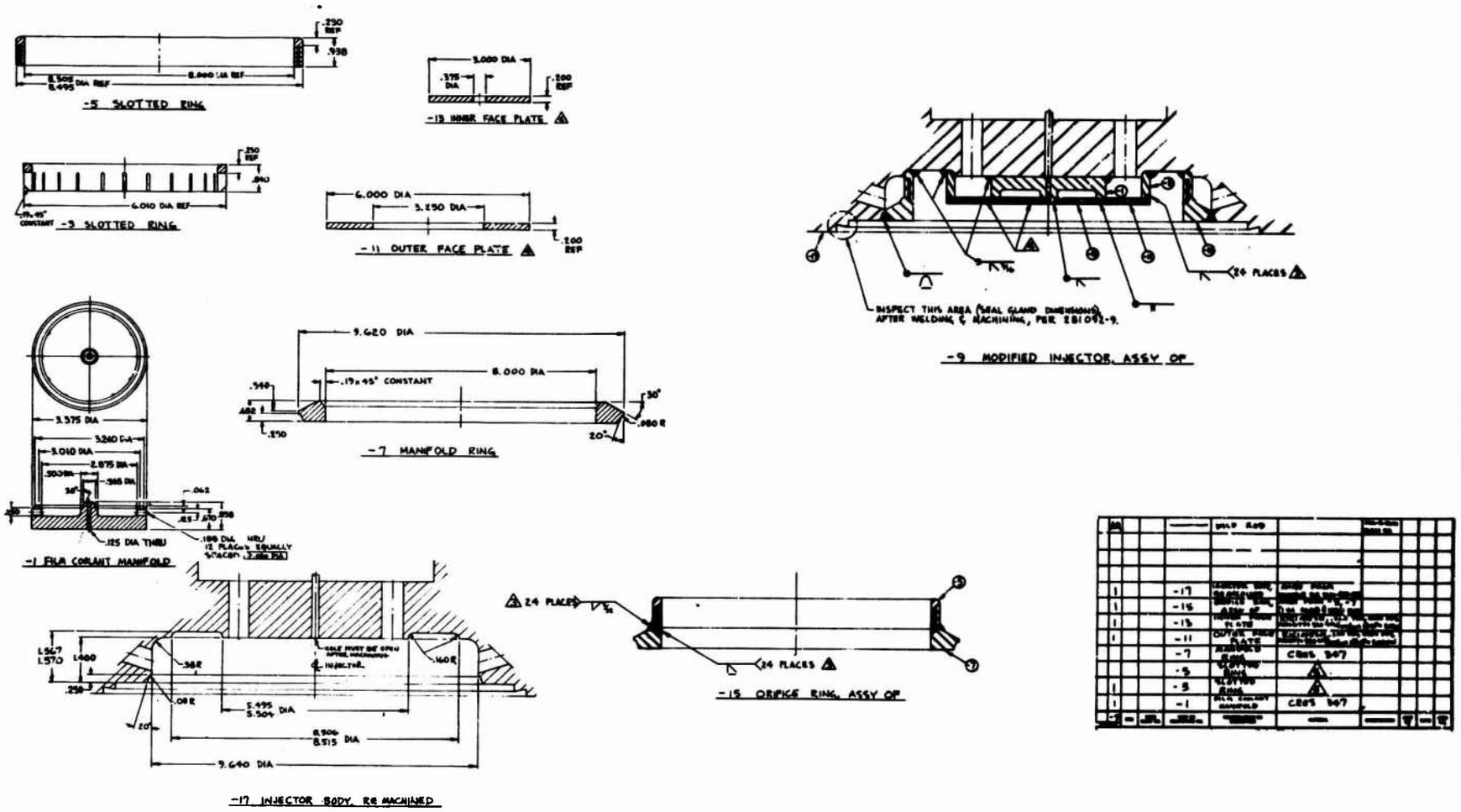

Figure VI-E-8

Book One

Vortex Injector with Porous Face

FEATURES	ORIGINAL DESIGN	INJECTOR MODIFICATION NUMBER I	II	
A. INJECTOR ELEMENT				
1. Basic element configuration	Recessed face	Recessed face	Recessed face	NOTES: ⚠1 Values shown are calculated values obtained from test data during the uncooled chamber program injector evaluation tests.
2. Momentum ratio				
a. Actual	3.32			
b. Designed	2.2	2.2	2.2	
3. Inner oxidizer element				
a. Type	Radial slots	Tangential slots	Radial slots	
b. No slots	24	24	24	⚠2 L* was 70 inches total on this test. All other tests used 100 inches total L*
c. Slot length	.688	.688	.688	
d. Slot width	.107	.093	.107	
e. Velocity (ft/sec)	109	121.0	108	
f. K_{wo} *	5.30	5.74	6.60	
4. Outer fuel element				Nominal design points for this injector was: MR 2:1 momentum ratio 2.2
a. Type	Tangential slots	Tangential slots	Tangential slots	
b. No. slots	24	24	24	
c. Slotllength	.080	.080	.080	
d. Slot width	.688	.688	.688	
e. Velocity (ft/sec)	87.6	105.0	87.6	
f. K_{we}*	4.36	4.36	4.22	
B. INNER INJECTOR FACE AREA				
1. Basic protective device	Ablative cap held in place with epoxy	Ablative cap held in place with cap screws.	Ablative cap steel reinforced screwed in place	
C. OUTER INJECTOR FACE AREA				
1. Basic protective device	None	None	None	
D. L* LINER MATERIAL	Atj. graphite	Ablative line	Ablative line	
E. INJECTOR PERFORMANCE ⚠2	94.9 ⚠1	No valid steady state information was obtained.	No valid steady state information was obtained.	
F. TYPE OF FAILURE	A. Ablative face cap. destroyed B. Erosion of oxidizer ring.	Gas generator malfunction & L* graphite liner eroded	Ablative ox. center cap failed on start & eroded in premix chamber	

* As Determined by Hydrotest

Vortex Injector Design Data Summary (u)

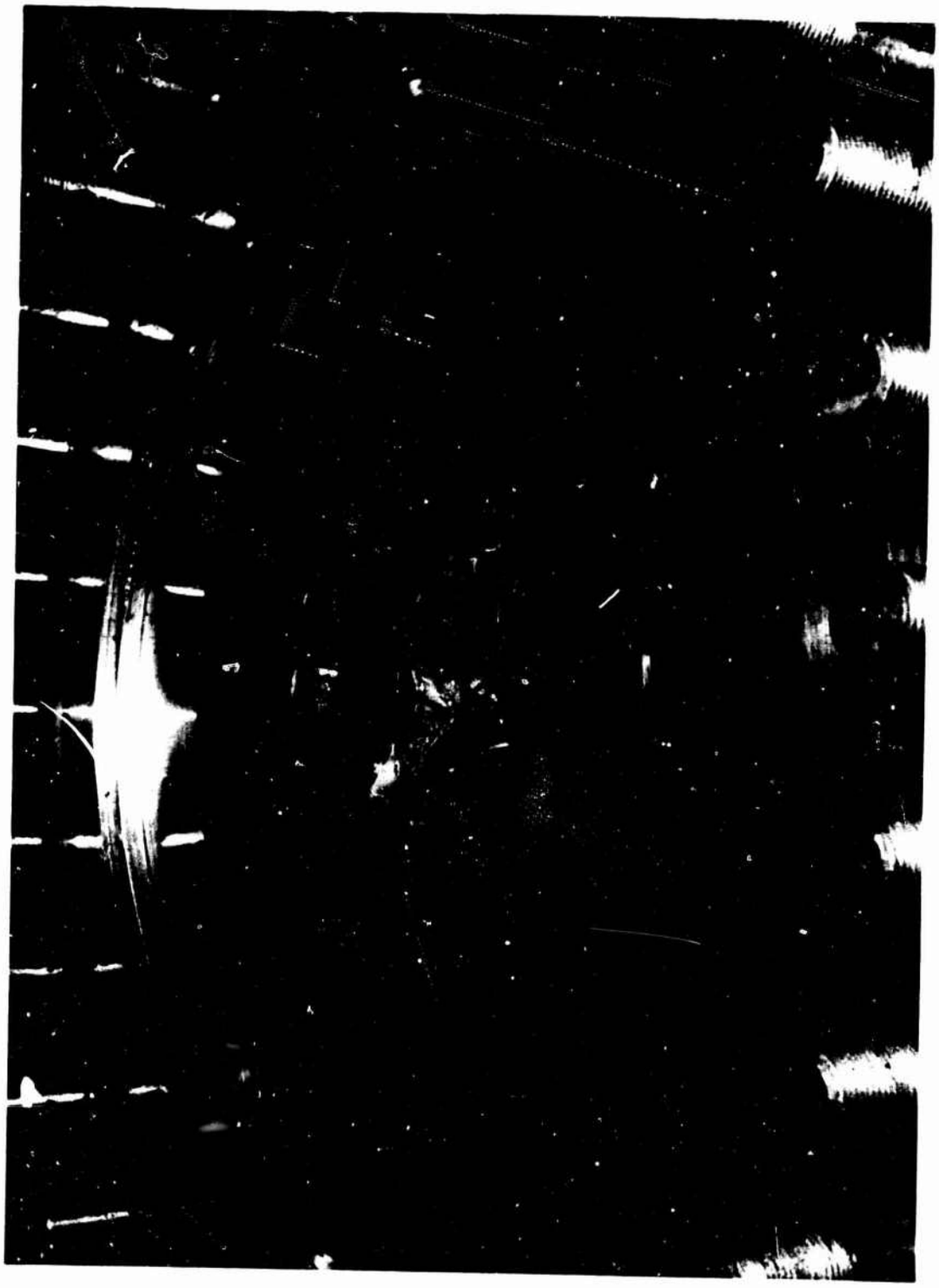

Vortex Injector, Original Design, Posttest Condition (u)

Figure VI-B-10

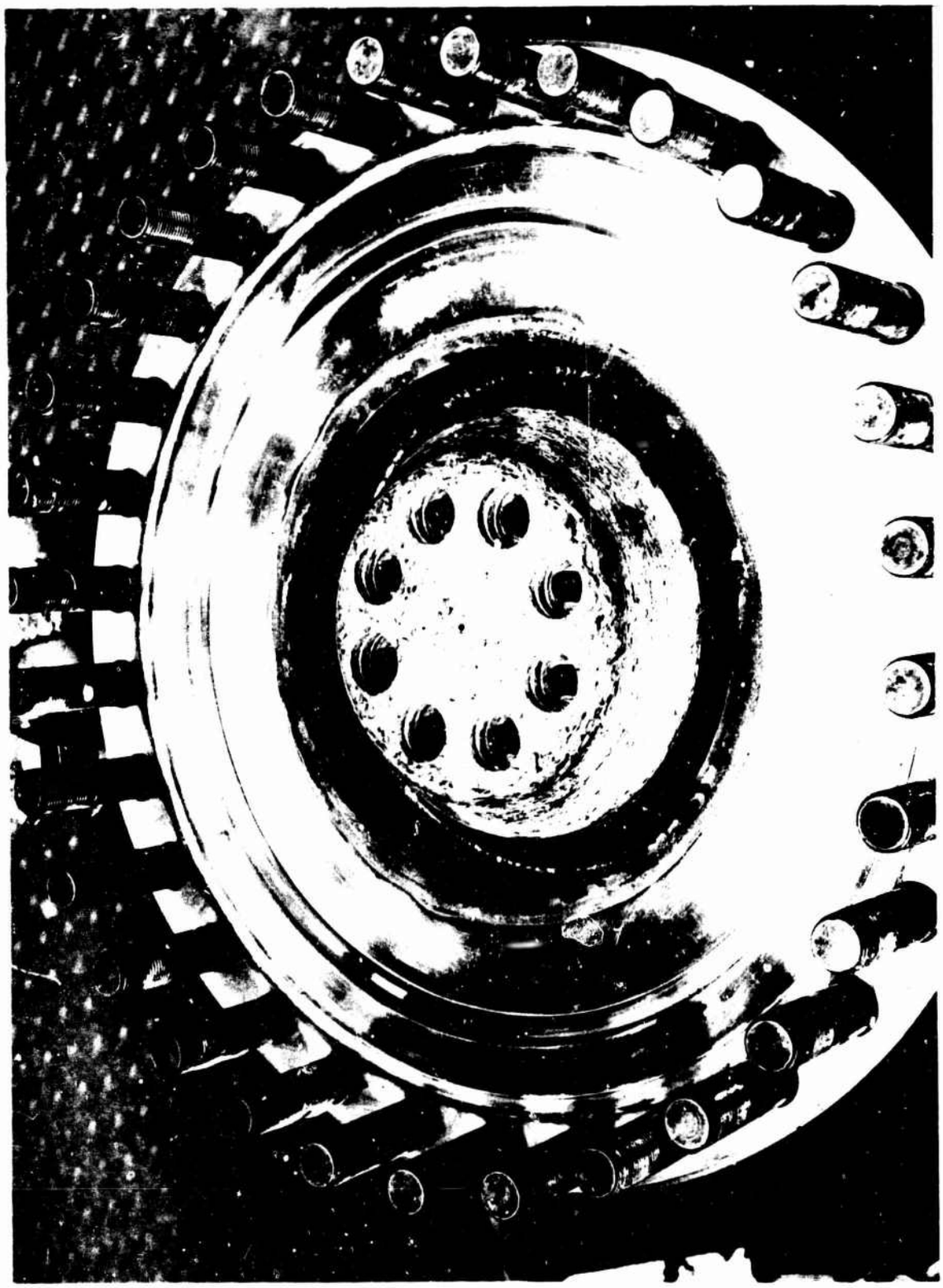

Mod 1 Vortex Injector, Pretest Condition

Figure VI-B-11

Mod 1 Vortex Injector, Posttest Condition

Figure VI-B-12

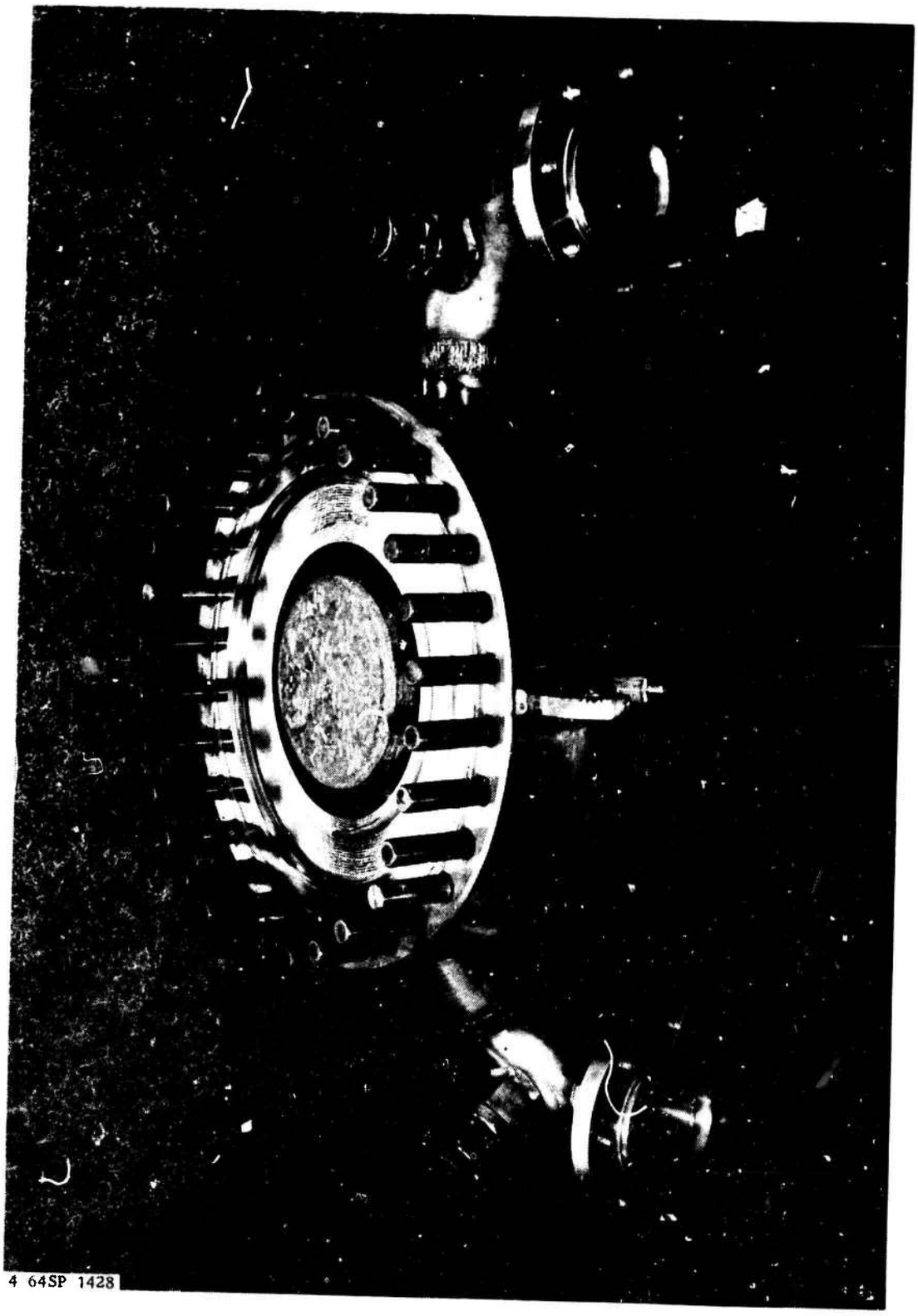

Mod 2 Vortex Injector, Pretest Condition

Figure VI-B-13

Mod 2 Vortex Injector, Closeup View, Pretest Condition

Figure VI-B-14

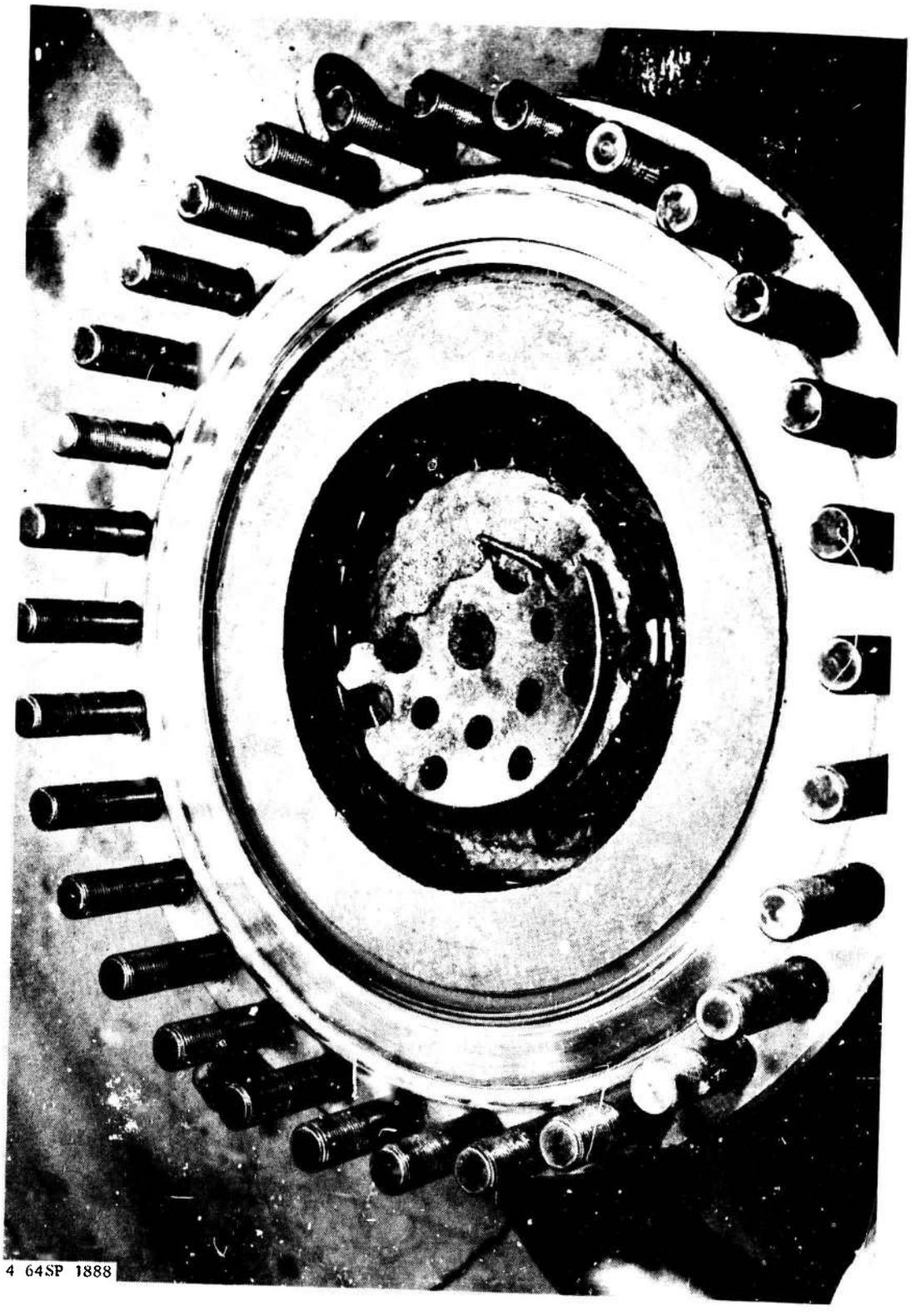

Mod 2 Vortex Injector, Posttest Condition

Figure VI-B-15

Mod 2 Vortex Injector, Closeup View, Posttest Condition

Figure VI-B-16

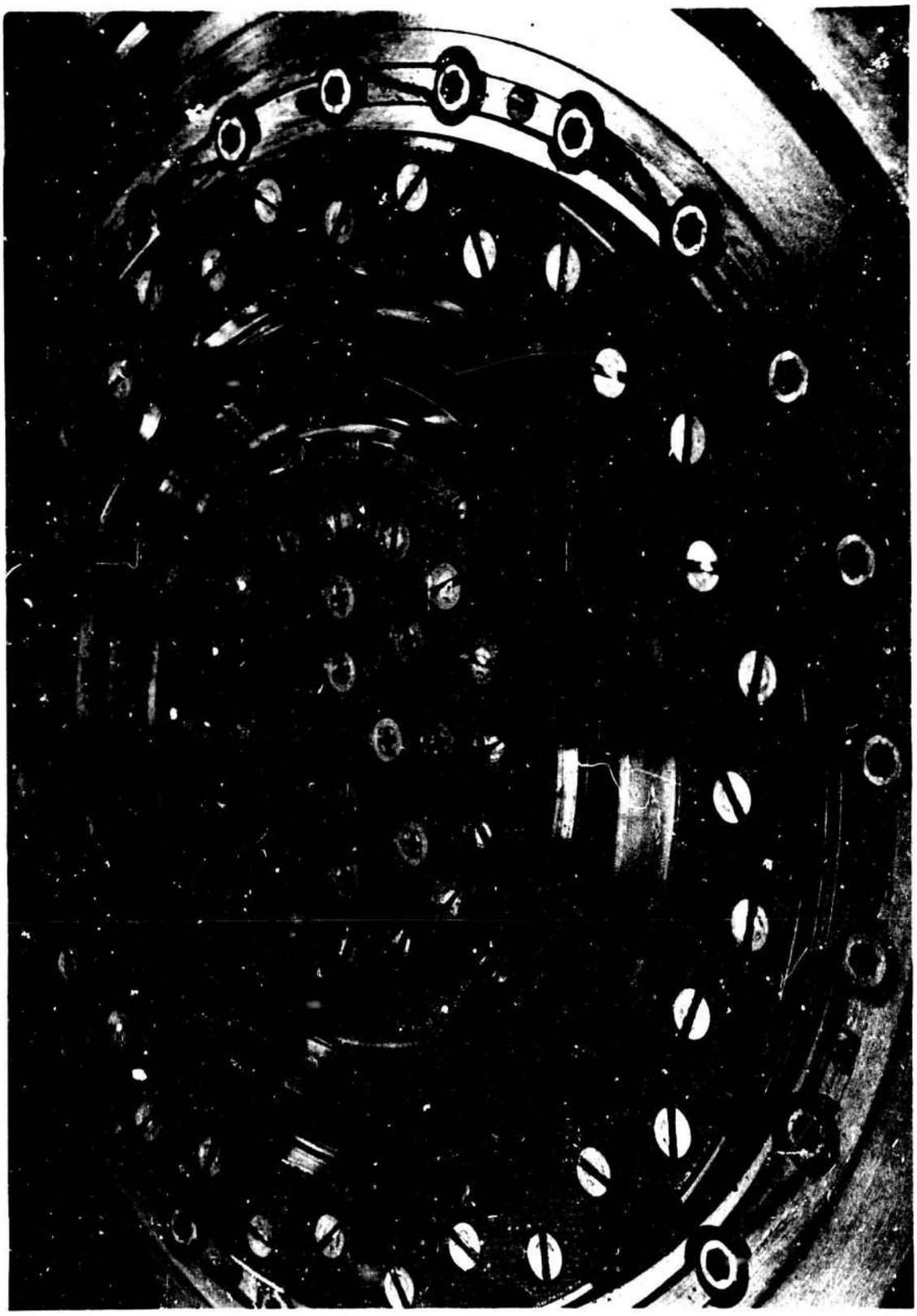

Improved Concentric Ring Injector

Figure VI-B-17

MANUF. NO. NUMBER	ORIGINAL	I	II	III	IV	V	VI	VII	VIII
FEATURE									
A. INJECTOR ELEMENT									
1. BASIC ELEMENT CONFIGURATION	RECESSED FACE	RECESSED FACE CERAMIC	RECESSED FACE-COATED	RECESSED FACE-COATED	RECESSED FACE-COATED	PROTRUDING ORIFICE	PROTRUDING ORIFICE	PROTRUDING ORIFICE	PROTRUDING ORIFICE
2. MOMENTUM RATIO 1	1.55	1.35	1.68	1.47	1.75	1.38	1.69	2.42	2.84
3. INNER ORIFICER ELEMENT:									
A. SLOT WIDTH	.0800	.0630	.080	.080	.080	.040	.040	.080	.040
B. TYPE	ANNULAR SLOTS	ANNULAR SLOTS	ANNULAR RING	ANNULAR RING	ANNULAR RING	ANNULAR RING	ANNULAR RING	ANNULAR RING	ANNULAR RING
C. VELOCITY (FT/SEC) 1	139	119	119	100	111	115	139	134	139
4. OUTER ORIFICER ELEMENT									
A. SLOT WIDTH	.0424	.0424	.041	.041	.041	0.84	0.88	0.88	0.080
B. TYPE	ANNULAR SLOTS	ANNULAR SLOTS	ANNULAR RING	ANNULAR RING	ANNULAR RING	ANNULAR RING	ANNULAR RING	ANNULAR RING	ANNULAR RING
C. VELOCITY (FT/SEC) 1	139	119	119	100	111	115	139	134	139
5. ORIFICER K_M 3	10.35	10.9	8.21	8.21	7.86	7.39	7.39	7.16	7.14
6. FUEL ELEMENT:									
A. SLOT WIDTH	.080	.072	.072	.072	.072	.070	.070	.070	.070
B. TYPE	ANNULAR RING	ANNULAR RING	ANNULAR RING	ANNULAR RING	ANNULAR RING	ANNULAR RING	ANNULAR RING	ANNULAR RING*	ANNULAR RING
C. VELOCITY (FT/SEC) 1	135	147	97	121	121	139	137	89	89
D. FUEL K_M 3	9.36	9.17	6.88	6.88	5.99	5.74	5.74	5.74	5.91
B. OUTER INJECTOR FACE AREA									
1. BASIC PROTECTIVE DEVICE	ATJ GRAPHITE	ABLATIVE	COATING & ABLATIVE	ABLATIVE & STEEL REINFORCED	RIGIMESH-FLAT FACE	RIGIMESH-FLAT FACE	RIGIMESH-FLAT FACE	RIGIMESH-45° CONE	RIGIMESH-FLAT FACE & FILM COOLING
2. RIGIMESH DATA:									
A. FLOW RATE, (LB/SEC-H_2O_4)	NONE	NONE	NONE	NONE	2.0	14.1	14.1	38.2	14.1
B. %TOTAL H_2O_4 FLOW	NONE	NONE	NONE	NONE	1.8	12.4	12.4	18.4	12.4
3. PERIPHERAL FILM COOLING	NONE	NONE	NONE	NONE	NONE	NONE	NONE	NONE	YES
A. FLOW RATE, (LB/SEC-H_2O_4)	NONE	NONE	NONE	NONE	NONE	NONE	NONE	NONE	3.4
B. % TOTAL H_2O_4 FLOW	NONE	NONE	NONE	NONE	NONE	NONE	NONE	NONE	3.0
C. INNER INJECTOR FACE AREA									
1. BASIC PROTECTIVE DEVICE	ATJ GRAPHITE	ABLATIVE	COATING & ABLATIVE-STEEL REINFORCED	ABLATIVE-STEEL REINFORCED	RIGIMESH-FLAT FACE	RIGIMESH-FLAT FACE	RIGIMESH-FLAT FACE	RIGIMESH-FLAT FACE	RIGIMESH-FLAT FACE
2. RIGIMESH DATA:									
A. FLOW RATE, (LB/SEC-H_2O_4)	NONE	NONE	NONE	NONE	1.6	8.0	8.0	8.0	8.0
B. % TOTAL H_2O_4 FLOW	NONE	NONE	NONE	NONE	1.4	7.0	7.0	7.0	7.0
D. INJECTOR PERFORMANCE (NOMINAL)	93.6 2	94.0	95.0	95.4	97.4	92.2	94.7	95.0	98.0
E. TYPE FAILURE	A. ELEMENT EROSION B. FACE EROSION	A. ELEMENT EROSION B. FACE EROSION	ABLATIVE FACE EROSION	A. EROSION OF OUTER ABLATIVE RING B. ELEMENT EROSION	A. RIGIMESH EROSION B. ELEMENT EROSION	PERIPHERAL EROSION OF OUTER ORIFICER RING	PERIPHERAL EROSION OF OUTER ORIFICER RING	PERIPHERAL EROSION OF OUTER ORIFICER RING	NONE

NOTES:

1. VALUES SHOWN ARE CALCULATED VALUES OBTAINED FROM TEST DATA DURING UNCOOLED CHAMBER PROGRAM INJECTOR EVALUATION TESTS. NOMINAL DESIGN POINTS FOR INJECTOR WAS OR 2.1, MOMENT. RATIO 2.0, INJECTION VELOCITY (ALL BASIC ELEMENTS/INJECTION) 140-130 FT/SEC, W_o = 114 LB/SEC, W_f = 54 LB/SEC
2. L* WAS 70 INCHES TOTAL ON THIS TEST. ALL OTHER TESTS USED 100 INCHES TOTAL L*.
3. VALUES SHOWN ARE CALCULATED FROM HYBRID TEST DATA.

Vortex Injector Design Data Summary (u)

Figure VI-B-18

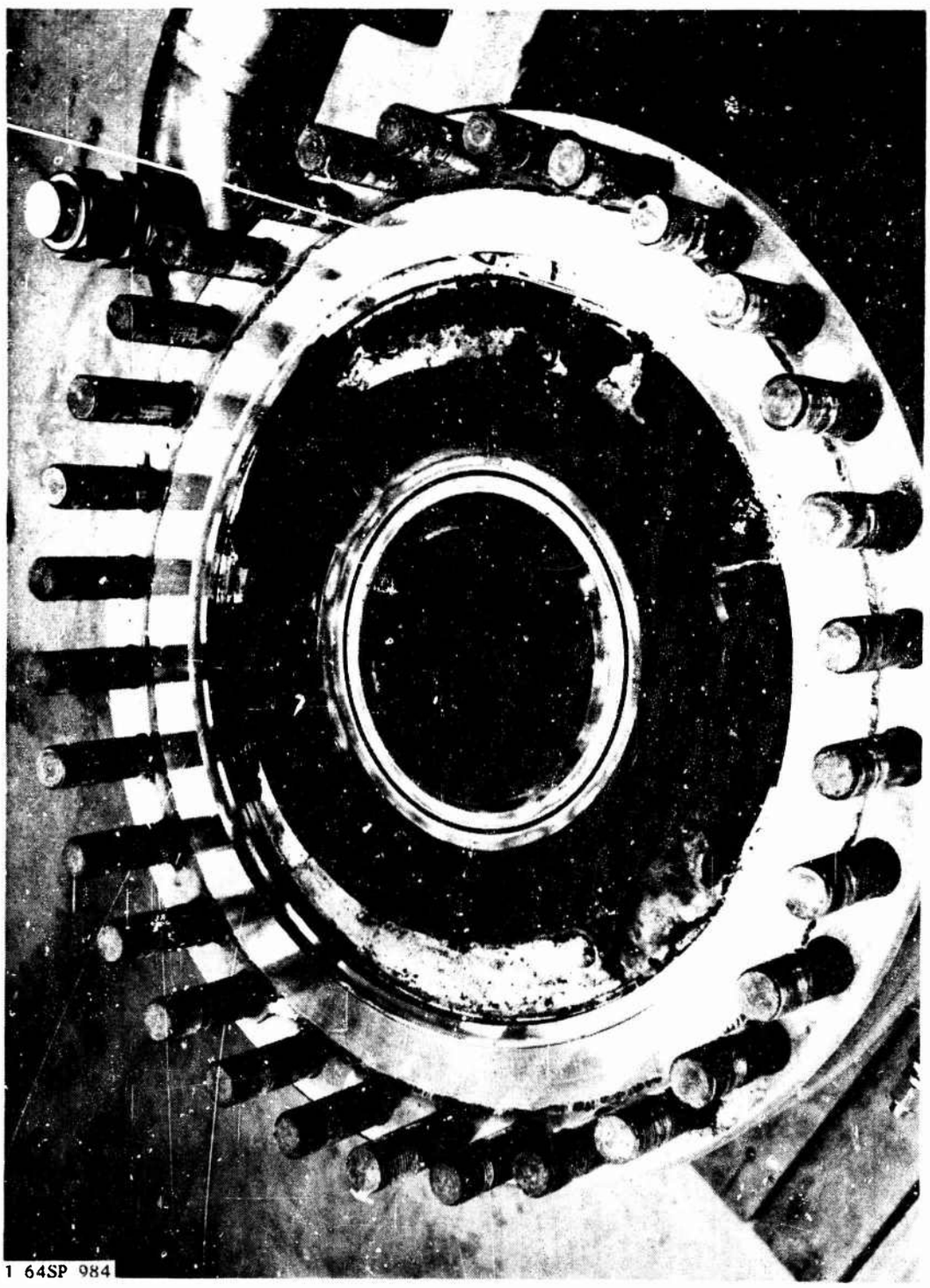

Concentric Ring Injector, Original Design, Posttest Condition

Figure VI-B-19

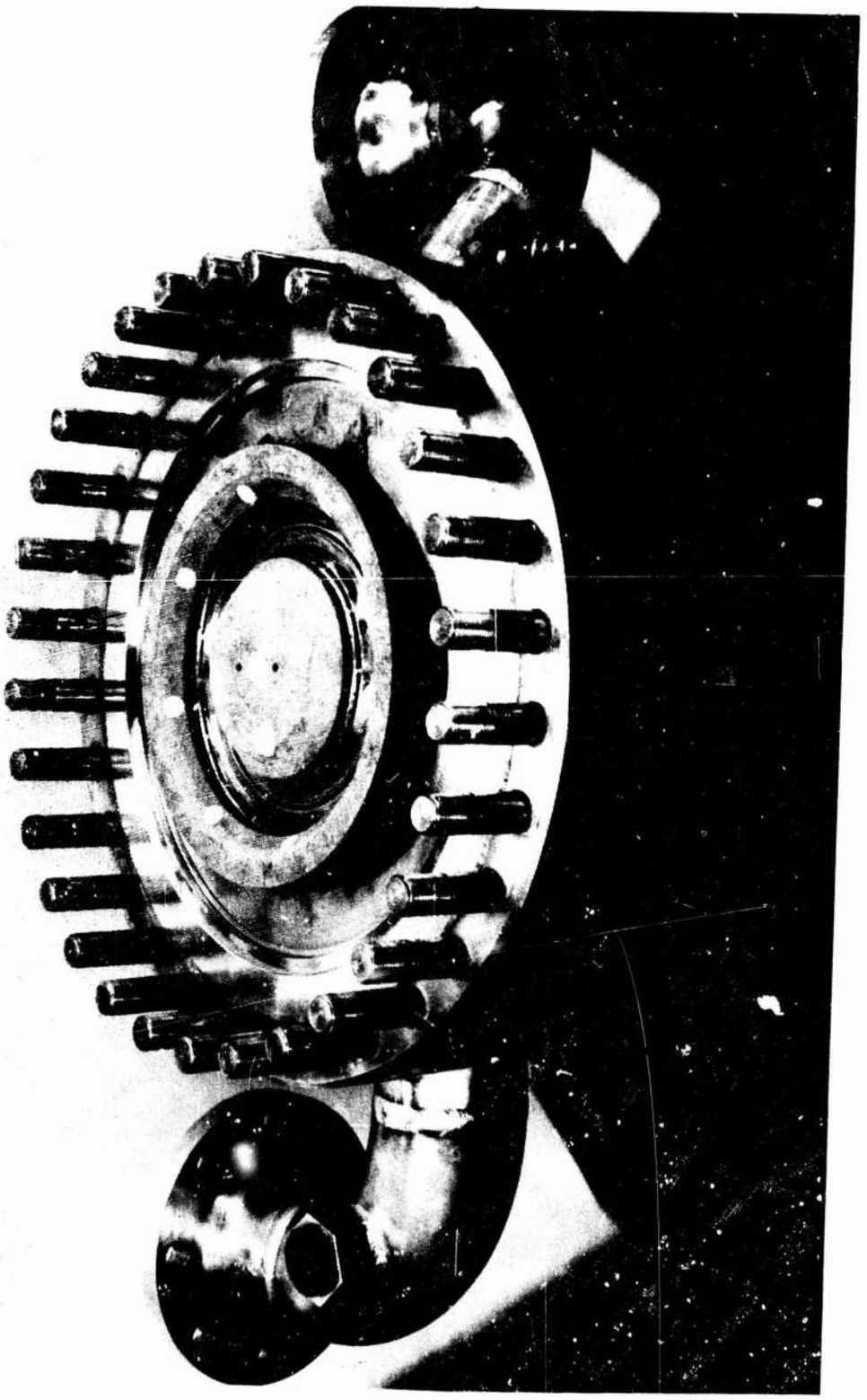

64SP 2765

Mod 1 Concentric Ring Injector, Pretest Condition

Figure VI-B-20

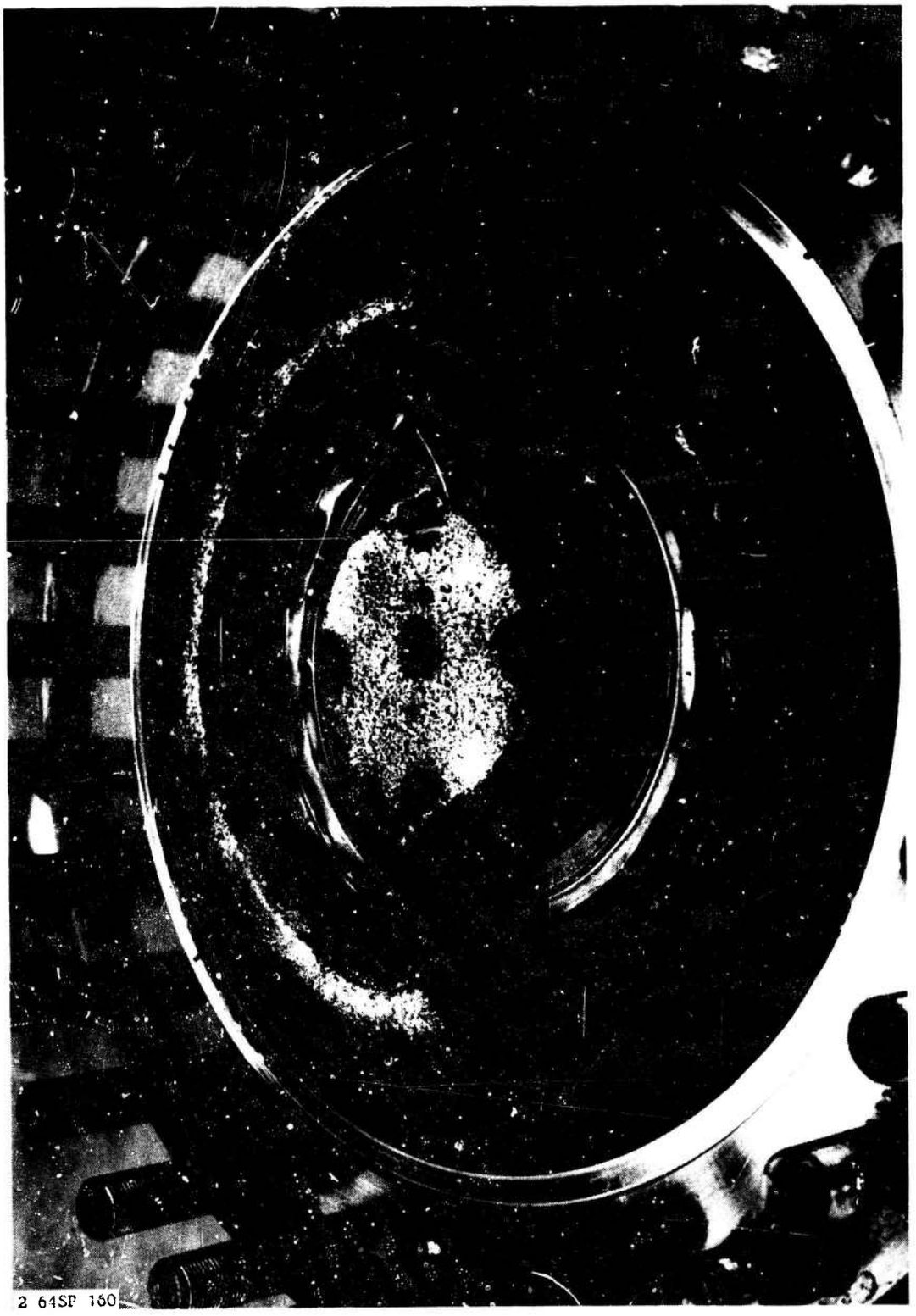

Mod 1 Concentric Ring Injector, Posttest Condition

Figure VI-B-21

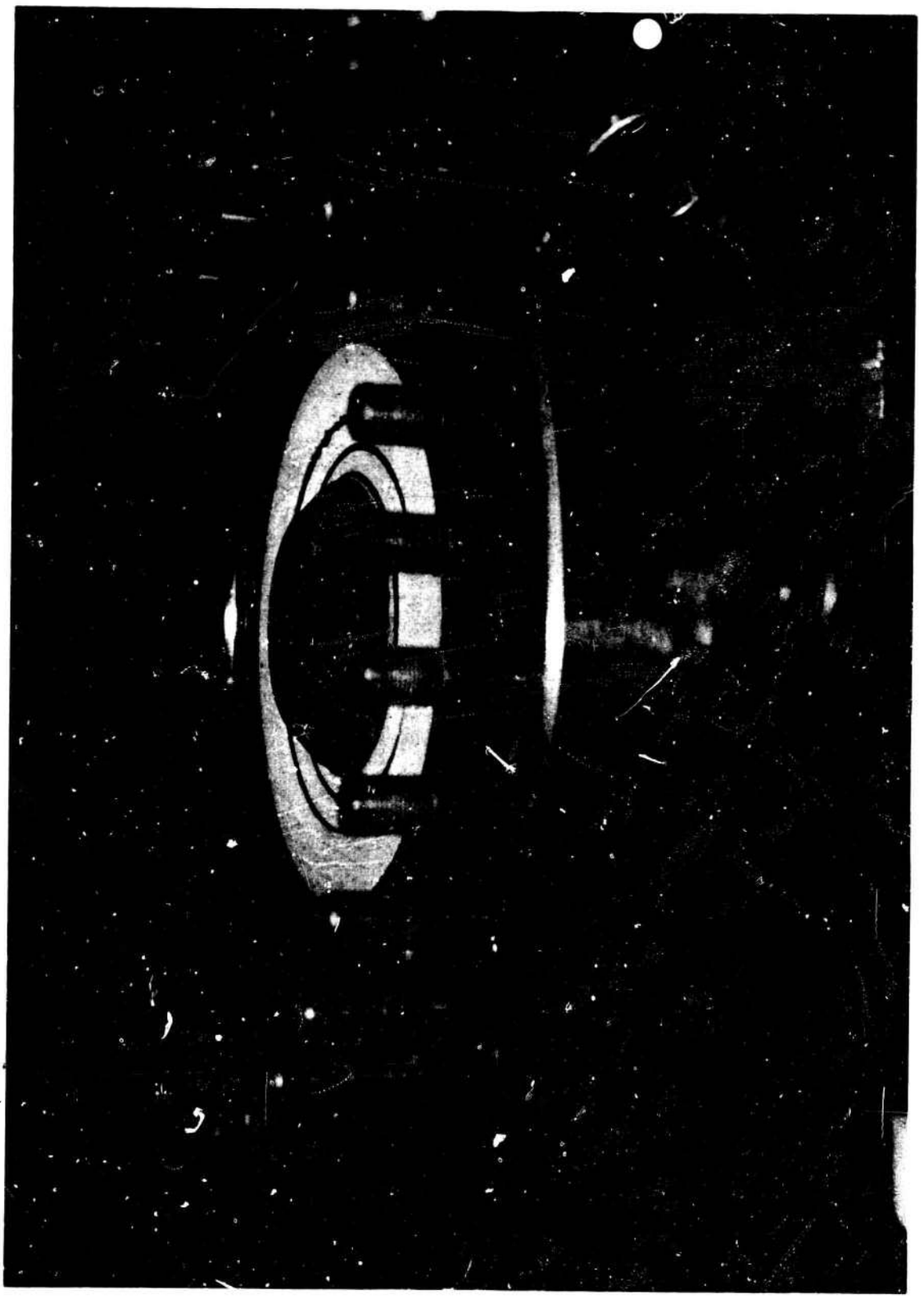

Mod C Concentric Ring Injector, Pretest Condition

Figure VI-B-22

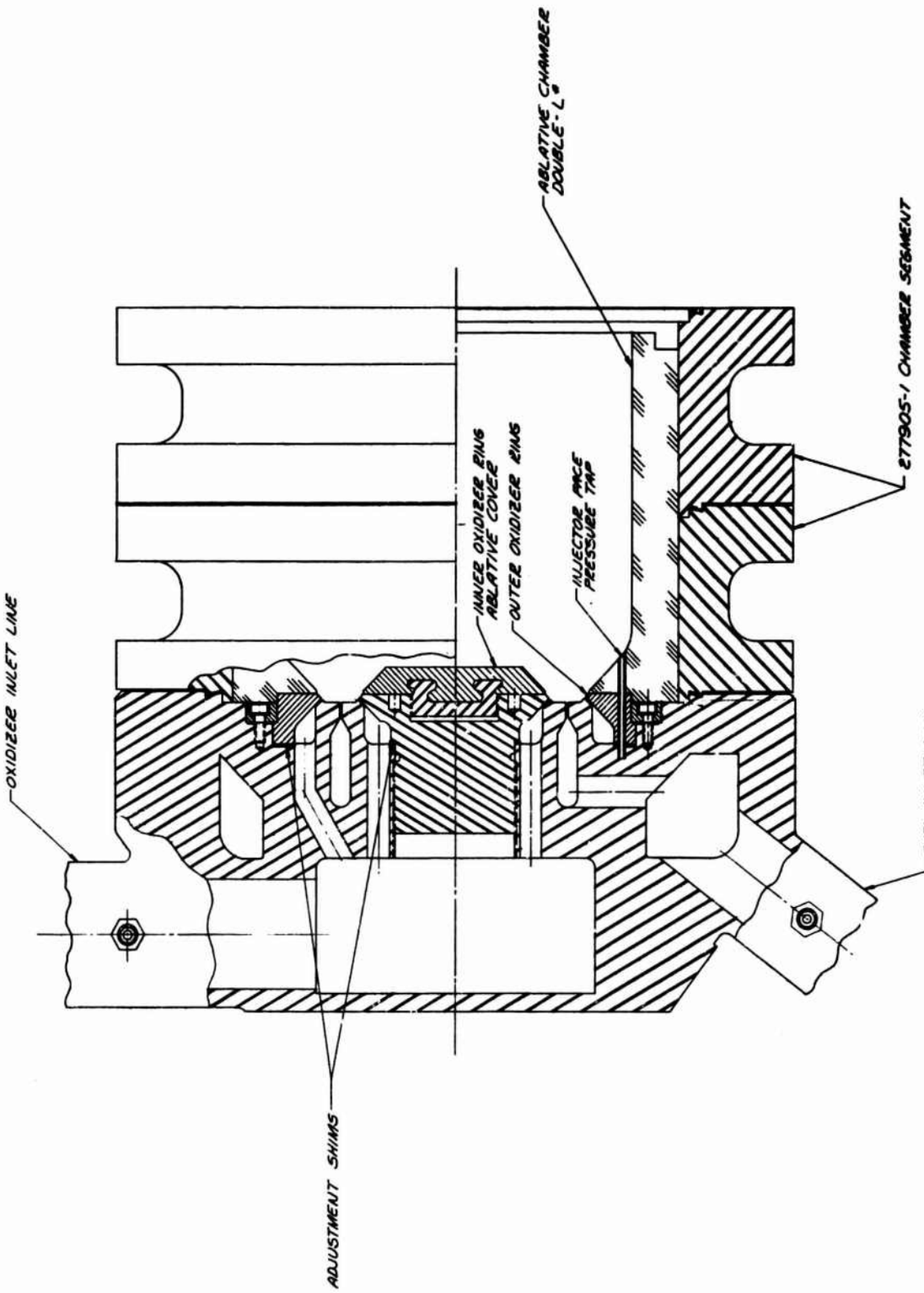

Mod 2 Concentric Ring Injector Design

Figure VI-B-23

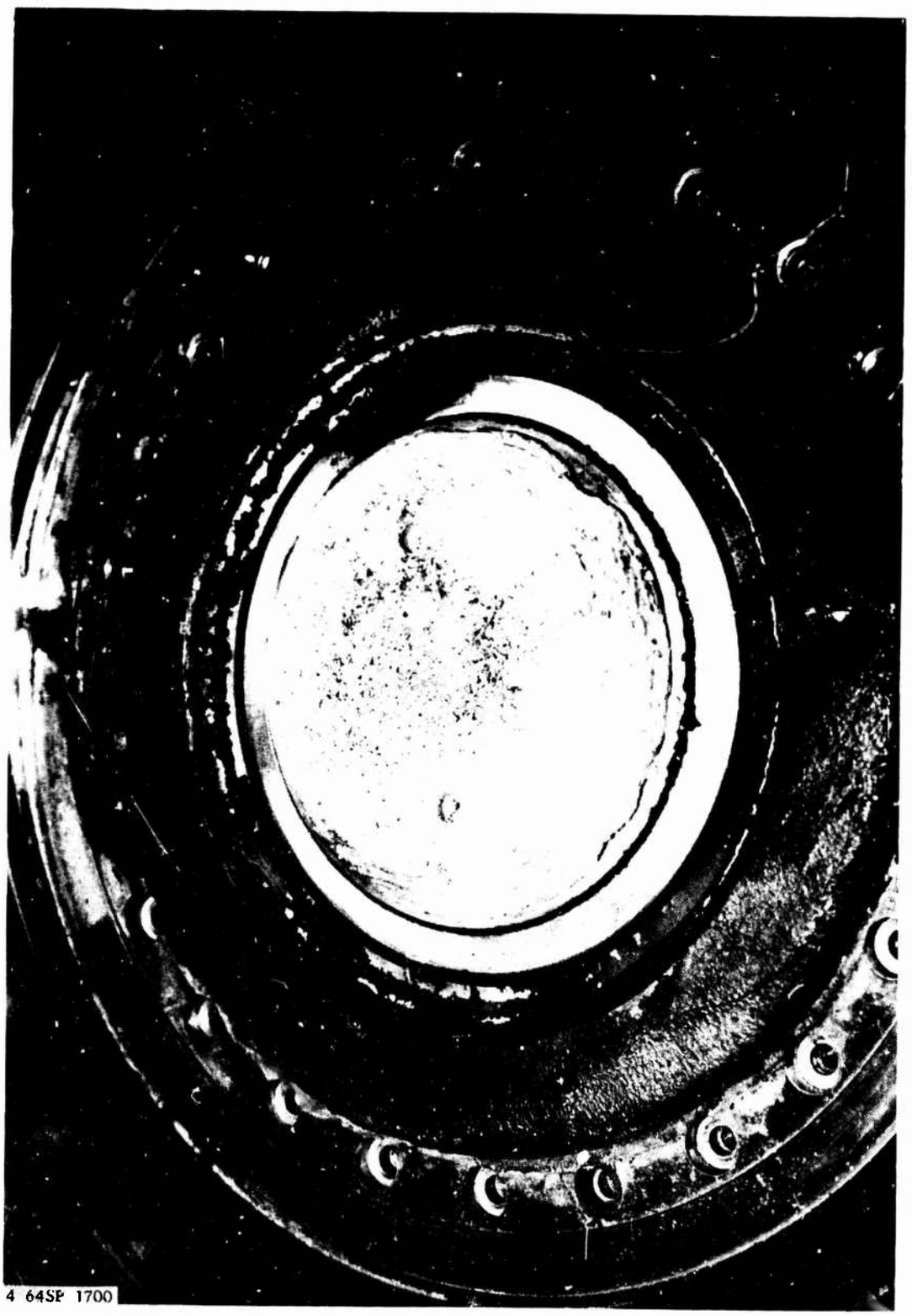

Mod 2 Concentric Ring Injector, Posttest Condition

Figure VI-B-24

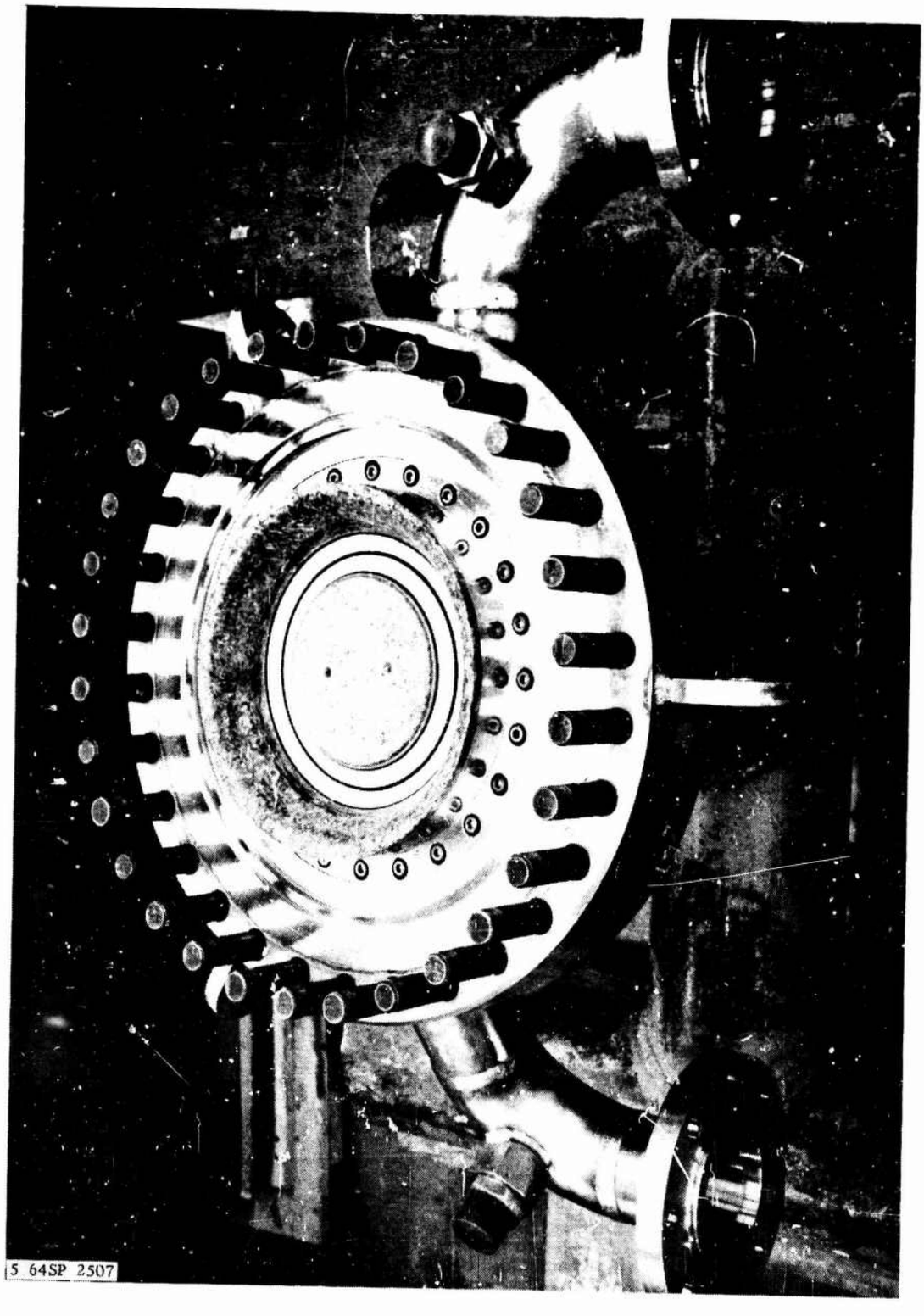

Mod 3 Concentric Ring Injector, Pretest Condition

Figure VI-B-25

Mod 3 Concentric Ring Injector, Posttest Condition

Figure VI-B-26

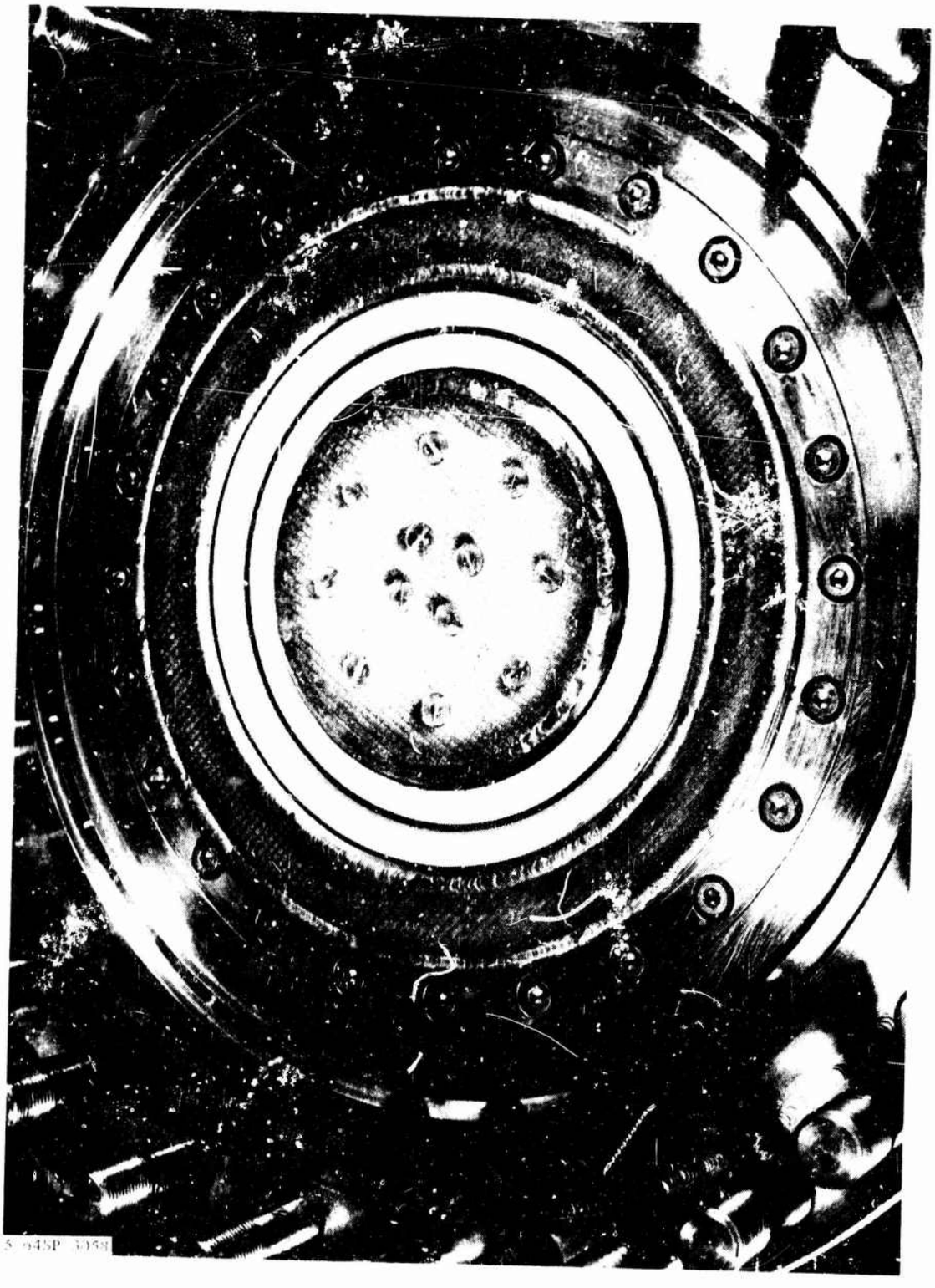

Mod IV Concentric Ring Injector, Pretest Condition

Figure VI-B-27

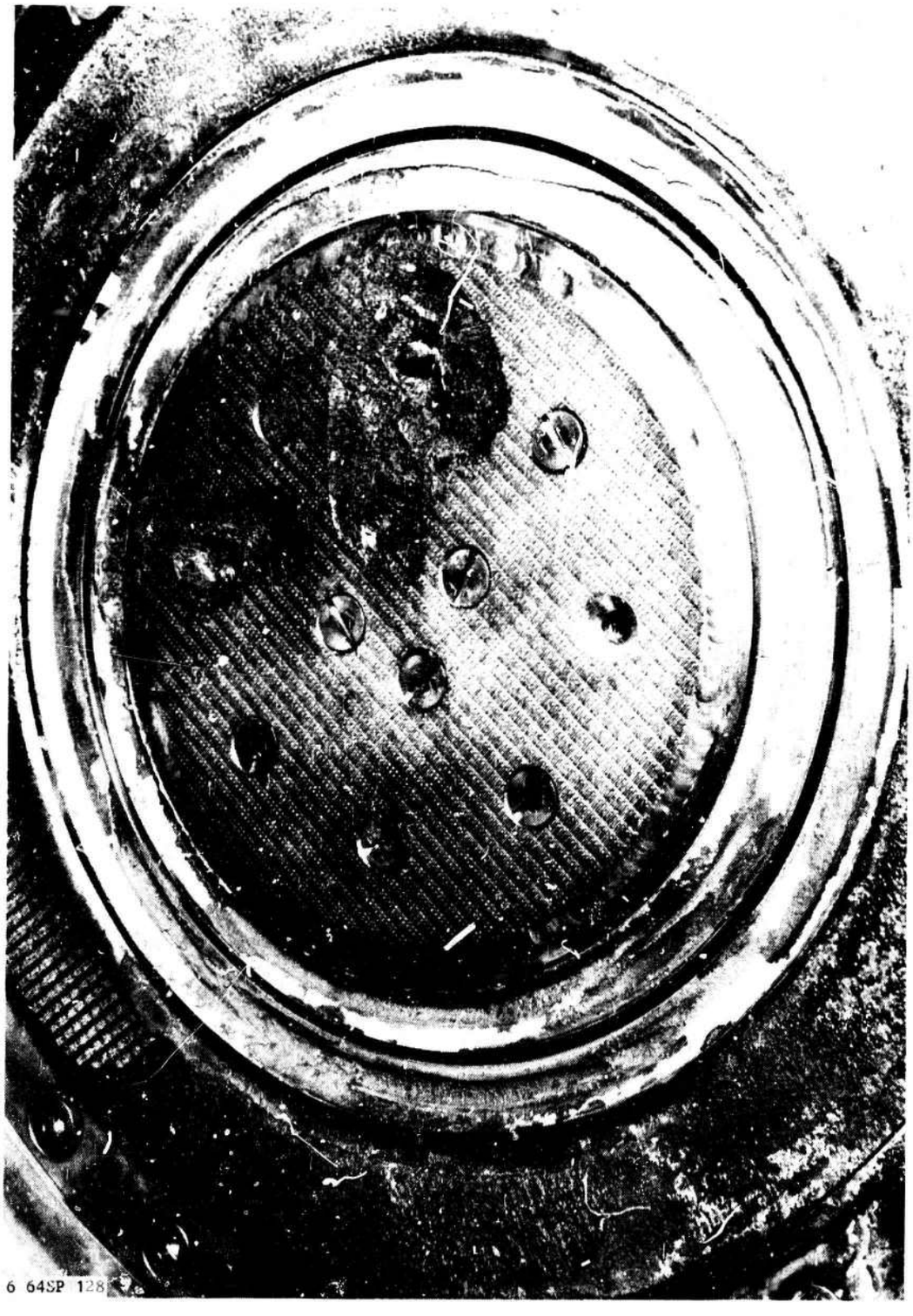

Mod IV Concentric Ring Injector, Posttest Condition

Figure VI-B-28

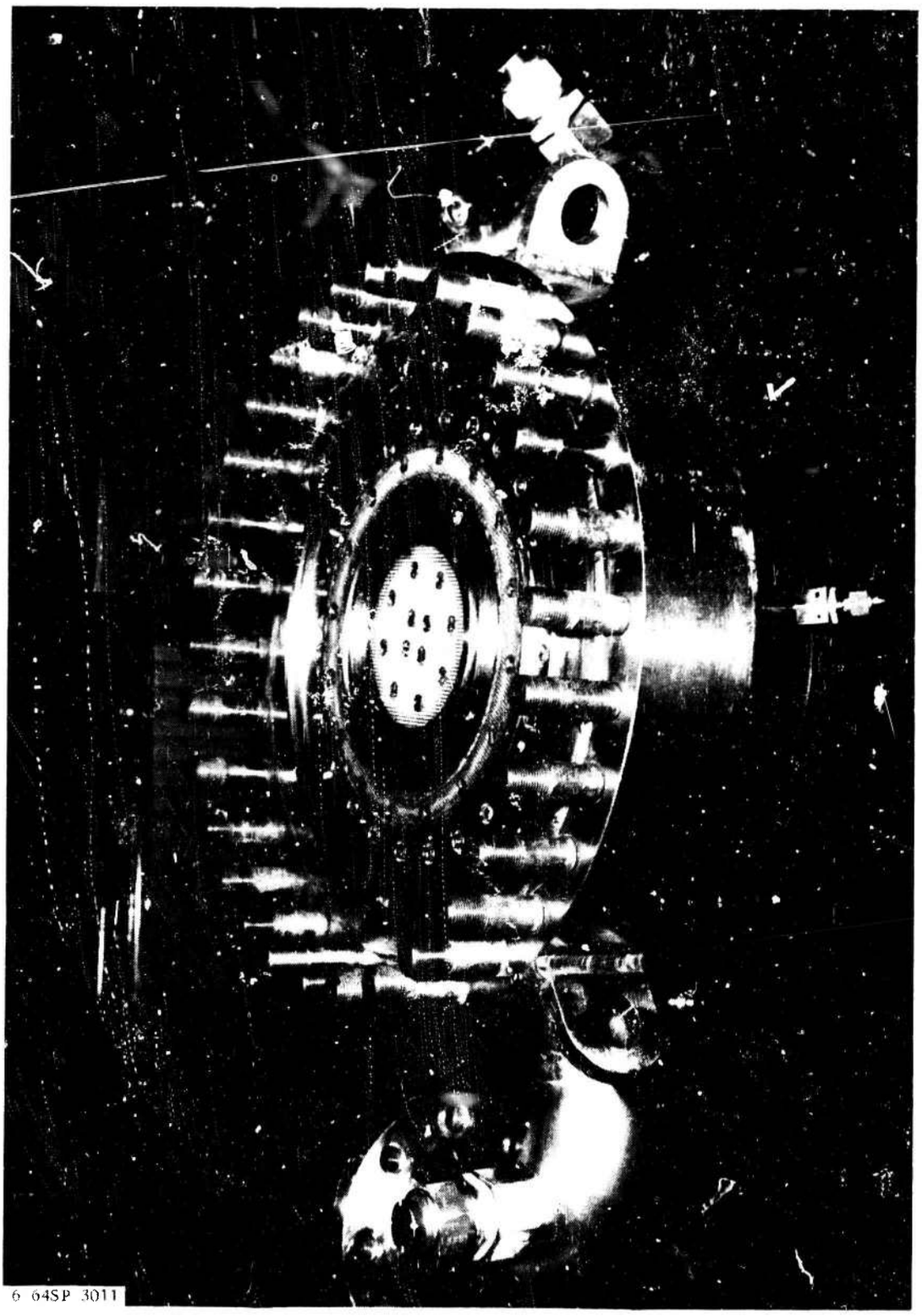

Mod V Concentric Ring Injector, Pretest Condition

Figure VI-B-29

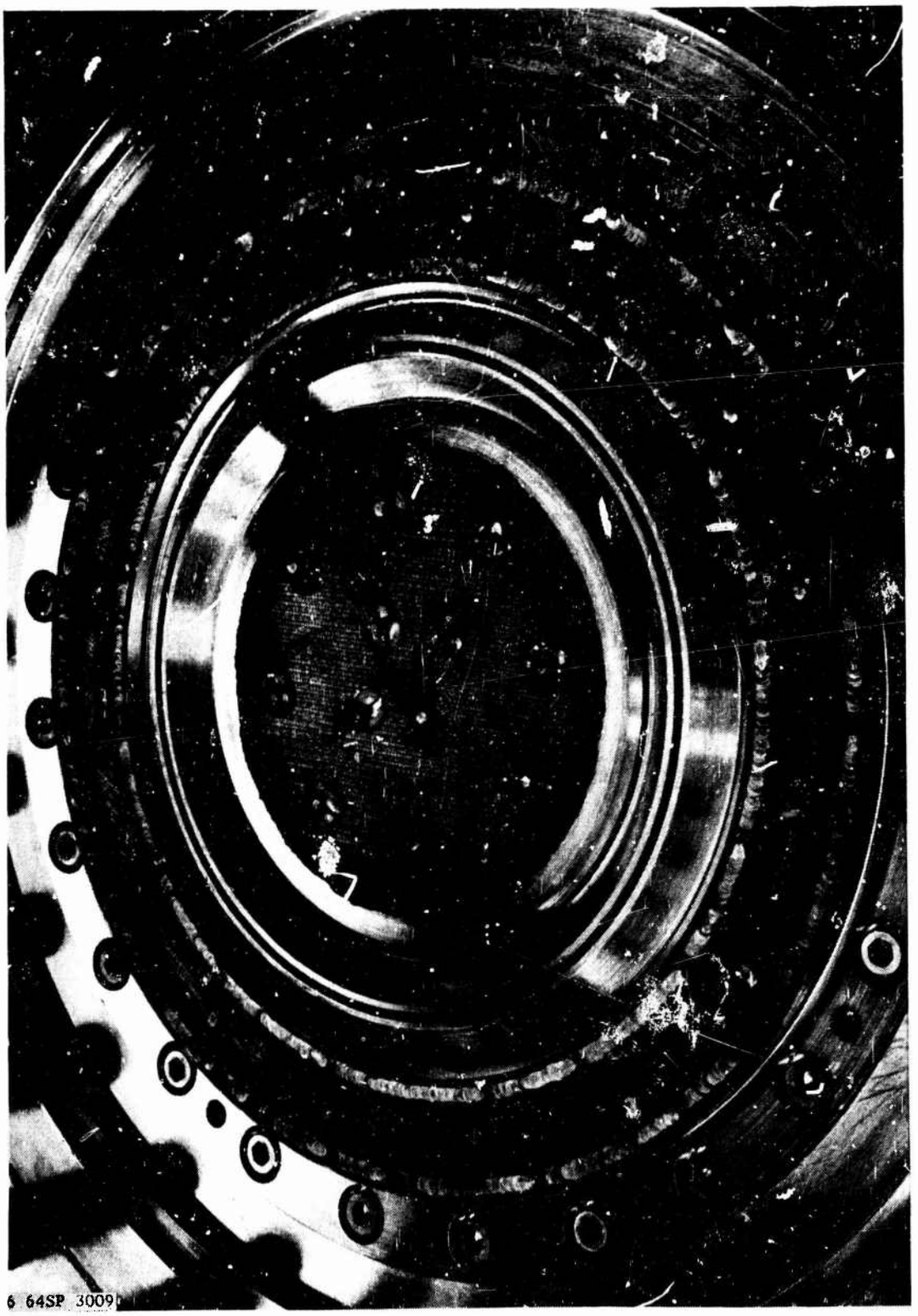

Mod V Concentric Ring Injector, Closeup View, Pretest Condition

Figure VI-B-30

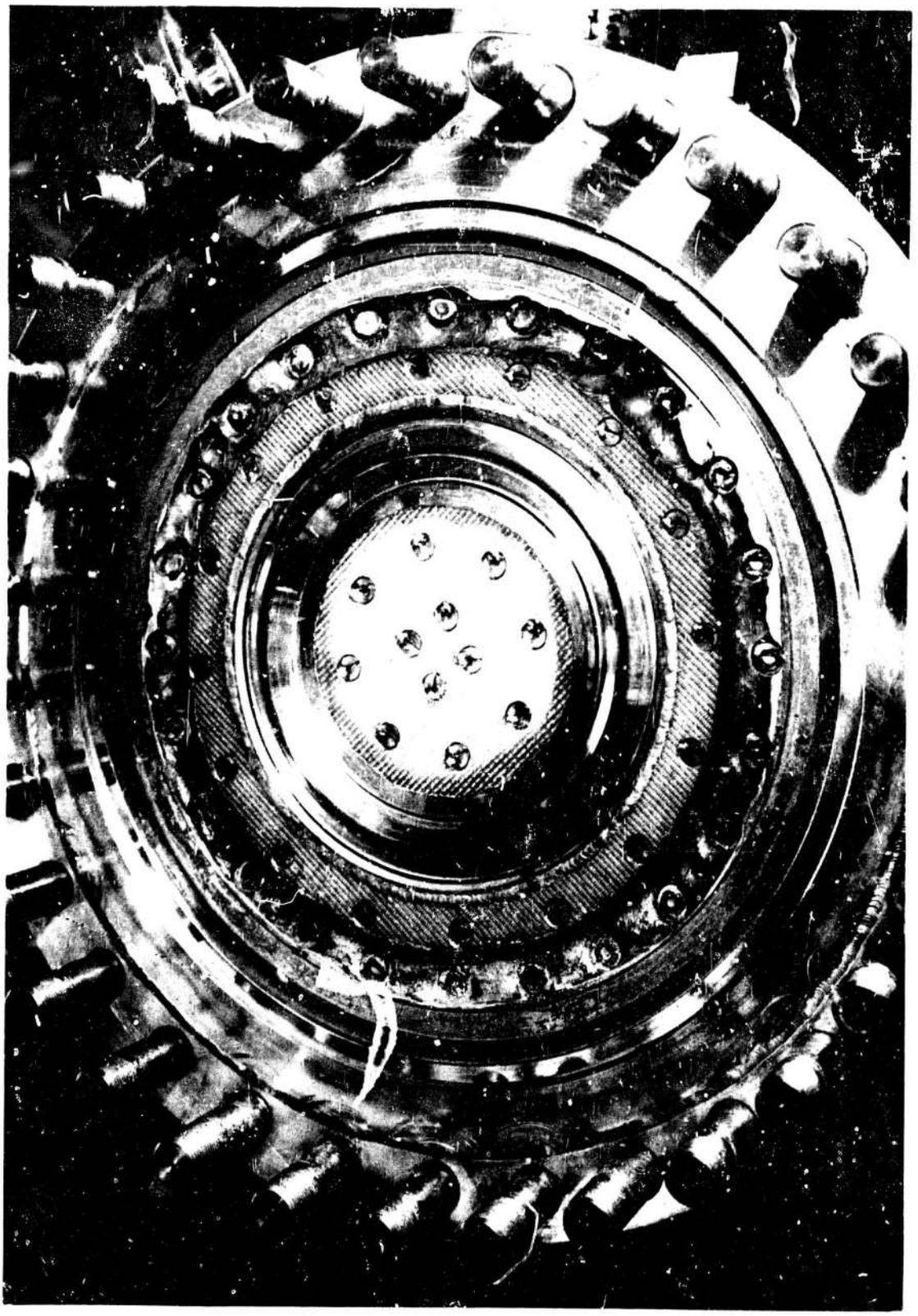

Mod V Concentric Ring Injector, Posttest Condition

Figure VI-B-31

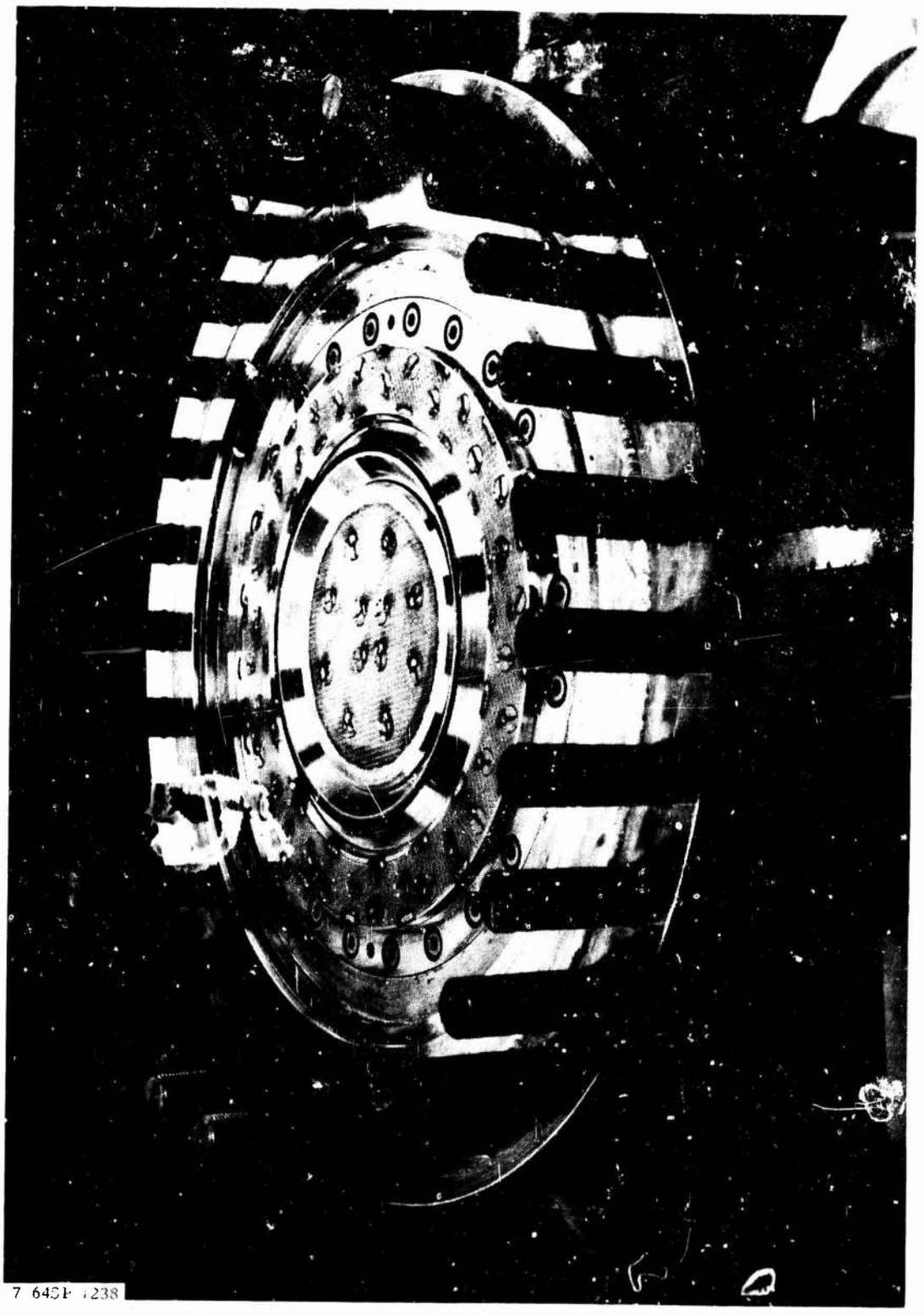

Mod VI Concentric Ring Injector, Pretest Condition

Figure VI-B-32

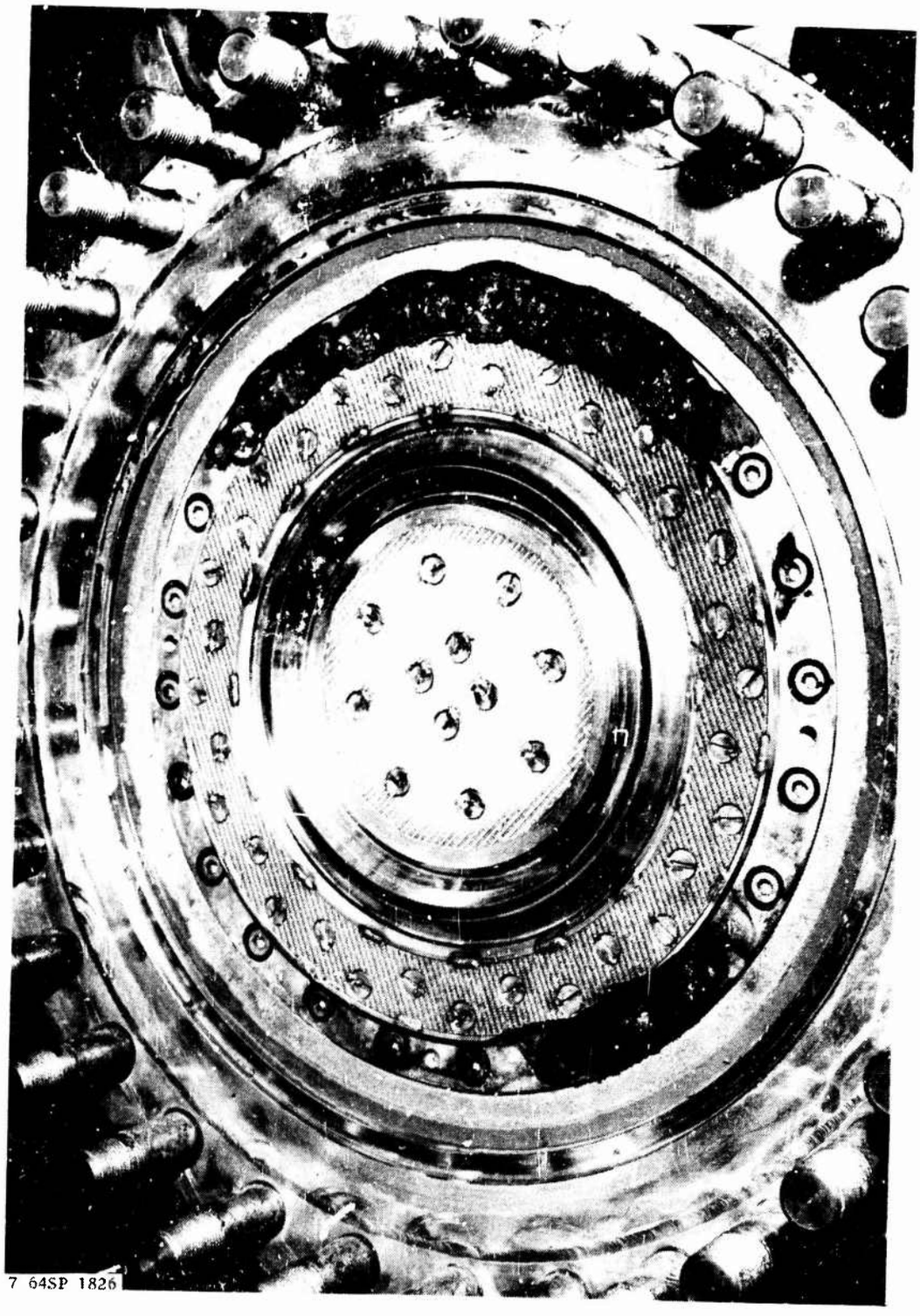

Mod VI Concentric Ring Injector, Posttest Condition

Figure VI-B-33

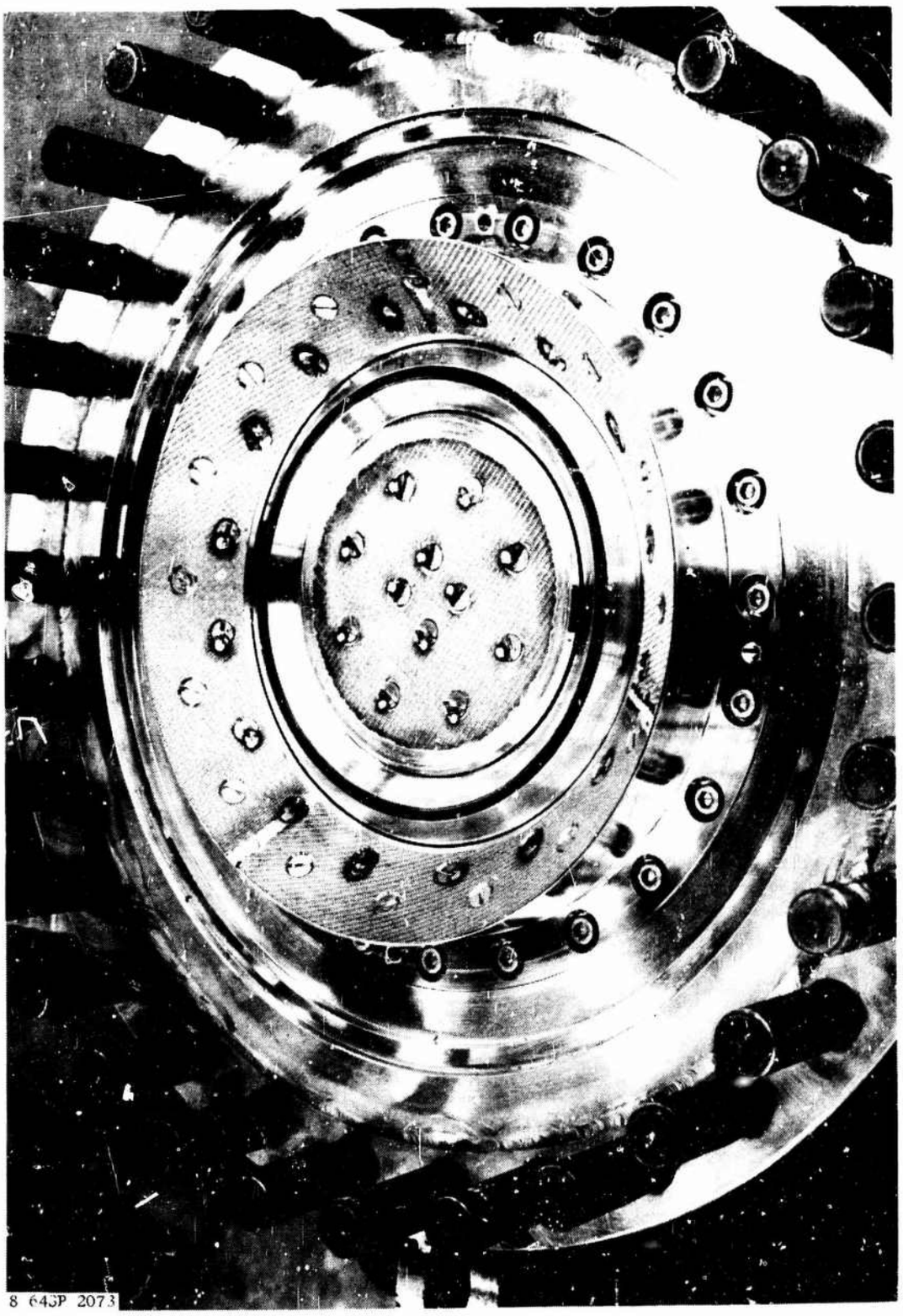

Mod VII Concentric Ring Injector, Pretest Condition

Figure VI-B-34

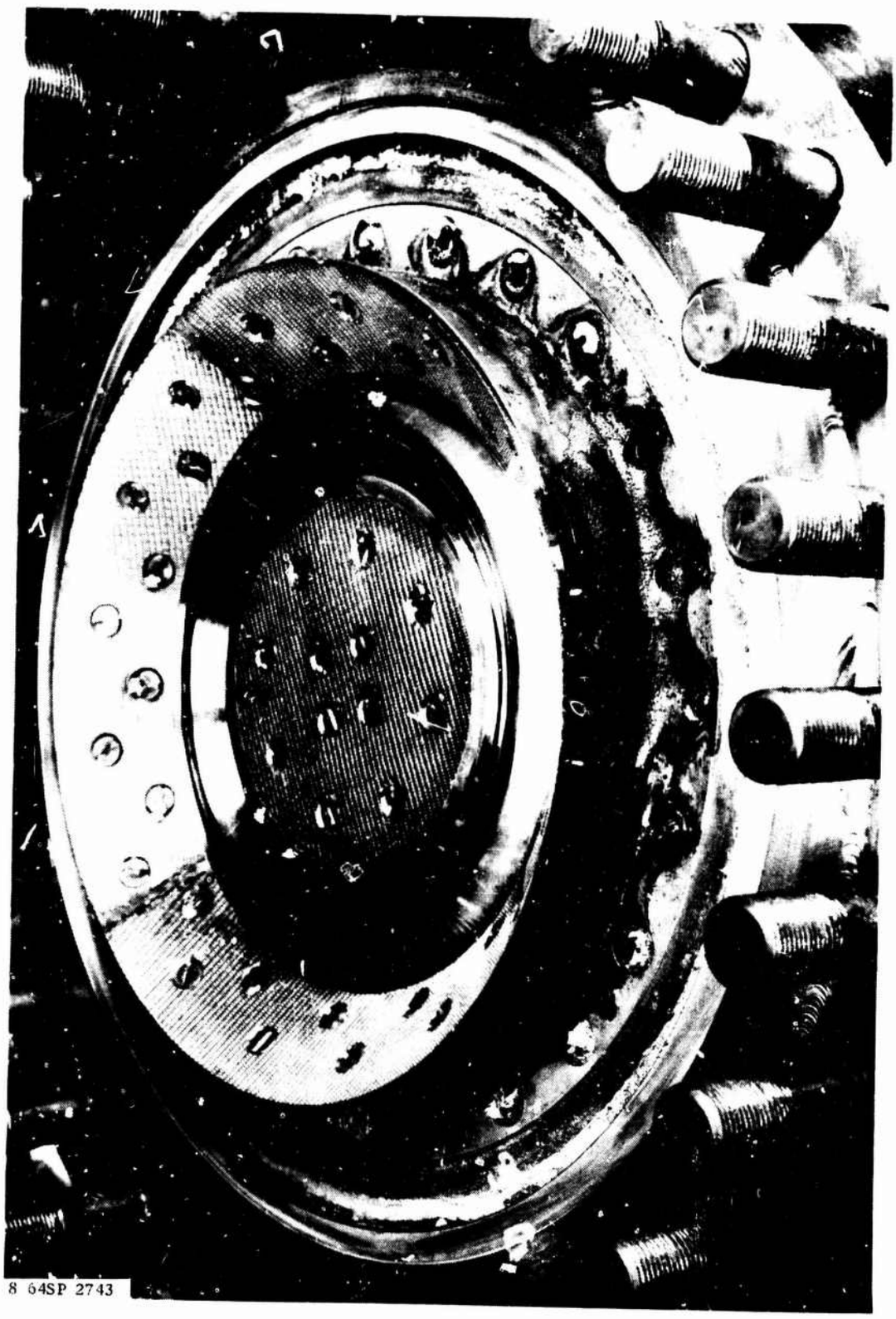

Mod VII Concentric Ring Injector, Posttest Condition

Figure VI-B-35

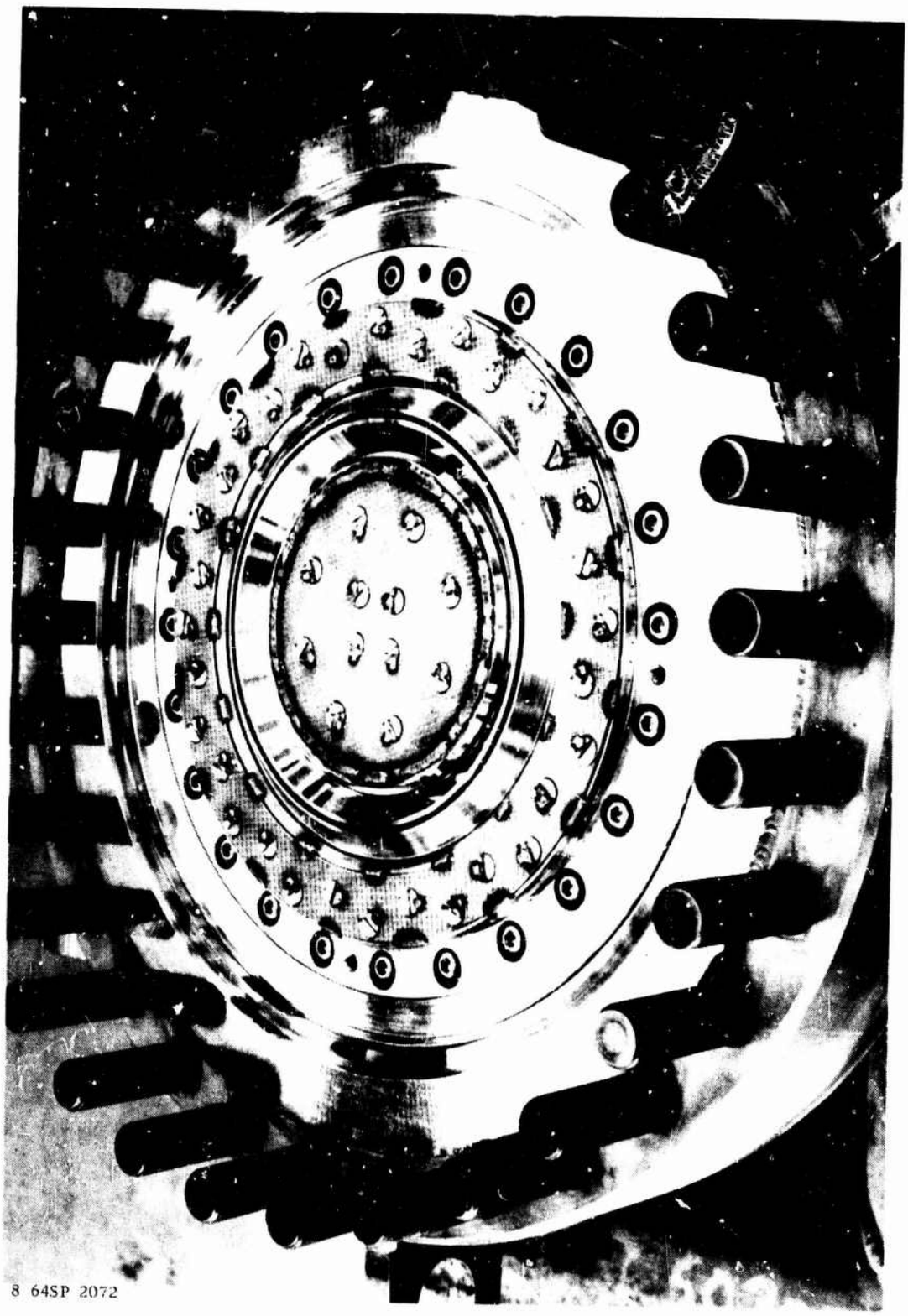

Mod VIII Concentric Ring Injector, Prefire Condition

Figure VI-B-36

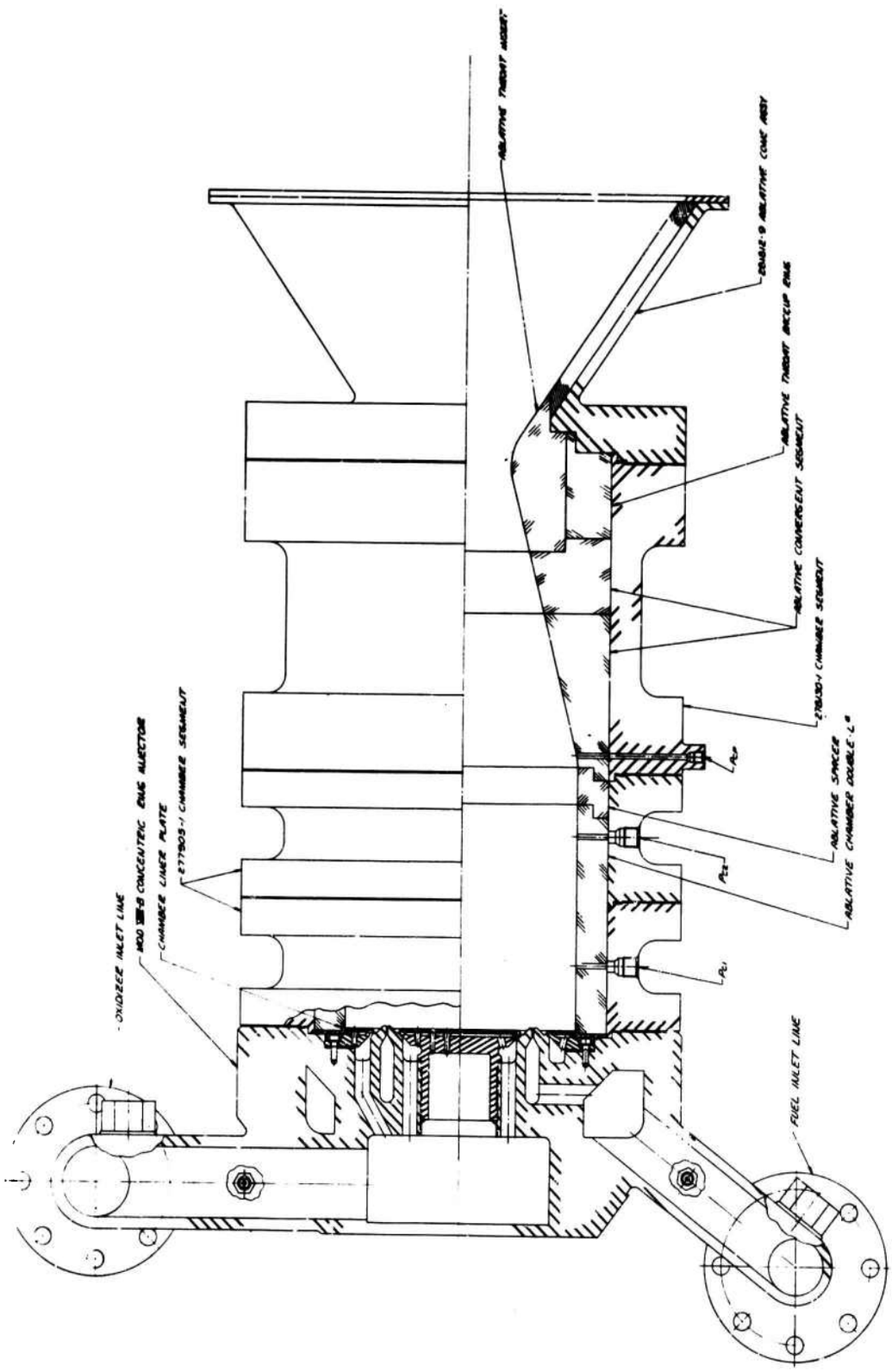

Uncooled TCA Design with Mod VIII Concentric Ring Injector

Figure VI-B-37

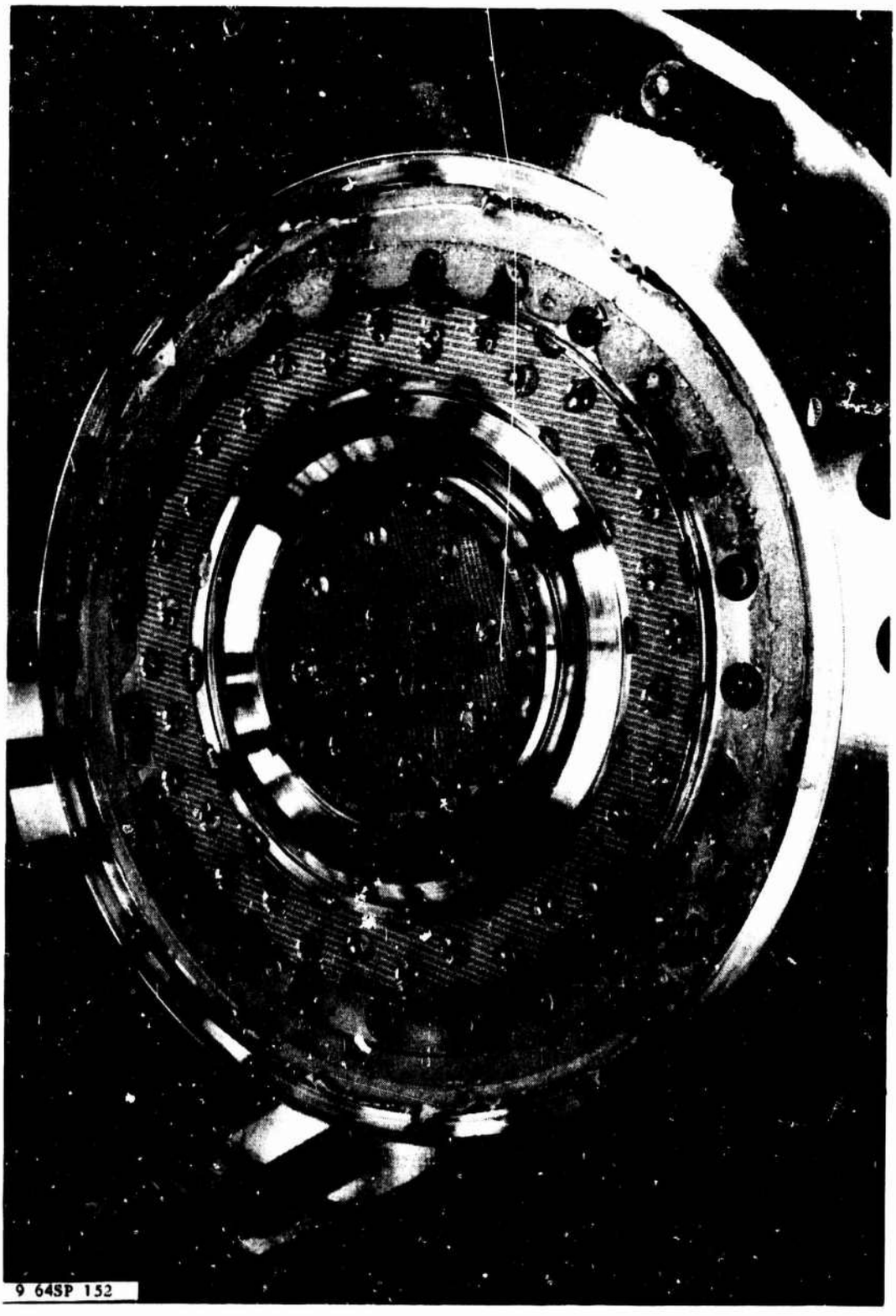

Mod VIII Concentric Ring Injector, Posttest Condition

Figure VI-B-38

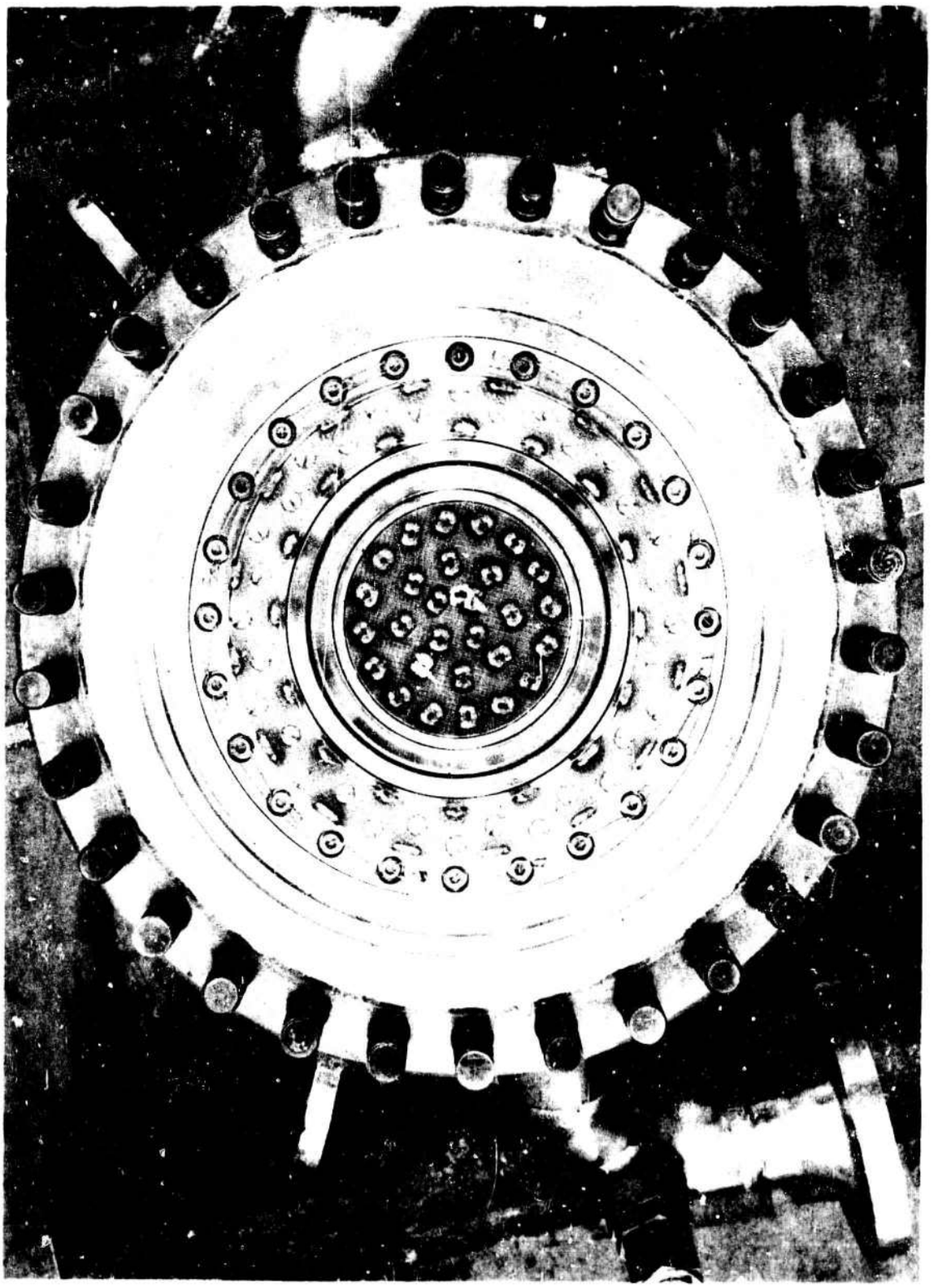

Mod VIIIA Concentric Ring Injector, Pretest Condition

Figure VI-B-39

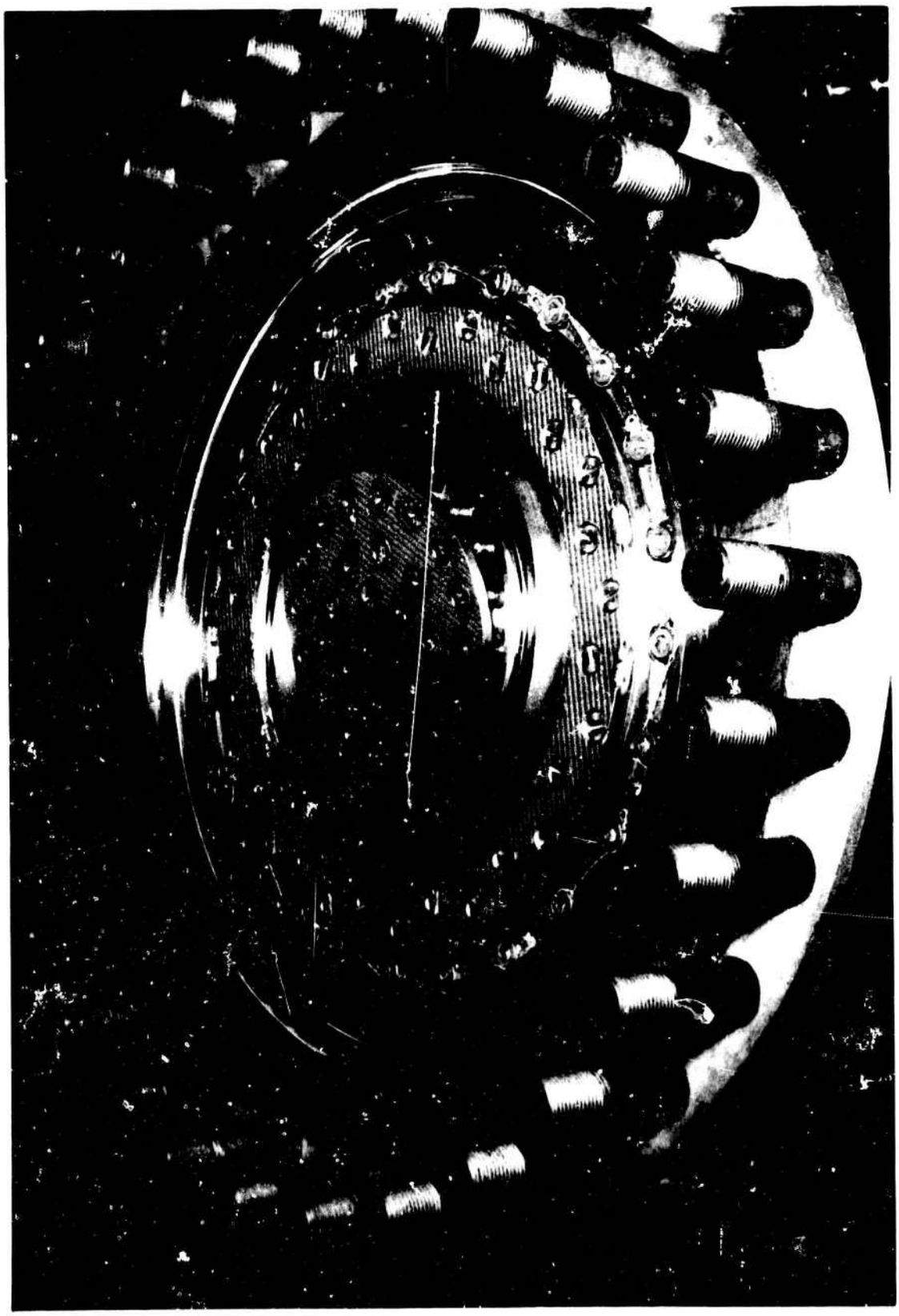

Mod VIIIA Concentric Ring Injector, Posttest Condition

Figure VI-B-40

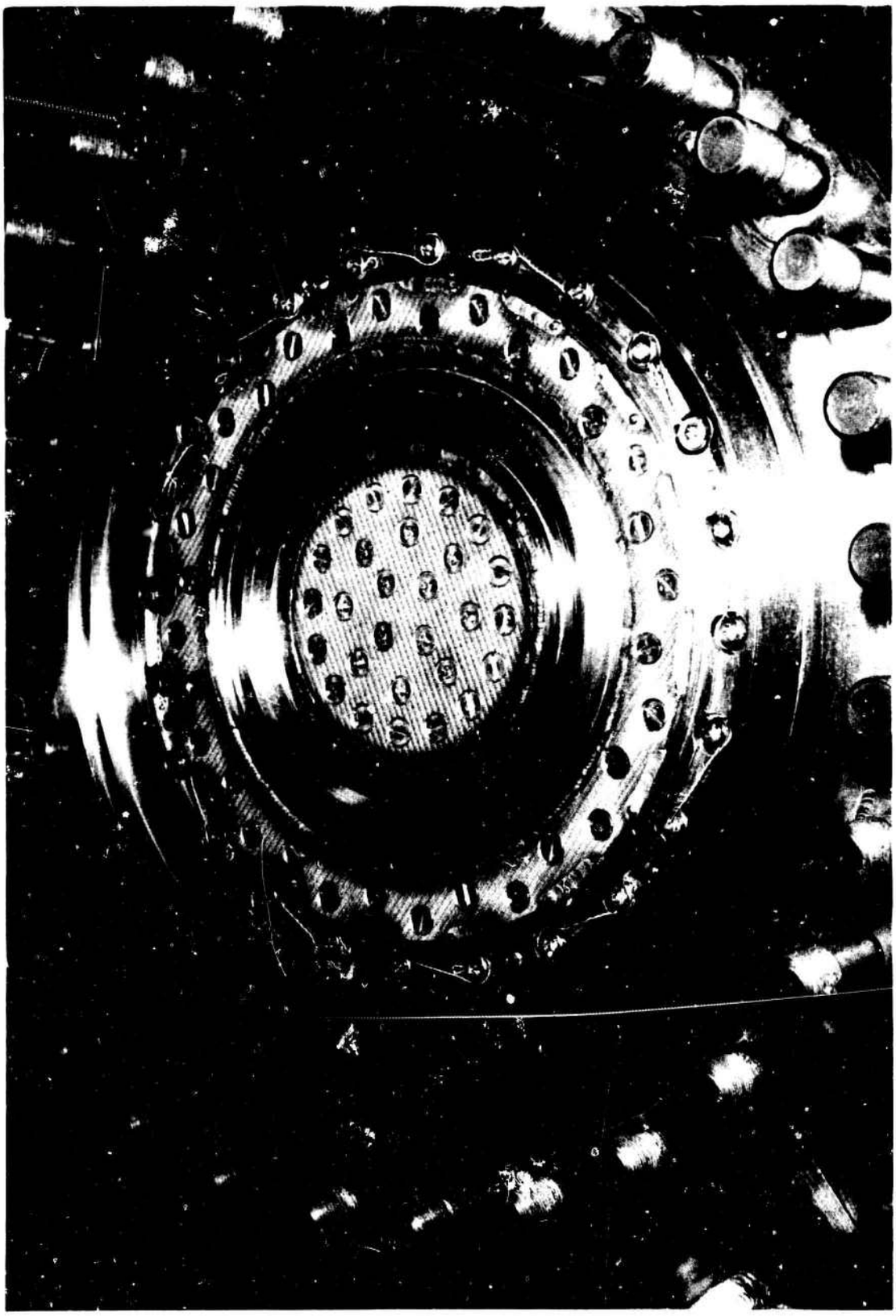

Mod VIIIB Concentric Ring Injector, Pretest Condition

Figure VI-B-41

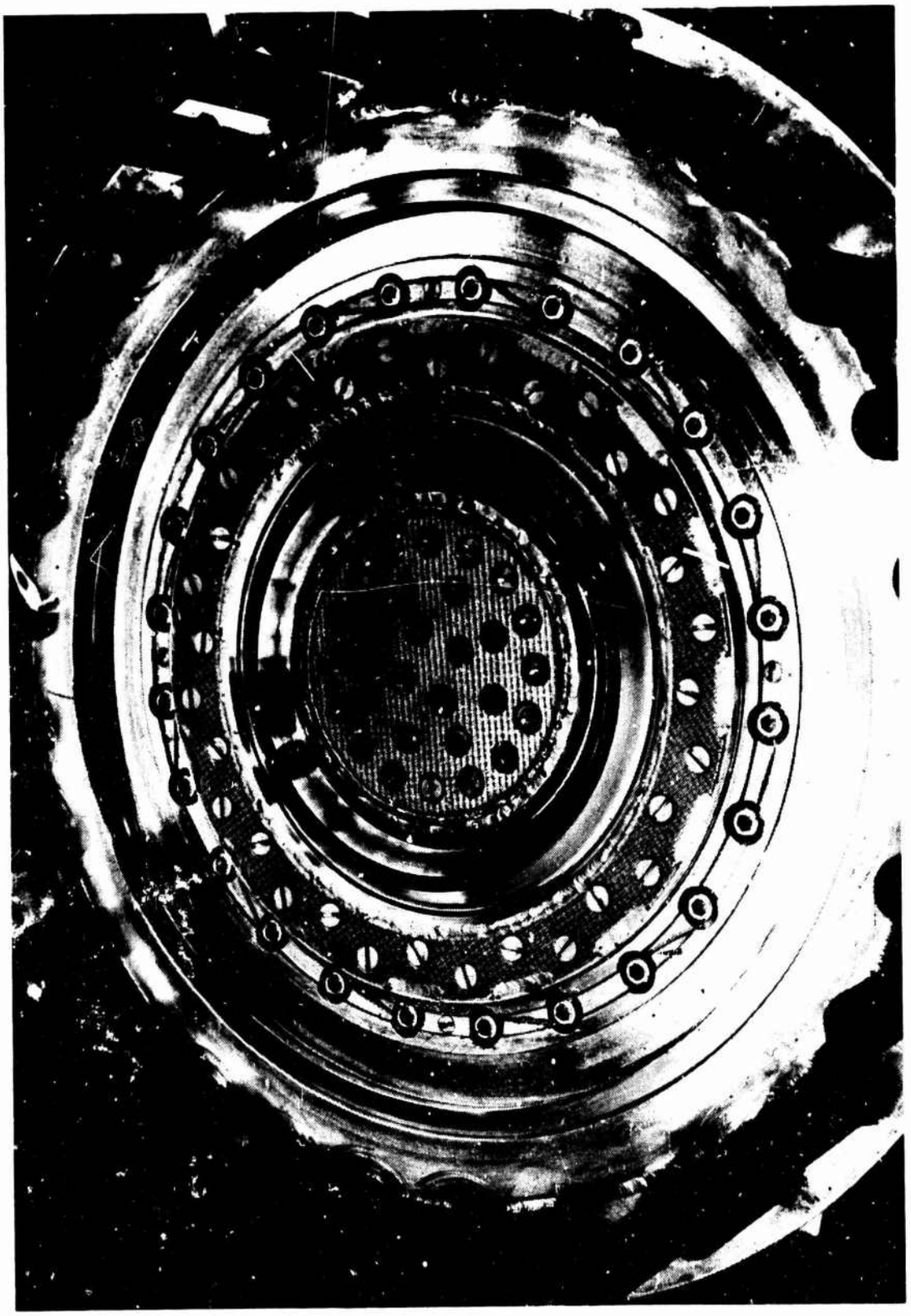

Mod VIIIB Concentric Ring Injector, Posttest Condition

Figure VI-B-42

NOTES:

1. ADJUST OXIDIZER RING TO DIMS SHOWN BY SHIMS AS SHOWN
2. T.S WELD PER AGC 40331
3. DYE PENETRANT INSPECT WELDS PER MIL-I-6866 TYPE OPTIONAL ACCEPTANCE LEVEL PER AGC-4006 CLASS II

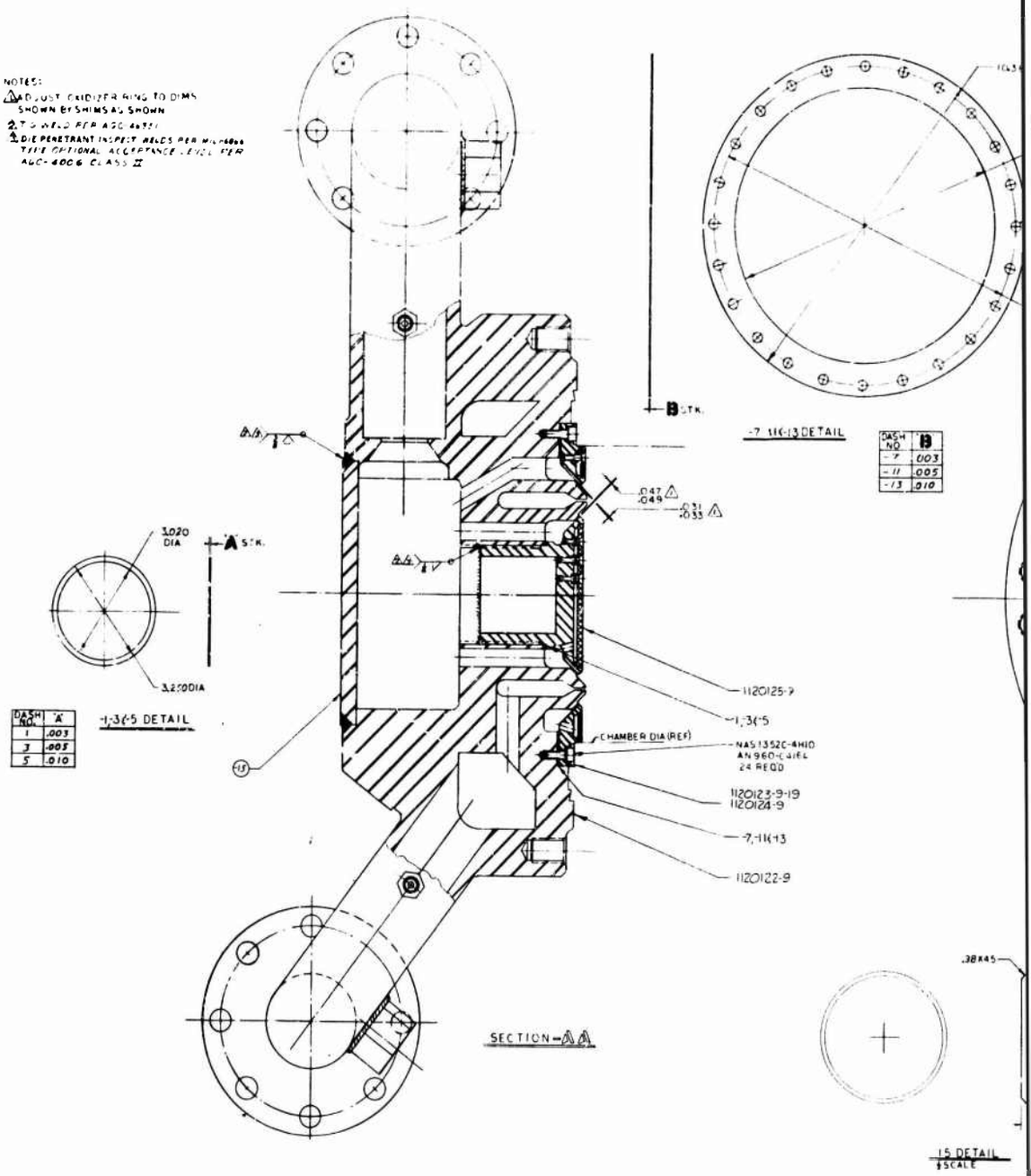

DASH NO	B
-7	.003
-11	.005
-13	.010

DASH NO	A
1	.003
3	.005
5	.010

1,3K-5 DETAIL

1

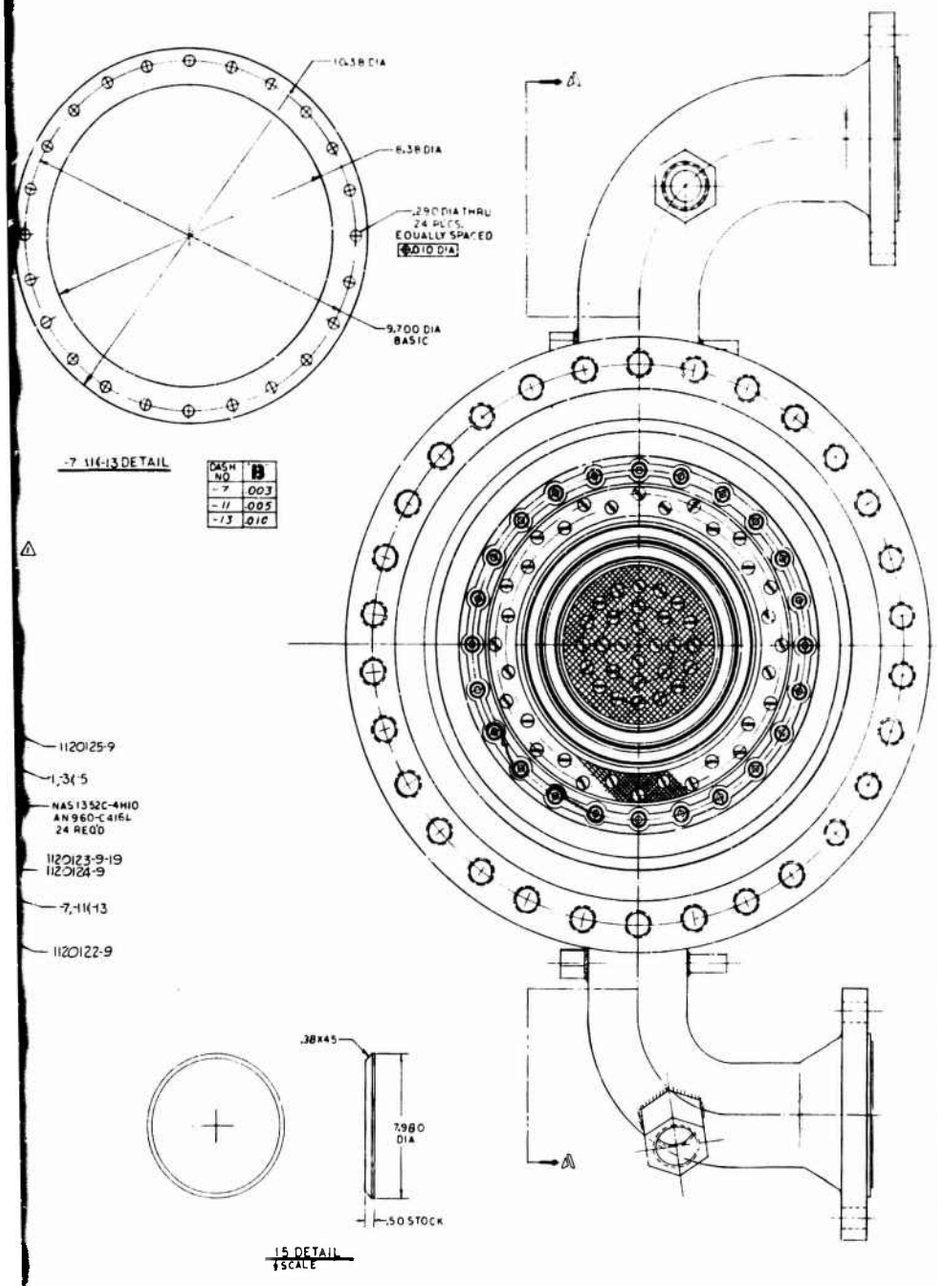

1			1120124-19	RING-OUTER OXIDIZER				11
	1		1120123-19	RING-OUTER OXIDIZER				10
AR	AR	AR	MS20995N32	WIRE-LOCK				9
1	1	1	-15	PLATE .50 R8.00 DIA CRES 347	005763			8
24	24	24	AN960-C416	WASHER				7
24	24	24	NAS1352-4H10	SOC. HD. CAP SCREW				6
AR	AR	AR	-7,-11(-13	SHIM-OUTER RING-OXID.	304 CRES			5
AR	AR	AR	-1,3(-5	SHIM-INNER RING-OXID.	304 CRES			4
		1	1120123-9	RING-OUTER OXIDIZER				3
1	1	1	1120125-9	RING-INNER OXIDIZER				2
1	1	1	1120229	BODY-INJECTOR ASSY				1

1120121-9

2

Mod VIII B Concentric Ring Injector (u)

Figure VI-B-43, Sheet 1 of 5

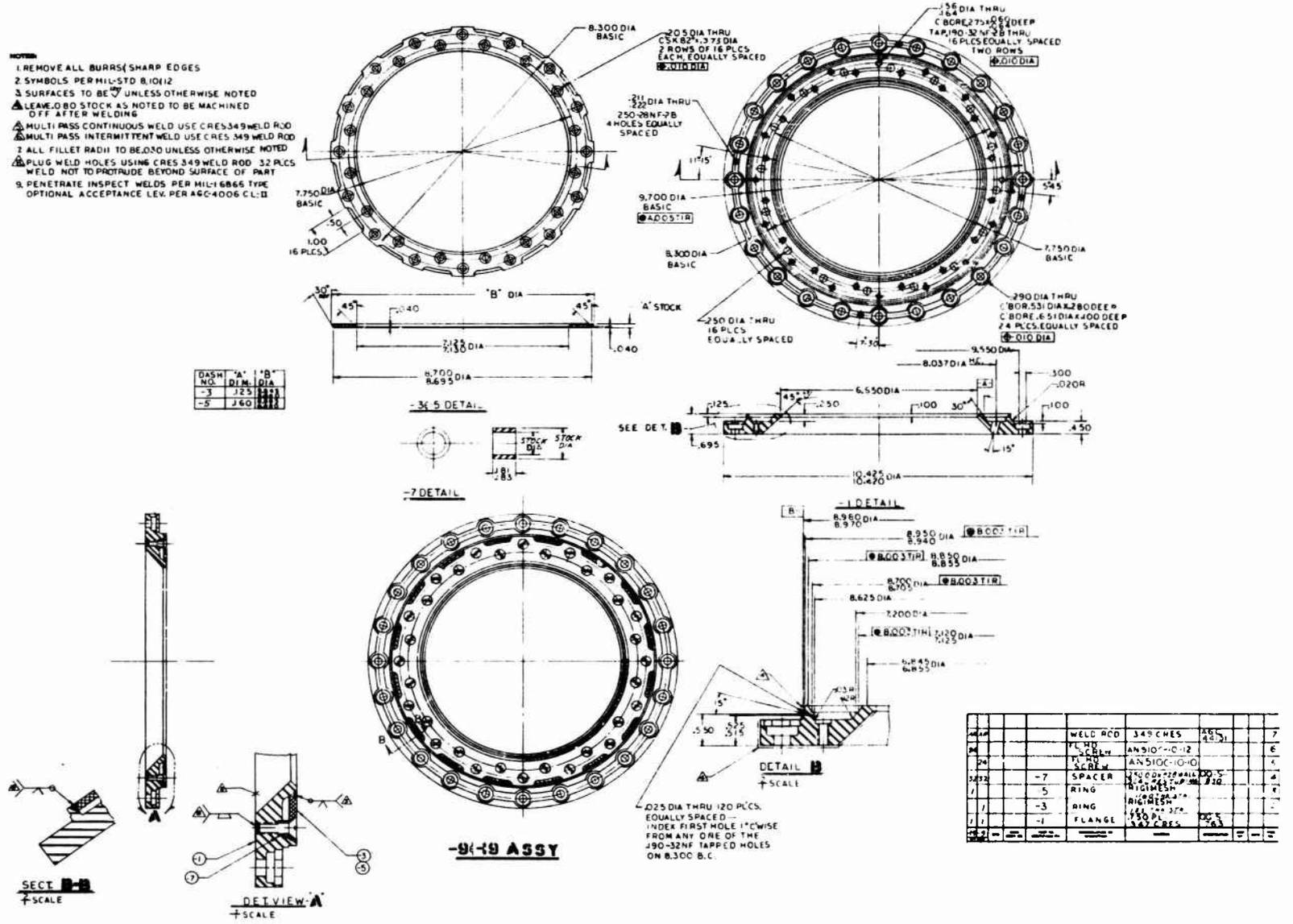

Figure VI-B-43, Sheet 2 of 5

Mod VIIIB Concentric Ring Injector

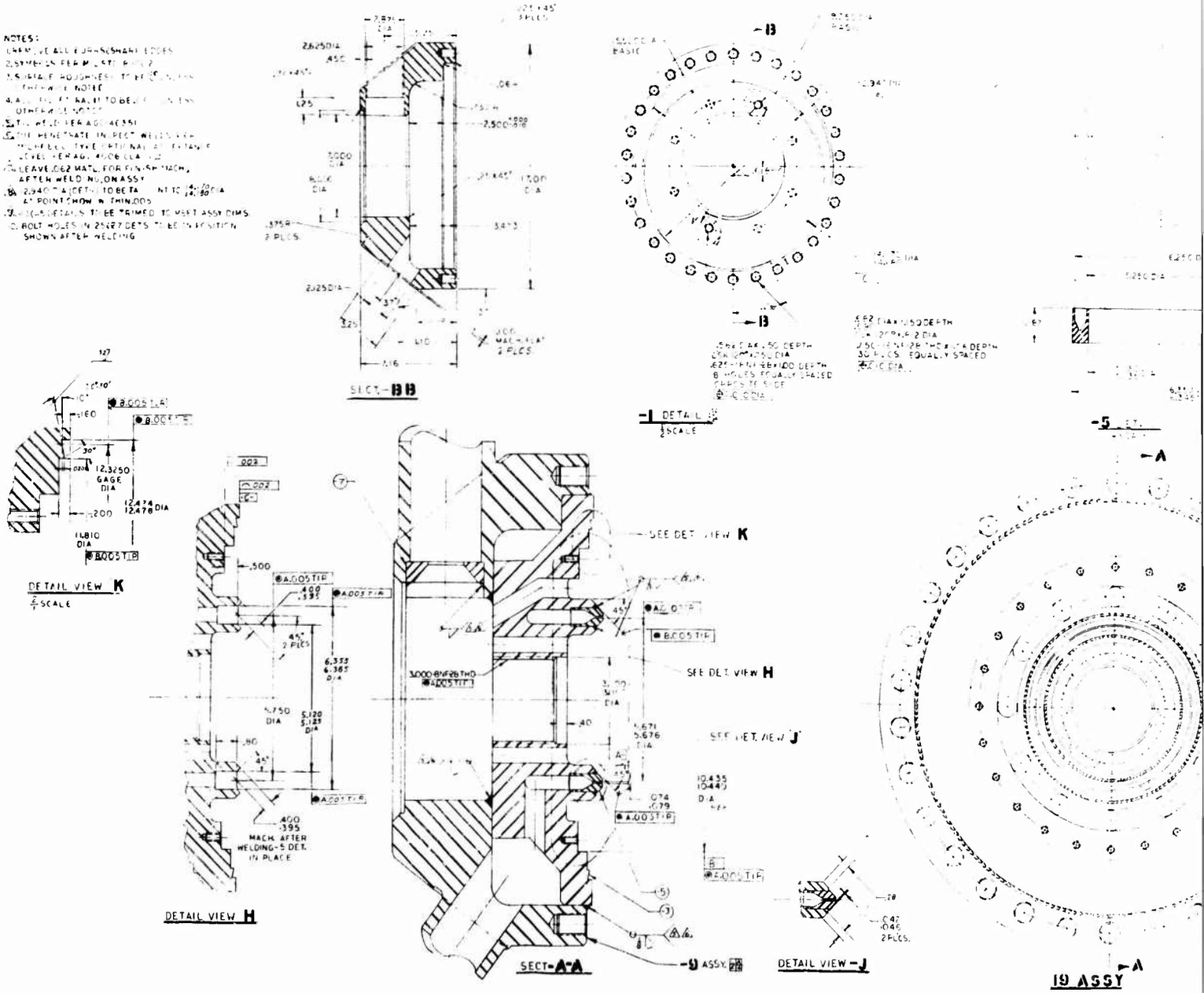
SECT-BB
DETAIL VIEW K
DETAIL VIEW H
SECT-AA
DETAIL VIEW J
SEE DET. VIEW K
SEE DET. VIEW H
SEE DET. VIEW J
19 ASSY

1

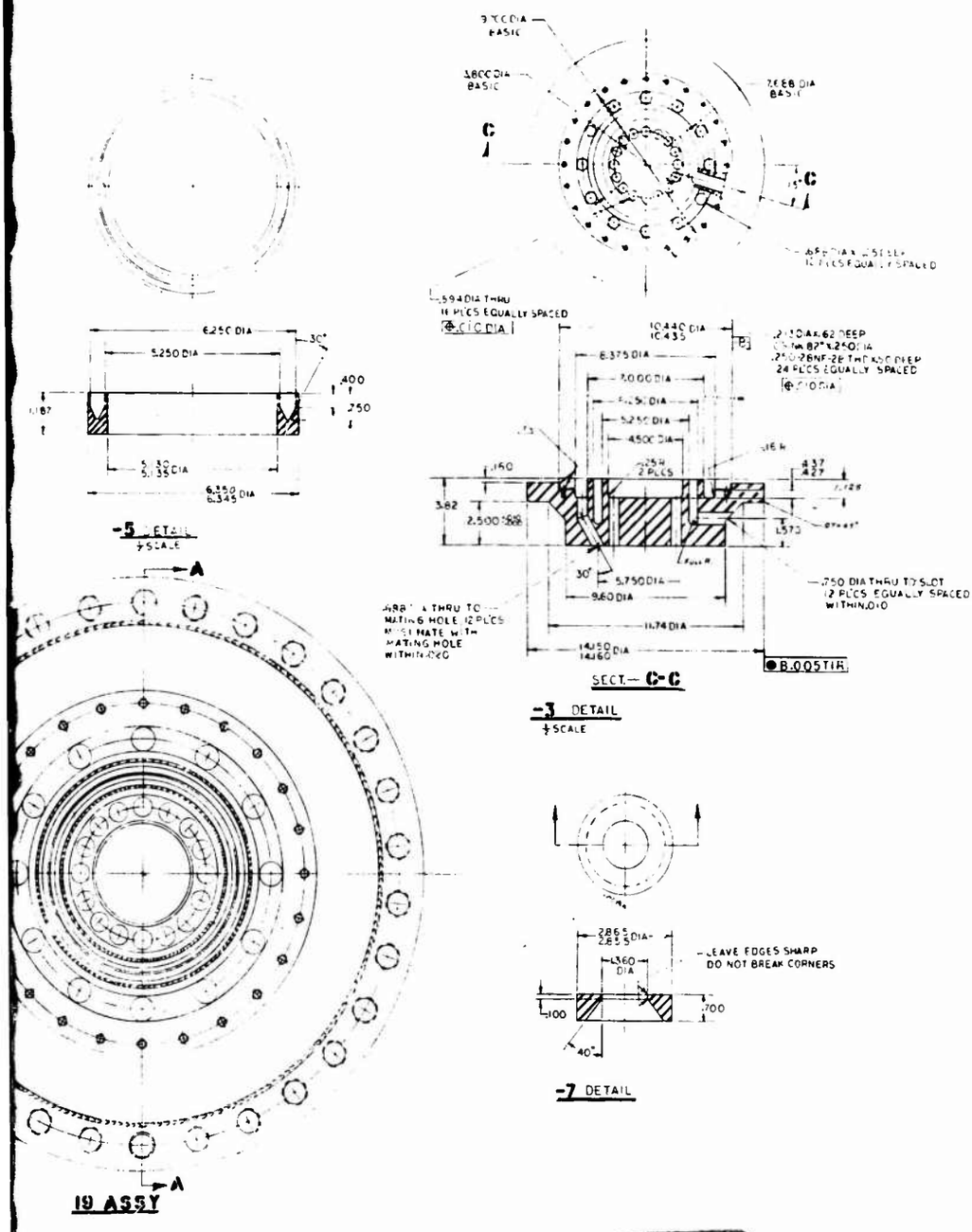

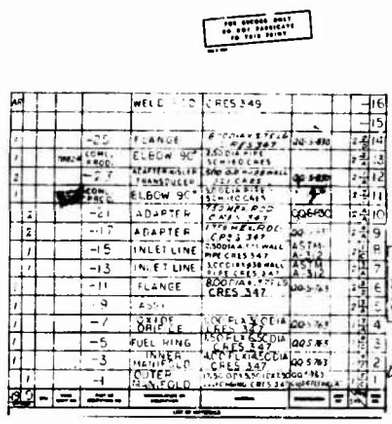

Mod VIII B Concentric Ring Injector

Figure VI-B-43, Sheet 3 of 5

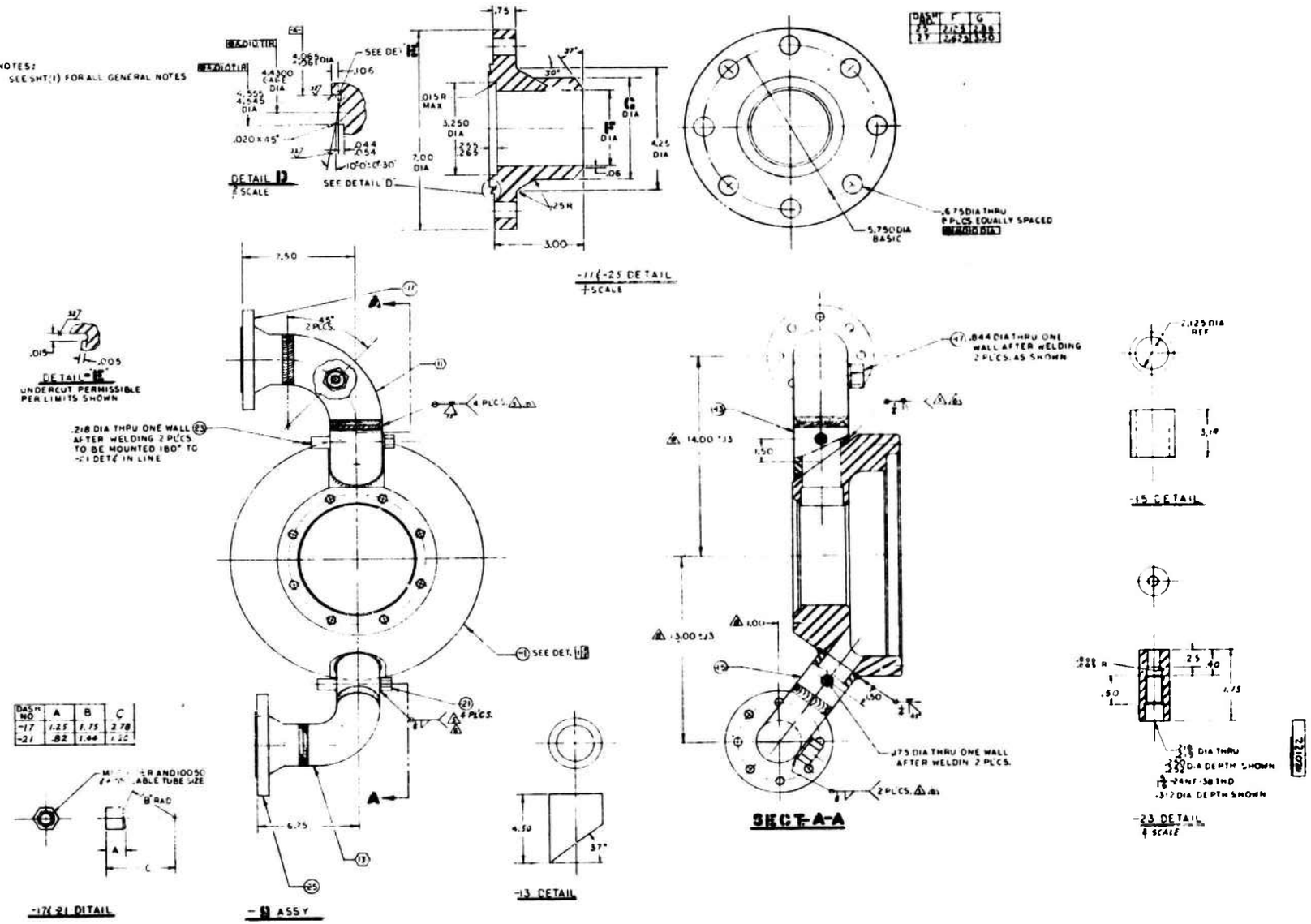

Figure VI-B-43, Sheet 4 of 5

Book One

Mod VIII B Concentric Ring Injector

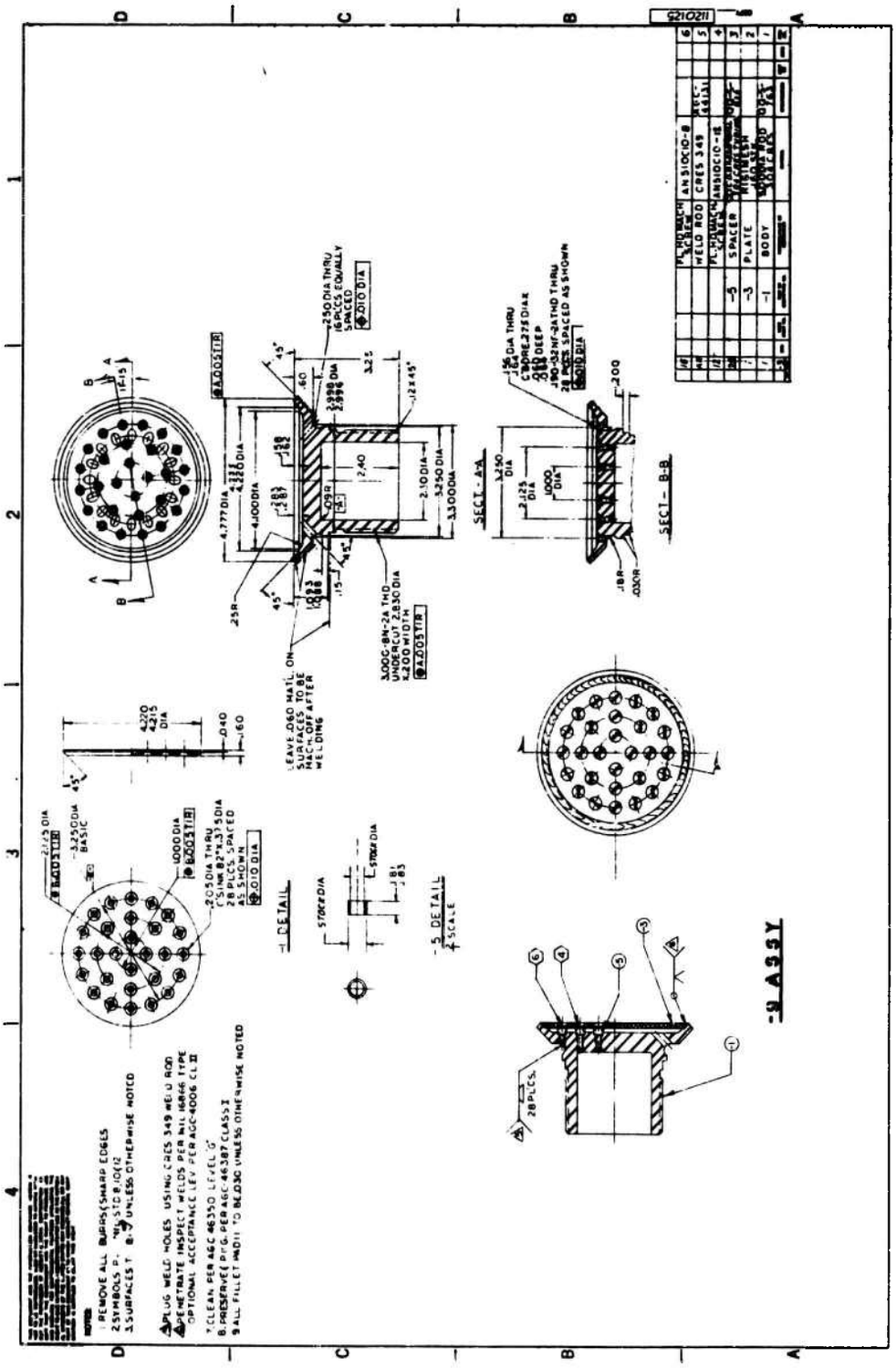

Figure VI-B-43, Sheet 5 of 5

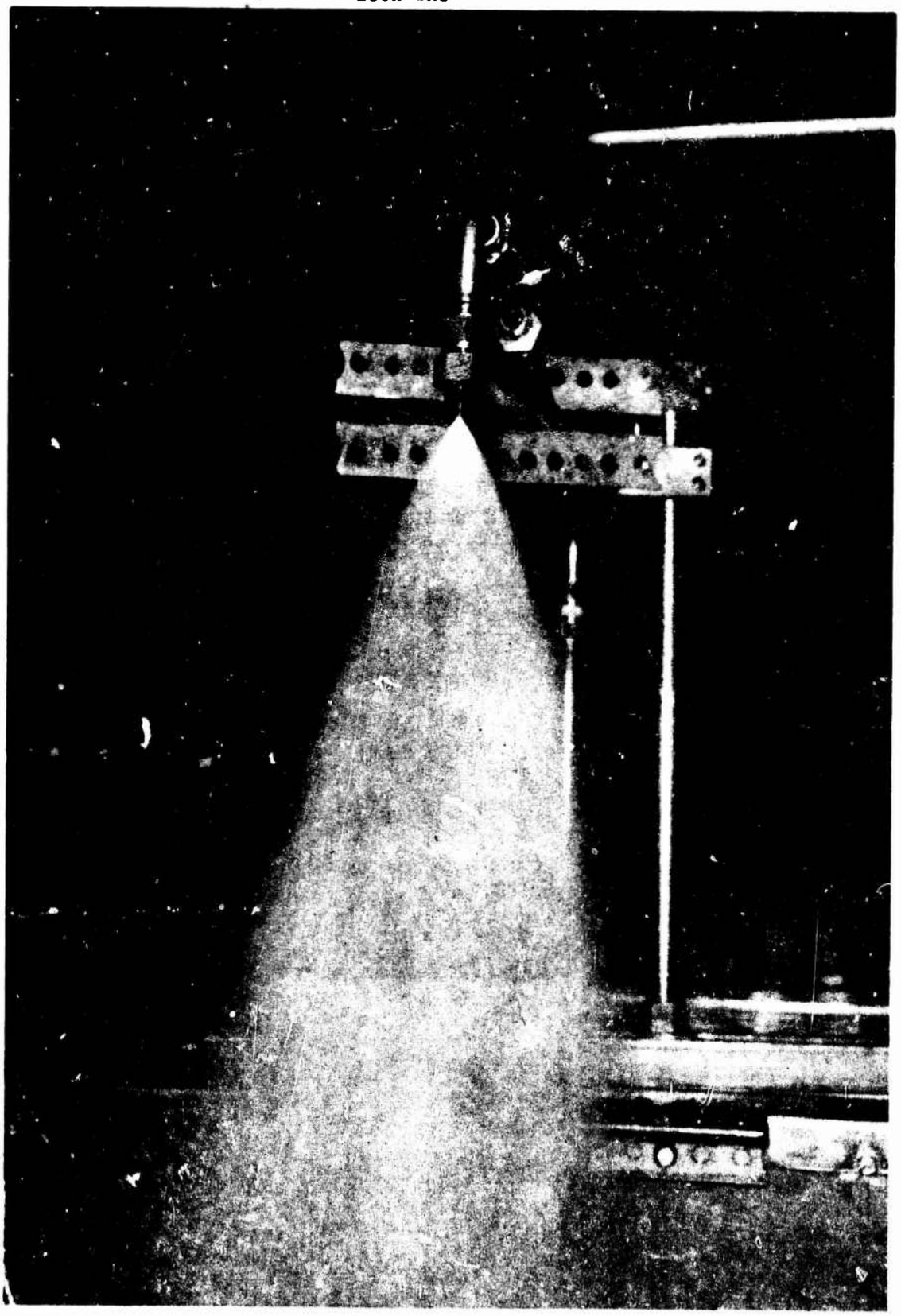

Water Flow Test of Fuel Spray Nozzle

Figure VI-B-44

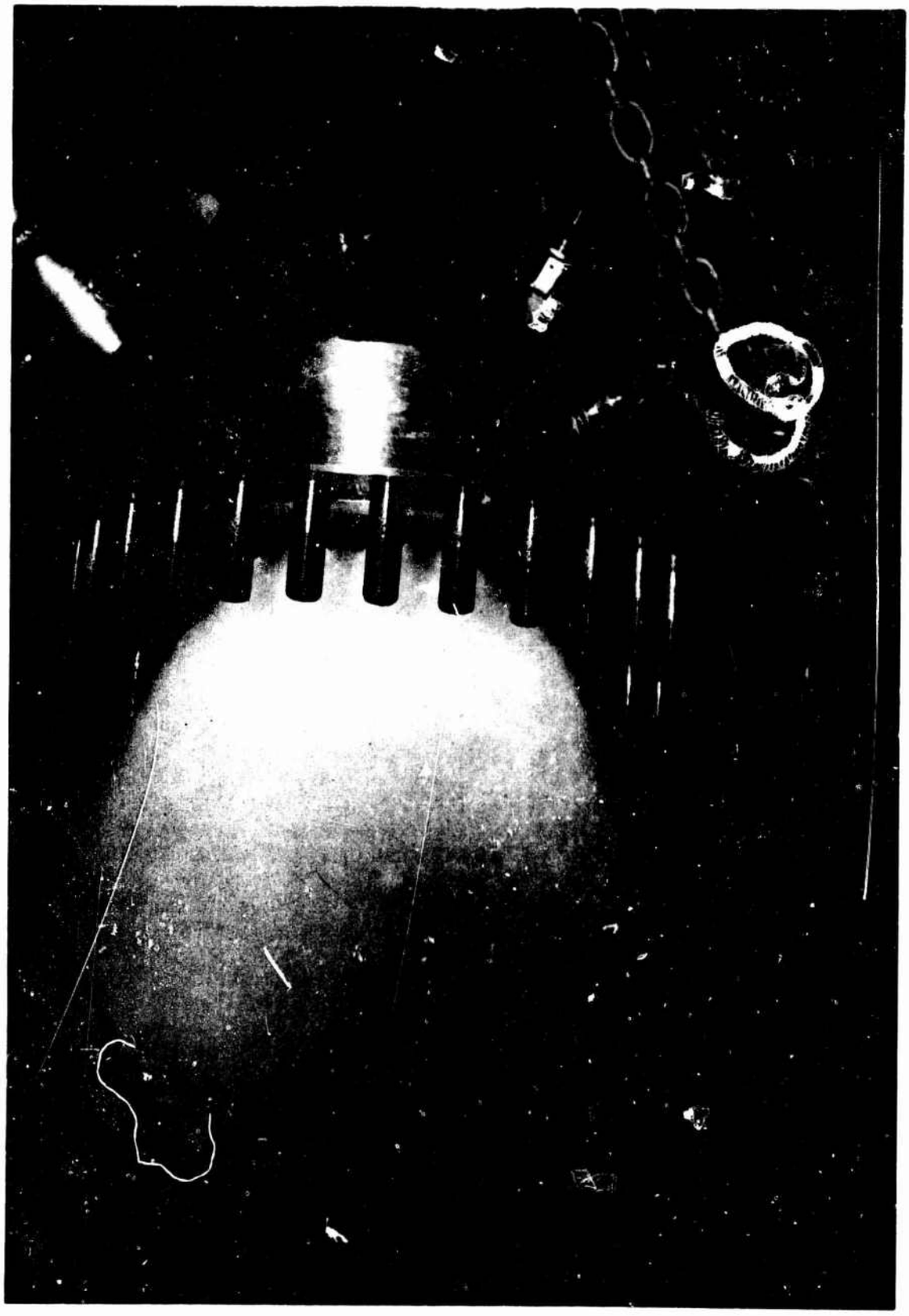

Water Flow Test of Transpiration-cooled Injector Fuel Circuit Only

Figure VI-B-45

Water Flow Test of Transpiration-cooled Injector, Oxidizer Circuit Only

Figure VI-B-46

Water Flow Test of Transpiration-cooled Injector, Fuel and Oxidizer Circuits Flowing at Rated Conditions

Figure VI-B-47

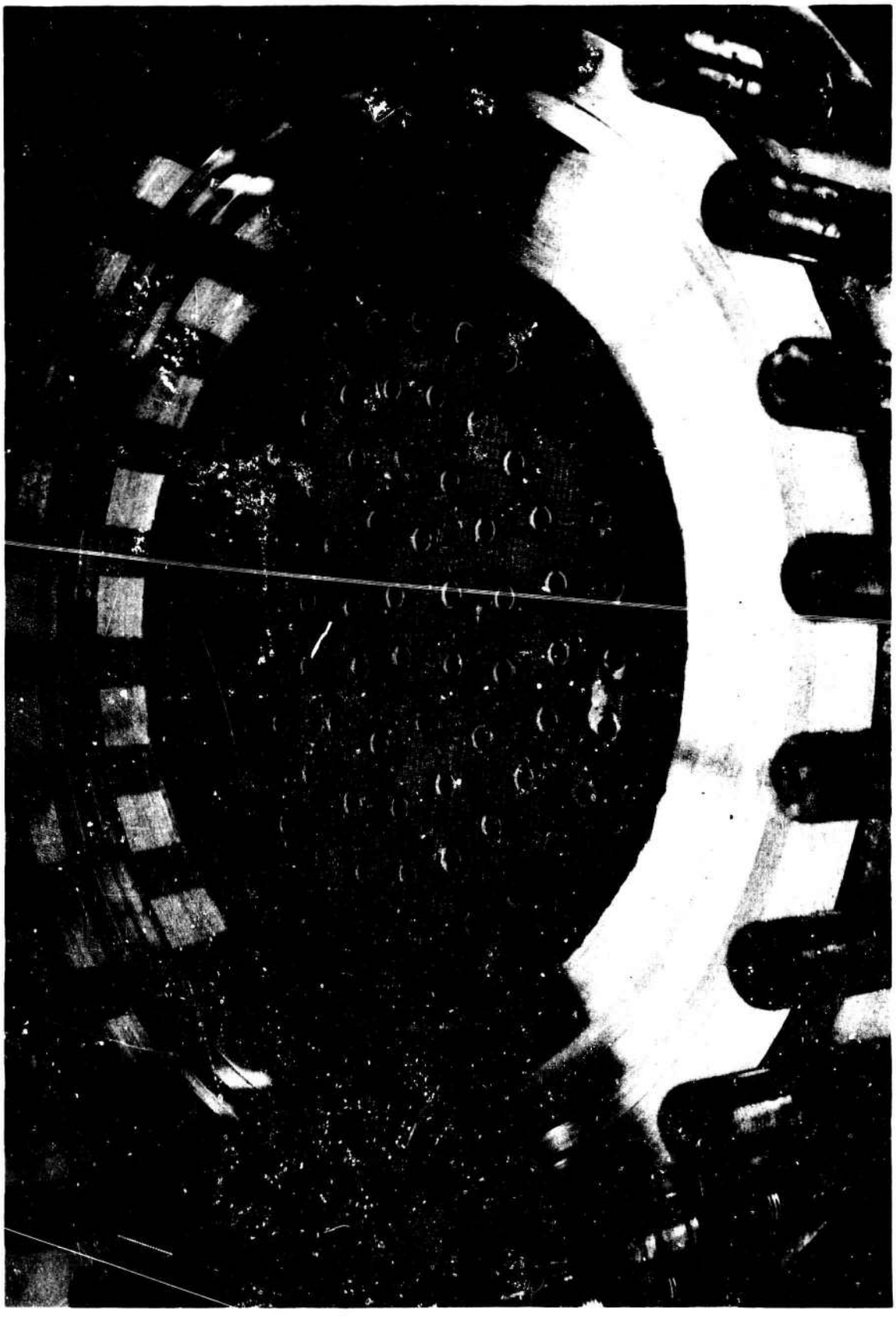

Transpiration-cooled Injector, Posttest Condition

Figure VI-B-48

INJECTOR	ORIGINAL DESIGN TEST 1.2-02-YAM-037	ORIGINAL DESIGN TEST 1.2-02-YAM-037
FEATURES		
A. INJECTOR ELEMENT		
1. Basic element configuration		
2. Oxidizer element		
a. type	Flat rigimesh face	Flat regimesh face
b. Velocity (Ft/sec)	121.2	118.2
c. Surface area sq. in		
d. K_W	6.33	6.33
3. Fuel element		
a. Type		
b. No. of elements	84	84
c. Velocity ft/sec	58.4	55.0
d. K_W	4.38	4.38
B. INJECTOR PERFORMANCE (Nominal)	- -	99
C. TYPE OF FAILURE	Successful test of injector, but ablative throat insert mechanically failed during startup.	None

Transpiration-cooled Injector Design Data Summary (u)

Figure VI-B-49

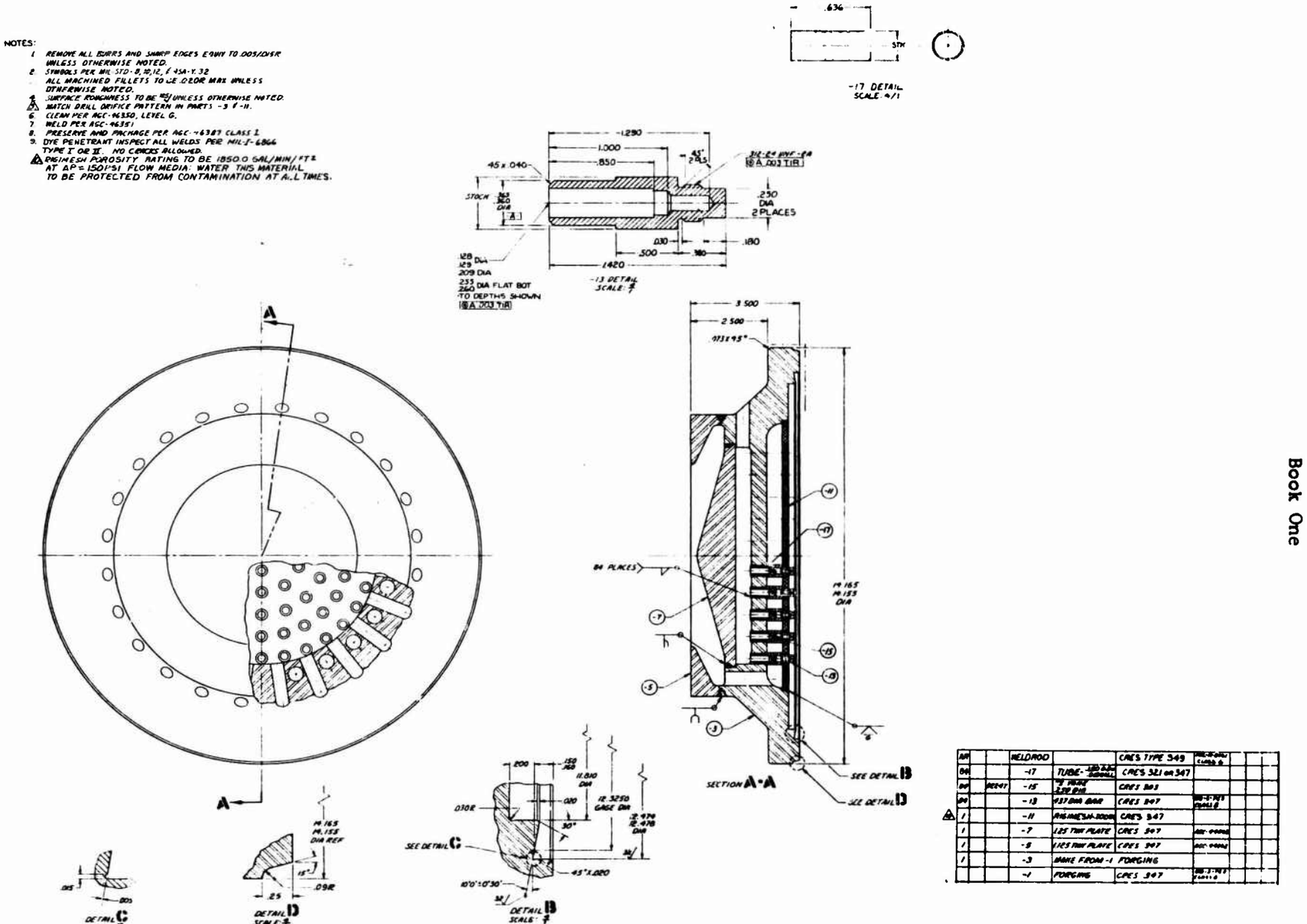

		WELDROD		CRES TYPE 349	
		-17	TUBE-	CRES 321 or 347	
		-15		CRES 301	
		-13		CRES 347	
		-11		CRES 347	
		-7		CRES 347	
		-5		CRES 347	
		-3		CRES 347	
		-1	FORGING	CRES 347	

Figure VI-B-50, Sheet 1 of 2

Transpiration-cooled Injector Fabrication Drawings (u)

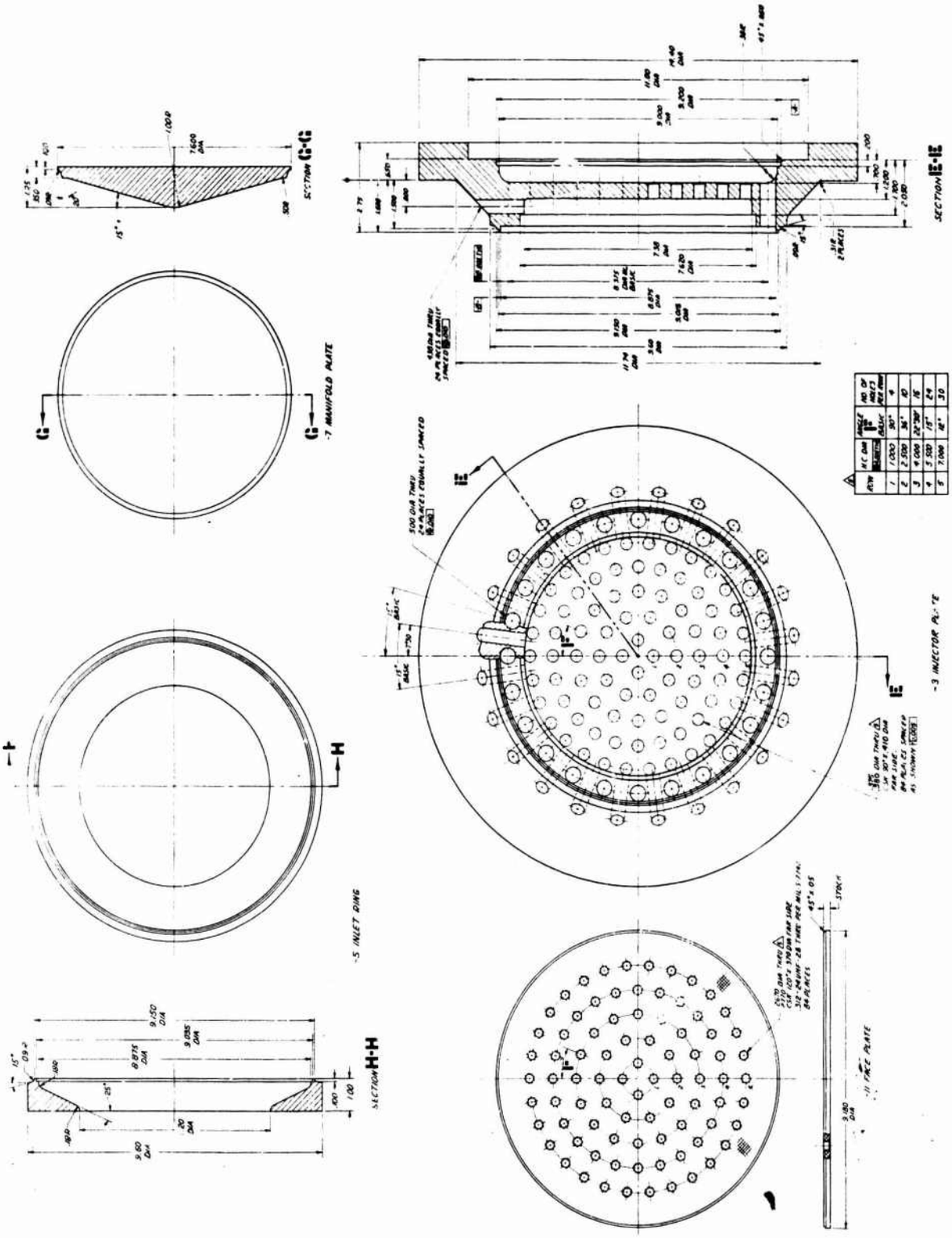

Transpiration-cooled Injector Fabrication Drawings (u)

Figure VI-B-50, Sheet 2 of 2

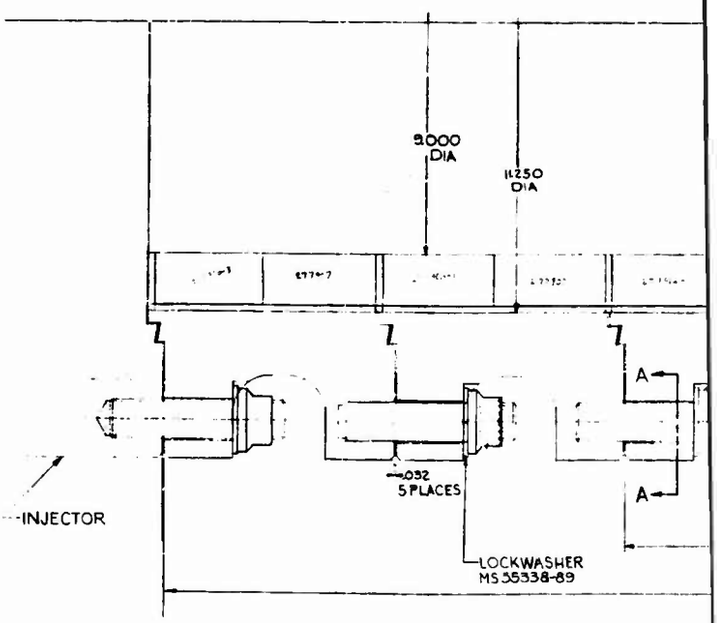
9.000
DIA
11.250
DIA
A
A
.032
5 PLACES
INJECTOR
LOCKWASHER
MS 35338-89

1

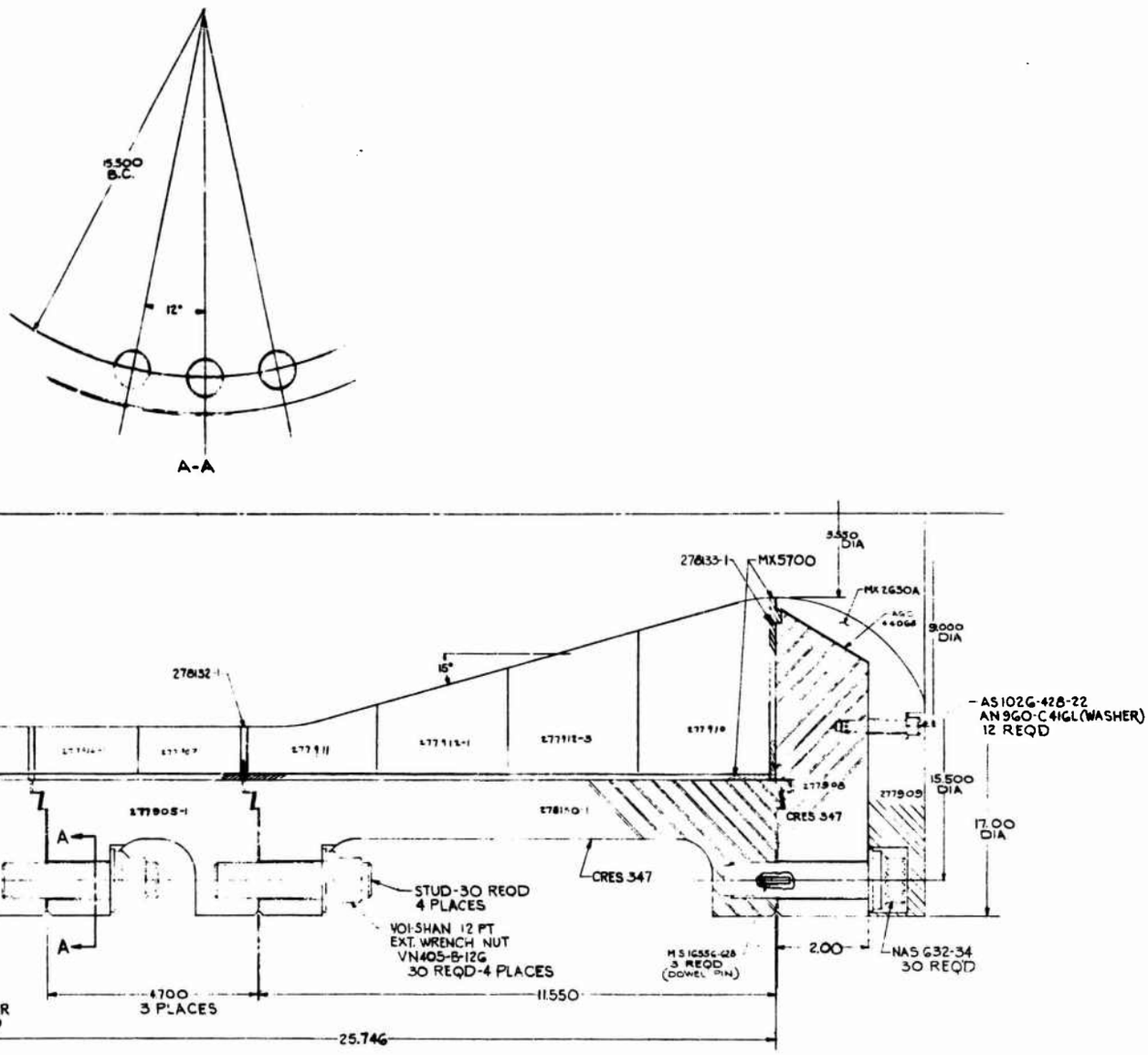

Uncooled Thrust Chamber Design

Figure VI-C-1

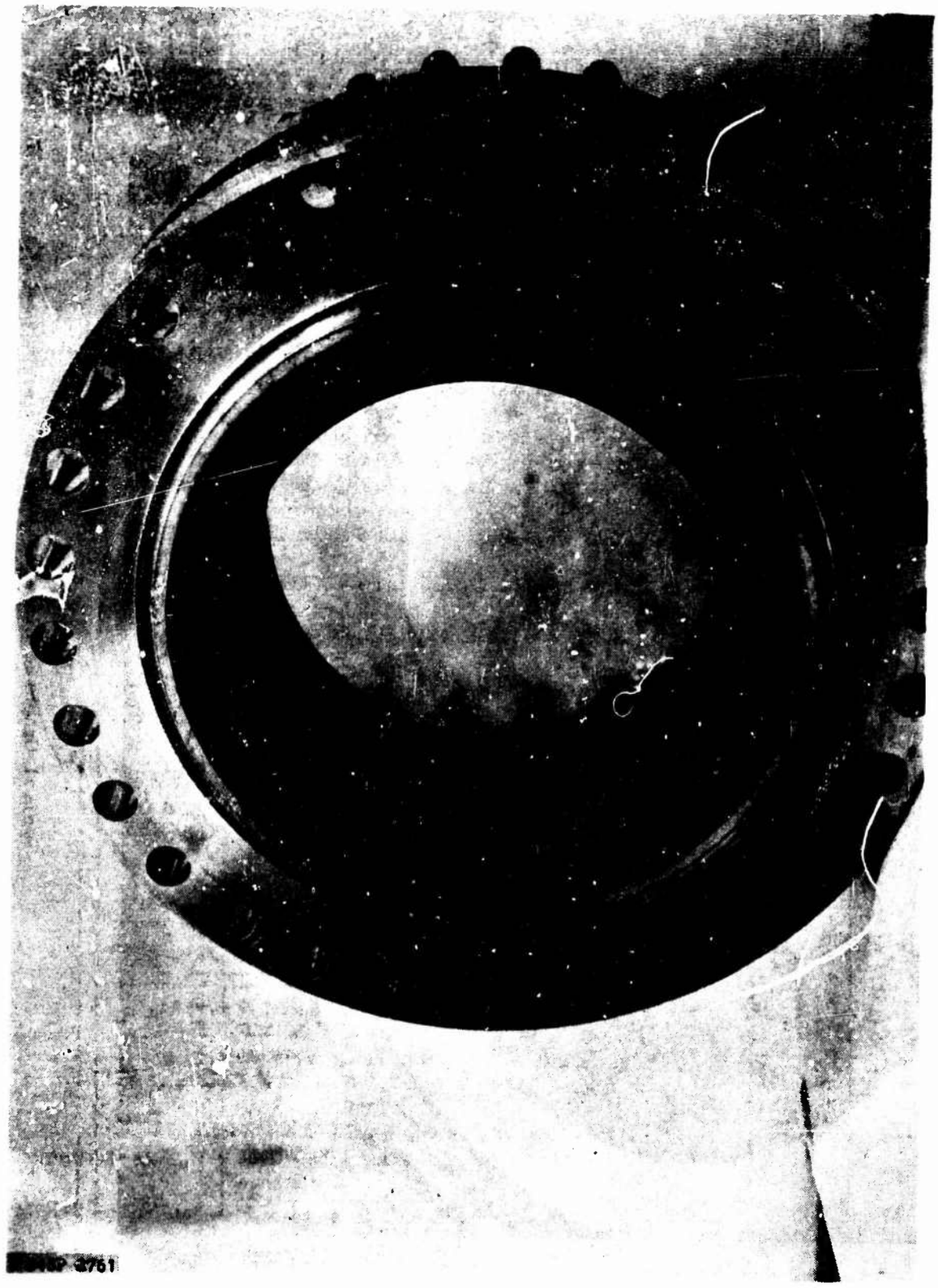

Graphite-Lined L* Segment, Pretest Condition

Figure VI-C-2

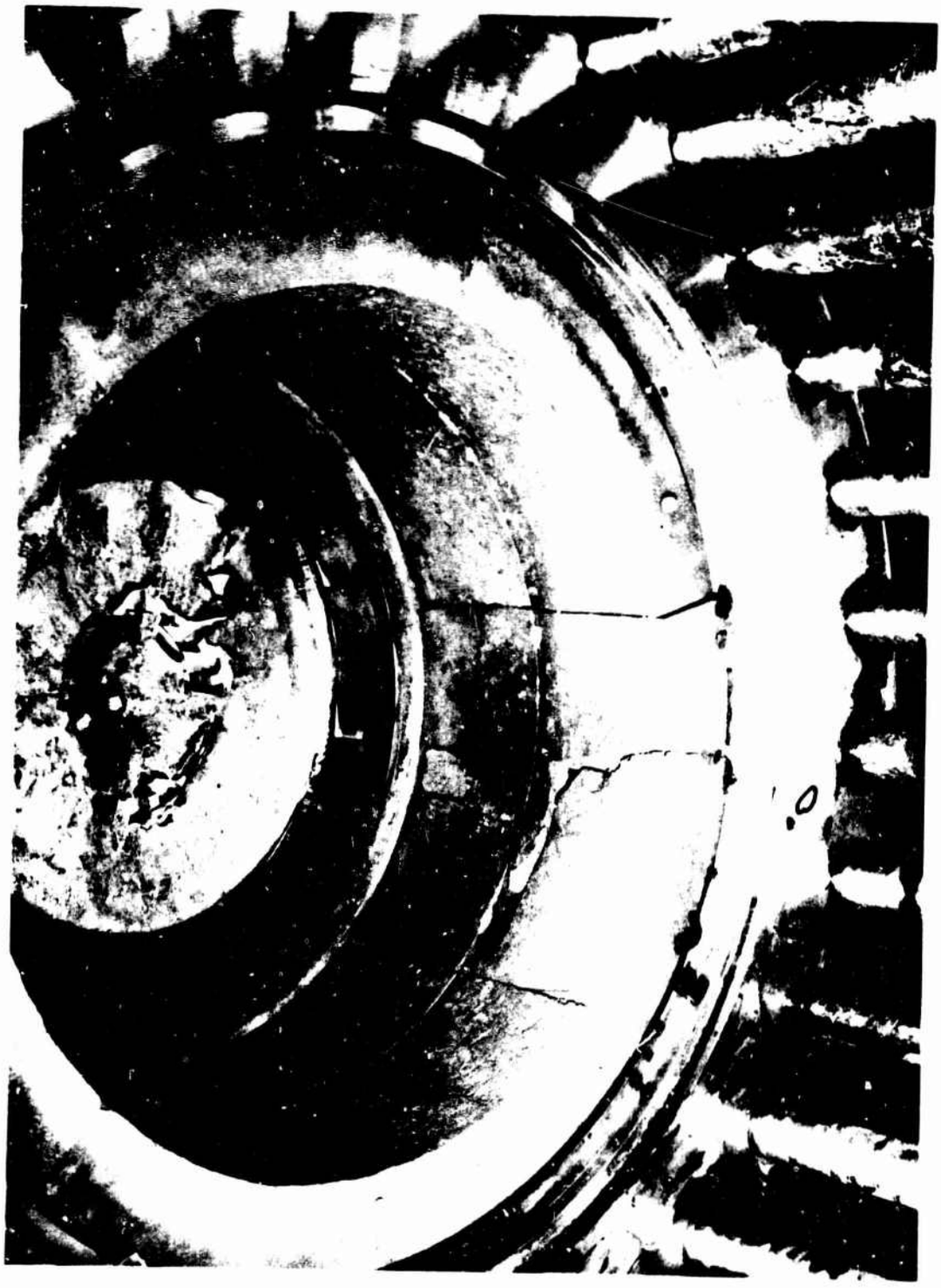

Typical Graphite Liner Failure

Figure VI-C-3

Graphite-lined Convergent and Throat Segment, Posttest Condition

Figure VI-C-4

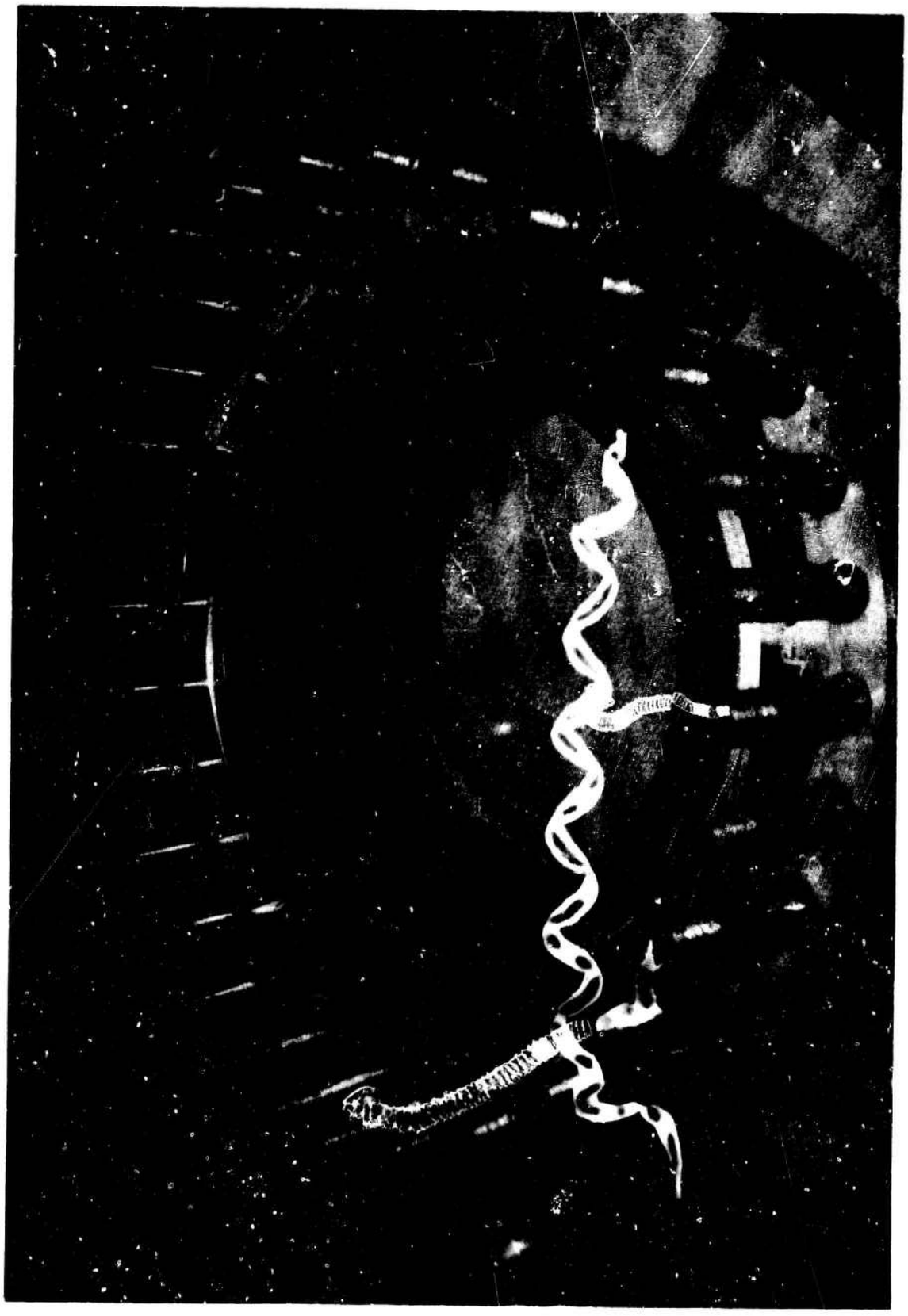

Coated Graphite L* Segment, Posttest Condition

Figure VI-C-5

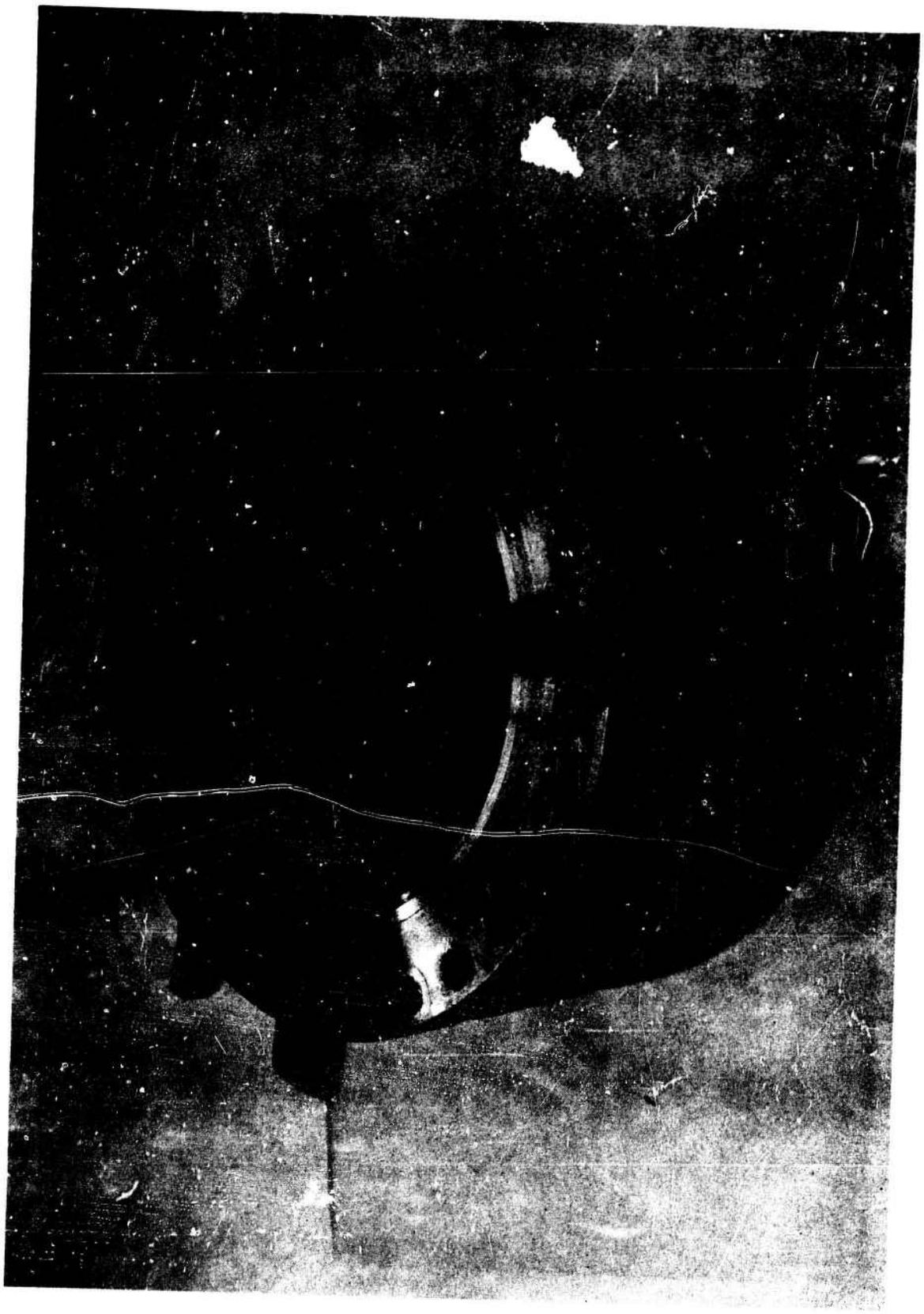

L* Segment Lined with MX 4566 Ablative Material, Pretest Condition

Figure VI-C-6

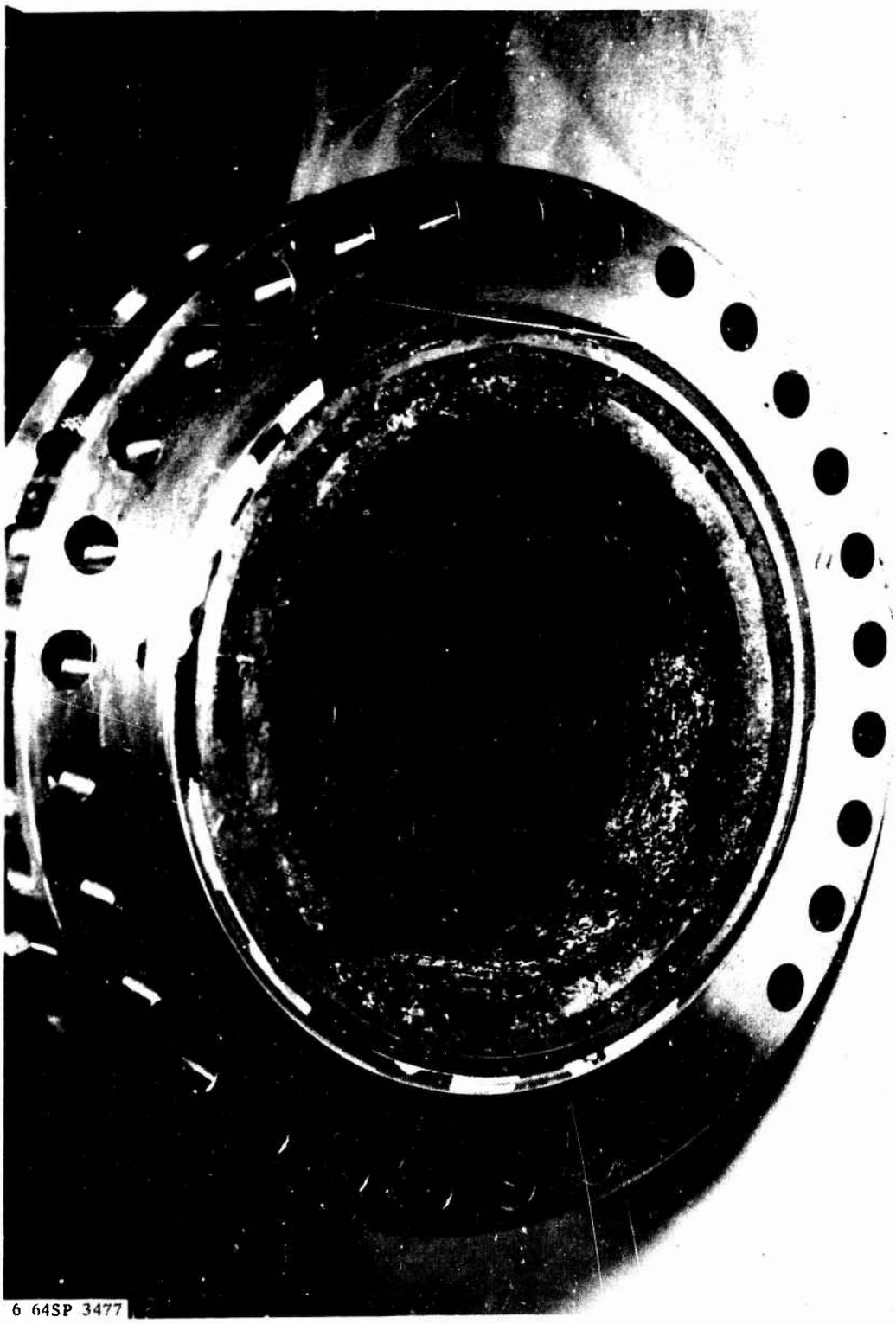

MX 4566 Ablative L* Segment, Posttest Condition

Figure VI-C-7

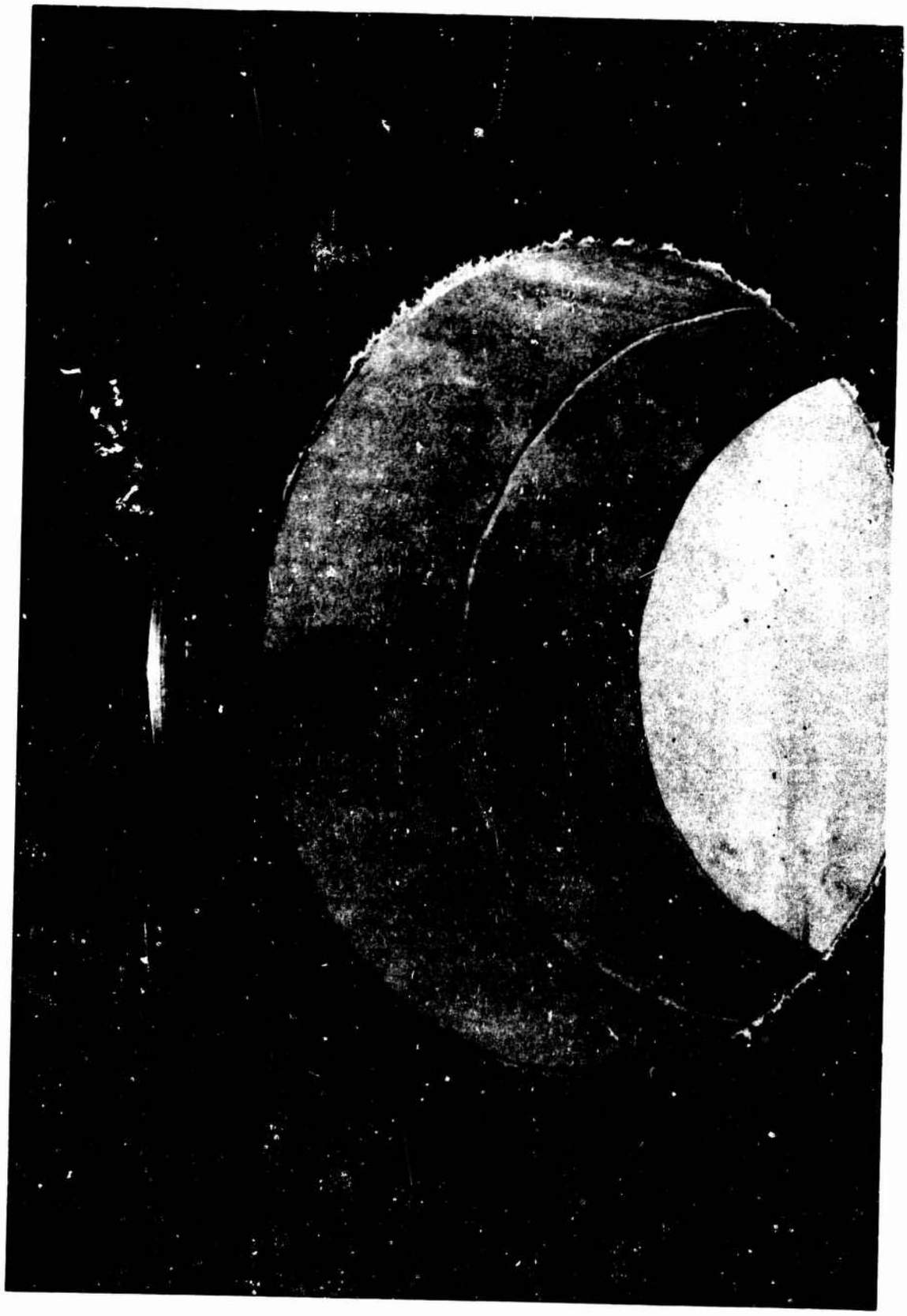

150 RPD Ablative L* Segment, Posttest Condition

Figure VI-C-8

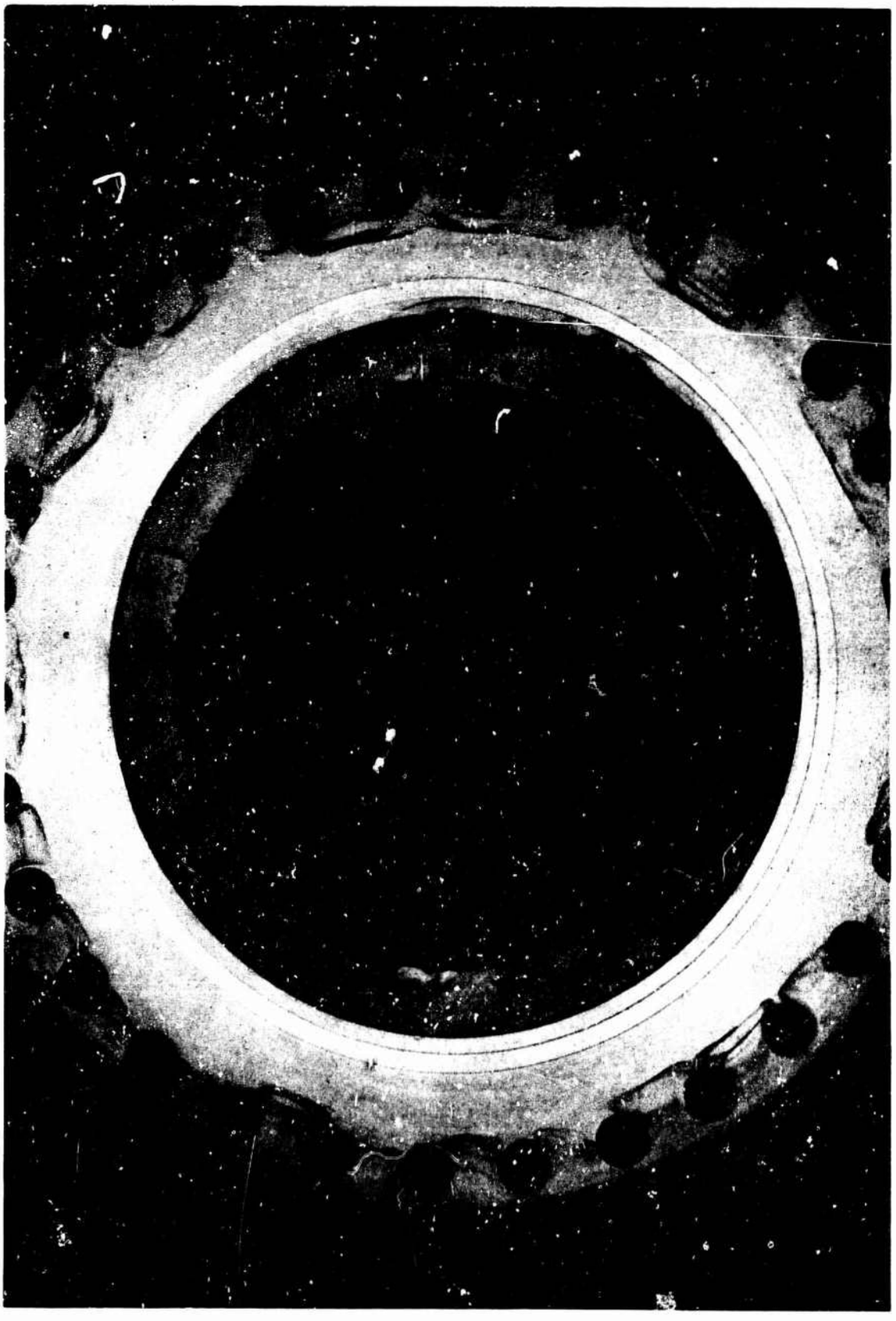

ZTA Convergent Segment and ATJ Throat Insert, Posttest Condition

Figure VI-C-9

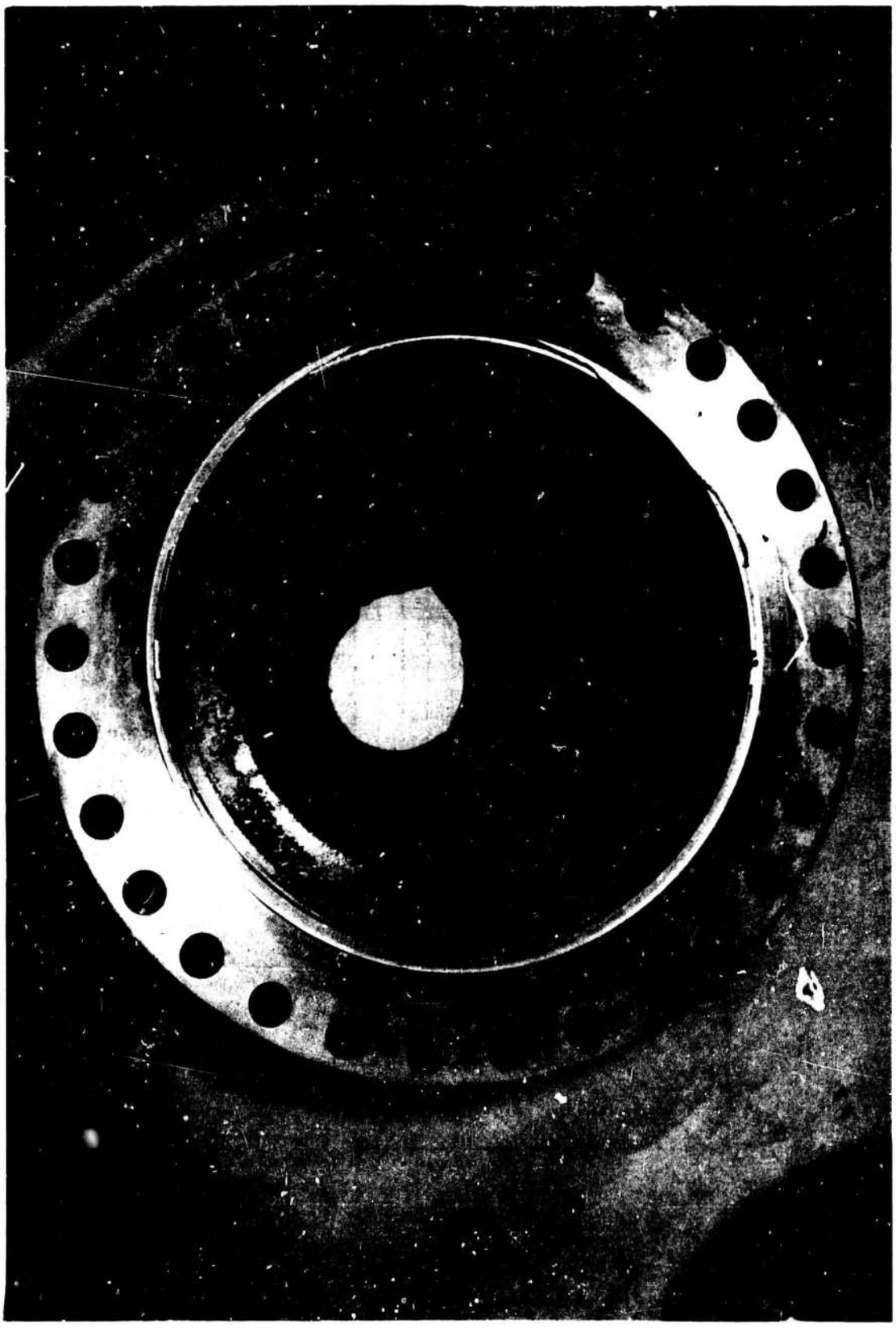

Ablative Convergent Section with ZTA Graphite Throat, Posttest Condition

Figure AI-C-10

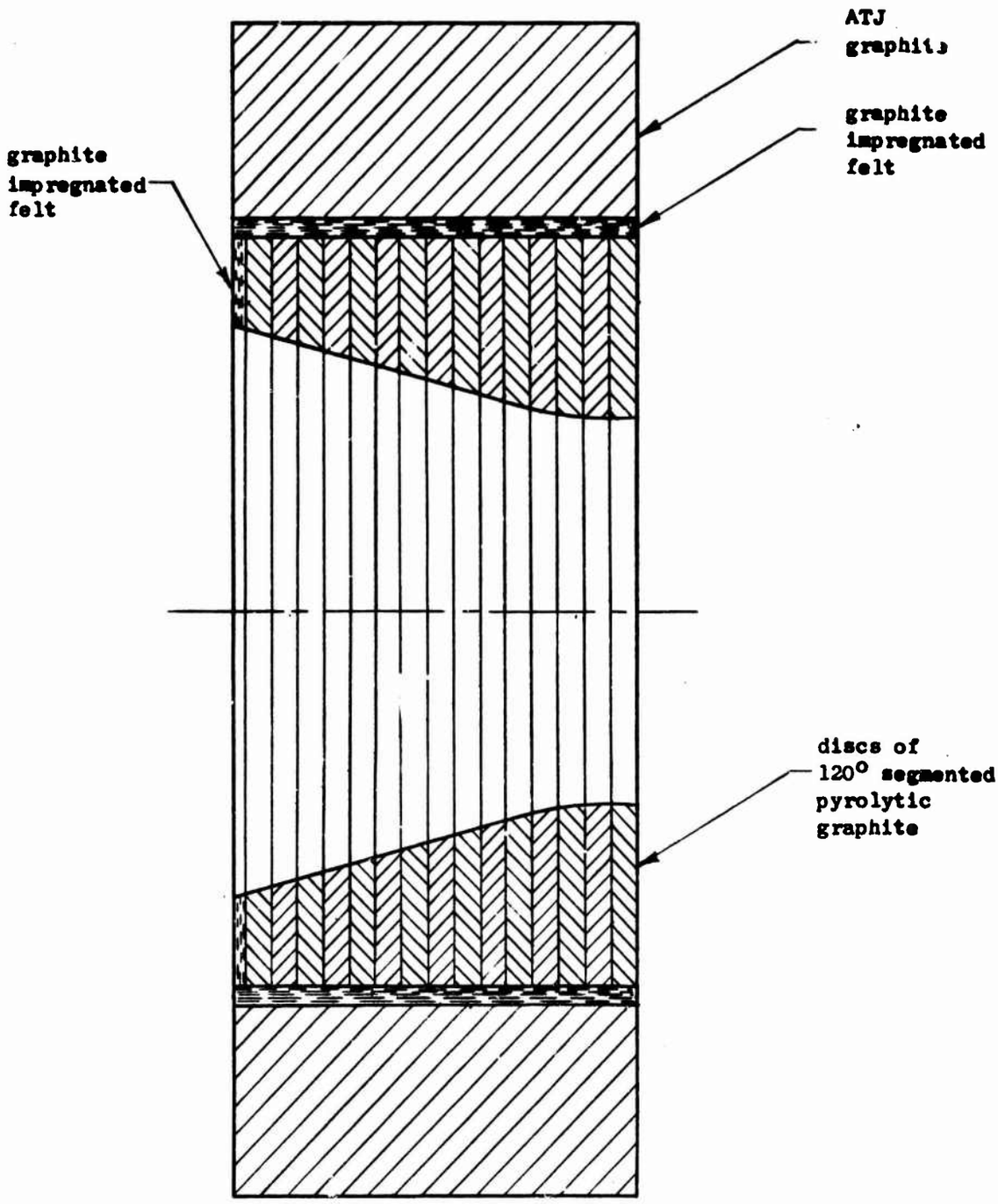

Pyrolytic Graphite Throat Insert Design

Figure VI-C-11

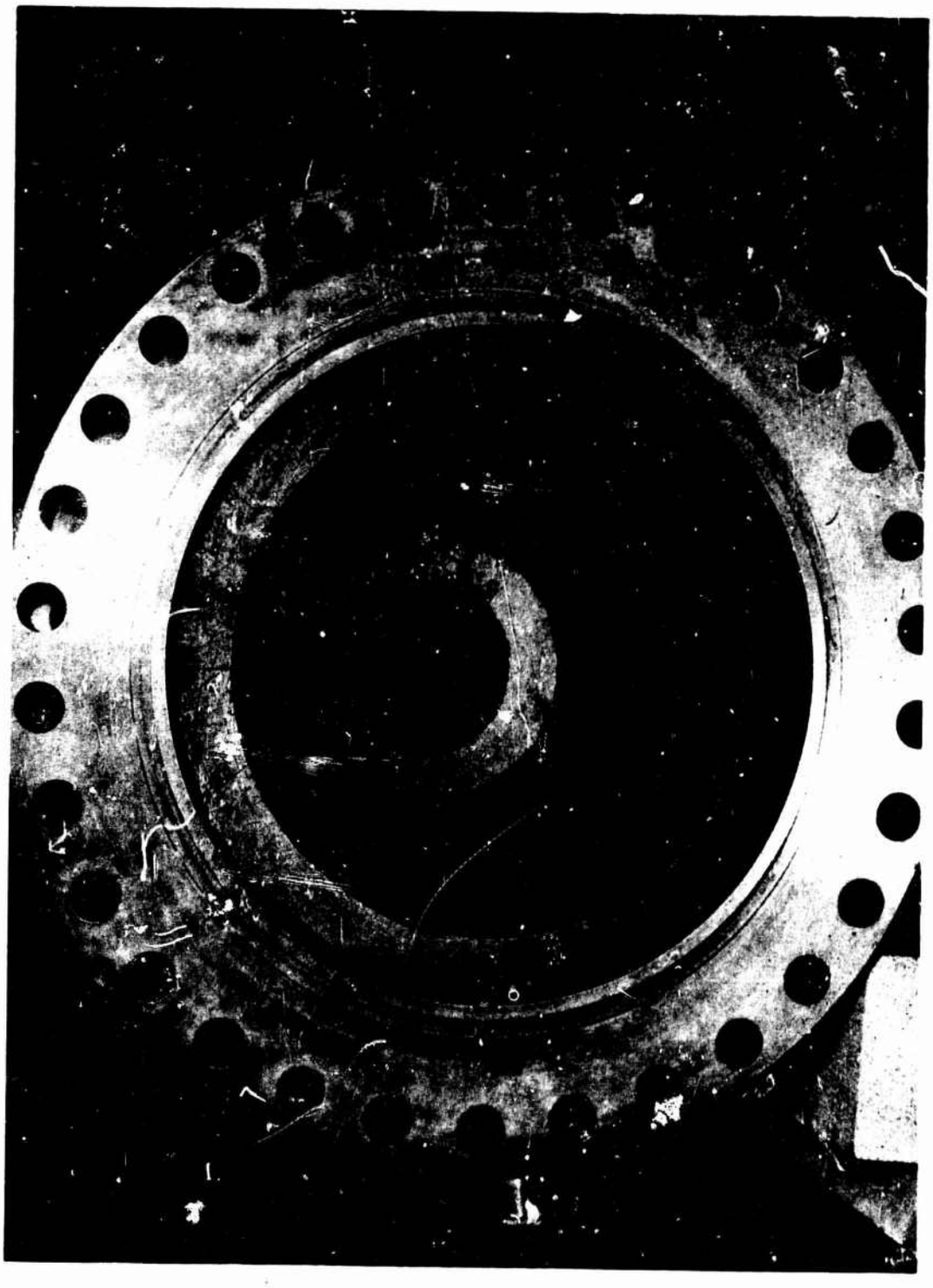

Pyrolytic Graphite Throat, Posttest Condition, Test 1.2-01-YAM-006 (u)

Figure VI-C-12

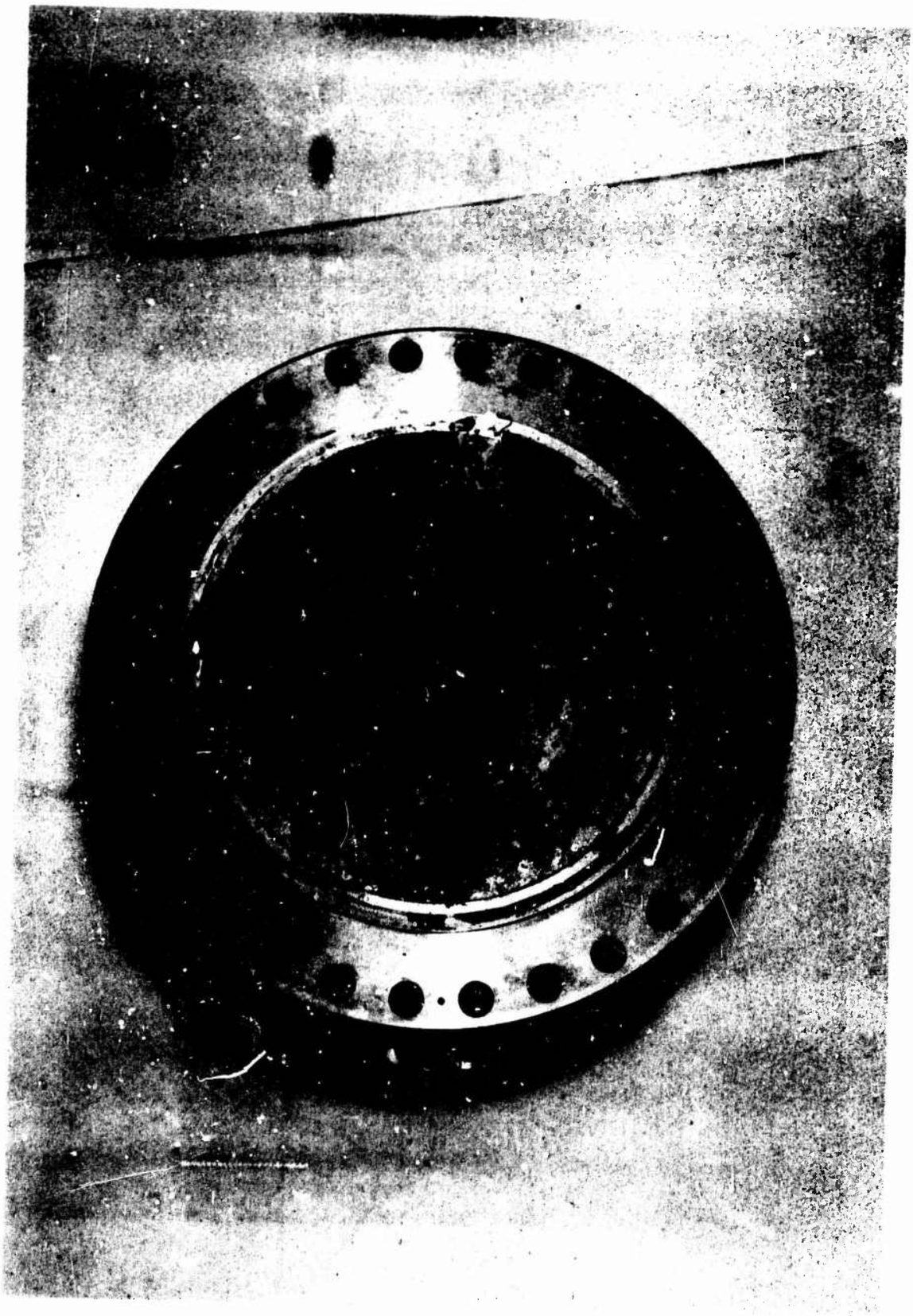

Pyrolytic Graphite Throat, Posttest Condition, Test 1.2-01-YAM-009

Figure VI-C-13

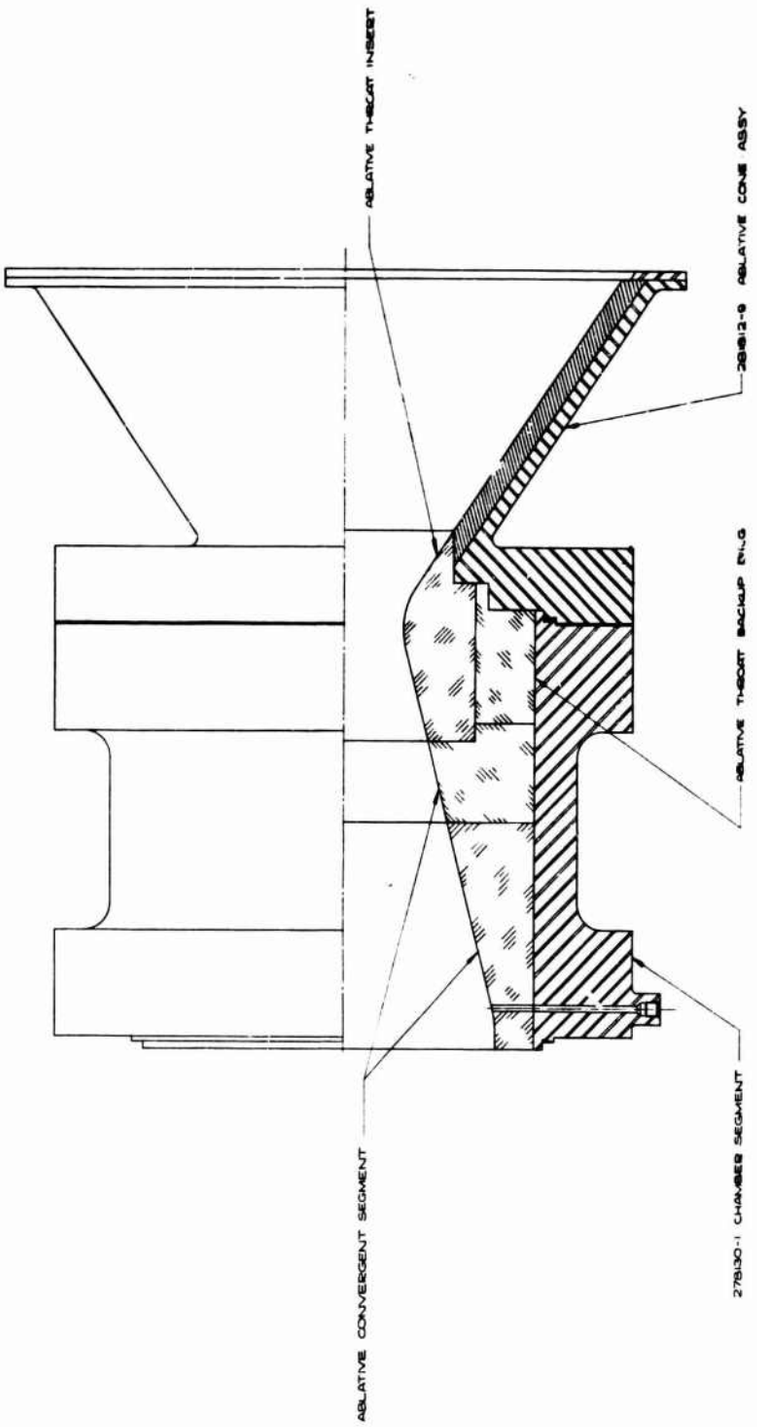

Ablative Throat Insert Design

Figure VI-C-14

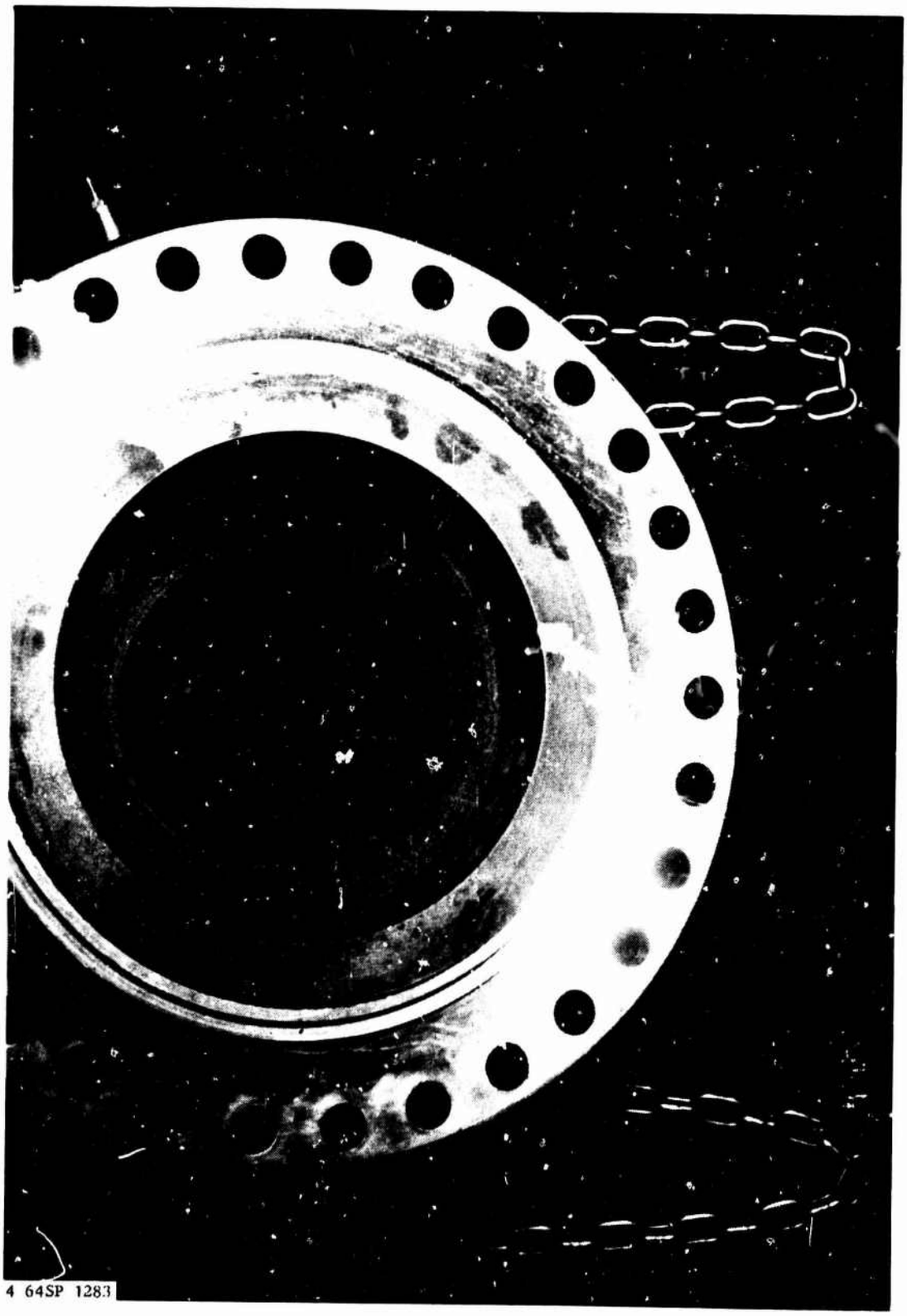

Ablative Convergent and Throat Segment, Pretest Condition

Figure VI-C-15

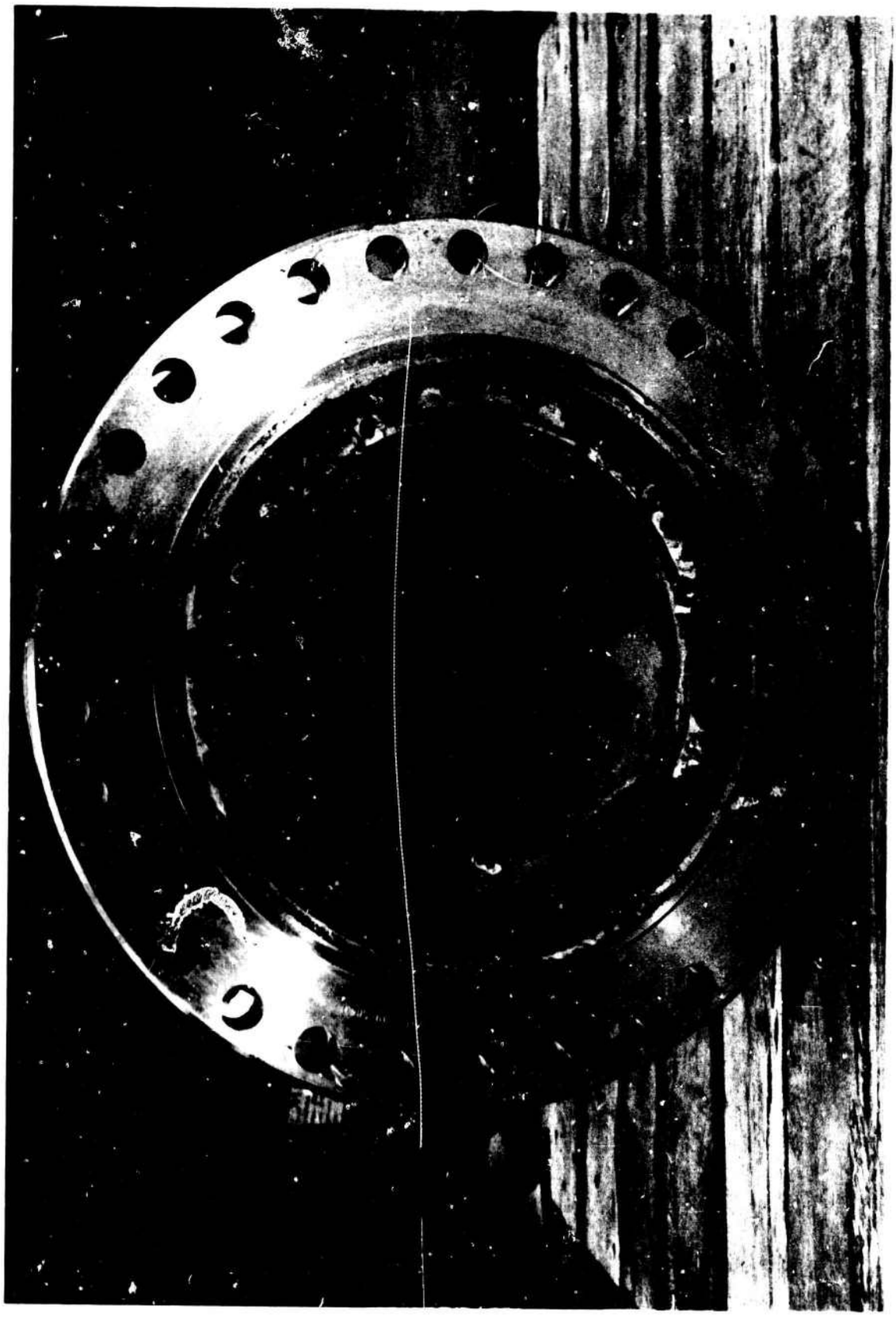

Ablative Convergent and Throat Segment, Posttest Condition

Figure VI-C-16

Graphite Cloth Throat Insert, Posttest Condition

Figure VI-C-17

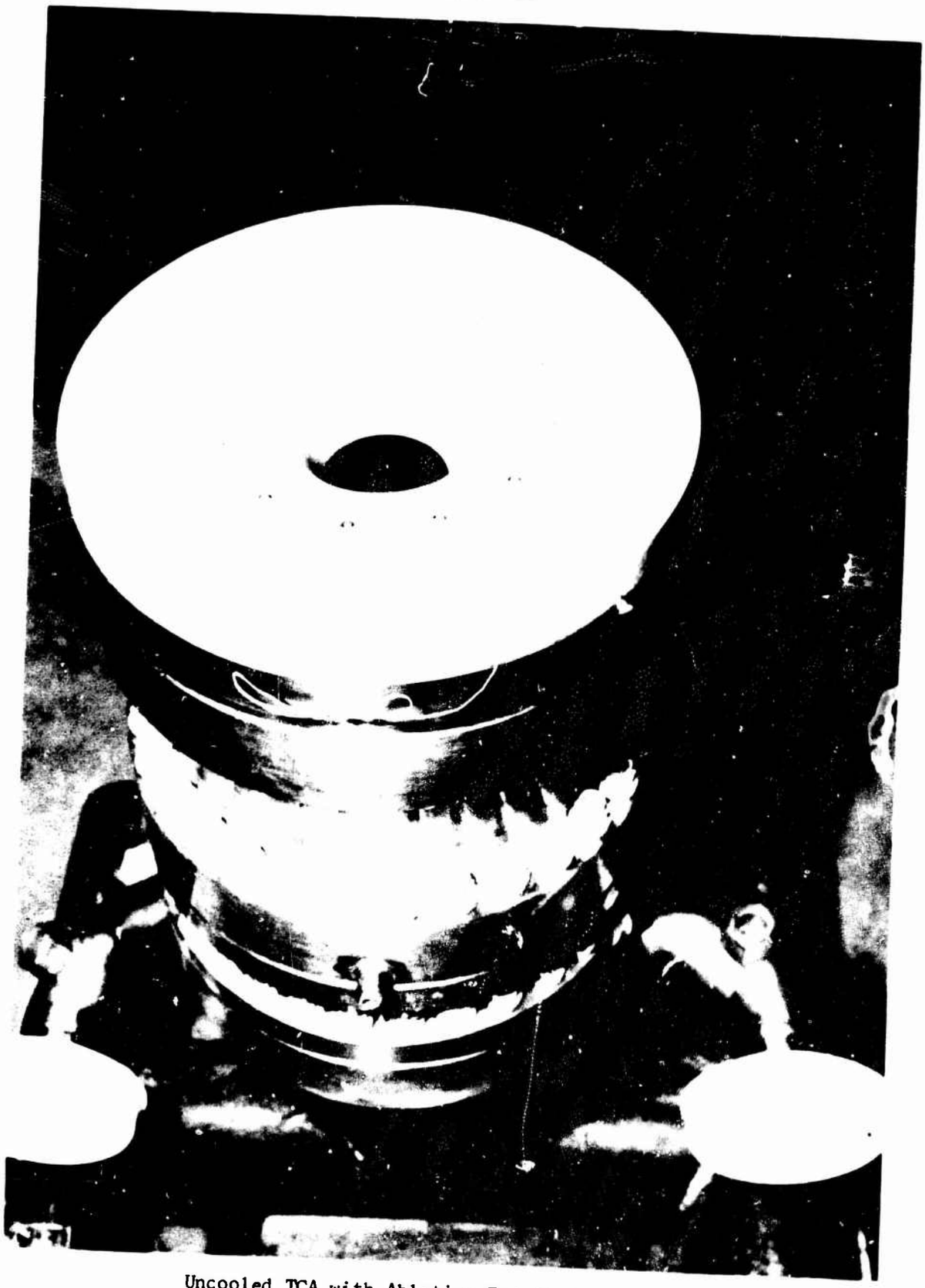

Uncooled TCA with Ablative End Closure Assembly

Figure VI-C-18

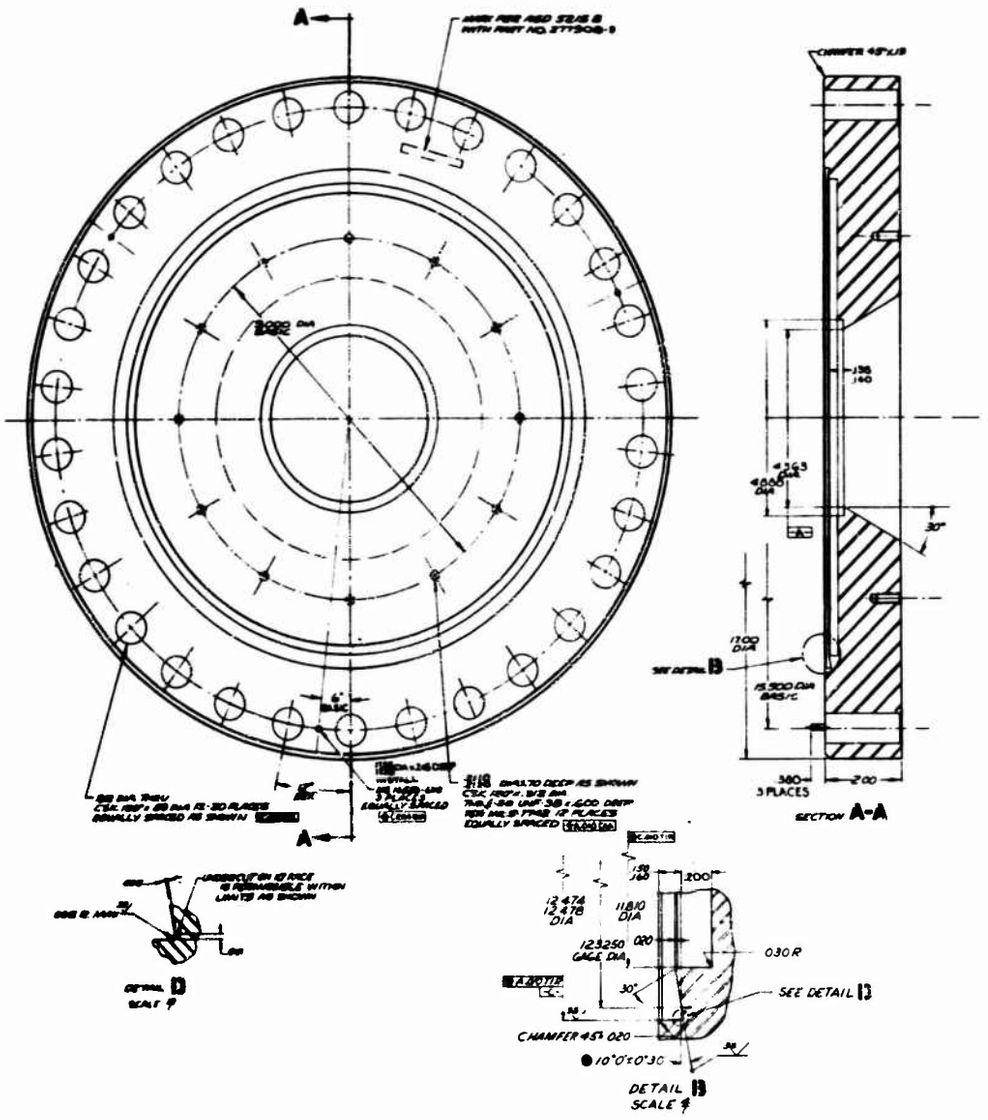

End Plate

Figure VI-C-19

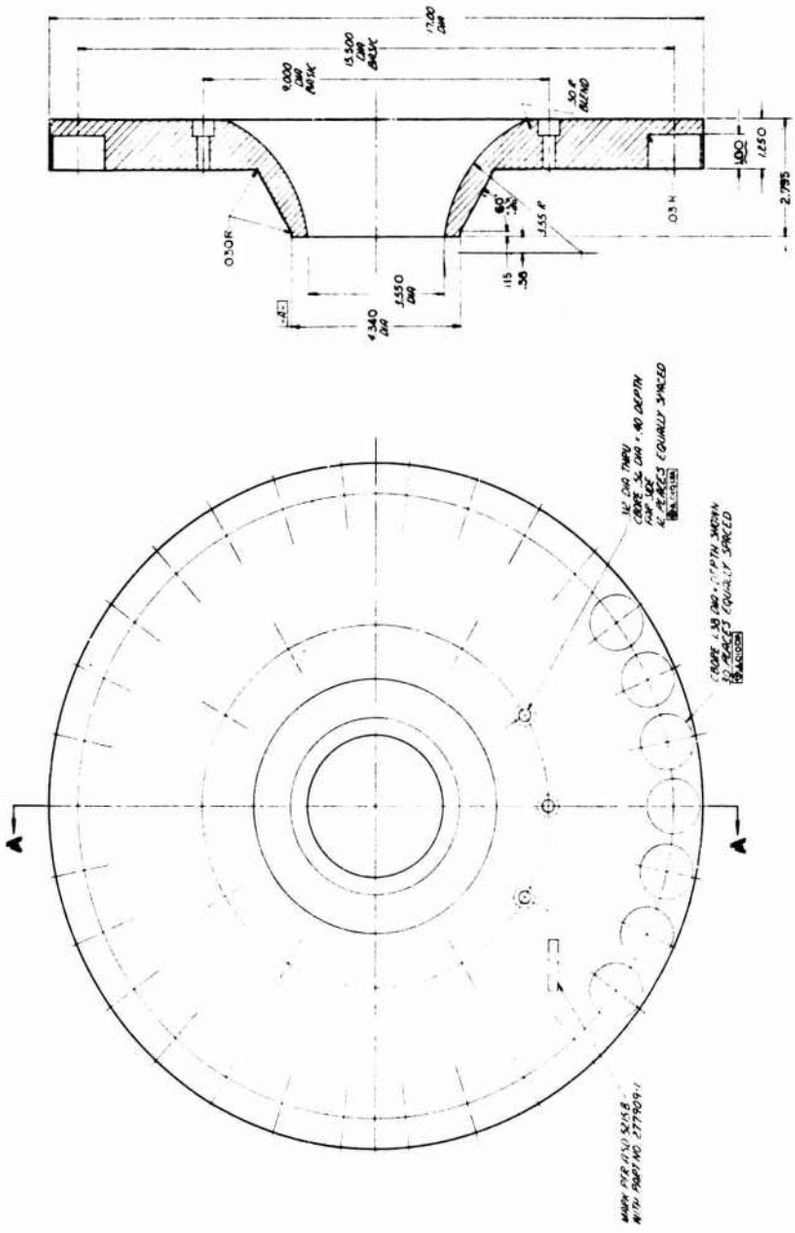

Ablative Protective Cover

Figure VI-C-20

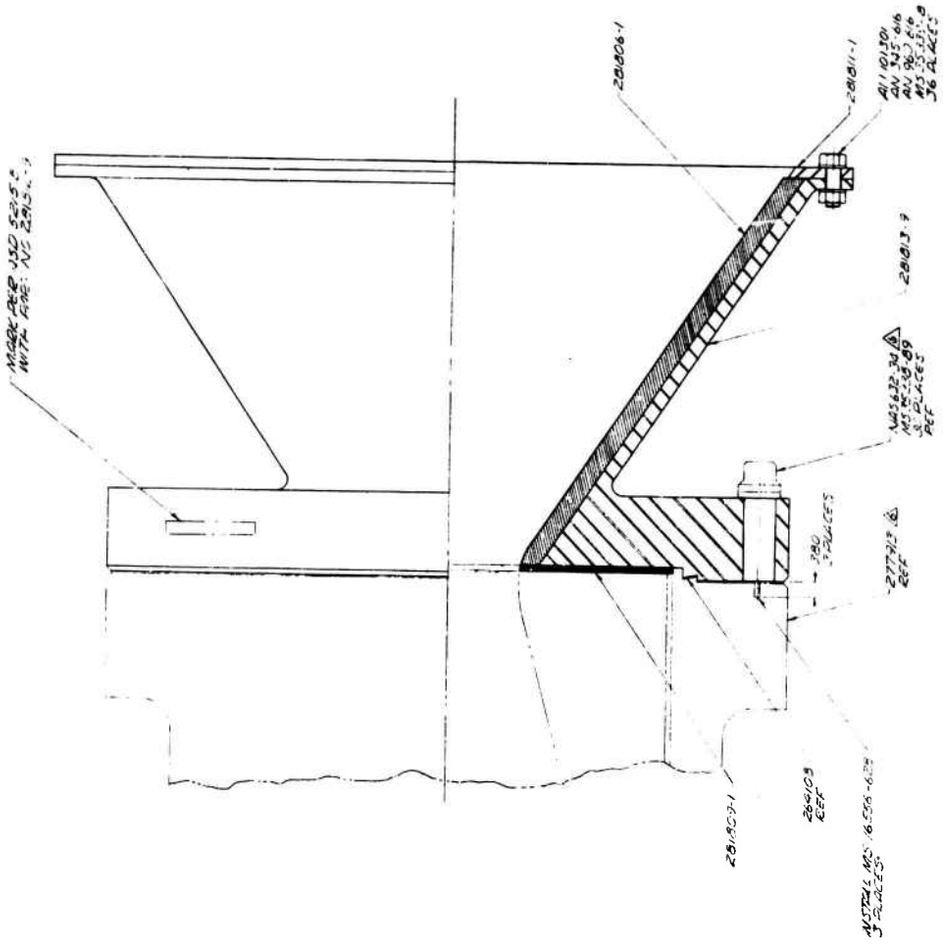

Ablative Exit Cone Design

Figure VI-C-21

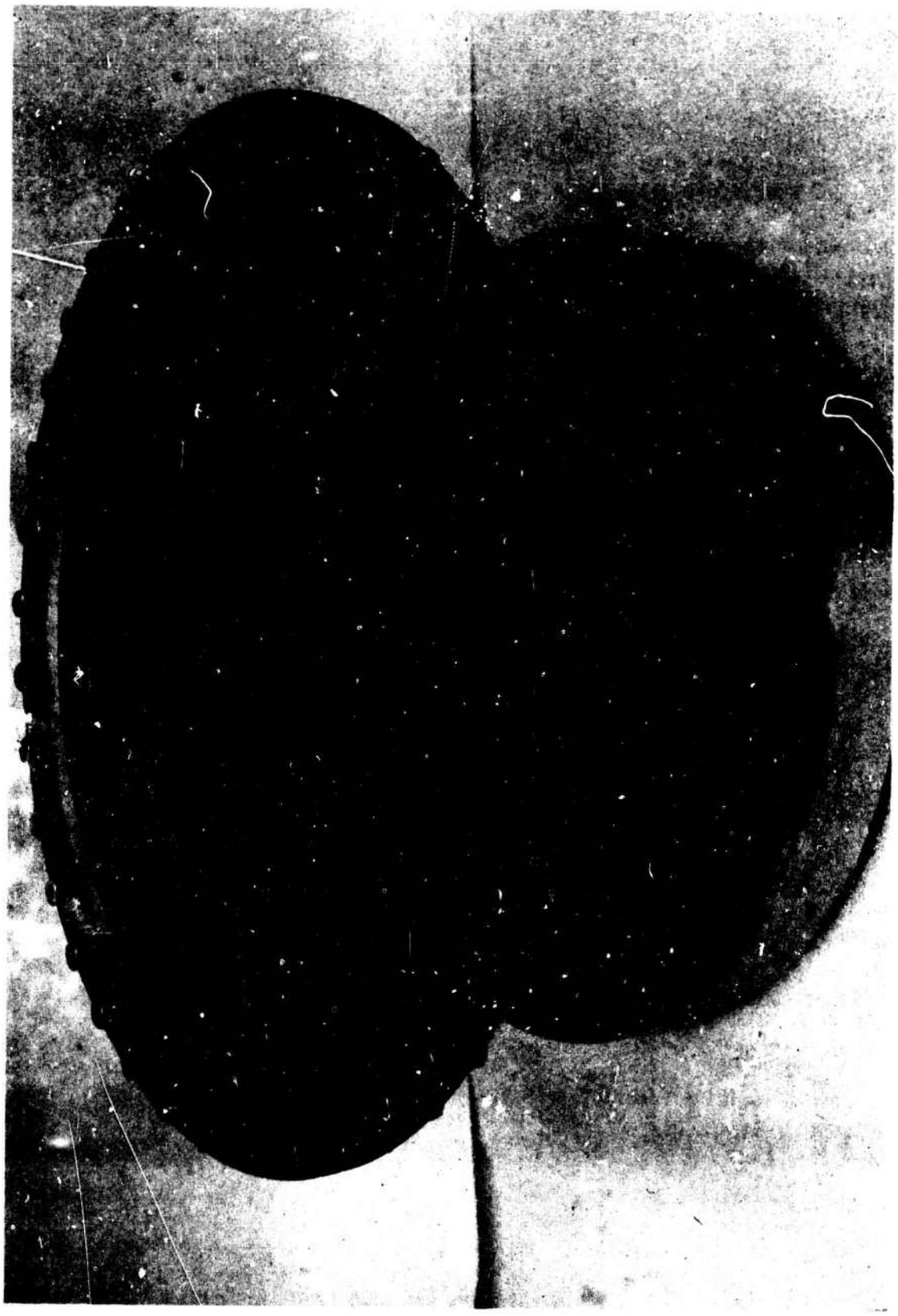

Ablative Exit Cone

Figure VI-C-22

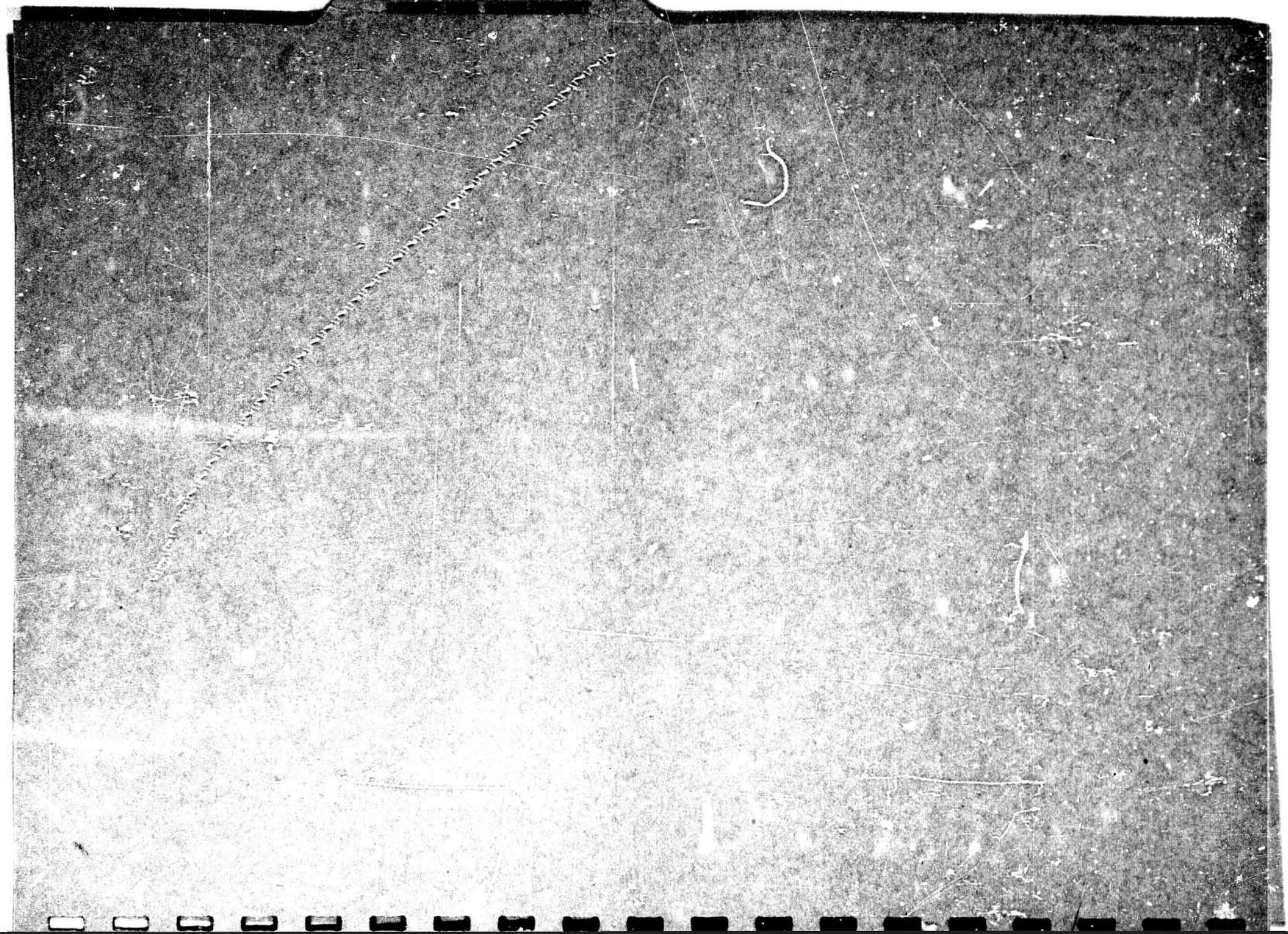

VII. COOLED THRUST CHAMBER DESIGN AND DEVELOPMENT

The basic objective of the Cooled Chamber Program was to investigate thrust chamber cooling techniques to determine the best cooling methods applicable to thrust chambers operating at high chamber pressures. To achieve this objective, a design and analytical investigation was first conducted in which each of the prospective cooling concepts was analyzed. The 3000-psia chamber pressure, 50,000-lb thrust chamber design was used as the model for the investigation. Some of the cooling concepts considered were eliminated as the result of this investigation; others were selected for detailed hardware design and evaluation by testing. To permit simultaneous evaluation of different cooling concepts in the experimental test program, all hardware components were designed as segments of the total thrust chamber. These segments included the cylindrical portion of the chamber, the convergent and throat section, the expansion nozzle down to the area ratio for optimum expansion at sea-level and a high area-ratio skirt extension. The segments were usable in combination with portions of the uncooled chamber hardware to permit evaluation of each cooling concept by itself, or in combination with other cooled hardware segments. A schematic showing the segments joined together to form the total thrust chamber is shown in Figure VII-A-1.

A detailed discussion of the cooling methods investigation is presented in Section VII,A below. All of the preliminary designs and analytical cooling studies conducted for the various cooling concepts considered are presented in this section. As a result of the cooling methods investigation, specific hardware was designed, fabricated and tested in the experimental program. Discussions for each of these components, including description of design, development testing, and analysis of the test results are presented in Sections VII,B through VII,F. Thrust chamber performance obtained with the experimental hardware is presented as a consolidated discussion and is given in Section VIII.

VII, Cooled Thrust Chamber Design and Development (cont.)

A. COOLING METHODS INVESTIGATION

To determine the best cooling methods for high-chamber-pressure thrust chambers, studies were made of several cooling concepts, individually and in various combinations. Following a preliminary investigation, the following concepts were selected for detailed analysis: regenerative cooling, film cooling, transpiration cooling, thermal barrier coatings, high-temperature materials, cooling by hot gas, vortex cooling, and ablative cooling.

1. Regenerative Cooling

Regenerative cooling is currently the most conventional cooling technique used in pump-fed liquid rocket engines. Existing engines that use N_2O_4/AeroZINE 50 propellants use the fuel (AeroZINE 50) as the regenerative coolant. The heat transfer properties of the N_2O_4 at the subcritical pressures at which these engines operate are relatively poor, making oxidizer regenerative cooling unattractive. However, in recent analytical and experimental work conducted by both Rocketdyne and Aerojet, it was determined that supercritical N_2O_4 is a very good regenerative coolant because of the endothermic dissociation of N_2O_4 at these pressures. At the time of the cooling methods investigation in this program, the heat transfer characteristics of supercritical N_2O_4 were not known; therefore AeroZINE 50 was the primary propellant considered for cooling the high heat-transfer region of the thrust chamber. However, oxidizer regenerative cooling of the expansion nozzle was considered (and subsequently selected for experimental evaluation).

A comprehensive study of regenerative cooling the thrust chamber with fuel was performed. Three thrust chamber designs were analyzed: a thick-wall tube bundle, a thin-wall tube bundle, and a smooth-wall drilled chamber. A summary of these analyses is given in the following paragraphs. The results of these analyses showed that regenerative cooling by itself is not sufficient to cool a high chamber pressure rocket thrust chamber; but it can be used in combination with other cooling technique, such as film cooling, or thermal barrier coatings.

VII, A, Cooling Methods Investigation (cont.)

a. Thick-Wall Tube Bundle

This thrust chamber, shown in Figure VII-A-2, is designed so that the tubes can withstand the pressure drop from the coolant passage to the outside of the thrust chamber without additional support required for the outside of the tube. It is a double-pass configuration, and has a characteristic length (L*) of 100 in. AeroZINE 50 is the regenerative coolant. The gas side of the tubes is protected by a thermal barrier coating.

Wall temperatures were computed for values of coating thermal resistance (t/k) of 80, 200, and 400 $in.^2$-sec-°F/Btu. Values of the allowable recovery temperature were then calculated and plotted as a function of chamber axial distance, shown in Figure VII-A-3. These curves indicate the maximum recovery temperature which can be allowed throughout the chamber for each value of thermal resistance without exceeding the assumed limiting temperature conditions of 3100°F coating surface temperature, 1700°F coating tube interface temperature, and 600°F inside tube wall temperature. Wherever the allowable recovery temperature is less than the existing gas recovery temperature, the gas temperature in the chamber boundary layer must be reduced by means of film cooling. Several methods of introducing film coolant into the combustion chamber were investigated; AeroZINE 50 was used as the film coolant. The method which required the minimum amount of film cooling, while still maintaining a practical design, is the injection of the coolant at four stations in the chamber, as shown in Figure VII-A-4. Twenty lb/sec, or 35% of the available fuel, is required for film cooling. Five lb/sec is injected in each of the four stations.

b. Thin-Wall Tube Bundle

In the thin-wall tube bundle design (Figure VII-A-5), the tube walls are designed to withstand only the pressure drop from the inside of the tubes to the inside of the combustion chamber. Therefore, the thrust chamber must have external reinforcing, such as steel or aluminum jacket, to make it operative.

VII, A, Cooling Methods Investigation (cont.)

It was hoped that the use of the thin walls would allow significantly higher heat transfer rates into the coolant, thereby reducing the film cooling flow rate requirement. However, the heat transfer analysis showed that with a coating thermal resistance (t/k) of 360 $in.^2$-sec-°F/Btu, approximately 20 lb/sec of film cooling is still required. This is because the resistance of the coating is much greater than the resistance of the tube wall; therefore, the difference in tube wall resistance obtained the changing tube thickness does not significantly change the overall resistance.

c. Smooth-Wall Thrust Chamber

In this design (Figure VII-A-6), the coolant passages are drilled in a stainless-steel shell. The convergent-throat-divergent contour is hyperbolic and is derived by the generation of a hyperboloid by straight lines. This construction is used successfully in the Agena engine. Since the regenerative passages are drilled, they are limited to a fixed circular area throughout the thrust chamber. Because of the chamber contour, it is therefore necessary to route the coolant passages in layers around the throat.

The heat-transfer characteristics of this thrust chamber are similar to that of the tube bundle thrust chambers described above and theoretically require a similar amount of film cooling to maintain proper temperatures of the coating and chamber wall. The main potential advantage of this design is that more uniform distribution of film cooling over the chamber surface can be obtained because of the smooth wall. In a conventional tube bundle, the film coolant has a tendency to flow off the crowns of the tubes and into the valleys between the tubes. Another potential advantage of the drilled construction is that it may be easier to maintain a coating on the chamber wall. This is because of the comparatively rigid construction of the inner wall as compared to the flexible wall of the conventional tube bundle.

VII, A, Cooling Methods Investigation (cont.)

The heat transfer analyses performed for the chambers described above show that relatively high film coolant flow rates are required. At very high pressures a relatively small amount of the total heat is able to be absorbed by regenerative cooling in the convergent and throat section of the nozzle. It was therefore concluded that in an advanced high pressure engine, a cooling technique other than regenerative plus film cooling will result in the optimum design for the throat region. In the chamber section, however, regenerative cooling together with a reasonable amount of film cooling is adequate. Below the throat at an area ratio of approximately 3:1, the chamber can be cooled by regenerative cooling alone. It was calculated that effective cooling could be obtained in this region using N_2O_4 as the regenerative coolant (endothermic effects of N_2O_4 not included). It was therefore decided to evaluate by experimental test an AeroZINE 50 cooled chamber L* segment and an N_2O_4 cooled expansion nozzle segment. For the chamber L* segment, both tube and drilled construction were considered. The layouts of each are shown in Figures VII-A-7 and VII-A-8, respectively. It was decided to use the smooth-wall concept because of the potential advantages cited above. The detailed design and the test experience are discussed in Section VII,B. The N_2O_4 regeneratively cooled expansion nozzle is discussed in Section VII,E.

2. Film Cooling

Liquid film-cooling with one of the propellants is the conventional supplemental cooling method for reducing local heat fluxes to acceptable levels that can be handled by regenerative cooling. The disadvantage of this cooling method is the thrust chamber performance loss produced by inefficient use of the propellant used for film cooling. The film coolant flow rate (and resultant performance loss) can be minimized by introducing the coolant into the chamber at multiple locations in the amounts locally required (rather than all from the injector face) and by maintaining good coolant distribution of the injected coolant on the wall of the thrust chamber.

VII, A, Cooling Methods Investigation (cont.)

Prior to this program no data existed which described the performance losses associated with film cooling high-pressure storable propellant thrust chambers, or the effectiveness of film cooling for removing heat from the chamber wall. In order to determine the effects of coolant injection location and quantity on coolant efficiencies and performance, it was decided to design and experimentally test a film coolant convergent and throat segment. To allow maximum flexibility in the program, use of either propellant as a coolant and multiple individually controlled injection stations were established as design criteria. The preliminary design is shown in Figure VII-A-9. The detailed design of this component and the test program conducted on the resultant hardware are discussed in Section VII,D, below.

3. Transpiration Cooling

Transpiration cooling is theoretically the most efficient form of film cooling. In this technique, the coolant flows directly through the chamber wall, which is constructed of a porous material. Because the film is distributed evenly over the entire area to be cooled, the technique is extremely efficient; and as a result, minimum engine performance degradation from the film coolant occurs. The problems associated with this method are plugging of the low porosity wall and vapor-lock effect caused by hot spots--conditions that propagate themselves until failure occurs. At the time of the investigation, the endothermic behavior of the N_2O_4 oxidizer was not known. Consequently, N_2O_4 was believed to be a relatively poor coolant and it was not considered in this application. The AeroZINE 50 fuel was not considered to be a satisfactory transpiration coolant because of the plugging characteristics associated with this carbonacious fuel. On this basis it was decided not to test the transpiration cooling concept in thrust chamber hardware in this program. However, based upon the recent heat-transfer characteristics data for N_2O_4 as well as new fabrication concepts for transpiration cooled chambers, transpiration cooling of storable propellant high-pressure rocket engines with N_2O_4 now appears feasible.

VII, A, Cooling Methods Investigation (cont.)

4. Coatings

Thermal barrier coatings can be used to reduce the heat flux and film cooling requirements of regeneratively cooled thrust chambers. The problems with coatings have historically been the maintaining of the coating on the chamber wall and the compatibility of the coating material with the combustion gases. At the time of the cooling concepts methods investigation of this program, coating development was being directed toward gradated ceramic-type coatings. Pure ceramic materials have drastically different coefficients of expansion than that of materials used for thrust chamber tubes. Because of this, the coatings separate from the chamber wall and are destroyed during the engine start transient. The gradated coatings were an attempt to overcome this problem through coating layers of materials which had different coefficients of expansion to produce a coating having a constantly varying coefficient of expansion which matched that of the parent material on one side and that of the ceramic material on the other.

Coatings of this type were evaluated in laboratory tests for application to the regeneratively cooled L* segment. Three suppliers: Advanced Technology Laboratories, Pyroco Co., and Aerojet-General Corporation provided 3-in.-long coated tubes for test evaluation. All coatings were gradated nichrome zirconia and nichrome thoria. The specimens were tested for layer thickness, thickness uniformity and thermal shock. Based upon these tests, it was decided to use a nichrome zirconia coating for the L* segment.

Following this investigation and prior to the time for coating the L* segment, an entirely new approach to coatings was developed by Aerojet-General under the Titan Product Improvement Program, Contract AF 04(694)-212. These coatings are refractory metal alloys, flame-sprayed to the combustion chamber. The thermal shock characteristics of this new family of coatings are vastly superior to the ceramic-type coatings; however, the oxidiation resistance of the coatings is relatively poor, making oxidizer film cooling questionable. Based on the recent coating development, it was decided to coat the regeneratively cooled L* segment using the new coating. Application of the coating to this hardware is discussed in Section VII,B.

VII, A, Cooling Methods Investigation (cont.)

5. High-Temperature Materials

Materials, such as pyrolytic graphite or tungsten can withstand very high temperatures without loss of mechanical strength. The use of these materials in combination of regenerative and/or film cooling was therefore investigated. It was found, however, that these materials are not compatible with the products of combustion of the storable propellants, and because of their brittleness, are marginal in their ability to survive the start transient of a high chamber pressure thrust chamber. Various methods of protection were investigated but none was found to be sufficient to ensure a reasonable degree of confidence. This concept was therefore abandoned.

6. Hot-Gas Cooling

Hot-gas cooling is essentially film cooling using relatively cool gases. A thrust chamber design using this cooling technique in combination with regenerative cooling and high-temperature materials was investigated. The design, shown in Figure VII-A-10, is a regeneratively cooled tube bundle chamber having an inner liner made of a high-temperature refractory material. The thrust chamber injector is separated into two sections. The central portion, through which most of the propellants are injected, operates at thrust chamber design mixture ratio. In the outer portion of the injector, fuel-rich gases are produced which flow down the thrust chamber in the annulus between the liner and the tube bundle. This gas provides cooling, and together with the liner, establishes a thermal barrier between the combustion gases and the regenerative tubes. The liner is made of a refractory material designed to operate at a much higher temperature than is possible with the steel material of the tube bundle.

Heat-transfer analyses performed with this chamber showed the concept to be impractical even with large quantities of hot-gas film coolant. Liner temperature was higher than the upper design temperature limit for refractory materials (3200°F

for tungsten; above this temperature the recrystallization characteristics cause the material to rapidly become brittle). Perforated liners were evaluated in which some of the hot gas from the annular chamber was allowed to flow through the liner into the main chamber to provide some film cooling on the hot-gas side of the liner. Liner temperatures were still in excess of acceptable values. It was concluded that this concept only moved the heat transfer problem from the tubes of a conventional regeneratively cooled chamber to the liner in this chamber. Furthermore, the required quantity of hot-gas film coolant is more than that required by conventional liquid film cooling of a regeneratively cooled thrust chamber. Therefore, this concept was eliminated from further consideration.

7. Vortex Cooling

The cooling effect of vortex injectors was first reported by Thiokol Chemical Corporation under Contract AF 04(611)-5682.* In this concept, fuel is injected tangentially onto an injector premix wall and the oxidizer is impinged radially from the center into the fuel. At the point of contact, fuel particles react with some of the oxidizer and undergo a density change. The centrifugal force replaces the low density fuel particles with the heavier oxidizer particles. As the combusting fuel particles migrate through the oxidizer toward the center of the thrust chamber, a vortex is formed. As long as the vortex is maintained, the centrifugal force tends to keep the cooler gases near the wall, and thus reduces the heat flux to the wall. Furthermore, since the fuel migrates through the oxidizer, better mixing and high combustion efficiency is obtained. Theoretically, the higher the vortex velocity the better the cooling and combustion efficiency. In practice, however, this is not true, since recirculation losses become prohibitive. At very high vortex velocities the recirculation of the combustion gases caused by the vortex can extend down into the throat region of the thrust chamber. When this happens the aerodynamic throat is smaller than the physical throat, a single stagnation pressure at the throat is not maintained, and a performance loss results.

*Vortex Combustion, Thiokol Chemical Corporation Report, Contract AF 04(611)-5682, April 1961.

VII, A, Cooling Methods Investigation (cont.)

In the High Chamber Pressure Rocketry Program, the vortex principle was further investigated in both the uncooled and the cooled thrust chamber programs. The uncooled program evaluated a conventional type of vortex injector. In the Cooled Chamber Program an investigation was conducted of the application of the vortex principle to a unique injector design in which the injector is located on the thrust chamber wall. Two conceptual designs of an L* segment were prepared (Figures VII-A-11 and VII-A-12). In the first design (Figure VII-A-11) 50% of the propellants is injected through a conventional vortex injector similar to that used with the uncooled thrust chamber. The remaining propellants are injected tangentially through four separate injection stations which are parallel to the chamber axis. Through these injectors 40% of the propellants is injected at design mixture ratio and 10% of the propellants is injected near the contour section of the nozzle at a mixture ratio of 0.085, producing a layer of relatively cool fuel-rich gases (1950°F) through the throat. In the second design (Figure VII-A-12) the total propellants are injected tangentially onto the chamber wall through 776 orifices. Of these orifices, 576 are oxidizer inlets and 200 are fuel inlets. Twenty-four of the fuel orifices located in the last injection row next to the convergent section are larger to provide a fuel-rich layer on the wall of the convergent and throat portion of the thrust chamber. A forward closure is attached over the top of the chamber where the injector normally is located. This closure can either be regeneratively cooled, film cooled, transpiration cooled, or ablative cooled. The design is illustrated with a regeneratively cooled face in Figure VII-A-12 and with an ablative face in Figure VII-A-13.

It was decided to evaluate the second design concept experimentally in the cooled chamber test program. The detailed design and test experience with this component is given in Section VII,C.

8. Ablative Cooling

Ablative cooling of thrust chambers is being successfully used in current storable propellant engines operating at very low chamber pressures (e.g., Transtage, P_c = 100 psia; Apollo; P_c = 100 psia). At high chamber pressures, however,

VII, A, Cooling Methods Investigation (cont.)

the heat transfer rates in the chamber and throats are so severe that prohibitively high erosion rates of the ablative materials occur, rendering the cooling concept completely unacceptable for long-duration firings. For very short durations, ablative materials are satisfactory, and were very successfully used in this program for uncooled chamber testing (see Section VI).

Ablative cooling can be used in the expansion nozzle portion of the chamber below the area ratio point where the heat fluxes are reduced to acceptable values. For this program an ablative nozzle extending from an area ratio of 21:1 to an area ratio of 70:1 was designed and test-fired. It is discussed in Section VII,F.

VII, Cooled Thrust Chamber Design and Development (cont.)

B. REGENERATIVELY COOLED CHAMBER SEGMENT

1. Design Description and Fabrication

The drilled L* segment, shown in Figure VII-B-1, is regeneratively cooled by fuel. It is a smooth-wall double-pass configuration, incorporating 192 1/8-in.-dia coolant passages. The fuel velocity in the passages is 128 ft/sec at the rated flow of 57 lb/sec. The manifolding is divided into 60° pie-sectors so that up and down flow is by alternate sectors instead of through every other hole. This arrangement was selected because of the space limitations in the segmented hardware. The design layout of the L* segment is shown in Figure VII-A-8.

The Cooling Methods Investigation showed that regenerative cooling alone is inadequate for cooling high chamber pressure engines, but must be supplemented with film cooling and/or a thermal barrier coating. A heat transfer analysis was performed to determine what film cooling flow rates were required to supplement the regenerative cooling with and without a coating. Fuel was assumed as the film coolant. With 100% of the rated fuel weight flow being circulated through the segment, and employing temperature limitations of 3100°F, 1700°F, and 600°F on the thermal barrier coating outer surface, the interface between chamber and coating, and the liquid-side wall temperature, respectively, theoretical calculations indicated that 3.8 lb/sec of fuel film coolant is required to cool the drilled chamber segment. If no thermal barrier coating is used and the limits of 1700°F and 600°F are placed on the gas-side wall temperature and the liquid-side wall temperature, respectively, 10 lb/sec of fuel film coolant is required. It was decided to evaluate both coated and uncoated configurations in the program.

The selected coating was of the metal-base type recently developed under the Improved Titan Predevelopment Program, Contract AF 04(694)-212. This family of coatings has demonstrated far superior performance to the gradated nichrome-zirconia type coatings considered earlier in the program. The specific coating selected for the L* segment was 85% tungsten, 12% zirconium oxide, and 3% silicon, by weight.

VII, B, Regeneratively Cooled Chamber Segment (cont.)

Design thickness was 0.090 in., which produced a thermal resistance (t/k) of 680 in.^{2}-sec-°F/Btu. This coating was applied to one of the two L* segments fabricated. It was deposited in 26 layers on the chamber wall by plasma-arc spraying. Actual thickness after application was 0.092 in.

The appearance of the coating as deposited is shown in Figure VII-B-2. The dark region is due to dampness. During the deposition process molten tungsten freezes immediately upon impact, and as a result high compressive residual stresses are present. In this instance, after deposition the liner was beginning to shrink away from the stainless-steel wall because of the high residual stress; it was possible to insert a 5-mil wire to a depth of 1/2 in. at several points at each end of the liner into the interface region. Other factors which contributed to the slight separation are the large thickness of the coating, 0.092 in., the smooth internal cylindrical geometry, which provides less bonding area and stress relieving than a tube bundle cooled structure, and the many thermal shocks experienced during the 26 passes required in the deposition process.

The finished hardware is shown assembled to the concentric-ring injector in Figure VII-B-3. Figure VII-B-1 shows the three metal skin-temperature thermocouples, installed 120° apart at the base of the segment at the coating-wall interface; the readings from these thermocouples, together with the coolant inlet and outlet temperatures, were used to calculate the heat-transfer conditions in the L* segment during testing.

2. Development Testing and Results

Three tests were performed using the drilled L* segment: Tests 1.2-02-YAM-030, -031, and -034. In the first two, the coated segment was evaluated; in the last test, the same hardware was tested with the coating removed. Each of these tests is discussed in the following paragraphs:

VII, B, Regeneratively Cooled Chamber Segment (cont.)

a. Test 1.2-02-YAM-030

This test, conducted on 22 March 1965, was a short-duration checkout test of the drilled L* segment hardware. The thrust chamber assembly consisted of the Mod VIII concentric-ring injector, drilled L* segment, an ablative L* segment, an ablative convergent and throat segment, and an ablative end-cover. Approximately 3.5 lb/sec of oxidizer film cooling from the outer periphery of the injector was applied to the L* segment wall. The test duration from FS-1 to FS-2 was 2.139 sec, of which 0.439 sec was at the steady state chamber pressure of 2573 psia. The test was successful, and no hardware damage occurred. There was no evidence of loss of thermal barrier or regression from oxidizer attack. There were several blue areas near the exit end of the segment, but there was no apparent thickness loss.

Examination of the fuel outlet temperature and coating-metal interface temperature measurements showed that the component did not reach thermal steady-state condition during the test. These temperature data and the chamber pressure are shown as functions of time in Figure VII-B-4.

A heat-transfer analysis to determine the firing duration required to achieve thermal steady-state condition was then conducted using the Aerojet-General transient conduction computer program 8057. This analysis used the actual chamber pressure transient and steady-state flow rates obtained in Test 1.2-02-YAM-030. The results of this analysis, shown in Figure VII-B-5, indicated that thermal steady-state condition could be achieved within a test duration of about 3.0 sec. Based on the results of this heat-transfer analysis, the duration of the next test (Test 1.2-02-YAM-031) was extended to 3.5 sec.

Examination of the fuel outlet temperature data obtained in Test 1.2-02-YAM-030 indicated that the response of the 22-gage chromel and alumel wire (approximately 0.025-in. dia) used in fabricating the 1/8-in.-dia thermocouples was too slow. A fuel bulk temperature rise of only 2°F was indicated at the end of the test. Higher-response thermocouples having a sheath diameter of 0.040 in. and constructed using 0.006-in. chromel and alumel wire were fabricated and installed for Test 1.2-02-YAM-031.

VII, B, Regeneratively Cooled Chamber Segment (cont.)

b. Test 1.2-02-YAM-031

The second test of the coated drilled L* segment was conducted on 29 March 1965. It ran for 3.02 sec at a chamber pressure of 2456 psia. The test was successful; no hardware damage occurred. Thermal steady-state condition was achieved just prior to shutdown. Temperature data for this test are shown in Figure VII-B-6.

The duration required to achieve complete steady-state condition appears to be longer than indicated by the transient conduction analysis discussed previously. This is probably due in part to the one-dimensional conduction assumption used in the analysis; also, the cold nitrogen purge employed in the fuel system prior to firing may also be a factor. The fuel inlet and outlet thermocouples indicate that the nitrogen temperature in the fuel system ranged from 10°F to 32°F just prior to FS-1. The low coolant passage wall temperatures produced by the cold gas therefore initially cool the fuel as it flows through the segment.

The fuel bulk temperature rise in the L* segment indicated by TFK-I (fuel inlet temperature) and TFK-O-1 (fuel outlet temperature) was 10.5°F. The readings of thermocouple TFK-O-2 (another fuel outlet temperature) were considered invalid because it yielded consistently low values throughout the test. These data, along with the measured fuel flow rate of 51.1 lb/sec, indicate a total heat-transfer rate of 370 Btu/sec. Analysis of the L* segment using Aerojet-General film cooling computer program 8034 yielded a calculated total heat transfer rate of 302 Btu/sec (8.6°F bulk rise)--about 18% less than the experimental value. This analysis was conducted assuming the heat-transfer coefficient calculated from the Bartz equation between the film coolant and segment wall and twice this value for the heat-transfer coefficient between the mainstream gas and film coolant.

The coating-metal interface temperature calculated for the downstream end of the segment in the above analysis is 610°F. The measured values range from 790°F (TSK-1) to 1285°F (TSK-2). The calculated coating gas-side wall temperature is 3380°F. No measurement of this temperature was attempted.

VII, B, Regeneratively Cooled Chamber Segment (cont.)

The thermal barrier again showed good performance. There was no general surface regression visible. There was some chipping at the injector end of the point of impingement of the film cooling. The fracture edges were rough and brittle; oxidation or corrosion did not appear to be a factor. The chipping was confined to within 3/8 in. of the end of the liner and to a depth ranging from 5 mil to full thickness. The cause for the chipping was not positively ascertained, but could have been from oxidizer impingement forces or mechanical movement of the liner. It was found upon disassembly that the entire liner was free to move axially 0.150 in. and rotate $\pm$ 50° angularly. Since the internal diameter of the L* segment was tapered slightly larger at the injector end, slipping of the liner downstream would force the coating inward and possibly cause the observed chipping.

Since the coating was now loose from the chamber wall, the bond thermal resistance during future firings would be unknown; furthermore, the loose coating might structurally fail during the shock of the start transient and damage adjacent hardware. It was therefore decided to remove the coating and retest the L* segment in its uncoated configuration.

c. Test 1.2-02-YAM-034

A parametric heat-transfer analysis was performed for the uncoated L* segment prior to Test -034. The results are shown in Figure VII-B-7. Maximum recommended operating heat flux for supercritical AeroZINE 50 to prevent burnout is 4.4 Btu/in.^{2} sec at 3000 psia. To stay below this limit, 7 to 14 lb/sec of N_2O_4 film cooling would be required, based on simple Bartz and twice-Bartz correlations, respectively. Wall temperatures at either of these flow rates were below acceptable maximum values.

Film cooling from the concentric-ring injector is 3.5 lb/sec N_2O_4. However, an additional 14 lb/sec of N_2O_4 is transpired through the outer Rigimesh ring, which certainly gives some added protection along the chamber wall.

VII, B, Regeneratively Cooled Chamber Segment (cont.)

Based upon the previous test results of the coated segment and the excellent condition of the posttest hardware, it was decided to test the uncoated L* segment with no additional film cooling applied.

Test 1.2-02-YAM-034 was conducted on 20 April 1965. Total test duration was 3.58 sec of which 1.6 sec was at a steady-state chamber pressure of 2475 psia. No hardware damage occurred. The uncoated L* segment, regeneratively cooled with fuel, was located just below the concentric-ring injector. Ablative hardware was used downstream.

The important test parameters for this test are shown in Figure VII-B-8. The L* segment wall temperature thermocouple, which was located at the base of the segment, rose initially to 2500°F, and then decayed to 1500°F, where it became steady just prior to shutdown. The high initial reading must have been caused by start transient conditions, since the hardware could not have withstood this temperature under steady-state conditions.

Because of the thermocouple location, the recorded temperature is not fully representative of the regeneratively cooled wall temperature. It is located at the base of the segment in the end-closure ring, which has a wall thickness of 0.030 in.; the regenerative coolant passes through this ring at 50 ft/sec. The main passage wall is 0.020 in. thick; fluid velocity is 62 ft/sec. The recorded temperature was corrected for this difference; the calculated actual wall temperature was 1300°F. At this temperature the N_2O_4 film cooling rate would be between 3 to 7 lb/sec, depending on whether simple or twice-Bartz is assumed. This is in good agreement with the actual coolant amount used. Because of the cooling supplied by the outer Rigimesh ring from the injector face, it was concluded that the twice-Bartz correlation more nearly approximated actual chamber conditions. At 7 lb/sec, chamber heat flux would then be 8 Btu/in.^{2} sec, which was above the recommended maximum value. No burnout occurred, however.

VII, Cooled Thrust Chamber Design and Development (cont.)

C. VORTEX CHAMBER SEGMENT

1. Description of Design

The vortex chamber segment is a propellant injection device that differs from conventional rocket engine injectors in that all propellant is injected through the chamber wall rather than at forward end of the combustion chamber through a conventional injector face. A reduction of chamber surface area to be cooled, the reduction of heat transfer to the chamber wall due to the vortexing action of the combusting gases, and the possibility of high injector combustion efficiency are the salient features of this design.

The vortex chamber segment design is illustrated in Figure VII-A-13. All propellant is injected through 1176 injection holes drilled tangentially through the chamber wall. These holes are vertically aligned on the chamber wall, producing 48 rows of holes. The rows are manifolded in such a way that the alternate rows of holes inject oxidizer (24 rows) while the remaining rows of holes inject fuel. Each fuel row contains 25 holes; each oxidizer row contains 24 holes. Fuel and oxidizer holes are 0.054 and 0.064 in. in diameter, respectively. Injection velocity was 100 ft/sec in both circuits. Injector pressure drops of 150 and 225 psi were designed for the fuel and oxidizer circuits, respectively. An additional hole in each fuel row is provided at the aft end of the chamber segment, next to the convergent portion of the nozzle, to provide a fuel-rich layer of propellant downstream on the chamber wall. Fuel and oxidizer holes in adjacent rows are not in line, but are purposely staggered from one another to promote propellant mixing and good combustion efficiency. The vertical rows of alternate fuel and oxidizer holes inject sheets or layers of propellant, and thus film-cool the injection surface as well as mix the propellants.

At the base of the vortex L* segment, four thermocouples are installed, equally spaced from one another to monitor the surface temperature of the injector face.

VII, C, Vortex Chamber Segment (cont.)

At the forward end of the segment, the area normally occupied by the injector in a conventional rocket engine, a steel closure plate is provided. This closure is protected from the combustion chamber gas by an ablative cover-plate that is mechanically fastened in place.

Inlet manifolding to the segment is provided by using the conventional injector inlet manifold housing. Internal manifolding of the segment is complex and separation between fuel and oxidizer circuits is dependent upon interchannel welding.

2. Development Testing

One vortex L* segment was fabricated; two tests were conducted with this unit. Total chamber L* was 70 in. The test objectives were to evaluate the design as an injector and as a cooling device. Unfortunately, failures unrelated to the injector or cooling principles of the design occurred in both tests; in the first test the graphite throat liner was lost during the start transient; in the second test, an interchannel propellant leak developed in the segment manifolds just after steady-state was reached--damaging the unit beyond repair. However, valid steady-state data were obtained in the latter test. Specific summary details for each test are discussed in the following paragraphs.

The completed vortex chamber segment is shown in Figures VII-C-1 and -2 as it appeared prior to the first test. This segment was assembled to a chamber containing an ATJ graphite convergent and throat segment; the assembly was tested on 11 January 1964 during Test 1.2-01-YAM-007. This test was designed to operate at a chamber pressure of 3000 psia for 1.65 sec. The test was prematurely terminated at FS-1 + 0.918 sec by the combustion stability monitor (CSM), an engine malfunction shutdown device. The graphite convergent and throat segments were severely damaged; the vortex L* segment sustained minor damage. The ablative face cover failed, and a number of oxidizer orifice tubes installed in the injector face came loose and bent into the main stream. The extent of the damage is illustrated in Figures VII-C-3, VII-C-4 and VII-C-5. High-speed photographic records verified that

VII, C, Vortex Chamber Segment (cont.)

the graphite failed early during the start transient--initiating the shutdown. After minor repairs, the vortex L* was restored to its original condition and was available for retesting. Figure VII-C-6 illustrates the vortex L* segment after repairs had been completed.

Test 1.2-01-YAM-010 was conducted on 11 February 1964. A scheduled duration was 1.75 sec at a chamber pressure of 3000 psia as planned. The test was prematurely shut down at FS-1 + 1.264 sec by the high transient pressure shutdown device (HTPSD).

Severe test hardware damage was sustained. Damage occurring to the vortex L* segment included failure of the ablative injector face cover by delamination (Figure VII-C-7) and mechanical failure of the chamber-injector face over an approximate 90° sector (Figure VII-C-8). Evidence of severe burning of metal was visible on the injector face.

3. Test Data Analysis and Conclusions

The analysis of the test records of the second test showed that this component was destroyed by a detonation in the segment manifold resulting from an interchannel propellant leak. On the injection orifice surface in an area approximately 180° opposite the point of interchannel leakage, there was no damage or injector erosion. Data were obtained from all four of the skin temperature thermocouples used in the test hardware, as shown in Figure VII-C-9. Two thermocouples were located in an area severely damaged by the detonation and subsequent erosion. The data obtained from these two thermocouples is not considered valid. Maximum temperatures from these two thermocouples were 1027°F and 2315°F. The third thermocouple was located in an area of only slight damage; it reached a maximum temperature of 918°F. The fourth thermocouple was located in an area where no damage or erosion occurred. The maximum temperature recorded by this thermocouple was 273°F. Near the location of the thermocouples that recorded high temperatures there is an indication (by erosion) that flames,

VII, C, Vortex Chamber Segment (cont.)

rather than liquid, were passing through the injection orifices. Thus, it is believed that the temperature recorded by the fourth thermocouple (273°F) is the only thermocouple that truly indicates the surface temperature of the design.

There was an excellent time correlation between the indication of the detonation as shown by the oscillograph of injector fuel and oxidizer pressure, and the rapid temperature rise of the thermocouple directly in the burnout area as recorded on the Millisadic printout.

Based on the data from Test -010, the performance of the vortex L* segment appears to be superior to that of the concentric-ring injector. A combustion efficiency of 94% at an L* of 70 in. was obtained in that test, compared with 82% with the concentric-ring injector at the same L*. Because of the limited data, however, more testing is required before conclusions relative to its performance characteristics can be made.

On the basis of the limited test experience gained with the vortex L* segment during this program, the following comments can be made.

(a) Interchannel welding should be avoided whenever possible.

(b) The vortex L* segment shows a potential as a high performance injector for short characteristic chamber lengths (L*).

(c) The vortex injector may have merit as a chamber cooling device (low temperatures were present on the injector face in the area unaffected by interchannel leakage).

(d) Further development testing would be required to determine the performance and cooling merits of the vortex chamber segment.

D. FILM-COOLED CONVERGENT AND THROAT SEGMENT

The cooling methods investigation showed that regenerative cooling in the convergent and throat section of a high-pressure combustion chamber required large amounts of supplemental film cooling to maintain the wall temperature within acceptable limits. It was calculated that at a chamber pressure of 5000 psia, only 15% of the total heat can be removed by regenerative cooling. Therefore, a great need existed for film cooling design data, including the thrust chamber performance loss resulting from film cooling, as well as the effectiveness of the coolant in cooling the chamber wall. To provide this data, a film-cooled convergent and throat chamber segment was designed and tested in the Cooled Chamber Program.

The design of the cooled convergent and throat segment is discussed in Section VII,D,1, below. A summary of the test results with this component is given in Section VII,D,2. The detailed test program performed is discussed in Section VII,D,3. Using the test data obtained, the effects of film cooling on thrust chamber performance were determined and defined in a mathematical model; also, a correlation defining the efficiency of the film cooling for cooling the chamber wall was established. The results of these studies are given in Section VIII, Thrust Chamber Performance.

1. Description of Design

The "cooled throat" design (Figure VII-D-1) uses tangentially injected film coolant as the method of cooling. It is well established that maximum effectivenss of film cooling is obtained when the coolant is injected in the same direction as that of the adjacent main gas stream; this results in minimum shearing of the coolant boundary layer with the main stream and helps maintain the coolant on the chamber wall. During the design phase of this program, the vortex injector, which produces a tangentially directed spiraling motion of the main gas stream on the chamber wall, was given the highest promise for success; therefore, tangential injection of the film coolant was selected. But the concentric-ring injector subsequently proved

VII, D, Film-Cooled Convergent and Throat Segment (cont.)

superior, which, when used with the cooled throat segment, initially resulted in relatively poor distribution of the coolant on the wall. Significant improvement in distribution was obtained through a design change in the segment; this is discussed later in this section.

The film coolant is injected through approximately 400 injection orifices equally spaced in each of 18 circumferential rows and spaced 0.80 in. apart longitudinally. Of these, 16 rows were located above the throat diameter, and two rows were below. Flow control to each row of injection slots is accomplished by orifices in the inlet line to each supply channel. With this design, coolant flow rate in each local portion of the chamber can be varied until the maximum allowable wall temperature is reached. To provide temperature information, two thermocouples were located between each injector section. One of these was welded to the chamber just below the gas-side surface; the other measured the wall temperature between the individual feed manifolds near the liquid surface. The thermocouple locations are shown in Figure VII-D-2.

The chamber was designed so that either fuel or oxidizer could be used as the film coolant. In the test program performed, oxidizer was the coolant used. An analysis was performed to predict the required amount of film coolant when using either of the propellants. For comparative purposes, calculations were also performed using water. The results, together with the assumptions made, are shown in the table below.

Coolant	Water	AeroZINE 50	Nitrogen Tetroxide
Flow Rate Required, lb/sec	15	43	35
% of Total Propellant	9	25	20

VII, D, Film-Cooled Convergent and Throat Segment (cont.)

Assumptions:

1. Incident heat flux calculated using h_g from Bartz equation and T_o equal to 700°F (sat. temp of water at 3000 psia).

2. The radiant heat flux is zero.

3. Spontaneous decomposition of AeroZINE 50 occurs at 500°F.

4. Spontaneous decomposition of nitrogen tetroxide occurs at 700°F.

5. Water does not decompose.

6. Gas stream properties evaluated at 3000 psia and M.R. = 2.0.

7. The distribution of liquid coolant is 100% efficient.

Two units were fabricated; both were used in the test program. The fabricated hardware is shown in Figures VII-D-3 and -4.

2. Summary of Test Program

The overall test objective of the cooled convergent and throat segment was to obtain performance and heat-transfer data for film cooling with liquid N_2O_4 in high-chamber-pressure engines. The basic approach followed was to initially overcool the hardware, and then in progressive tests reduce the film cooling flow rate until burnout occurred.

VII, D, Film-Cooled Convergent and Throat Segment (cont.)

Twenty-three tests were attempted using the cooled throat segment; of these 13 yielded valid data, two yielded invalid data but reached a steady-state operating point, and eight were malfunction shutdowns which occurred before any significant chamber pressure was attained. The first test was performed on 9 October 1964, and the final test on 19 May 1965. All tests used the Mod VIII concentric-ring injector. Chamber L* was 100 in.; of this, the throat segment supplied 40 in., and two 30-in. ablative L* segments, located above the throat segment, supplied the remainder. During the course of the testing program, four expansion nozzles were used with the segment: an ablative exit cone of area ratio 8.28:1, a regeneratively cooled nozzle of area ratio 21:1, the regeneratively cooled nozzle in combination with an ablative nozzle extension of 70:1, and a 21:1 ablative exit cone.

The program objectives for the cooled convergent and throat segment were achieved. Film cooling was reduced from a maximum of 58 lb/sec to 36 lb/sec, at which point throat burnout occurred. Using a second unit of identical design, film cooling was again progressively reduced until burnout occurred at 33 lb/sec. The burned portion of the second chamber, which included the section from feed channels 12-16, was subsequently machined out and replaced with an ablative insert. This unit was then retested; in this test, slightly less film cooling was used in the remaining channels than had been used in the test before (18.4 lb/sec versus 20.8 lb/sec, channels 1-11). Erosion in the convergent portion of the chamber occurred.

From these tests, the minimum film cooling requirements for both the chamber and throat sections of the chamber were determined. At the time the throat was designed, predicted minimum flow rate for N_2O_4 was 35 lb/sec, which is very close to the experimental value. However, the design analysis assumed perfect distribution of film coolant on the chamber wall; actual distribution obtained was relatively poor, as evidenced by the heat marks on the chamber. Therefore, the film cooling capabilities of N_2O_4 are somewhat better than predicted.

VII, D, Film-Cooled Convergent and Throat Segment (cont.)

The performance and heat-transfer data obtained during these tests were used to establish mathematical models which can be used as design data for future high-pressure designs in which film cooling is used. A discussion of this effort is given in Section VIII.

3. Detailed Test Program

The tests conducted with the cooled throat segment can be logically grouped into five test series. Each of these test series is discussed in the following paragraphs. Predicted and actual film coolant flow rates for each test in which steady-state data were recorded are tabulated in Figure VII-D-5. Wall temperature data for each test are given in Figure VII-D-6. Summarized test parameters are specified in the cumulative testing summary, Figure II-A-2.

a. Test Series 1: Tests 1.2-02-YAM-011 through -015

This was the first group of tests conducted with the cooled throat segment. The primary test objectives were to evaluate the structural adequacy of the hardware, determine thrust chamber performance at a relatively high film coolant flow rate, and to determine the test duration required to achieve thermal steady state condition in the chamber. The 8.28:1 ablative exit cone was used with the throat segment. Nominal chamber pressure desired was 3000 psia.

Of the five tests conducted, Tests -012, -014, and -015 yielded valid data. Tests -011 and -013 were malfunction shutdowns; steady-state chamber pressure was not achieved in either test. The planned film cooling flow rate for all tests was 45 lb/sec; actual flow rates were 46.7, 45.0, and 41.8 lb/sec for the three valid tests. No hardware damage occurred in any test; however, poor film cooling distribution was evident by heat marks on the chamber wall, as shown in the posttest photographs, Figures VII-D-7, and -8.

VII, D, Film-Cooled Convergent and Throat Segment (cont.)

The first test was run for the relatively short duration of 1.865 sec. At FS-2 the thermocouples located in the chamber wall did not reach steady-state conditions. In the next two tests the test duration was extended to 2.37 and 4.03 sec, respectively in an effort to reach thermal steady-state condition. After reviewing the temperature data, it was concluded that the thermocouples were not recording true surface temperature conditions. These thermocouples were 1/8 in. dia., and were welded into the chamber wall 0.075 in. below the surface in the large heat-sunk area of the chamber.

Based upon these three tests, it was decided to modify the instrumentation for obtaining wall surface temperatures and to attempt to improve the film coolant distribution on the chamber wall. The revised thermocouples design is shown in Figure VII-D-2. In the new design, the thermocouple is located directly on the surface, with a 0.003-in. air gap separating it from the heat sink mass. It was thought that perhaps the reponse of the 1/8-in.-dia thermocouple was to slow; therefore it was decided to evaluate both 1/8-in.-dia. and high-response 0.040-in.-dia thermocouples in the next test series on a trial basis. Two of each size thermocouples were installed for the next test series.

The film cooling distribution pattern on the chamber wall showed that the film cooling was being washed downstream before it traveled very far in the tangential direction. As the mainstream velocity increased, the amount of tangential coverage became less and less until at the throat, almost no tangential component was present. It an attempt to correct this problem, a modified design was made wherein a circumferential groove would be machined around the chamber at each injection plane, encompassing all the orifices in that plane. With this design, the film coolant could flow inside the groove, undisturbed by the main gas stream, and then spill into the chamber as a sheet rather than as individual streams. It was decided to incorporate this modification, on a trial basis, into the hardware for the next test series. Grooves 0.030-in. deep by 0.090-in. wide were machined into injection stations 1 through 9, and at 11, 13, 15, as shown in Figure VII-D-9.

VII, D, Film-Cooled Convergent and Throat Segment (cont.)

Following modification of the throat segment, it was returned to the test area for further testing. Heat marks on the chamber wall caused by the previous tests had been removed by the use of sandpaper.

b. Test Series 2: Tests 1.2-02-YAM-016 through -020

The objectives of this test series were to (1) evaluate the hardware modifications made as a result of the previous tests, (2) attain thermal steady-state conditions, and (3) begin reducing film cooling flow rate. Five tests were performed in this series, in which Tests -017, -018 and -020 yielded valid data. Tests -016 and -019 were malfunction shutdowns prior to ignition in the chamber. Nominal chamber pressure was again 3000 psig, and the 8.28:1 exit cone was used with the throat segment. Planned coolant flow rate for the first test was again 45 lb/sec; the planned test duration was 3.0 sec. The first valid test, Test -017, was fired on 26 November 1964. No hardware damage occurred on this test. Posttest inspection of the hardware showed no indication of heat marks; on this basis it was concluded that the grooving of the injection channels significantly improved film cooling distribution. Examination of the test records also showed that thermal steady-state in the chamber was reached at approximately FS-1 + 2.25 sec. The thermocouple design modification proved completely successful, and showed excellent response. No significant difference between the 1/8-in.-dia and the 0.040-in.-dia configurations was evident. Temperature traces obtained with the new thermocouple design, together with traces from other thermocouples in the chamber of the original configuration, are shown in Figure VII-D-10. TTs-5 in this plot is one of the new designs; TTs-1, -13, and -9 are of the older configuration.

Actual coolant flow rate obtained in Test -017 was 57.8 lb/sec; this was reduced to 49.4 lb/sec in Test -018. These flows were higher than expected because the "dishpan" orifices controlling flow to the individual coolant channels had been installed backwards, changing the orifice C_D. Chamber condition following these tests was excellent, with no heat marks appearing on the chamber wall. Coolant flow rate was then reduced to 37 lb/sec in Test -020, which caused burnout

VII, D, Film-Cooled Convergent and Throat Segment (cont.)

in the throat region. During this test, coolant feed channels 2, 4, 6, 8, and 10 were completely blocked to permit investigation of effective cooling length. All erosion occurred below these stations, however. The damaged hardware is shown in Figures VII-D-11, VII-D-12 and VII-D-13. Slight heat marks were evident in the upper chamber, but not to the degree experienced prior to grooving the channels. It was therefore concluded that the grooves did not provide uniform distribution but improved it significantly over the non-grooved configuration.

c. Test Series 3: Test 1.2-02-YAM-021

Cooled throat SN 2 was tested for the first time in Test -021. The configuration was identical to that of SN 1, except that based on previous results, high-response thermocouples were used throughout, and grooves were machined in all of the coolant channels. The 21:1 area ratio oxidizer regeneratively cooled exit nozzle was assembled to the throat segment and tested for the first time in this test. The assembly is shown on the test stand in Figure VII-D-14. To accommodate the pressure drop in the exit nozzle, the oxidizer pump discharge pressure was raised from 3515 to 4450 psia. A new oxidizer pump impeller designed to furnish the higher pressure was used in this test.

The test was terminated at FS-1 + 2.197 by explosion of the oxidizer pump. A discussion of the oxidizer pump failure is given in Section XII. The only damage to the thrust chamber assembly was the rupture of three 2-in.-dia flex lines which supplied propellants to the exit cone. One of the rupture lines is shown in Figure VII-D-15.

Valid steady-state data was obtained in this test prior to the pump explosion. Coolant flow rate in this test was 35.7 lb/sec; all coolant channels were flowing. Heat marks in the chamber were not severe. Posttest condition of the cooled throat is shown in Figures VII-D-16 and VII-D-17. Very slight erosion was present, which resulted from an off-mixture-ratio condition in the chamber following the pump failure. This erosion was repaired prior to the next test.

VII, D, Film-Cooled Convergent and Throat Segment (cont.)

As a result of the pump failure, it was decided to lower chamber pressure to approximately 2600 psia, which corresponds to 4650 psia pump discharge pressure when the exit nozzle is used. This is the safe upper limit for the original oxidizer pump configuration.

d. Test Series 4: Tests 1.2-02-YAM-022 through -029, -032, and -033

The refurbished TCA assembly was returned to the test area, and testing was resumed on 15 February 1965. The regeneratively cooled exit nozzle was again tested in conjunction with the cooled throat segment. In one test, Test -029, the ablative expansion nozzle skirt was also added, bringing the total area ratio to 70:1. Nominal chamber pressure was 2600 psia.

Ten tests were conducted in this test series, of which five produced valid data at rated chamber pressure; these included Tests -023, -025, -027, -029, and -033. Three of the invalid tests, Tests -026, -028, and -030, were malfunction shutdowns; in Test -022, one of the 2-in.-dia flex lines to the regeneratively cooled exit nozzle ruptured during the start transient, which caused reduced weight flow and chamber pressure throughout the test. Except for the broken line, no damage was sustained. In Test -024, the gas generator valve did not open completely, resulting in reduced chamber pressure of 2304 psig. Except for the low chamber pressure, this was a valid test. Coolant weight flow was 34.6 lb/sec. No hardware damage occurred.

In the five valid tests, film coolant weight flow was progressively reduced in the following steps: 42.9, 38.9, 36.0, 34.3, and 33.1 lb/sec. Prior to the last test, the hardware was removed for inspection. It is shown in Figures VII-D-18 and -19. Heatmarks indicating uneven film cooling distribution are plainly visible. In Test -033, conducted on 14 April 1965, severe erosion of the throat was experienced below the twelfth injection plane. The tubes of the regeneratively cooled exit cone were also burned out near the throat-exit nozzle interface. The damaged hardware is shown in Figures VII-D-20, -21, -22, and -23.

VII, D, Film-Cooled Convergent and Throat Segment (cont)

The burnout conditions of throat segment SN 1 with those of SN2 were compared. Failure with SN 1 occurred with 36.6 lb/sec coolant weight flow; chamber pressure was 2809 psia. SN 2 failed with 35.1 lb/sec at 2615 psia. Only a portion of the film coolant injection stations were grooved for improved film cooling distribution in SN 1, whereas all were grooved in SN 2. It was concluded that the combination of lower chamber pressure and better film cooling distribution accounted for the somewhat lower flow rate prior to burnout being obtained with SN 2.

Testing with the throat segment thus far had determined the minimum film cooling flow rates for the throat area of the chamber. No erosion had ever occurred in the upper convergent portion of the chamber. To determine how close to marginal conditions this upper section was operating, it was decided to remove the eroded section of the throat of SN 2, replace it with an ablative insert, and continue testing. The modified throat design is shown in Figure VII-D-24. The burned tubes of the exit cone were also machined out and replaced by an ablative liner, as shown in Figure VII-D-25.

e. Test Series 5: Tests 1.2-02-YAM-035 and -036

Testing with the repaired thrust chamber assembly was resumed on 18 May 1965. Test -035 was a malfunction; Test -036 yielded valid data. It was planned to introduce approximately the same film coolant flow rate into the chamber as was introduced in those same channels during the previous test, which was 20.8 lb/sec. Actual flow rate achieved in Test -036 was 18.4 lb/sec, slightly below the intended amount. Chamber pressure was 2616 psia. Erosion over the entire length of the cooled portion of the chamber occurred on this test, as shown in Figures VII-D-26 and -27. Thus the decrease of 2.4 lb/sec in film cooling flow rate from the previous test was enough to cause burnout, which showed the convergent portion of the chamber had been operating near the lower limit in the previous test.

VII, D. Film-Cooled Convergent and Throat Segment (cont.)

As a result of the test program, it was concluded that minimum film cooling conditions in both the convergent and throat portions of the chamber had been established. The percentage of film cooling used, based on total propellant flow rate, varied from 11 to 24%. This was a sufficiently broad range to establish a correlation of film cooling flow rate with thrust chamber performance. This correlation was developed into a mathematical model which is usable to predict performance for advanced high-pressure engines using combined regenerative and film cooling. It is presented in Section VIII, below. The model is currently being used in Aerojet-General "Advanced Storable Engine Program," Contract AF 04(611)-10830.

VII, Cooled Thrust Chamber Design and Development (cont.)

E. REGENERATIVELY COOLED EXPANSION NOZZLE

Results of the cooling methods investigation showed that regenerative cooling with N_2O_4 was feasible below an area ratio of approximately 3:1. To demonstrate this cooling technique, a regeneratively cooled expansion nozzle was designed, fabricated, and test-evaluated as part of the Cooled Chamber Program.

1. Description of Design

The cooled expansion nozzle (Figure VII-E-1) is a tube bundle design using oxidizer as the regenerative coolant. It is a double-pass configuration, composed of 68 tapered tubes reinforced by a steel jacket. The nozzle contour is a 15° half-angle cone, extending from an area ratio of 2.5 to an area ratio of 21. The contour was based on the ultimate use of this nozzle in combination with a high area-ratio ablative cooled skirt, and is a truncated section of an optimum Rao nozzle of area ratio 183. The design details are shown in Figure VII-E-2.

The results of the heat-transfer analysis performed for this design are shown in Figure VII-E-3. The analysis was based upon the assumption that no film cooling or thermal barrier coating are used between the steel tubes and the gas stream. It can be seen that the gas-side wall temperature at the upper end of the nozzle segment (2.0 in. down from the throat) is 1875°F, decreasing to 1700°F (the upper design temperature limit) for the outside tube wall at 2.9 in. from the throat. Since this nozzle was scheduled for testing only in conjunction with the film-cooled throat segment, it was determined that the slight amount of film coolant required by the top inch of the nozzle would be available from the throat film coolant.

2. Development Testing

Nine tests were conducted using the oxidizer regeneratively cooled expansion nozzle: Tests 1.2-02-YAM-021 through -028, and Test 1.2-02-YAM-033. In

VII, E, Regeneratively Cooled Expansion Nozzle (cont.)

all tests, the nozzle was tested in conjunction with the film-cooled throat. Detailed conditions for each of the tests are reported in the discussion of the throat segment, Section VII,D.

The regeneratively cooled expansion nozzle operated satisfactorily in all tests, and demonstrated oxidizer regenerative cooling of the expansion nozzle of a high-pressure engine. During Test -033 severe erosion of the throat segment occurred, which subsequently caused the expansion nozzle tube bundle to burn out. The exit nozzle was in no way responsible for this failure. The posttest condition of the nozzle is shown in Figure VII-D-23. To allow continued testing of a repaired throat segment with a 21:1 area ratio nozzle, the damaged tubes of the expansion nozzle were machined out and replaced by an ablative liner. Figure VII-D-25 shows the hardware in this configuration. This nozzle was subsequently used in Test 1.2-02-YAM-036.

3. Test Data Analysis

Test data analyses were performed for the five valid thrust chamber tests: 1.2-02-YAM-023 through -025, and Tests -027 and -029. In Test -022 only one of the two required thermocouples operated, Tests -026 and -028 were invalid tests, and Test -033 supplied invalid data due to upstream erosion of the throat segment.

The inlet and outlet temperatures of the coolant, plotted as a function of time, are shown in Figures VII-E-4 through VII-E-8. The inlet temperature exceeds the outlet temperature at the beginning of the tests, because prior to hot-fire, the oxidizer coolant is heated by the turbopump, and then is subsequently cooled by the relatively cold tubes. As soon as fire develops in the chamber, an inversion of these temperatures takes place. The bulk temperature rise of the coolant was approximately 10°F in all tests. Assuming no film cooling from the throat segment, predicted bulk rise was from 50 to 75°F, depending on thrust chamber mixture ratio. The actual bulk rise recorded was determined to be reasonable for the high oxidizer film cooling flow rates being used on the throat segment above.

VII, Cooled Thrust-Chamber Design and Development (cont.)

F. ABLATIVE EXPANSION NOZZLE

1. Description of Design

The ablative expansion nozzle was designed as a nozzle extension to the cooled thrust chamber. Using this extension, it was planned to obtain data for a high area ratio thrust chamber operating at high chamber pressure. The contour selected, (Figure VI-A-1) was an optimum Rao nozzle extending to an area ratio of 183. The area ratio was selected because it was sufficiently high to obtain the desired data and also provided a nozzle exit diameter which matched an existing diffuser at Aerojet (a diffuser is required for large area ratio nozzles tested at sea-level to prevent flow separation).

The ablative nozzle extension is shown in Figure VII-F-1. It is of three-piece construction, including an ablative liner of wrapped asbestos, a wrapped fiberglass structural shell, and a steel flange for attaching the ablative nozzle to the regeneratively cooled expansion nozzle at the 21:1 area ratio interface.

Prior to testing with this component, an analysis was conducted to determine what performance differences could be expected from the use of the nozzle extension. Performance increases from two sources are possible: first, a large area-ratio nozzle flowing fully inherently provides higher vacuum performance because of the increased area on which the internal nozzle pressure acts; secondly, in large area-ratio nozzles, film cooling introduced in the chamber has a greater chance to combine and burn with the main exhaust gases before being exhausted into the atmosphere, which results in some performance recovery. Analysis showed that even at very high area ratios (such as the 183:1 area ratio nozzle skirt), the performance recovery to be expected was approximately 1%, while the inherent performance increase resulting from the high area-ratio was approximately 8.8%. Based upon these facts, it was determined that, considering the accuracy of the test stand and the relatively

VII, F, Ablative Expansion Nozzle (cont.)

large performance increase inherent with the large nozzle, the chances of measuring isolated performance increases resulting from film cooling recombination were practically impossible. Therefore, it was decided to reduce the area ratio to a value where flow separation would not occur when the thrust chamber was tested without a diffuser. This would result in a cost savings to the program by eliminating the requirement for modifications and activation of the diffuser, and still would provide demonstration of an ablative skirt and yield performance data at a relatively high area ratio. The ablative nozzle, which had already been fabricated to the 183:1 area ratio configuration, was therefore cut off to 70:1, the 3-sigma limit of the predicted flow separation area ratio of 90:1. The nozzle is shown after modification in Figure VII-F-2.

2. Test Experience and Results

The ablative nozzle extension was used in one test firing, Test 1.2-02-YAM-009. This test was of short duration, having a steady-state chamber pressure period of 0.6 sec. Following the test, the nozzle was in perfect condition. A discussion of the performance obtained in this test is given in Section VIII.

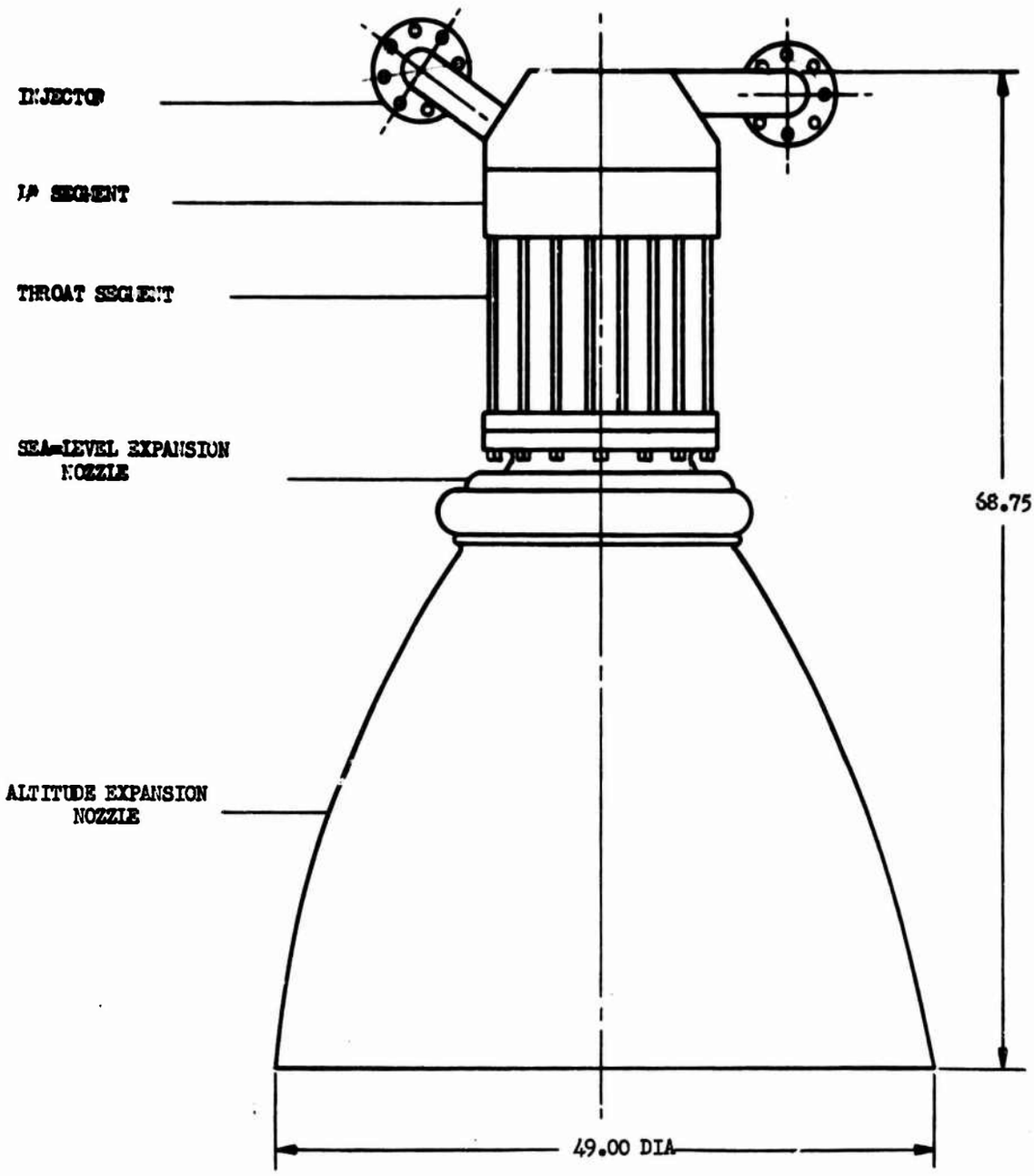

Segmented Cooled Thrust Chamber Assembly

Figure VII-A-1

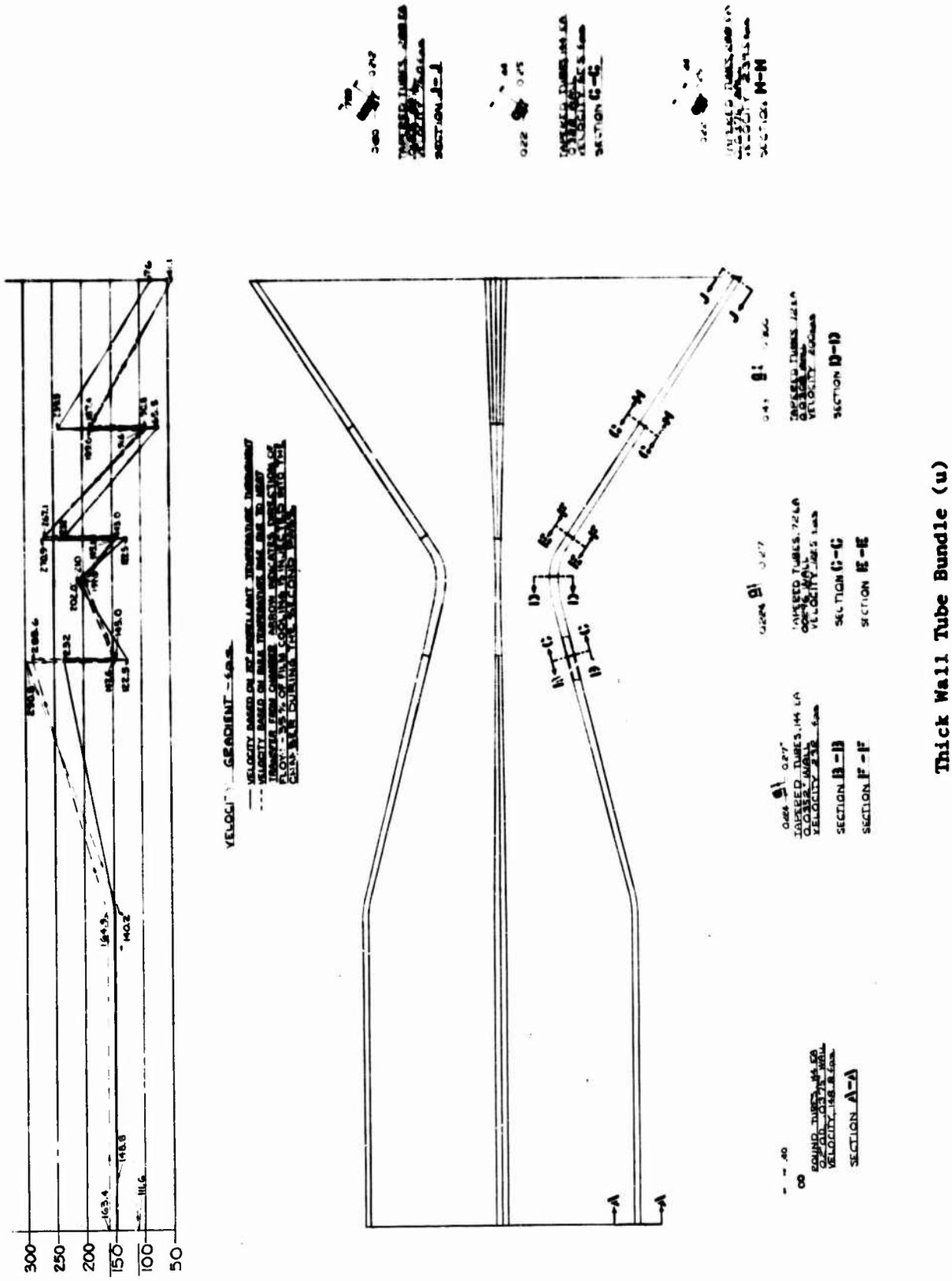

Thick Wall Tube Bundle (u)

Figure VII-A-2

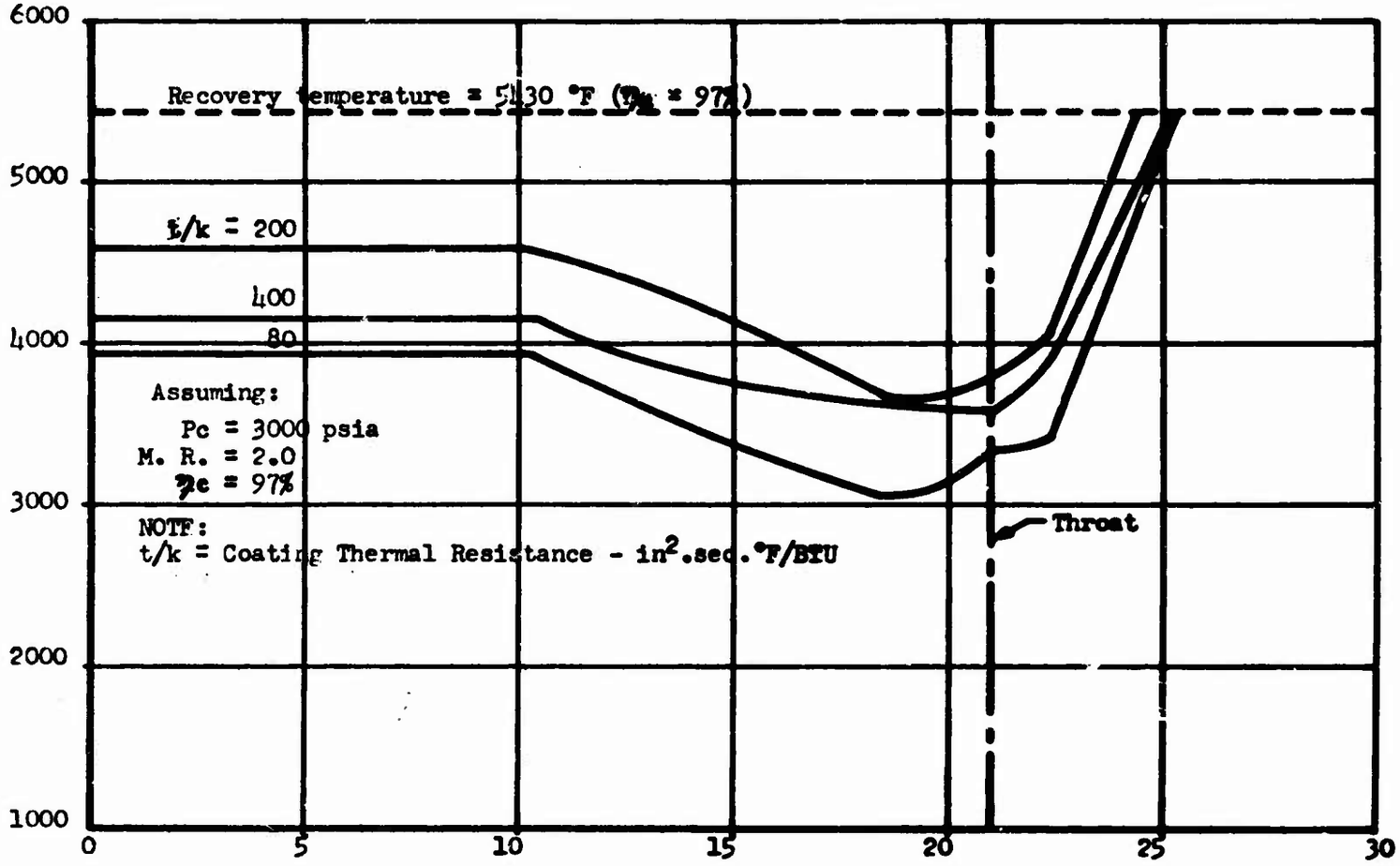

Tube Bundle Allowable Recovery Temperature vs Axial Distance
for Various t/k

Figure VII-A-3

Book One

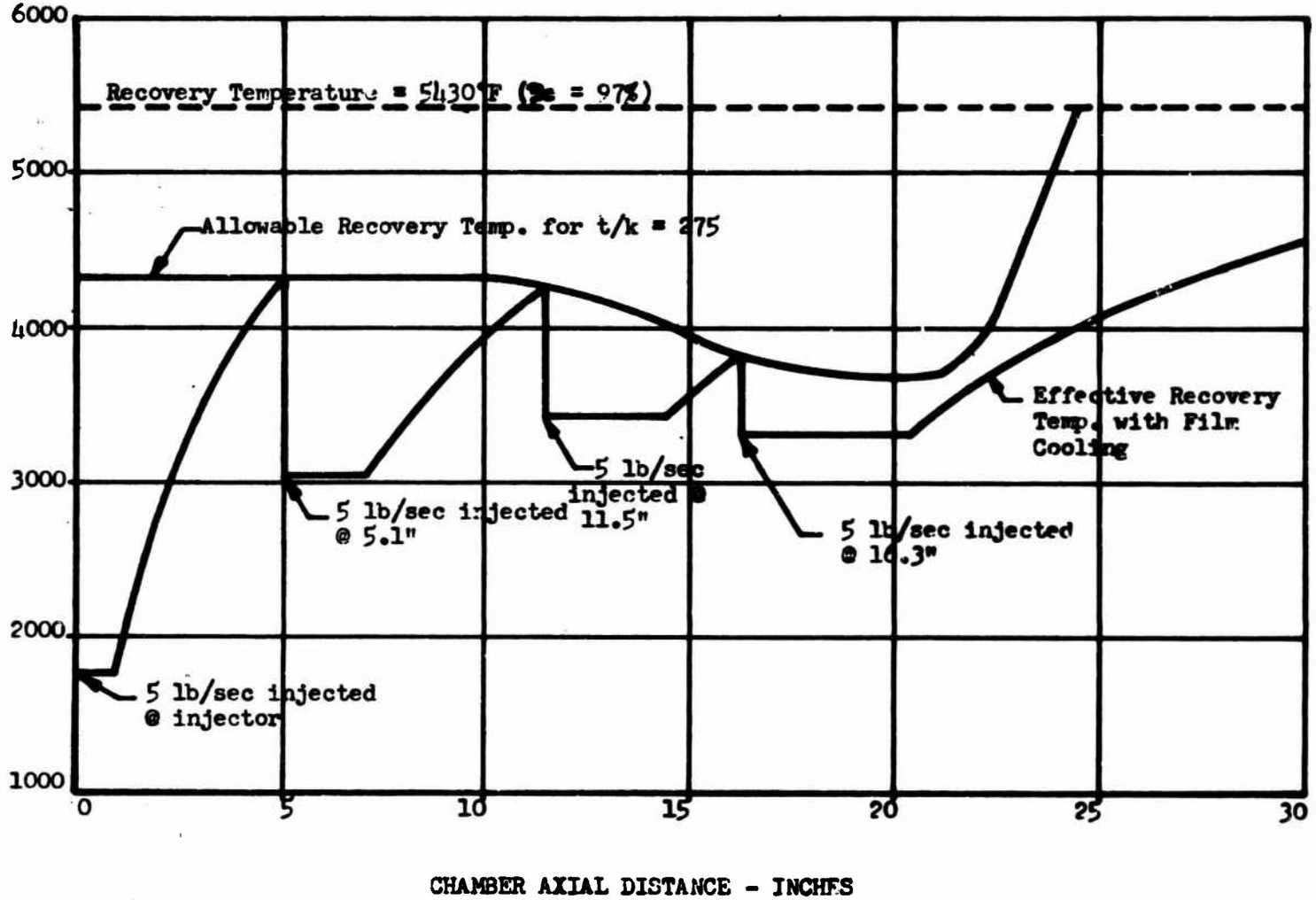

Figure VII-A-4

Tube Bundle Allowable Recovery Temperature vs Axial Distance
for t/k = 275

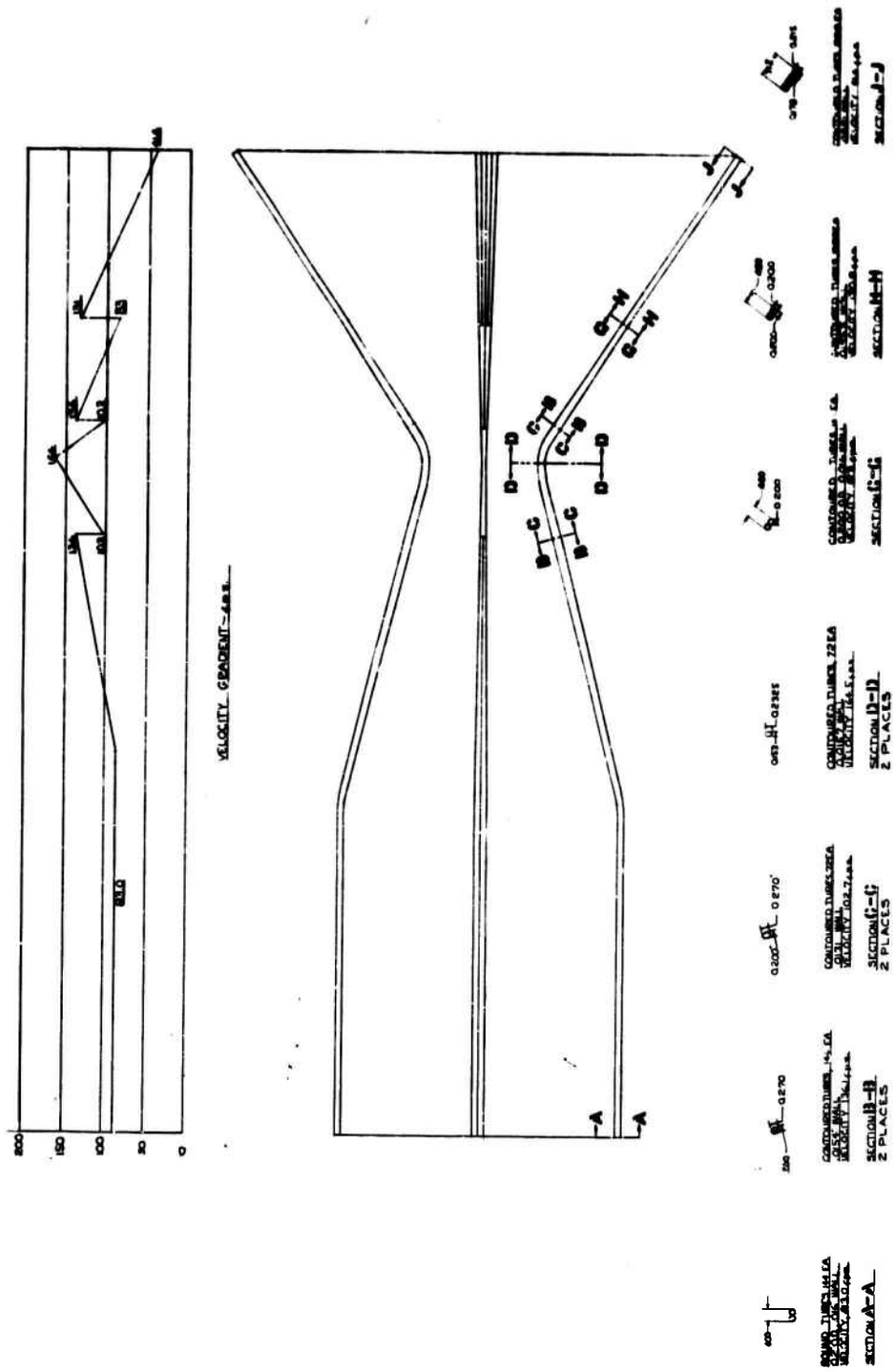

Thin Wall Tube Bundle (u)

Figure VII-A-5

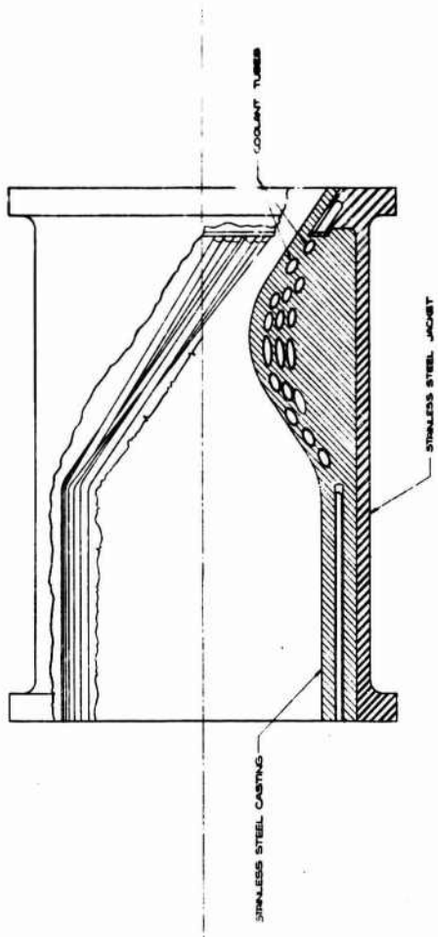

Drilled Chamber Concept

Figure VII-A-6

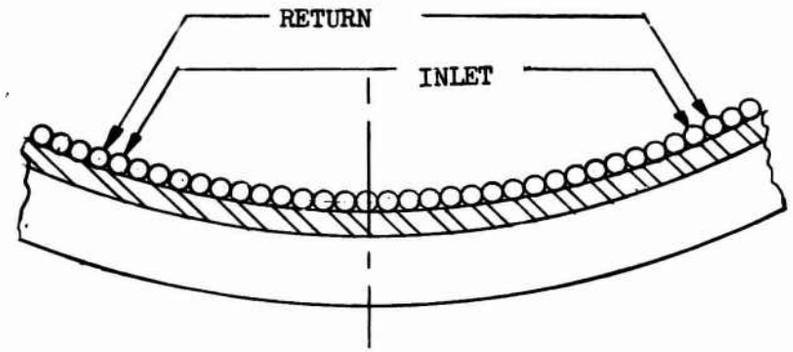

SECTION
36 OF 192 TUBES SHOWN

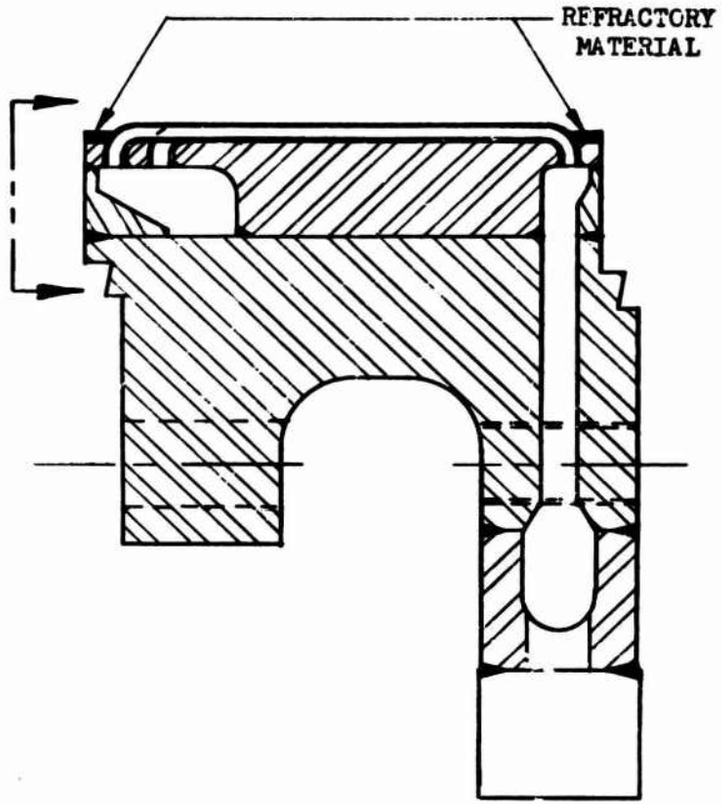

Figure VII-A-7

Segment--Cooled; Tube Concept

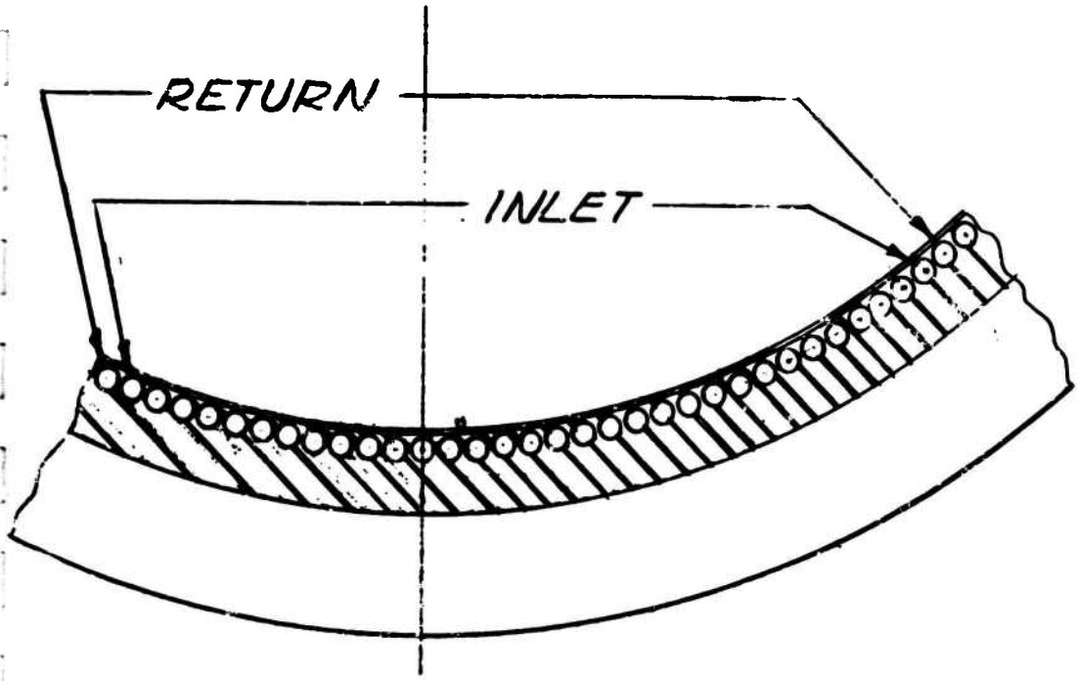

SECTION D-D
SCALE 1/1

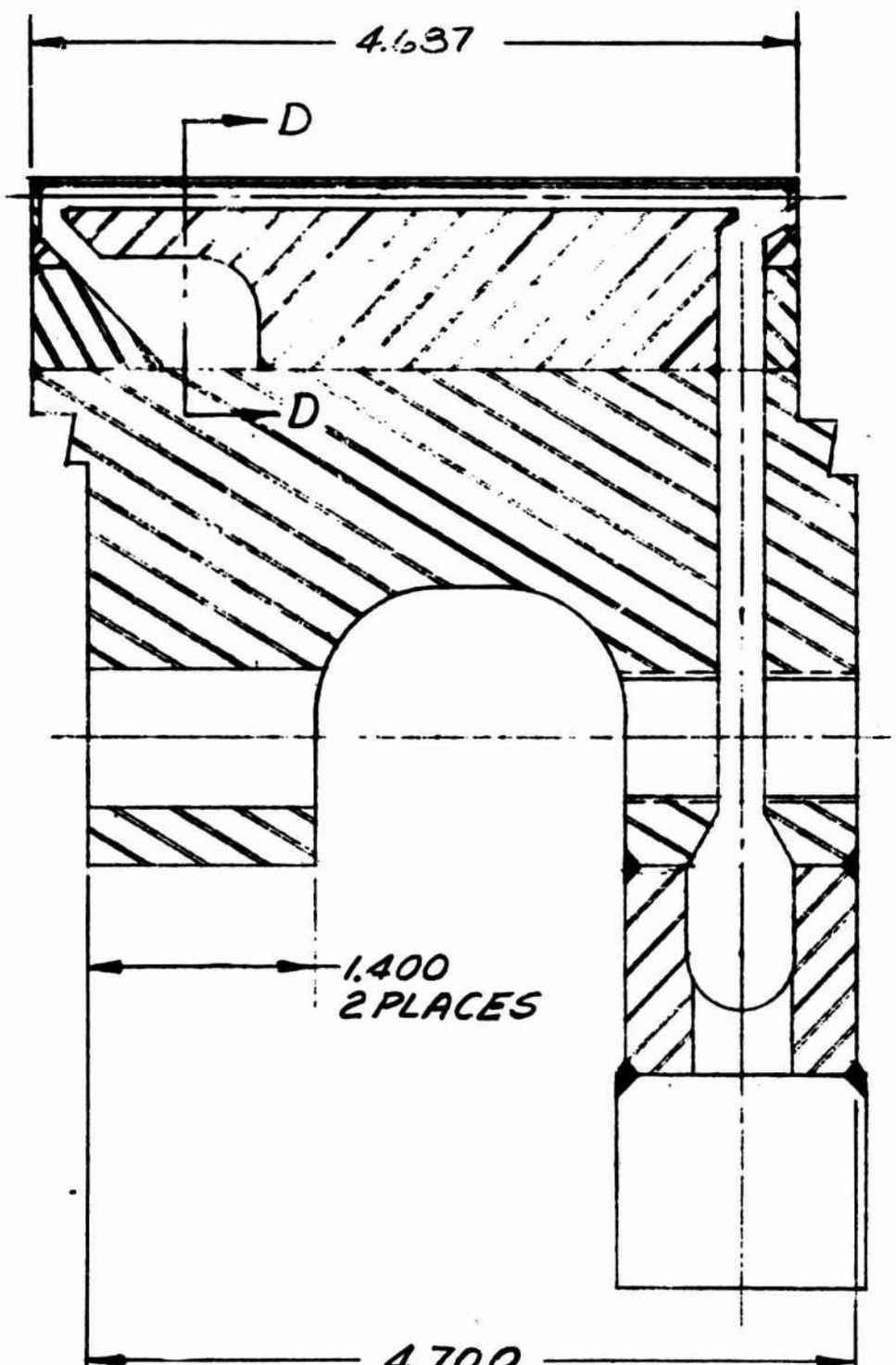

Segment--Cooled; Drilled Concept

Figure VII-A-8

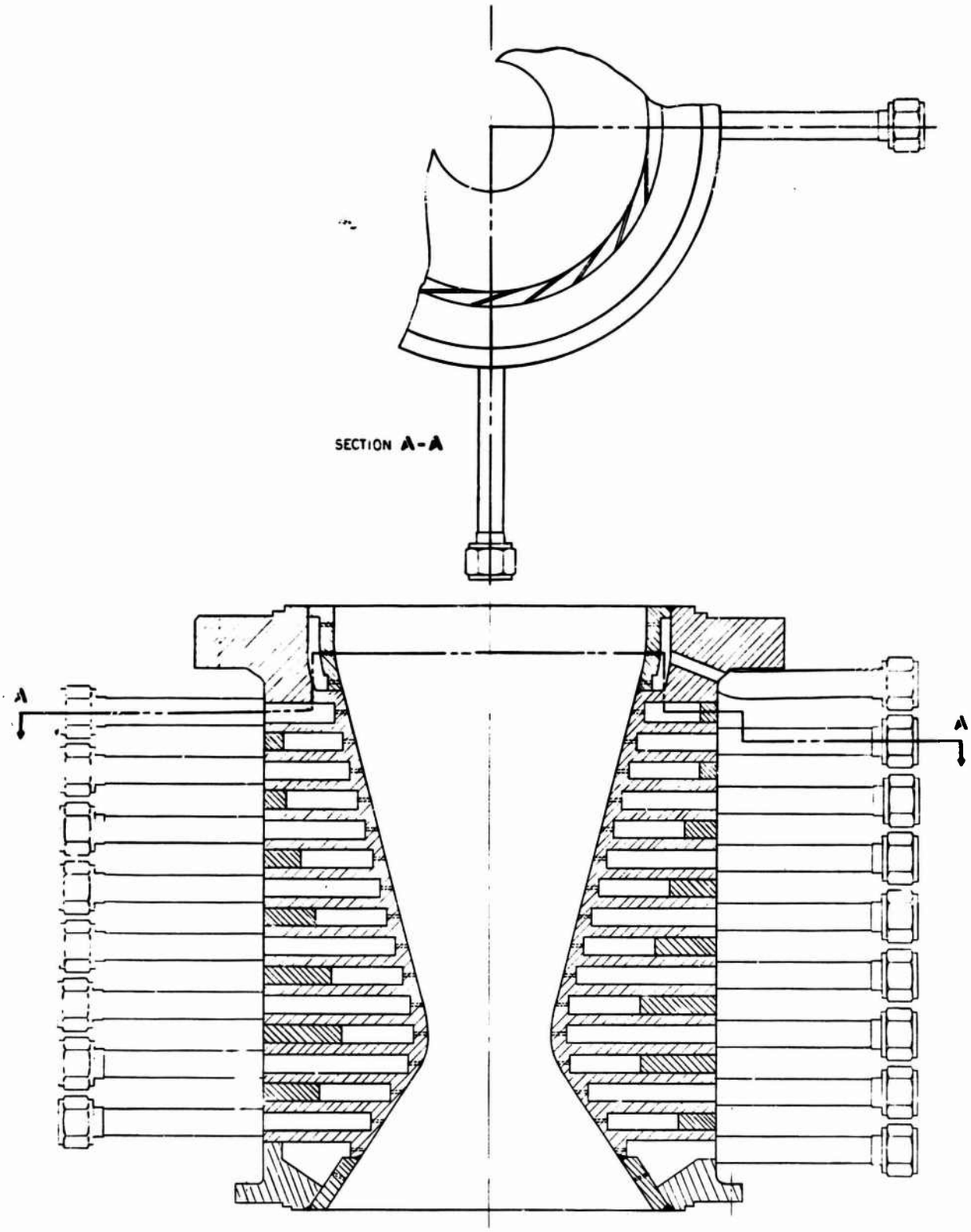

Cooled Throat Segment--Conceptual Design

Figure VII-A-9

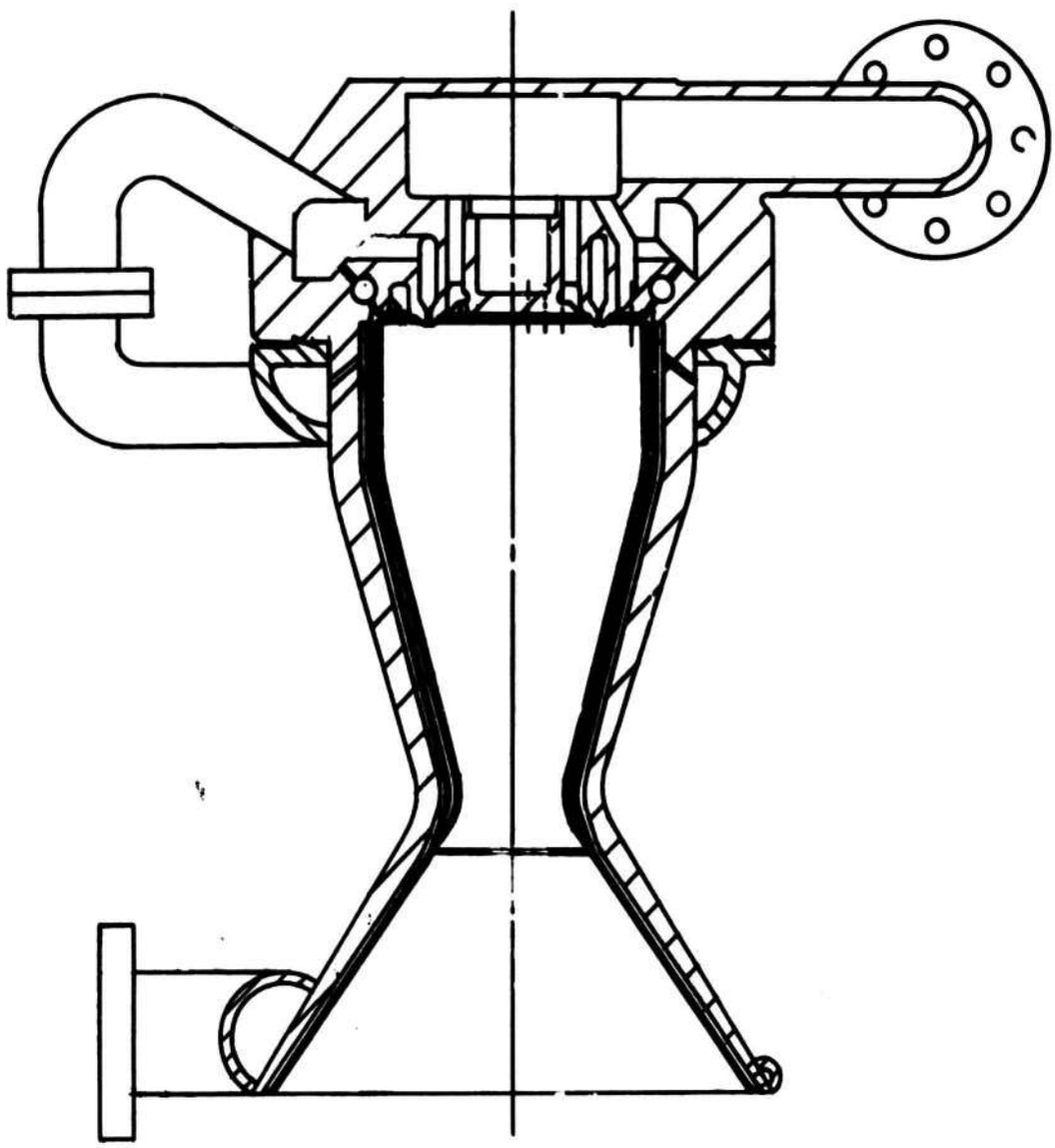

Hot Gas Cooling Concept (with Refractory Liner)

Figure VII-A-10

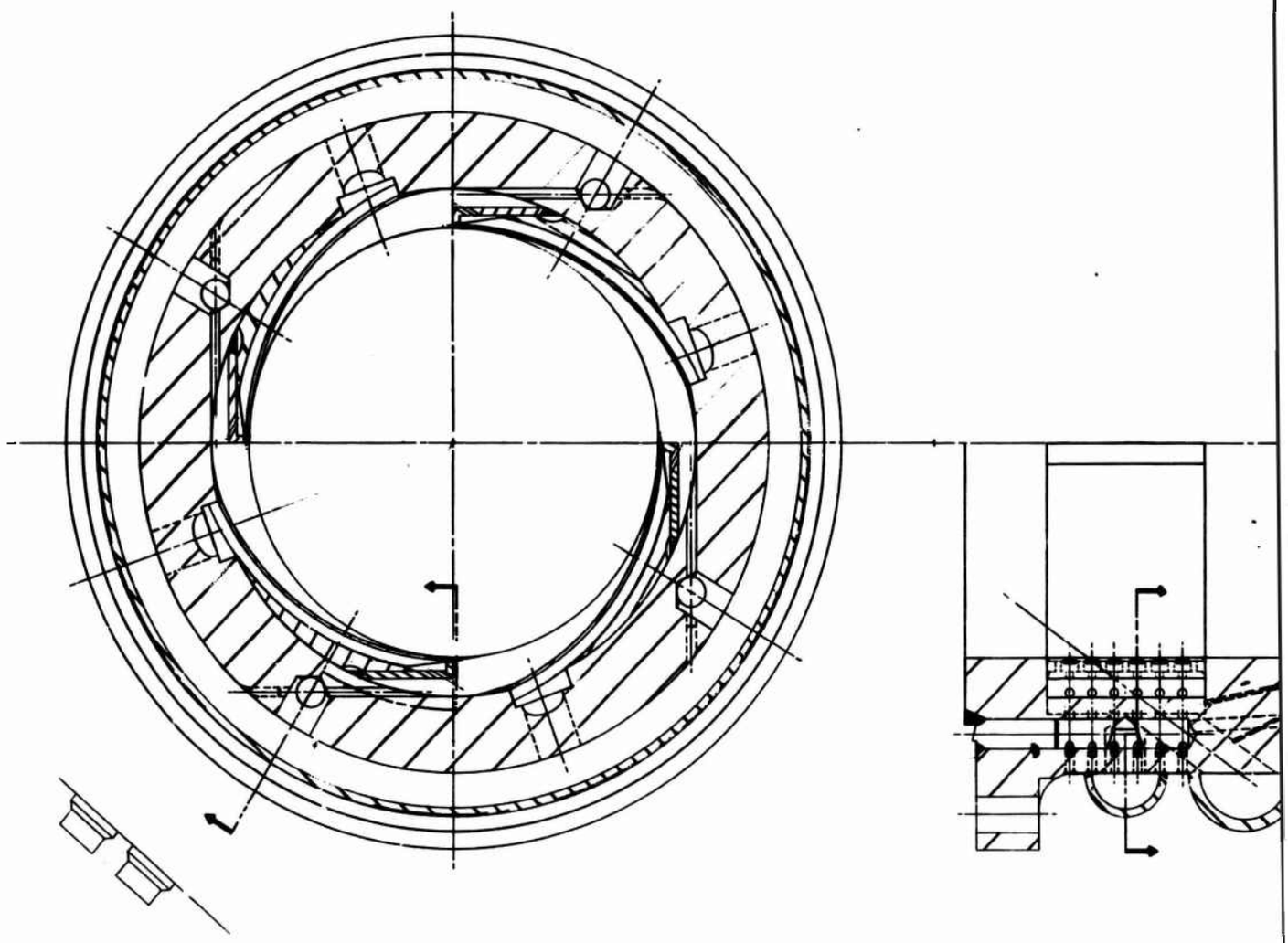

1

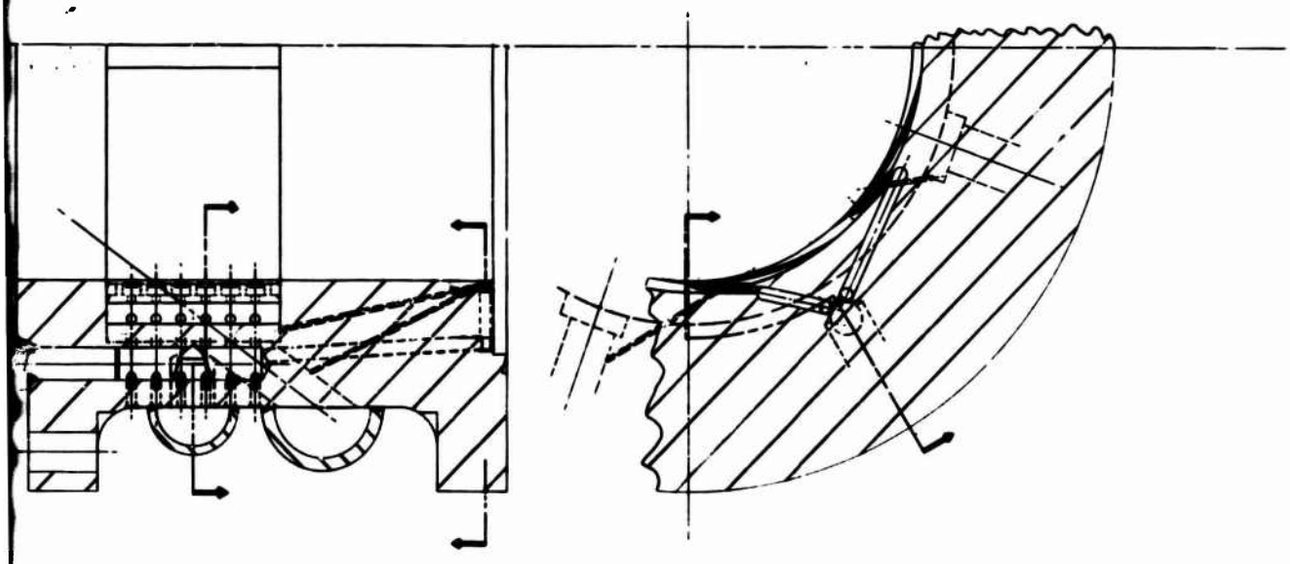

2

Vortex Chamber Segment Design No. 1

Figure VII-A-11

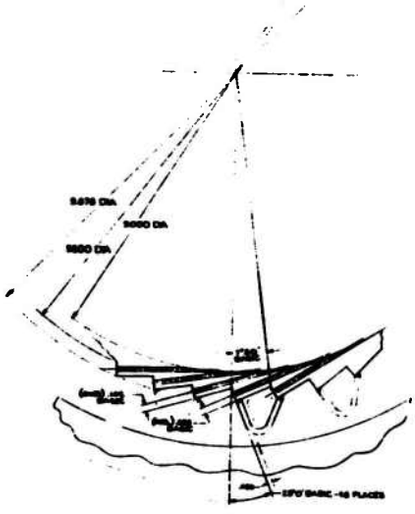

SECTION B-B'
SCALE: ¼

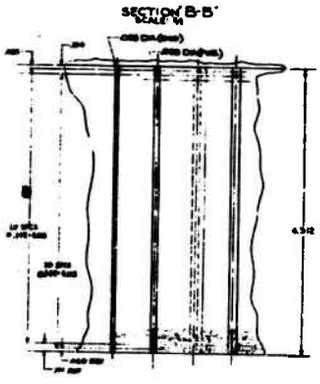

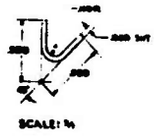

SCALE: ¼

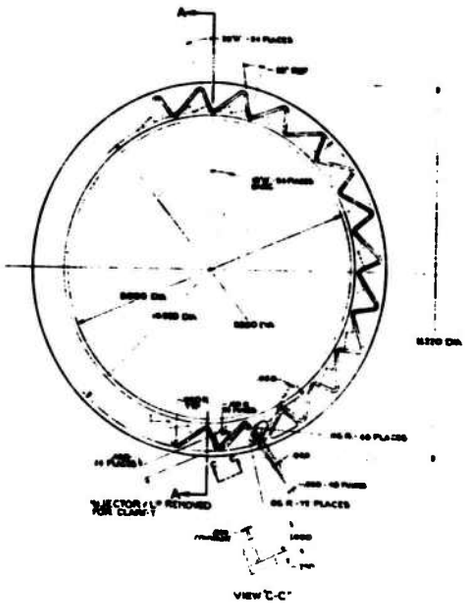

VIEW 'C-C'

1

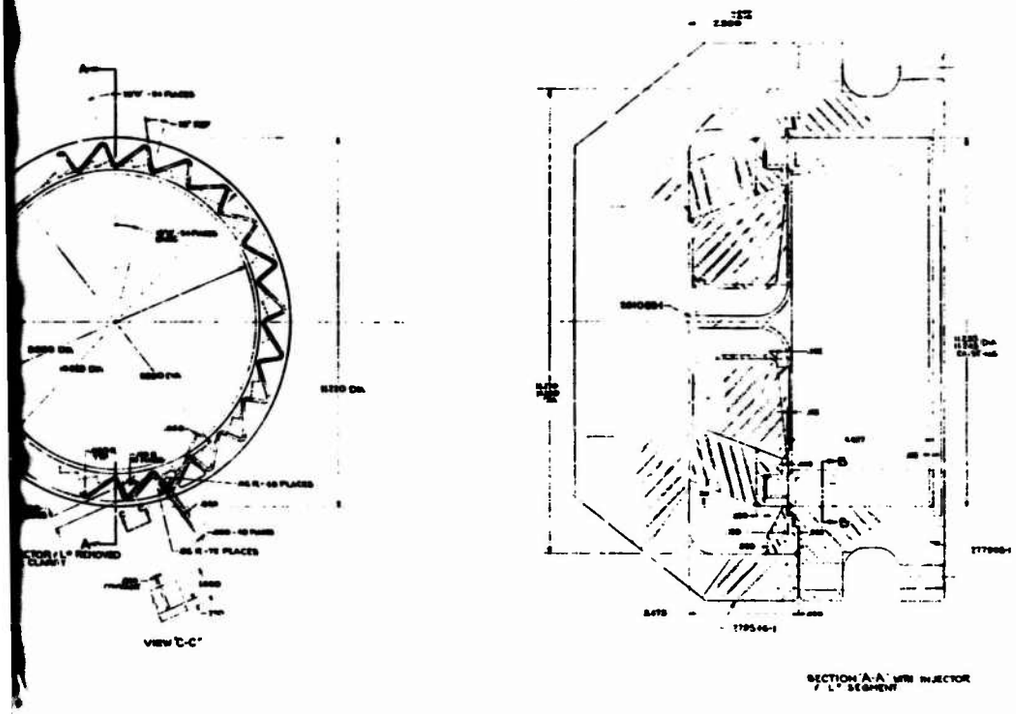

2

Vortex Chamber Segment Design No. 2 (u)

Figure VII-A-12

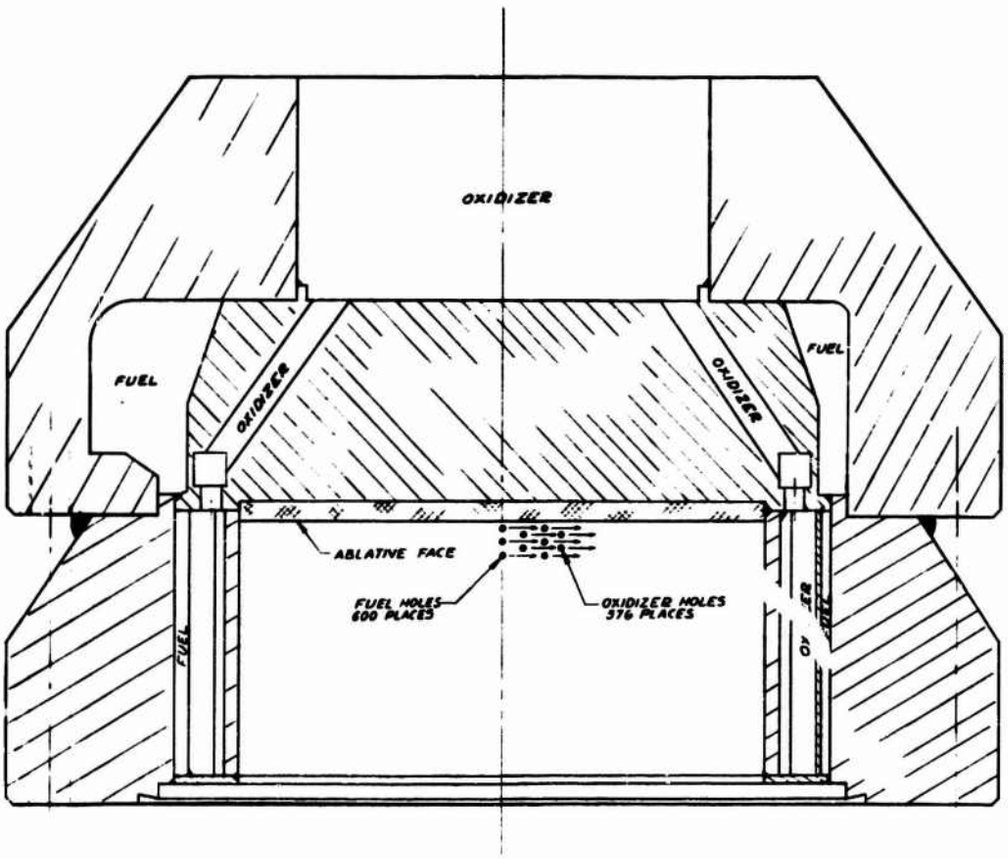

Vortex Chamber Segment Design

Figure VII-A-13

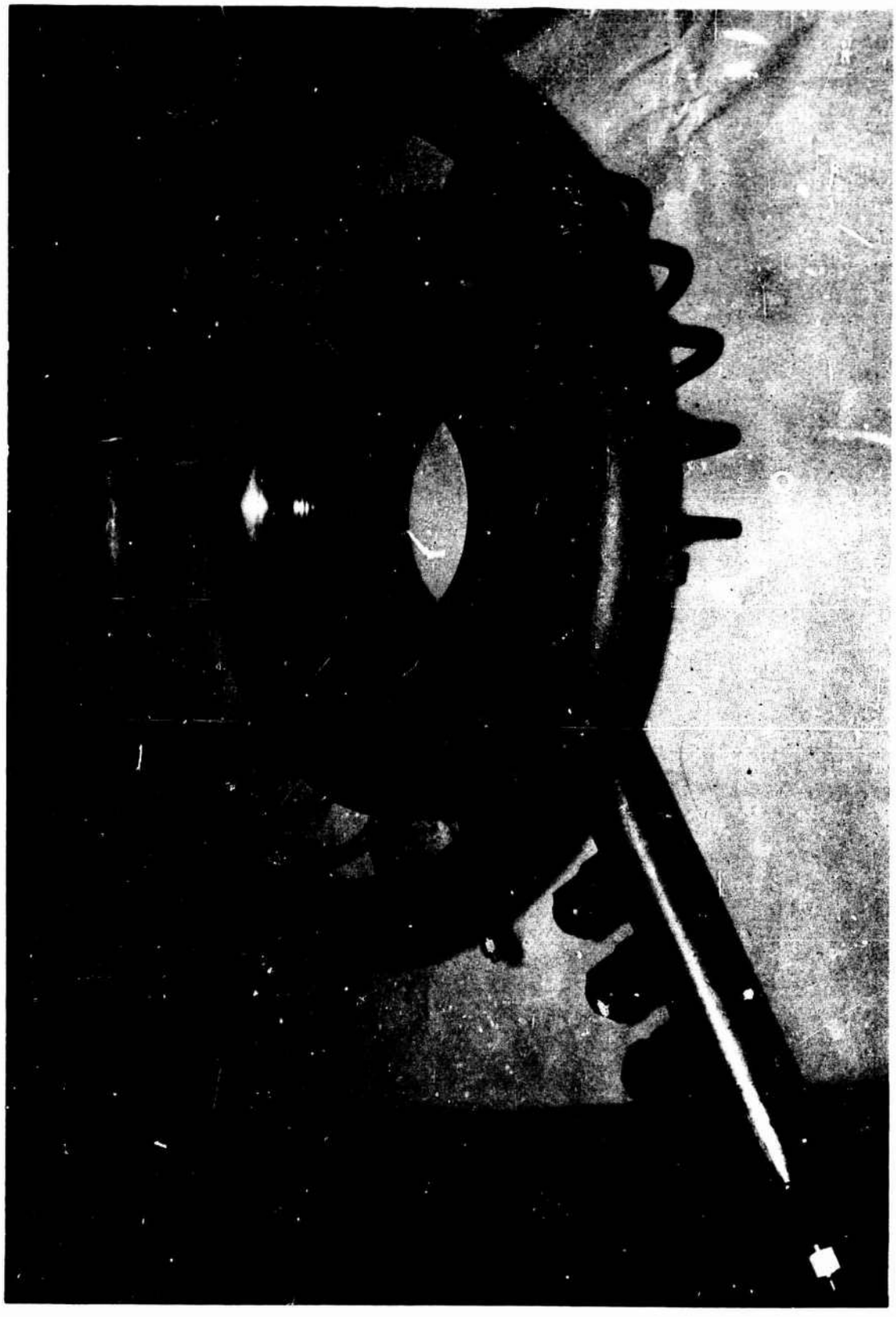

Coated Drilled L* Segment

Figure VII-B-1

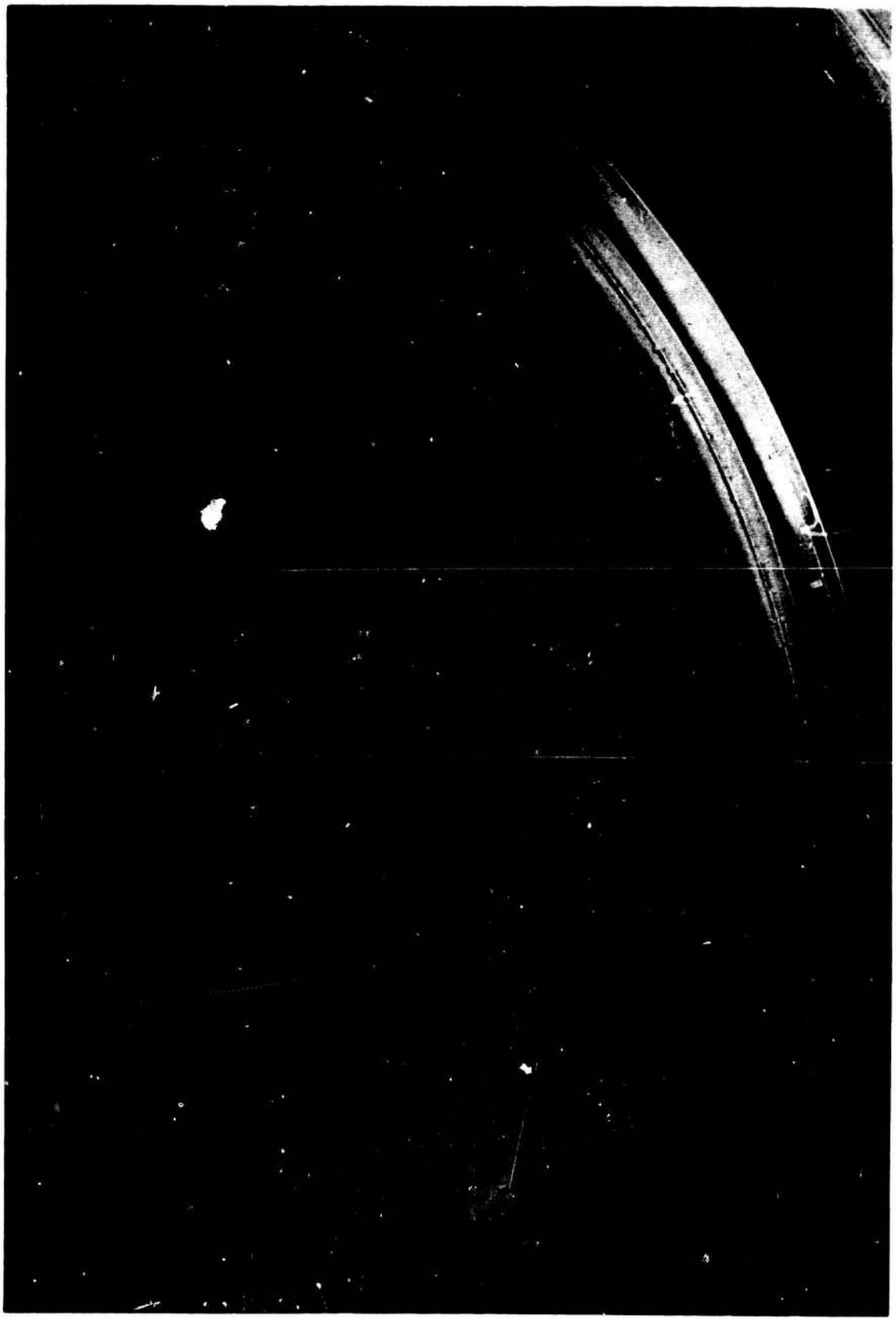

Close-up of Coated Drilled L* Segment

Figure VII-B-2

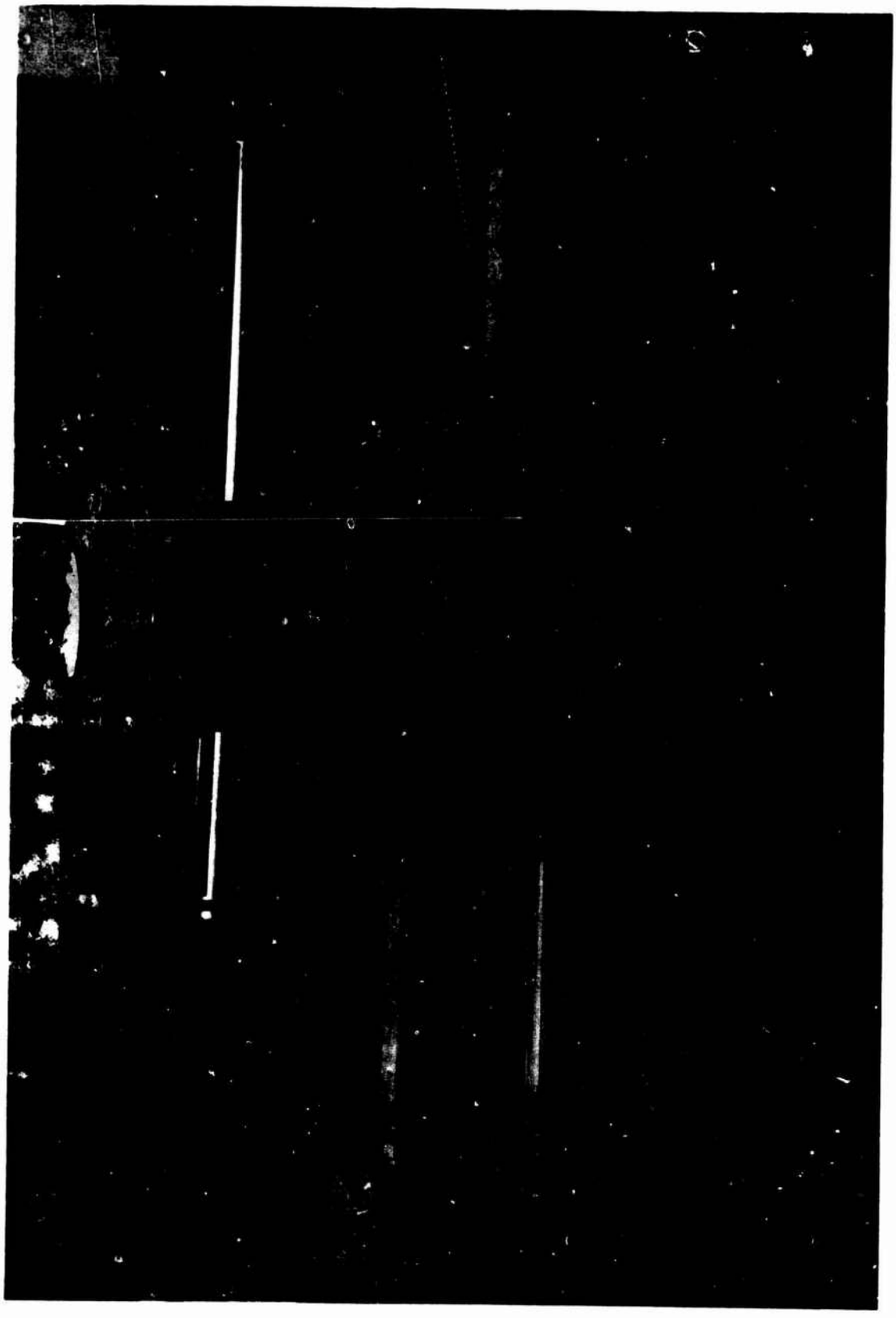

Mod VIII-B Concentric Ring Injector and Drilled L* Segment Assembly

Figure VII-B-3

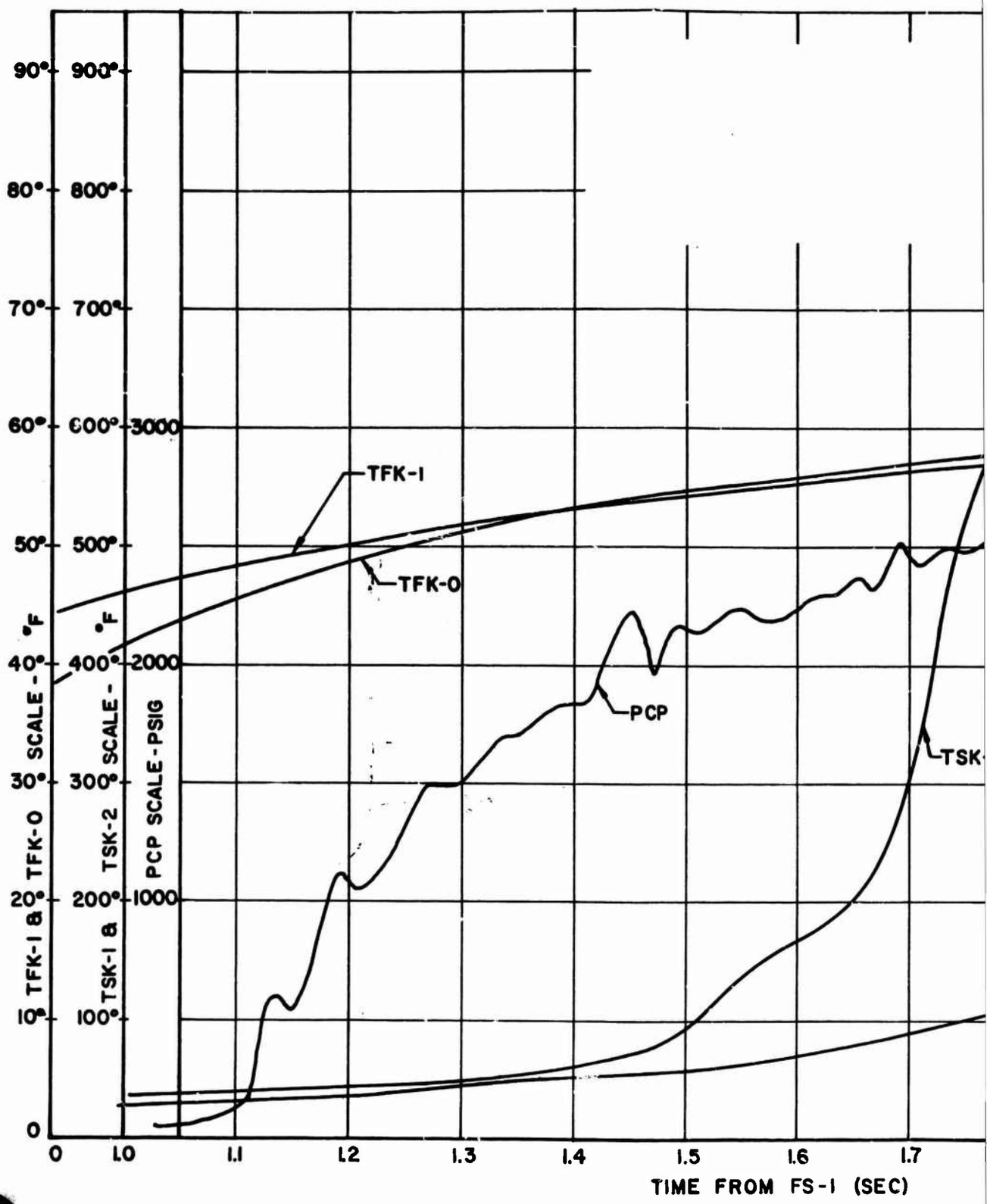
TFK-1
TFK-0
PCP
TSK
TFK-1 & TFK-0 SCALE - °F
TSK-1 & TSK-2 SCALE - °F
PCP SCALE-PSIG
TIME FROM FS-1 (SEC)
0
10°
20°
30°
40°
50°
60°
70°
80°
90°
100°
200°
300°
400°
500°
600°
700°
800°
900°
1000
2000
3000
1.0
1.1
1.2
1.3
1.4
1.5
1.6
1.7

1

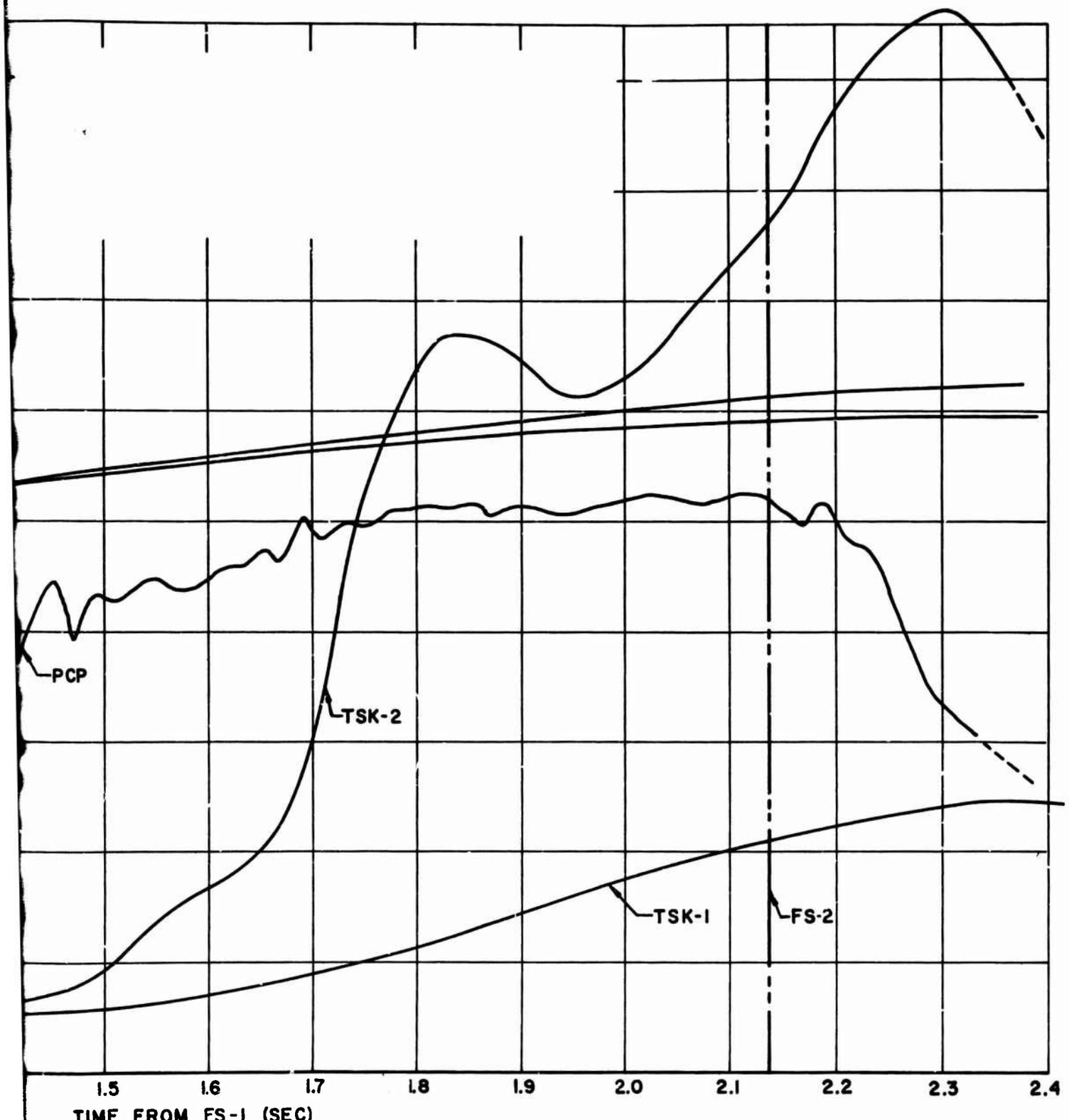

2

Pressure and Temperature Test Data, 1.2-02-YAM-030 (u)

Figure VII-B-4

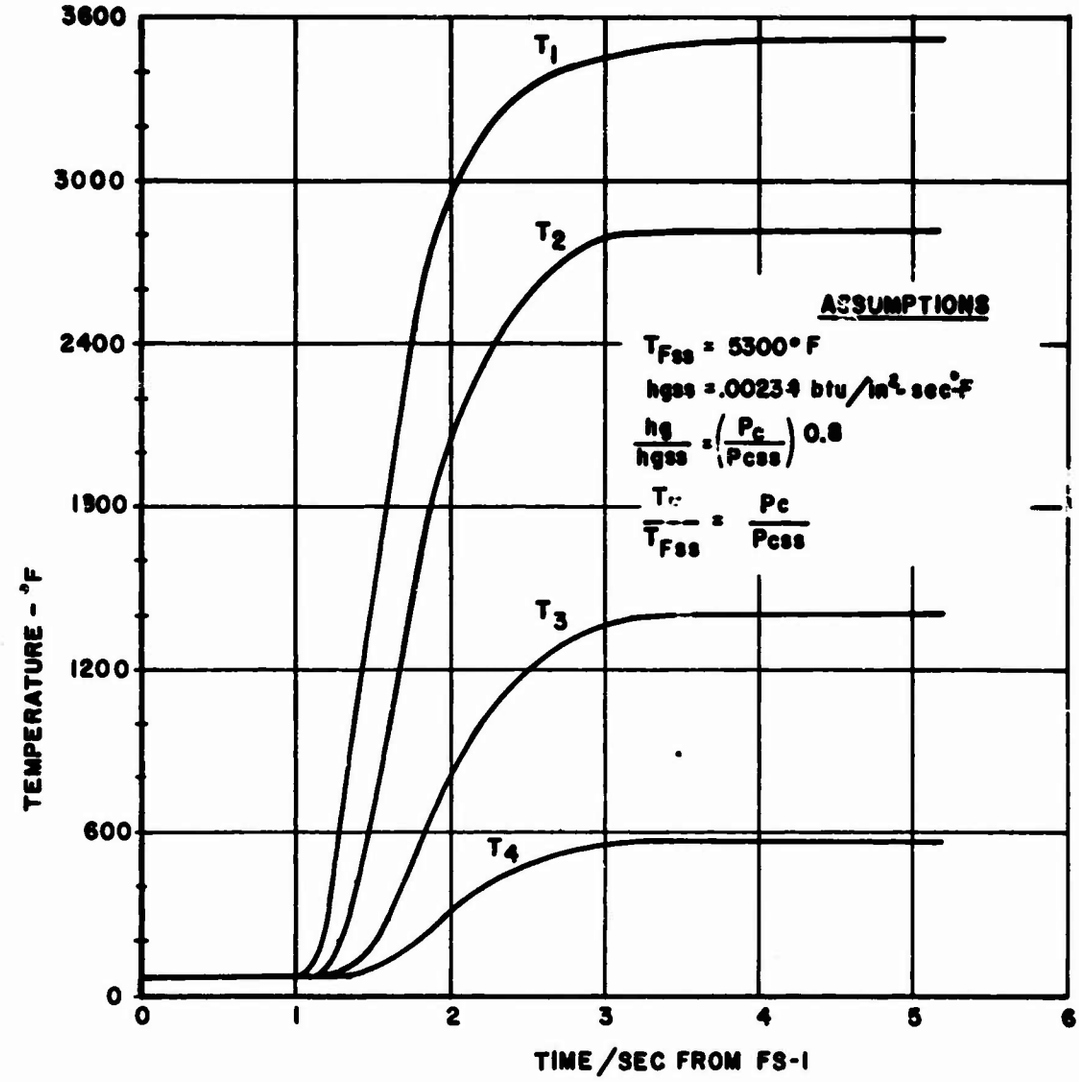

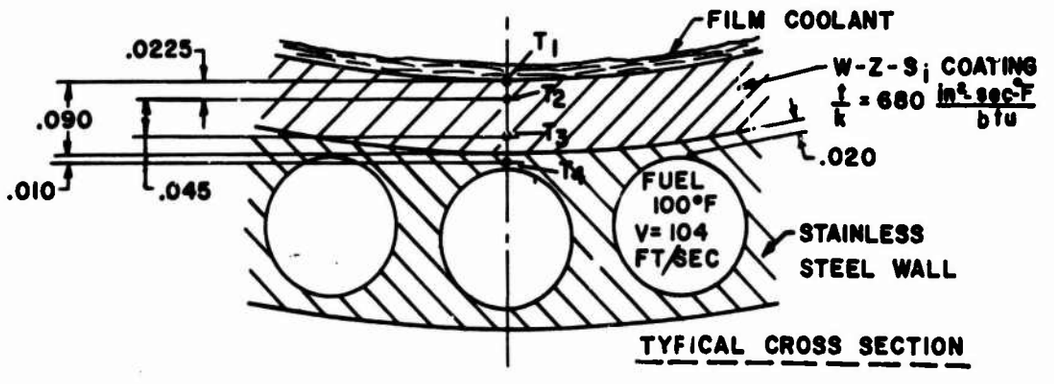

Transient Conduction Analysis for the Regeneratively Cooled L* Segment

Figure VII-B-5

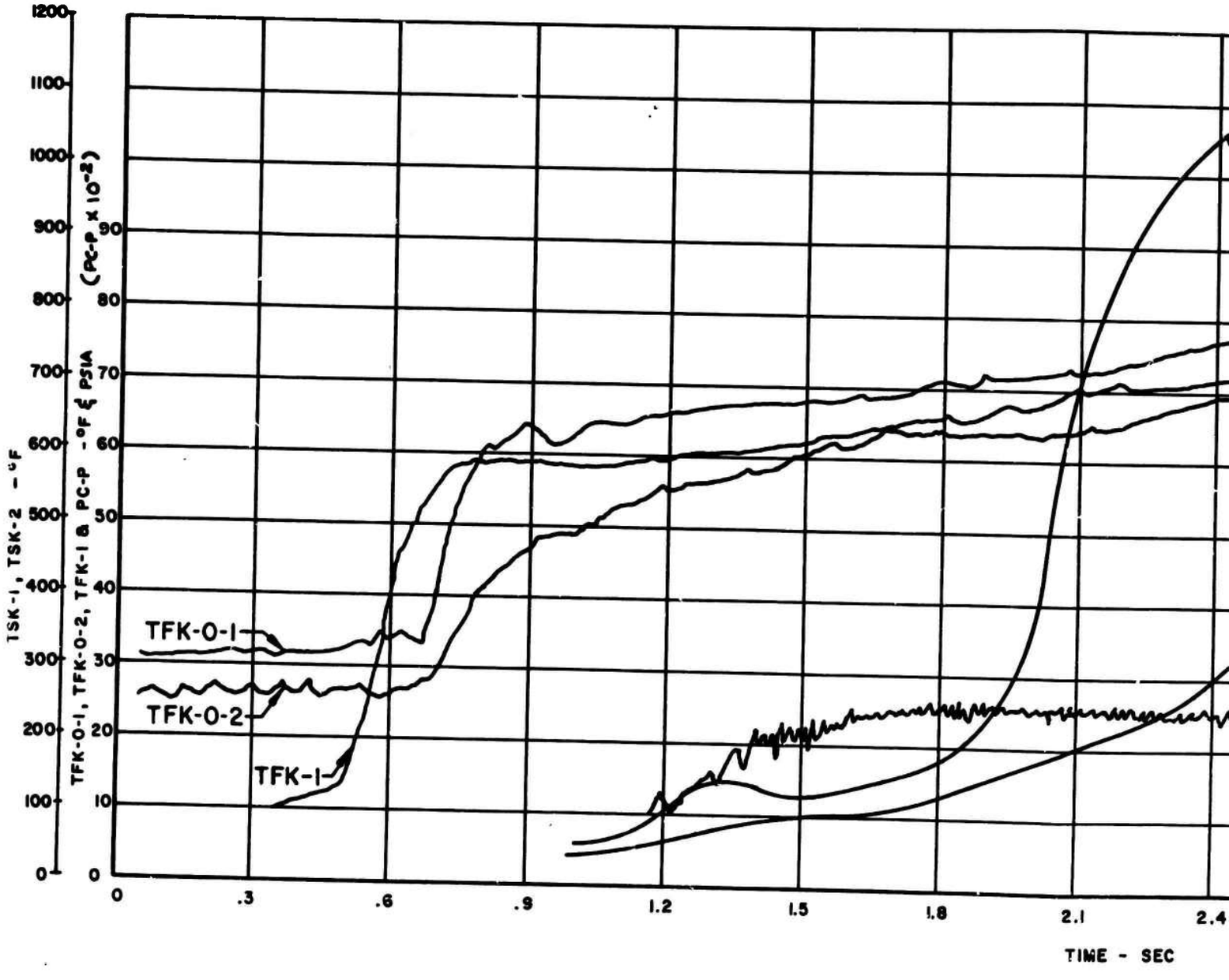
TSK-1, TSK-2 - °F
TFK-0-1, TFK-0-2, TFK-1 & PC-P - °F & PSIA
(PC-P x 10⁻²)
TFK-0-1
TFK-0-2
TFK-1
TIME - SEC
0
.3
.6
.9
1.2
1.5
1.8
2.1
2.4
100
200
300
400
500
600
700
800
900
1000
1100
1200
10
20
30
40
50
60
70
80
90

1

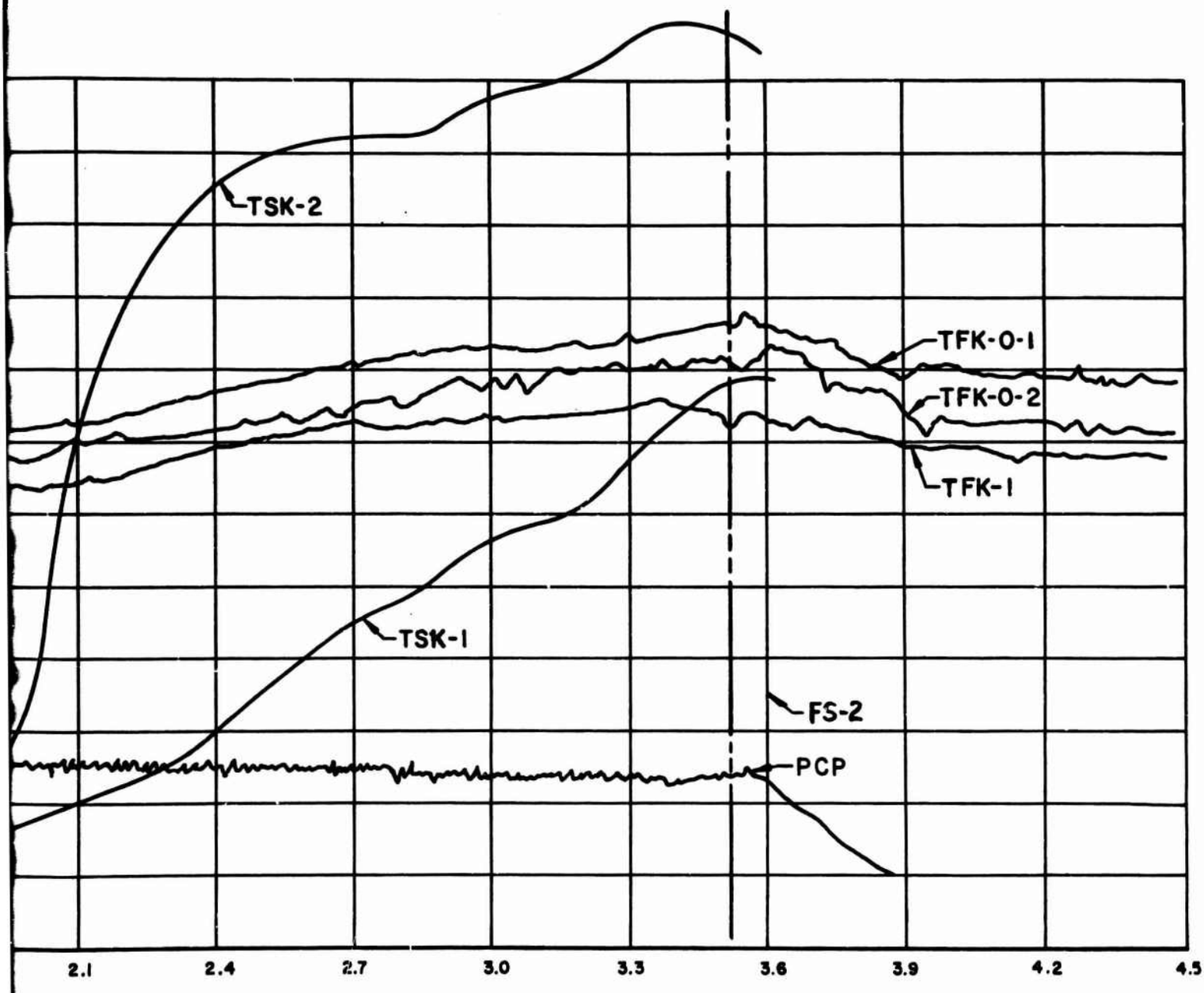

2

Pressure and Temperature vs Time, Test 1.2-02-YAM-031 (u)

Figure VII-B-6

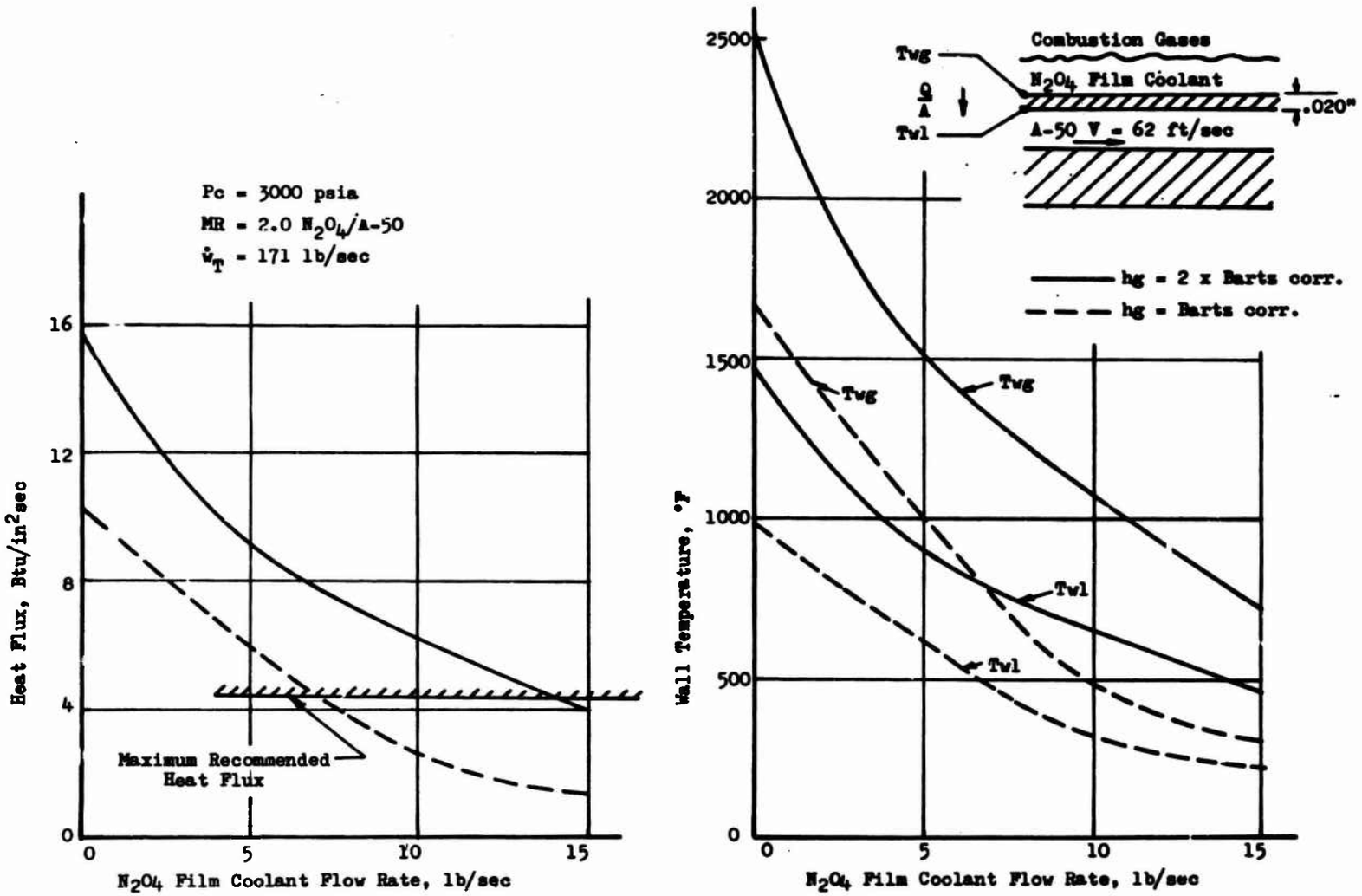

Figure VII-B-7

Theoretical Wall Temperature and Heat Flux vs Coolant Weight Flow
for Uncoated Drilled L* Segment

Book One

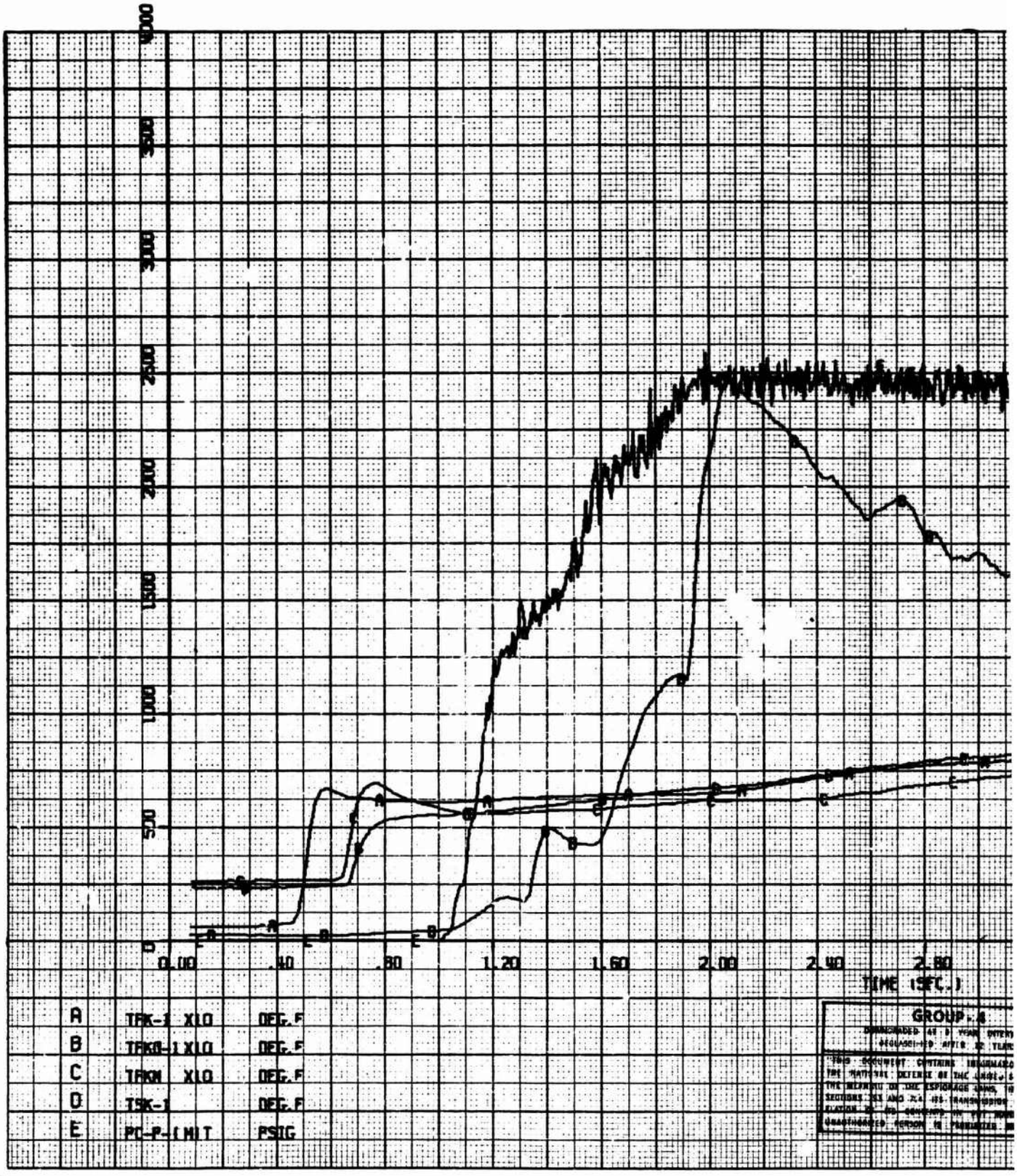
4000
3500
3000
2500
2000
1500
1000
500
0
0.00
.40
.80
1.20
1.60
2.00
2.40
2.80
TIME (SEC.)
A TRK-1 X10 DEG. F
B TRKO-1 X10 DEG. F
C TRKN X10 DEG. F
D TSK-1 DEG. F
E PC-P-LIMIT PSIG
GROUP - 4

1

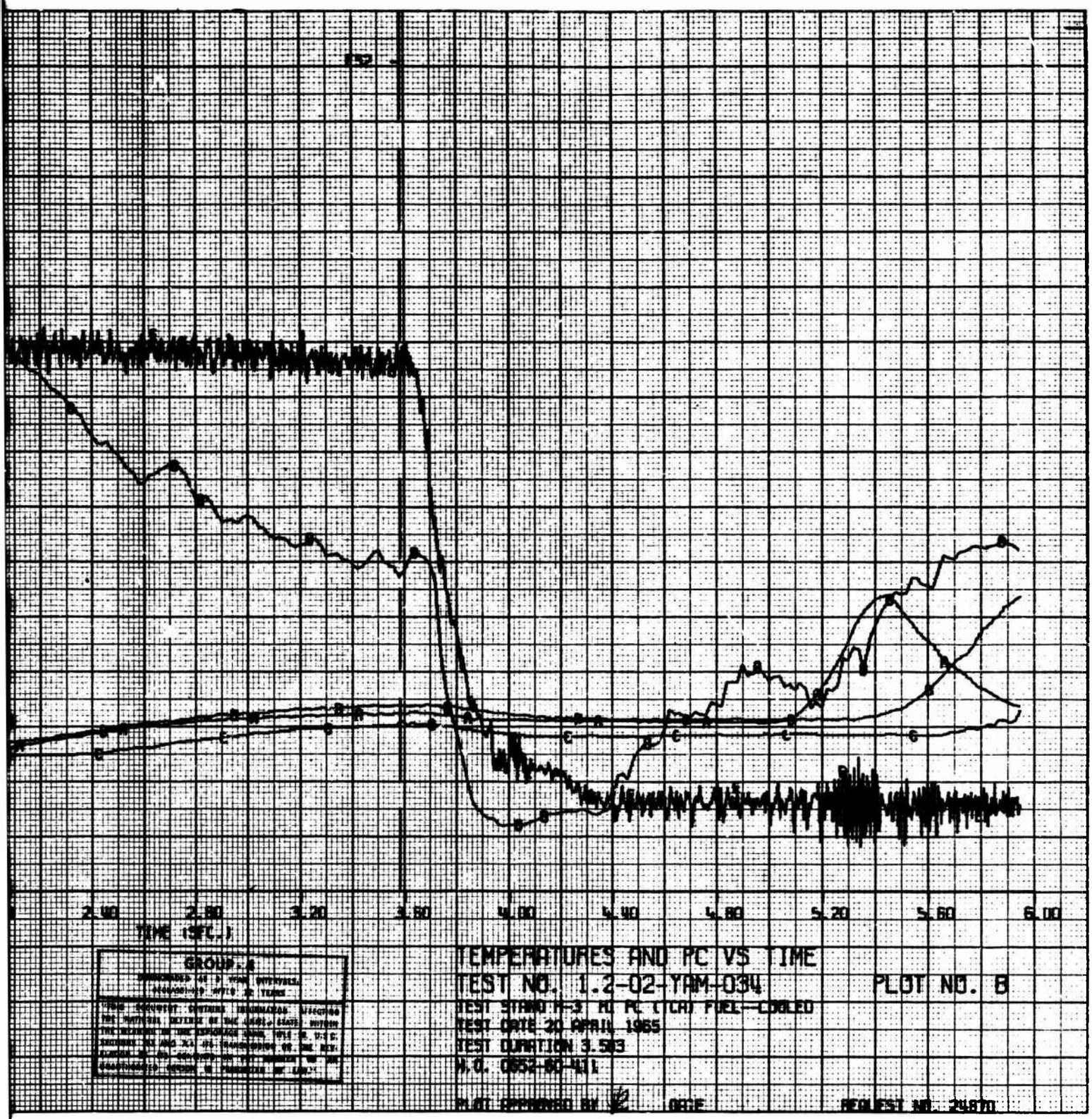

Pressure and Temperature vs Time, Test 1.2-02-YAM-034 (u)

Figure VII-B-8

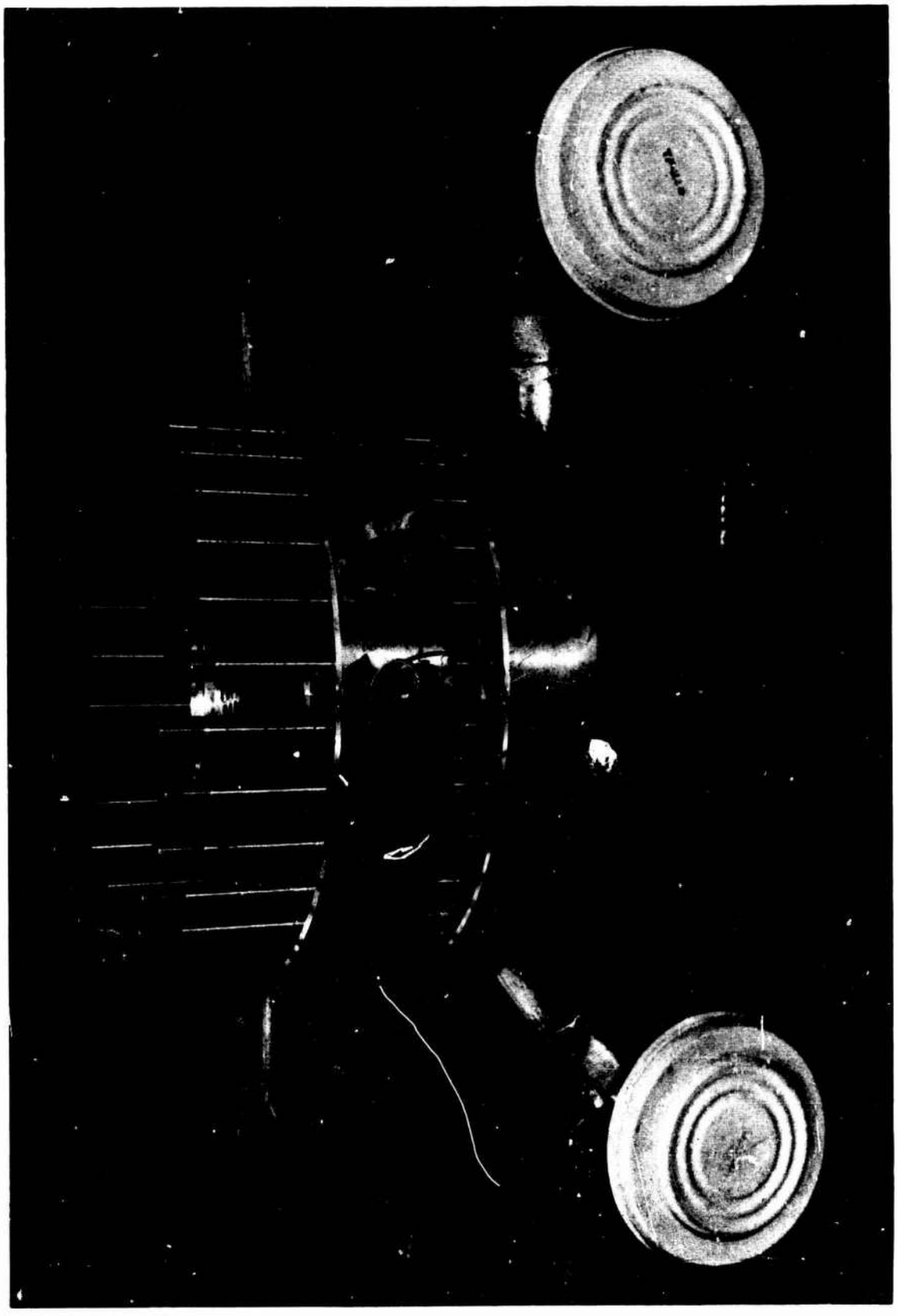

Vortex Chamber Segment

Figure VII-C-1

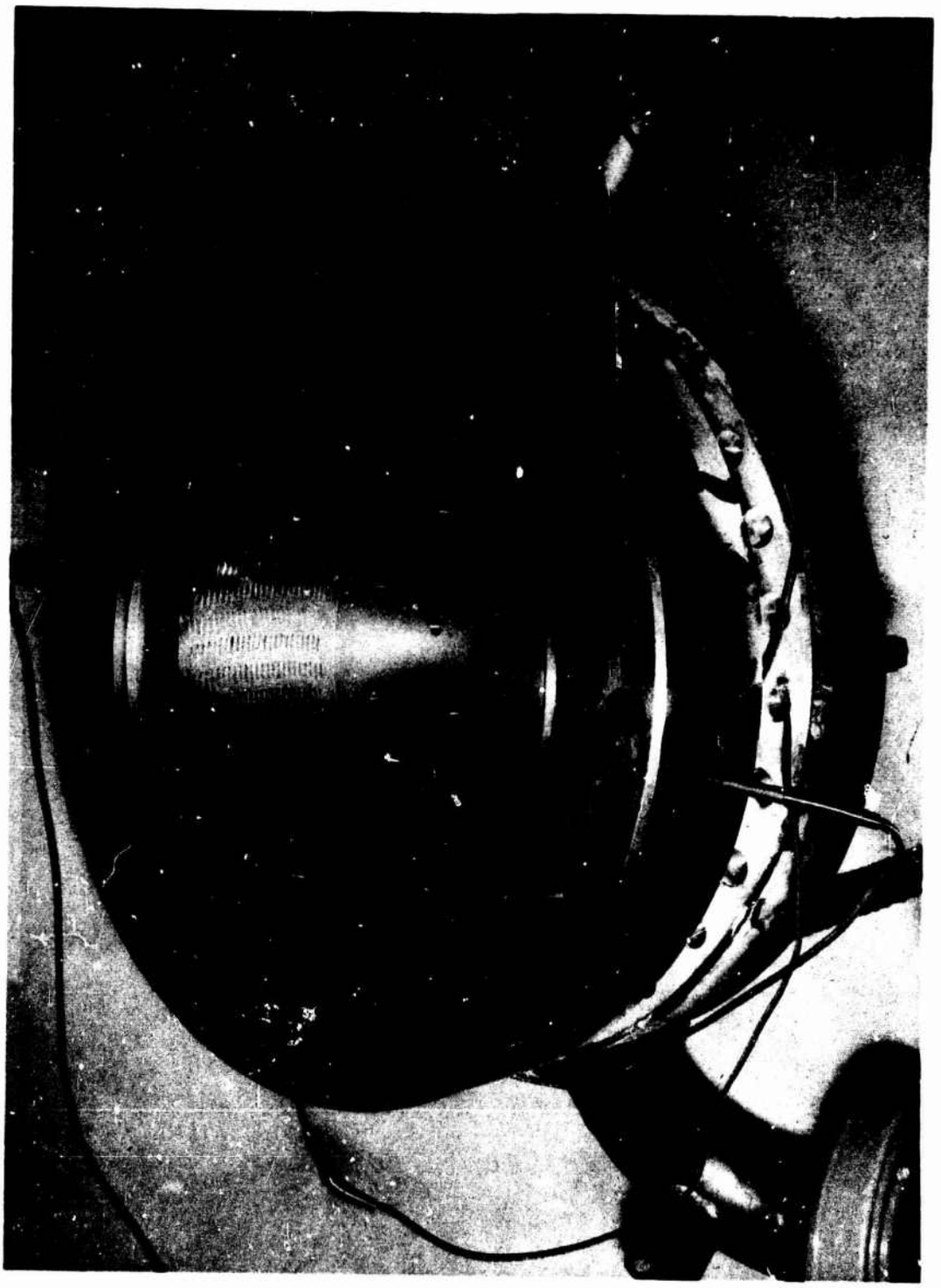

Internal View, Vortex Chamber Segment (u)

Figure VII-C-2

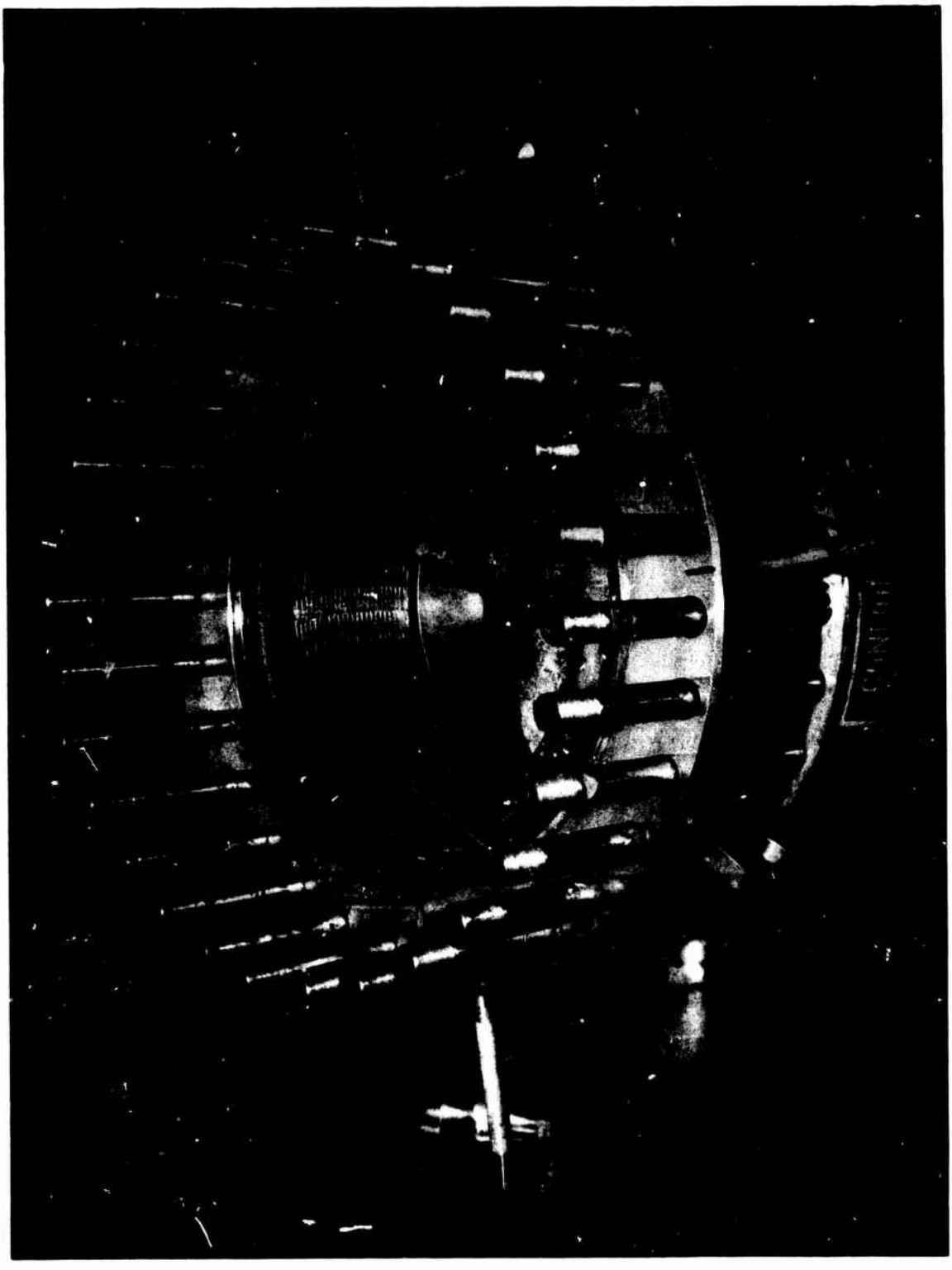

Vortex Chamber Segment, Posttest 1.2-01-YAM-007 (u)

Figure VII-C-3

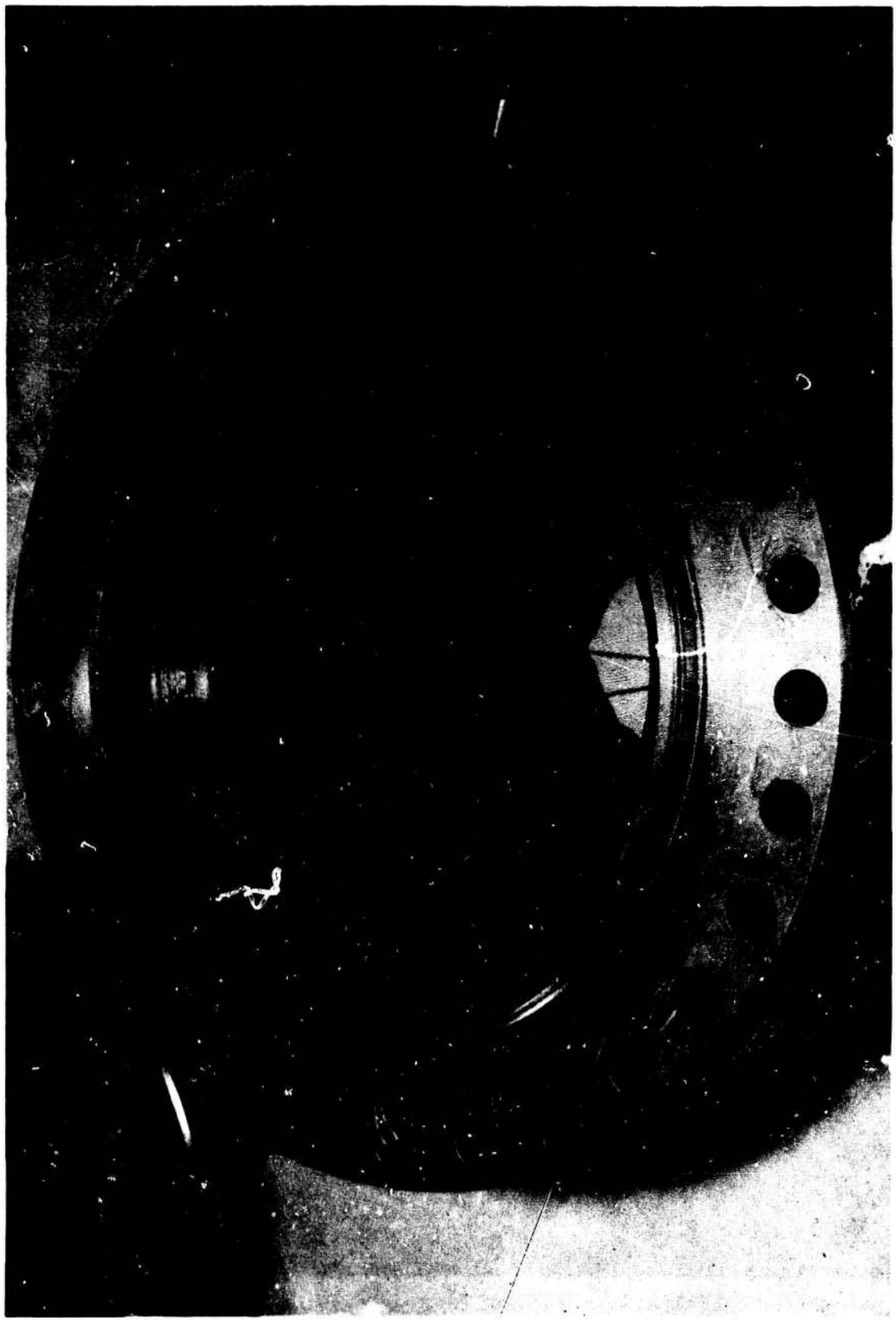

Graphite Convergent and Throat Segment, Posttest 1.2-01-YAM-007

Figure VII-C-4

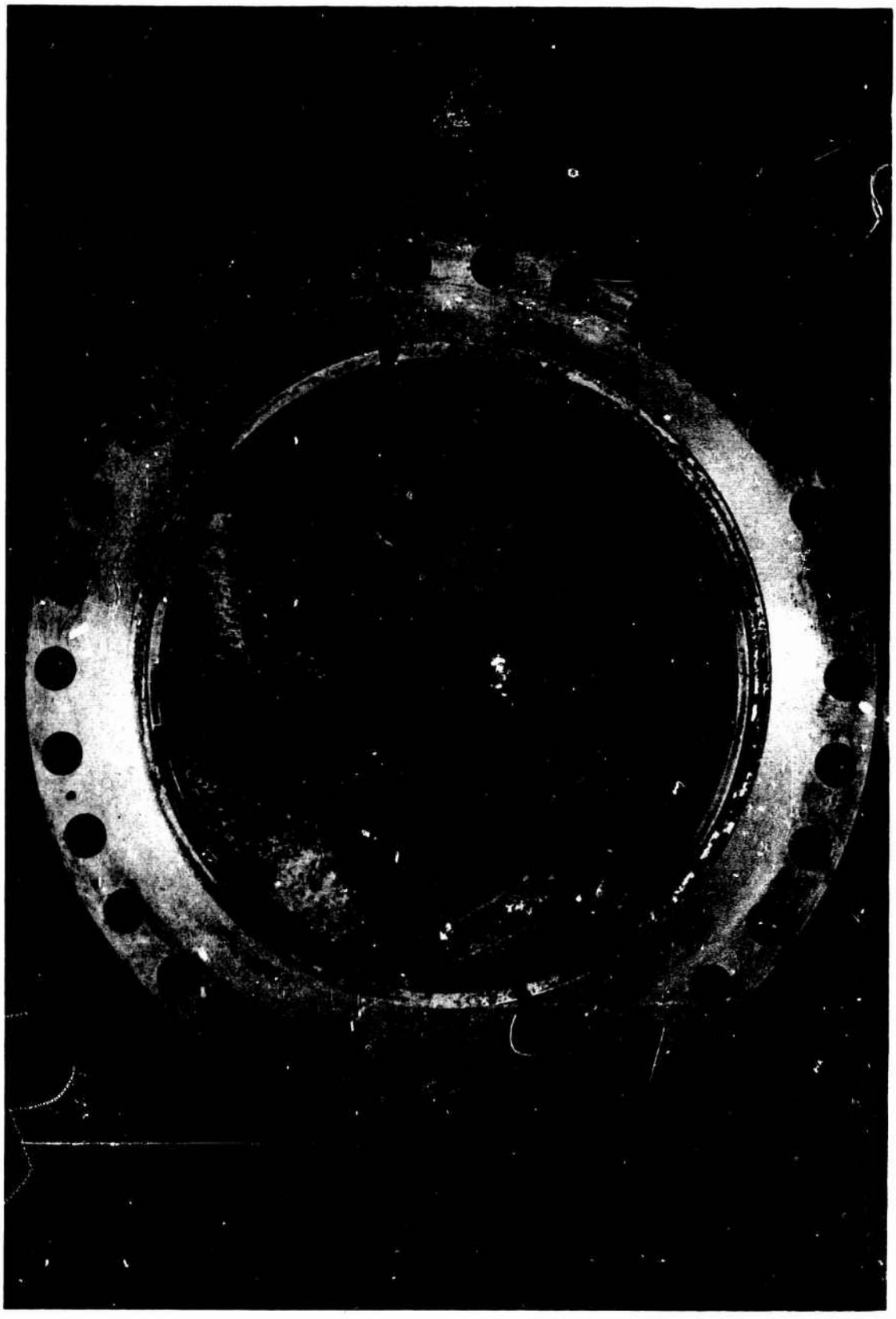

Graphite Throat, Posttest 1.2-01-YAM-007

Figure VII-C-5

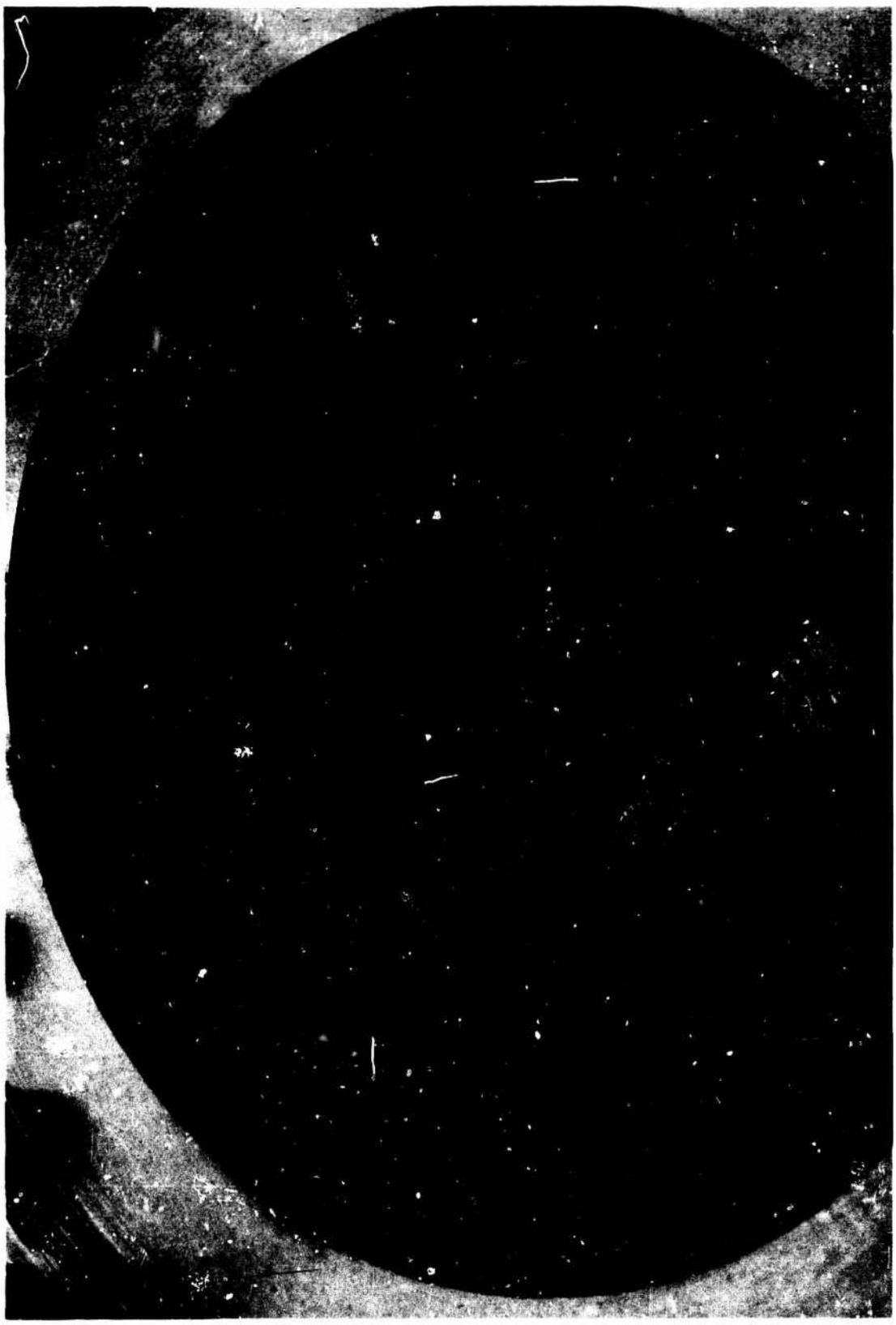

Repaired Vortex Chamber Segment, Pretest 1.2-01-YAM-010

Figure VII-C-6

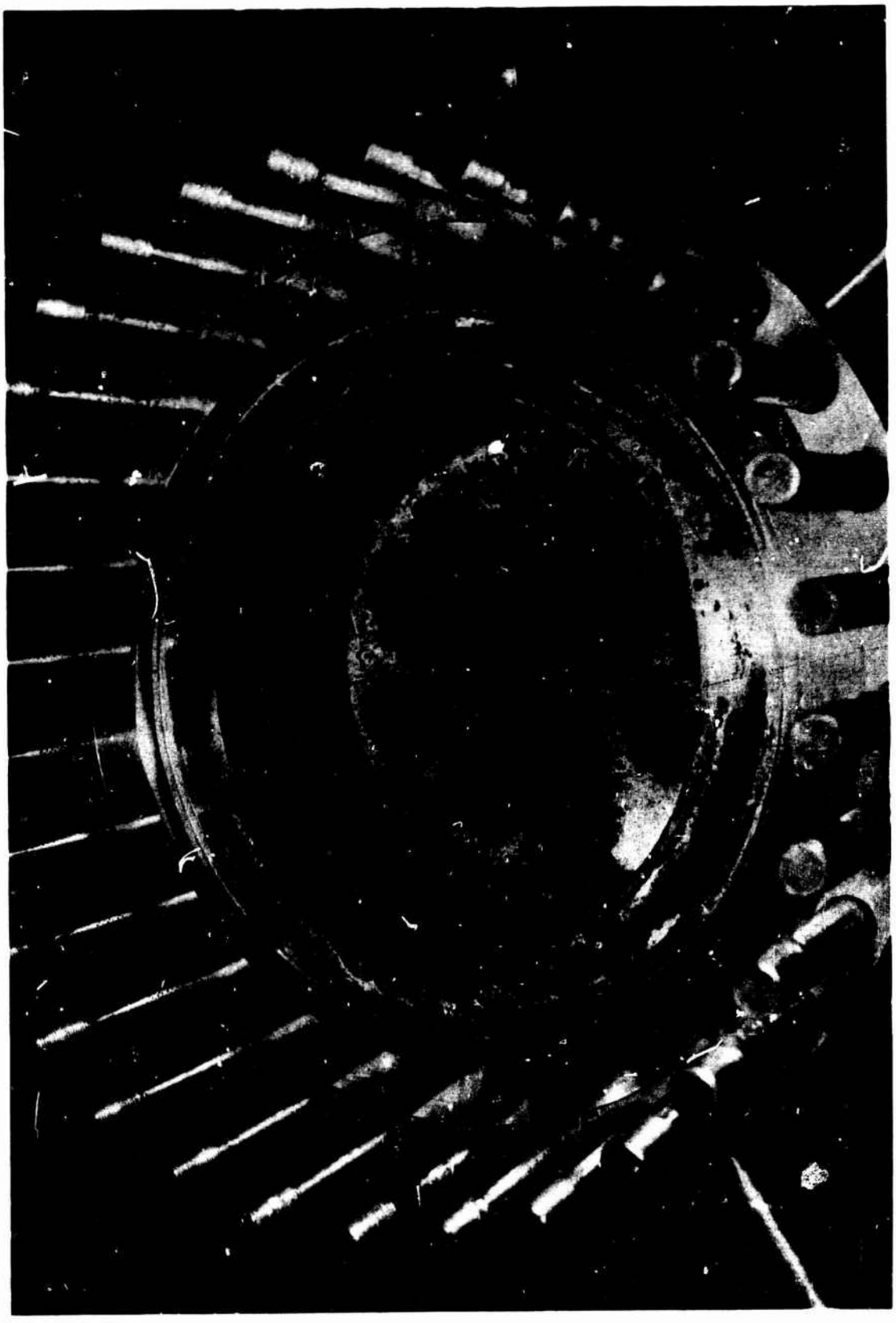

Vortex Chamber Segment Close-up, Posttest 1.2-01-YAM-010

Figure VII-C-7

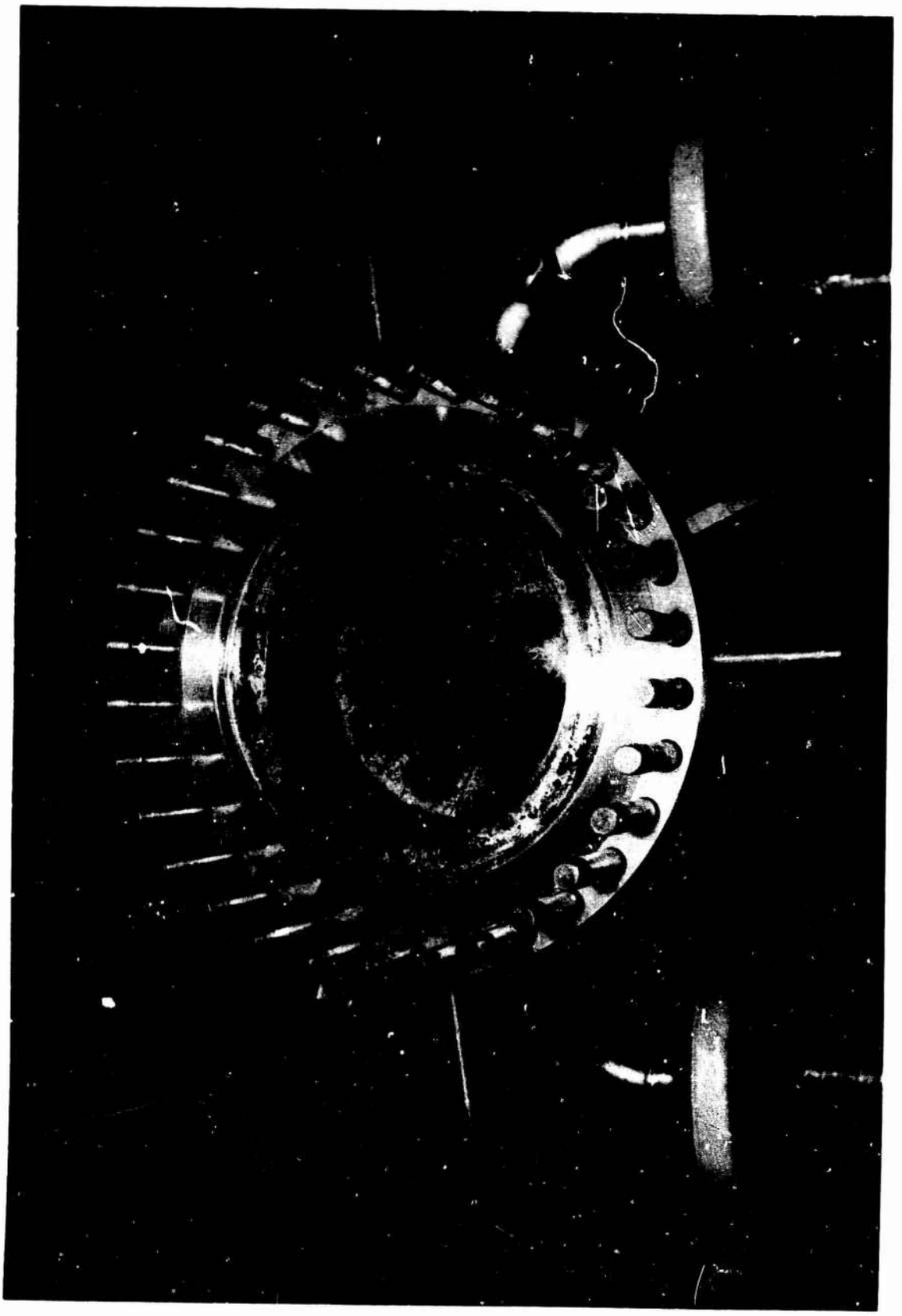

Vortex Chamber Segment, Posttest 1.2-01-YAM-010

Figure VII-C-8

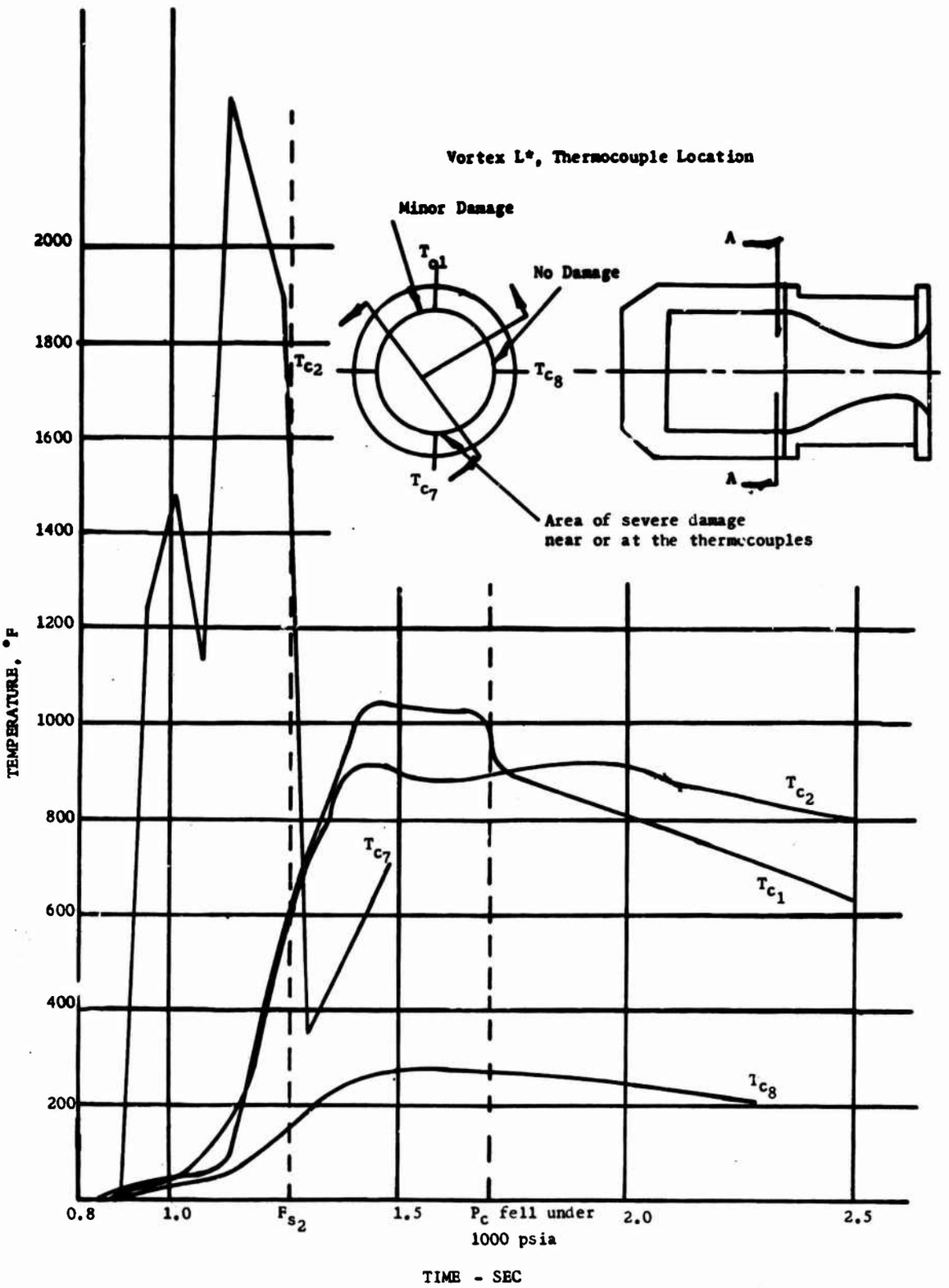

Vortex L* Thermocouple Data, Test 1.2-01-YAM-010

Figure VII-C-9

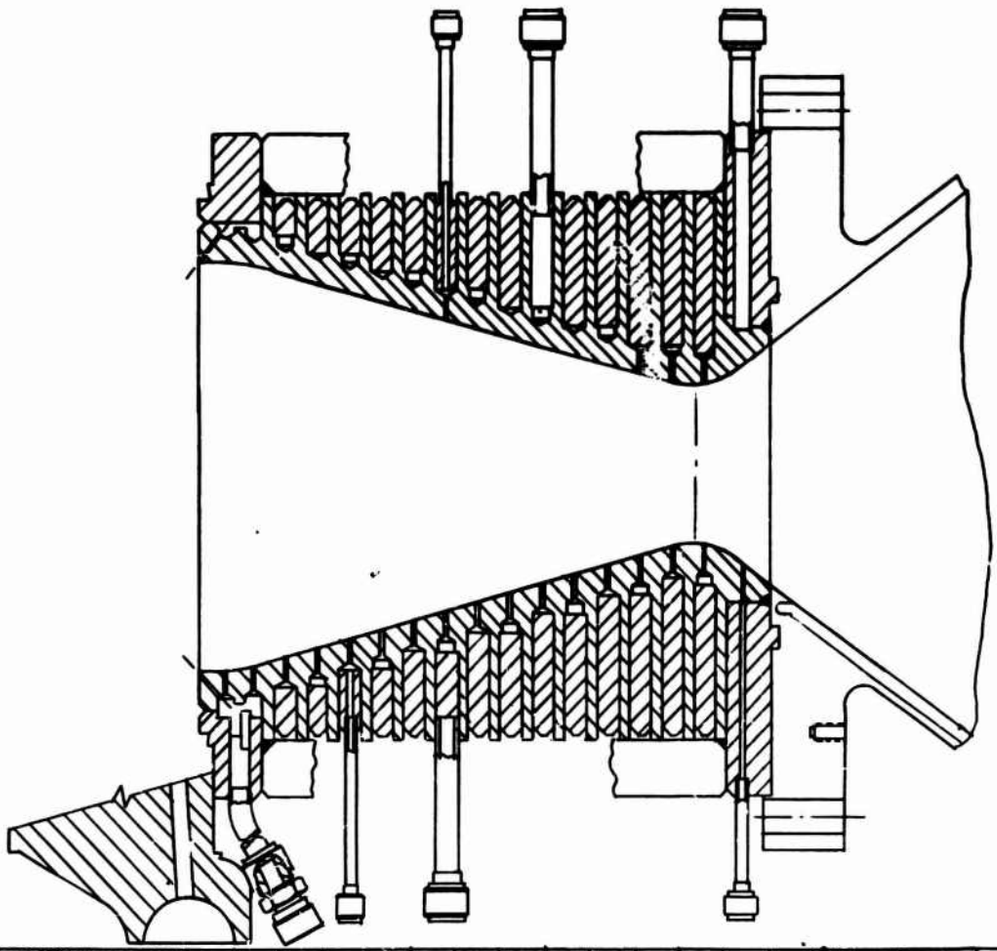

LOCATION PLANE REF		1	2	3	4	5	6	7	8	9	10	11	12	13	14	15'	16	THROAT	17	18
DIA		9.70	9.00	8.82	8.40	8.00	7.60	7.20	6.80	6.40	6.00	5.60	5.20	4.80	4.40	4.00	3.68	.355	.364	.418
DISTANCE FROM THROAT		11.550	10.950	10.785	9.535	8.785	8.035	7.285	6.535	5.785	5.035	4.285	3.535	2.785	2.035	1.285	.535	.000	.215	1.110
HOLE DATA																				
NO.		24	24	24	23	22	21	20	19	18	17	16	15	14	13	12	12		12	14
DIA		.052	.052	.052	.052	.052	.055	.055	.055	#53	#53	#52	#51	#51	#51	.070	.070		.082	.082
DRILL SIZE		55	55	55	55	55	54	54	54	53	53	1/16	52	51	51	50	50		45	45
TOTAL AREA IN²		#50	#50	#50	#48	#46	#49	#47	#44	#49	#47	#48	#47	#49	#46	#46	#46		#35	.0740
LENGTH SHORTEST		1.80	1.45	1.41	1.30	1.33	1.31	1.33	1.21	1.20	1.20	1.13	1.09	1.01	1.05	1.00	0.92		0.92	1.22
MANIFOLDS																				
AREA IN²	INLET	← .471 →			.095 ←												→ .095		.1510	.1700
	OUTLET	← .293 →			.0235 ←												→ .0235		#23	#23
AREA IN² SUPPLY	RECTANGULAR ENTRANCE	← .9006 →			.1875 ←												→ .1875		.1875	.221
TUBE *	TUBE	← .1269 →																		
	SIZE	← 1/2 X .049 WALL →																		
	LENGTH	← 4.50 →																		

Cooled Throat Segment, Final Design (u)

Figure VII-D-1

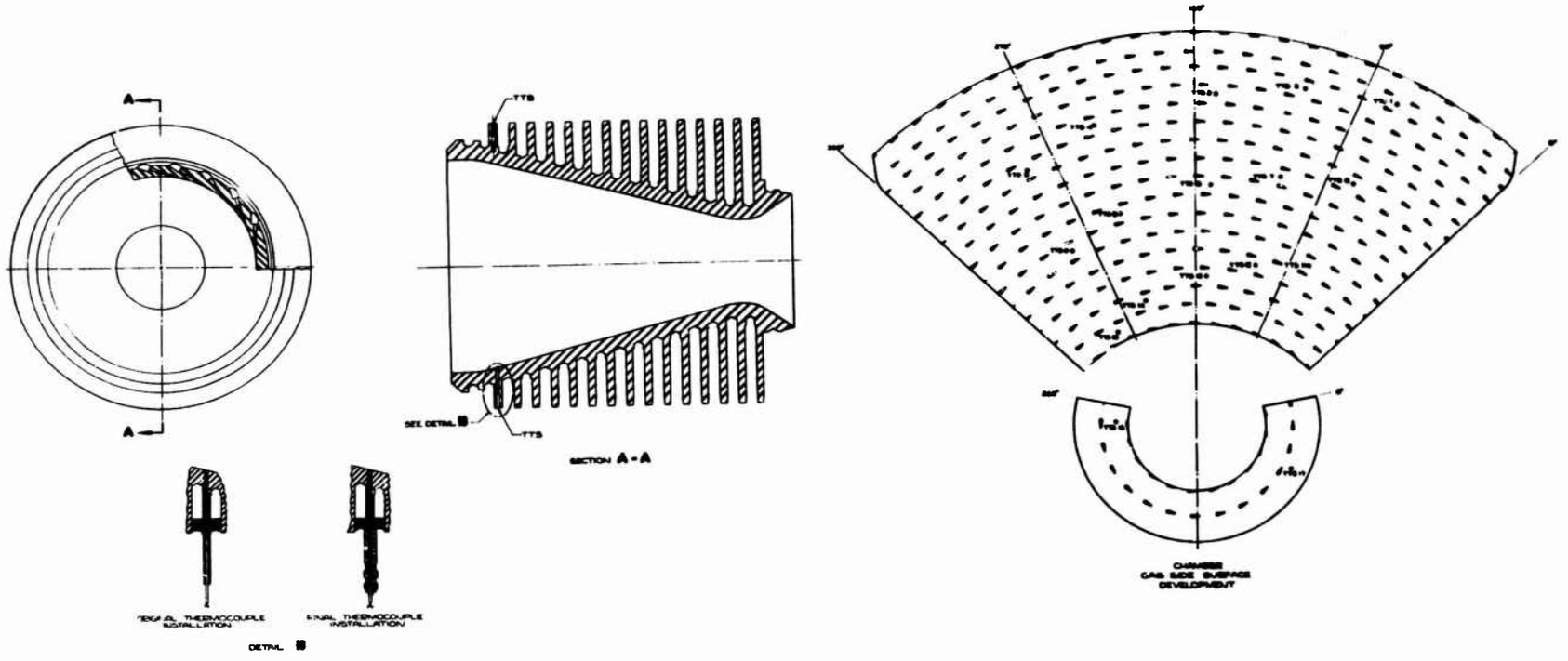

Figure VII-D-2

Thermocouple Location and Installation Technique

Book One

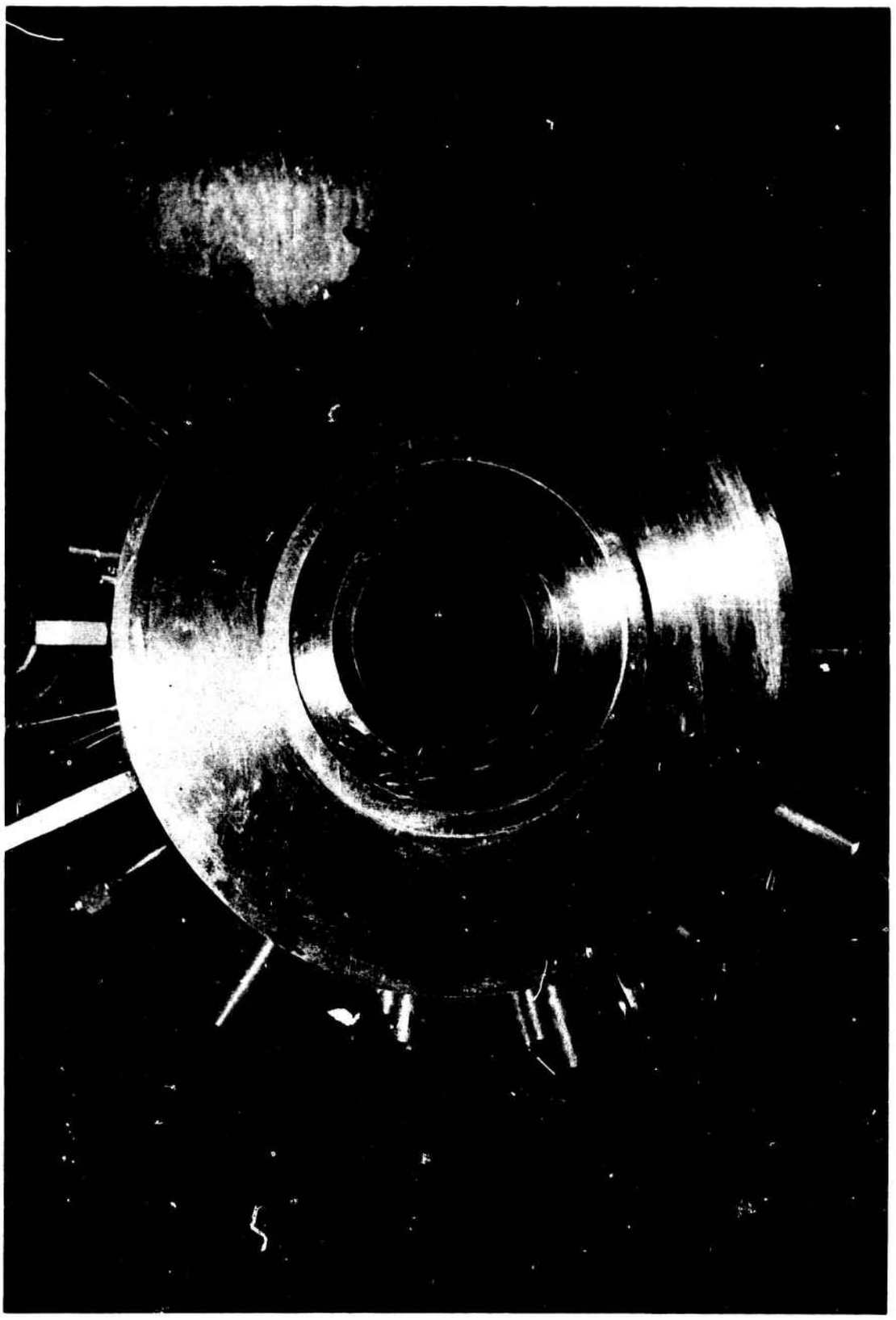

Cooled Throat Segment, Aft View

Figure VII-D-3

Figure VII-D-4

		10-19-64		11-2
		1.2-02-YAM-015		1.2-02
		Predicted Coolant Flow Rate lb/sec	Actual Coolant Flow Rate lb/sec	Predicted Coolant Flow Rate lb/sec
		6.435	6.450	6.435
		2.43	2.445	2.43
		2.43	2.215	2.43
		2.43	2.240	2.43
		2.43	1.912	2.43
		2.475	2.260	2.475
		2.475	2.130	2.475
		2.475	2.175	2.475
		2.475	2.170	2.475
		2.475	2.270	2.475
	)	2.475	2.190	2.475
	0	2.43	2.340	2.43
	0	2.43	2.050	2.43
	00	2.43	2.240	2.43
	15	2.925	2.935	2.925
	370	3.780	3.850	3.780
	.005	45.00	41.872	45.00
		4595		45
		86.2		86.
		4.034		3.0
	est M-012	Same as Test 1.2-02-YAM-012		Same as 02-YAM-(channels 9 & 11, 17 & 18 TTS-4 & .040 dia thermocc -5, -11 .125 dia thermocc
Remarks	S/N-1	S/N-1		S/N-1

Notes: (1) Test 1.2-02-YAM-011 was first test of the oxidizer film cooled convergent and throat
(2) Tests where no useful data were obtained include: Tests 1.2-02-YAM-011/10-8-64, -01
(3) Single Point Data.
(4) All sixteen orifices were installed backwards.
(5) Orifice in channel No. 1 was installed backwards.

19-64		11-26-64		11-30-64		12-2-64		1-9-65	
02-YAM-015		1.2-02-YAM-017		1.2-02-YAM-018		1.2-02-YAM-020		1.2-02-YAM-021	
ed te	Actual Coolant Flow Rate lb/sec	Predicted Coolant Flow Rate lb/sec	Actual Coolant Flow Rate lb/sec	Predicted Coolant Flow Rate lb/sec	Actual Coolant Flow Rate lb/sec	Preticted Coolant Flow Rate lb/sec	Actual Coolant Flow Rate lb/sec	Predicted Coolant Flow Rate lb/sec	Actual Coolant Flow Rate lb/sec
	6.450	6.435	3.457	6.435	8.359(5)	7.626	8.582	6.235	4.353
	2.445	2.43	2.702	1.701	1.841	0	0	2.911	2.434
	2.215	2.43	2.764	2.430	2.592	2.874	3.467	2.607	2.236
	2.240	2.43	2.829	1.701	2.250	0	0	2.241	1.007
	1.912	2.43	2.750	2.430	2.510	2.897	3.300	2.738	2.305
	2.260	2.475	2.783(4)	1.732	2.043	0	0	1.295	2.031
	2.130	2.475	2.673	2.475	2.498	2.960	3.345	2.629	2.214
	2.175	2.475	2.709	1.732	2.297	0	0	2.954	2.506
	2.170	2.475	2.910	2.475	2.497	2.948	3.056	1.126	0.934
	2.270	2.475	3.188	1.732	2.117	0	0	3.149	2.618
	2.190	2.475	2.857	2.475	2.552	2.468	2.357	2.136	1.753
	2.340	2.43	3.001	2.430	2.42	2.566	2.511	2.672	2.158
	2.050	2.43	2.729	2.430	2.468	4.823	2.169	2.582	1.191
	2.240	2.43	2.963	2.430	2.277	2.483	1.872	2.749	2.045
	2.935	2.925	5.116	2.925	3.452	3.494	2.250	2.912	2.502
	3.850	3.780	7.443	3.780	7.397	6.831	3.688	3.954	3.456
	41.872	45.00	57.874	41.313	49.393	33.652	36.597	43.898	35.713
4595		4536		4358		5165(3)		4732	
86.2		86.2		81.3		92.3(3)		85.4	
.034		3.022		2.524		2.067		2.197	
as Test 2-YAM-012		Same as Test 1.2-02-YAM-012 except channels 2 through 9 & 11, 13, 15, 17 & 18 were grooved. TTS-4 & TTS-7 were .040 dia high-response thermocouples & TTS-3, -5, -11 & -14 were .125 dia high-response thermocouples.		Same as Test 1.2-02-YAM-017		Same as Test 1.2-02-YAM-017		All injection stations grooved, 17 high-response thermocouples installed (.125 dia).	
		S/N-1		S/N-1		S/N-1, throat severely eroded		S/N-2, slight erosion of throat due to off M/R condition. OTPA failure.	

led convergent and throat segment, conducted on 10-8-64.
2-02-YAM-011/10-8-64, -013/10-16-64, -016/11-26-64, -019/12-2-64, -026/3-5-65, -028/3-12-65.

Cumulative Summary of Coolant Flow Rates, Cooled Convergent and Throat Segment Tests (u)

Figure VII-D-5, Sheet 1 of 3

Test Date		2-15-65		2-19-65		2-26-65		3
Test No.		1.2-02-YAM-022		1.2-02-YAM-023		1.2-02-YAM-024		1.2-
Coolant Feed Channel No.	Coolant Injection Station No.	Predicted Coolant Flow Rate lb/sec	Actual Coolant Flow Rate lb/sec	Predicted Coolant Flow Rate lb/sec	Actual Coolant Flow Rate lb/sec	Predicted Coolant Flow Rate lb/sec	Actual Coolant Flow Rate lb/sec	Predict Coolant Flow Ra lb/sec
1	1,2,3	4.966	4.070	4.966	5.253	5.24	4.704	5.
2	4	1.843	1.147	1.843	1.951	1.00	0.906	1.
3	5	1.539	.964	1.539	1.627	1.62	1.458	1.
4	6	1.850	1.165	1.850	1.955	1.63	1.465	1.
5	7	2.276	1.430	2.276	2.545	1.67	1.445	1.
6	8	1.130	.715	1.130	1.208	1.77	1.601	1.
7	9	2.253	1.420	2.253	2.409	1.88	1.703	1.
8	10	2.329	1.477	2.329	2.484	1.91	1.716	1.
9	11	1.862	1.172	1.862	1.994	1.99	1.802	1.
10	12	2.145	1.351	2.145	2.301	2.28	2.045	2.
11	13	1.607	.989	1.607	1.666	2.31	2.108	2.
12	14	2.212	1.443	2.212	2.429	2.35	2.133	2.
13	15	2.665	1.728	2.665	2.871	2.80	2.571	2.
14	16	2.749	1.797	2.749	2.955	2.95	2.681	2.
15	17	4.782	3.684	4.782	5.347	3.01	2.709	3.
16	18	3.928	2.574	3.928	3.915	3.85	3.552	3.
Total Coolant Weight Flow		40.136	27.126	40.136	42.910	38.27	34.599	38.2
Calculated C* ft/sec		2012.2		4874.4		4205.8		48
% of Theoretical C*		37.3		90.5		73.2		
FS_1 to FS_2 Duration		2.678		2.953		3.514		3
Configuration of Cooled Convergent and Throat Segment		Same as Test 1.2-02-YAM-021		Same as Test 1.2-02-YAM-021		Same as Test 1.2-02-YAM-021		Same as T YAM-021
Remarks		S/N-2 High Pressure Flexible Line from Oxidizer Manifold to Exit Cone Failed During Test. Low P_c Obtained		S/N-2 Valid Test. All Test Hardware in Refireable Condition.		S/N-2 Gas Generator valve did not open completely, P_c of approximately 2400 psi was obtained, no hardware damage.		S/N-2 Valid Test Hardware i Condition.

-26-65		3-2-65		3-8-65		3-15-65			
02-YAM-024		1.2-02-YAM-025		1.2-02-YAM-027		1.2-02-YAM-029		1.2-02-YAM-033	
od te	Actual Coolant Flow Rate lb/sec	Predicted Coolant Flow Rate lb/sec	Actual Coolant Flow Rate lb/sec	Predicted Coolant Flow Rate lb/sec	Actual Coolant Flow Rate lb/sec	Predicted Coolant Flow Rate lb/sec	Actual Coolant Flow Rate lb/sec	Predicted Coolant Flow Rate lb/sec	Actual Coolant Flow Rate lb/sec
	4.704	5.24	5.336	3.924	3.799	3.78	3.73	3.72	3.78
	0.906	1.00	1.028	1.376	1.347	1.38	1.36	1.39	1.40
	1.458	1.62	1.655	1.371	1.340	1.30	1.29	1.30	1.34
	1.465	1.63	1.662	1.350	1.322	1.32	1.30	1.33	1.35
	1.445	1.67	1.635	1.788	1.762	1.81	1.79	1.83	1.86
	1.601	1.77	1.811	1.811	1.771	1.78	1.76	1.83	1.87
	1.703	1.88	1.429	1.603	1.563	1.56	1.54	1.51	1.54
	1.716	1.91	1.955	1.845	1.810	1.83	1.80	1.80	1.84
	1.802	1.99	2.035	1.815	1.780	1.73	1.71	1.72	1.73
	2.045	2.28	2.315	1.992	1.953	1.96	1.94	1.93	1.97
	2.108	2.31	2.375	2.189	2.142	2.14	2.11	2.09	2.14
	2.133	2.35	2.395	2.815	2.750	2.74	2.71	2.72	2.80
	2.571	2.80	2.882	3.187	3.120	2.96	2.92	2.90	2.94
	2.681	2.95	2.984	3.249	3.207	2.98	2.93	2.90	2.93
	2.709	3.01	2.999	3.473	3.428	3.02	2.98	1.76	1.77
	3.552	3.85	3.911	3.022	2.940	2.47	2.44	1.79	1.81
	34.599	38.27	38.907	36.809	36.034	34.77	34.30	32.52	33.08
205.8		4890.6		4823.3		4745		4475	
73.2		91.1		90.6		93.2		86.9	
3.514		3.506		3.522		3.001		3.524	
est 1.2-02-		Same as Test 1.2-02-YAM-021		Same as Test 1.2-02-YAM-021		Same as Test 1.2-02-YAM-02?		Same as Test 1.2-02-YAM-21	
ator valve pen complete approximate si was no hardware		S/N-2 Valid Test. All Test Hardware in Refireable Condition.		S/N-2 Valid Test. All Test Hardware in Refireable Condition.		S/N-2 Valid Test. All Test Hardware in Refireable Condition.		Channels 12 through 16 eroded beyond repair during this test	

Cumulative Summary of Coolant Flow Rates, Cooled Convergent and Throat Segment Tests (u)

Figure VII-D-5, Sheet 2 of 3

Test Date: 5-19-65

Test No.		1.2-02-YAM-036	
Coolant Feed Channel No.	Coolant Injection Station No.	Predicted Coolant Flow Rate lb/sec	Actual Coolant Flow Rate lb/sec
1	1, 2, 3	3.48	3.03
2	4	1.41	1.25
3	5	1.29	1.14
4	6	1.33	1.17
5	7	1.78	1.57
6	8	1.79	1.54
7	9	1.56	1.39
8	10	1.81	1.61
9	11	1.72	1.54
10	12	1.94	1.78
11	13	2.55	2.36
12	14	0	0
13	15	0	0
14	16	0	0
15	17	0	0
16	18	0	0
Total coolant weight flow, lb/sec		20.71	18.38
% of theoretical c*		91 to 96.5	
FS_1 to FS_2 duration, sec		2.580	
Configuration of Cooled Convergent and Throat Segment		Ablative liner in the throat from channels 12 through 16	
Remarks		Remaining channels (1 through 11) eroded during this test	

Cumulative Summary of Coolant Flow Rates, Cooled Convergent and Throat Segment Tests (u)

Figure VII-D-5, Sheet 3 of 3

Book One

Test Date		10/9/64				10/16/64			
Test Number		1.2-02-YAM-012				1.2-02-YAM-014			
Coolant Feed Channel No.	Coolant Injection Station No.	Thermocouple Number	* T_{avg} (°F)	T_{max} @ Time (°F) (sec)	** T_{TS-2} (°F)	* T_{avg} (°F)	T_{max} @ Time (°F) (sec)	** T_{TS-2} (°F)
1	1,2	TTS-1	98	193 @ 7.5	133	130	256 @ 2.8	189
1	3	TTS-2	84	186 @ 2.8	105	112	217 @ 3.0	163
2	4	TTS-3	98	223 @ 2.3	143	---	Invalid	---
3	5	TTS-4	118	357 @ 2.6	194	186	440 @ 3.0	309
4	6	TTS-5	---	No Hook Up	---	---	No Hook Up	---
5	7	TTS-6	127	278 @ 2.3	185	172	320 @ 3.0	250
6	8	TTS-7	---	No Hook Up	---	331	722 @ 2.9	365
7	9	TTS-8	106	180 @ 3.0	135	135	209 @ 3.0	175
8	10	TTS-9	132	305 @ 2.3	198	191	369 @ 3.0	285
9	11	TTS-10	104	193 @ 2.3	140	138	233 @ 2.9	191
10	12	TTS-11	---	Erratic	---	---	Not Working	---
11	13	TTS-12	91	137 @ 3.1	116	111	178 @ 3.0	146
12	14	TTS-13	97	176 @ 2.5	128	129	221 @ 2.9	181
13	15	TTS-14	---	No Hookup	---	---	No Hookup	---
14	16	TTS-15	109	216 @ 2.3	154	130	261 @ 2.9	213
15	17	TTS-16	129	243 @ 2.4	73	193	307 @ 2.8	276
16	18	TTS-17	---	No Hookup	---	---	No Hookup	---
Remarks		* T_{avg} During Period 1.27 - 1.77 **TS-2 @ 1.865 sec Original design hardware, slow response instrumentation (all thermocouples), junction 0.073 in. below surface, no grooving of injection stations. Throat Assy S/N-1				* T_{avg} During Period 1.35 - 2.37 **TS-2 @ 2.373 sec Same hardware as Test 1.2-02-012. Throat Assy S/N-1			

Notes: (1) Test 1.2-02-YAM-011 was the first test of the oxidizer film cooled convergent and throat segment. (2) Tests where no useful data were obtained include: Tests 1.2-02-YAM-011 on 10/8/64, -013 on 10/16/64, -016 on 11/26/64, -019 on 12/2/64, -026 on 3/5/65, -028 on 3/12/65.

Test Date	10/19/64			11/26/64			11/30/64		
Test Number	1.2-02-YAM-015			1.2-02-YAM-017			1.2-02-YAM-018		
Thermocouple Number	* T_{avg} (°F)	T_{max} @ Time (°F) (sec)	** T_{TS-2} (°F)	* T_{avg} (°F)	T_{max} @ Time (°F) (sec)	** T_{TS-2} (°F)	* T_{avg} (°F)	T_{max} @ Time (°F) (sec)	** T_{TS-2} (°F)
TTS-1	303	357 @ 4.5	333	220	294 @ 3.4	268	172	234 @ 3.0	200
TTS-2	281	332 @ 4.5	314	111	128 @ 3.1	127	79	88 @ 2.6	86
TTS-3	---	Invalid	---	---	Invalid	---	---	Not Working	---
TTS-4	456	617 @ 4.6	333	773	913 @ 2.7	854	---	Invalid	---
TTS-5	---	No Hookup	---	491	528 @ 2.1	480	631	1729 @ 2.6	718
TTS-6	369	438 @ 4.7	419	193	262 @ 3.1	245	191	234 @ 3.1	218
TTS-7	549	642 @ 4.4	610	---	Invalid	---	---	No Hookup	---
TTS-8	242	280 @ 4.3	264	183	237 @ 2.3	214	167	212 @ 3.1	184
TTS-9	406	312 @ 4.7	434	337	447 @ 3.0	395	306	418 @ 2.9	350
TTS-10	258	318 @ 4.3	289	185	249 @ 3.0	219	151	204 @ 3.1	172
TTS-11	---	Invalid	---	---	Not Working	---	---	No Hookup	---
TTS-12	212	249 @ 4.5	234	---	Not Working	---	---	Erratic	---
TTS-13	---	Invalid	---	176	236 @ 3.4	215	157	208 @ 3.0	175
TTS-14	---	No Hookup	---	---	Erratic	---	---	No Hookup	---
TTS-15	280	358 @ 4.6	314	212	273 @ 3.5	247	256	348 @ 3.1	290
TTS-16	384	417 @ 4.4	410	180	203 @ 3.1	199	228	283 @ 2.9	247
TTS-17	---	No Hookup	---	---	Erratic	---	---	No Hookup	---
Remarks	* T_{avg} During Period 3.00 - 4.00 sec **TS-2 @ 4.033 sec Same hardware as Test 1.2-02-YAM-012. Throat Assy S/N-1			* T_{avg} During Period 2.00 - 3.00 sec **TS-2 @ 3.022 sec Same hardware as Test 1.2-02-YAM-012 except channels 2 through 9 & 11, 13, 15, 17 & 18 were grooved. TT-4 & TTS-7 were 0.040 dia. high response thermocouples & TTS-3, -5, -11 & -14 were 0.125 dia. high response thermocouples. Throat Assy S/N-1.			* T_{avg} During Period 2.00 - 2.50 sec **TS-2 @ 2.324 sec Same hardware as Test 1.2-02-YAM-017. Throat Assy S/N -1		

Cumulative Summary of Skin Temperatures, Cooled Convergent and Throat Segment Tests

Figure VII-D-6, Sheet 1 of 3

Test Date	12/2/64			1/9/65			2/15/65		
Test Number	1.2-02-YAM-020			1.2-02-YAM-021			1.2-02-YAM-022		
Thermocouple Number	* T_{avg} (°F)	T_{max} @ Time (°F) (sec)	** T_{TS-2} (°F)	* T_{avg} (°F)	T_{max} @ Time (°F) (sec)	** T_{TS-2} (°F)	* T_{avg} (°F)	T_{max} @ Time (°F) (sec)	** T_{TS-2} (°F)
TTS-1	118	182 @ 2.5	154	444	1070 @ 2.1	1062	---	Erratic	---
TTS-2	73	101 @ 2.7	88	252	796 @ 2.3	738	1565	Erratic	1449
TTS-3	---	Not Working	---	234	483 @ 2.1	483	2216	Erratic	---
TTS-4	300	634 @ 1.3	419	699	Erratic	934	---	Erratic	---
TTS-5	1229	2227 @ 2.4	1185	263	605 @ 2.3	584	---	Erratic	---
TTS-6	186	313 @ 2.5	268	567	1329 @ 2.3	1305	---	Not Working	---
TTS-7	76	90 @ 1.4	71	530	1104 @ 2.1	1044	---	Not Working	---
TTS-8	193	202 @ 2.5	175	244	610 @ 2.3	520	256	738 @ 6.3	262
TTS-9	348	415 @ 2.3	368	---	Not Working	---	341	989 @ 3.0	351
TTS-10	107	191 @ 3.2	147	416	903 @ 2.1	903	375	929 @ 6.3	388
TTS-11	---	No Hookup	---	307	537 @ 2.1	537	279	712 @ 6.4	281
TTS-12	---	Not Working	---	395	708 @ 2.2	627	478	867 @ 5.0	501
TTS-13	122	361 @ 2.8	205	410	791 @ 2.2	739	516	1024 @ 6.3	530
TTS-14	---	Erratic	1612	651	Erratic	1800	46	54 @ 6.3	48
TTS-15	1909	Erratic	---	556	1257 @ 2.2	1170	---	No Hookup	---
TTS-16	1492	Erratic	2299	296	961 @ 2.4	726	---	Erratic	---
TTS-17	---	No Hookup	---	123	185 @ 2.1	185	120	123 @ 2.7	121
Remarks	* T_{avg} During Period 1.47-1.97 sec **TS-2 @ 2.067 sec Same hardware as Test 1.2-02-YAM-017, throat burnout occurred. Throat Assy S/N-1			* T_{avg} During Period 1.60-2.10 sec **TS-2 @ 2.197 sec All injection stations grooved, 17 high response thermocouples installed (.125 dia). OTPA failed, slight erosion of throat due to off M/R condition. Thermal steady state not achieved. Throat Assy S/N-2			* T_{avg} During Period 2.35-2.65 sec **TS-2 @ 2.678 sec Same hardware configuration as Test 1.2-02-YAM-021. High pressure flex line from oxidizer manifold to exit cone failed during test. Low P_c obtained. Throat Assy S/N-2		

Test Date	2/19/65			2/26/65			3/2/65		
Test Number	1.2-02-YAM-023			1.2-02-YAM-024			1.2-02 YAM-025		
Thermocouple Number	* T_{avg} (°F)	T_{max} @ Time (°F) (sec)	** T_{TS-2} (°F)	* T_{avg} (°F)	T_{max} @ Time (°F) (sec)	** T_{TS-2} (°F)	* T_{avg} (°F)	T_{max} @ Time (°F) (sec)	** T_{TS-2} (°F)
TTS-1	410	486 @ 3.1	439	383	392 @ 3.4	392	481	602 @ 3.6	563
TTS-2	610	849 @ 3.1	798	1104	1138 @ 3.6	1130	798	829 @ 3.5	826
TTS-3	339	419 @ 3.1	394	580	600 @ 3.6	596	687	708 @ 3.7	745
TTS-4	577	688 @ 3.0	677	434	462 @ 3.4	448	585	623 @ 3.6	613
TTS-5	441	513 @ 3.0	489	481	496 @ 3.2	491	611	627 @ 3.4	625
TTS-6	572	784 @ 3.1	714	1026	1149 @ 3.6	1101	1244	1330 @ 3.7	1313
TTS-7	1295	1730 @ 2.9	1730	1578	1686 @ 2.9	1538	1848	1992 @ 2.5	1824
TTS-8	467	523 @ 3.0	515	564	579 @ 3.5	579	693	724 @ 3.6	706
TTS-9	1010	1110 @ 2.8	1106	1151	1179 @ 3.5	1179	---	Erratic	---
TTS-10	601	720 @ 2.9	677	553	589 @ 3.1	559	796	858 @ 3.4	775
TTS-11	441	4[illegible] @ 3.0	467	439	445 @ 3.1	445	504	519 @ 3.6	510
TTS-12	536	[illegible] @ 3.1	600	498	[illegible] @ 3.4	600	800	900 @ 3.6	800
TTS-13	465	487 @ 2.8	481	431	433 @ 3.0	424	495	556 @ 7.8	499
TTS-14	871	1043 @ 3.0	1013	919	932 @ 3.6	922	1048	1071 @ 3.4	1071
TTS-15	---	No Hookup	---	---	Erratic	---	802	870 @ 3.6	850
TTS-16	453	637 @ 3.1	585	572	610 @ 3.5	606	691	731 @ 3.6	717
TTS-17	148	157 @ 3.0	156	149	151 @ 3.2	151	161	163 @ 3.3	162
Remarks	*T_{avg} During Period 2.40 - 2.90 sec **TS-2 @ 2.953 sec Same hardware configuration as Test 1.2-02-YAM-021. Valid test, all test hardware in refireable condition. Good readings from all but one thermocouple. Throat Assy S/N-2			*T_{avg} During Period 3.00 - 3.50 sec **TS-2 @ 3.514 sec Same hardware configuration as Test 1.2-02-YAM-021. Valid test, all test hardware in refireable condition. Throat Assy S/N-2			*T_{avg} During Period 3.00 - 3.50 sec **TS-2 @ 3.506 sec Same hardware configuration as Test 1.2-02-YAM-021. Valid test, all test hardware in refireable condition. Throat Assy S/N-2		

Cumulative Summary of Skin Temperatures, Cooled Convergent and Throat Segment Tests

Figure VII-D-6, Sheet 2 of 3

Test Date	3/9/65			3/15/65			
Test Number	1.2-02-YAM-027			1.2-02-YAM-029			
Thermocouple Number	* T_{avg} (°F)	T_{max} @ Time (°F) (sec)	** T_{FS-2} (°F)	* T_{avg} (°F)	T_{max} @ Time (°F) (sec)	** T_{FS-2} (°F)	
TTS-1	492	546 @ 3.6	529	476	563 @ 3.1	544	
TTS-2	1014	1377 @ 3.7	1040	802	988 @ 3.2	922	
TTS-3	671	731 @ 3.7	715	498	646 @ 3.2	591	
TTS-4	611	654 @ 3.4	617	---	No Readout	---	
TTS-5	699	730 @ 3.5	730	---	Erratic	---	
TTS-6	1263	1348 @ 3.7	1311	999	1149 @ 3.2	1035	
TTS-7	2001	2125 @ 3.4	2035	2041	2105 @ 2.9	1834	
TTS-8	690	721 @ 3.5	719	596	646 @ 3.1	631	
TTS-9	613	1418 @ 2.2	590	---	Erratic	---	
TTS-10	634	725 @ 2.7	622	583	631 @ 2.8	921	
TTS-11	631	647 @ 3.2	625	547	593 @ 3.1	573	
TTS-12	580	613 @ 3.7	601	443	533 @ 3.2	515	
TTS-13	468	532 @ 7.6	450	447	468 @ 3.0	468	
TTS-14	990	1019 @ 3.5	1018	949	954 @ 3.0	932	
TTS-15	1124	1181 @ 3.4	1131	672	736 @ 3.2	727	
TTS-16	638	659 @ 3.7	646	---	Erratic	---	
TTS-17	158	159 @ 3.2	159	155	160 @ 3.0	159	
Remarks	*T_{avg} During Period 3.02 - 3.52 sec **FS-2 @ 3.522 sec Same hardware configuration as test 1.2-02-YAM-021. Valid test, all test hardware in refirable condition. Throat Assy S/N-2			*T_{avg} During Period 2.70 - 3.00 sec ** FS-2 @ 3.008 sec Same hardware configuration as test 1.2-02-YAM-021. Valid test, all test hardware in refirable condition. Throat Assy S/N-2			

Test Date			4/14/65			5/19/65		
Test Number			1.2-02-YAM-033			1.2-02-YAM-036		
Coolant Feed Channel No.	Coolant Injection Station No.	Thermocouple Number	* T_{avg} (°F)	T_{max} @ Time (°F) (sec)	** T_{FS-2} (°F)	* T_{avg} (°F)	T_{max} @ Time (°F) (sec)	** T_{FS-2} (°F)
1	1,2	TTS-1	699	790 @ 3.05	460	1475	1570 @ 2.75	1537
1	3	TTS-2	933	1040 @ 3.08	630	1660	1666 @ 2.41	1651
2	4	TTS-3	535	580 @ 3.11	385	1396	2310 @ 2.81	1471
3	5	TTS-4	685	710 @ 3.30	682	895	1105 @ 2.88	943
4	6	TTS-5	428	460 @ 3.17	360	585	604 @ 2.77	594
5	7	TTS-6	1191	1360 @ 3.10	760	1238	1250 @ 2.73	1229
6	8	TTS-7	1089	1160 @ 3.13	860	2308	Erratic	-
7	9	TTS-8	660	790 @ 3.15	407	1004	1080 @ 2.82	1025
8	10	TTS-9	1142	1170 @ 2.92	1105	1595	1666 @ 2.72	1645
9	11	TTS-10	617	680 @ 3.05	490	630	705 @ 2.82	643
10	12	TTS-11	453	500 @ 3.03	362	600	Erratic	797
11	13	TTS-12	475	510 @ 3.08	404	-	Erratic	-
12	14	TTS-13	1071	Erratic	1053			
13	15	TTS-14	945	1010 @ 3.08	846			
14	16	TTS-15	1314	Erratic	652			
15	17	TTS-16	1870	Erratic	1480			
16	18	TTS-17	167	250 @ 2.90	145			
			*T_{avg} During Period 2.920 to 3.420 sec **FS-2 @ 3.524			*T_{avg} During Period 2.200 to 2.500 sec **FS-2 @ 2.586 sec		

Cumulative Summary of Skin Temperatures, Cooled Convergent and Throat Segment Tests

Figure VII-D-6, Sheet 3 of 3

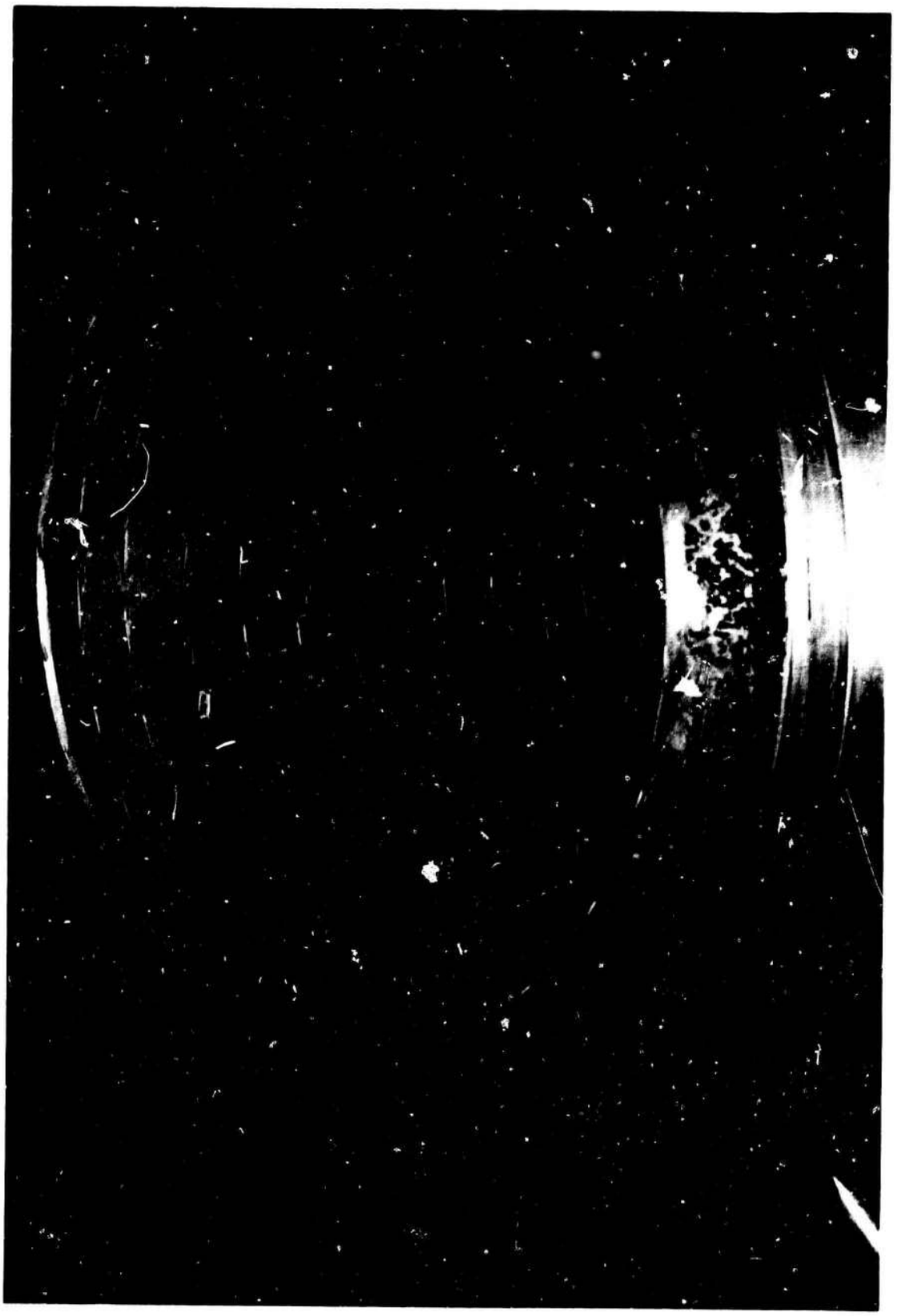

Cooled Throat, Posttest 1.2-02-YAM-012

Figure VII-D-7

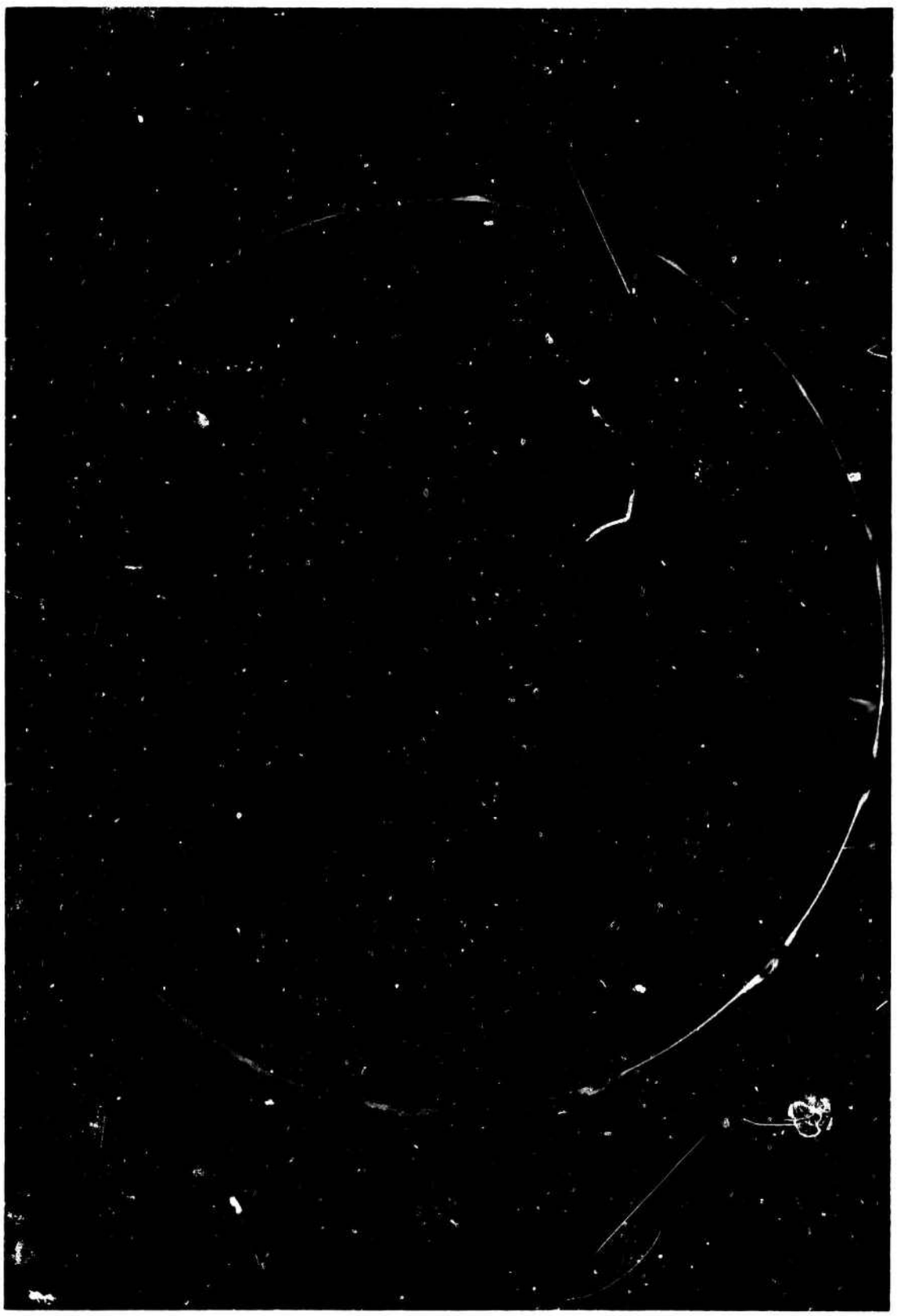

Cooled Throat Segment and Ablative Exit Cover, Posttest 1.2-02-YAM-012

Figure VII-D-8

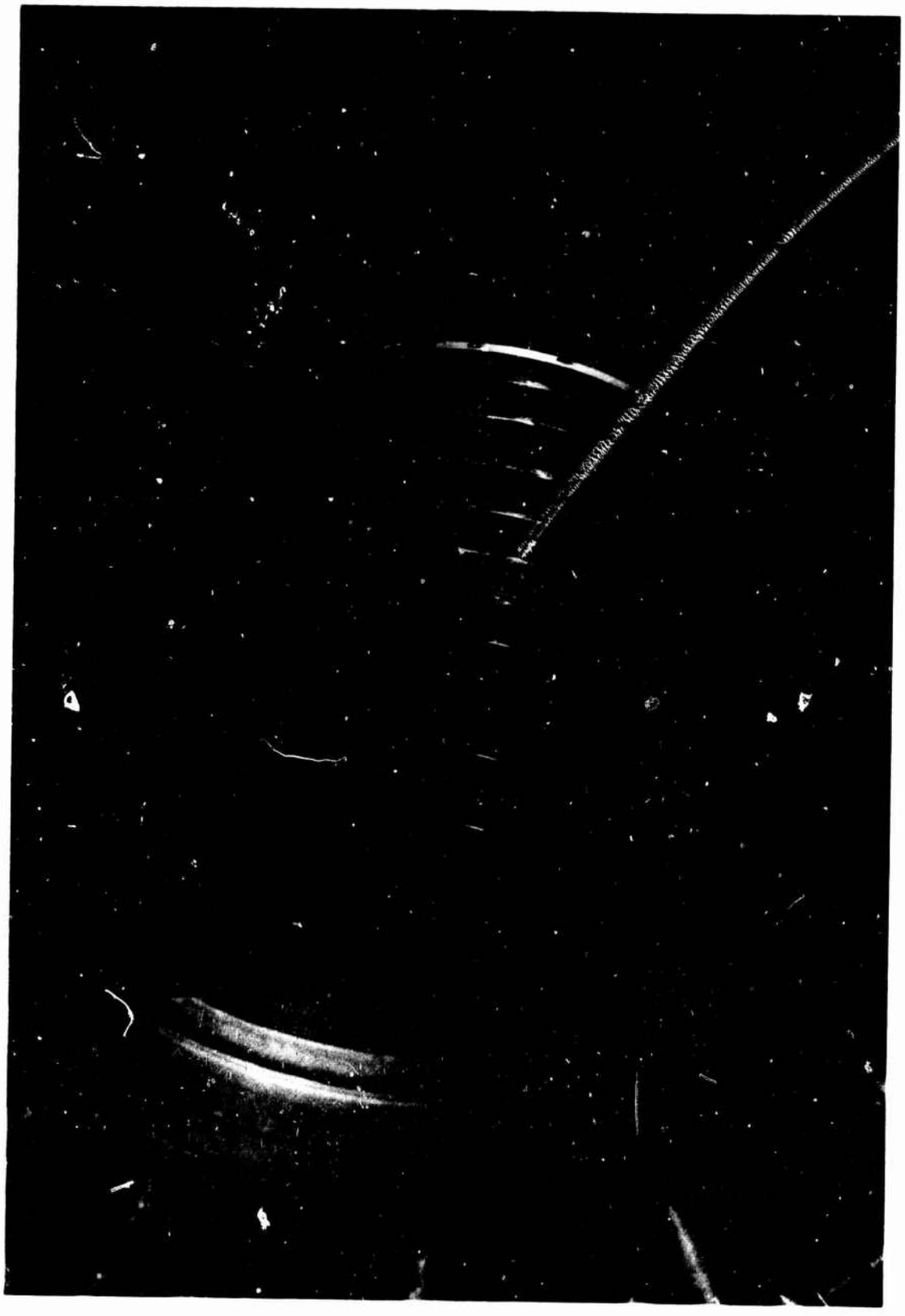

Grooved Cooled Convergent Section, Pretest 1.2-02-YAM-020

Figure VII-D-9

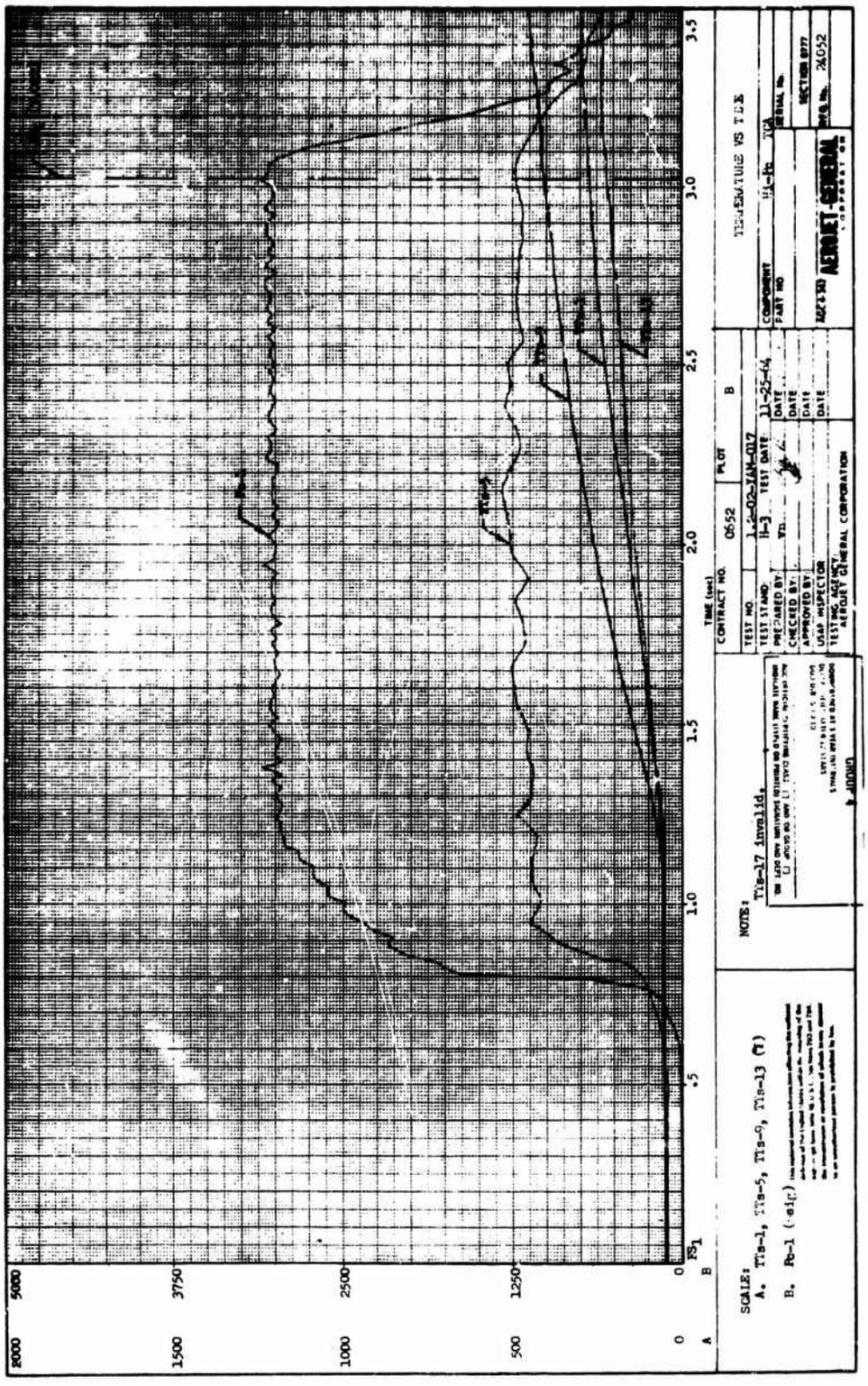

Temperature Data, Test 1.2-02-YAM-017, Showing Response of Old and New Thermocouple Design (u)

Figure VII-D-10

Cooled Throat, Posttest 1.2-02-YAM-020

Figure VII-D-11

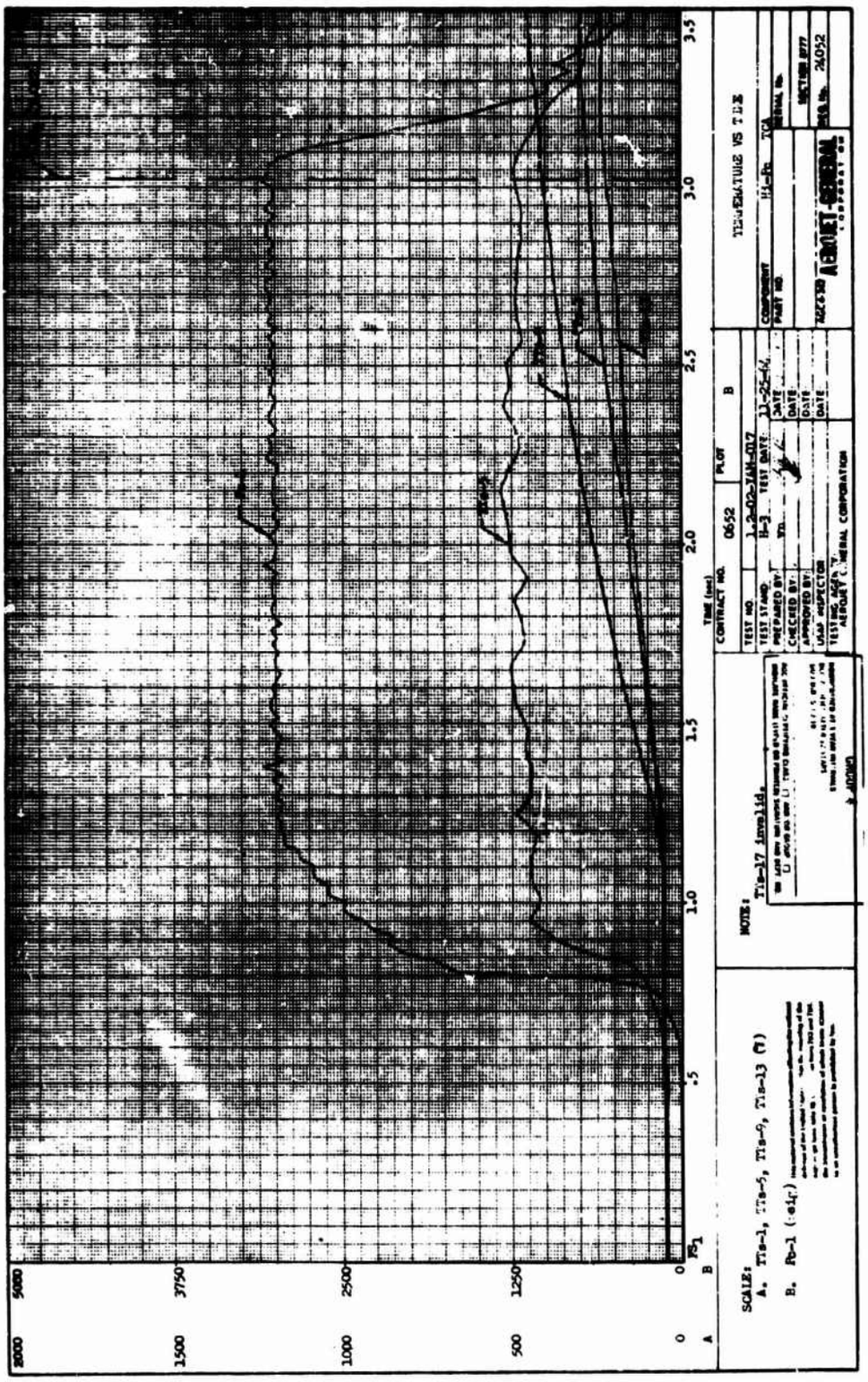

Temperature Data, Test 1.2-02-YAM-017, Showing Response of Old and New Thermocouple Design (u)

Figure VII-D-10

Close-up of Cooled Throat, Posttest 1.2-02-YAM-020

Figure VII-D-12

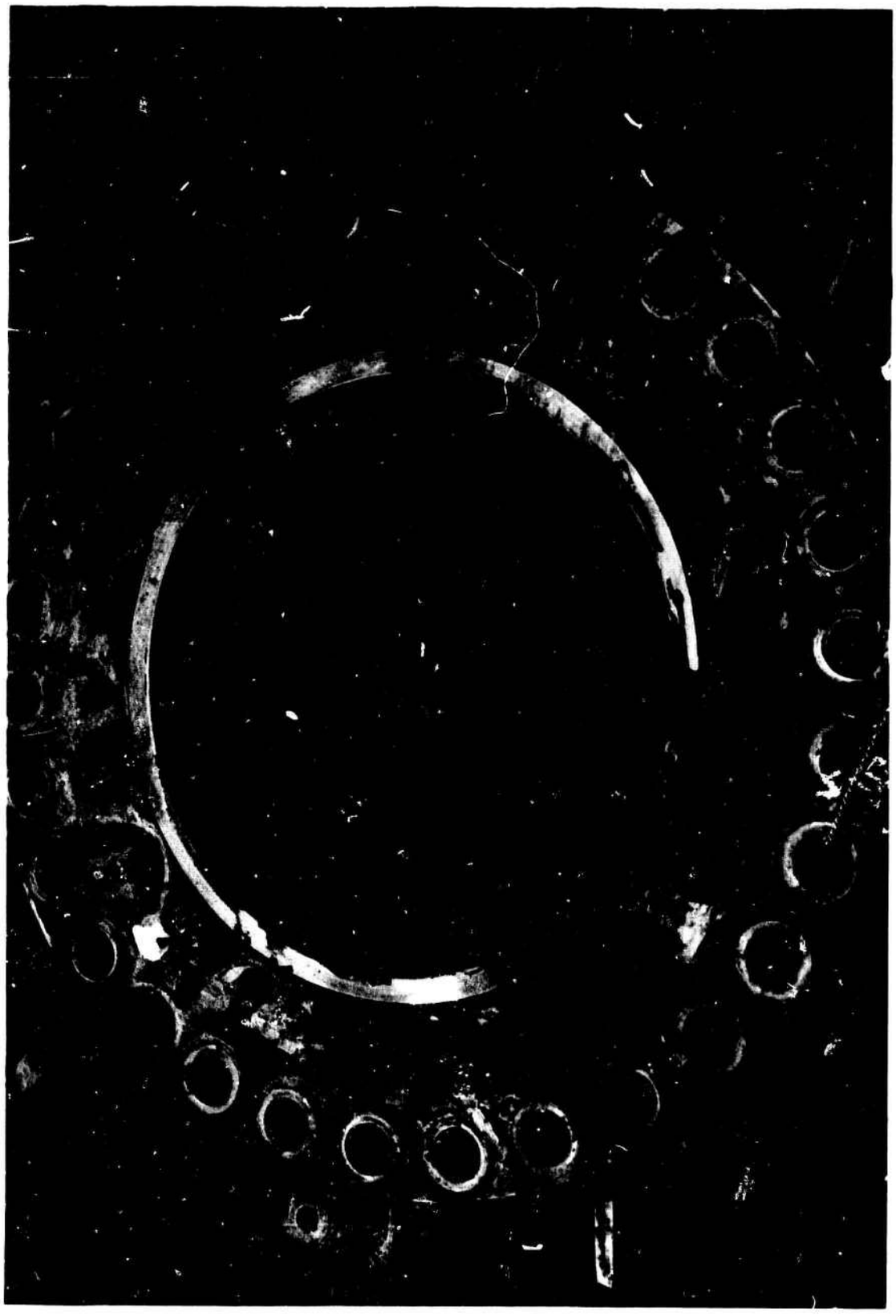

Aft View, Cooled Throat, Posttest 1.2-02-YAM-020

Figure VII-D-13

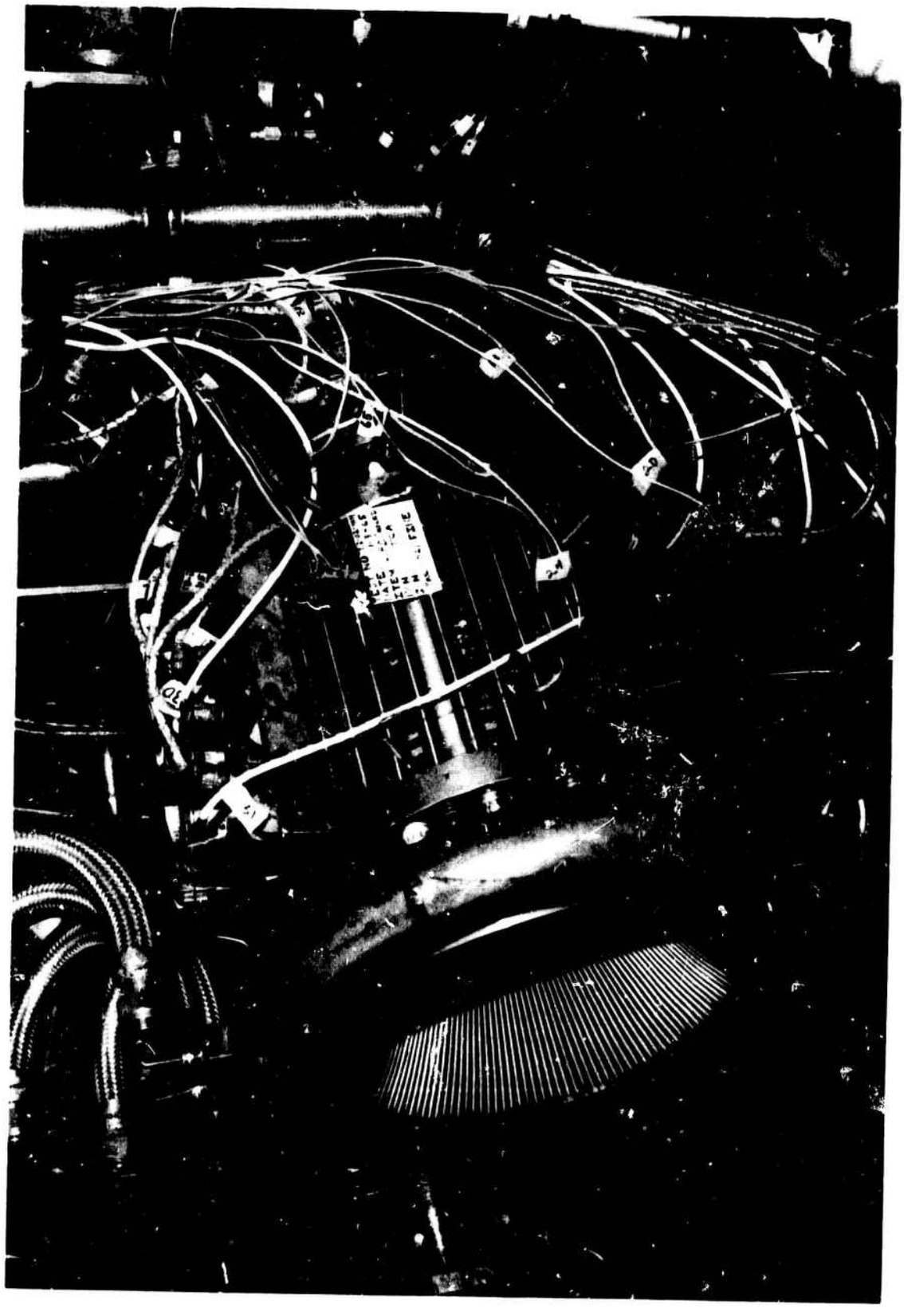

Cooled Throat and Regeneratively Cooled Sea-Level Expansion Nozzle,
Pretest 1.2-02-YAM-021

Figure VII-D-14

Ruptured Flexible Hose, Posttest 1.2-02-YAM-021

Figure VII-D-15

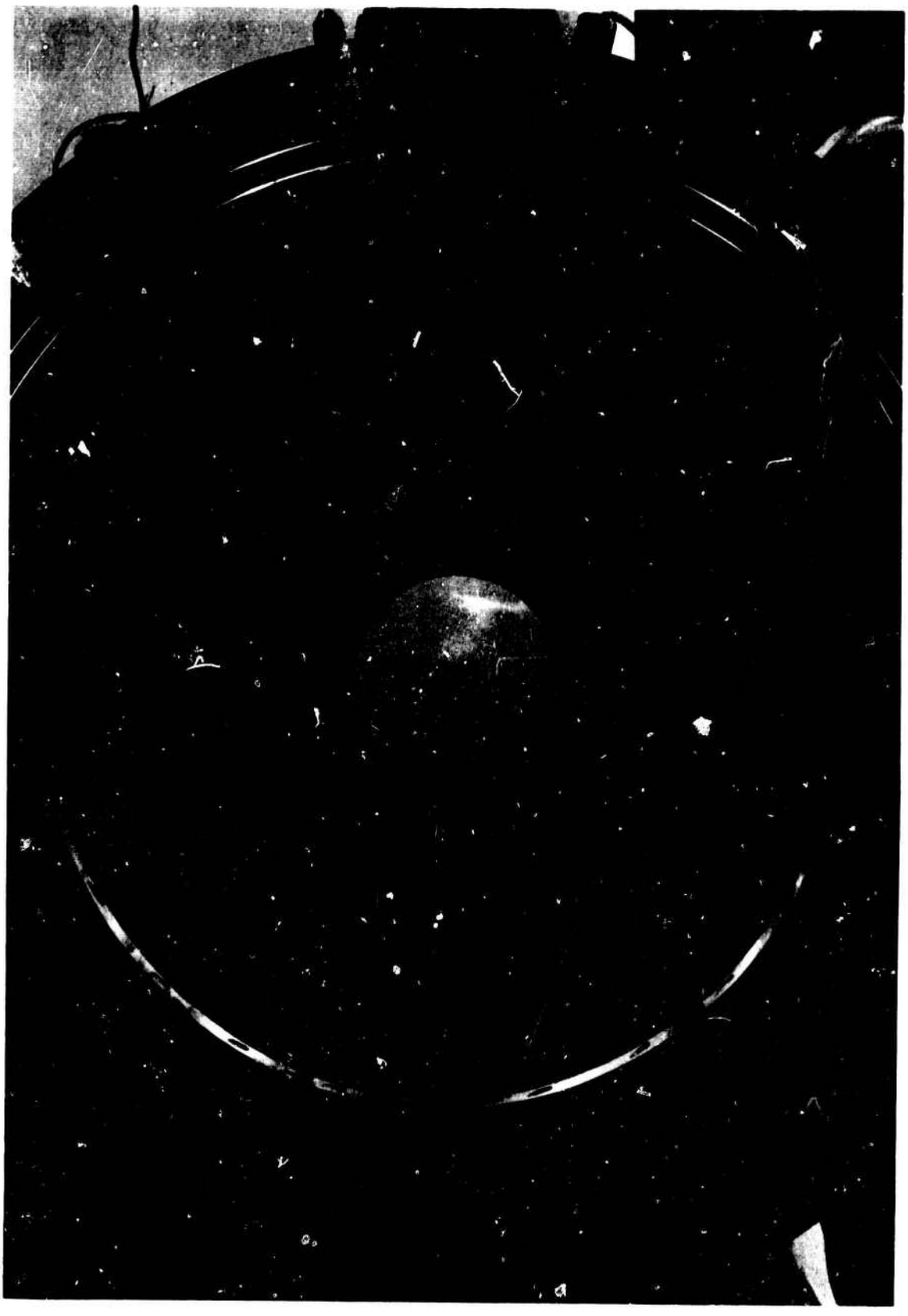

Front View, Cooled Throat, Posttest 1.2-02-YAM-021

Figure VII-D-16

Aft View, Cooled Throat, Fosttest 1.2-02-YAM-021

Figure VII-D-17

Front View, Cooled Throat after Nine Tests

Figure VII-D-18

Oxidizer Regeneratively Cooled Expansion Nozzle after Nine Tests

Figure VII-D-19

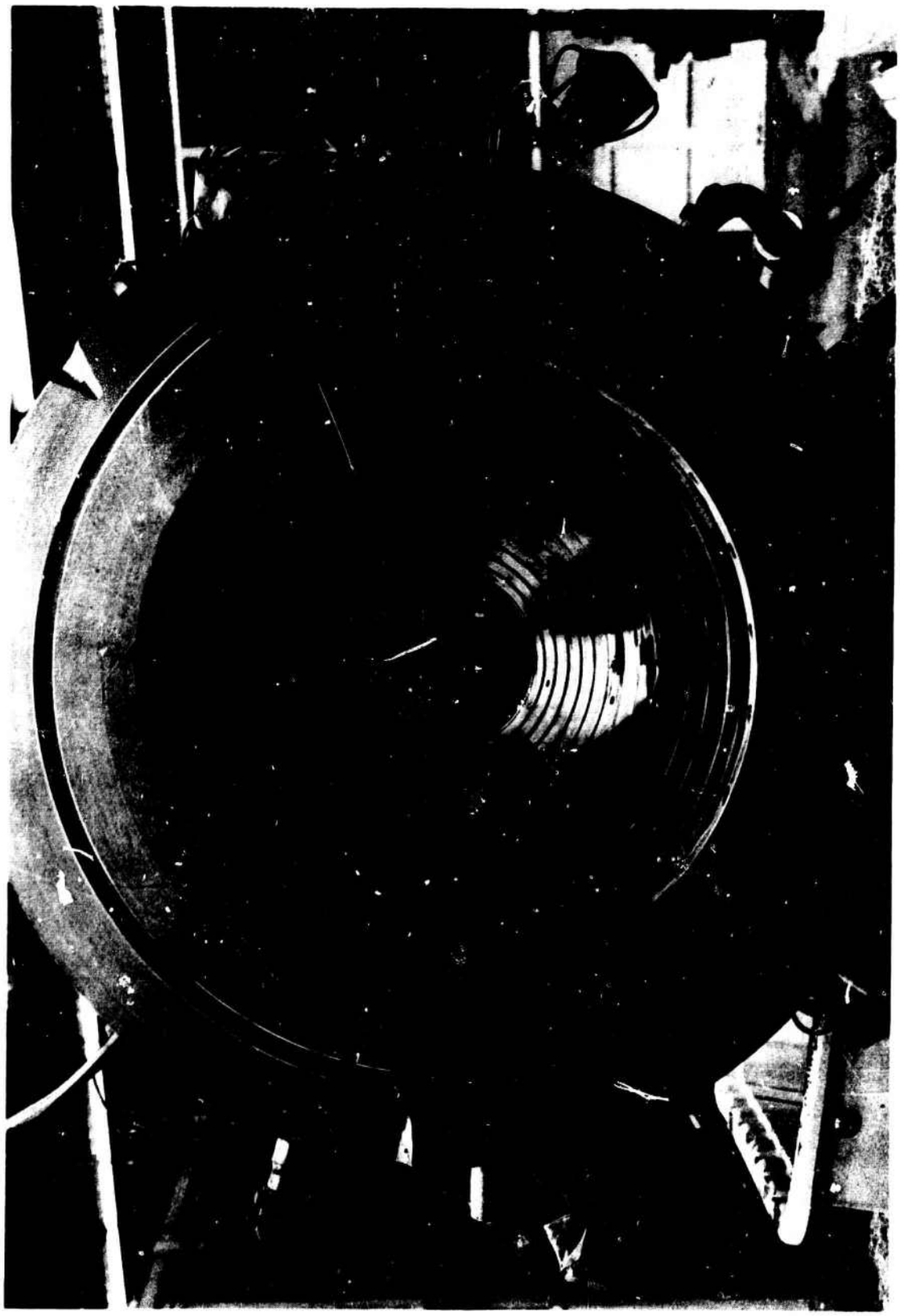

Front View, Cooled Throat, Posttest 1.2-02-YAM-033

Figure VII-D-20

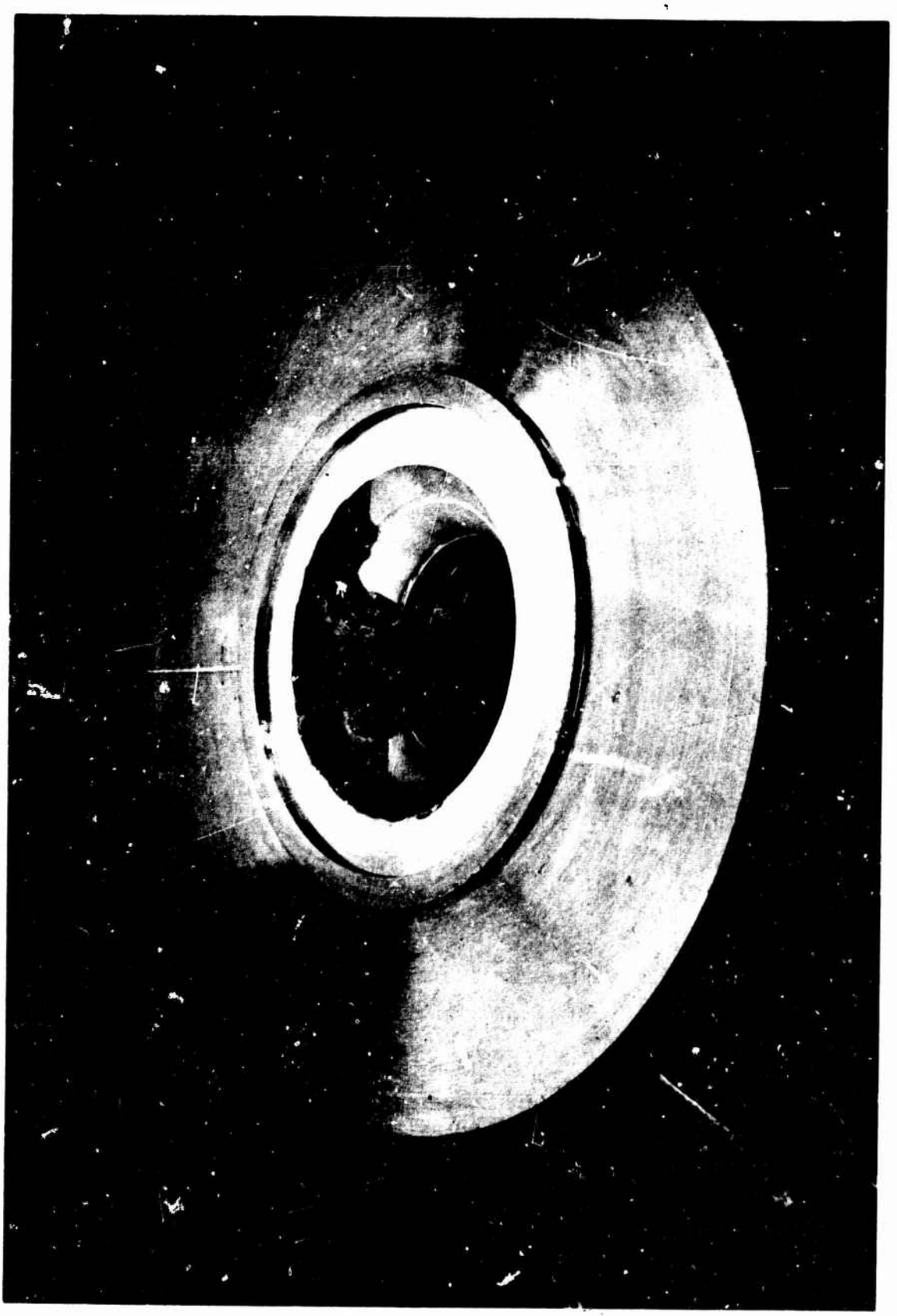

Aft View, Damaged Cooled Throat, Posttest 1.2-02-YAM-033

Figure VII-D-21

Close-up of Damaged Throat Segment, Posttest 1.2-02-YAM-033

Figure VII-D-22

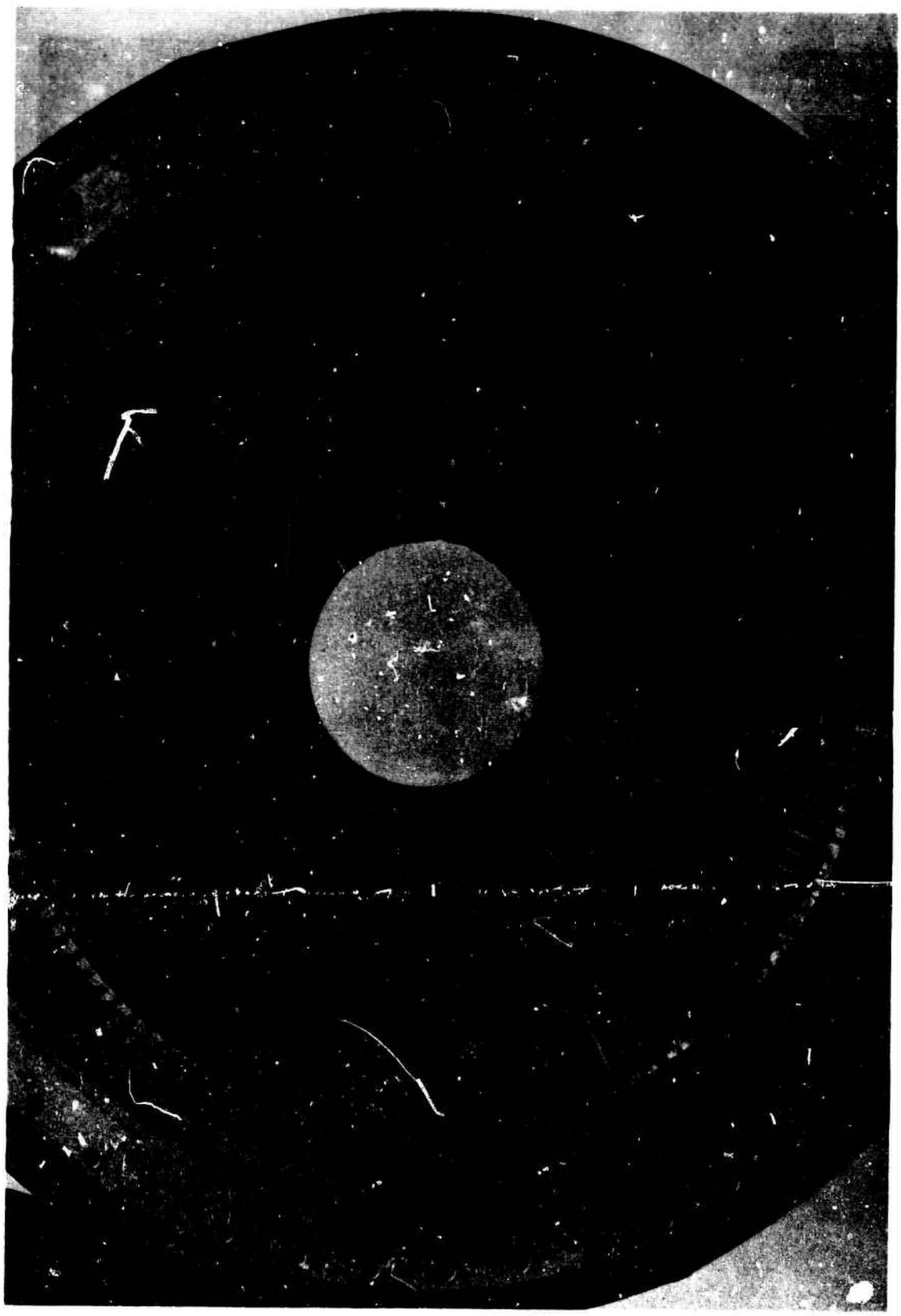

Damaged Oxidizer Regeneratively Cooled Sea-Level Expansion Nozzle,
Posttest 1.2-02-YAM-033

Figure VII-D-23

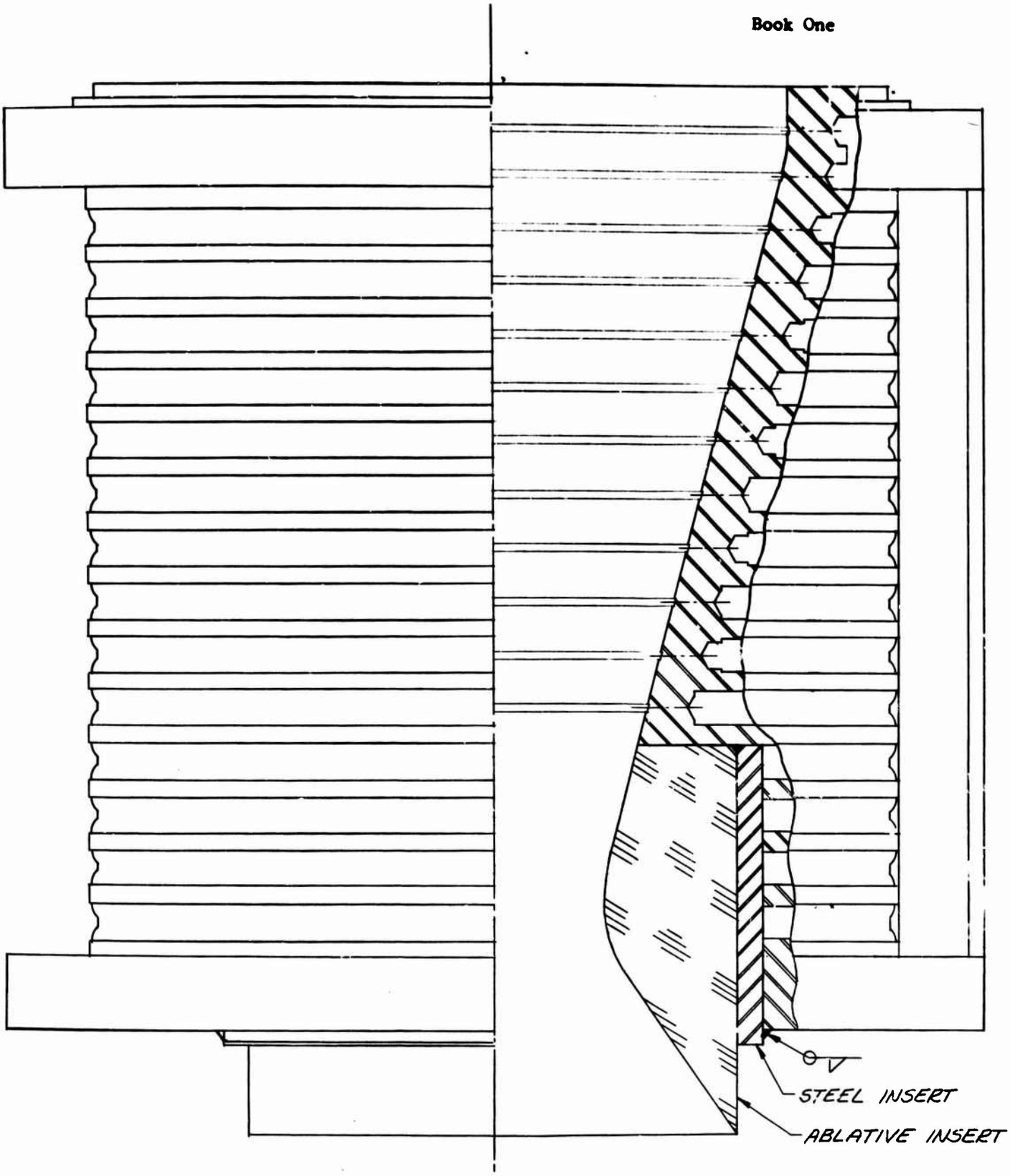

Modification of Cooled Convergent and Throat Segment to Incorporate Ablative Throat

Figure VII-D-24

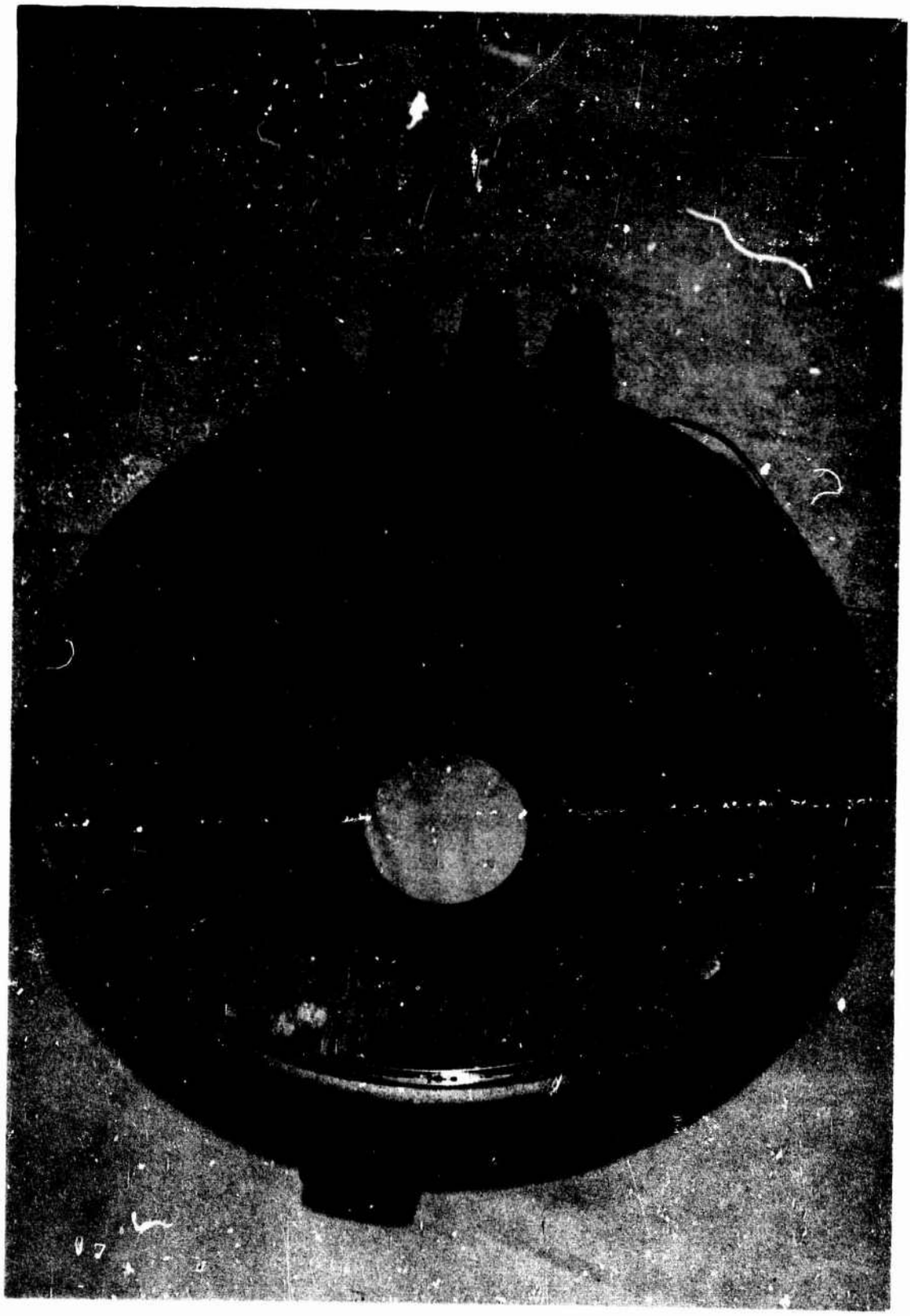

Modification of Regeneratively Cooled Exit Nozzle to Uncooled Nozzle Using Ablative Insert

Figure VII-D-25

Damaged Cooled Throat, Posttest 1.2-02-YAM-036

Figure VII-D-26

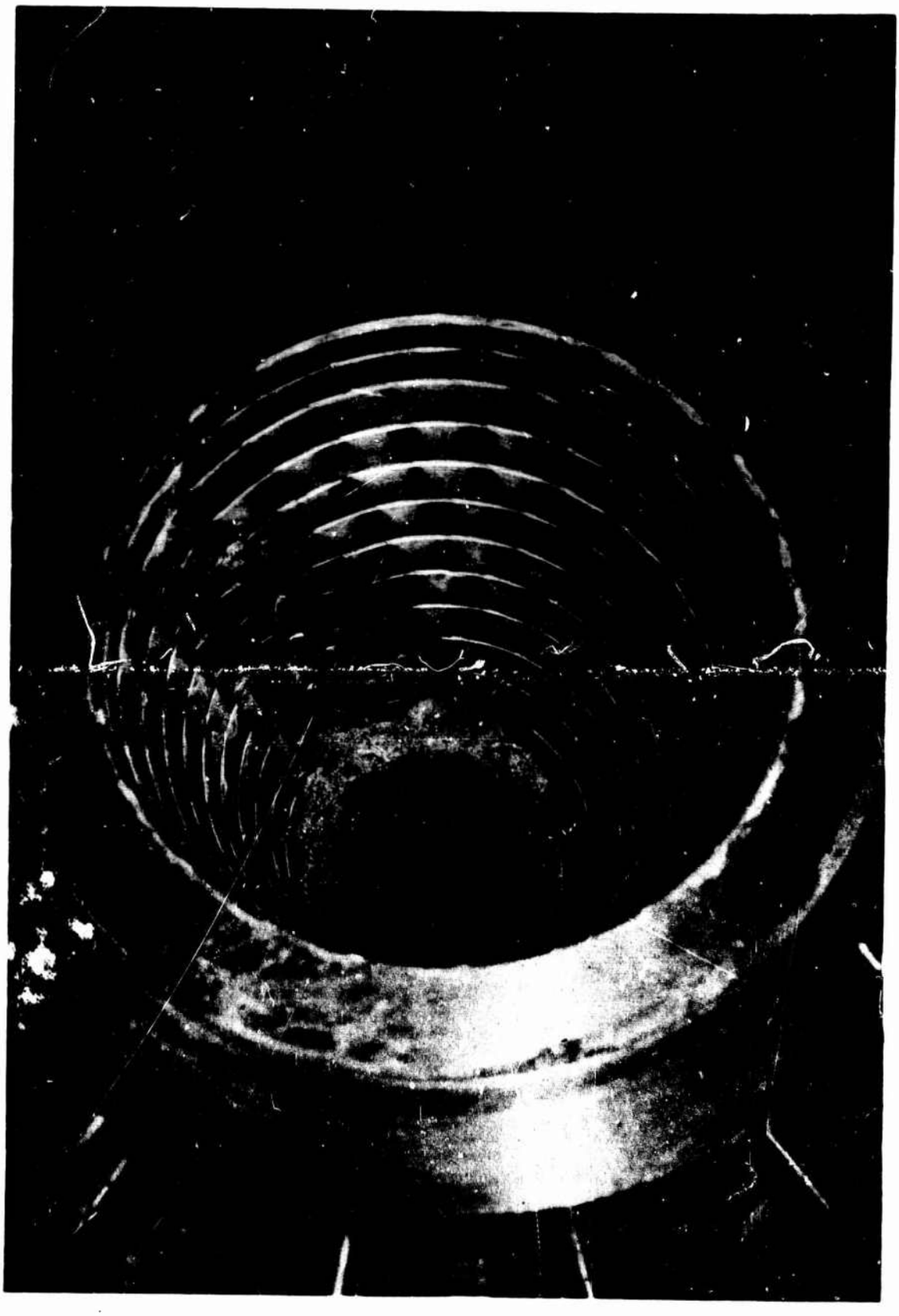

Close-up of Damaged Cooled Throat, Posttest 1.2-02-YAM-036

Figure VII-D-27

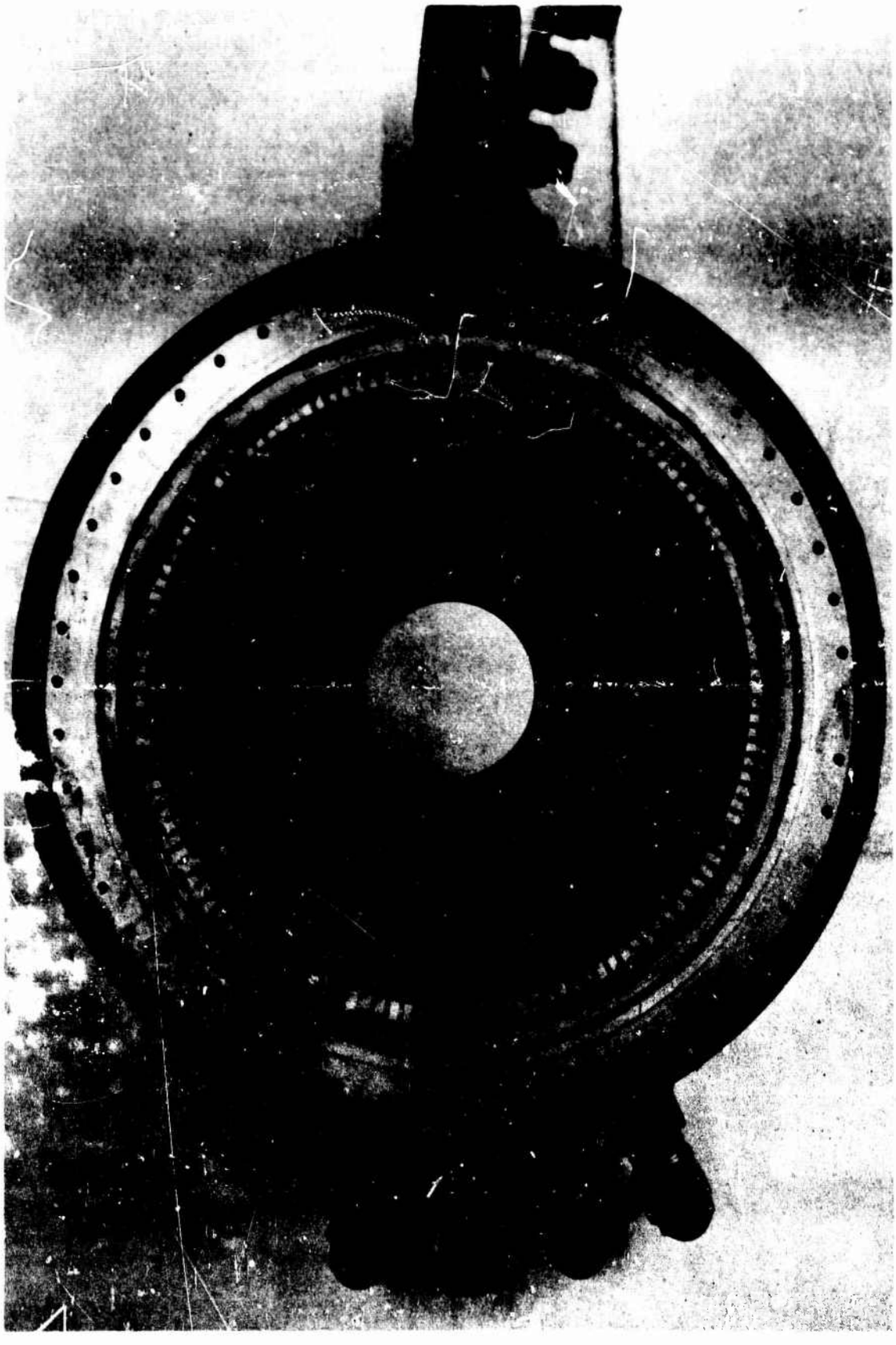

Oxidizer Regeneratively Cooled Expansion Nozzle

Figure VII-E-1

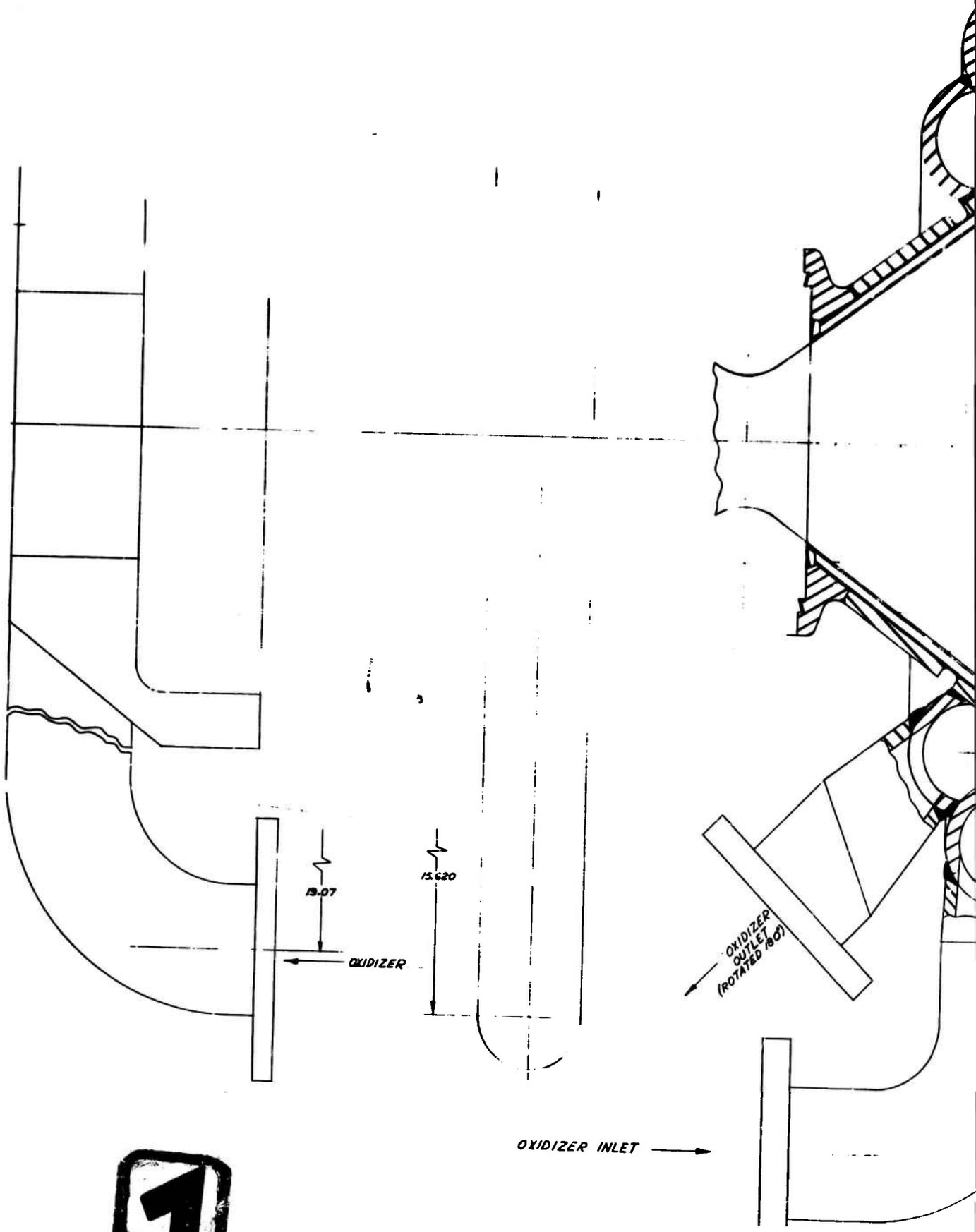
13.07
13.620
OXIDIZER
OXIDIZER OUTLET (ROTATED 180°)
OXIDIZER INLET

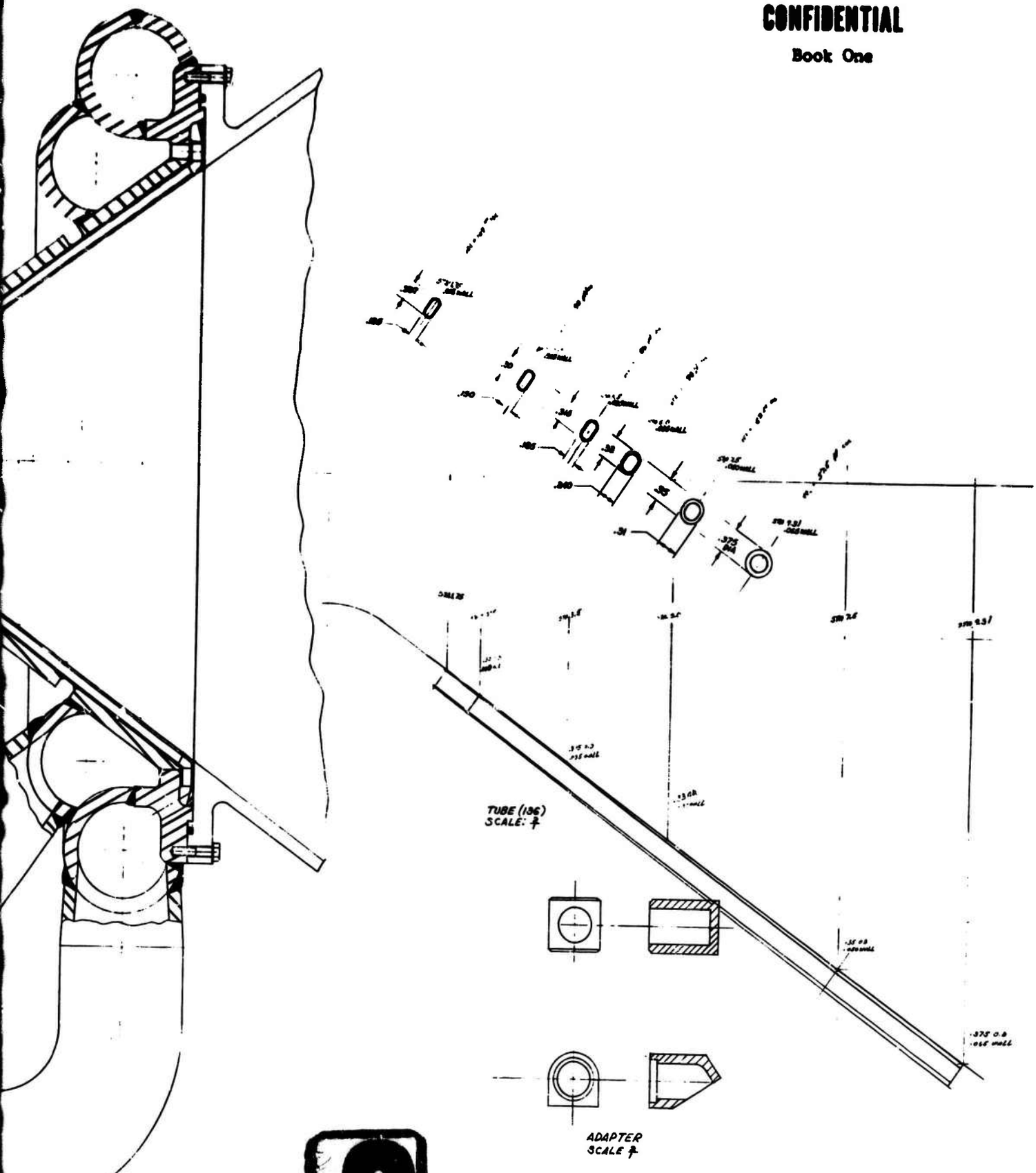

Cooled Expansion Nozzle Design (u)

Figure VII-E-2

NOTE: 1. P_c = 3000 psia
2. MR = 2.0

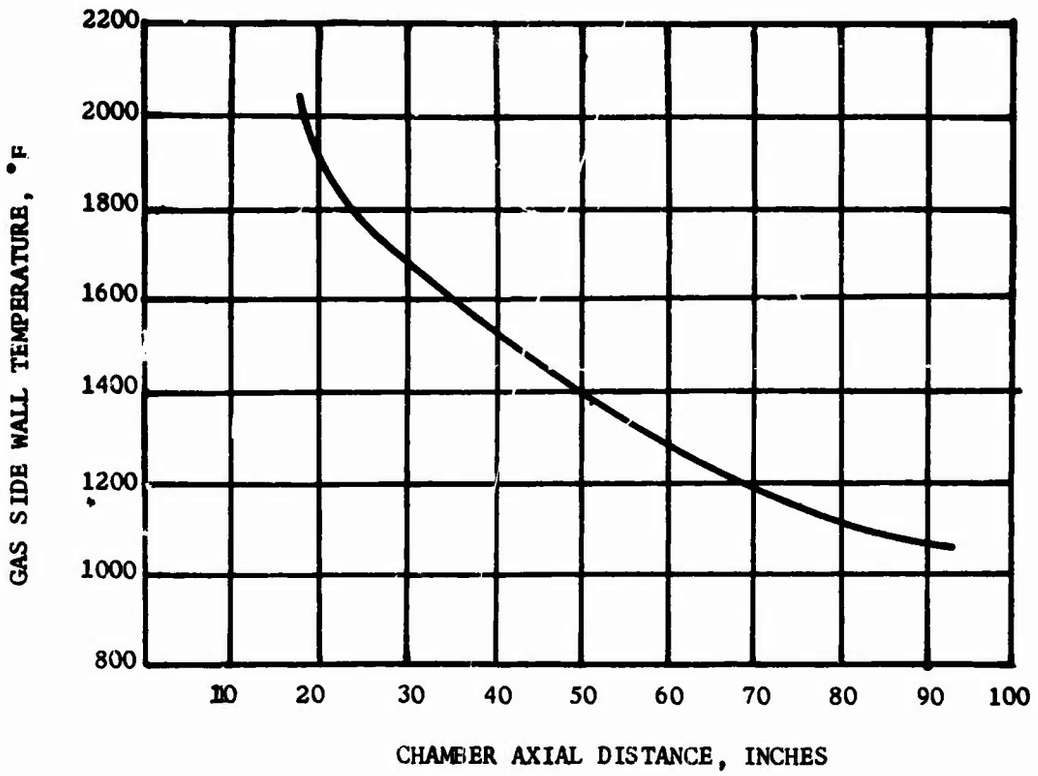

Gas-Side Wall Temperature vs Chamber Distance, Oxidizer Regeneratively Cooled Sea-Level Expansion Nozzle

Figure VII-E-3

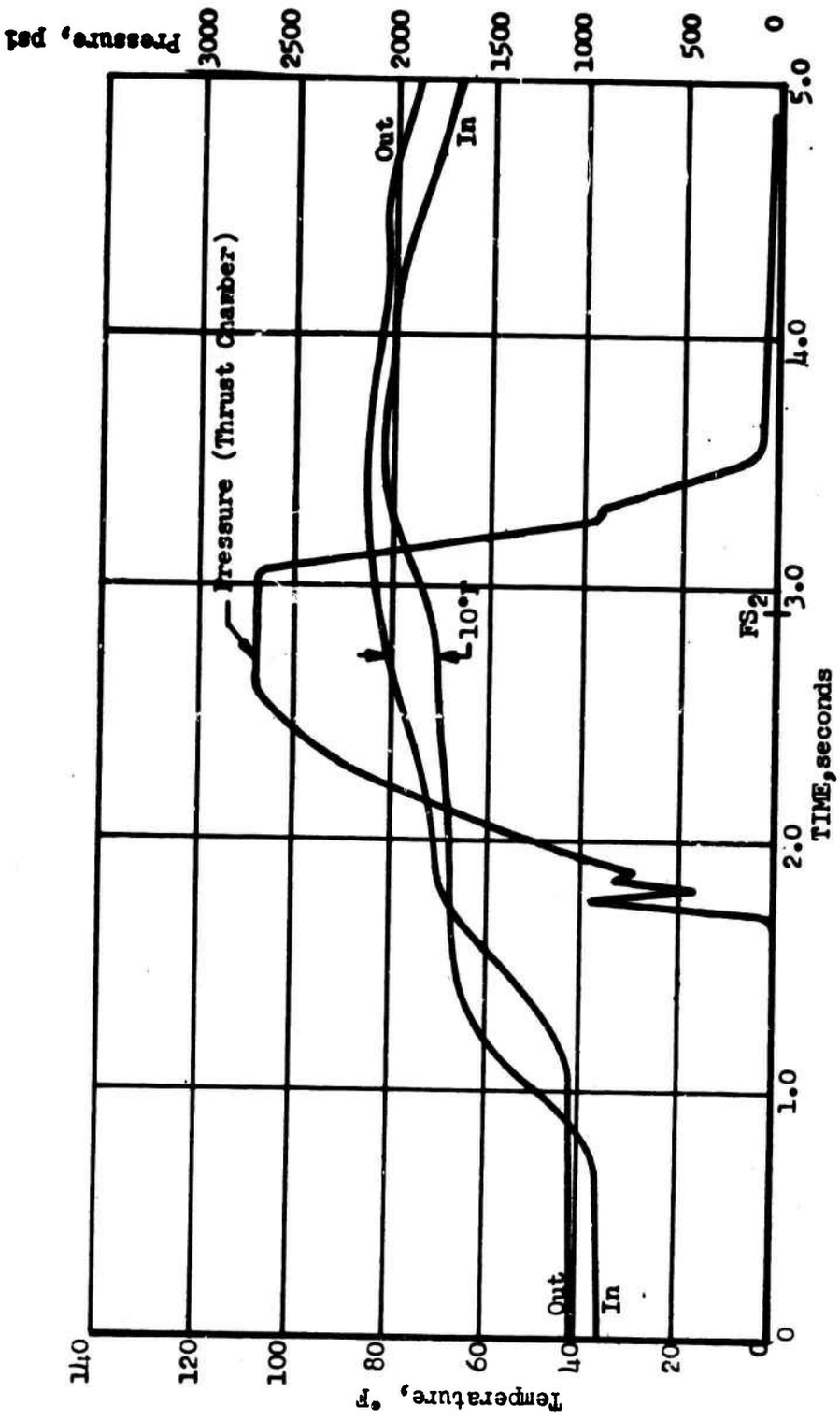

Plot of Exit Cone Coolant Inlet and Outlet Temperature and Thrust Chamber Plenum Pressure vs Time, Test 1.2-02-YAM-023

Figure VII-E-4

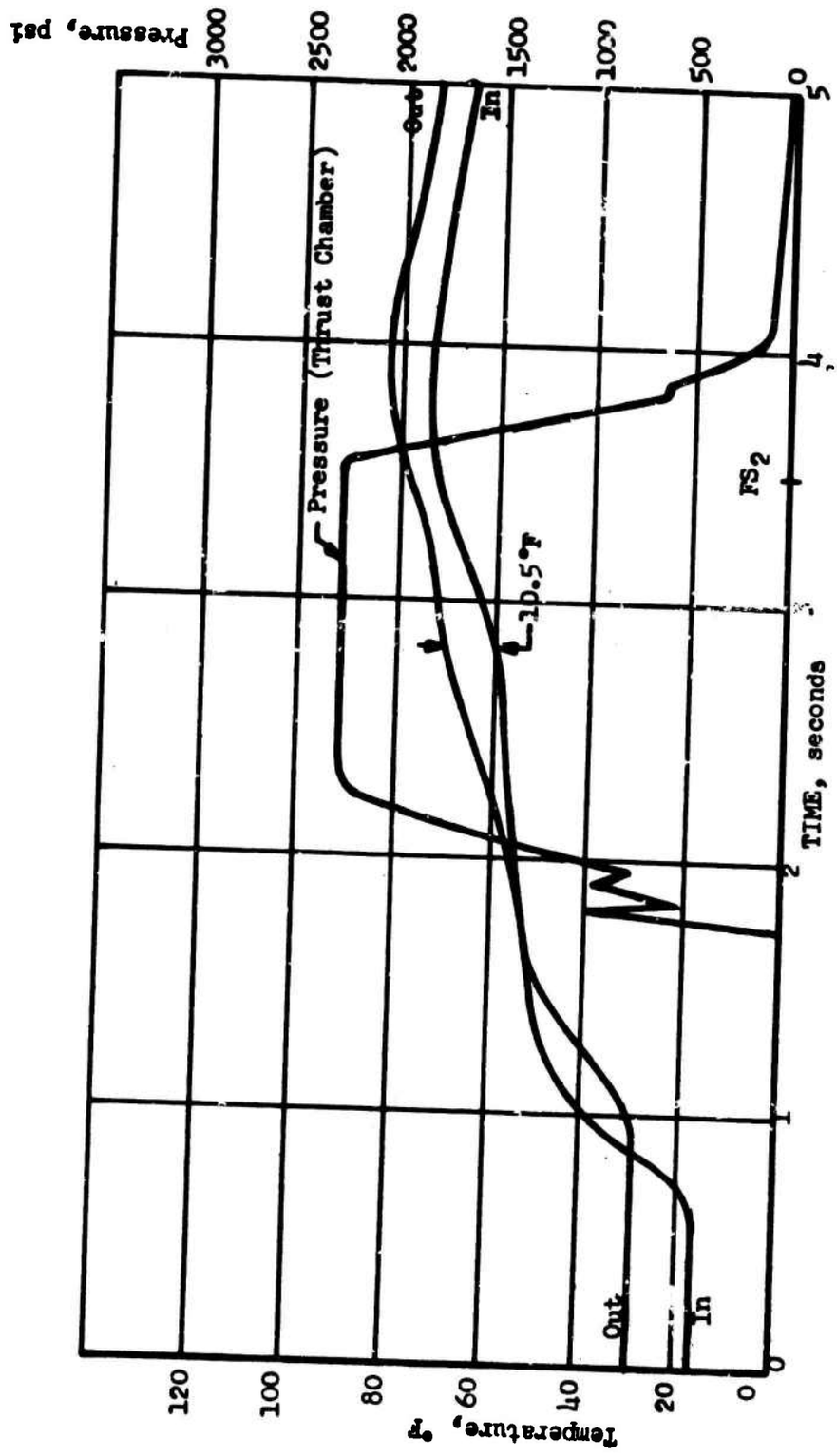

Plot of Exit Cone Coolant Inlet and Outlet Temperature and Thrust Chamber Plenum Pressure vs Time, Test 1.2-02-YAM-024

Figure VII-E-5

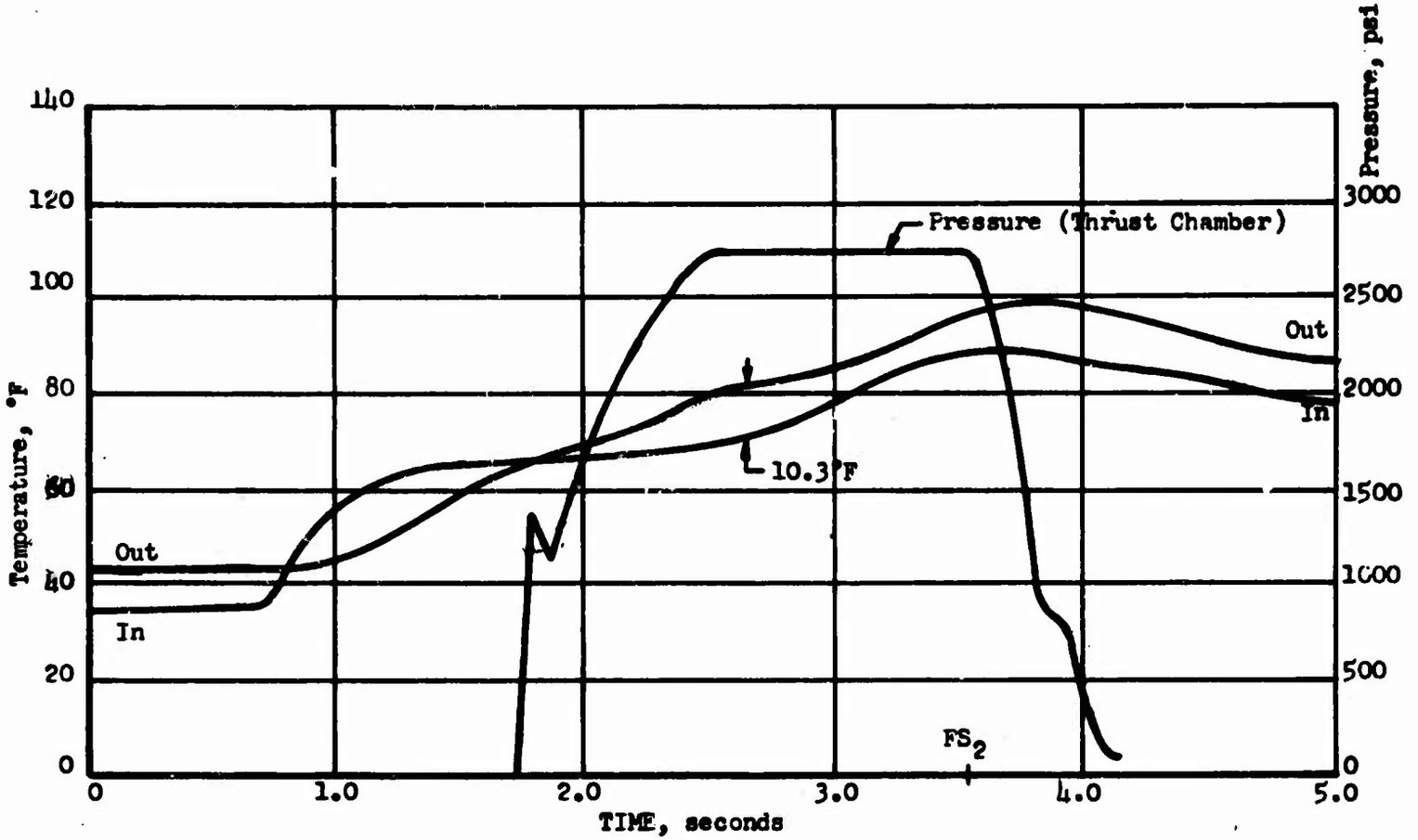

Figure VII-E-6

Plot of Exit Cone Coolant Inlet and Outlet Temperature and Thrust Chamber Plenum Pressure vs Time, Test 1.2-02-YAM-025

Book One

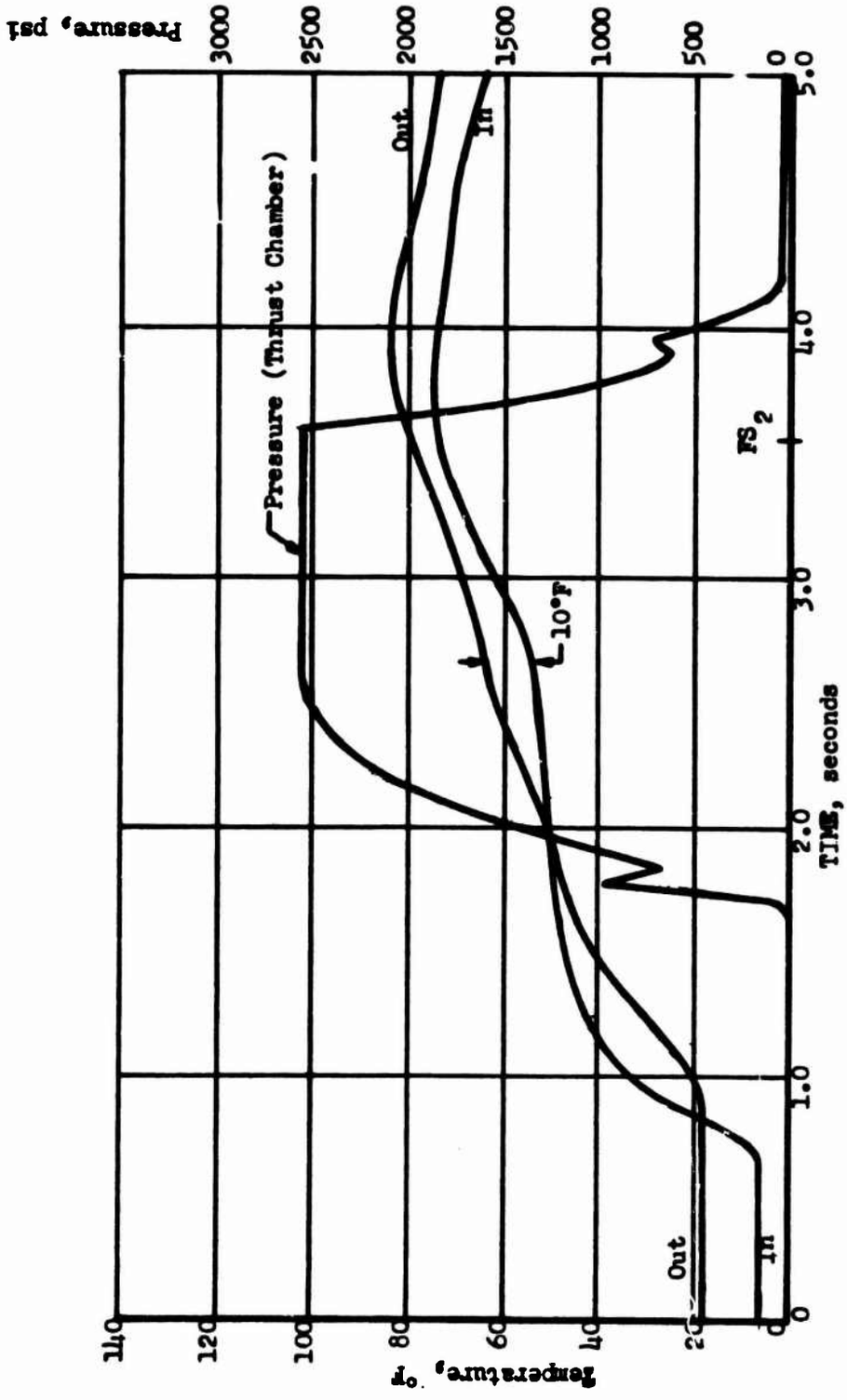

Plot of Exit Cone Coolant Inlet and Outlet Temperature and Thrust Chamber Plenum Pressure vs Time, Test 1.2-02-YAM-027

Figure VII-E-7

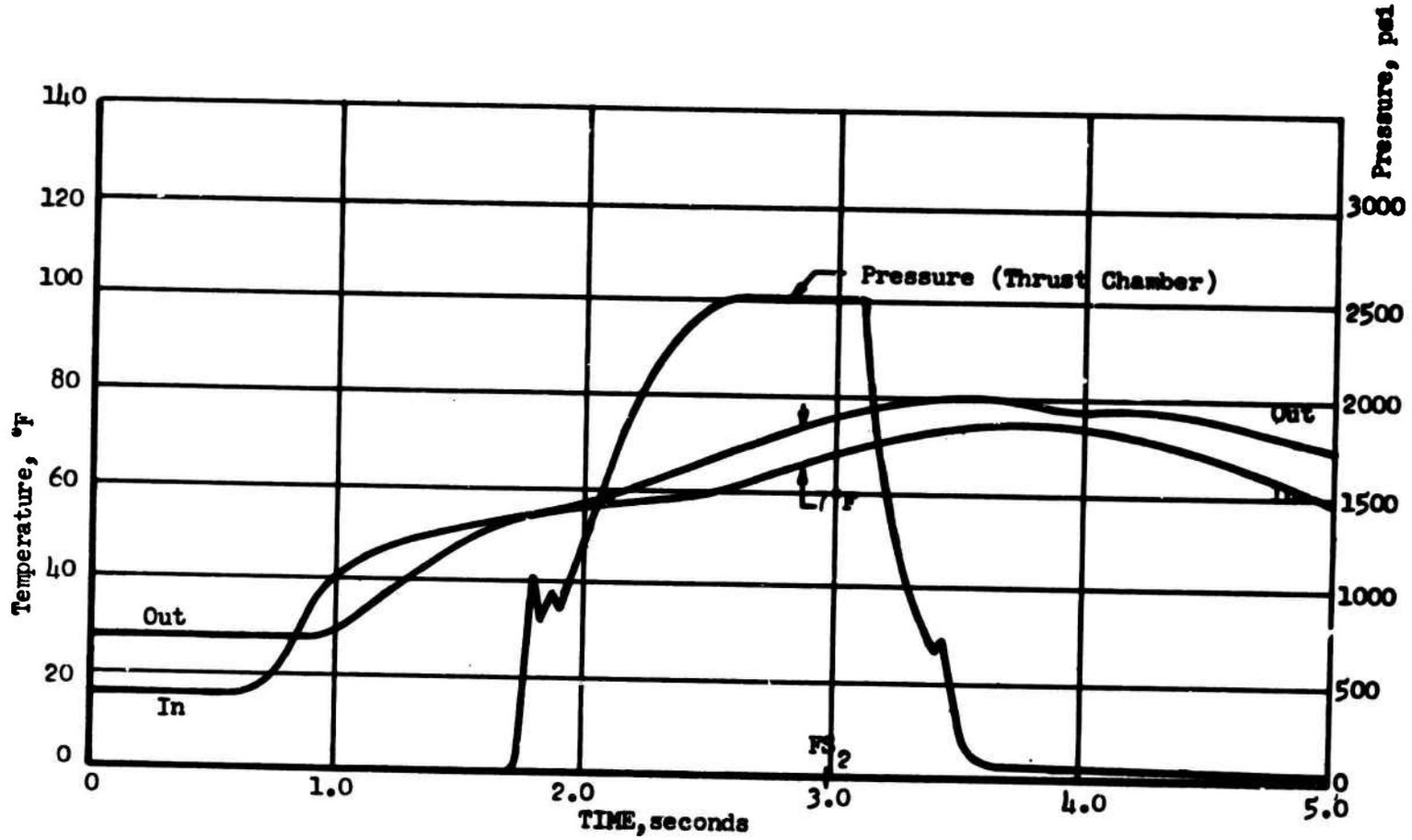

Figure VII-E-8

Plot of Exit Cone Coolant Inlet and Outlet Temperature and Thrust Chamber Plenum Pressure vs Time, Test 1.2-02-YAM-029

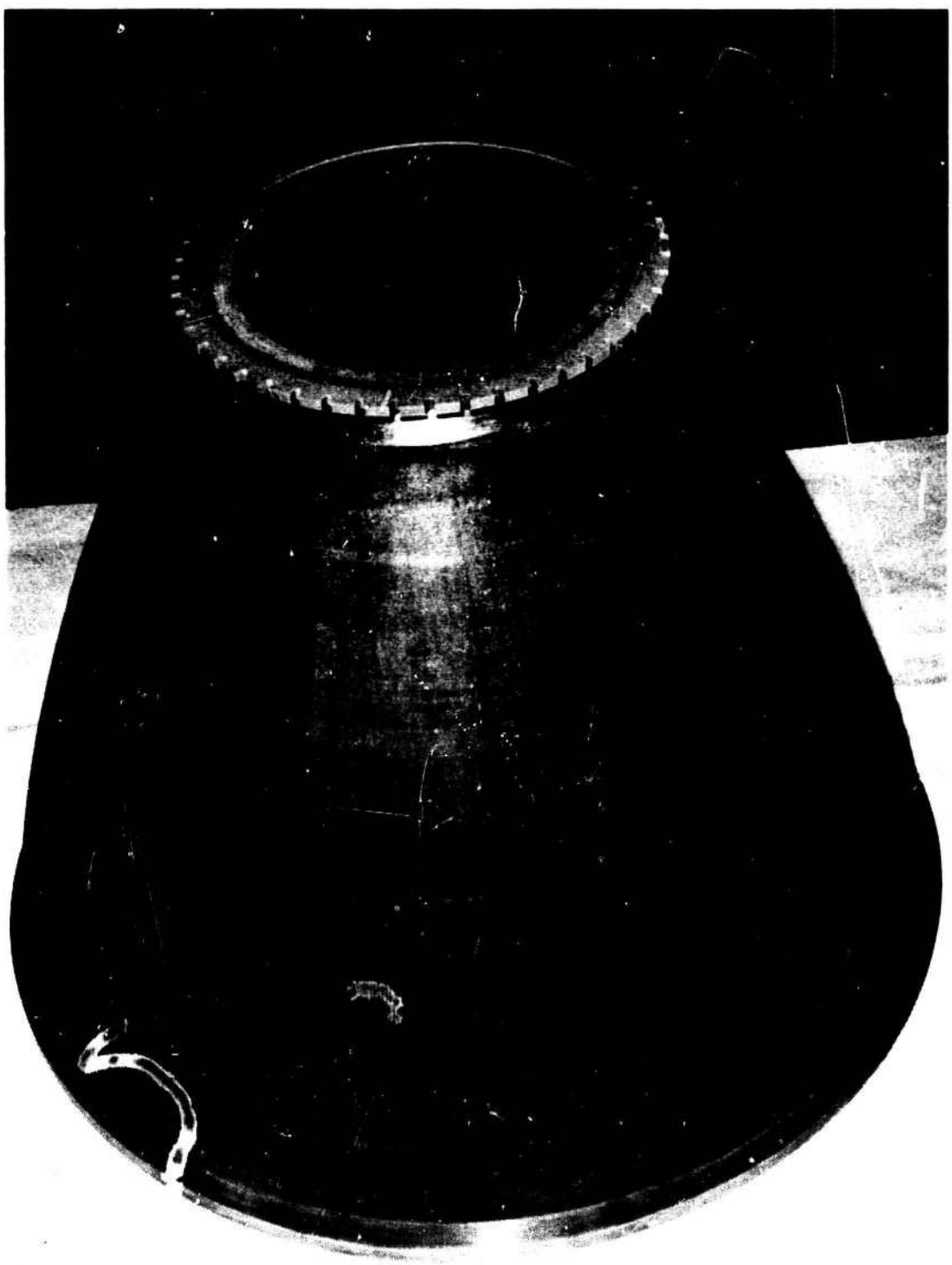

4-64SP 1931

Ablative Nozzle Extension

Figure VII-F-1

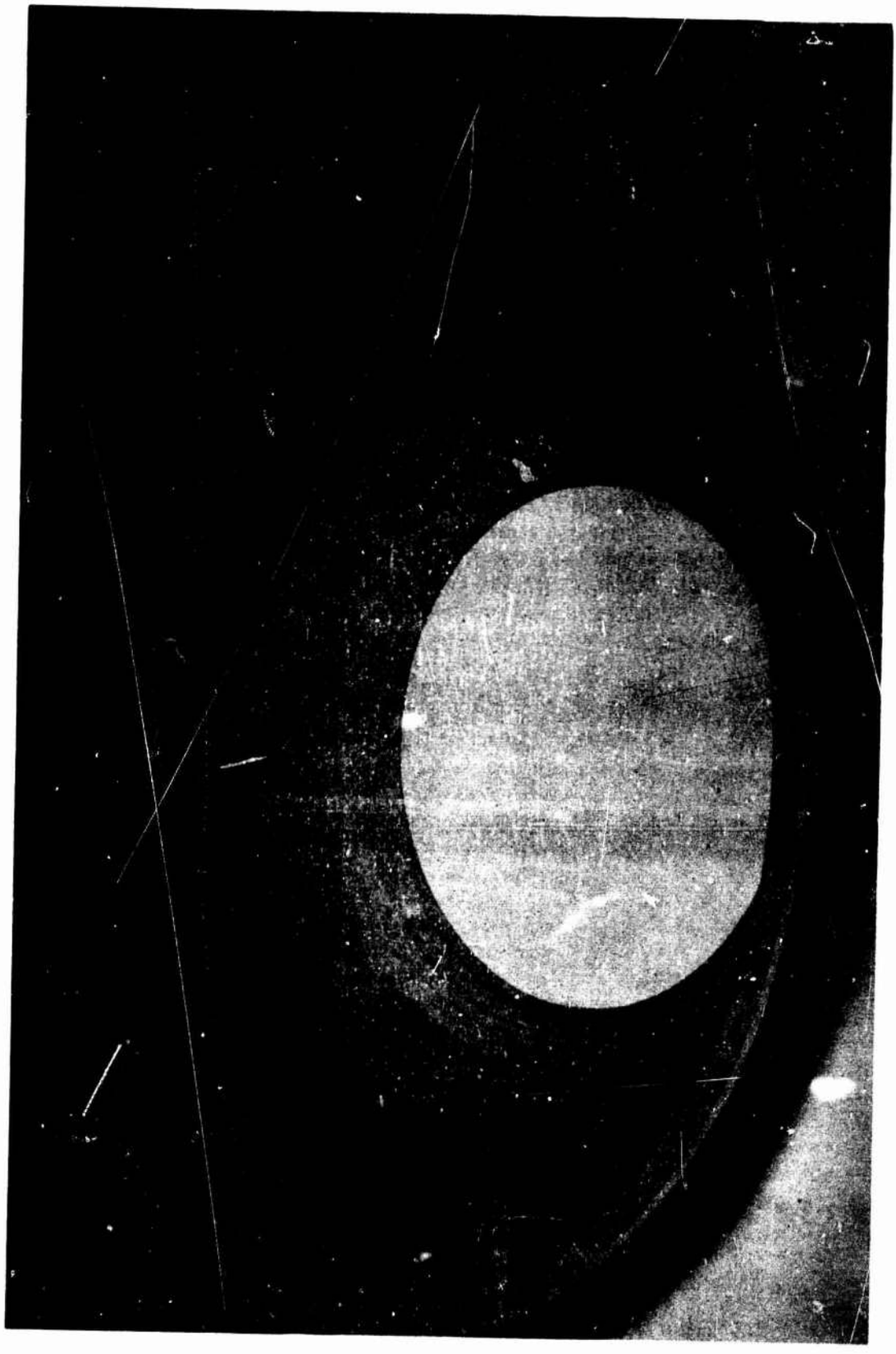

Modified Ablative Nozzle Extension

Figure VII-F-2